Validering van reactiviteitsdescriptoren
voor de beschrijving van chemische reacties

Assessment of Reactivity Descriptors
for the Study of Chemical Reactions

Karen Hemelsoet

Promotoren: prof. dr. M. Waroquier, dr. ir. V. Van Speybroeck
Proefschrift ingediend tot het behalen van de graad van
Doctor in de Ingenieurswetenschappen

Vakgroep Subatomaire en Stralingsfysica
Voorzitter: prof. dr. D. Ryckbosch
Faculteit Wetenschappen
Academiejaar 2006 - 2007

UNIVERSITEIT
GENT

ISBN 978-90-8578-139-4
NUR 928, 913
Wettelijk depot: D/2007/10.500/13

Dit onderzoekswerk werd uitgevoerd binnen het Centrum voor Moleculaire Modellering

Woord vooraf

Het schrijven van dit boek vormt de bekroning van een zeer intensieve periode en traditiegetrouw zou ik verschillende mensen willen vermelden die een belangrijke rol hierin hebben gespeeld.

In de eerste plaats wens ik mijn promotor Prof. Michel Waroquier te bedanken. Zijn enthousiaste manier van lesgeven hebben initieel mijn interesse in kwantummechanica gewekt en daarnaast bewonder ik hem voor zijn enorme inzet om een goede professionele omkadering te bieden. Onder zijn leiding is het Centrum voor Moleculaire Modellering snel uitgegroeid tot een jonge en dynamische groep, waarin een brede waaier aan onderwerpen aan bod komt. De enorme groei van onze onderzoeksgroep is eveneens te danken aan Dr. Veronique Van Speybroeck. Ondanks een grote werkdruk is zij steeds bereid om iedereen te helpen met kleine of grotere problemen. Naarmate mijn doctoraatswerk vorderde, leunden de onderwerpen steeds dichter aan bij haar expertisegebied en ik kon steeds rekenen op haar ondersteuning en hulp. Ik ben haar daar zeer dankbaar voor. De theoretische kennis van Prof. Dimitri Van Neck blijft verbazen en toch maakt ook hij altijd tijd vrij om jonge onderzoekers te helpen.

Daarnaast heb ik ook de kans gekregen om samen te werken met mensen van buiten onze onderzoeksgroep. Ik wens Prof. Guy B. Marin en Prof. Marie-Françoise Reyniers van het Laboratorium voor Petrochemische Techniek van de Universiteit Gent te bedanken voor de samenwerkingen die geleid hebben tot verschillende papers. Prof. Paul Geerlings en Prof. Frank De Proft van de Vrije Universiteit Brussel ben ik eveneens zeer erkentelijk voor de samenwerking. Niet alleen zijn zij ware experts op het gebied van conceptuele DFT, de door hun georganiseerde conferenties – zoals DFT2003 en het Reactivity Symposium 2006 – betekenden een grote stimulans. De samenwerking met Prof. Chris V. Stevens en Dr. Kristof Moonen was zeer leerrijk en wakkerde mijn interesse voor de scheikundige context aan. I also would like to acknowledge Prof. Paul Ayers, another expert within the field of reactivity indices, for the enlightening answers to many questions. I hope we can collaborate somewhere in the future. And finally, I wish to thank Prof. Leo Radom from the University of Sydney, Australia, and all the members of his research group, in particular Dr. Damian Moran. Not only for their kind hospitality during my visit in 2006, but also for the enjoyable, fruitful and very professional collaboration.

Verder dank ik ook al mijn collega's voor de goede werksfeer, in het bijzonder Peter, David en mijn zeer fijne (ex-)bureaugenoten Yves, Karel, Toon en Bart. Toon en Bart hebben de laatste tijd met heel wat nervositeit moeten omgaan en ze waren een grote steun. De immense groei van ons computerpark zorgen ervoor dat Toon en Ewald er soms een tweede dagtaak bijhebben en toch blijven zij steeds bereid om alle kleine pc-problemen op te lossen, ik apprecieer hun hulp enorm. Ook de mannen van het atelier en Rudi wens ik te danken omdat zij altijd hulp bieden aan de niet-zo-handigen onder ons, waaronder (helaas) mezelf.

Op persoonlijk vlak waren de afgelopen jaren minstens even intens. Het opboksen tegen de verkeerdelijke veronderstelling dat doctoreren een veredeld studentenleven is, heeft heel wat energie gekost, maar ik denk dat het toch gelukt is. Tussen alle drukte in waren er gelukkig de ontspannende momenten met Katrijn, Kelly en Petra. Bedankt! Mijn ouders zou ik ook willen bedanken voor alle steun gedurende de afgelopen jaren en het bezorgen van een warme thuis. Mijn zus Nele, tante Leen, tante Lulu en de mama van Lode dank ik eveneens voor alle aanmoedigingen en de praktische hulp.

Tenslotte zijn er nog twee bijzondere mensen, die alles vervolledigen en zinvol maken. Lode en Arjan, jullie staan letterlijk en figuurlijk het dichtst bij mij. Lode, jij geeft mijn leven zoveel kleur en maakt elke dag de moeite waard. Ik ben blij dat ik je tegengekomen ben, want anders had ik je mijn leven lang gemist. Sinds de geboorte van Arjan is de uitdaging en het geluk nog zoveel groter. Arjan, je bent een ongelooflijke bron van plezier en tederheid, ik hoop dat je heel gelukkig wordt.

Contents

List of Tables

List of Figures

Nederlandstalige Samenvatting

Op dit ogenblik is een brede waaier aan veeldeeltjestechnieken voorhanden om moleculaire systemen en chemische reacties, van zowel wetenschappelijk als industrieel belang, te bestuderen. Essentieel voor een dergelijke beschrijving zijn ab initio-methoden, waarmee zonder enige empirische input de grondtoestandsenergie en verschillende fysische en chemische eigenschappen kunnen berekend worden. Binnen deze ab initio-methoden kan een onderscheid gemaakt worden tussen op de golffunctie gebaseerde technieken (zoals Hartree-Fock) en dichtheidsfunctionaaltheorie (DFT). In deze doctoraatsthesis ligt de nadruk op de laatste methode. DFT vormt nl. een sterk theoretisch kader voor de introductie van belangrijke chemische concepten en is tevens een belangrijk computationeel werktuig aangezien er accurate en betrouwbare resultaten bekomen worden tegenover een haalbare computationele inspanning. DFT is gebaseerd op de basistheorema's van Hohenberg en Kohn en de introductie van ééndeeltjesorbitalen door Kohn en Sham zorgde voor een praktisch berekeningsschema waarin de exchange-correlatie functionaal de enige onbekende is.

In dit doctoraatswerk werden DFT-gebaseerde reactiviteitsindicatoren gevalideerd voor een brede waaier aan chemische reacties die voorkomen in zeer uiteenlopende toepassingsgebieden. De chemische potentiaal, de globale hardheid en de globale zachtheid worden gebruikt om de reactiviteit van een volledige, geïsoleerde molecule te bespreken of om een verzameling van gelijkaardige systemen met elkaar te vergelijken. De Fukui functie wordt gebruikt als een intra-moleculaire descriptor terwijl de lokale zachtheid inter-moleculaire informatie kan verschaffen over regioselectiviteit. Om het nut van voorgaande grootheden goed te kunnen testen worden zij geïmplementeerd binnen goedgekende chemische principes, zoals de equalisatie van de electronegativiteit, het principe van maximale hardheid en het hard/zacht zuur/base of HSAB-principe. De validering van de bekomen resultaten gebeurt a.d.h.v. een vergelijking met ab initio thermodynamische en kinetische grootheden. In het algemeen hebben DFT-gebaseerde reactiviteitsdescriptoren hun nut reeds bewezen voor de interpretatie van een groot aantal experimentele en/of theoretische resultaten. Het blijft echter een grote uitdaging om op voorhand te voorspellen of zij succesvol zullen zijn of zullen falen voor een specifieke reactie. Om werkelijk gebruik te kunnen maken van deze indicatoren als een onafhankelijk en voorspellend instrument zijn eenvoudige richtlijnen nodig die aangeven welke indicatoren een grote kans hebben om de correcte reactiviteit aan te geven. De reactiviteitsdescriptoren beschrijven elektronische effecten op basis van informatie van enkel de reactanten; ze zijn echter niet in staat om sterische effecten in rekening te brengen. De inherente beperkingen moeten steeds in het achterhoofd gehouden worden. In dit doctoraatswerk wordt er b. v. in de transitietoe-

standen van bepaalde bimoleculaire radicalaire reacties sterke sterische hinder ondervonden, wat leidt tot hoge reactiebarrières. Op basis van de definities kan er verwacht worden dat de descriptoren hier niet gebruikt kunnen worden om additionele informatie te bieden over de chemische reactiviteit en dit werd inderdaad waargenomen.

De grootste groep van onderzochte toepassingen bestaat uit radicalaire reacties. De meerderheid van deze radicalaire reacties treedt op tijdens cokesvorming, een neveneffect van thermisch kraken van koolwaterstoffen. Cokes is een grafietachtige residulaag die gevormd wordt op de binnenste reactorwand van de krakingsoven. Gebruik makend van transitietoestandstheorie werden waterstofabstracties door een aanvallend methylradicaal aan polyaromatische systemen zeer intensief bestudeerd, resulterend in accurate, betrouwbare en tegelijkertijd computationeel haalbare thermodynamische en kinetische resultaten. Andere bestudeerde bimoleculaire radicalaire reacties zijn additions van gasfaseradicalen aan kleine olefines en de initiatie- en eerste propagatiestappen van de polymerisatiereacties die leiden tot de vorming van polyethyleen en polyvinylchloride. In het algemeen werd vastgesteld dat de radicalaire Fukui functie erin slaagt om de geprefereerde reactiesite aan te duiden. Dit toont duidelijk het belang aan van de grensorbitalen voor dit specifieke reactietype. Het lokale HSAB-principe kon eveneens succesvol toegepast worden en correcte reactiviteitssequenties werden bekomen wanneer gelijkaardige moleculen met elkaar vergeleken werden. De lokale zachtheid is bijgevolg een geschikte indicator voor de studie van bimoleculaire radicaire reacties. Het succes van de lokale descriptoren is in schril contrast met het gebruik van de globale grootheden. Het globaal HSAB-principe slaagt er niet in de correcte reactiviteitssequenties aan te duiden en het gebruik van globale descriptoren wordt bijgevolg afgeraden bij de studie van bimoleculaire radicalaire reacties. Naast deze bimoleculaire reacties werden er ook unimoleculaire radicalaire reacties bestudeerd. In deze gevallen slaagt de radicalaire Fukui functie er niet in om de correcte reactiesite voor cyclisatie aan te duiden. De onderzochte cyclisaties stemmen overeen met een gebonden elektronentransfertproces: tijdens de reactie blijft het spingetal constant, terwijl het totale elektronenaantal wel wijzigt op lokaal niveau. De spin-gepolariseerde Fukui functie werd aangewend en deze grootheid was inderdaad succesvol.

In dit doctoraatswerk werden ook bimoleculaire reacties onderzocht die optreden binnen zeolietkatalyse, nl. interacties tussen kleine probemoleculen (zowel apolair als polair) en zeolietclusters. Naast de traditionele zuivere-zuurstofcluster werd ook de invloed van de substitutie van een zuurstofbrug door een aminegroep nagegaan. Het globaal HSAB-principe is enkel in staat om de interacties tussen de clusters en de apolaire moleculen correct te beschrijven. De interacties met de polaire moleculen worden gedomineerd door polaire bijdragen en aangezien deze niet in rekening genomen worden in het HSAB-principe is de globale zachtheid geen geschikte indicator voor dit specifieke reactietype. Ook vanuit lokaal standpunt treden er veel problemen op. Het

complexe reactiemechanisme van deze geconcerteerde reacties, waarbij de aanval aan de zure en aan de basische site simultaan gebeurt, kan niet beschreven worden gebruik makend van de geteste lokale indicatoren. In het algemeen is er nog verder onderzoek nodig voor de correcte beschrijving van multiple-site interacties. De polaire probemoleculen zijn harde systemen, en de lokale hardheid is eventueel een geschiktere index. Tot op heden is de berekening van deze grootheid echter nog problematisch en is er geen praktisch schema beschikbaar.

Een laatste toepassing was de unimoleculaire cyclisatie van een anion dat aanleiding geeft tot de vorming van een vierring, nl. de β-lactamring. Deze reactie vormt een uitstekend voorbeeld om competitieve reactiepaden te bestuderen, aangezien initieel de vorming van een stabiele zesring verwacht wordt. Het anionreactant is zeer zacht en de Fukui functie slaagt erin het geprefereerde atoom voor cyclisatie, nl. dit dat aanleiding geeft tot de vierring, aan te duiden als het meest reactief. Wanneer het anionreactant gebruikt werd binnen bimoleculaire reacties, b. v. protonatiereacties, is de lokale zachtheid een geschikte descriptor om de waargenomen regioselectiviteit te beschrijven.

In dit doctoraatswerk werd tevens een belangrijk voordeel van het gebruik van reactiviteitsindicatoren onderzocht, nl. de lage computationele kost van deze grootheden. In de eerste plaats gebruiken zij enkel informatie bekomen op basis van de reactanten. Een zeer uitgebreide studie toont aan dat reactiviteitssequenties gebaseerd op globale descriptoren in grote mate onafhankelijk zijn van het gebruikte berekeningsniveau. Verschillende theoretische methoden – gaande van Hartree-Fock tot de nieuwste ontwikkelingen binnen dichtheidsfunctionaaltheorie – werden getest voor zowel geometrieoptimalisatie als energieberekeningen. De grote onafhankelijkheid van het berekeningsniveau draagt bij tot de betrouwbaarheid van de onderzochte conceptuele grootheden die in het algemeen een belangrijke toegevoegde waarde bieden aan thermodynamische en kinetische grootheden.

Summary

At present, a plethora of techniques is available to study molecular systems and chemical reactions. In this light, ab initio many body techniques enable us, without any experimental input, to compute molecular energetics and a whole range of chemical properties. A twofold classification can be made, separating wave function based methods (such as Hartree-Fock) from density functional theory (DFT). In this thesis, the focus mainly lies on the density functional method, both from a conceptual as computational viewpoint - for the latter, one of the reasons being its excellent cost-to-performance ratio. The formulation of the Hohenberg-Kohn theorems in 1964 provided the starting point for the fast development of fundamental DFT, yielding all basic ingredients for a complete many-body theory. In a next step, Kohn and Sham introduced orbitals within the formalism, paving the way to a breakthrough of DFT as an important computational tool within modern chemistry. In addition to these developments, much attention has been paid to the insights DFT can give into chemical reactivity. In particular, the density functional methodology provides an excellent framework to define a variety of well-known chemical concepts.

In this thesis, the applicability of several fundamental DFT-based reactivity indicators has been tested for a variety of reactions occurring in diverse domains of chemistry. The chemical potential, global hardness and global softness are used to discuss the reactive behavior of one single molecule or a set of related molecules, providing reactivity sequences for the latter. The Fukui function is used as an intra-molecular descriptor, whereas the local softness can provide inter-molecular reactivity information about regio selectivity. In order to test the usefulness of the aforementioned properties, they are usually used in conjunction with well-known chemical principles such as the electronegativity equalization, the principle of maximum hardness and the hard and soft acids and bases (HSAB) principle. A validation of the results is obtained through comparison with ab initio thermodynamic and kinetic data. In general, DFT-based concepts have proven to be of great use in the interpretation of a variety of experimental and theoretical results. It remains nevertheless challenging to make predictions about their success or failure for specific types of interactions. In order to rely on the indicators as independent and/or predictive tools for the description of chemical reactivity, there is need for practical guidelines describing which indicators are suitable for a certain problem. The descriptors probe electronic interactions, however it is clear that they do not monitor other effects, such as steric contributions. Whenever the indicators are tested, their limitations must a priori be kept in mind. For instance, some of the reactions studied in this work exhibit high reaction barriers due to large steric hindrance effects between the two reactants and thus, the indicators are not expected to

be successful.

The largest group of applications concerns radical reactions. The majority of them occur during the formation of coke, which is a side process of thermal cracking of hydrocarbons. Radical systems are particularly interesting and challenging. However so far only a handful of papers examined and discussed their behavior using reactivity descriptors. In the specific case of hydrogen abstraction reactions at polyaromatic species by a methyl radical, accurate, reliable and yet affordable thermodynamic and kinetic data have been obtained. Other studied bimolecular radical reactions are addition reactions of radicals to small olefins and the initiation and first propagation steps within the polymerization process of polyethylene and poly(vinylchloride). Overall, it can be concluded that the radical Fukui function is capable of indicating the preferred site of reaction. This clearly indicates the importance of frontier orbital effects for this specific type of interaction. The local HSAB principle was also successfully applied, leading to correct reactivity sequences when related molecules were compared with each other. Hence the local softness is a suitable indicator for studying bimolecular radical reactions. This is in accordance with earlier suggestions and with the categorization of Klopman, as the larger radicals are characterized by high global softness values. Whereas the local viewpoint leads to satisfactory results, the global HSAB principle fails for some specific bimolecular radical reactions and is therefore not recommended. In addition to these bimolecular reactions, two examples of unimolecular radical cyclization reactions have also been studied. For these reactions, the Fukui function is used to describe the intra-molecular regio selectivity. However, the correct site of cyclization could not be indicated. Since these reactions correspond to a constrained charge transfer – the spin number remains constant, whereas the total number of electrons changes at a local level – the spin-polarized reactivity descriptors, and in particular the spin-polarized Fukui function has been tested and indeed, its usefulness is demonstrated.

A second group of studied bimolecular reactions correspond to typical reactions occurring within zeolite catalysis. The small probe molecules are characterized as hard systems, and both polar and apolar representatives were chosen. The zeolite catalyst was modelled by a small 5-tetrahedral cluster, and in addition to the traditional oxygen-bridged cluster the influence of amine substitution was tested. These reactions were difficult to describe using DFT-based reactivity descriptors. The global HSAB principle fails for the interactions with the polar molecules, as in these cases polarization effects – which are not included in the purely electron transfer process – are dominant. In contrast, the reactions between the zeolite clusters and the apolar molecules do follow the HSAB rule. From a local point of view, the complex mechanism of these concerted reactions, occurring simultaneously at the acid and basic site of the zeolite framework, could not be specified based on local descriptors. Multiple-site interactions in general remain a domain for further research. In addition, the local hardness might be more suitable to describe interactions with hard

molecules, although at present the calculations remain troublesome and no practical scheme is presented yet.

A final application concerns a unimolecular ionic cyclization reaction leading to the formation of a four-membered β-lactam ring. This is an example in which competing pathways can take place because the formation of the more stable six-membered ring, instead of the strained four-membered ring, is initially expected. The anion reactant is a very soft species and the traditional local indicator, i. e. the Fukui function, succeeds in correctly predicting the preferred reaction path. Therefore the indicator adds to the unravelling of the origin of the experimentally observed cyclization preference. Moreover, extension to bimolecular reactions using this anion reactant also revealed the successful applicability of the local softness, as also these results were in correspondence with reaction barriers obtained at 0 Kelvin.

In this thesis, one of the main advantages of using reactivity descriptors was accentuated, in particular their low computational cost. Not only do they solely require information from the reactants, but it was furthermore demonstrated that reactivity sequences are mainly independent of the level of theory used for geometry optimizations as well as for single-point energy calculations. An extended set of theoretical procedures, ranging from simple ab initio methods such as Hartree-Fock, over a very popular and successful functional, to the latest class of highly promising methods. The observation of level-of-theory independency for the calculation of the global descriptors is highly reassuring and adds to the reliability of DFT-based reactivity indicators. It must however be emphasized that overall the perturbative approach should be used complementary to information obtained from thermodynamics and kinetics.

Part I

Assessment of Reactivity Descriptors for the Study of Chemical Reactions

1

General Introduction

Since the beginning of quantum mechanics, there has been an interest in how the mathematical formalism and physical concepts of this theory can be used to describe the chemical bonding. Without discussing the entire evolution of chemical reactivity, some milestones are pointed out. An initial description was based on the electronic quantum theory of organic chemistry (Lewis-dot structures), which was generalized by Coulson and Longuet-Higgins. In a next stage, symmetry rules for the molecular orbitals were established for predicting the course of a reaction. In this light, the frontier orbital theory (FMO) of Fukui and the Woodward-Hoffmann rules can be situated. Furthermore, Pearson postulated, based on experimental observations, the hard and soft acids and bases (HSAB) principle. At present, a plethora of techniques is available to study molecular systems and chemical reactions. For instance, ab initio many body techniques enable us, without any experimental input, to compute molecular energetics and a whole range of chemical properties. A twofold classification can be made, separating wave function based methods (such as Hartree-Fock) from density functional theory (DFT). Both methodologies had a huge impact on chemical research, as was also recognized in 1998 by awarding the Nobel Prize for Chemistry to Prof. J. A. Pople and Prof. W. Kohn, the protagonists of wave function quantum chemistry and DFT, respectively.

In this thesis, the focus mainly lies on the density functional method, both from a conceptual as computational viewpoint - for the latter, one of the reasons being its excellent cost-to-performance ratio. The formulation of the Hohenberg-Kohn theorems in 1964 provided the starting point for the fast development of fundamental DFT, yielding all basic ingredients for a complete many-body theory. In a next step, Kohn and Sham introduced orbitals within the formalism, paving the way to a breakthrough of DFT as an important computational tool within modern chemistry. In addition to these developments, much attention has been paid to the insights DFT can give into chemical reactivity. In particular, the density functional methodology provides an excellent

framework to define a variety of well-known chemical concepts, such as the chemical potential, hardness and softness.

Within DFT, every chemical reaction can in theory be completely described through changes in the electron density. However, it is sometimes more useful and convenient to change the fundamental variables to the external potential and the total number of electrons. Reactivity indicators of DFT are defined in this way, and these properties form an important subject of this thesis. More precisely, the indicators represent response functions of the total electronic energy to perturbations in the nuclear configuration (corresponding to the external potential) or total electron number. These 'model' or 'universal' perturbations are thought to capture the essence of the attacking species, without the requirement of more detailed information. Since we are dealing with the first terms within a Taylor-series expansion, they will be most reliable when the perturbation is small, so that higher-order effects are negligible. Therefore, the indicators are most appropriate for describing geometries in which the reactants are well separated, so that the perturbations under consideration are relatively weak.

From a more traditional point of view, reactivity can be studied using chemical thermodynamics and kinetics. So far, and keeping in mind the increasing computer facilities, many efforts have been made to obtain accurate results for reaction barriers, reaction enthalpies and rate constants. Therefore, high-level, and computationally very demanding, many body techniques have been developed and tested. The kinetic rate constants are usually computed by applying transition state theory (TST) or extensions of it. The original formulation is, although rather old and conceptually simple, still very successful. TST uses static structure properties of three distinct states of the system (the reactants, products and transition state).

Clearly, it is now possible to study chemical reactivity from two different viewpoints: using thermodynamic and kinetic properties on one hand and using DFT-based reactivity descriptors on the other. In this thesis, it is thoroughly examined to what extent both approaches can be combined in a complementary way, and to what extent the DFT-based indicators can be treated as an independent, predictive, intuitive tool. In this light, it is useful to make some preliminary remarks about the advantages and disadvantages of the perturbative perspective. One of the main advantages of the reactivity descriptors is that the required calculations are computationally less intensive – but also less detailed – because all information is obtained through study of the reactants only. According to this procedure, only information about the onset of the chemical reaction is obtained, and therefore the indicators are expected to be successful especially in the case of a transition state whose structure is similar to the reactant (early transition structure according to the Hammond's postulate). Another advantage is the possibility to discuss the problem of regio selectivity. And finally, due to the general nature of the definitions provided within the perturbative approach, the broad area of application is definitely

another point which adds to its success. In addition to the above-mentioned advantages, conceptual DFT also encounters some drawbacks. First of all, it remains challenging to provide general guidelines to predict the success (or failure) of the descriptors. In addition, the model is very useful to obtain qualitative information. It however remains very approximate in a quantitative sense. Consequently, the focus usually lies on exploring trends in chemical reactivity, rather than obtaining accurate quantitative data. Up till now, most papers on the interpretative use of reactivity indicators focussed on obtaining intra- and intermolecular reactivity trends. A comparison with experimental data was initially made, whereas at present the predictive results are compared with accurate thermodynamic and/or kinetic ab initio quantities.

In this thesis, the interpretative use of DFT-based reactivity indicators is thoroughly investigated for a variety of chemical compounds and reactions. The applications are inspired by research topics which are conducted within the Center of Molecular Modeling (Head Prof. M. Waroquier). As a first application, radical reactions are selected. The majority of the studied interactions can be situated in the growth process of a coke layer occurring within the thermal cracking process of hydrocarbons. This work is performed in collaboration with the Laboratorium voor Petrochemische Techniek (Head Prof. G. B. Marin) of the University of Ghent. A part of this work specifically focusses on obtaining accurate and reliable thermodynamic and kinetic results and is done in collaboration with the research group of Prof. L. Radom of the University of Sydney in Australia. In general, radical reactions form challenging test cases for the applicability of reactivity descriptors, as the charge transfer between a radical and a neutral molecule is a more complex phenomenon compared with the transfer between two ions, two neutral systems or between an ion and a neutral system. So far, only a handful of papers examined radical systems and/or reactions using reactivity descriptors. The applicability of reactivity descriptors for these interactions is studied in collaboration with the Research Group of General Chemistry (Head Prof. P. Geerlings) of the Free University of Brussels. A second group of applications are typical acid-base reactions occurring in the heterogeneous catalysis using zeolites. In the pores of these periodic materials, reactions between small probe molecules and the zeolite framework take place. It is investigated which effects (electrostatic, frontier-orbital,...) dominate the interactions and which description (hard-hard or soft-soft) is most appropriate to examine the chemical reactivity. Consequently, it is interesting to see which reactivity indicators will be applicable to correctly describe these complex multiple-site interactions. A final set of applications corresponds to cyclization reactions, and both radical and ionic interactions are investigated. The experimental data of these examples are provided by the research groups of Prof. C. V. Stevens and Prof. N. De Kimpe of the University of Ghent. The radical cyclization is additionally examined using spin-polarized concepts in collaboration with the research group of Prof. P. Geerlings and Prof. F. De Proft. The unimolecular nature of these interactions provides another extra ingredient and the suitability of various descriptors is probed.

This thesis is structured as follows: in the next chapter the theoretical background of DFT-based reactivity indicators and their implementation into important principles on one hand and chemical kinetics on the other, is given. Chapter 3 summarizes the results, obtained within the three different fields of application (as mentioned above). Chapter 4 contains a general conclusion and some brief comments on further perspectives. The second part of this work (Part II) contains the original papers, published or in press, in which a more detailed discussion of the results is presented.

2

Theoretical Background

2.1 DFT-based reactivity descriptors: definitions and calculation

DFT-based reactivity indicators represent the response of a system to a specific perturbation. This perturbation might be a change in the total number of electrons N or in the nuclear configuration $v(\mathbf{r})$. Assuming functional differentiability of the total electronic energy E with respect to N (at fixed $v(\mathbf{r})$) and/or with respect to $v(\mathbf{r})$ (at fixed N), the indicators are defined as derivatives of $E[N, v(\mathbf{r})]$ (1). Hence, a series of response functions is obtained. The Taylor series expansion of $E[N, v(\mathbf{r})]$ is written as:

$$\begin{aligned} E[N, v(\mathbf{r})] &= E_0 + \Delta N (\frac{\partial E}{\partial N})_{v(\mathbf{r})} + \frac{1}{2}(\Delta N)^2 (\frac{\partial^2 E}{\partial N^2})_{v(\mathbf{r})} \\ &+ \int (\frac{\partial E}{\partial v(\mathbf{r})})_N \Delta v(\mathbf{r}) d\mathbf{r} + \Delta N \int (\frac{\partial^2 E}{\partial N \partial v(\mathbf{r})}) v(\mathbf{r}) d\mathbf{r} \\ &+ \frac{1}{2} \int (\frac{\partial^2 E}{\partial v(\mathbf{r}) \partial v(\mathbf{r}')}) \Delta v(\mathbf{r}) \Delta v(\mathbf{r}') d\mathbf{r} d\mathbf{r}' + \dots \end{aligned}$$

The question of whether E is differentiable to N was earlier investigated (2–7), since for realistic systems such as isolated atoms and molecules, N necessarily represents an integer value. However, extensions to fractional particle numbers were introduced, and two different approaches can be distinguished: the fractional occupation numbers method developed by Janak (4) versus a thermodynamic extension of Perdew et al. (5), Perdew and Levy (8) and von Barth (9). In the latter approach it was proven that the E versus N curve consists of straight line segments. Consequently, N-derivative discontinuities will show up and three distinct classes of indicators appear, according to a nucleophilic ($dN > 0$), electrophilic ($dN < 0$) and radical ($dN = 0$) attack. Moreover, higher-order derivatives are identically zero. In practice, the Taylor expansion

of the energy functional (given above) is usually truncated at second order, and hence a quadratic interpolation is obtained.

The functional derivatives, up to second order (n=2), are schematically depicted in Table 2.1. It is immediately clear that three categories can be distinguished (10): global indicators, local indicators and kernels (or two-point indicators). The first group represents characteristics of the system as a whole, whereas the second group corresponds to values which vary from point to point. The latter group represents the response at a certain position $\mathbf{r}$ to a perturbation at another position $\mathbf{r}'$. All definitions are given at 0 Kelvin, however a generalization of DFT to finite temperatures is possible and was made by Mermin (11).

					$E[N, v(\mathbf{r})]$					
			↙				↘			
n=1			μ					$\rho(\mathbf{r})$		
		↙		↘			↙		↘	
n=2	η				$f(\mathbf{r})$					$\chi_1(\mathbf{r}, \mathbf{r}')$

↙ ≡ $(\frac{\partial}{\partial N})_{v(\mathbf{r})}$ and ↘ ≡ $(\frac{\partial}{\partial v(\mathbf{r})})_N$

Table 2.1: Schematical overview of the reactivity indicators.

An overview of the definitions of DFT-based indicators is given in Table 2.2. In the remainder of this section a brief discussion of their properties is given. In addition, the extension to a spin-polarized system is also addressed and finally, some descriptors used within the context of aromaticity are presented. For a comprehensive and extended review about both the theoretical aspects as well as applications, we refer to recent work by Geerlings, De Proft and Langenaeker (12).

2.1.1 Global descriptors

Global descriptors are used to discuss the reactive behavior of one single molecule or a set of related molecules, providing reactivity sequences for the latter.

The first order derivative towards N equals the *chemical potential* μ. It is the cornerstone of conceptual DFT as it provides a chemical interpretation for the Lagrange-multiplier used in the Euler equation $(v(\mathbf{r}) + \frac{\partial F_{HK}[\rho]}{\partial \rho(\mathbf{r})} = \mu)$ (13). The aforementioned relationship points out that the chemical potential is the effective electrostatic potential experienced by the electron density. Hence, this quantity characterizes the escaping tendency of the electron cloud from the equilibrium state (14). The chemical potential was also recognized to be equal to a long-standing and important chemical concept, in particular the electronegativity χ $(\mu = -\chi)$ (15; 16).

The second order derivative towards N equals the *global hardness* η (17).

Global indicators	*Local indicators*
$\mu = (\frac{\partial E}{\partial N})_{v(\mathbf{r})}$	$\rho(\mathbf{r}) = (\frac{\partial E}{\partial v(\mathbf{r})})_N$
$\eta = \frac{1}{2}(\frac{\partial^2 E}{\partial N^2})_{v(\mathbf{r})} = \frac{1}{2}(\frac{\partial \mu}{\partial N})_{v(\mathbf{r})}$	$\eta(\mathbf{r}) = \frac{1}{2}(\frac{\partial \mu}{\partial \rho(\mathbf{r})})_{v(\mathbf{r})}$
$S = \frac{1}{2\eta} = (\frac{\partial N}{\partial \mu})_{v(\mathbf{r})}$	$s(\mathbf{r}) = (\frac{\partial \rho(\mathbf{r})}{\partial \mu})_{v(\mathbf{r})}$
$\omega = \frac{\mu^2}{2\eta}$	$f(\mathbf{r}) = (\frac{\partial^2 E}{\partial N \partial v(\mathbf{r})}) = (\frac{\partial \rho(\mathbf{r})}{\partial N})_{v(\mathbf{r})} = (\frac{\partial \mu}{\partial v(\mathbf{r})})_N$
$\nu = \frac{2\eta}{\mu^2}$	
$\lambda_N = \exp(-\frac{1}{10}(\mathrm{sgn}(\eta+\mu)\left(\frac{(\eta+\mu)^2}{2\eta}\right)))$	
$\lambda_E = \exp(-\frac{1}{10}(\frac{(\mu-\eta)^2}{2\eta}))$	
Kernels	
$\chi_1(\mathbf{r},\mathbf{r}') = (\frac{\partial^2 E}{\partial v(\mathbf{r}) v(\mathbf{r}')})_N$	
$\eta(\mathbf{r},\mathbf{r}') = \frac{\partial^2 F[\rho]}{\partial \rho(\mathbf{r}) \partial \rho(\mathbf{r}')}$	
$s(\mathbf{r},\mathbf{r}') = -\frac{\partial \rho(\mathbf{r}')}{\partial u(\mathbf{r})} = -\frac{\partial \rho(\mathbf{r})}{\partial u(\mathbf{r}')}$	

Table 2.2: Definitions of reactivity indicators.

This quantity characterizes the resistance towards charge transfer, and is correlated to the stability of the reagent (18; 19). The global hardness was found – within an orbital approach using Koopmans' theorem (20) – to be related to the energy gap between the occupied and unoccupied orbitals. The reciprocal of the global hardness is the *global softness* S, which was identified to be a measure of polarizability (21). It is generally accepted that small, non polarizable, and highly charged species behave as hard reagents, while larger, more polarizable, and less charged species act as soft. Both quantities reflect on initial work that was performed by Pearson, studying generalized Lewis acid-base reactions (22):

$$\mathrm{A}+ : \mathrm{B} \quad \rightleftarrows \quad \mathrm{A} - \mathrm{B}$$

where A is a Lewis acid or electron pair acceptor and B a Lewis base or electron pair donor. Recently, Ayers suggested that the electronic chemical potential can be used as a measure of the intrinsic strength of acids and bases (23).

In the majority of the studies published in literature so far, the global descriptors are computed applying the simple finite difference method (FD) and taking the arithmetic average of the left- and right-hand-side derivatives (using the quadratic interpolation for E versus N) (1). The vertical ionization potential IP and electron affinity EA consequently form the basic quantities. The disadvantage of this conceptually simple method is that it necessitates three energy calculations (corresponding to the N, $N-1$ and $N+1$ system). In addition with possible stability problems of the $N+1$ and/or $N-1$ structures, use of orbital energies, applying Koopmans' theorem to approximate the FD method, might be more appropriate. This particular theorem states that the ionization potential and electron affinity of an N-electron system can be identified

with the orbital energy of the highest occupied molecular orbital (HOMO) and lowest unoccupied molecular orbital (LUMO), respectively (20). This approximation is basically applicable when orbital relaxation effects can be neglected upon addition or removal of an electron. It is important to keep in mind that usage of this theorem in combination with DFT methods should be treated with care as the Kohn-Sham orbitals have no sound physical meaning. Komorowski et al. developed an analytical method of calculation, using coupled perturbed Hartree-Fock equations (24). It is important to note that one should be very careful when results, obtained using various methods, are compared with each other. For the calculation of the hardness, other specific methodologies were developed, e.g. using the hardness kernel (vide supra) (25) or an MO-resolved hardness tensor (26). Developments within the atoms-in-molecules (AIM) (27) or equalization of electronegativity (28; 29) context should also be mentioned. The working equations, used in this thesis to calculate the global indicators, are summarized in Table 2.3.

	FD Method	Koopmans' theorem
μ	$-(IP+EA)/2$	$(\epsilon_{\text{HOMO}}+\epsilon_{\text{LUMO}})/2$
η	$(IP-EA)/2$	$(\epsilon_{\text{LUMO}}-\epsilon_{\text{HOMO}})/2$
S	$(IP-EA)^{-1}$	$(\epsilon_{\text{LUMO}}-\epsilon_{\text{HOMO}})^{-1}$

Table 2.3: Simple methods of calculations for the global indicators.

In recent years, other indicators were introduced to describe the ability of a molecule to accept or donate electrons, i.e. the electrophilic or nucleophilic behavior, respectively. These properties can be identified as combinations of μ and η. In this light, the *electrophilicity* ω is defined as the change in energy that occurs when a reagent is placed in contact with the perfect nucleophile (that is, a reservoir of electrons with zero chemical potential and zero hardness) (30–32). The definition is reported in Table 2.2 and it is clear that it is in agreement with chemical intuition, yielding that a good electrophile is a molecule with a low value of μ and a small η. The reciprocal quantity is the *nucleophilicity* ν, defined as $\nu = 1/\omega$ (32; 33). The *nucleofugality* λ_N characterizes the ability to accept an entire electron from a system, whereas the *electrofugality* λ_E is the ability to donate an entire electron to a system (34).

2.1.2 Local descriptors

Local descriptors provide direct information about the site-selectivity within a molecule and indicate at which site the reaction preferentially will occur.

Using standard perturbation techniques, the first order derivative to $v(\mathbf{r})$ (at fixed N) is shown to equalize the *electron density* $\rho(\mathbf{r})$. Relative information about $\rho(\mathbf{r})$ can be obtained using the *shape factor* $\sigma(\mathbf{r}) = \rho(\mathbf{r})/N$ (35).

The shape factor, which is normalized to 1, redistributes the total number of electrons. Analogous to the canonical and grand-canonical ensembles, the isomorphic and grand-isomorphic ensembles can be used, using $[N,\sigma(\mathbf{r})]$ and $[\mu,\sigma(\mathbf{r})]$ as the basic variables, respectively (36). The shape factor is also applied when the 'similarity' of charge distributions is studied and in this light, various similarity indices have been proposed (37–45).

The second order, mixed derivative equals the *Fukui function* $f(\mathbf{r})$ (46; 47). This quantity is normalized to 1 and can be seen as an intra-molecular descriptor. The Fukui function generalizes the frontier molecular orbital concept (FMO) developed by Fukui in 1952, in which the importance of the frontier orbitals (highest occupied and lowest unoccupied or HOMO and LUMO) is pointed out (48–50). This connection is explicitly shown in the following equations, taking into account the N-discontinuity problem using the FD method (step 1) and freezing all orbitals, with exception of the frontier orbitals (step 2):

$$\begin{aligned} f^+(\mathbf{r}) &\approx \rho_{N+1}(\mathbf{r}) - \rho_N(\mathbf{r}) \approx \rho_{\text{LUMO}}, \\ f^-(\mathbf{r}) &\approx \rho_N(\mathbf{r}) - \rho_{N-1}(\mathbf{r}) \approx \rho_{\text{HOMO}}, \\ f^0(\mathbf{r}) &\approx (\rho_{N+1}(\mathbf{r}) - \rho_{N-1}(\mathbf{r}))/2 \approx (\rho_{\text{LUMO}} + \rho_{\text{HOMO}})/2. \end{aligned}$$

The direct link between the Fukui functions and the frontier orbitals was also shown by Yang et al. (51):

$$\begin{aligned} f^+(\mathbf{r}) &= \lim_{\delta\to 0^+} \frac{\partial \rho_{M+\delta}(\mathbf{r})}{\partial N} = \sum_{i=1}^{M} \frac{\partial}{\partial N} |\psi_i(\mathbf{r})|^2 + |\psi_{\text{LUMO}}|^2, \\ f^-(\mathbf{r}) &= \lim_{\delta\to 0^-} \frac{\partial \rho_{M+\delta}(\mathbf{r})}{\partial N} = \sum_{i=1}^{M-1} \frac{\partial}{\partial N} |\psi_i(\mathbf{r})|^2 + |\psi_{\text{HOMO}}|^2. \end{aligned}$$

For the calculation of this three-dimensional quantity, various methodologies have been proposed, providing alternatives for the FD method. First of all, a gradient expansion for $f(\mathbf{r})$ was developed, however this method was only applied for atomic systems (52–54). The variational principle for chemical hardness (25) yields that $f(\mathbf{r})$ is found as the function that minimizes the hardness kernel (vide supra) (55; 56). The practical usage of this method is hampered by problems related to the accurate calculation of the hardness kernel. Nalewajski et al. proposed a method, based on a single Kohn-Sham calculation, where an extra term is added to the frontier orbital term (57). This extra term accounts for orbital relaxation effects.

The *local softness* $s(\mathbf{r})$ is another frequently used local indicator, describing inter-molecular site reactivity as it contains all information of the $f(\mathbf{r})$ indicator combined with global information (58). The correlation between both quantities ($s(\mathbf{r}) = Sf(\mathbf{r})$) is easily obtained by applying the chain rule.

In general, practical use of these three-dimensional reactivity descriptors

remains quite prohibitive and therefore, condensed values are applied, giving an approximate value for the local indicator at the position of an atomic center. Using the FD method, the following equations are obtained (59):

$$\begin{aligned} f_k^+ &= \tilde{q}_k(N+1) - \tilde{q}_k(N) \quad \text{and} \quad s_k^+ = S(\tilde{q}_k(N+1) - \tilde{q}_k(N)), \\ f_k^- &= \tilde{q}_k(N) - \tilde{q}_k(N-1) \quad \text{and} \quad s_k^- = S(\tilde{q}_k(N) - \tilde{q}_k(N-1)), \\ f_k^0 &= (\tilde{q}_k(N+1) - \tilde{q}_k(N-1))/2 \quad \text{and} \quad s_k^0 = S(\tilde{q}_k(N+1) - \tilde{q}_k(N-1))/2. \end{aligned}$$

In these equations $\tilde{q}_k(N)$ is the electron population on the k^{th} atom of the molecule with N electrons. This population can be calculated using various population analysis methods such as Mulliken (60), Natural Population Analysis (NPA) (61), Hirshfeld (62), AIM (3) and others based on the electrostatic potential (e.g. CHELPG (63) and MK (64; 65)). The influence of the population analysis method on the resulting condensed values is non-negligible, and a substantial amount of studies addressed this topic (66–73). Related works, developing other methods of calculation for these atomic Fukui functions and softness values should also be mentioned (74–80). According to Ayers et al. the condensed Fukui functions are, in the context of a variational approach to chemical reactivity, even more instructive indicators of molecular site reactivity than the actual Fukui function (81).

Computing condensed descriptors sometimes lead to negative values, and although this is rather counterintuitive there is no theoretical reason why this should not be acceptable. Roy et al. attributed these negative values to relaxation effects and improper population analysis techniques (82–85). Ayers et al. found that a requirement for obtaining positive Fukui functions consists in the diagonal dominance of the hardness matrix (81). This is in accordance with findings of Bultinck et al. who stated that when using the EEM scheme one always finds positive Fukui functions for not too heavily distorted geometries (86). In order to overcome the issue of negative condensed Fukui functions, new indicators, i.e. the *relative nucleophilicity* ($= s^-/s^+$) and *relative electrophilicity* ($= s^+/s^-$) were introduced (87; 88).

Within the context of hard and soft species, a local hardness indicator $\eta(\mathbf{r})$ is also of interest. The original definition (Table 2.2) was suggested in analogy with the soft counterpart (89). However, this definition is problematic as it is in contrast with the first theorem of Hohenberg and Kohn, where the one-one relationship between $\rho(\mathbf{r})$ and $v(\mathbf{r})$ is proven (90). An alternative expression for $\eta(\mathbf{r})$ was therefore given (91; 92):

$$\eta(\mathbf{r}) = \frac{1}{2N} \int \frac{\partial^2 F_{\text{HK}}}{\partial\rho(\mathbf{r})\partial\rho(\mathbf{r}')} \lambda(\rho(\mathbf{r}'))d\mathbf{r}'$$

with F_{HK} the universal (as it is independent of $v(\mathbf{r})$) Hohenberg-Kohn functional and $\lambda(\rho(\mathbf{r})) = \rho(\mathbf{r})$ or $\lambda(\rho(\mathbf{r})) = Nf(\mathbf{r})$. The latter choice however leads to the somehow unrealistic and unphysical result that $\eta(\mathbf{r}) = \eta$, suggesting that the local descriptor equalizes the global one (91; 92).

2.1.3 Kernels

Kernels or two-point indicators are nonlocal quantities, depending on two spatial positions $\mathbf{r}$ and $\mathbf{r}'$. They can be associated with local responses to local perturbations.

Within a perturbational approach, responses to changes in $v(\mathbf{r})$ have been extensively studied by Senet (80; 93) and Fuentealba et al. (94–96). The *first-order response function* $\chi_1(\mathbf{r}, \mathbf{r}')$ is of particular interest. This property is also known as the polarizability kernel $P(\mathbf{r}, \mathbf{r}')$.

The *softness kernel* $s(\mathbf{r}, \mathbf{r}')$ was introduced by Berkowitz and Parr (97), using the modified potential $u(\mathbf{r}) = v(\mathbf{r}) - \mu = -\frac{\partial F_{\text{HK}}[\rho]}{\partial \rho}$. An interesting relationship between the softness kernel and linear response function can be obtained:

$$\chi_1(\mathbf{r}, \mathbf{r}') \quad = \quad -s(\mathbf{r}, \mathbf{r}') + \frac{s(\mathbf{r})s(\mathbf{r}')}{S}.$$

From a theoretical and algorithmic point of view, kernels have known a lot of attention, however, so far, numerical studies are very scarce. One of the reasons is that an explicit form for the *hardness kernel* $\eta(\mathbf{r}, \mathbf{r}')$ remains troublesome (98; 99). Its form must be (100):

$$\eta(\mathbf{r}, \mathbf{r}') \quad = \quad \frac{1}{|\mathbf{r} - \mathbf{r}'|} + R(\mathbf{r}, \mathbf{r}'),$$

where the first part represents the classical Coulombic part, and the second term includes contributions from the kinetic, exchange and correlation energy functionals.

From the definitions in Table 2.2, it is clear that the softness and hardness kernel $\eta(\mathbf{r}, \mathbf{r}')$ are related through the following relationship, indicating their reciprocity:

$$\int s(\mathbf{r}, \mathbf{r}')\eta(\mathbf{r}', \mathbf{r}'')d\mathbf{r}' \quad = \quad \delta(\mathbf{r} - \mathbf{r}'').$$

2.1.4 Spin-polarized generalizations

The standard density functional theory can be extended to spin-polarized DFT (SP-DFT) in order to describe systems with a more generalized potential, such as a magnetic field $\mathbf{B}(\mathbf{r})$ in addition to the usual scalar potential $v(\mathbf{r})$ (101–103). The total electronic energy can be expressed in terms of the electron and spin density, $\rho(\mathbf{r})$ and $\rho_S(\mathbf{r})$:

$$E[\rho(\mathbf{r}), \rho_S(\mathbf{r})] \quad = \quad F[\rho(\mathbf{r}), \rho_S(\mathbf{r})] + \int \rho(\mathbf{r})v(\mathbf{r})d\mathbf{r} - \mu_B \int \mathbf{B}(\mathbf{r})\rho_S(\mathbf{r})d\mathbf{r},$$

with $F[\rho(\mathbf{r}), \rho_S(\mathbf{r})]$ the universal functional (the sum of the kinetic energy and the electron-electron repulsion energy) and μ_B the Bohr magneton. Minimization of the energy functional with respect to $\rho(\mathbf{r})$ and $\rho_S(\mathbf{r})$, under the normalization constraints:

$$\begin{aligned} \int \rho(\mathbf{r}) d\mathbf{r} &= \int \rho^{\uparrow}(\mathbf{r}) d\mathbf{r} + \int \rho^{\downarrow}(\mathbf{r}) d\mathbf{r} = N^{\uparrow} + N^{\downarrow} = N, \\ \int \rho_S(\mathbf{r}) d\mathbf{r} &= \int \rho^{\uparrow}(\mathbf{r}) d\mathbf{r} - \int \rho^{\downarrow}(\mathbf{r}) d\mathbf{r} = N^{\uparrow} - N^{\downarrow} = N_S, \end{aligned}$$

yields the following fundamental equations for the Lagrange multipliers:

$$\begin{aligned} \mu_N &= (\frac{\partial E}{\partial \rho(\mathbf{r})})_{\rho_S(\mathbf{r}),\mathbf{B}(\mathbf{r})} = (\frac{\partial F}{\partial \rho(\mathbf{r})})_{\rho_S(\mathbf{r}),\mathbf{B}(\mathbf{r})} + v(\mathbf{r}), \\ \mu_S &= (\frac{\partial E}{\partial \rho_S(\mathbf{r})})_{\rho(\mathbf{r}),v(\mathbf{r})} = (\frac{\partial F}{\partial \rho_S(\mathbf{r})})_{\rho(\mathbf{r}),v(\mathbf{r})} - \mu_B \mathbf{B}(\mathbf{r}). \end{aligned}$$

These quantities have been identified with the chemical and spin potential, respectively. Note that in this definition of μ_N (in contrast to the non polarized description), the derivative is taken at constant spin number N_S.

Analogous to spin-restricted conceptual DFT, a perturbative approach can be used, according to changes in N (describing charge-transfer processes), N_S (describing spin-polarization processes), $v(\mathbf{r})$ or $\mathbf{B}(\mathbf{r})$ (104–113). This methodology yields definitions for various global, local and nonlocal reactivity descriptors. An overview of the basic global and local quantities is given in Table 2.4; the nonlocal properties are left out, as – due to their computational complexity – no numerical results have been reported so far.

Global indicators	*Local indicators*
$\mu_N = (\frac{\partial E}{\partial N})_{N_S,v(\mathbf{r}),\mathbf{B}(\mathbf{r})}$	$\rho(\mathbf{r}) = (\frac{\partial E}{\partial v(\mathbf{r})})_{N,N_S,\mathbf{B}(\mathbf{r})}$
$\mu_S = (\frac{\partial E}{\partial N_S})_{N,v(\mathbf{r}),\mathbf{B}(\mathbf{r})}$	$\rho_S(\mathbf{r}) = -\frac{1}{\mu_B}(\frac{\partial E}{\partial \mathbf{B}(\mathbf{r})})_{N,N_S,v(\mathbf{r})}$
$\eta_{NN} = (\frac{\partial \mu_N}{\partial N})_{N_S,v(\mathbf{r}),\mathbf{B}(\mathbf{r})}$	$f_{NN}(\mathbf{r}) = (\frac{\partial \mu_N}{\partial v(\mathbf{r})})_{N,N_S,\mathbf{B}(\mathbf{r})}$
$\eta_{NS} = (\frac{\partial \mu_N}{\partial N_S})_{N,v(\mathbf{r}),\mathbf{B}(\mathbf{r})}$	$f_{SN}(\mathbf{r}) = (\frac{\partial \mu_N}{\partial \mathbf{B}(\mathbf{r})})_{N,N_S,v(\mathbf{r})} = -\mu_B(\frac{\partial \rho_S}{\partial N_S})_{N,v(\mathbf{r}),\mathbf{B}(\mathbf{r})}$
$= (\frac{\partial \mu_S}{\partial N})_{N_S,v(\mathbf{r}),\mathbf{B}(\mathbf{r})} = \eta_{SN}$	
$\eta_{SS} = (\frac{\partial \mu_S}{\partial N_S})_{N,v(\mathbf{r}),\mathbf{B}(\mathbf{r})}$	$f_{NS}(\mathbf{r}) = (\frac{\partial \mu_S}{\partial v(\mathbf{r})})_{N,N_S,\mathbf{B}(\mathbf{r})} = (\frac{\partial \rho}{\partial N_S})_{N,v(\mathbf{r}),\mathbf{B}(\mathbf{r})}$
	$f_{SS}(\mathbf{r}) = (\frac{\partial \mu_S}{\partial \mathbf{B}(\mathbf{r})})_{N,N_S,v(\mathbf{r})} = -\mu_B(\frac{\partial \rho_S}{\partial N_S})_{N,v(\mathbf{r}),\mathbf{B}(\mathbf{r})}$

Table 2.4: Definitions of spin-polarized reactivity indicators.

For the second-order derivatives, η_{NN} is the equivalent of the hardness in the spin-restricted case, except (as for the first-order derivative μ_N) that the derivative is taken at constant N_S. The spin hardness η_{SS} is evaluated at constant N and provides information about different valence states of the system. The four variants of the Fukui function describe the regio selectivity. It is important to note that the functional derivatives, as defined within SP-DFT, should be treated with utmost care. Within a spin-polarized framework, the

mapping between $[\rho(\mathbf{r}), \rho_S(\mathbf{r})]$ and $[v(\mathbf{r}), \mathbf{B}(\mathbf{r})]$ is not unique (114). However, it is shown that this non uniqueness is removed when N_S and N are kept constant, which is the case in this perturbative approach.

The spin potential μ_S and spin hardness η_{SS} can be used to describe the energy change between a reference ground state and an excited state. During this process, the number of electrons and external potential remain constant. The spin potential can be calculated as follows (note, again, the analogy with the spin-unrestricted situation):

$$\mu_S^+ \approx \frac{\epsilon^\alpha_{\mathrm{LUMO}} - \epsilon^\beta_{\mathrm{HOMO}}}{2}, \quad \mu_S^- \approx \frac{\epsilon^\alpha_{\mathrm{HOMO}} - \epsilon^\beta_{\mathrm{LUMO}}}{2},$$

with $\epsilon^\alpha_{\mathrm{HOMO}}$, $\epsilon^\beta_{\mathrm{HOMO}}$, $\epsilon^\alpha_{\mathrm{LUMO}}$ and $\epsilon^\beta_{\mathrm{LUMO}}$ the orbital energies of the spin-up and spin-down HOMO and LUMO orbitals, respectively. The first equation corresponds to an increase in the spin number, whereas the latter corresponds to a decrease in N_S. The spin hardness can be evaluated as:

$$\eta^0_{SS} \approx \frac{\mu_S^-(M') - \mu_S^+(M)}{2},$$

with (M') the system of higher multiplicity, and (M) the system of lower multiplicity. The atomic spin Fukui functions can be computed using the HOMO and LUMO shape factors (104; 105):

$$\begin{aligned} f^-_{NN,k} &= \frac{1}{2}(\sigma_k^{\mathrm{HOMO},\uparrow} + \sigma_k^{\mathrm{HOMO},\downarrow}), \\ f^+_{NN,k} &= \frac{1}{2}(\sigma_k^{\mathrm{LUMO},\uparrow} + \sigma_k^{\mathrm{LUMO},\downarrow}). \end{aligned}$$

These shape factors can be calculated within a molecular spin orbital approximation, using different partitioning schemes.

Early applications involve atomic systems and the topic of chemical binding (112). Furthermore, charge redistribution between states of different multiplicities (107), singlet-triplet gaps (108) and some chemical reactions (115) such as cyclizations (116), were discussed. In this thesis, spin-polarized DFT will be used to discuss cyclization reactions, in which a constrained charge transfer takes place. This work is performed in collaboration with the research group of Prof. Geerlings and Prof. F. De Proft of the Free University of Brussels (VUB).

2.1.5 Descriptors of aromaticity

It has been shown by Parr et al. that reactivity indices (and in particular the hardness) can also be used as indicators of aromaticity (117–121). This observation is based on the fact that both hardness and aromaticity are measures of high stability and low reactivity. Another important characteristic of aromaticity is the possibility to sustain induced ring currents. Various criteria are used

to describe the aromatic character of molecules (122; 123). The *diamagnetic susceptibility anisotropy* $\triangle\chi$, the *chemical shift* δ and the *Nucleus Independent Chemical Shift* (NICS) are among the most popular magnetic descriptors. The first (size-dependent) descriptor is defined as the difference between the out-of-plane component χ_3 and the average of the in-plane components χ_1 and χ_2. The chemical shift equals $\delta = \sigma_{TMS} - \sigma$, with σ the isotropic part of the shielding tensor and tetra methylsilane (TMS) the reference molecule. This property mainly monitors local effects and to a much lesser extent global ones (like ring currents) (124). The NICS is the absolute magnetic shielding in the center of a ring and consists of a diamagnetic and a paramagnetic contribution (125–127). It was recommended to use the NICS values calculated at 1 $\mathring{A}$ above the ring centers as aromaticity index, rather than the NICS values computed in the ring centers (126; 127). The main advantage of the NICS is that they are less dependent on the ring size and that they do not require a reference system, however they cannot be used for quantifying local aromaticity (128; 129). Recent work on aromaticity involves the usage of multicenter bond indices, which characterize the concept of extended delocalized bonding (130–136).

2.2 Principles

The aforementioned definitions of reactivity descriptors within a rigorous framework such as DFT provided the means to come up with a more mathematical and conceptual background for several renowned chemical principles. These principles, i.e. the equalization of electronegativity of Sanderson, the hard and soft acids and bases principle and the principle of maximum hardness, were initially well-known from experimental observations.

2.2.1 Equalization of electronegativity

Sanderson postulated that, upon molecule formation, the electronegativities of the constituent atoms must equalize, yielding a molecular electronegativity which equals the geometric mean of the original atomic electronegativities (137–140). The model only takes into account changes of the total electron number N, consequently neglecting other perturbations. In this simple case, the number of electrons that flow (ΔN) is proportional to the electronegativity difference ($\Delta\chi$ or equivalently $\Delta\mu$), whereas the binding energy ΔE is proportional to its square. The main goal of the principle is to obtain molecular charge distributions (and partial atomic charges arise quite naturally) with relatively little computational effort. However, this original formulation suffers from the severe drawback that all atoms of a given element will have the same atomic charge within a molecule. Therefore, the principle has been further developed into more sophisticated electronegativity schemes, such as the electronegativity equalization method (EEM) of Mortier et al. (28; 141; 142), which can be

used for the practical (fast) estimation of atomic charges for large molecules (143–145).

2.2.2 HSAB principle

The hardness and softness descriptors have known widespread attention, due to their importance within the well-known hard and soft acids and bases (HSAB) principle. Pearson originally proposed this principle in 1963 (22; 146–148), and it was quickly recognized as an important and fundamental chemical principle with special utility in inorganic chemistry. The principle indicates that hard acids prefer binding with hard bases (often forming bonds with substantial ionic character) and soft acids prefer to coordinate with soft bases (often forming bonds with substantial covalent character). The principle can be applied at a global ($S_A = S_B$, interaction between system A and system B) and local ($s_{Ai} = s_{Bj}$, interaction between atom i of system A and atom j of system B) level. The applicability of the local version remains somewhat controversial, as in some cases a non reactive site is indicated (149; 150). The softness-matching criterion in the case of multiple sites of interaction remains a challenging subject, and further research is necessary. Some working equations have been proposed, and generalized by Ponti (151). For the interaction between atom i of system A and atom j of system B, in combination with the interaction between atom k of system A and atom l of system B, the following quantity should be minimized:

$$\Delta s \quad = \quad (|s_{Ai} - s_{Bj}|^n + |s_{Ak} - s_{Bl}|^n)^{1/n}, \qquad n = \pm 1, \pm 2, \ldots .$$

Several attempts to prove the HSAB principle by minimizing the energy change ΔE were suggested in the literature (152–154). They differ in the extent of used approximations, e.g. incorporation of contributions due to changes in the external potential $v(\mathbf{r})$. Generally speaking, the binding energy ΔE can be written as separate contributions, and investigation of these terms results in a greater understanding of the applicability of the principle (23; 149; 155):

$$\triangle E \quad = \quad \triangle E_{covalent} + \triangle E_{electrostatic} + \triangle E_{polarisation}$$

with

$$\begin{aligned} \triangle E_{covalent} &= \triangle E_v + \triangle E_\mu \\ &\approx -\frac{1}{4}\frac{(\mu_A - \mu_B)^2}{\eta_A + \eta_B} - \frac{1}{2}\frac{\lambda}{S_A + S_B}. \end{aligned}$$

The first term represents a charge-transfer process, equalizing the chemical potentials of the interacting systems at constant external potential $v(\mathbf{r})$. The second term on the other hand represents a reshuffling or rearrangement process at constant chemical potential μ. Among other propositions for both terms, the working equations suggested by Gazquez et al. are given, with λ a constant

involving the effective number of valence electrons and the proportionality constant between S_{AB} and $S_A + S_B$ (153; 154). This covalent contribution is taken into account when proving the HSAB principle, consequently neglecting the other terms:

$$\triangle E_{electrostatic} = \int d\mathbf{r}\rho_A(\mathbf{r})\triangle v_A(\mathbf{r}) + \int d\mathbf{r}\rho_B(\mathbf{r})\triangle v_B(\mathbf{r}) + \triangle V_{nn},$$

$$\begin{aligned}\triangle E_{polarisation} &= \int\int d\mathbf{r}d\mathbf{r}'\chi_A(\mathbf{r},\mathbf{r}')\triangle v_A(\mathbf{r})\triangle v_A(\mathbf{r}') \\ &+ \int\int d\mathbf{r}d\mathbf{r}'\chi_B(\mathbf{r},\mathbf{r}')\triangle v_B(\mathbf{r})\triangle v_B(\mathbf{r}').\end{aligned}$$

In the first equation, $\triangle V_{nn}$ equals the nuclear-nuclear repulsion interaction. Ayers recently reinvestigated the mathematical foundations of the HSAB principle. First of all, the double-exchange reaction ($A_hB_s + A_sB_h \rightleftarrows A_hB_h + A_sB_s$, with A_h representing a hard acid, B_s a soft base and so on) was shown to be exothermic, providing a simple proof for the HSAB principle as indeed this implies that the equilibrium of the exchange reaction lies to the right (155). Electron-transfer effects favor the formation of the soft-soft product, whereas electrostatic effects favor the formation of the hard-hard product (23). In this light, the categorization into two types of reactions, according to the hard or soft character of the reactants, leads to a better understanding of the HSAB principle and its validity. This twofold classification is obviously similar to that of Klopman, who made a distinction between charge controlled and frontier orbital controlled reactions (156). The latter group corresponds to the formation of covalent bonds, associated with partial electron transfer from the highest occupied orbital of the base to the lowest unoccupied orbital of the acid. The first group can be associated with ionic bonding, dominated by the electrostatic attraction between the acid and the base.

2.2.3 PMH principle

According to the principle of maximal hardness (PMH), molecules will rearrange themselves to achieve maximal hardness. This principle was initially formulated by Pearson (157–159). A formal proof was given by Parr and Chattaraj (160), however relying on the constancy of μ and $v(\mathbf{r})$, which is in practice an unrealistically severe demand. Nevertheless, the principle was also validated by other authors (18; 161). In this light, Liu and Parr used a second-order functional expansion of $E[N, v(\mathbf{r})]$ to reach the conclusion that the larger the hardness, the lower the energy (161). As a consequence of the aforementioned correlation between softness and polarizability, the principle of minimum polarizability might provide a useful alternative (162). Many numerical studies, investigating isolated systems (163–168) or reactions (162; 169; 170), were performed. It was recently shown by Chattaraj and Ayers that the maximum

hardness principle implies the HSAB rule (171). Indeed, when the right part of the double-exchange reaction $A_hB_s + A_sB_h \rightleftarrows A_hB_h + A_sB_s$ is harder, this corresponds to a state of higher stability, which is a manifestation of the HSAB principle.

As a corollary of the PMH, the transition state of a reaction should exhibit minimal hardness (169). When studying hardness variations along the reaction path (hardness profiles), the activation hardness

$$\Delta\eta_{\text{act}} = \eta_{\text{reactant}} - \eta_{\text{transition state}}$$

might be a useful quantity (120). The smaller the activation hardness, the easier a reaction should occur. A vast amount of studies has focussed on this topic, both on applying the PMH to obtain more information about the transition structure as well as to study the directionality of a reaction (172–177). We note that the latter feature, in case of exchange reactions, can also be addressed by the HSAB principle.

2.3 Chemical kinetics

In this work, rate constants $k(T)$, with T the temperature, are computed using Transition State Theory (TST) (178–183). TST is based on several assumptions. First of all, the phase space between the reactant and product species is divided by a surface, which intersects the minimum-energy path at the transition structure (TS). This structure corresponds to a first-order saddle point. In order words, at this point the energy reaches a maximum value in the reaction coordinate, whereas it corresponds to a minimum conformation in all other degrees of freedom. It is furthermore assumed that every trajectory that passes the dividing surface from the reactant side eventually forms products (nonrecrossing rule) and that the reactant equilibrium maintains a Boltzmann energy distribution. For a bimolecular reaction $A + B \rightarrow C + D$, the following expression is obtained (182; 183):

$$k(T) \quad = \quad \frac{k_B T}{h} \frac{q_\ddagger / V}{(q_A/V)(q_B/V)} \mathrm{e}^{-\frac{\Delta E_0^\ddagger}{k_B T}}$$

where k_B is the Boltzmann constant, h is Planck's constant, V is the reference volume in which the translational part of the partition function is evaluated, q_A, q_B and $q_\ddagger$ relate to the molecular partition functions of the reactants (A and B) and transition structure (TS), respectively, and $\Delta E_0^\ddagger$ is the ZPVE -corrected energy difference between the TS and the reactants (i.e. the reaction barrier) at 0 K. The TST method has known deficiencies. In particular, it does not account for the recrossing effects that are important in the high temperature region and it cannot adequately model the quantum mechanical tunneling effects that are sometimes significant in the low temperature region.

The link with the macroscopic quantities – the pre-exponential factor A and activation barrier E_a – found in the Arrhenius rate law is made by a linear fit of $\ln k(T)$ values, calculated for a range of temperatures, versus $1/T$. The explicit equation for the Arrhenius rate coefficient:

$$k(T) \quad = \quad A \exp(-\frac{E_a}{RT}),$$

(with R the universal gas constant) makes clear that the activation energy corresponds to the slope of the linear fit, whereas the pre-exponential factor is obtained as the intercept with the $\ln k(T)$ axis.

In order to obtain accurate results for the rate constants, high-level ab initio methods are applied to calculate the microscopic quantities, i.e. the reaction barrier $\Delta E_0^{\ddagger}$ and the partition functions for the reactants and TS. In the remainder of this section, we briefly discuss two refinements to the standard formulation of TST. In particular tunneling contributions and internal rotations are summarized, as these were applied in the application section of this thesis.

2.3.1 Tunneling corrections

The effect of quantum mechanical tunneling through the potential energy barrier can be included in the transmission coefficient (or Boltzmann tunneling factor) $\kappa(T)$, which is introduced as an extra factor within the original equation for the rate coefficient $k(T)$. In addition to the tunneling of particles with an energy lower than the potential barrier, nonclassical reflection effects (corresponding to destructive interference which prevents the reaction to happen, although the system's energy is higher than the barrier) also occur. Both effects are taken into account to calculate κ. However, as the low energy states have a larger occupancy than the high energy ones, the tunneling tends to dominate the reflection effect. Consequently, the quantum mechanical corrections result in an increase of the rate coefficient ($\kappa(T) > 1$). According to Truhlar et al. (184), $\kappa(T)$ can be written as:

$$\kappa(T) \quad = \quad \frac{\int_{E=0}^{\infty} P(E) \mathrm{e}^{-\frac{E}{k_B T}} dE}{\int_{E^{\ddagger}}^{\infty} \mathrm{e}^{-\frac{E}{k_B T}} dE} = \frac{\mathrm{e}^{\frac{E^{\ddagger}}{k_B T}}}{k_B T} \int_{E=0}^{\infty} P(E) \mathrm{e}^{-\frac{E}{k_B T}} dE,$$

with $E^{\ddagger}$ the threshold energy and $P(E)$ the transmission probability.

Several calculation schemes have been developed, and in particular the analytic solutions of Wigner and Eckart have been widely used. In the first method, the classical potential energy barrier is replaced by a parabolic barrier (185):

$$V(x) \quad = \quad V_0 - \frac{1}{2} m \omega^{\ddagger} x^2,$$

where V_0 is the energy at the top of the barrier, and $\omega^{\ddagger}$ is the imaginary frequency of the TS. The Wigner tunneling correction is then given by:

$$\kappa(T) = 1 + \frac{1}{24}(\hbar\omega^{\ddagger}\beta)^2$$

with $\beta = 1/(k_B T)$. Thus, the Wigner correction only requires the imaginary frequency of the TS. However, since this method only accounts for contributions near the top of the barrier, the tunneling effect is often grossly underestimated. Eckart used a more realistic exponential fit to model the barrier (186):

$$V(s) = a\frac{e^{\alpha(s-s_0)}}{1+e^{\alpha(s-s_0)}} + b\frac{e^{\alpha(s-s_0)}}{(1+e^{\alpha(s-s_0)})^2} + c$$

with

$$s_0 = -\frac{1}{\alpha}\ln(\frac{a+b}{b-a}).$$

The parameter α is called the range parameter and can be calculated using the classical barrier height, the imaginary frequency and the reduced mass of the tunneling species. The coefficients a, b and c are also entirely determined through properties of the reactants, products and TS. This method is (as is the Wigner method) compatible with TST, as the Eckart function is completely described using properties of the three stationary points along the reaction path. The Eckart method often overestimates the tunneling effect. However, this error is sometimes compensated for by the corner cutting effect, resulting in a good agreement with experimental data. More sophisticated and computationally demanding calculation schemes are also available (187–189).

2.3.2 Internal rotations

In order to evaluate the molecular partition function q, the various motions corresponding to an M-atomic system are assumed to be decoupled:

$$q = q_{elec}q_{trans}q_{rot}q_{vib}.$$

As the Born-Oppenheimer approximation holds, the electronic contribution q_{elec} can be approximated by 1 or 2, for a neutral/ionic or radical system, respectively. The translational q_{trans} factor can be evaluated using the expression for an ideal gas. The rotational part needs special attention. Within the Harmonic Oscillator (HO) model all the internal (vibrational) motions are approximated as independent harmonic oscillators, assuming that only small deviations from the reference structure take place, and that the potential energy is quadratic in all variables. The corresponding partition function q_{vib} is obtained as a product of contributions of the form:

$$q_{vib,i} = \frac{e^{-\frac{h\nu_i}{2k_B T}}}{1-e^{-\frac{h\nu_i}{k_B T}}}$$

for each of the internal modes i ($i = 1, \ldots, 3M - 6$ for a non-linear molecule). This expression is however not adequate to describe internal rotations, which correspond to a non-quadratic potential energy surface, giving rise to large amplitude vibrations with significant structural changes.

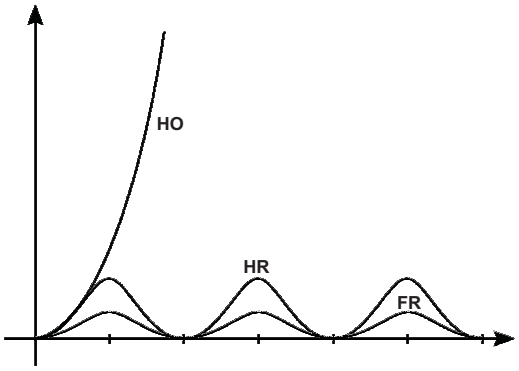

Figure 2.1: Potential energy corresponding to various descriptions of internal movement.

In the extreme case of a very low potential energy barrier, the Free Rotor (FR) model can be used (190; 191). Consequently, the HO partition function of this free-rotor mode is replaced by the following expression:

$$q_{FR} = \frac{1}{\sigma_{int}} \sqrt{\frac{k_B T \pi}{h\nu}} = \frac{1}{\sigma_{int}} \sqrt{\frac{2 k_B T \pi I_m}{\hbar^2}},$$

where σ_{int} is the symmetry number of the internal rotation, and I_m is the reduced moment of inertia. The intermediate regime can be described using a Hindered Rotor (HR) model (192–194). In this work the following approximative scheme is used: the one-dimensional potential into the torsional angle is determined by several stationary points, which correspond to a full geometry optimization. Through these stationary points, a k_{max}-term Fourier expansion is fitted:

$$V_m(\phi_m) = \sum_{k=1}^{k_{max}} \frac{1}{2} V_{mk}(1 - \cos(k\phi_m)).$$

When the potential energy function has high symmetry, the Fourier-series converges very rapidly and only a small number of harmonics is needed. In general, the HR partition function for each internal rotation m is obtained after solving the Schrödinger equation for the energy values $\epsilon_m(k)$ and using this equation:

$$q_{HR} = \frac{1}{\sigma_{int}} \sum_k g_k(m) \exp(-\frac{\epsilon_k(m)}{k_B T})$$

where $g_k(m)$ is the degeneracy of the energy level $\epsilon_k(m)$ and σ_{int} the symmetry number of the internal rotation.

The one-dimensional potential energy curves of the various descriptions are illustrated in Figure A.1. Summarizing, by analyzing the vibrational spectrum of the molecule, some low-lying modes can be identified as internal rotations. These torsional motions are treated in a specific way (as FR or HR), whereas all other modes correspond to harmonic oscillators. Hence, a mixed harmonic oscillator/free rotor (HO/FR) or harmonic oscillator/hindered rotor (HO/HR) scheme is used to describe the internal movement. In recent studies on various radical reactions, the importance of correctly describing hindered internal rotations in order to obtain reliable partition functions was demonstrated (195; 196).

3

Applications: an Overview

3.1 Radical reactions within the formation process of coke

3.1.1 Introduction

Steam cracking or pyrolysis of hydrocarbons is considered as the main production process of light olefins such as ethene and propene, species which are key components in the chemical industry. Among other applications, their derivatives are used for the production of thermoplastics, fibers, foams, etc. which have known a growing demand in recent years. In commercial cracking units, paraffinic hydrocarbon feedstocks - of which ethane and naphta are the most common - are cracked following a complex radical chain mechanism. The feedstock passes in the cracking furnace through a radiation, transition and convection section, respectively. In the radiation section a carbonaceous residue is however formed on the reactor walls (197). This residue, or coke, decreases the efficiency of the cracking unit and an increase of the input heat and inlet pressure is necessary to retain a constant conversion level and selectivity. The formation of coke is therefore highly undesirable. As an ultimate consequence of the coke deposit the unit has to be taken out of production for decoking, in which the coke is burnt off with a controlled air-steam mixture. According to experimental observations, coke is essentially being formed following three different mechanisms. Firstly, there is a catalytic mechanism where a thin, filamentous layer is formed on the reactor wall (198). Secondly, a heterogeneous, non-catalytic mechanism leads to a more dense graphite-like coke matrix (199). This mechanism consists of radical reactions between the coke surface on one hand and gaseous coke precursors on the other. Thirdly, in particular circumstances (at very high temperatures or using heavy feedstocks) a homogeneous, non-catalytic mechanism is also observed. It is reported that

for the temperature intervals relevant in the steam cracking units, the heterogeneous, non-catalytic mechanism is the most important (200).

The Laboratorium voor Petrochemische Techniek (LPT) (Head Prof. G. B. Marin) has a longstanding tradition in the development of single event (SE) microkinetic models for a variety of processes. The thermal cracking model has been intensively studied, whereas the growth process of coke is less explored. The thesis of ir. S. Wauters is a reference work for the SE microkinetic model of coke (201–203). As kinetic parameters are needed in the network, ab initio molecular modeling can give a valuable contribution. In this light, a lot of work was performed at the Center of Molecular Modeling (CMM) during the last years (191; 195; 204–209). The coke layer is known to exhibit graphite-like characteristics, and there is an experimentally observed similarity between the coke formation process and aromatization. Therefore coke is represented by a polyaromatic structure consisting of conjugated six-membered rings (210). The growth of the coke layer is described using a model based on elementary reactions, similar to a model designed by Frenklach et al. to describe the formation of soot, using polycyclic aromatic hydrocarbons (PAHs) (211–214). More recently, Vereecken et al. (215) have studied the growth of PAHs incorporating five-membered rings, which can also act as possible intermediates for the formation of nonplanar systems, including fullerenes. However, at present there is no incorporation of five-membered rings in the model of coke formation. In the present model, five classes of reversible reactions can be distinguished: hydrogen abstraction, substitution, gas phase olefin addition to radical surface species, gas phase radical addition to olefinic bonds and cyclization (203). The fundamental nature of these elementary steps allows general applicability of the model. Initial radical surface species are created as a result of hydrogen abstraction reactions by gaseous radical precursors. Subsequently, addition of these surface species to a gas phase olefin and ultimately, cyclization or dehydrogenation lead to the formation of a new ring and the incorporation of carbon atoms or coke. The entire mechanism is illustrated in Figure 3.1.

In earlier ab initio calculations, the coke layer was usually modelled using one single benzene ring. However, the influence of the environment can be investigated by means of an extended set of various PAHs. The importance of PAHs in general can hardly be overestimated, as they are among the most studied organic compounds (216; 217). They play a key role in a large number of different areas as they are both naturally occurring and anthropogenic. PAHs are the largest known class of chemical carcinogens and mutagens (218–221). They are present in atmospheric aerosols and many celestial objects such as meteorites, planetary nebulae, reflection nebulae and active galaxies (222–225). Recent work has reported on spectroscopic evidence for the existence of PAHs in interstellar space (226). Their importance in the formation process of hollow-cage fullerenes is also known (227–229). As mentioned earlier, PAHs are key intermediate products in soot formation and coal conversion processes (203; 230–233). Additional important information about PAHs can also be obtained

by studying their aromatic characteristics (117; 122; 123; 234).

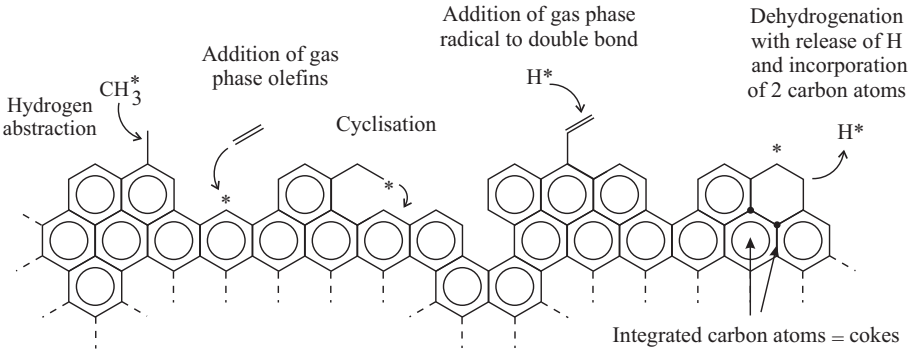

Figure 3.1: Elementary radical reactions enabling the growth of the coke surface (203).

In this work, information about the chemical reactivity of several of the aforementioned elementary reactions is obtained using thermodynamics/kinetics on one hand, and using DFT-based reactivity descriptors on the other. The first aspect has also been studied by other researchers, among others Radom and coworkers focussed on radical addition reactions. Additions to carbon-carbon double and/or triple bonds (235–239), and methyl radical additions to C=O and C=S double bonds were investigated (240; 241). The delicate balance between the various factors governing reaction kinetics and thermochemistry for this reaction type has been demonstrated both experimentally and theoretically (242–244).

In general, studies on the DFT-based reactivity indicators of radical species and reactions have so far been very limited. Pioneering work on reactions of free radicals has been done by Pearson (245). Global and local reactivity indicators were calculated for a variety of open-shell systems (246–250). Radical addition reactions were most intensively studied. Chandra and Nguyen (251) tested the HSAB principle for the addition of free radicals to olefins using the condensed values of the Fukui function and softness. Generally, the attack takes place at the less substituted carbon atom of the double bond. However, no general correlation could be found between local softness values and barrier heights. The exceptional behavior of the addition mechanism of fluoromethyl radicals to fluoroethylenes was investigated in detail by Korchowiec and Uchimaru (250). Hydrogen abstraction reactions between a radical and a neutral system were also investigated by Chandra et al., who found good correlations between the hardness and the activation energy in case of interactions between the OH radical and halomethane compounds (249). Nguyen et al. used the global and local softness as well as the electronegativity to rationalize hydrogen abstraction from methane and propene by various radicals. They also investigated the re-

giochemistry of radical additions to (substituted) propenes and the condensed softness was found to be a suitable descriptor (252). Overall, they could not find a particular descriptor that correlates well with the barrier heights for the two types of investigated radical reactions. Hydrogen abstraction reactions of the ethynyl radical with hydrogen compounds were also studied (253). It was shown that the strengths of the X-H bonds are dominant reaction parameters, and no correlations between other reactivity descriptors and barrier heights were obtained. Difficulties in the present definitions of local radical indicators were demonstrated by examining a variety of radical addition reactions (254). An isolated study on hardness and polarizability profiles for intramolecular proton transfer in water dimer radical cation represents an example of the applicability of reactivity indicators for weak interactions (255). A new interest into radical reactions originated with the development of spin-polarized reactivity descriptors (see section 2.1.4). So far, some radical cyclization reactions were already studied (256) (for more details, see ***Paper XI***).

In addition to the elementary reactions occurring in the coke formation process, the kinetics of related radical reactions, in particular the free-radical polymerization processes of ethene (leading to polyethylene or PE) and vinyl chloride (leading to poly(vinyl chloride) or PVC) were also investigated. PE and PVC represent the top most produced plastics in the world. The polymerization mechanism consists of initiation, propagation, chain transfer to small molecules and termination. The applicability of reactivity indicators on the initiation and first propagation steps was studied, providing another example for bimolecular radical reactions. The detailed discussion can be found in ***Paper VII***.

In this section, ab initio calculations are performed on three types of elementary classes occurring in the coke formation process. These calculations provide the opportunity to obtain the required levels of insight and understanding for model genesis. This information must in particular contribute to an efficient design of clean and practical combustion devices such as engines and incinerators, and for a maximal run length of steam cracking units. Hydrogen abstraction reactions by a methyl radical are thoroughly investigated, starting with an extended level of theory (LOT) study on the reference reaction at benzene (subsection 3.1.2). In a next step (subsection 3.1.3), the investigated class of species is broadened to a large selection of various PAHs, allowing to elaborate on the influence of the polyaromatic environment on the thermodynamic and kinetic parameters. The importance of the hydrogen abstractions in the coke growth process is stressed, since they initiate the radical species which lead to the cascade of radical reactions. Furthermore, there is evidence that they are the rate determining step in the coking process, due to the low concentration of available methyl radicals in the process gas (257–259). It is important to note that the addition of the methyl radical to benzene, followed by consecutive hydrogen abstractions, represents a competitive pathway, also creating initial surface radicals. This route is however not investigated here,

this work is in progress at the CMM. An overview of ab initio results obtained at the CMM within the growth process of coke can be found in ***Paper VI***. Subsection 3.1.4 focusses on reactivity information obtained from DFT-based reactivity descriptors. The hydrogen abstraction reactions, as well as inter and intra molecular additions, and some free radical polymerization reactions are discussed. The reactivity of the isolated compounds and the preferred reaction site is studied using global and local indicators, respectively. Finally, we are particularly interested in reactivity sequences and in the applicability of the HSAB principle, and correlations with thermodynamic and/or kinetic results are reported whenever possible.

3.1.2 LOT dependence of thermodynamics and kinetics for hydrogen-abstraction reactions

An extended level of theory (LOT) study is performed on the hydrogen abstraction reaction at benzene, serving as a reference for abstraction at polybenzenoid species (Figure 3.2) (***Paper I***). This work was done in collaboration with the research group of Prof. L. Radom, who has a large expertise in the study of radical reactions. The performance of a broad variety of DFT and HF/post-HF methods, in conjunction with various double- and triple-zeta Pople basis sets, is assessed.

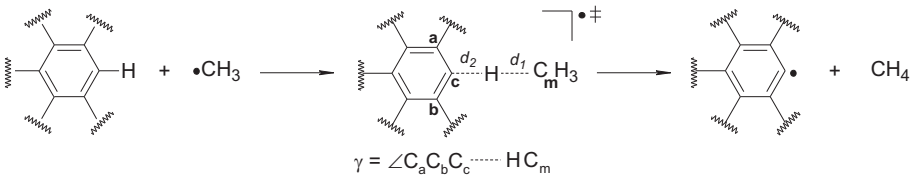

Figure 3.2: Hydrogen abstraction by the methyl radical from a model PAH to form an aryl radical plus methane. The forming bond length (d_1), breaking bond length (d_2), and out-of-plane angle (γ = angle between the $C_aC_bC_c$ plane and the H-CH_3 line) of the transition structure are highlighted.

First of all, the sensitivity of the optimized geometry on the LOT is profoundly examined. Frequencies are computed at the same level of theory to provide zero-point vibrational energies (ZPVEs) and to confirm the nature of the stationary points. Secondly, single-point energy calculations are performed for each geometry at the URCCSD(T)/6-311+G(*d,p*) level in order to evaluate the quality of the optimized structures. Thirdly, using the B3-LYP/6-31+G(*d,p*) and BMK/6-31+G(*d,p*) optimized geometries, reaction enthalpies and barriers are computed using various standard DFT methods in combination with the 6-31G(*d*), 6-31+G(*d,p*) and 6-311+G(*3df,2p*) basis sets. The CBS-QB3 (260; 261), G3(MP2)-RAD (262), G3-RAD (263; 264) and W1 (265) high-level composite procedures are also applied.

Geometries

The optimized TS geometries show that at all levels, the forming bond is modestly shorter than the breaking bond (average difference approximately 0.07 $\AA$), which is consistent with a late TS and in accordance with the reaction endothermicity. Using URCCSD(T)/6-311+G(*d,p*) single-point energies calculated on the different optimized geometries, the basis set effect is found negligible and the choice of the quantum chemical method also has little influence. However for the phenyl radical a relatively large range of $\sim$ 15 kJ mol^{-1} is obtained. This is entirely due to the UMP2 results which are submitted to large spin contamination encountered in the unrestricted description of radical reactions. Overall, it is found that QCISD, CCSD and BMK are attractive choices for optimizing the equilibrium structures in the benzene hydrogen-abstraction reaction. From the viewpoint of computational advantage, the BMK method is therefore preferred. In this light, the popular B3-LYP functional is also found suitable for obtaining good geometries, whereas BB1K and MPW1K are less good from this perspective. When the URCCSD(T)/6-311+G(*d,p*) energies are used to calculate reaction enthalpies and barriers, we see relatively little variation, indicating significant error cancellation. Geometries obtained with the DFT functionals, for example, lead to URCCSD(T) endothermicities that lie within the range 29.2 $\pm$ 0.2 kJ mol^{-1}, and barriers of 78.5 $\pm$ 0.4 kJ mol^{-1}. The heavily spin-contamined methods show poor values for both the enthalpy and the barrier. It is overall concluded that the sensitivity of geometry optimization on LOT is limited.

Reaction enthalpies and barriers

Reaction enthalpies ΔH_{298} and reaction barriers $\Delta E_0^{\ddagger}$ are calculated using the B3-LYP/6-31+G(*d,p*) and BMK/6-31+G(*d,p*) geometries, using scaled ZPVEs and thermal corrections (266–269). A selection of the results is given in Table 3.1.

The composite W1 procedure is chosen as the benchmark method, as it is known – when evaluated with a large test set of thermochemical data – to generally give agreement with experiment to within 2 kJ mol^{-1} (265). The calculated reaction enthalpy at 0 K of 34.5 kJ mol^{-1} is in close agreement with the experimental value reported by Tokmakov et al. (270). G3-RAD and G3(MP2)-RAD predict enthalpies and barriers in good agreement with the W1 value, whereas the CBS-QB3 leads to a somewhat larger deviation, which may be associated with the spin contamination in the UMP2 wave function that is used in CBS-QB3 for the phenyl radical.

Inspection of the data resulting from standard DFT methods (Table 3.1) shows that there is a non-negligible basis-set effect. The 6-31G(*d*) basis set appears to be too small for obtaining accurate data, in particular significantly

Method	ΔH_{298}	$\Delta E_0^{\ddagger}$	ΔH_{298}	$\Delta E_0^{\ddagger}$
	B3-LYP geometry		BMK geometry	
W1 (0 K)	34.5	72.4		
W1 (298 K)	34.1			
G3-RAD	35.4	72.5		
G3(MP2)-RAD	37.1	73.8		
CBS-QB3	42.1	77.6		
URCCSD(T)/6-311+G(*3df,2p*)	33.8	72.9	33.2	73.4
MPW1K/6-31G(*d*)	27.1	69.5	27.0	69.5
BB1K/6-31G(*d*)	21.7	64.4	21.6	64.5
BMK/6-31G(*d*)	23.4	63.5	23.2	63.6
MPW1K/6-31+G(*d,p*)	33.4	73.0	33.3	73.0
BB1K/6-31+G(*d,p*)	28.5	69.4	28.4	69.4
BMK/6-31+G(*d,p*)	29.8	67.7	29.7	67.8
UB3LYP/6-311+G(*3df,2p*)	30.5	66.2	30.0	66.8
RB3LYP/6-311+G(*3df,2p*)	30.0	68.4	29.5	69.0
MPW1K/6-311+G(*3df,2p*)	33.4	74.1	33.3	74.1
BB1K/6-311+G(*3df,2p*)	28.7	71.0	28.6	71.0
BMK/6-311+G(*3df,2p*)	30.1	71.5	29.6	72.0
Tokmakov et al. (0 K) (270)	36.8 ± 3.8			
G2M(CC,MP2) (0 K) (270)	43.1	81.9		

Table 3.1: Barriers ($\Delta E_0^{\ddagger}$) and Reaction Enthalpies (ΔH_{298}) for the Benzene Abstraction Reaction (kJ mol^{-1}).

underestimating the ΔH_{298} W1 benchmark value. Inclusion of diffuse functions results in an improvement in the calculated MPW1K, BB1K and BMK enthalpies by about 6-7 kJ mol^{-1}. However, a further upgrade to the larger 6-311+G(*3df,2p*) basis set has only a minor effect. A similar effect is observed for the barriers. The average increase in barriers from 6-31G(*d*) to 6-31+G(*d,p*) is now approximately 4 kJ mol^{-1}, while increasing the basis set to 6-311+G(*3df,2p*) results in an extra shift of about 2 kJ mol^{-1}.

Of the non-composite procedures, the computationally most expensive method, URCCSD(T)/6-311+G(*3df,2p*), clearly performs the best. It is also found that the large-basis-set DFT methods generally underestimate the benchmark enthalpy and barrier. The MPW1K functional shows an exceptional behavior for the barriers and the obtained results are very close to the benchmark values. B3-LYP underestimates the barrier by about 6 kJ mol^{-1}, RB3-LYP shows a modest improvement over UB3-LYP, reducing the deviation from W1 to about 4 kJ mol^{-1}. BB1K and MPWB1K, developed especially for kinetics

applications, perform well. However, BMK shows the best performance of the DFT methods, giving barriers within 1 kJ mol^{-1} of the benchmark value.

Kinetic parameters and rate constants

The kinetic parameters E_a and A are determined in the temperature range of 600 to 800 K, in which experimental data are available. Tunneling corrections on one hand and the internal rotation of the methyl group around the forming/breaking bond on the other are taken into account to refine the original TST results (see section 2.3). For the studied abstractions a small torsional frequency (ν_m) is obtained for the specific mode. The corresponding rotational barrier is very low, a mixed HO/FR model is therefore applied to calculate $k(T)$. This results in a decrease of about 3 kJ mol^{-1} for E_a, which is quite small compared with the 38 kJ mol^{-1} range when the various methods are compared with each other. In contrast, A varies significantly, with a difference of almost one order of magnitude depending on whether the rotation of the methyl group is handled using the HO/FR or HO model. This is a consequence of the erroneous HO partition function which is especially important for the pre-exponential factor. However, this strong correlation disappears when the methyl torsion is treated as a free rotor (HO/FR model) and A now fluctuates within a small range. Eckart tunneling corrections are also included, accounting for a substantial decrease by approximately 5 kJ mol^{-1} for E_a, whereas the A values are only minorly influenced.

Comparison with experimental data allows for further assessment of the computational methods. Two experimental data sets are available, obtained by Krech and Price (271) and Zhang et al. (272) in the temperature intervals 744-800 K and 650-770 K, respectively. A large discrepancy exists between the kinetic parameters deduced from the two experiments. These differences partly arise because the temperature range in which the experiments were carried out is quite narrow, meaning that a large extrapolation is required to obtain the Arrhenius kinetic parameters. Due to these large discrepancies, high-level composite procedure are applied, providing a valuable alternative in the search for accurate benchmark values. Using high-level composite results as benchmarks for the present application suggests that BB1K, MPW1K, BMK and URCCSD(T) in combination with the 6-311+G(*3df,2p*) basis set (and using BMK/6-31+G(*d,p*) geometries and frequencies) lead to accurate and reliable results.

Finally, the accuracy of the theoretical model is assessed by comparing directly the experimental and theoretical rate constants in the relevant temperature range. Even methods that fail in reproducing a good estimate of E_a and A separately give quite good estimates of the rate constants due to compensation effects between the kinetic parameters. All composite procedures show an excellent performance. In addition, it is found that the computationally

feasible two-component methods using BB1K, MPW1K or BMK energies (obtained with the 6-311+G(*3df,2p*) basis set) and BMK/6-31+G(*d,p*) geometries and frequencies give very good agreement with the experimental rates.

3.1.3 Thermodynamics and kinetics for hydrogen-abstraction reactions on PAHs by a methyl radical

The influence of the local environment of the abstraction site on thermodynamic and kinetic parameters of hydrogen-abstraction reactions by a methyl radical is investigated (***Paper II***). This work was also performed in collaboration with the research group of Prof. L. Radom. A test set of 16 polyaromatic hydrocarbons (PAHs) is used, and abstractions at various sites of these PAHs are considered. All reactants are depicted in Figure 3.3. Based on the extended LOT study performed on the reference reaction at benzene (subsection 3.1.2), the BMK/6-311+G(*3df,2p*)//B3-LYP/6-311G(*d,p*) method is chosen, as this level provides accurate results and is yet affordable for calculations on molecules of moderately large size. Our test set of PAHs can be divided into two sub-categories. The first group includes the series of linear acenes, consisting of benzene (**B**), naphthalene (**N**), anthracene (**A**), tetracene (**T**) and pentacene (**P**). The other group consists of non-linear structures, including phenanthrene (**PH**), benzo[c]phenanthrene (**BPH**), dibenzo[c,g]phenanthrene (**DBPH**), benz[a]anthracene (**BA**), dibenz[a,j]-anthracene (**DBA**), coronene (**C**), benzo[a]naphth[2,1-j]anthracene (**BNA**), benzo[a]phenanthro[3,4-j]anthracene (**BPHA**), pyrene (**PYR**), perylene (**PER**) and benzo[ghi]perylene (**BPER**). In the remainder of the discussion, the notation PAH-X refers to the abstraction of hydrogen atom X from the polycyclic aromatic hydrocarbon PAH. It is also important to stress that throughout this entire work, the notation X//Y corresponds to a geometry calculation at level Y, followed by a single-point energy calculation at level X. In the case when both the geometry and energy calculations are performed at the same level of theory X, the simple notation X is used.

Geometries

As concluded in section 3.1.2, the geometries are almost independent of the level used for the optimization. Thus, available B3-LYP/6-311G(*d,p*) geometries are utilized. We note that all the product radicals are of the σ-type, with the unpaired electron almost completely localized on a single carbon atom (273). A key geometrical feature is the planarity of most of the reactant PAHs and product aryl radicals. Four exceptions are found among the PAH molecules, specifically **BPH**, **DBPH**, **BNA** and **BPHA**. Because of steric repulsive interactions between a pair of closely-positioned hydrogen atoms, these molecules show significant deviations from planarity. The nonplanarity is to a large ex-

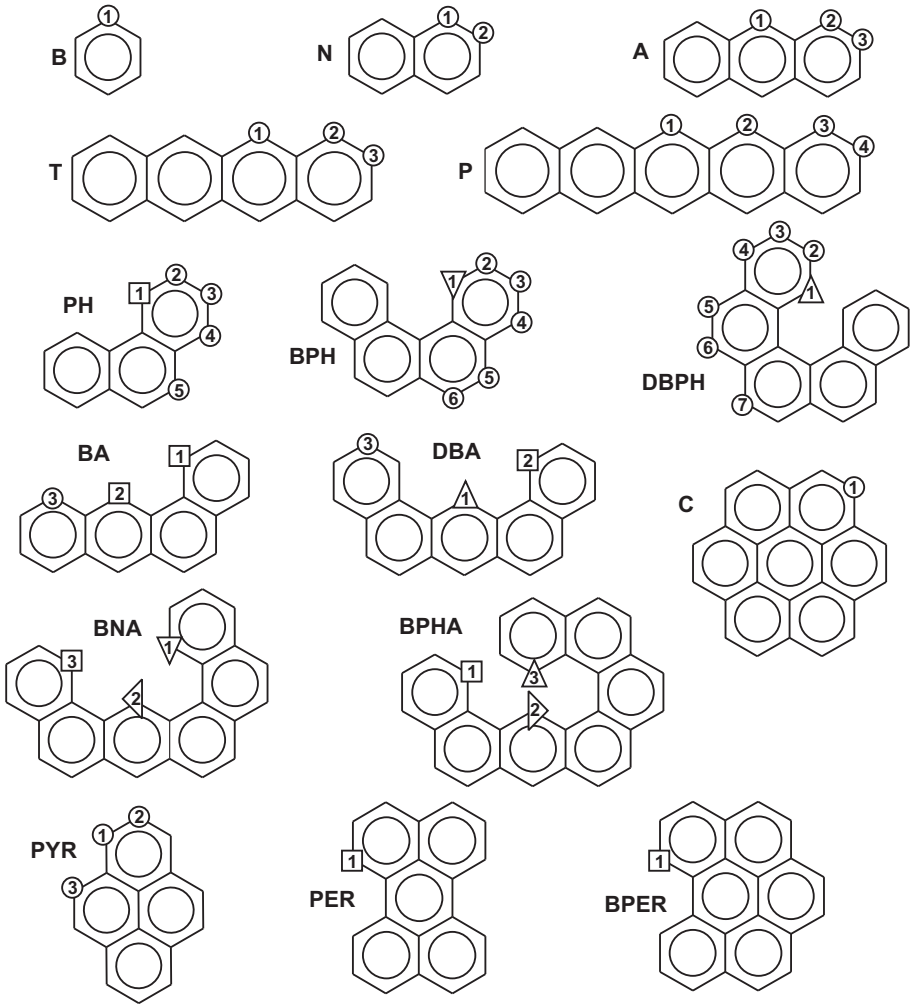

Figure 3.3: Schematic representation of PAHs. The sites where hydrogen abstraction is considered are numbered. The sites are labelled on the basis of the hydrogen-abstraction enthalpy classifications (see text) ($\bigcirc$ for B sites,$\square$ for PH sites,∇ for BPH sites,$\triangle$ for DBPH sites,$\triangleleft$ for BNA sites and $\triangleright$ for BPHA sites).

tent removed (in the case of **BPH**-1, **BNA**-1 and **BNA**-2) or significantly reduced (in the case of **DBPH**-1, **BPHA**-2 and **BPHA**-3) when the aryl radicals are formed, following the abstraction of a hydrogen atom. Other important geometrical features in the PAHs and the product radicals are the changes in the bond distances and angles at the hydrogen-abstraction site. The perturbations associated with the removal of a hydrogen atom lead to a shortening of the adjacent C-C bonds by approximately 0.02 $\AA$, as well as a widening of

the bond angle at the carbon from which abstraction has taken place by about 6°. Analogous to the benzene abstraction, in most TSs the forming bond is modestly shorter than the breaking bond (average difference approximately 0.07 $\AA$), being consistent with a late TS and in accordance with the reaction endothermicity. Only **DBA**-1, **BNA**-2 and **BPHA**-2 are found to be exceptions to this rule, due to the more folded geometrical structure. It can also be seen that for the abstraction of hydrogen atoms located at some of the more congested sites of the PAHs, the approaching methyl radical is forced to follow an out-of-plane pathway. This is basically due to steric hindrance between the incoming methyl radical and the closely-positioned hydrogen atoms.

Reaction Enthalpies and Barriers

The hydrogen-abstraction enthalpies ΔH_{298} lie within a broad range between -1.8 (**BNA**-2) and +34.3 (**A**-1, **T**-1) kJ mol^{-1}. The reactions are endothermic, with the exception of the **BNA**-2 reaction, which is slightly exothermic. A clustering of the reaction enthalpies into six groups (**B**-, **PH**-, **DBPH**-, **BPHA**-, **BPH**-, **BNA**- and **BPA**-like sites) is observed, this classification of the various hydrogen atoms is illustrated in Figure 3.3. From the Figure, it is also clear that the present classification corresponds to a qualitative description of the local environment of the sites. Detailed analysis of the linear acenes reveals that a further division into three categories is possible, corresponding to **B**-, **N**- and **A**-like sites. The latter group is found to exhibit the largest ΔH_{298} values in the particular molecule being considered. It is concluded overall that the reaction enthalpies for abstraction at the more congested sites correspond to smaller (less positive or more negative) enthalpy values, due to a relief from steric hindrance upon creation of the radical.

The hydrogen-abstraction barriers at 0 K ($\Delta E_0^{\ddagger}$) are relatively high, lying between 70.8 (**P**-4) and 89.2 (**DBA**-1) kJ mol^{-1}. It can be seen that the steric hindrance effects that the methyl radical encounters when approaching the abstraction site become very important for the more congested sites. The most striking examples of such increased barriers are seen for the abstractions at **DBA**-1, **BA**-2, **BNA**-2 and **BPHA**-2, with barriers amounting to 89.2, 82.9, 80.7 and 82.2 kJ mol^{-1}, respectively.

Inspection of the above properties shows that there is no general correlation between the ΔH_{298} and $\Delta E_0^{\ddagger}$ results. Indeed, a large scattering is observed when these quantities are plotted (Figure 3.4 (a)). We conclude that greater congestion generally leads to reduced reactivity for hydrogen abstraction by a methyl radical (because the site becomes less accessible), in contrast to the greater reactivity that would have been anticipated to accompany the lower reaction enthalpies (relief of steric strain) with a normal (Bell-Evans-Polanyi) reactivity-enthalpy relationship (274; 275). Nevertheless for the series of linear acenes, the Bell-Evans-Polanyi relationship does hold reasonably well (Figure

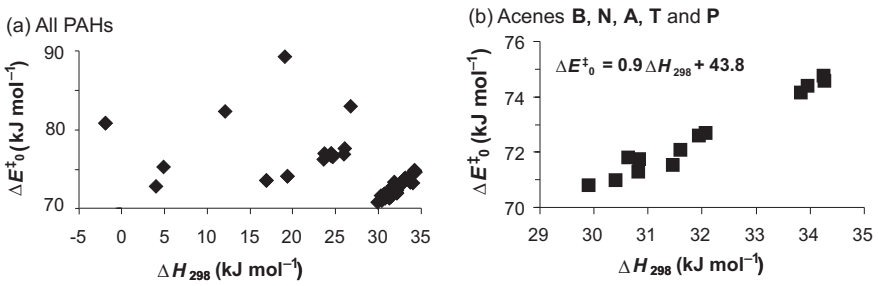

Figure 3.4: Reaction barriers at 0 K ($\Delta E_0^{\ddagger}$) versus reaction enthalpies at 298 K (ΔH_{298}) for hydrogen-abstraction reactions at various sites of (a) all the PAHs examined and (b) only the series of linear acenes (BMK/6-311+G(*3df,2p*)//B3-LYP/6-311G(*d,p*)).

3.4 (b)), as for these uncongested regions, the approaching methyl radical does not suffer from increased steric hindrance effects in the transition structure.

Kinetic Parameters and Rate Constants

Rate constants $k(T)$, and corresponding activation energies E_a and pre-exponential factors A, for the reactions between the various PAHs and methyl radical are calculated in the relevant temperature interval of 700-1100 K. Two refinements are taken into consideration (see 2.3): the effect of tunneling corrections on one hand, and a refined description of the low-energy torsion of the methyl group in the TSs on the other. The latter effect corresponds to replacing the standard HO partition function for the particular mode by a Free Rotor (FR) or Hindered Rotor (HR) partition function, for uncongested or congested sites, respectively. The contributions of both refinements are summarized in Table 3.2. It is observed that both effects are non-negligible.

	IR model	Eckart tunneling	overall
$(E_a)_i - (E_a)_f$	3.3	4.5	7.8
A_f/A_i	0.4	0.7	0.3
$k_f/k_i\,(700)$	0.6	1.6	1.0
$k_f/k_i\,(900)$	0.5	1.4	0.7
$k_f/k_i\,(1100)$	0.5	1.2	0.6

Table 3.2: Effect of refinements on the activation energy E_a (in kJ mol^{-1}), pre-exponential factor A and rate constant $k(T)$ at various temperatures. The subscripts i and f refer to the initial (without refinement) and final (with refinement) values, respectively.

Generally speaking, E_a is influenced by both refinements in a similar manner, whereas A is predominantly influenced by a more accurate description of the internal rotation. Both the barrier and pre-exponential factor decrease as a consequence of the refinements. These effects act in the opposite direction on the resulting rate coefficient $k(T)$ (Table 3.2): as a result of tunneling the rate coefficients increase, whereas the more accurate description of the internal rotation leads to a decrease of the $k(T)$ values. Overall, it turns out that the latter effect is dominant: the final $k(T)$ values (taking into account the two refinements) are lower than the original TST results. An increase in temperature makes this effect more clear, as the tunneling contribution becomes less important.

Inspection of $k(T)$ for the category of linear acenes reveals two interesting features, as illustrated in Figure 3.5(a). Firstly, it is seen that abstractions of a hydrogen atom located at a central ring are the slowest, approximately three times slower than abstraction at benzene. Secondly, a convergent behavior of the kinetic parameters and rate constants with increasing PAH size is observed. Comparison of the kinetic parameters E_a and A for the abstraction reactions at **B**-1, **N**-1, **A**-1, **T**-1 and **P**-1 shows that convergence is already reached for both parameters in the **A** molecule. It thus appears sufficient to take into account three six-membered rings in order to adequately model the kinetics of the linear acenes.

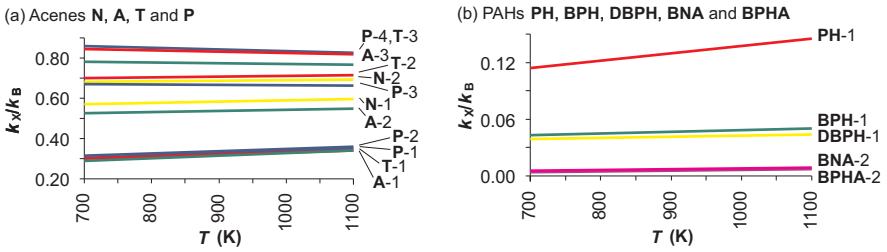

Figure 3.5: Rate constants for the hydrogen abstractions at (a) linear acenes and (b) PAHs **PH**, **BPH**, **DBPH**, **BNA** and **BPHA** (BMK/6-311+G(*3df,2p*)//B3-LYP/6-311G(*d,p*)).

Inspection of $k(T)$ for the non-linear PAHs (Figure 3.5(b)) first of all reveals that the calculated values for the less congested PAH molecules, e.g. **PH**, are higher than those for the congested sites at all temperatures. It is also noted that for the abstraction at these (congested) non-**B**-like sites the variation in E_a and A is larger than in the series of linear acenes. The A values clearly support the conclusion that the abstraction becomes more difficult as the PAH abstraction site becomes more congested. In addition, the E_a values for the very congested sites **BNA**-2 and **BPHA**-2 are substantially higher. As a final remark, we note that comparison of the **PH**-1 and **BPER**-1 results indicates

that the deviations between the rate parameters for the two abstraction reactions are small. This leads to the conclusion that adding an extra layer to the coke surface model has little influence on the kinetic results.

3.1.4 Reactivity descriptors versus thermodynamics and kinetics

Reactivity Descriptors of PAHs

The ionization potential IP, electron affinity EA, and derived global indicators μ, η and S are calculated for the set of PAHs introduced in previous section (Figure 3.3), using B3-LYP/6-311G(*d,p*) optimized geometries. First of all, the performance of the B3-LYP and BMK functionals (used for the single-point energy calculations) is tested, both functionals are combined with the large 6-311+G(*3df,2p*) basis set. The influence is found to be very limited, and no qualitative changes are obtained for the reactivity sequence of the PAHs. Therefore, only the BMK results are retained, the μ and S values are given in Table 3.3.

PAH	μ	S	PAH	μ	S
B	-3.857	2.477 *(2.626)*	**BA**	-3.836	3.959 *(3.854)*
N	-3.814	3.184 *(3.261)*	**DBA**	-3.849	3.956 *(3.996)*
A	-3.828	3.945 *(3.939)*	**BNA**	-3.848	4.251 *(-)*
T	-3.850	4.731 *(4.610)*	**BPHA**	-3.827	4.293 *(-)*
P	-3.867	5.523 *(5.195)*	**C**	-3.806	3.900 *(3.990)*
PH	-3.778	3.339 *(3.570)*	**PYR**	-3.786	3.836 *(3.929)*
BPH	-3.833	3.689 *(3.720)*	**PER**	-3.824	4.532 *(4.545)*
DBPH	-3.808	3.792 *(-)*	**BPER**	-3.822	4.192 *(4.031)*

Table 3.3: μ (eV) and S (au^{-1}), calculated at BMK/6-311+G(*3df,2p*)//B3-LYP/6-311G(*d,p*) level. Available experimental S are given between parentheses.

From Table 3.3, all optimized species can be considered as soft, ranging between 2.477 and 5.523 au^{-1}. The S results match very well their experimental counterparts. This excellent agreement is mainly due to error cancellation between the IP and EA contributions. For the series of linear acenes, an increase in molecular size corresponds to an increase of the EA value. In combination with decreasing IP values, this behavior is also observed for S, demonstrating a higher reactivity for the larger linear molecules (in agreement with other studies (276–278)).

From a local viewpoint, the radical Fukui function $f^0(\mathbf{r})$ is plotted for a selection of PAHs in Figure 3.6. Identification of the most reactive sites – and in particular the most reactive hydrogen atoms – within the hydrocarbon

molecules is clearly not straightforward. The **T** molecule is a representative of the series of linear acenes, whereas **DBPH** and **BPHA** represent non-linear PAH. The $f^0(\mathbf{r})$ isosurface of **T** shows a scarcely varying behavior: the lobes surrounding the hydrogen atoms all look very similar, suggesting that it is hard to distinguish between the reactivity of these atoms. The variations are somewhat larger for the non-linear PAHs, however, they remain limited for the B-like sites. Nevertheless, the three-dimensional radical Fukui function of **DBPH** clearly indicates that the hydrogen atoms at congested positions (e.g. position 1) exhibit a low reactivity. In the case of **BPHA** it is observed that several hydrogen atoms are now characterized by a low reactivity, which is due to the more folded structure of the molecule.

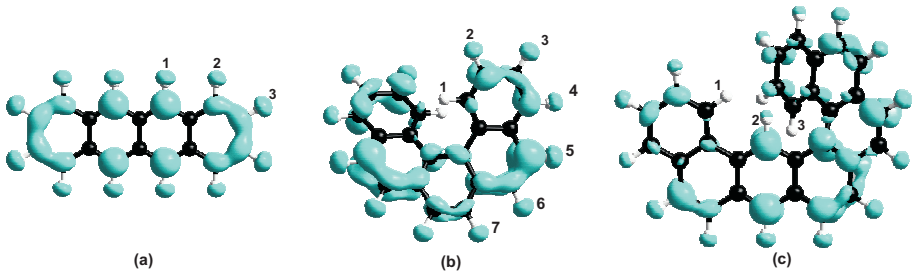

Figure 3.6: Isosurfaces of the radical Fukui function $f^0(\mathbf{r})$ for (a) **T** ,(b) **DBPH** and (c) **BPHA**.

In the following paragraphs, three types of elementary reactions occurring within the coke growth process are studied from the viewpoint of DFT-based reactivity indicators. An in depth discussion can be found in ***Papers III, IV and V***, whereas ***Paper VII*** discusses related radical addition reactions within the free-radical polymerization processes of PE and PVC. The applicability of the DFT-based reactivity indicators was investigated in collaboration with Prof. P. Geerlings and Prof. F. De Proft, who have a large expertise in the field of conceptual DFT. The polymerization reactions were studied in collaboration with Prof. M. F. Reyniers of the Laboratorium voor Petrochemische Techniek.

Hydrogen Abstraction Reactions

The first investigated class of radical reactions are hydrogen abstraction reactions at PAHs by a methyl radical, as thoroughly studied in 3.1.3. All properties are calculated using the BMK/6-311+G(*3df,2p*)//B3-LYP/6-311G(*d,p*) level of theory. We investigate the applicability of the HSAB principle, both from a global and local viewpoint, comparing barriers at 0 Kelvin (obtained in 3.1.3) with softness differences.

Firstly, following a global approach, $\Delta E_0^{\ddagger}$ values are compared with ΔS

results, which correspond to the differences between S of the PAH molecule on one hand (tabulated in Table 3.3) and S of the attacking methyl radical (2.741 au^{-1}) on the other. There is manifestly no meaningful correlation between the two quantities. Secondly, from a local perspective, $\Delta E_0^{\ddagger}$ values are compared with $\Delta s_{C,H_i}$ results, which correspond to the differences between s_H of the various hydrogen atoms of the PAH molecule on one hand and s_C of the carbon atom of the methyl group (2.849 au^{-1}) on the other. The CHELPG population analysis method was used to compute the condensed-to-atoms values. The first goal is to examine whether the indicators succeed in correctly indicating the preferred hydrogen for abstraction within a particular PAH molecule. As reported in previous paragraph, based on the $f^0(\mathbf{r})$ isosurfaces, the differences between the reactive behavior of the hydrogen atoms for the series of linear acenes are very small. However, inspection of the condensed softness values results in the observation that the minimal $\Delta s_{C,H_i}$ value can be assigned to the hydrogen atoms located at the outer rings. Thus, the local HSAB principle suggests that abstraction of hydrogen atoms located at the outer rings is preferred. This was also concluded based on the reaction barriers at 0 Kelvin. This correct behavior seems also valid for the non-linear series, but there are some pertinent exceptions. Furthermore, when inspecting intermolecular reactivity sequences comparing all PAH molecules, it is seen that generally speaking a correlation between the local softness differences and the barriers is obtained. The exceptions to the HSAB principle indicate that the dominant factors for these particular reactions are not hard/soft acid/base considerations. Indeed (as earlier discussed), steric hindrance effects between the incoming methyl radical and the PAH molecule cause exceptional high barriers, which the reactivity descriptors can not explain.

Addition Reactions

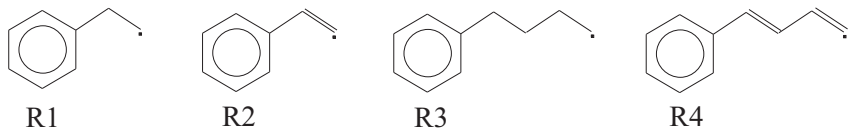

Figure 3.7: Reactant radicals involved in the addition reactions.

The second investigated class concerns addition reactions of hydrocarbon radicals to small gas phase components, such as ethylene, propene, ethyne and propyne. The reactant radicals are depicted in Figure 3.7: the ethylbenzene radical (R1), phenylacetylene radical (R2), butylbenzene radical (R3) and 1-phenyl-1,3-butadiene-4-yl radical (R4) are studied. Reaction barriers and local softness differences, computed at B3-LYP/6-311G(*d,p*), are given in Table 3.4, all additions are found to be exothermic. The condensed-to-atoms local de-

scriptors were obtained using the NPA population analysis scheme. In this case the Δs values correspond to the minimal differences between the s_C of the carbon atom of the radical center on one hand and the s_C of the carbon atoms of the olefin on the other.

An important question is which olefins are the most reactive towards addition, allowing the growth of the coke network. Furthermore, we investigate whether the indicators can provide accurate information about the regio selectivity and about which reaction pathways are preferred.

		ethylene	*ethyne*	*propene*	*propyne*
R1	$\Delta E_0^\ddagger$	31.02	32.51	30.49	39.28
	Δs	0.948	1.267	0.947	1.238
R2	$\Delta E_0^\ddagger$	18.74	23.77	25.60	32.23
	Δs	0.677	0.996	0.675	0.967
R3	$\Delta E_0^\ddagger$	35.93	39.77	35.99	-
	Δs	0.890	1.210	0.889	1.180
R4	$\Delta E_0^\ddagger$	-	34.55	28.41	-
	Δs	0.804	1.123	0.802	1.094

Table 3.4: Reaction barriers at 0 Kelvin ($\Delta E_0^\ddagger$, kJ mol^{-1}, including scaled ZPVEs) and local softness differences (Δs, au^{-1}) for the addition reactions, calculated at the B3-LYP/6-311G(d,p) level of theory.

Several conclusions can be made:

- The site-reactivity of the non-symmetric molecules propene and propyne is in accordance with predictions from steric considerations (cf. the Markovnikov rule for neutral addition reactions): the addition of the radical will preferentially occur at the least substituted carbon atom involved in the double, respectively triple bond. The preferred pathway gives rise to a secondary radical which is more stable than a primary radical.

- The Δs values serve as a measure for the reactivity of the different precursors and it is seen that the Δs values are in agreement with the $\Delta E_0^\ddagger$. The softness indicators support the observation that addition to precursors exhibiting a double bond is favored relative to triple bonds. It was previously reported that the slower addition of carbon-centered radicals to alkynes in comparison with similarly substituted alkenes is a general feature (244), and this topic was intensively investigated in ref. (238). In addition, the deviations between the Δs values of the reactions with ethylene (ethyne) and reactions with propene (propyne) are small. This is due to the fact that condensed reactivity indices only provide information concerning a limited molecular region. The chain length is of little importance here and the methyl substituent in the chain does not substantially

influence the reactivity index of the relevant carbon atom for addition, as this carbon atom is mainly influenced by the double, respectively triple bond.

- On basis of the Δs values, we conclude that R2 is more reactive than R4, followed by R3 and R1. This is in line with chemical intuition since R2 and R4 are both vinylic radicals and are more reactive than the primary radicals R1 and R3. The $\Delta E_0^{\ddagger}$ results are indeed much lower for additions of R2, emphasizing the large reactive character of this radical.
- No correlation can be found between the HSAB predictions and the reaction enthalpies (not tabulated). Moreover, no meaningful agreement could be found between the ΔH_r and $\Delta E_0^{\ddagger}$ values, as would be expected based on a normal Bell-Evans-Polanyi relationship (274; 275).

Cyclization Reactions

The third investigated class corresponds to unimolecular radical reactions, in particular cyclization reactions. The reactants consist of an aromatic nucleus of conjugated benzene rings (a maximum of 4 aromatic rings is considered) and an attached alkyl chain with the appropriate number of carbons to allow cyclization. Five ring closing reactions are studied, starting from the **B**-RE, **N**-RE, **A**-RE, **PH**-RE and **BPH**-RE, they are schematically depicted in Figure 3.8. These reactant structures are formed during the coke formation process after several appropriate addition reactions.

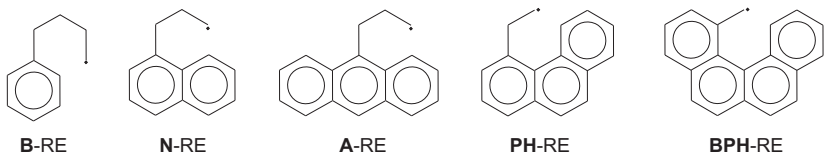

Figure 3.8: Reactant radicals involved in the cyclization reactions.

First of all, we report the failure of the radical Fukui function $f^0(\mathbf{r})$ in predicting the correct carbon atom for cyclization. Note that the Fukui function is used, instead of the local softness, as the reactions are unimolecular. In this light, applicability of the standard DFT-based indicators for unimolecular radical reactions will be further discussed in section 3.3. Valuable alternative reactivity indicators can be defined within a spin-polarized framework. Due to the presence of the aromatic nucleus in the examined reactant radicals, descriptors of aromaticity can also provide helpful information. The latter approach is explored here: a correlation between aromatic descriptors (see 2.1.5) on one hand and the reaction barriers at 0 Kelvin on the other is investigated. To

compare various reactions, a suitable normalization is required for the magnetic susceptibility anisotropy χ and the proton chemical shift δ, since these properties are size-dependent. We therefore introduce the relative dimensionless parameters R and T:

$$R = \frac{\triangle\chi(TS) - \triangle\chi(RE)}{\triangle\chi(RE)},$$
$$T = \frac{\delta(TS) - \delta(RE)}{\delta(RE)},$$

where δ represents the average chemical proton shift of the protons attached to the aromatic nucleus. Thus, both properties R and T are mainly determined by the aromatic behavior of the nucleus. An overview of the results, calculated at B3-LYP/6-311G(*d,p*), is given in Table 3.5.

In general it is seen that the relative indices R and T behave similarly. Comparison between these magnetic parameters and $\Delta E_0^{\ddagger}$ indicates that the smaller the aromaticity difference between the aromatic nucleus in the transition state and reactant (the smaller R and T), the lower the reaction barrier for cyclization. This demonstrates the importance of the aromaticity change of the aromatic nucleus during the course of the reaction in order to describe the kinetics of the studied cyclization reactions. Overall, a high barrier for cyclization is found for the largest reactant (**BPH**-RE). The properties R and T illustrate that for this reaction the aromaticity increases when going to the transition state (positive sign), because during the reaction the molecule becomes more planar since the radical corresponds to a benzylic type.

	B-RE	**N**-RE	**A**-RE	**PH**-RE	**BPH**-RE
R	-16.34	-15.19	-7.51	-5.18	2.99
T	-7.68	-7.30	-5.96	-2.10	0.88
$\Delta E_0^{\ddagger}$	51.79	49.11	41.39	33.43	50.03

Table 3.5: Calculated relative magnetic descriptors ($\times 10^{-2}$) and reaction barriers (kJ mol^{-1}) for cyclization reactions (B3-LYP/6-311G(*d,p*)).

3.1.5 Conclusions

Various reactions which are important in the radical growth process leading to coke have been studied. Besides obtaining accurate thermodynamic and kinetic results for one of the elementary steps in the coke network, we have focussed on the interpretative use and applicability of DFT-based reactivity indicators. The descriptors were applied in order to obtain correct information on the reactive behavior as well as reactivity sequences of the involved compounds and reactions.

Hydrogen abstraction reactions by a methyl radical were profoundly examined. These reactions create initial surface radicals in the coke network, and they are known to determine the global coking rate. An extended set of theoretical procedures (both wave function and density functional based) used for calculating accurate and yet cost-effective thermodynamic and kinetic parameters has been evaluated. The influence of two theoretical refinements, in particular inclusion of Eckart tunneling corrections and a more accurate description of the low-lying internal rotation around the forming/breaking bond, is also assessed. The abstraction at benzene is taken as a reference to obtain a suitable level of theory for further computations on the polyaromatic structures. High-level ab initio methods, and in particular W1, were used as a benchmark level whenever experimental results were unavailable or unreliable. It was found that the methods used for geometry optimization are less important, although HF and several post-HF methods lead to inaccurate results. The methods used for single-point energy calculations however showed larger variations. Overall it has been observed that accurate reaction barriers, enthalpies and kinetic data can be obtained using the low-cost BMK/6-311+G(*3df,2p*)//B3-LYP/6-311G(*d,p*) method.

In a next step, this method was chosen to study a comprehensive set of polyaromatics, modelling the coke surface. The influence of the local environment on the thermodynamic and kinetic data of the corresponding hydrogen abstraction reactions by a methyl radical was hereby investigated. It was found that congested sites in the PAHs correspond to lower reaction enthalpies (relief of strain upon creation of the radical), whereas the reaction barriers are higher (steric hindrance). This behavior is opposed to a normal Bell-Evans-Polanyi relationship. However, analysis of the sub-set of linear acenes does indicate a good correlation between reactivities and reaction enthalpies, because abstraction at these uncongested locations does not exhibit steric hindrance effects in the transition structures. The kinetic results support these conclusions.

Furthermore, analysis of the reactive characteristics of various polyaromatics by means of global reactivity descriptors showed that all compounds can be considered as soft (both using the B3-LYP, as well as the BMK functional) and good agreement with experimental data was obtained. For the series of linear acenes, an increased reactivity was found for the larger species. The applicability of the local HSAB principle for the bimolecular radical reactions was shown: predictions based on the HSAB principle are overall in good agreement with reaction barriers at 0 Kelvin. The local softness is well-suited to predict the preferred site for abstraction or addition, respectively. In case of cyclization reactions of alkyl chains at an aromatic nucleus, the aromaticity change of the aromatic nucleus during the reaction is the determining reactivity factor and thus the magnetic indices correlate well with the reaction barriers. The limitations of the descriptors are also reported, as they fail to explain exceptional high barriers for the abstraction reactions (due to steric hindrance effects in the transition structures) and a correlation with thermodynamic properties (such

as reaction enthalpies) was in general not obtained.

3.2 Typical reactions in small zeolite clusters

3.2.1 Introduction

Zeolites are microporous crystalline aluminosilicates, built from corner-sharing SiO_4 and AlO_4 tetrahedra. These solid-state catalysts portray a wide variety of properties and applications, due mainly to their shape-selectivity and Brönsted acid sites ≡Si-OH-Al≡, in combination with neighboring Lewis base sites ≡Si-O-Al≡ (279). We have modeled the zeolite by cutting out a small fragment from the zeolite catalyst, forming a cluster of 5 tetrahedral atoms (T-atoms=Al or Si) (280; 281). In addition to a traditional acidic zeolite cluster, we will also compare results with amine substituted zeolites (282). The various 5T clusters are depicted in Figure 3.9.

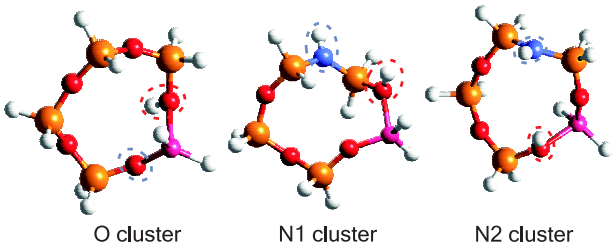

Figure 3.9: Optimized cluster geometries at B3-LYP/6-31G(d) level of theory, with acid site (red dotted line) and basic site (blue dotted line). For the O and N1 clusters both active sites are located on the same tetrahedron, while for the N2 cluster, the acid and base sites are further separated.

The appeal of nitrogen-substituted zeolites is mainly based on the minor change on molecular level (substituting a single oxygen bridge by a N-H bridge), yet which leads to completely different reactivity profiles. Earlier ab initio calculations showed that the amine-based zeolites are catalytically more active than the conventional analogue with O linkages (283; 284). Therefore, these catalysts represent a new class of highly promising materials. We study the formation of an alkoxide or an equivalent alkylammonium species, an archetypal step in zeolite chemistry for which both acid and basic sites play a crucial role. We specifically study the interaction of chloromethane, methanol, ethylene and propene with the clusters (285). In a traditional zeolite with only oxygen bridges, both sites are located near the aluminum defect. Amine moieties on the other hand cannot be located next to this aluminum, in order to prevent

protonation of the ≡Si-NH-Al-OH-Si≡ bridge to a less reactive ≡Si-NH_2-Al-O-Si≡ connection.

Firstly, the sensitivity of global reactivity descriptors on the applied computational method is investigated (***Paper VIII***). A strong level-of-theory dependence of the reactivity descriptors would almost certainly undermine their reliability. Relevant works investigating the performance of different theoretical procedures for describing reactivity-related properties are, however, rather scarce. For the global indicators, only De Proft et al. previously studied the effect of different theoretical methods on the electronegativity and hardness (286). Using the G2 thermochemical data set, they concluded that all DFT methods perform better than the high-level coupled cluster method. A superior behavior was demonstrated for the B3-LYP and B3-PW91 functionals in particular. Additionally, Jalbout et al. (287; 288) reported the excellent performance of the CBS-QB3 and G3B3 methods for a set of heteronuclear and homonuclear diatomic molecules. In an early work by Chattaraj et al. , comparing HF and MP2 results, the effect of correlation was found to be important for the validity of the HSAB principle in the case of soft-soft interactions, whereas interactions involving the hard Ag^+ acid could be sufficiently described using the far less time-consuming HF level (165).

Secondly, we assess whether DFT-based reactivity descriptors are capable of providing reliable information about typical reactions between small molecules and different zeolite frameworks (***Paper IX***). The investigated systems are bifunctional in the sense that the acid and basic sites are both located on framework atoms, either being oxygen bridges or an oxygen and a nitrogen bridge in case of an amine substituted zeolite. To the best of our knowledge only Vos et al. studied reactivity indicators on similar systems although limited to solely oxygen bridges to predict reaction preference for the alkylation of toluene and benzene (289; 290). Other works mainly focussed on cation-exchanged zeolites (291–301).

3.2.2 LOT dependence of global DFT-based reactivity descriptors

The influence of both basis set size and electronic structure method on global reactivity indicators is thoroughly investigated, using various small probe molecules and zeolite clusters (Figure 3.9) as a case study (***Paper VIII***). The global indicators are calculated using the finite difference method. The performance of the MPWB1K (302) and BMK functionals (303), representing the latest class of hybrid metafunctionals - which are primarily known for their successful description of kinetic properties - is assessed for the very first time, and comparison is made with Hartree-Fock and B3-LYP results. Since the electron affinity shows a large sensitivity to basis set – as the addition of the electron entails a profound change in the spatial extent of the wave function of the

anion (304) – a broad variety of Gaussian Pople and Dunning basis sets was tested. The main interest is to qualitatively investigate whether reactivity sequences remain unchanged when different levels of theory are used. First of all, it is important to note that the influence of the computational method on the geometry optimization was assessed, using B3-LYP, BMK and MPWB1K optimized structures in combination with the 6-31G(d) and/or 6-31+G(*d,p*) basis set. The influence was found to be very limited, and therefore, the choice of the low-cost B3-LYP/6-31G(d) optimized geometries was warranted.

Small probe molecules

The four probe molecules (chloromethane, methanol, ethylene and propene) have been used as a test case because experimental IP data are available. In addition, QCISD(T)/6-311++G(*3df,2p*)//B3-LYP/6-31G(d) benchmark values were used to investigate the experimentally non-accessible quantities μ and η. Overall, the functional sensitivity is found to be small. From an interpretative point of view, μ can be applied to characterize the relative electrophilic or nucleophilic behavior of the involved molecules. All basis sets including diffuse functions succeed in a correct prediction of the stronger electrophilic behavior of the polar molecules (methanol and chloromethane) and a more nucleophilic behavior for the apolar molecules (ethene and propene). The electrophilicity indicator ω is more appropriate in this light, and leads to the same conclusion. Overall, we find that accurate results can be obtained using either one of B3-LYP, BMK or MPWB1K DFT functionals, in combination with a basis set of double-zeta or triple-zeta quality, augmented with both diffuse and polarization functions. In order to obtain reliable results, the importance of adding diffuse functions should be stressed.

Reactivity indicators: purely oxygen-bridged zeolites

Values of μ and η are obtained for the isolated, purely oxygen-bridged zeolite reactant (O cluster in Figure 3.9), testing four electronic structure methods and nine basis sets. All methods indicate the relatively hard character of this catalyst (η values range between 4.81 and 6.22 eV). Inclusion of diffuse functions gives rise to a decrease with approximately 0.40 eV for η. Comparison between all results leads to the conclusion that, for the basis set dependence, a double-zeta basis set, augmented with one set of diffuse functions and polarization functions, seems sufficient for a reliable calculation of the global properties.

Global softness differences ΔS and activation hardnesses $\Delta\eta_{\text{act}}$, corresponding to the interactions between the purely oxygen-bridged cluster and the four small probe molecules were also computed, using the same extended set of theoretical levels. Firstly, we find the absolute values of HF to differ substantially from the DFT results, the BMK and MPWB1K results being very similar. Sec-

ondly, the lack of diffuse functions will most often lead to higher ΔS and $\Delta\eta_{\mathrm{act}}$ values. Thirdly, it is important to note that reactivity sequences corresponding to the various probe molecules and based on these properties may alternate, according to the used theoretical method.

Reactivity sequences: amine-modified zeolites

It is investigated whether the reactive ordering of the three zeolite model clusters (Figure 3.9) is independent of the level of theory applied for the single-point energy calculations. The hardness sequence $\eta(O) > \eta(N2) > \eta(N1)$ is retained for all investigated levels and indicates that substitution of an oxygen bridge by an amine group lowers the hardness, increasing the reactivity of the amine-modified cluster.

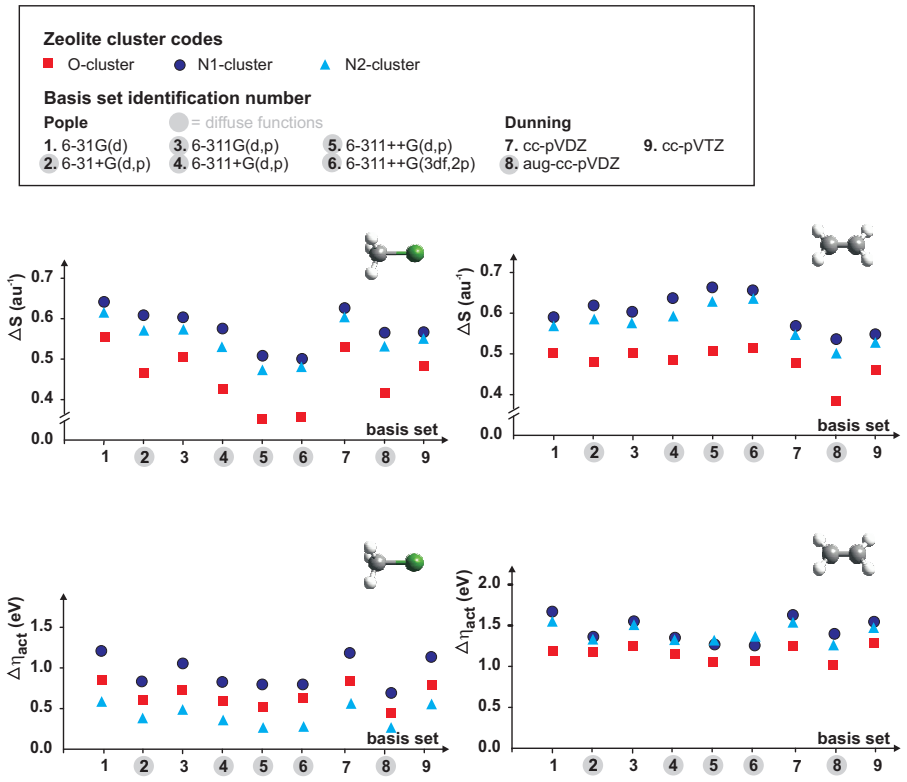

Figure 3.10: Global softness differences and activation hardnesses for the interaction between the various clusters and chloromethane and ethylene, calculated using the BMK functional.

As in previous paragraph, ΔS and $\Delta\eta_{\text{act}}$ values were calculated. The small polar probe molecules are also identified as hard, whereas the apolar molecules show intermediate values. Hence all interactions can be characterized as hard-hard. Chloromethane and ethylene are chosen as a reference for the polar and apolar species, respectively. The reactivity sequence $\Delta S(N1) > \Delta S(N2) > \Delta S(O)$ is found throughout, for interactions with both chloromethane and ethylene. The reactivity sequence based on $\Delta\eta_{\text{act}}$ is different for the two tested probe molecule. For chloromethane, the following sequence is obtained: $\Delta\eta_{\text{act}}(N1) > \Delta\eta_{\text{act}}(O) > \Delta\eta_{\text{act}}(N2)$, whereas for ethylene we find: $\Delta\eta_{\text{act}}(N1) > \Delta\eta_{\text{act}}(N2) > \Delta\eta_{\text{act}}(O)$. A minor level-of-theory dependence is reported, as all DFT methods perform very similar. The ordering, obtained with the BMK functional, is illustrated in Figure 3.10. The HF results are more scattered and more sensitive to the applied basis set.

3.2.3 Reactivity descriptors versus thermodynamics and kinetics

The interpretative use of the DFT-based descriptors (global and local) for studying the aforementioned hard-hard interactions between the small probe molecules and the three zeolite catalysts is further elaborated (***Paper IX***). Correlations with energetic results are investigated, using energy barriers calculated at 0 Kelvin ($\Delta E_0^{\ddagger}$) as tabulated in Table 3.6. All calculations are performed at the B3-LYP/6-31G(d) level of theory, which was shown to give intermolecular energies and vibrational frequencies similar to those obtained using MP2 by Zygmunt et al. Previous paragraph showed that this level of theory is sufficient when the main focus lies with studying the reactivity ordering of the clusters and their corresponding reactions.

	$\Delta E_0^{\ddagger}$	ΔS	$\Delta\eta_{\text{act}}$	$\Delta E_0^{\ddagger}$	ΔS	$\Delta\eta_{\text{act}}$
	CH3Cl			CH3OH		
O	169.9	0.653	0.635	199.8	0.717	1.094
N1	220.3	0.773	1.080	165.8	0.838	0.720
N2	117.5	0.747	0.458	150.3	0.811	0.556
	C2H4			C3H6		
O	96.6	0.528	1.096	86.0	0.419	1.454
N1	141.0	0.648	1.494	117.6	0.540	1.880
N2	124.3	0.622	1.354	119.6	0.513	1.840

Table 3.6: Barriers, ZVPE included (kJ/mol), softness differences (au^{-1}) and activation hardnesses (eV) for chemisorption reactions.

Firstly, the applicability of the global HSAB principle is investigated. We find that no correlation exists between ΔS and $\Delta E_0^{\ddagger}$ for the reaction with

the polar molecules chloromethane and methanol. The failure of the HSAB is possibly a corollary of the derivation of the HSAB rule, which was obtained through optimization of the covalent contribution of the interaction energy, and therefore partially neglecting other effects such as polarization. In contrast, the softness matching criterion is successful for the reactions with the apolar guest molecules ethylene and propene.

Secondly, we already mentioned that the principle of maximum hardness is incapable of differentiating between the reactivities of the various probe molecules. However, when the reactivities of the various zeolite catalysts are compared, an excellent correlation between $\Delta\eta_{\mathrm{act}}$ and $\Delta E_0^{\ddagger}$ is observed.

Thirdly, site-selectivity is studied using local properties. Since the reactions are characterized as hard-hard, the atomic charges and electrostatic energy were calculated and they are found to correctly indicate the acid site within all three zeolite clusters. Furthermore, in Figure 3.11 three-dimensional iso-surfaces of frontier-related properties are plotted for the purely oxygen-bridged cluster. The frontier orbitals HOMO and LUMO correctly indicate the basic and acid site, respectively. The only exception is found in the case of the N1 cluster, where the basic character of the nitrogen site is not recognized. In addition, the Fukui function governing electrophilic attack ($f^-(\mathbf{r})$) is investigated. This property contains more detailed information, nevertheless, the Fukui function iso-surface of the O cluster is not concentrated on a specific region and therefore does not succeed in predicting the basic site for this cluster. For the N1 and N2 clusters, the basic oxygen can be identified, but the nitrogen site only shows significant basic character for the N2 cluster.

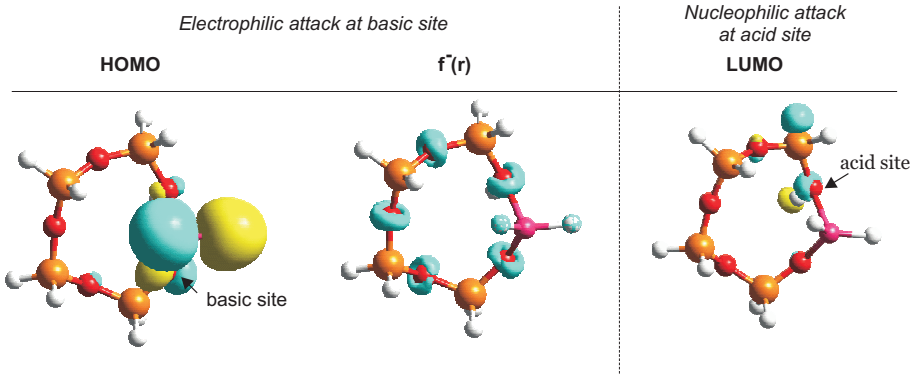

Figure 3.11: Iso-surfaces (value 0.2) of the HOMO, the Fukui function ($f^-(\mathbf{r})$) for electrophilic attack and the LUMO for the O cluster.

3.2.4 Conclusions

The level of theory dependence of global DFT-based reactivity descriptors has been thoroughly assessed, taking large inorganic zeolite clusters as well as small polar and apolar probe molecules as a test case. The performance of HF and three DFT methods, in particular B3-LYP, BMK and MPWB1K, has been investigated. These four methods were combined with nine different basis sets. The reactivity of three zeolite models containing both oxygen and amine bridges has been studied and special attention was given to their mutual reactivity ordering.

The sensitivity of the global hardness (and consequently the global softness differences) and the activation hardness to the applied level of theory, is overall found to be very limited. We find similar performance for the three investigated DFT functionals, with the BMK and MPWB1K results particularly close to each other. The HF results are more scattered and sensitive to the applied basis set. Comparison between the three zeolite clusters shows that for the studied hard-hard interactions, reactivity sequences are mainly independent of DFT functional and/or basis set used.

Furthermore, the reactivity sequences obtained using the reactivity descriptors are overall in agreement with sequences based on ab initio reaction energies. An exception is found for the interactions between the oxygen-bridged zeolite cluster and the polar molecules, where the reactivity ordering is not in accordance with the HSAB principle. This failure is possibly due to a partial neglect of polarization effects in the derivation of the principle. It is nevertheless illustrated that the reactivity properties, and in particular the Fukui function and local softness, can also be applied to correctly describe hard-hard interactions. They provide additional information to the atomic charges and electrostatic energy, which are more frequently used to describe interactions between hard species. The excellent agreement between the activation hardness and energy barriers for all studied reactions is also remarkable, indicating the necessity of taking into account transition state effects for the interaction with polar molecules.

3.3 Ring closing reactions

3.3.1 Introduction

As a final category of applications, two cyclization reactions have been studied. In both examples competing pathways occur, and it is interesting to examine whether DFT-based indicators can distinguish between these routes. The reactions have been investigated in collaboration with the research groups of Prof. C. V. Stevens and Prof. N. De Kimpe of the University of Ghent, who mainly

focussed on the experimental part. In addition, one of the cyclization reactions was elaborated on using spin-polarized reactivity descriptors, in collaboration with the research group of Prof. P. Geerlings and Prof. F. De Proft of the Free University of Brussels. In this thesis, the focus lies on the validation of reactivity descriptors and as such, the detailed reaction mechanisms will not be discussed, these can be found in the original papers.

General and simple guidelines for the regio selectivity of ring closure in alicyclic compounds have been introduced by Baldwin (305). They correctly describe the majority of the ring forming processes encountered in this type of chemical species (306–313). However, various counterexamples have already been given in literature (314–316). According to the Baldwin rules, ring closures can be classified into exo and endo types, corresponding to a bond breaking outside or inside the ring, respectively. Next, they classify reactions by the type of electrophilic site (digonal, trigonal or tetragonal). Finally, they state that orbital overlap requirements for the formation of bonds only favor certain combinations of ring size and the aforementioned parameters.

As a first example, the cyclization of azaheterocyclic aminophosphonates is studied (***Paper X***), where a remarkable preference toward a four-membered over a six-membered ring was observed (317–319). This is quite surprising because the latter species is known to be energetically favored, as it is characterized by smaller ring strains (320). Analogous work on similar ring closures is very scarce (321–324). The influence of various factors, such as the reaction environment (325) and substituents (326; 327) are also expected to be important. The main motivation for studying the present reaction lies in the pharmaceutical importance of the β-lactam ring as part of several important antibiotics, including penicillin (328).

As a second example, cascade cyclization reactions of nitrogen- and carbon-centered radical species are studied (***Paper XI***). These domino reactions start from the ring opening of the N-alkenyl-2-aziridinylmethyl radical and ultimately can lead to pyrrolizidines or indolizidines (329–332). These reactions exhibit large synthetic potential, as experimental results already showed their importance in the efficient synthesis of pyrrolizidines. In contrast, indolizidines could ultimately not be formed. Ab initio calculations contributed to the unravelling of the origin of these observations, indicating that the route toward indolizidines is characterized by a higher barrier of approximately 35 kJ mol^{-1} (329). The similar process, starting from the ring opening of 2-oxiranylmethyl and cyclopropylmethyl radicals, has been studied in detail in the literature (333–339). In the specific case when dealing with radical species, Beckwith et al. constructed some practical guidelines considering the influence of steric and electronic factors on the regio selectivity, among others stating the preference for exo-cyclizations and the importance of substituents (340). Other works also contributed to a better understanding of the regio selectivity in the cyclization of alkyl- and aryl-substituted radicals (341–349).

3.3.2 Cyclization of functionalized aminophosphonates

The origin of a peculiar ring closure of functionalized aminophosphonates toward four-membered phosphone-β-lactams, instead of the more stable six-membered ring, has been investigated (***Paper X***) (317–319). Figure 3.12 depicts a schematical overview of the reaction mechanism. When N-chloroacetyl-1-aminoal-kenyl phosphonate is treated with a base, a phosphorus-stabilized anion is formed, which can be represented by two canonical resonance contributors. Comparison between these two structures indicate that the α-canonical anion has a higher reactivity than the γ-canonical anion. After detachment of the chlorine ion (attached at carbon atom 5), the ring closure can occur at the α-carbon atom 1 (leading to the formation of the four-membered ring) or at the γ-carbon atom 3 (leading to the formation of the six-membered ring). Figure 3.12 also depicts the gas phase anion reactant.

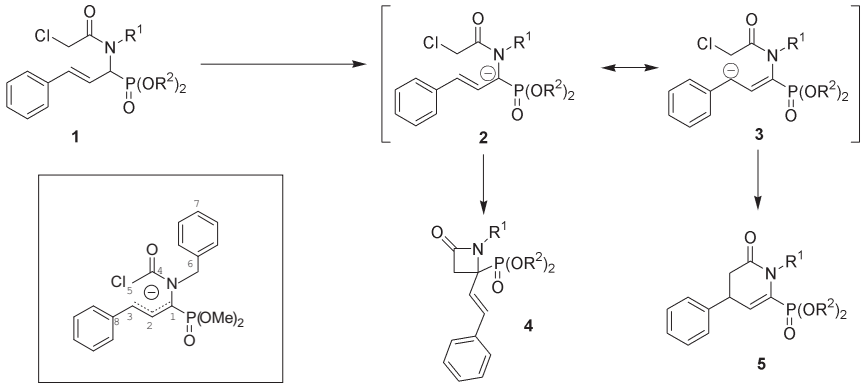

Figure 3.12: Reaction scheme. Inset: anion reactant, with indication of atoms which are important during the cyclization reaction.

Inspection of the geometrical parameters, such as bond lengths and dihedral angles, of the energetically most favored structure suggests a preference for the formation of the four-membered ring. The crucial bond lengths of the reactant are given in Figure 3.13. In addition, the transition structures of the competing pathways also seem to be in favor of formation of the four-membered ring. The optimized conformers, using B3-LYP/6-31+G(d), are depicted in Figure 3.13, calculated bond lengths and dihedral angles are also given. An important geometrical parameter that changes during the ring closure is the $C_2C_1NC_4$ dihedral angle (numbering, see Figure 3.12). Detailed investigation of the transition state, and of the internal rotation around the $C_1 - N$ bond shows that this rotation is significantly hindered (illustrated in Figure 3.14(a), calculated at the B3-LYP/3-21+G(d) level of theory). Moreover, the Figure clearly demonstrates that the rotational potential is strongly asymmetric. The

energy needed to reach the precursor suitable for four- or six-membered ring closure amounts to 15 and 38 kJ mol^{-1}, respectively. Therefore, rotation toward the γ-carbon atom is disfavored. It has been shown that extra ingredients, such as substituents, taking into account the transmetalation effects or solvent interactions, do not change the observed preference for the four-membered ring.

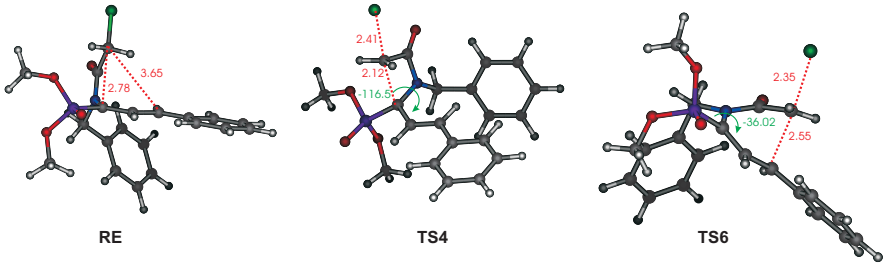

Figure 3.13: Optimized conformers of the anion reactant (RE) and the transition structures leading to the four- (TS4) and six-membered (TS6) ring, respectively.

The observed site selectivity in this ambident nucleophile is further rationalized by inspecting appropriate DFT-based reactivity indicators. The global hardness, local softness and Fukui function, were calculated for the most stable conformer, using the B3-LYP/6-31+G(d) level of theory. For the computation of the condensed Fukui and softness values, the natural population analysis (NPA) and CHELPG scheme were applied. The global indicators strongly emphasize the soft character of the studied anion, with $\eta = 2.74$ eV. Furthermore, the reactions are intramolecular S_N2 cyclization reactions, and the Fukui function for electrophilic attack ($f^-(\mathbf{r})$) is believed to indicate the most favorable site. Using the condensed-to-atoms values, the α-carbon atom is found to be the softest center whereas the γ-carbon atom is somewhat harder, suggesting that cyclization preferentially occurs at the α-position. This is also illustrated in Figure 3.14(b), where the three-dimensional iso-surface of $f^-(\mathbf{r})$ is visualized. It is concluded that the specific reaction is an example of a frontier-orbital controlled reaction, and the Fukui function is an appropriate indicator to describe the site selectivity.

	NPA		CHELPG	
atom	f_k^-	s_k^-	f_k^-	s_k^-
C_1 (or C_α)	0.27	1.32	0.37	1.86
C_3 (or C_γ)	0.23	1.16	0.35	1.72

Table 3.7: Condensed Fukui function and softness, calculated at B3-LYP/6-31+G(d), using the NPA and CHELPG schemes.

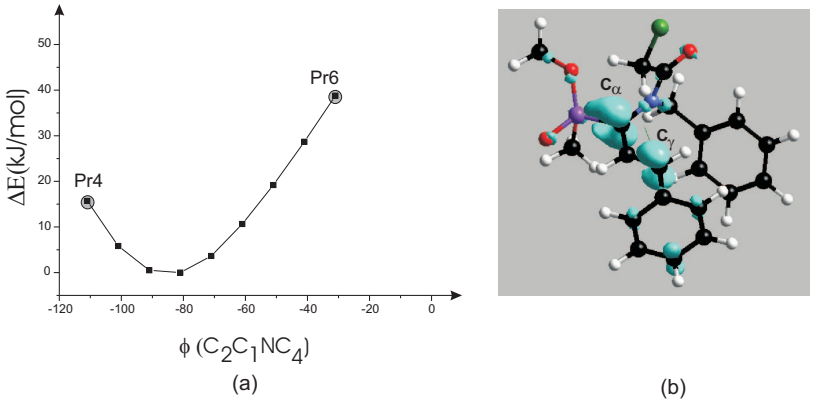

Figure 3.14: (a)Part of the rotational potential in terms of the $C_2C_1NC_4$ dihedral angle. The precursors for four- and six-membered ring formation (Pr4 and Pr6) are indicated by a grey circle. (b)Iso-surface (value 0.005) of the Fukui function for electrophilic attack at the most stable conformer of the anion, which is the precursor for four-membered ring formation.

In contrast to the discussed unimolecular reaction, experimental observations about the site-selectivity in case of a bimolecular reaction, in particular protonation and trapping with methyl iodide, report that these reactions occur at the γ-position. The protonation reaction is – due to the hard character of the proton – charge-controlled and is therefore expected to occur preferentially at the most electronegative center. This is indeed the γ-atom in our case, as most of the negative charge is located at this position. Methyl iodide is a soft electrophile, however application of hard and soft arguments from a local point of view also leads to an agreement between experiment and computational results: the intermediately hard carbon atom of methyl iodide will react with the hard γ-carbon atom of the anion.

3.3.3 Nitrogen- and carbon-centered radicals in cascade cyclizations

The radical cascade cyclization of N-alkenyl-2-aziridinylmethyl radicals has been studied (***Paper XI***) (329). A cyclization reaction of a nitrogen-centered radical takes place, leading to the formation of a five-membered ring for a pentenyl chain or or six-membered ring in the case of a hexenyl chain (Figure 3.15). In the following step, a bicyclic skeleton is formed (cyclization of a carbon-centered radical), after which the radical cascade terminates into azabicyclic

compounds. Experimental data reported on the preference for intramolecular addition of the radical center to the 5-exo-carbon atom, resulting in the formation of the smaller ring. Activation barriers, calculated at the same level of theory of the energetics, confirmed this observation. The applicability of reactivity descriptors, calculated using B3-LYP/6-311++G(d,p) single-point energy calculations, is tested. For the condensed-to-atoms values of the Fukui functions, the NPA scheme was used.

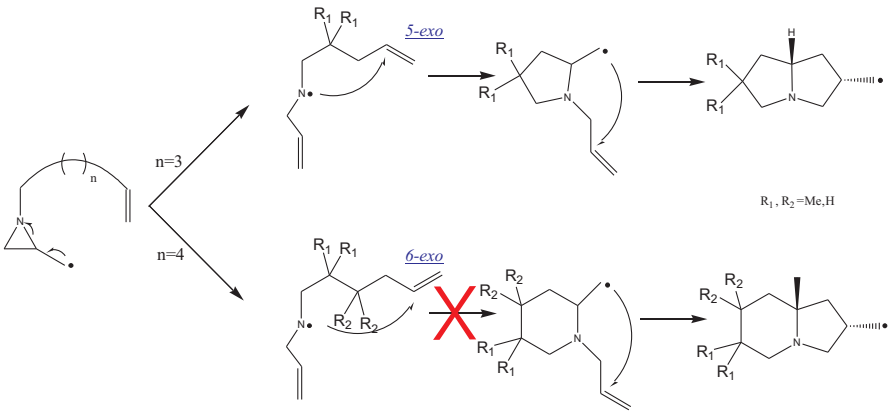

Figure 3.15: Cascade cyclizations of nitrogen- and carbon-centered radicals

The condensed-to-atoms counterparts of the radical Fukui function $f^0(\mathbf{r})$ indicate that the f_k^0 value for the 6-exo-carbon atom is always higher than the value for the 5-exo-carbon atom. Hence, the Fukui function predicts an attack which is in disagreement with the experimental observations. Taking into account the details of an intramolecular addition mechanism, more insight into the origin of this failure (which is basically the failure of the local HSAB principle) is obtained. In the studied reaction, part of the molecule acts as an electron acceptor and another part as an electron donor. Thus, from a local point of view, the number of electrons N changes. However, the spin state of the system, characterized by N_S, remains constant. As mentioned in the theoretical section (subsection 2.1.4), spin-polarized DFT offers a valuable alternative to describe the chemical reactivity for systems in which a constrained charge transfer (N_S constant) occurs. The polarized Fukui function $f_{NN}(\mathbf{r}) = (\frac{\partial \rho(\mathbf{r})}{\partial N})_{N_S, v(\mathbf{r}), \mathbf{B}(\mathbf{r})}$ is used to investigate the regio selectivity. Indeed, using the spin-polarized condensed-to-atoms values $f_{NN,k}^0$, it is found that the better matching always corresponds to the 5-exo-carbon atom of the double bond. It is concluded that the 5-exo-ring closure is correctly predicted applying spin-polarized descriptors.

As a final remark, we note that the aforementioned cyclization reaction is

analogous to the cyclization reaction occurring in the coke formation process. Indeed, also for the latter process the traditional non-polarized indicators could not be applied successfully. In contrast, for the cyclization of functionalized aminophosphonates (discussed in previous subsection 3.3.2) the Fukui function was found to be a suitable descriptor to describe the regio selectivity. However, during the course of this reaction a chlorine ion is detached from the original anion reactant, and therefore N_S is not kept constant.

3.3.4 Conclusions

The site-selectivity of two unimolecular cyclization reactions has been investigated. In the first example, the remarkable selectivity of a phosphorus-stabilized anion leading to the formation of a four-membered, instead of a six-membered ring has been investigated. The Fukui function is found to be a suitable descriptor, as it correctly indicates the α-carbon to be the preferred atom for cyclization. In addition, bimolecular reactions, such as proton trapping, can also be correctly described by applying hard-soft acid-base considerations. In the second example, radical cascade reactions leading to the exclusive formation of pyrrolizidines have been studied. In this case, the Fukui function is found to fail in predicting the correct regio selectivity. However, in this reaction, the charge transfer is constrained (as the spin multiplicity is kept constant during the course of the reaction) and hence, spin-polarized indicators offer a valuable alternative. It is indeed found that the spin-polarized Fukui function succeeds in correctly describing the preferred site for cyclization.

4

General Conclusions and Perspectives

In this thesis, the applicability of several fundamental reactivity indicators, defined within the framework of density functional theory, has been tested for a variety of reactions occurring in diverse domains of chemistry. The chemical potential, global hardness and global softness are used to discuss the reactive behavior of one single molecule or a set of related molecules, providing reactivity sequences for the latter. The Fukui function is used as an intra-molecular descriptor, whereas the local softness can provide inter-molecular reactivity information about regio selectivity. In order to test the usefulness of the aforementioned properties, they are usually used in conjunction with well-known chemical principles such as the electronegativity equalization, the principle of maximum hardness and the hard and soft acids and bases (HSAB) principle. A validation of the results is obtained through comparison with ab initio thermodynamic and kinetic data. In general, DFT-based concepts have proven to be of great use in the interpretation of a variety of experimental and theoretical results. It remains nevertheless challenging to make predictions about their success or failure for specific types of interactions. In order to rely on the indicators as independent and/or predictive tools for the description of chemical reactivity, there is need for practical guidelines describing which indicators are suitable for a certain problem. The descriptors probe electronic interactions, however it is clear that they do not monitor other effects, such as steric contributions. Whenever the indicators are tested, their limitations must a priori be kept in mind. For instance, some of the reactions studied in this work exhibit high reaction barriers due to large steric hindrance effects between the two reactants and thus, the indicators are not expected to be successful.

The largest group of applications concerns radical reactions. The majority of them occur during the formation of coke, which is a side process of thermal cracking of hydrocarbons. Radical systems are particularly interesting and

challenging, however so far only a handful of papers discussed their behavior using reactivity descriptors. In the specific case of hydrogen abstraction reactions at polyaromatic species, accurate, reliable and yet affordable thermodynamic and kinetic data have been obtained. Other investigated bimolecular radical reactions are addition reactions of radicals to small olefins and the initiation and first propagation steps within the polymerization process of polyethylene and poly(vinylchloride). Overall, it can be concluded that the radical Fukui function is capable of indicating the preferred site of reaction. This clearly indicates the importance of frontier orbital effects for this specific type of interaction. The local HSAB principle was also successfully applied, leading to correct reactivity sequences when related molecules were compared with each other. Hence the local softness is a suitable indicator for studying bimolecular radical reactions. This is in accordance with earlier suggestions and with the categorization of Klopman, as the larger radicals are characterized by high global softness values. Whereas the local viewpoint leads to satisfactory results, the global HSAB principle fails for some specific bimolecular radical reactions and is therefore not recommended. In addition to these bimolecular reactions, two examples of unimolecular radical cyclization reactions have also been studied. For these reactions, the Fukui function is used to describe the intra-molecular regio selectivity. However, the correct site of cyclization could not be indicated. Since these reactions correspond to a constrained charge transfer – the spin number remains constant, whereas the total number of electrons changes at a local level – the spin-polarized reactivity descriptors, and in particular the spin-polarized Fukui function has been tested and indeed, its usefulness is demonstrated.

The study of radical reactions might benefit from taking into account more detailed information considering the reaction mechanism. At present, a radical attack is described by taking the arithmetic average of the indicators for electrophilic and nucleophilic attack. In practice however, the various radical reaction mechanisms differ quite a lot, as is illustrated in this work: radical hydrogen abstraction reactions are basically very different from radical addition reactions, and so on. Therefore, it is suggested that the definitions for the indicators describing a radical reaction are specific weighted averages, taking into account the nucleophilic or electrophilic character of the reaction partners. Further research is also required on the applicability of the spin-polarized formulation of conceptual density functional theory. This work is in progress at the research group of Prof. P. Geerlings and Prof. F. De Proft.

A second group of studied bimolecular reactions correspond to typical reactions occurring within zeolite catalysis. The small probe molecules are characterized as hard systems, and both polar and apolar representatives were chosen. The zeolite catalyst was modelled by a small 5-tetrahedral cluster, and in addition to the traditional oxygen-bridged cluster the influence of amine substitution was tested. These reactions were difficult to describe using DFT-based reactivity descriptors. The global HSAB principle fails for the interactions with the polar molecules, as in these cases polarization effects – which are not

included in the purely electron transfer process – are dominant. In contrast, the reactions between the zeolite clusters and the apolar molecules do follow the HSAB rule. From a local point of view, the complex mechanism of these concerted reactions, occurring simultaneously at the acid and basic site of the zeolite framework, could not be specified based on local descriptors. Multiple-site interactions in general remain a domain for further research. In addition, the local hardness might be more suitable to describe interactions with hard molecules, although at present the calculations remain troublesome and no practical scheme is presented yet.

A final application concerns a unimolecular ionic cyclization reaction leading to the formation of a four-membered β-lactam ring. This is an example in which competing pathways can take place because the formation of the more stable six-membered ring, instead of the strained four-membered ring, is initially expected. The anion reactant is a very soft species and the traditional local indicator, i. e. the Fukui function, succeeds in correctly predicting the preferred reaction path. Therefore the indicator adds to the unravelling of the origin of the experimentally observed cyclization preference. Moreover, extension to bimolecular reactions using this anion reactant also revealed the successful applicability of the local softness, as also these results were in correspondence with reaction barriers obtained at 0 Kelvin.

In this thesis, one of the main advantages of using reactivity descriptors was accentuated, in particular their low computational cost. Not only do they solely require information from the reactants, but it was furthermore demonstrated that reactivity sequences are mainly independent of the level of theory used for geometry optimizations as well as for single-point energy calculations. An extended set of theoretical procedures, ranging from simple ab initio methods such as Hartree-Fock, over a very popular and successful functional, to the latest class of highly promising methods. The observation of level-of-theory independency for the calculation of the global descriptors is highly reassuring and adds to the reliability of DFT-based reactivity indicators. It must however be emphasized that overall the perturbative approach should be used complementary to information obtained from thermodynamics and kinetics.

Part II

Papers

Paper I

An assessment of theoretical procedures for predicting the thermochemistry and kinetics of hydrogen abstraction by methyl radical from benzene

Hemelsoet K. , Moran D. , Van Speybroeck V. ,
Waroquier M. and Radom L.

J. Phys. Chem. A, **2006**, *110*, 8942–8951

8942 *J. Phys. Chem. A* **2006,** *110,* 8942−8951

An Assessment of Theoretical Procedures for Predicting the Thermochemistry and Kinetics of Hydrogen Abstraction by Methyl Radical from Benzene

Karen Hemelsoet,[†,‡] Damian Moran,*[,‡] Veronique Van Speybroeck,*[,†] Michel Waroquier,[†] and Leo Radom*[,‡]

Center for Molecular Modeling, Ghent University, Proeftuinstraat 86, B-9000 Gent, Belgium, and School of Chemistry and ARC Centre of Excellence in Free Radical Chemistry and Biotechnology, University of Sydney, Sydney, NSW 2006, Australia

Received: March 23, 2006; In Final Form: May 13, 2006

The reaction enthalpy (298 K), barrier (0 K), and activation energy and preexponential factor (600−800 K) have been examined computationally for the abstraction of hydrogen from benzene by the methyl radical, to assess their sensitivity to the applied level of theory. The computational methods considered include high-level composite procedures, including W1, G3-RAD, G3(MP2)-RAD, and CBS-QB3, as well as conventional ab initio and density functional theory (DFT) methods, with the latter two classes employing the 6-31G(d), 6-31+G(d,p) and/or 6-311+G(3df,2p) basis sets, and including ZPVE/thermal corrections obtained from 6-31G-(d) or 6-31+G(d,p) calculations. Virtually all the theoretical procedures except UMP2 are found to give geometries that are suitable for subsequent calculation of the reaction enthalpy and barrier. For the reaction enthalpy, W1, G3-RAD, and URCCSD(T) give best agreement with experiment, while the large-basis-set DFT procedures slightly underestimate the endothermicity. The reaction barrier is slightly more sensitive to the choice of basis set and/or correlation level, with URCCSD(T) and the low-cost BMK method providing values in close agreement with the benchmark G3-RAD value. Inspection of the theoretically calculated rate parameters reveals a minor dependence on the level of theory for the preexponential factor. There is more sensitivity for the activation energy, with a reasonable agreement with experiment being obtained for the G3 methods and the hybrid functionals BMK, BB1K, and MPW1K, especially in combination with the 6-311+G-(3df,2p) basis set. Overall, the high-level G3-RAD composite procedure, URCCSD(T), and the cost-effective DFT methods BMK, BB1K, and MPW1K give the best results among the methods assessed for calculating the thermochemistry and kinetics of hydrogen abstraction by the methyl radical from benzene.

1. Introduction

Hydrogen-abstraction reactions are ubiquitous in chemistry and biology and have been studied in such diverse areas as cosmology, combustion science, and the polymer industry. For example, the initiation step in coke formation,[1] an industrially important side process of thermal hydrocarbon cracking, is hydrogen abstraction.[2−4] To model these potentially complex reaction processes, calculations on some of the contributing elementary reactions are advisable, as they provide the opportunity to obtain the required levels of insight and understanding for model genesis.[5−8] In the present paper, we will focus on the abstraction of hydrogen from benzene by the methyl radical (see Figure 1), as this represents a fundamental point of comparison for radical-mediated hydrogen abstractions from the benzenoid components of polycyclic aromatic hydrocarbons (PAHs).[9,10] PAHs are of general interest, as some are known carcinogens,[11] and they are formed as byproducts during the incomplete combustion of organic substances such as coal, oil, and waste.[12−15] Of related relevance to radical-abstraction reactions are radical-addition processes,[16−18] where a delicate balance between the various factors governing reaction kinetics and thermochemistry has been demonstrated both experimentally and theoretically.[19]

Hydrogen-abstraction reactions have been the subject of numerous computational studies.[2,20−23] Of most relevance to the present investigation is the comprehensive work of Tokmakov et al.,[22] who examined the reaction of phenyl radical with methane (i.e., the reverse of the reaction of benzene plus methyl radical) at the G2M(CC,MP2) level of theory and reported an exothermicity at 0 K of 43.1 kJ mol^{-1} and a barrier of 38.8 kJ mol^{-1} for the process. Their predicted G2M(CC,MP2) exothermicity is approximately 6.3 kJ mol^{-1} greater than experiment, which they attributed[22] to the highly spin-contaminated unrestricted wave function of the phenyl radical[24,25] (leading to the energy of the phenyl radical being overestimated). Also of interest is the recent assessment study by Coote,[23] who found MPW1K/6-311+G(3df,2p) to be a reliable, yet cost-effective, theoretical method for modeling the hydrogen-abstraction reactions of carbon-centered radicals. In a related radical study,[17] we found that the geometries, frequency factors, and temperature corrections for a series of radical-addition reactions to C=C and C≡C bonds were relatively insensitive to the level of theory, while reaction enthalpies and barrier heights were very sensitive to the method employed.[17] As the aromatic ring might have a substantial influence on these quantities, the conclusions

* Authors to whom correspondence should be addressed. E-mail: dmoran@chem.usyd.edu.au; veronique.vanspeybroeck@ugent.be; radom@chem.usyd.edu.au.
[†] Ghent University.
[‡] University of Sydney.

10.1021/jp061823z CCC: $33.50
Published on Web 06/29/2006

obtained from these previous studies on radical reactions involving nonaromatic species might not necessarily be applicable to the present investigation.

For the reaction of benzene with the methyl radical ($C_6H_6 + \bullet CH_3 \rightarrow \bullet C_6H_5 + CH_4$), relevant data from two experiments are available.[26,27] Using a flow-tube experiment with either dimethylmercury or dimethylcadmium as the $\bullet CH_3$ source, Krech and Price[26] measured a rate constant of $k(T) = 6.3 \times 10^4\ e^{(-4680/T)}\ m^3\ mol^{-1}\ s^{-1}$ within the temperature range 744−800 K. More recently, Zhang et al.[27] conducted a steady-state analysis of CH_4 formation during pyrolysis of C_2H_4 in the presence of C_6H_6 at temperatures of 650−770 K, leading to a rate constant $k(T) = 2.0 \times 10^6\ e^{(-7580/T)}\ m^3\ mol^{-1}\ s^{-1}$. However, both the slope and the intercept for $1/T \rightarrow 0$ of the rate curves in these two experiments show substantial differences, and therefore, so do the activation energies and the preexponential factors. These differences may at least partly be associated with the narrow temperature ranges used for the extrapolations.

As noted above, the reverse of the benzene abstraction reaction, i.e., $CH_4 + \bullet C_6H_5 \rightarrow \bullet CH_3 + C_6H_6$, has been examined experimentally by Tokmakov et al.,[22] who used the complementary methods of pyrolysis/Fourier transform IR spectroscopy and pulsed-laser-photolysis/mass spectrometry. They reported a rate constant $k(T)$ for this process of $6.0 \times 10^6\ e^{(-6201/T)}\ m^3\ mol^{-1}\ s^{-1}$ in the temperature range 600−980 K. They also noted the disparity between the kinetic parameters reported by Krech and Price[26] and Zhang et al.[27] Other experimental data for the reverse of the benzene abstraction reaction have been obtained by Heckmann et al.[28] and Duncan et al.[29]

In recent years, there has been significant testing of a wide range of theoretical procedures for their ability to obtain reliable and accurate reaction thermochemistry and kinetics. Density functional theory (DFT) methods have often been found to provide an excellent cost-to-reliability performance and have therefore seen increased popularity.[30] B3-LYP is undoubtedly the most widely used DFT functional,[31] but its limitations—including the troublesome description of unstable structures such as transition structures (TSs), especially when polar effects are important—are also potentially problematic for hydrogen-abstraction reactions.[2,21,23,32,33] Recent studies on benchmark systems have shown that the new hybrid metafunctionals such as BMK,[34] MPWB1K,[35] and TPSS1KCIS[36] perform better than B3-LYP in certain situations.[37]

The main goal of the current work is to examine the influence of level of theory on optimized geometries, reaction enthalpies at 298 K (ΔH_{298}), barriers ($\Delta E_0^{\ddagger}$), activation energies (E_a), preexponential factors (A), and rate constants (k) for the abstraction of hydrogen from benzene by the methyl radical. This study will serve as a reference for further work on larger polyaromatic systems, and in this respect, we will focus particularly on identifying accurate and yet affordable computational methods that might be suitable for modeling the hydrogen-abstraction reactions of a broad variety of benzenoid hydrocarbons. As part of the study, the influence of level of theory on rate constants is also investigated, and comparison is made with experimental data. Although the characteristics and reactive behavior of benzene and other PAHs[3,8,10] have been previously investigated, this study represents the first systematic assessment of the performance of theory for calculating the thermochemical and kinetic properties of the hydrogen-abstraction reaction between benzene and the methyl radical.

2. Theoretical Procedures

Molecular orbital theory[38] and density functional theory (DFT)[39] calculations were performed using the *Gaussian 03*,[40] *Molpro 2000.6*,[41] and *ACES II*[42] program packages. Unless noted otherwise, calculations on radicals were performed with an unrestricted open-shell wave function. The "U" prefix is often omitted, though it is sometimes included for emphasis. In the limited number of cases where a restricted open-shell wave function was used, this is indicated by an "R" prefix. The frozen-core approximation was used throughout, except where full calculations were required as part of a standard composite method.

Geometries were optimized at the BP86, BLYP, B3-P86, B3-LYP, B3-PW91, MPW1K, BB1K, MPWB1K, BMK, UHF, RHF, UMP2, UQCISD, and UCCSD levels of theory, in conjunction with the 6-31G(d) and 6-31+G(d,p) basis sets. The B3-LYP and CCSD methods were also used in combination with the 6-31G(d,p) and/or 6-311G(d,p) basis sets. Harmonic vibrational frequencies were computed at the same level of theory as the geometry optimization and used (after appropriate scaling) to provide zero-point vibrational energies (ZPVEs) and to confirm the nature of the stationary points. Single-point energy calculations were performed for each geometry at the URCCSD(T)/6-311+G(d,p) level, with the calculated total energies allowing the quality of the optimized structures to be evaluated.

Using the B3-LYP/6-31+G(d,p) and BMK/6-31+G(d,p) optimized geometries, hydrogen-abstraction barriers and reaction enthalpies were computed using a variety of standard DFT methods in combination with the 6-31G(d) and 6-31+G(d,p) basis sets. In addition to these small-basis-set calculations, UB3-LYP, RB3-LYP, B3-PW91, MPW1PW91, MPW1K, BB1K, MPWB1K, BMK, UHF, RHF, UMP2, RMP2, and the UR-CCSD(T) procedure of Molpro were also used with the 6-311+G(3df,2p) basis set. The barriers and reaction enthalpies were also computed with the CBS-QB3,[43] G3(MP2)-RAD,[44] and G3-RAD[45] high-level composite procedures. The reaction enthalpy was also computed with the W1 procedure,[46] which has been found, when evaluated with a large test set of thermochemical data, to generally give agreement with experiment to within 2 kJ mol^{-1}.[46]

We applied transition state theory (TST)[47] to calculate the rate constants using the expression[48]

$$k(T) = \kappa \frac{k_B T}{h} \frac{q_{\ddagger}/V}{(q_A/V)(q_B/V)} e^{-(\Delta E_0^{\ddagger}/k_B T)} \quad (1)$$

where κ is the tunneling coefficient, k_B is the Boltzmann constant, h is Planck's constant, V is the reference volume in which the translational part of the partition function is evaluated, q_A, q_B, and $q_{\ddagger}$ relate to the molecular partition functions of the reactants (A and B) and transition structure (TS), respectively, and $\Delta E_0^{\ddagger}$ is the ZPVE-corrected energy difference between the TS and the reactants (i.e., the reaction barrier) at 0 K. To calculate the tunneling coefficient, κ, the Wigner[49] and Eckart[50] methods were tested, representing simple procedures that only need to consider the reaction stationary points and are therefore compatible with TST. In general, the Eckart method is considered to be superior to the Wigner approximation,[51] as the latter depends solely on the imaginary frequency of the TS and can grossly underestimate the effect of tunneling. The Eckart approximation, on the other hand, is found often to overestimate the tunneling contribution, especially at very low temperature.[51]

The link with the macroscopic quantities found in the Arrhenius rate law is made by a linear fit to a set of $k(T)$ values calculated using eq 1 for a range of temperatures. One refinement in our theoretical treatment comes from the observa-

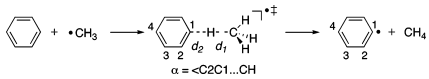

Figure 1. Hydrogen abstraction from benzene by the methyl radical to form the phenyl radical plus methane. The forming bond length (d_1), breaking bond length (d_2), and torsional angle (α) of the transition structure are highlighted.

tion that the TS of the reaction between benzene and methyl radical has a very-low-frequency vibration, corresponding to internal rotation of the methyl group about the forming bond. As a result, the free rotor (FR) approximation is used to model this mode.[52] In a recent study on radical-addition reactions, we demonstrated the importance of correctly describing hindered internal rotations in order to obtain reliable partition functions.[6,53] In the present case, we use a mixed harmonic oscillator/free rotor (HO/FR) model, in which all the internal motions except for the methyl torsion in the TS are approximated as independent harmonic oscillators and the corresponding partition functions are obtained as a product of contributions of the form

$$q_{\mathrm{vib},i} = \frac{\mathrm{e}^{-(h\nu_i/2k_\mathrm{B}T)}}{1 - \mathrm{e}^{-(h\nu_i/k_\mathrm{B}T)}} \qquad (2)$$

for each of the internal modes i ($i = 1, ..., 3N - 6$ for a nonlinear molecule). For the internal motion of the methyl group in the TS, the standard HO contribution is replaced by a manually constructed FR partition function given by

$$q_{\mathrm{FR}} = \frac{1}{\sigma_{\mathrm{int}}}\sqrt{\frac{k_\mathrm{B}T\pi}{h\nu}} = \frac{1}{\sigma_{\mathrm{int}}}\sqrt{\frac{2k_\mathrm{B}T\pi I_\mathrm{m}}{\hbar^2}} \qquad (3)$$

where σ_{int} is the symmetry number, and I_m is the reduced moment of inertia.

Another important consideration for an accurate description of reaction kinetics and thermochemistry is the use of ZPVE and thermal-correction scaling factors,[54] as they provide a means for accounting for systematic deviations between measured and computed frequency-dependent properties.[21,36,54−56] Published scaling factors for the thermal correction to the enthalpy are not available for the hybrid meta-DFT functionals, and a value of 0.98 is used.

3. Results and Discussion

3.1. Geometries. The hydrogen abstraction from benzene by a methyl radical to form the phenyl radical plus methane is shown in Figure 1. Three of the geometric parameters vary significantly during the course of the reaction. These are the forming (d_1) and breaking (d_2) bond lengths and the torsional dihedral angle (α) of a C−H bond of the methyl group with respect to the plane of the aromatic ring.

The geometries of the reactants, products, and TSs were optimized at various levels of theory.[57] Considering the TS geometry first, we see from Table 1 that, at all levels of theory, d_1 is modestly shorter than d_2 (average difference approximately 0.07 Å), which is consistent with a "late" (in the Hammond sense) TS and in accordance with the reaction endothermicity. The bond lengths d_1 and d_2 show a moderate dependence on the quantum chemical method used, which has also been noted in reports for other hydrogen-abstraction reactions.[23] For example, with the 6-31+G(d,p) basis set, values of d_1 range from 1.254 Å (MP2) to 1.325 Å (UHF), while values of d_2 range from 1.358 Å (RHF) to 1.398 Å (UMP2). There are also only modest differences associated with the choice of basis set, with

TABLE 1: Calculated Torsional Angle (α) and Forming (d_1) and Breaking (d_2) Bond Lengths in the Transition Structure for Hydrogen Abstraction from Benzene by Methyl Radical[a]

level of theory	α (°)	d_1 (Å)	d_2 (Å)
BP86/6-31G(d)	17.4	1.327	1.372
BP86/6-31+G(d,p)	15.5	1.311	1.388
BLYP/6-31G(d)	16.5	1.335	1.373
BLYP/6-31+G(d,p)	15.3	1.320	1.388
B3-P86/6-31G(d)	18.5	1.307	1.367
B3-P86/6-31+G(d,p)	15.7	1.294	1.379
B3-LYP/6-31G(d)	18.5	1.316	1.369
B3-LYP/6-31G(d,p)	16.7	1.313	1.371
B3-LYP/6-31+G(d,p)	15.2	1.304	1.382
B3-LYP/6-311G(d,p)	22.2	1.307	1.379
B3-PW91/6-31G(d)	16.4	1.310	1.368
B3-PW91/6-31+G(d,p)	16.7	1.298	1.380
MPW1K/6-31G(d)	16.0	1.296	1.363
MPW1K/6-31+G(d,p)	15.6	1.286	1.373
BB1K/6-31G(d)	17.4	1.304	1.355
BB1K/6-31+G(d,p)	16.5	1.294	1.365
MPWB1K/6-31G(d)	16.5	1.302	1.354
MPWB1K/6-31+G(d,p)	16.0	1.291	1.364
BMK/6-31G(d)	21.4	1.313	1.363
BMK/6-31+G(d,p)	21.5	1.302	1.375
UHF/6-31G(d)	30.1	1.332	1.360
UHF/6-31+G(d,p)	18.5	1.325	1.365
RHF/6-31G(d)	30.1	1.303	1.353
RHF/6-31+G(d,p)	30.1	1.298	1.358
MP2/6-31G(d)	30.2	1.274	1.385
MP2/6-31+G(d,p)	30.3	1.254	1.398
QCISD/6-31G(d)	31.4	1.310	1.370
QCISD/6-31+G(d,p)	30.3	1.292	1.372
CCSD/6-31G(d)	[b]	1.310	1.370
CCSD/6-31+G(d,p)	[b]	1.292	1.372
CCSD/6-311G(d,p)	[b]	1.296	1.374

[a] See Figure 1 for definitions of α, d_1, and d_2. [b] For the sake of computational efficiency, the CCSD optimizations were carried out with C_s symmetry, i.e., α = 0°.

6-31+G(d,p) consistently producing TSs with somewhat shorter forming-bond and longer breaking-bond lengths than 6-31G(d). The method and basis set used for optimization does have a significant effect on the torsion angle α, with values ranging from about 15° to 30° (see Table 1). However, this is simply the result of an almost free rotor motion for the methyl group in the TS, with barriers to rotation of 0.1 kJ mol^{-1} or less.[58]

For the reactants and products, the effect of variation in theoretical procedure and basis set is generally similar in the closed-shell/radical pairs, i.e., methane/methyl radical and benzene/phenyl radical. An exception is found with the UMP2 structures for the phenyl radical. For example, the UMP2/6-31+G(d,p) values are 1.357 (C1−C2), 1.376 (C2−C3), and 1.373 (C3−C4) Å, significantly shorter than the BMK/6-31+G(d,p) values of 1.383 (C1−C2), 1.410 (C2−C3), and 1.403 (C3−C4) Å. In contrast, C−C bond lengths in benzene are very similar at the two levels: 1.399 (UMP2/6-31+G(d,p)) and 1.402 (BMK/6-31+G(d,p)) Å. The anomalous UMP2 results for the phenyl radical reflect the strong spin contamination in the UMP2/6-31+G(d,p) wave function ($\langle S^2 \rangle = 1.230$).

The effect of the variation in optimized geometries on computed energies was assessed by performing single-point energy calculations on each structure at the URCCSD(T)/6-311+G(d,p) level of theory (see Figure 2). We can see that use of geometries optimized with either the 6-31G(d) or 6-31+G(d,p) basis set leads to very similar URCCSD(T) energies for virtually all the theoretical procedures. In addition, in the case of methyl radical and methane, the choice of the quantum chemical method used to optimize the geometry has little influence, leading to modest variations of less than 1.0 kJ

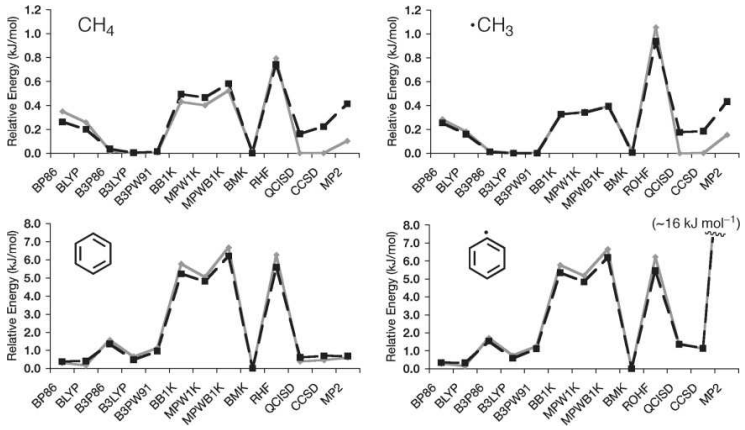

Figure 2. Variation in URCCSD(T)/6-311+G(d,p) total energies calculated for geometries optimized using a variety of levels of theory for methane, methyl radical, benzene, and phenyl radical. DFT, RHF, QCISD, CCSD, and MP2 methods were used in conjunction with the 6-31G(d) (solid gray line) and 6-31+G(d,p) (dashed black line) basis sets. The zero level is taken as the lowest energy obtained for a particular species with the particular basis set. The MP2 results for the heavily spin-contaminated phenyl radical are off-scale, with relative energies of approximately 16 kJ mol^{-1}, and are therefore not included.

mol^{-1} in the URCCSD(T) total energies. In contrast, the variations in total energies for benzene and the phenyl radical span ranges of ~7 and ~16 kJ mol^{-1}, respectively! If the UMP2 phenyl radical result is set aside, the results in Figure 2 show that the URCCSD(T) energy trends for the phenyl radical parallel those for benzene. The exceptional URCCSD(T)//UMP2 energy for the phenyl radical is associated with the effect on the UMP2-optimized geometry of the heavy spin contamination, as noted above. The large $\langle S^2 \rangle$ of the phenyl radical has been previously noted (UHF/6-31G(d) $\langle S^2 \rangle = 1.4$),[25] with the RCCSD(T) energy lying 9 kJ mol^{-1} below the UCCSD(T) value. Spin contamination is always a potential hazard in unrestricted descriptions of radical reactions.

The QCISD- and CCSD-optimized structures (in combination with the 6-31+G(d,p) basis set) for methane, methyl radical, and benzene are among the best on the URCCSD(T)/6-311+G-(d,p) surface, as also are the BMK structures (see Figure 2). BMK also produces the structure with the lowest URCCSD-(T)/6-311+G(d,p) energies for the phenyl radical, so it is clearly an attractive choice for optimizing the equilibrium structures in the benzene hydrogen-abstraction reaction. Figure 2 equally illustrates that the popular B3-LYP functional is also suitable for obtaining good geometries for stationary points of the studied reaction. BB1K and MPW1K are less good from this perspective.

When the URCCSD(T)/6-311+G(d,p) energies corresponding to the various optimized structures are used to calculate reaction enthalpies and barriers (Table 2), we see relatively little variation, indicating significant error cancellation. Geometries obtained with the DFT functionals, for example, lead to URCCSD(T) endothermicities that lie within the range 29.2 ± 0.2 kJ mol^{-1} and barriers of 78.5 ± 0.4 kJ mol^{-1}. The heavily spin-contamined (as indicated by the $\langle S^2 \rangle$ values of the transition structure and the phenyl radical) UHF, QCISD, and UCCSD geometries lead to endothermicities and barriers that lie somewhat below and above this range, respectively. The UMP2 geometries on the other hand show poor values for both the enthalpy and the barrier.

TABLE 2: Effect of Geometry on URCCSD(T)/6-311+G(d,p) Barriers (kJ mol^{-1}) and Reaction Enthalpies (kJ mol^{-1})

geometry	enthalpy[a]	barrier[a]	$\langle S^2 \rangle^b$	$\langle S^2 \rangle^c$
BP86/6-31G(d)	29.2	78.3	0.756	0.756
BP86/6-31+G(d,p)	29.1	78.4	0.755	0.756
BLYP/6-31G(d)	29.2	78.5	0.755	0.755
BLYP/6-31+G(d,p)	29.1	78.6	0.755	0.755
B3-P86/6-31G(d)	29.2	78.4	0.760	0.759
B3-P86/6-31+G(d,p)	29.3	78.5	0.759	0.759
B3-LYP/6-31G(d)	29.2	78.4	0.759	0.757
B3-LYP/6-31G(d,p)	29.2	78.4	0.759	0.757
B3-LYP/6-31+G(d,p)	29.3	78.5	0.759	0.757
B3-LYP/6-311G(d,p)	29.3	78.5	0.759	0.757
B3-PW91/6-31G(d)	29.2	78.1	0.760	0.760
B3-PW91/6-31+G(d,p)	29.3	78.5	0.760	0.760
MPW1K/6-31G(d)	29.3	78.9	0.770	0.769
MPW1K/6-31+G(d,p)	29.3	78.8	0.769	0.768
BB1K/6-31G(d)	29.2	78.5	0.763	0.762
BB1K/6-31+G(d,p)	29.4	78.7	0.763	0.761
MPWB1K/6-31G(d)	29.2	78.4	0.764	0.762
MPWB1K/6-31+G(d,p)	29.3	78.5	0.763	0.762
BMK/6-31G(d)	29.1	78.2	0.761	0.760
BMK/6-31+G(d,p)	29.1	78.3	0.761	0.760
UHF/6-31G(d)	24.8	73.9	1.423	1.433
UHF/6-31+G(d,p)	25.5	74.6	1.378	1.397
RHF/6-31G(d)	28.8	78.0	0.750	0.750
RHF/6-31+G(d,p)	28.8	78.0	0.750	0.750
UMP2/6-31G(d)	45.3	97.2	1.244	1.260
UMP2/6-31+G(d,p)	44.4	95.5	1.211	1.230
UQCISD/6-31G(d)	30.1	79.6	1.391	1.396
UQCISD/6-31+G(d,p)	29.9	79.2	1.354	1.366
UCCSD/6-31G(d)	29.8	79.2	1.399	1.402
UCCSD/6-31+G(d,p)	29.6	79.0	1.372	1.372
UCCSD/6-311G(d,p)	29.6	79.0	1.387	1.394

[a] Without ZPVE correction. [b] DFT or HF $\langle S^2 \rangle$ value in the transition structure, optimized at the theoretical level indicated. [c] DFT or HF $\langle S^2 \rangle$ value in the phenyl radical, optimized at the theoretical level indicated.

TABLE 3: Barriers ($\Delta E_0^{\ddagger}$) and Reaction Enthalpies (ΔH_{298}) for the Benzene Abstraction Reaction (kJ mol^{-1})

	B3-LYP geometry[a]		BMK geometry[b]	
method	ΔH_{298}	$\Delta E_0^{\ddagger}$	ΔH_{298}	$\Delta E_0^{\ddagger}$
G3-RAD [c]	35.4	72.5		
G3(MP2)-RAD[c]	37.1	73.8		
CBS-QB3[c]	42.1	77.6		
W1 (0 K)[c]	34.5	72.4[f]		
W1 (298 K)[c]	34.1			
BP86/6-31G(d)	17.3	37.8	17.3	38.2
B-LYP/6-31G(d)	18.5	45.2	18.5	45.6
B3-P86/6-31G(d)	22.6	51.4	22.5	51.6
UB3-LYP/6-31G(d)	23.4	57.8	23.3	58.1
B3-PW91/6-31G(d)	22.4	57.0	22.3	57.2
MPW1K/6-31G(d)	27.1	69.5	27.0	69.5
BB1K/6-31G(d)	21.7	64.4	21.6	64.5
MPWB1K/6-31G(d)	22.2	62.4	22.0	62.4
BMK/6-31G(d)	23.4	63.5	23.2	63.6
MPW1K/6-31+G(d,p)	33.4	73.0	33.3	73.0
BB1K/6-31+G(d,p)	28.5	69.4	28.4	69.4
BMK/6-31+G(d,p)	29.8	67.7	29.7	67.8
UB3-LYP/6-311+G(3df,2p)	30.5	66.2	30.0	66.8
RB3-LYP/6-311+G(3df,2p)	30.0	68.4	29.5	69.0
B3-PW91/6-311+G(3df,2p	28.7	63.0	28.3	63.6
MPW1PW91/6-311+G(3df,2p)	29.9	63.3	29.4	63.9
MPW1K/6-311+G(3df,2p)	33.4	74.1	33.3	74.1
BB1K/6-311+G(3df,2p)	28.7	71.0	28.6	71.0
MPWB1K/6-311+G(3df,2p)	29.2	69.1	28.7	69.6
BMK/6-311+G(3df,2p)	30.1	71.5	29.6	72.0
UHF/6-311+G(d,p)	17.5	113.6		
UMP2/6-311+G(d,p)	139.0	179.2		
UCCSD(T)/6-311+G(d,p)	42.4	82.9		
RHF/6-311+G(d,p)	42.7	156.3		
URCCSD(T)/6-311+G(d,p)	33.5	74.1		
UHF/6-311+G(3df,2p)	17.6	114.9	15.5	114.1
UMP2/6-311+G(3df,2p)	141.2	180.8	143.9	184.4
RHF/6-311+G(3df,2p)	41.4	156.5	40.7	156.8
RMP2/6-311+G(3df,2p)	38.8	63.2	38.3	63.3
URCCSD(T)/6-311+G(3df,2p)	33.8	72.9	33.2	73.4
expt (298 K)[d]	35.5			
Tokmakov et al. (0 K)[e]	36.8 ± 3.8			
G2M(CC,MP2) (0 K)[e]	43.1	81.9		

[a] B3-LYP/6-31+G(d,p) geometries, scaled ZPVEs, and thermal corrections, unless otherwise indicated. [b] BMK/6-31+G(d,p) geometries, scaled ZPVEs, and thermal corrections. [c] Geometries, ZPVEs, and thermal corrections as prescribed for these methods. [d] Calculated from experimental heats of formation from ref 60 (see text). [e] From ref 22. [f] See Note Added in Proof.

3.2. Reaction Enthalpies and Barriers. ΔH_{298} and $\Delta E_0^{\ddagger}$ values for the reaction between benzene and methyl radical were calculated using the B3-LYP/6-31+G(d,p) and BMK/6-31+G(d,p) geometries, using scaled ZPVEs and thermal corrections (Table 3).[56,59] A variety of methods were used in combination with the 6-31G(d), 6-31+G(d,p), and/or 6-311+G(3df,2p) basis sets to calculate energies. These include BP86, B-LYP, B3-P86, B3-LYP (U and R), B3-PW91, MPW1K, BB1K, MPWB1K, BMK, MPW1PW91, RMP2, and URCCSD(T). In addition, a selection of high-level composite procedures were employed, with the computationally demanding W1 method representing the highest-level procedure included in this study. Also included in Table 3 are the experimentally derived values of ΔH_{298} = 35.5 kJ mol^{-1}, calculated using the 298 K enthalpies of formation of benzene (82.93 kJ mol^{-1}), methyl radical (145.69 kJ mol^{-1}), phenyl radical (339 kJ mol^{-1}), and methane (−74.87 kJ mol^{-1}),[60] and ΔH_0 = 36.8 ± 3.8 kJ mol^{-1}, calculated by Tokmakov et al.[22] using experimental C−H bond dissociation energies.

3.2.1. Reaction Enthalpies. The W1 procedure predicts a reaction enthalpy at 0 K of 34.5 kJ mol^{-1}, which is in close agreement with the experimental value reported by Tokmakov et al.[22] At 298 K, the W1 result amounts to 34.1 kJ mol^{-1}, though the good agreement with the experimental value (35.5 kJ mol^{-1}) might be somewhat fortuitous because of the considerable experimental uncertainty (±8 kJ mol^{-1}) in the experimental $\Delta H_{f,298}$ for phenyl radical.[60] In light of this experimental uncertainty, the high-level W1 result will be treated as our benchmark value.[61] G3-RAD and G3(MP2)-RAD predict enthalpies in good agreement with the W1 value, with deviations of 1.3 and 3 kJ mol^{-1}, respectively. CBS-QB3 leads to a somewhat larger deviation (of 8 kJ mol^{-1}) from the W1 benchmark value, which may be associated with the spin contamination in the UMP2 wave function that is used in CBS-QB3 for the phenyl radical.[61] As previously noted, the dependence of reaction enthalpies on the level of theory used for the geometry optimization is limited, with very similar ΔH_{298} values being obtained for the B3-LYP and BMK geometries.

Inspection of the data resulting from standard DFT methods (Table 3) shows that there is a nonnegligible basis-set effect. The 6-31G(d) basis set appears to be too small to obtain accurate thermochemical data, significantly underestimating the ΔH_{298} W1 benchmark value. For example, inclusion of diffuse functions results in an improvement in the calculated MPW1K, BB1K, and BMK enthalpies by about 6−7 kJ mol^{-1}. However, a further upgrade to the larger 6-311+G(3df,2p) basis set has only a minor effect.

Of the noncomposite procedures, the computationally most expensive method, URCCSD(T)/6-311+G(3df,2p), performs the best, predicting a reaction enthalpy of 33.8 kJ mol^{-1} with the B3-LYP/6-31+G(d,p) geometry. URCCSD(T) performs quite well for the reaction enthalpy even with the more modest 6-311+G(d,p) basis set, giving 33.6 kJ mol^{-1} for B3-LYP/6-31+G(d,p) geometries.[62] RMP2 in combination with the 6-311+G(3df,2p) basis set (see Table 3) overestimates the W1 benchmark enthalpy by about 4−5 kJ mol^{-1},[63] whereas the large-basis-set DFT methods underestimate the benchmark enthalpy by 0.7−5.4 kJ mol^{-1}. The MPW1K functional gives a reaction enthalpy of 33.4 kJ mol^{-1}, in combination with both the 6-31+G(d,p) and 6-311+G(3df,2p) basis sets, which is very close to the benchmark result.

We note from Table 3 that UHF and particularly UMP2 produce poor values of the reaction enthalpy, both with the 6-311+G(d,p) and 6-311+G(3df,2p) basis sets. This is presumably associated with the high spin contamination in the product phenyl radical in the unrestricted wave functions. The UCCSD(T) reaction enthalpy appears to be in better agreement with our benchmark value but is still somewhat overestimated.[61]

3.2.2. Reaction Barriers. The $\Delta E_0^{\ddagger}$ values are also included in Table 3. Unfortunately, W1 calculations on the TS are computationally too demanding with our currently available resources (but see Note Added in Proof). In the absence also of reliable experimental information, the G3-RAD $\Delta E_0^{\ddagger}$ value of 72.5 kJ mol^{-1} is used as the benchmark for comparison of results from other methods. The choice of G3-RAD is supported by a recent extensive study of hydrocarbon hydrogen-abstraction reactions,[23] in which excellent agreement was found between G3X-RAD and W1, with an MAD of just 0.9 kJ mol^{-1}.[64] Most theoretical procedures underestimate the G3-RAD benchmark barrier, with the exception of MPW1K, which leads to surprisingly higher barriers when compared with similar DFT methods. The CBS-QB3 method also overestimates the benchmark value (by approximately 5 kJ mol^{-1}). A basis-set effect similar to that described for the reaction enthalpies is observed for the barriers. The average increase in barriers from 6-31G(d) to 6-31+G-

TABLE 4: Calculated Rate Constants at Various Temperatures (k_{600}, k_{700}, k_{800}; m^3 mol^{-1} s^{-1}), Activation Energies (E_a, kJ mol^{-1}), and Preexponential Factors (A, m^3 mol^{-1} s^{-1}) for the Benzene Abstraction Reaction ($C_6H_6 + \bullet CH_3 \rightarrow \bullet C_6H_5 + CH_4$) in the Temperature Range 600−800 K[a]

level[b]	k_{600}	k_{700}	k_{800}	E_a	A
BP86/6-31G(d)	4.64×10^3	1.61×10^4	4.10×10^4	43.5	2.84×10^7
BP86/6-31+G(d,p)	2.00×10^3	7.96×10^3	2.25×10^4	48.3	3.20×10^7
BLYP/6-31G(d)	1.13×10^3	4.73×10^3	1.39×10^4	50.1	2.59×10^7
BLYP/6-31+G(d,p)	3.41×10^2	1.71×10^3	5.74×10^3	56.3	2.72×10^7
B3-P86/6-31G(d)	3.03×10^2	1.49×10^3	4.94×10^3	55.7	2.14×10^7
B3-P86/6-31+G(d,p)	1.59×10^2	8.81×10^2	3.18×10^3	59.7	2.51×10^7
B3-LYP/6-31G(d)	8.37×10^1	4.87×10^2	1.82×10^3	61.5	1.89×10^7
B3-LYP/6-31+G(d,p)	3.14×10^1	2.15×10^2	9.07×10^2	67.1	2.18×10^7
B3-PW91/6-31G(d)	8.99×10^1	5.21×10^2	1.95×10^3	61.4	1.99×10^7
B3-PW91/6-31+G(d,p)	4.75×10^1	3.08×10^2	1.25×10^3	65.3	2.30×10^7
MPW1K/6-31G(d)	8.48×10^0	6.63×10^1	3.10×10^2	71.8	1.51×10^7
MPW1K/6-31+G(d,p)	4.95×10^0	4.30×10^1	2.18×10^2	75.5	1.85×10^7
BB1K/6-31G(d)	3.29×10^1	2.19×10^2	9.04×10^2	66.1	1.87×10^7
BB1K/6-31+G(d,p)	1.55×10^1	1.18×10^2	5.44×10^2	71.0	2.35×10^7
MPWB1K/6-31G(d)	3.64×10^1	2.35×10^2	9.49×10^2	65.1	1.69×10^7
MPWB1K/6-31+G(d,p)	1.67×10^1	1.25×10^2	5.64×10^2	70.2	2.16×10^7
BMK/6-31G(d)	3.04×10^1	2.05×10^2	8.56×10^2	66.6	1.91×10^7
BMK/6-31+G(d,p)	1.47×10^1	1.12×10^2	5.17×10^2	71.1	2.27×10^7
B3-LYP/6-311+G(3df,2p)[c]	1.98×10^1	1.45×10^2	6.48×10^2	69.6	2.27×10^7
BB1K/6-311+G(3df,2p)[c]	8.54×10^0	7.07×10^1	3.45×10^2	73.8	2.27×10^7
MPW1K/6-311+G(3df,2p)[c]	4.68×10^0	4.22×10^1	2.20×10^2	76.8	2.27×10^7
BMK/6-311+G(3df,2p)[c]	6.99×10^0	5.95×10^1	2.97×10^2	74.8	2.27×10^7
URCCSD(T)/6-311+G(3df,2p)[c]	5.38×10^0	4.76×10^1	2.44×10^2	76.1	2.27×10^7
CBS-QB3[d]	1.90×10^0	1.96×10^1	1.12×10^2	81.4	2.32×10^7
G3(MP2)-RAD[d]	3.82×10^0	3.45×10^1	1.80×10^2	76.9	1.89×10^7
G3-RAD[d]	4.96×10^0	4.32×10^1	2.19×10^2	75.6	1.89×10^7
exptl[e]			1.81×10^2	38.9	6.30×10^4
exptl[f]		3.95×10^1		63.0	1.99×10^6

[a] Calculated using the mixed harmonic oscillator and free rotor (HO/FR) model; see text. [b] Geometries, energies, and frequencies computed at the same theoretical level unless otherwise noted. [c] Calculated using BMK/6-31+G(d,p) geometries and frequencies. [d] Geometries, ZPVEs, and thermal corrections as prescribed for these methods. [e] Ref 26. [f] Ref 27.

(d,p) is now approximately 4 kJ mol^{-1}, while increasing the basis set to 6-311+G(3df,2p) results in an extra shift of about 2 kJ mol^{-1}.

Examination of the large-basis-set results in more detail shows that, as with the calculated enthalpies, the URCCSD(T)/6-311+G(3df,2p) barriers are in close agreement with the benchmark value, differing by less than 1 kJ mol^{-1}. However, the performance of RMP2 is less good, with a deviation of approximately 9 kJ mol^{-1} from the G3-RAD value, consistent with previous observations for radical additions to alkynes,[17] but in contrast to other studies on radical addition[16,17] and abstraction[23] reactions.

For the large-basis-set DFT results in Table 3, the deviations from the G3-RAD barrier lie between +1.6 and −9.5 kJ mol^{-1}. B3-LYP underestimates the barrier by about 6 kJ mol^{-1}. This is consistent with the results of Tokmakov et al.[22] and more general observations[32] that B3-LYP tends to underestimate reaction barriers. As found in other studies,[23] RB3-LYP shows a modest improvement over UB3-LYP, reducing the deviation from G3-RAD to about 4 kJ mol^{-1}. B3-PW91 and MPW1PW91 show deviations of about 9 kJ mol^{-1}, indicating that their good performance for the radical additions of methyl, ethyl, and propyl radicals to ethylene[65] cannot be generalized to the hydrogen-abstraction reactions for aromatic systems. MPWB1K, BB1K, and MPW1K, developed especially for kinetics applications, perform well. However, BMK shows the best performance of the DFT methods, giving barriers within 1 kJ mol^{-1} of the benchmark value.

Even more so than with the reaction enthalpy, UHF and UMP2 produce very poor values of the abstraction barrier, both with the 6-311+G(d,p) and 6-311+G(3df,2p) basis sets, leading to values that are substantially higher than our benchmark value (Table 3). In this case, presumably high spin contamination in the TS leads to problems with the unrestricted wave function. Interestingly, RHF also gives very high barriers. Clearly, these methods are not suitable for studying this and related reactions. UCCSD(T) leads to only a slight overestimation of the barrier compared with our benchmark value.[61]

3.3. Kinetic Parameters and Rate Constants. The kinetic parameters, i.e., the activation energy E_a and preexponential factor A, which were obtained by means of the HO/FR model in the relevant temperature range 600−800 K, are presented in Tables 4 and 5 for the forward ($C_6H_6 + \bullet CH_3 \rightarrow \bullet C_6H_5 + CH_4$) and reverse ($\bullet C_6H_5 + CH_4 \rightarrow C_6H_6 + \bullet CH_3$) reactions, respectively. The tabulated results include Eckart tunneling correction factors. A selection of methods was tested, in combination with the 6-31G(d), 6-31+G(d,p), and/or 6-311+G(3df,2p) basis sets. The rate constants at temperatures of 600, 700, and 800 K are also listed.

3.3.1. Tunneling Corrections. The predicted TST rate constants include Eckart quantum mechanical tunneling corrections, calculated in the experimentally relevant temperature range 600−800 K. For the sake of comparison, the Wigner method was also used to calculate the tunneling corrections. The calculated correction factors all lie between 1.2 and 2.2, with the Eckart corrections generally a little larger than the Wigner corrections (see Table S4 of the Supporting Information). As a result of the tunneling corrections, the activation energies decrease by approximately 5 kJ mol^{-1}, but the preexponential factors are influenced to a smaller extent. The rate curves that include tunneling experience a relatively small upward shift (rate increase) compared with the classical rate curves. Using the Eckart model, average corrections of 63% at 600 K and 36% at 800 K are found for the rate constants $k(T)$.

3.3.2. The HO vs HO/FR Model. Because the torsional frequency (ν_m) corresponding to the internal rotation of the

TABLE 5: Calculated Rate Constants at Various Temperatures (k_{600}, k_{700}, k_{800}; m^3 mol^{-1} s^{-1}), Activation Energies (E_a, kJ mol^{-1}), and Preexponential Factors (A, m^3 mol^{-1} s^{-1}) for the Reverse ($\bullet C_6H_5 + CH_4 \rightarrow C_6H_6 + \bullet CH_3$) Reaction in the Temperature Range 600−800 K[a]

level[b]	k_{600}	k_{700}	k_{800}	E_a	A
BP86/6-31G(d)	5.29×10^4	1.18×10^5	2.14×10^5	27.9	1.42×10^7
BP86/6-31+G(d,p)	5.42×10^4	1.19×10^5	2.16×10^5	27.6	1.37×10^7
BLYP/6-31G(d)	1.62×10^4	4.20×10^4	8.56×10^4	33.2	1.26×10^7
BLYP/6-31+G(d,p)	1.21×10^4	3.23×10^4	6.73×10^4	34.2	1.15×10^7
B3-P86/6-31G(d)	1.08×10^4	2.91×10^4	6.13×10^4	34.7	1.13×10^7
B3-P86/6-31+G(d,p)	1.37×10^4	3.58×10^4	7.34×10^4	33.5	1.13×10^7
B3-LYP/6-31G(d)	3.53×10^3	1.10×10^4	2.58×10^4	39.7	1.01×10^7
B3-LYP/6-31+G(d,p)	3.48×10^3	1.08×10^4	2.53×10^4	39.6	9.74×10^6
B3-PW91/6-31G(d)	3.13×10^3	1.00×10^4	2.39×10^4	40.6	1.07×10^7
B3-PW91/6-31+G(d,p)	4.02×10^3	1.24×10^4	2.87×10^4	39.2	1.04×10^7
MPW1K/6-31G(d)	8.33×10^2	3.11×10^3	8.35×10^3	46.0	8.42×10^6
MPW1K/6-31+G(d,p)	1.26×10^3	4.44×10^3	1.15×10^4	44.1	8.68×10^6
BB1K/6-31G(d)	8.21×10^2	3.14×10^3	8.57×10^3	46.8	9.74×10^6
BB1K/6-31+G(d,p)	1.04×10^3	3.85×10^3	1.03×10^4	45.7	9.89×10^6
MPWB1K/6-31G(d)	1.43×10^3	5.08×10^3	1.31×10^4	44.2	1.01×10^7
MPWB1K/6-31+G(d,p)	2.31×10^3	7.73×10^3	1.91×10^4	42.1	1.07×10^7
BMK/6-31G(d)	1.10×10^3	4.03×10^3	1.07×10^4	45.4	9.85×10^6
BMK/6-31+G(d,p)	1.43×10^3	5.05×10^3	1.30×10^4	44.1	9.86×10^6
B3-LYP/6-311+G(3df,2p)[c]	2.26×10^3	7.50×10^3	1.84×10^4	41.8	9.86×10^6
BB1K/6-311+G(3df,2p)[c]	7.37×10^2	2.86×10^3	7.93×10^3	47.4	9.86×10^6
MPW1K/6-311+G(3df,2p)[c]	1.02×10^3	3.77×10^3	1.01×10^4	45.8	9.86×10^6
BMK/6-311+G(3df,2p)[c]	7.37×10^2	2.86×10^3	7.93×10^3	47.4	9.86×10^6
URCCSD(T)/6-311+G(3df,2p)[c]	1.15×10^3	4.18×10^3	1.10×10^4	45.2	9.86×10^6
CBS-QB3[d]	2.38×10^3	7.93×10^3	1.96×10^4	42.0	1.08×10^7
G3(MP2)-RAD[d]	2.06×10^3	6.93×10^3	1.72×10^4	42.4	1.01×10^7
G3-RAD[d]	1.90×10^3	6.74×10^3	1.62×10^4	42.8	1.01×10^7
exptl[e]	1.96×10^2	8.57×10^2	2.59×10^3	51.6	6.03×10^6
exptl[f]	1.47×10^3	4.11×10^3	8.91×10^3	36.0	1.99×10^6
exptl[g]	7.22×10^1	2.72×10^2	7.38×10^2	46.4	7.90×10^5

[a] Calculated using mixed harmonic oscillator and free rotor (HO/FR) model; see text. [b] Geometries, energies, and frequencies computed at the same level unless otherwise noted. [c] Calculated using BMK/6-31+G(d,p) geometries and frequencies. [d] Geometries, ZPVEs, and thermal corrections as prescribed for these methods. [e] Ref 22. [f] Ref 28. [g] Ref 29.

methyl group is very small (ν_m lies in the range 3.4−45.1 cm^{-1}; see Table S5 of the Supporting Information), the harmonic oscillator approach is inappropriate, and the free rotor model should therefore be used for the description of this mode. We have compared E_a and A values for the benzene abstraction reaction, calculated using the HO and HO/FR models at a variety of levels of theory, and these results are also included in Table S5. The E_a values within the HO model are found to lie in the range 46.4−78.4 kJ mol^{-1}, whereas within the HO/FR model, the range of values is 43.5−81.4 kJ mol^{-1} (see also Table 4). In general, there is a decrease of about 3 kJ mol^{-1} when going from the HO to the HO/FR model, which is quite small compared with the 38 kJ mol^{-1} range of activation energies. This indicates the limited influence on the activation energy E_a of the method used for treating internal rotations (particularly when there is only one such motion), which is in accordance with previous findings.[6] In contrast, the preexponential factor varies significantly, with a difference of almost 1 order of magnitude depending on whether the rotation of the methyl group is handled using the HO/FR or HO model. The large variation in the torsional frequency (ν_m) calculated by the various levels of theory flows through to the HO predictions of the preexponential factor A (Table S5). This is not surprising in light of eq 2. However, this strong correlation between ν_m and A disappears when the methyl torsion is treated as a free rotor (HO/FR model). The preexponential factor now fluctuates within a small range of 1.5×10^7 to 3.2×10^7 m^3 mol^{-1} s^{-1} (Table 4). Only the results obtained with the HO/FR model are discussed in the remainder of this paper.

3.3.3. Experiment vs Theory. For the forward reaction, two experimental data sets are available, obtained by Krech and Price[26] and Zhang et al.[27] in the temperature intervals 744−800 K and 650−770 K, respectively. A large discrepancy exists between the kinetic parameters deduced from the two experiments (see Table 4), with respective activation energies of 38.9 and 63.0 kJ mol^{-1} and preexponential factors of 6.30×10^4 and 1.99×10^6 m^3 mol^{-1} s^{-1}. This is a clear example in which there are large uncertainties associated with the E_a and A values deduced from the experimental rate equation, that arise partly because the temperature range in which the experiments were carried out is quite narrow. This means that a large extrapolation is required to obtain the Arrhenius kinetic parameters. Under these circumstances, our high-level theoretical results are likely to serve as better benchmarks. The CBS-QB3, G3(MP2)-RAD, and G3-RAD values for E_a lie in the range 75−82 kJ mol^{-1}, while the values for A lie in the range $(1.9-2.3) \times 10^7$ m^3 mol^{-1} s^{-1}. Using these as benchmarks then suggests that BB1K, MPW1K, BMK, and URCCSD(T) in conjunction with the 6-311+G(3df,2p) basis set and using BMK/6-31+G(d,p) geometries and frequencies perform well.

The accuracy of the theoretical model can also be assessed by comparing directly the experimental and theoretical rate constants in the relevant temperature range. A first remark in this respect concerns the differences between the rate constants obtained in the two experiments in the overlapping temperature range 744−770 K. Remarkably, despite the substantial differences in the derived E_a and A values, the rate constants of Krech and Price[26] are only a factor of 1.5 larger than the rate constants obtained by Zhang et al.[27] The uncertainties in the measured rate constants are much smaller than for the kinetic parameters A and E_a because of the difficult extrapolation required to derive the latter. We find that the majority of the theoretical methods predict rate constants to within a factor of 10 of the two experimental rate curves in the entire temperature range.

TABLE 6: Calculated $\langle f_k \rangle$ Values for the Forward ($C_6H_6 + \bullet CH_3 \rightarrow \bullet C_6H_5 + CH_4$) and Reverse ($\bullet C_6H_5 + CH_4 \rightarrow C_6H_6 + \bullet CH_3$) Reactions[a]

	forward reaction		reverse reaction		
level[b]	ref 26	ref 27	ref 22	ref 28	ref 29
B3-P86/6-31G(d)	25.10	37.31	35.88	7.09	108.19
B3-P86/6-31+G(d,p)	15.83	22.14	44.38	8.73	133.35
B3-LYP/6-31G(d)	9.02	12.28	13.27	2.67	40.59
B3-LYP/6-31+G(d,p)	4.37	5.47	13.03	2.62	39.83
B3-PW91/6-31G(d)	9.64	13.15	12.00	2.42	36.80
B3-PW91/6-31+G(d,p)	6.09	7.83	14.92	3.00	45.58
MPW1K/6-31G(d)	1.46	1.71	3.67	0.76	11.42
MPW1K/6-31+G(d,p)	1.01	1.12	5.27	1.08	16.32
BB1K/6-31G(d)	4.37	5.56	3.69	0.76	11.51
BB1K/6-31+G(d,p)	2.57	3.05	4.54	0.93	14.12
MPWB1K/6-31G(d)	4.62	5.96	6.03	1.23	18.66
MPWB1K/6-31+G(d,p)	2.68	3.21	9.23	1.87	28.40
BMK/6-31G(d)	4.14	5.22	4.77	0.98	14.81
BMK/6-31+G(d,p)	2.45	2.89	5.99	1.22	18.54
B3-LYP/6-311+G(3df,2p)[c]	3.09	3.73	8.96	1.82	27.56
BB1K/6-311+G(3df,2p)[c]	1.61	1.83	3.37	0.70	10.51
MPW1K/6-311+G(3df,2p)[c]	1.01	1.10	4.45	0.92	13.84
BMK/6-311+G(3df,2p)[c]	1.38	1.55	3.37	0.70	10.51
URCCSD(T)/6-311+G(3df,2p)[c]	1.13	1.24	4.94	1.01	15.34
CBS-QB3[d]	0.51	0.52	9.48	1.92	29.16
G3(MP2)-RAD[d]	0.83	0.90	8.26	1.68	25.45
G3-RAD[d]	1.02	1.13	7.70	1.57	23.76

[a] f_k is defined as k_{theory}/k_{expt}. The $\langle f_k \rangle$ values tabulated here are average values calculated with respect to all the available relevant experimental data. [b] Geometries, frequencies, and energies computed at a single theoretical level unless otherwise noted. [c] Calculated using BMK/6-31+G(d,p) geometries and frequencies. [d] Geometries, ZPVEs, and thermal corrections as prescribed for these methods.

To quantify the deviations of the theoretical rate constants with respect to the experimental values, a factor $f_k = k_{theory}/k_{experiment}$ is introduced. A value of f_k greater than 1.0 indicates that theory is overestimating the rate constant compared with experiment. The calculated f_k values with respect to both available experiments are given in Table S6 of the Supporting Information. A schematic overview of the error analysis based on f_k values is given in Table 6. The numbers listed are the average values of f_k in the relevant temperature ranges (744−800 K for Krech and Price and 650−770 K for Zhang et al.). We can see that the composite methods such as G3(MP2)-RAD and G3-RAD perform extremely well in predicting the rate constants, with $\langle f_k \rangle$ values in the range 0.83−1.13. Also, the two-component method URCCSD(T)/6-311+G(3df,2p)//BMK, which uses the BMK/6-31+G(d,p) geometries and frequencies, has comparable accuracy. Among the DFT-based methods that use the same functional and basis for both the geometry and single-point energy calculations, MPW1K performs the best. The two-component methods that use BB1K, MPW1K, and BMK energies (obtained with the 6-311+G(3df,2p) basis set) and BMK/6-31+G(d,p) geometries and frequencies also give very good agreement with the experimental rates. The latter levels are also computationally extendable to larger systems such as polyaromatics and thus represent attractive cost-effective methods.

For the reverse reaction, results for three experiments are available, conducted by Tokmakov et al.,[22] Heckmann et al.,[28] and Duncan et al.,[29] in the temperature ranges 600−980, 560−1410, and 550−680 K, respectively. It can be seen (Table 5) that in this case there is significant variation among the experimental rate constants. The rate constants of Heckmann et al.[28] are larger than the values of Tokmakov et al.[22] values by a factor of approximately 5, whereas the data reported by Duncan et al.[29] are smaller than the values of Tokmakov et al. by a factor of about 3. The experimental analysis depends in many cases on the rates of various simultaneous side reactions, and therefore there is significant and unquantifiable uncertainty in the experimental rate constants.

The values of the f_k factors with respect to all three experiments are included in Table S7 of the Supporting Information, and an overview is given in Table 6. The calculated f_k values for our best methods (CBS-QB3, G3(MP2)-RAD, and G3-RAD) suggest that the experimental results of Heckmann et al.[28] are the most reliable. MPW1K/6-31+G(d,p) as well as BB1K, MPW1K, BMK, and CCSD(T) with the 6-311+G(3df,2p) basis set and BMK/6-31+G(d,p) geometries and frequencies all perform well, as in the case of the forward benzene abstraction reaction.

4. Conclusions

In the present study, the performance of a variety of theoretical procedures in predicting thermodynamic and kinetic parameters for the hydrogen-abstraction reaction between benzene and the methyl radical has been assessed, leading to the following broad conclusions.

(1) Very good geometries for methane, methyl radical, benzene, and phenyl radical are produced by BMK in combination with the 6-31G(d) and 6-31+G(d,p) basis sets. These geometries are in fact as good as or even better than their B3-LYP or CCSD counterparts. In general, the variations in the URCCSD(T)/6-311+G(d,p) single-point energies as a function of the level of theory used for geometry optimization are systematic, and as a consequence, there is significant error cancellation when evaluating the reaction enthalpy and barrier with structures of apparent lower quality. More specifically, the barriers and enthalpies calculated using high-level single points on lower-level optimized structures typically lie within a range of less than 1.6 kJ mol^{-1}. The exceptions are for comparisons involving UMP2-optimized structures for phenyl radical, which suffer from heavy spin contamination.

(2) Reaction enthalpies calculated with G3-RAD and UR-CCSD(T)/6-311+G(3df,2p) are in excellent agreement with the W1 benchmark value. The lower-level MPW1K results are also remarkably good. Other lower levels of theory, such as RMP2, B3-LYP, MPWB1K, and BMK, in combination with the 6-311+G(3df,2p) basis set, predict reasonable reaction enthalpies.

(3) The reaction barriers are more sensitive to the level of theory employed. The effect of the basis set is more pronounced, and the 6-31G(d) basis-set results reflect a significant basis-set error. Using the G3-RAD value of $\Delta E_0^{\ddagger}$ as the benchmark, we find that MPW1K, BB1K, and BMK perform very well. The URCCSD(T)/6-311+G(3df,2p) method predicts reaction barriers in very good agreement with G3-RAD.

(4) Activation energies and preexponential factors for both the forward ($C_6H_6 + \bullet CH_3 \rightarrow \bullet C_6H_5 + CH_4$) and reverse ($\bullet C_6H_5 + CH_4 \rightarrow C_6H_6 + \bullet CH_3$) reactions have been calculated in the temperature range 600−800 K. The computed activation energies cover a broad range in the case of the forward reaction. The influence on the calculated E_a of the method used for treating internal rotations is limited to 3 kJ mol^{-1}, whereas for the preexponential factor, there is a much greater sensitivity to this choice. On the other hand, the activation energy is much more sensitive than the preexponential factor to the level of theory used, with the latter being practically independent of this choice. In light of experimental uncertainties, the high-level methods CBS-QB3, G3(MP2)-RAD, and G3-RAD serve as

secondary benchmarks and indicate that good results are obtained from BB1K, MPW1K, and BMK energies (obtained with the 6-311+G(3df,2p) basis set) and BMK/6-31+G(d,p) geometries and frequencies.

(5) Finally, rate constants calculated for both the forward and reverse reactions reveal that a large proportion of our theoretical methods succeed in predicting rates that deviate by less than a factor of 10 from the experimental values. The functionals BMK, BB1K, and MPW1K, when used with a BMK/6-31+G(d,p) geometry, along with G3-RAD and G3(MP2)-RAD provide the best agreement with experiment. The inclusion of the Eckart tunneling correction reduces the E_a by a maximum of 5.3 kJ mol^{-1} and the preexponential factor by a factor of 0.6. The HO/FR model reduces E_a by a maximum of 2.9 kJ mol^{-1} and the A value by a factor of 0.2. Together, these two effects make a maximum contribution of 8 kJ mol^{-1} to the activation energies and a tenfold change in the preexponential factors for the benzene abstraction reaction.

Acknowledgment. K.H. wishes to thank Professor Leo Radom and members of his research group for their kind hospitality during her stay at the University of Sydney in January−May 2005, where this work originated. D.M. thanks the University of Sydney for a Sesqui Postdoctoral Fellowship. V.V.S. and M.W. thank the Fund for Scientific Research − Flanders, the Research Board of Ghent University. L.R. thanks the Australian Research Council for a Discovery Grant, and funding from the ARC Centre of Excellence in Free Radical Chemistry and Biotechnology, and gratefully acknowledges generous allocations of computing time from the Australian Partnership for Advanced Computing, the Australian National University Supercomputing Facility, and the Australian Centre for Advanced Computing and Communication. Finally, we thank Professor Jan Martin for making the BMK functional available for our use.

Note Added in Proof: Since submission of this paper, we have been able to calculate a W1 value for the benzene abstraction barrier. The result (72.4 kJ mol^{-1}) supports our use within the paper of the G3-RAD barrier (72.5 kJ mol^{-1}, Table 3) as the benchmark.

Supporting Information Available: Optimized geometries (Table S1), effect of DFT integration grid on barriers, enthalpies, activation energies and preexponential factors (Table S2), total energies, zero-point vibrational energies, and thermal corrections (Table S3), Wigner and Eckart tunneling correction factors (Table S4), effect of model used for handling the methyl rotation and effect of level of theory on activation energies and preexponential factors for the benzene abstraction reaction (Table S5), and detailed error analysis for the benzene abstraction reaction (Table S6) and the reverse reaction (Table S7). This material is available free of charge via the Internet at http://pubs.acs.org.

References and Notes

(1) Wauters, S.; Marin, G. B. *Chem. Eng. J.* **2001**, *82*, 267.
(2) Saeys, M.; Reyniers, M. F.; Marin, G. B.; Van Speybroeck, V.; Waroquier, M. *J. Phys. Chem. A* **2003**, *107*, 9147.
(3) Hemelsoet, K.; Van Speybroeck, V.; Marin, G. B.; De Proft, F.; Geerlings, P.; Waroquier, M. *J. Phys. Chem. A* **2004**, *108*, 7281.
(4) Saeys, M.; Reyniers, M. F.; Van Speybroeck, V.; Waroquier, M.; Marin, G. B. *ChemPhysChem* **2006**, *7*, 188.
(5) (a) Van Speybroeck, V.; Van Neck, D.; Waroquier, M.; Wauters, S.; Saeys, M.; Marin, G. B. *Int. J. Quantum Chem.* **2003**, *91*, 384. (b) Van Speybroeck, V.; Van Neck, D.; Waroquier, M.; Saeys, M.; Wauters, S.; Marin, G. B. *J. Phys. Chem. A* **2000**, *104*, 10939.
(6) Van Speybroeck, V.; Borremans, Y.; Van Neck, D.; Waroquier, M.; Wauters, S.; Saeys, M.; Marin, G. B. *J. Phys. Chem. A* **2001**, *105*, 7713.
(7) Van Speybroeck, V.; Reyniers, M. F.; Marin, G. B.; Waroquier, M. *ChemPhysChem* **2002**, *3*, 863.
(8) Van Speybroeck, V.; Hemelsoet, K.; Waroquier, M.; Marin, G. B. *Int. J. Quantum Chem.* **2004**, *96*, 568.
(9) Gonzales, J. M.; Barden, C. J.; Brown, S. T.; Schleyer, P. v. R.; Schaefer, H. F.; Li, Q.-S. *J. Am. Chem. Soc.* **2003**, *125*, 1064, and references therein.
(10) Watson, M. D.; Fechtenkötter, A.; Müllen, K. *Chem. Rev.* **2001**, *101*, 1267.
(11) (a) *Polycyclic Aromatic Hydrocarbons and Astrophysics*; Léger, A., d'Hendecourt, L., Boccara, N., Eds.; NATO ASI Series, Series C 191; Reidel: Dordrecht, 1987. (b) Puget, J. L.; Léger A. *Annu. Rev. Astron. Astrophys.* **1989**, *27*, 161.
(12) Pope, C. J.; Marr, J. A.; Howard, J. B. *J. Phys. Chem.* **1993**, *97*, 11001.
(13) Richter, H.; Mazyar, O. A.; Sumathi, R.; Green, W. H.; Howard, J. B.; Bozzelli, J. W. *J. Phys. Chem. A* **2001**, *105*, 1561.
(14) Harris, S. J.; Weiner, A. M.; Blint, R. J. *Combust. Flame* **1988**, *72*, 91.
(15) (a) Frenklach, M.; Clary, D. W.; Gardiner, W. C.; Stein, S. E. *Proc. Combust. Inst.* **1984**, *20*, 887. (b) Frenklach, M.; Warnatz, J. *Combust. Sci. Technol.* **1987**, *51*, 265. (c) Frenklach, M.; Wang, H. In *Proceedings of the 23rd International Symposium on Combustion*; The Combustion Institute: Pittsburgh, PA, 1990; p 1559. (d) Frenklach, M. In *Proceedings of the 23rd International Symposium on Combustion*; The Combustion Institute: Pittsburgh, PA, 1996; p 2258.
(16) (a) Coote, M. L.; Wood, G. P. F.; Radom, L. *J. Phys. Chem. A* **2002**, *106*, 12124. (b) Gómez-Balderas, R.; Coote, M. L.; Henry, D. J.; Fischer, H.; Radom, L. *J. Phys. Chem. A* **2003**, *107*, 6082. (c) Henry, D. J.; Coote, M. L.; Gómez-Balderas, R.; Radom, L. *J. Am. Chem. Soc.* **2004**, *126*, 1732.
(17) Gómez-Balderas, R.; Coote, M. L.; Henry, D. J.; Radom, L. *J. Phys. Chem. A* **2004**, *108*, 2874.
(18) Saeys, M.; Reyniers, M. F.; Marin, G. B.; Van Speybroeck, V.; Waroquier, M. *AIChE J.* **2004**, *50*, 426.
(19) For a recent comprehensive review, see: Fischer, H.; Radom, L. *Angew. Chem., Int. Ed.* **2001**, *40*, 1340.
(20) (a) Basch, H.; Hoz, S. *J. Phys. Chem. A* **1997**, *101*, 4416. (b) Jursic, B. S. *Chem. Phys. Lett.* **1997**, *264*, 113. (c) Schimmel, P. H. A.; Ruttink, P. J. A.; de Jong, B. H. W. S. *J. Phys. Chem. B* **1999**, *103*, 10506. (d) Pu, J.; Truhlar, D. G. *J. Phys. Chem. A* **2005**, *109*, 773. (e) Lynch, B. J.; Fast, P. L.; Harris, M.; Truhlar, D. G. *J. Phys. Chem. A* **2000**, *104*, 4811. (f) Kang, J. K.; Musgrave, C. B. *J. Chem. Phys.* **2001**, *115*, 11040.
(21) Lynch, B. J.; Truhlar, D. G. *J. Phys. Chem. A* **2001**, *105*, 2936.
(22) Tokmakov, I. V.; Park, J.; Gheyas, S.; Lin, M. C. *J. Phys. Chem. A* **1999**, *103*, 3636.
(23) Coote, M. L. *J. Phys. Chem. A* **2004**, *108*, 3865.
(24) Mebel, A. M.; Lin, M. C.; Yu, T.; Morokuma, K. *J. Phys. Chem. A* **1997**, *101*, 3189.
(25) Nicolaides, A.; Smith, D. M.; Jensen, F.; Radom, L. *J. Am. Chem. Soc.* **1997**, *119*, 8083.
(26) Krech, M.; Price, S. J. W. *Can. J. Chem.* **1967**, *45*, 157.
(27) Zhang, H. X.; Ahonkhai, S. I.; Back, M. H. *Can. J. Chem.* **1989**, *67*, 1541.
(28) Heckmann, E.; Hippler, H.; Troe, J. *Symp. Int. Combust. Proc.* **1996**, *16*, 543.
(29) Duncan, F. J.; Trotman-Dickenson, A. F. *J. Chem. Soc.* **1962,** *52*, 4672.
(30) Kohn, W.; Becke, A. D.; Parr, R. G. *J. Phys. Chem.* **1996**, *100*, 12974.
(31) Becke, A. D. *J. Chem. Phys.* **1993**, *98*, 5648.
(32) Van Speybroeck, V.; De Kimpe, N.; Waroquier, M. *J. Org. Chem.* **2005**, *70*, 3674.
(33) Lingwood, M.; Hammond, J. R.; Hrovat, D. A.; Mayer, J. M.; Borden, W. T. *J. Chem. Theory Comput.* **2006**, *2*, 740.
(34) Boese, A. D.; Martin, J. M. L. *J. Chem. Phys.* **2004**, *121*, 3405.
(35) Zhao, Y.; Truhlar, D. G. *J. Phys. Chem. A* **2004**, *108*, 6908.
(36) Zhao, Y.; Lynch, B. J.; Truhlar, D. G. *Phys. Chem. Chem. Phys.* **2005**, *7*, 43.
(37) Zhao, Y.; González-García, N.; Truhlar, D. G. *J. Phys. Chem. A* **2005**, *109*, 2012.
(38) (a) Hehre, W. J.; Radom, L.; Schleyer, P. v. R.; Pople, J. A. *Ab Initio Molecular Orbital Theory*; Wiley: New York, 1986. (b) Jensen, F. *Introduction to Computational Chemistry*; Wiley: New York, 1999.
(39) Koch, W.; Holthausen, M. C. *A Chemist's Guide to Density Functional Theory*; Wiley-VCH: Weinheim, 2000.
(40) Frisch, M. J.; Trucks, G. W.; Schlegel, H. B.; Scuseria, G. E.; Robb, M. A.; Cheeseman, J. R.; Montgomery, J., J. A.; Vreven, T.; Kudin, K. N.;

Burant, J. C.; Millam, J. M.; Iyengar, S. S.; Tomasi, J.; Barone, V.; Mennucci, B.; Cossi, M.; Scalmani, G.; Rega, N.; Petersson, G. A.; Nakatsuji, H.; Hada, M.; Ehara, M.; Toyota, K.; Fukuda, R.; Hasegawa, J.; Ishida, M.; Nakajima, T.; Honda, Y.; Kitao, O.; Nakai, H.; Klene, M.; Li, X.; Knox, J. E.; Hratchian, H. P.; Cross, J. B.; Bakken, V.; Adamo, C.; Jaramillo, J.; Gomperts, R.; Stratmann, R. E.; Yazyev, O.; Austin, A. J.; Cammi, R.; Pomelli, C.; Ochterski, J. W.; Ayala, P. Y.; Morokuma, K.; Voth, G. A.; Salvador, P.; Dannenberg, J. J.; Zakrzewski, V. G.; Dapprich, S.; Daniels, A. D.; Strain, M. C.; Farkas, O.; Malick, D. K.; Rabuck, A. D.; Raghavachari, K.; Foresman, J. B.; Ortiz, J. V.; Cui, Q.; Baboul, A. G.; Clifford, S.; Cioslowski, J.; Stefanov, B. B.; Liu, G.; Liashenko, A.; Piskorz, P.; Komaromi, I.; Martin, R. L.; Fox, D. J.; Keith, T.; Al-Laham, M. A.; Peng, C. Y.; Nanayakkara, A.; Challacombe, M.; Gill, P. M. W.; Johnson, B.; Chen, W.; Wong, M. W.; Gonzalez, C.; Pople, J. A. *Gaussian 03*, revision C2; Gaussian, Inc.: Wallingford, CT, 2004.

(41) Werner, H.-J.; Knowles, P. J.; Amos, R. D.; Bernhardsson, A.; Berning, A.; Celani, P.; Cooper, D. L.; Deegan, M. J. O.; Dobbyn, A. J.; Eckert, F.; Hampel, C.; Hetzer, G.; Korona, T.; Lindh, R.; Lloyd, A. W.; McNicholas, S. J.; Manby, F. R.; Meyer, W.; Mura, M. E.; Nicklass, A.; Palmieri, P.; Pitzer, R.; Rauhut, G.; Schütz, M.; Stoll, H.; Stone, A. J.; Tarroni, R.; Thorsteinsson, T. *MOLPRO 2000.6*; University of Birmingham: Birmingham, U. K., 1999.

(42) Stanton, J. F.; Gauss, J.; Watts, J. D.; Nooijen, M.; Oliphant, N.; Perera, S. A.; Szalay, P. G.; Lauderdale, W. J.; Kucharski, S. A.; Gwaltney, S. R.; Beck, S.; Balková, A.; Bernholdt, D. E.; Baeck, K. K.; Rozyczko, P.; Sekino, H.; Hober, C.; Bartlett, R. J. *ACES II*; Quantum Theory Project; University of Florida: Gainsville, FL, 2005.

(43) (a) Ochterski, J. W.; Petersson, G. A.; Montgomery, J. A. *J. Chem. Phys.* **1996**, *104*, 2598. (b) Montgomery, J. A.; Frisch, M. J.; Ochterski, J. W.; Petersson, G. A. *J. Chem. Phys.* **2000**, *112*, 6532.

(44) Henry, D. J.; Parkinson, C. J.; Mayer, P. M.; Radom, L. *J. Phys. Chem. A* **2001**, *105*, 6750.

(45) (a) Henry, D. J.; Sullivan, M. B.; Radom, L. *J. Chem. Phys.* **2003**, *118*, 4849. (b) Henry, D. J.; Parkinson, C. J.; Radom, L. *J. Phys. Chem. A* **2002**, *106*, 7927.

(46) Martin, J. M. L.; Parthiban, S. In *Quantum Mechanical Prediction of Thermochemical Data*; Cioslowski, J., Ed.; Kluwer-Academic: Dordrecht, The Netherlands, 2001; pp 31−65.

(47) (a) Wynne-Jones, W. F. K.; Eyring, H. J. *J. Chem. Phys.* **1936**, *3*, 492. (b) Evans, M. G.; Polanyi, M. *Trans. Faraday Soc.* **1935**, *31*, 875. (c) Evans, M. G.; Polanyi, M. *Trans. Faraday Soc.* **1937**, *33*, 448.

(48) (a) Laidler, K. J. *Chemical Kinetics*; HarperCollins: New York, 1987. (b) McQuarrie D. A.; Simon, J. D. *Physical Chemistry − A Molecular Approach*; University Science Books: Sausalito, CA, 1997.

(49) Wigner, E. *J. Chem. Phys.* **1937**, *5*, 720.

(50) Eckart, C. *Phys. Rev.* **1930**, *35*, 1303.

(51) Truong, T. N.; Duncan, W. T.; Tirtowidjojo, M. *Phys. Chem. Chem. Phys.* **1999**, *1*, 1061, and references herein.

(52) Troe, J. *J. Chem. Phys.* **1977**, *66*, 4758.

(53) Van Cauter, K.; Van Speybroeck, V.; Vansteenkiste, P.; Reyniers, M. F.; Waroquier, M. *ChemPhysChem* **2006**, *7*, 131.

(54) Scott, A. P.; Radom, L. *J. Phys. Chem.* **1996**, *100*, 16502.

(55) Zhao, Y.; Lynch, B. J.; Truhlar, D. G. *J. Phys. Chem. A* **2004**, *108*, 2715.

(56) Values used in the present study for B3-LYP/6-31+G(d,p) are 0.9806 (ZPVE) and 0.9989 ($\Delta\Delta H$), while for BMK/6-31+G(d,p), they are 0.95 (ZPVE) and 0.98 ($\Delta\Delta H$).

(57) Geometries of reactants and products at the B3-LYP/6-31+G(d,p), BMK/6-31+G(d,p), and CCSD/6-31+G(d,p) levels are presented in Table S1.

(58) Since the rotation of the methyl group in the TS has a very low frequency, the effect of the DFT integration grid on the value of the computed frequencies was checked using the B3-LYP and BP86 functionals. However, as shown in Table S2, the results are independent of the integration grid used.

(59) The component absolute energies, ZPVEs, and thermal corrections are presented in Table S3 of the Supporting Information.

(60) http://webbook.nist.gov/chemistry.

(61) We note that W1 is based on the URCCSD(T) procedure of MOLPRO, as is G3-RAD and G3(MP2)-RAD. CBS-QB3, on the other hand, is based on the fully unrestricted UMP2 and UCCSD(T) procedures of Gaussian, together with a spin correction. The comparison of results among the various methods partly reflects this unrestricted/restricted treatment. The experimental reaction enthalpy values lie between those based on URCCSD-(T) and those based on spin-corrected UCCSD(T) but are closer to the former.

(62) Calculated from the vibrationless enthalpy in Table 2 and the ZPVE and $\Delta\Delta H$ corrections in Table S3 of the Supporting Information.

(63) We note that RMP2/6-31G(d,p) calculations lead to an enthalpy value of 34.6 kJ mol^{-1}, very close to the experimental value.

(64) For molecules containing only first-row elements, G3-RAD and G3X-RAD only differ in the choice of geometry and would give identical results in the present study (where prescribed geometries are used).

(65) Van Speybroeck, V.; Van Cauter, K.; Coussens, B.; Waroquier, M. *ChemPhysChem* **2005**, *6*, 180.

Paper II

Thermochemistry and kinetics of hydrogen abstraction by methyl radical from polycyclic aromatic hydrocarbons

Hemelsoet K. , Van Speybroeck V. , Moran D. ,
Marin G. B. , Radom L. and Waroquier M.

J. Phys. Chem. A, **2006**, *110*, 13624–13631

Thermochemistry and Kinetics of Hydrogen Abstraction by Methyl Radical from Polycyclic Aromatic Hydrocarbons

Karen Hemelsoet,*,†,‡ Veronique Van Speybroeck,† Damian Moran,‡,§ Guy B. Marin,|| Leo Radom,*,‡,§ and Michel Waroquier*,†

Center for Molecular Modeling, Proeftuinstraat 86, and Laboratorium voor Petrochemische Techniek, Krijgslaan 281-S5, Ghent University, B-9000 Ghent, Belgium, and School of Chemistry and ARC Centre of Excellence in Free Radical Chemistry and Biotechnology, University of Sydney, Sydney, NSW 2006, Australia

Received: August 9, 2006; In Final Form: October 12, 2006

Thermodynamic and kinetic properties relating to hydrogen abstraction by methyl radical from various sites in polycyclic aromatic hydrocarbons (PAHs) have been investigated. The reaction enthalpies (298 K), barriers (0 K), and activation energies and pre-exponential factors (700−1100 K), have been calculated by means of density functional theory, specifically with B3-LYP/6-311G(d,p) geometries, followed by BMK/6-311+G-(3df,2p) single-point energy calculations. For uncongested sites in the PAHs, a reasonable correlation is obtained between reactivities (as characterized by the reaction barriers) and reaction enthalpies. This is reflected in a Bell−Evans−Polanyi (BEP) relationship. However, for congested sites, abstraction is accompanied both by lower reaction enthalpies (due to relief of steric strain) and also by reduced reactivities (due to significantly increased steric hindrance effects in the transition structures), so that the BEP relationship does not hold. In addition, the reaction enthalpies and kinetic parameters for the series of linear acenes indicate that abstraction is more difficult from the central rings.

1. Introduction

Polycyclic aromatic hydrocarbons (PAHs) are widely studied organic molecules.[1,2] They play a key role in a large number of different areas as they are both naturally occurring and anthropogenic. PAHs are the largest known class of chemical carcinogens and mutagens.[3−5] They are present in atmospheric aerosols and many celestial objects such as meteorites, planetary nebulae, reflection nebulae, and active galaxies,[6−8] and recent work has reported spectroscopic evidence for the existence of PAHs in interstellar space.[9] Their importance in the formation process of hollow-cage fullerenes is also known.[10] In addition, PAHs are key intermediate products in soot formation and coal conversion processes.[11−14] They can arise as side products in steam cracking units used in the petrochemical industry for the production of light alkenes such as ethene and propene.[15] In this light, a quantitative understanding of the formation of PAH molecules is important for the efficient design of clean and practical combustion devices such as engines and incinerators and for a maximal run length of steam cracking units.

PAHs can grow by means of a radical reaction network. The model that begins with a phenyl radical, proposed by Frenklach et al.,[14] currently seems to be the most favored synthetic route. This model proposes a sequential addition of acetylene molecules to the phenyl radical to form mainly planar, naphthalene-like PAHs consisting of (substituted) six-membered rings. More recently, Vereecken et al.[16] have studied the growth of PAHs incorporating five-membered rings, which can also act as possible intermediates for the formation of nonplanar systems, including fullerenes. In the PAH growth processes, various classes of elementary reactions such as hydrogen abstraction, addition, cyclization, and dehydrogenation can be distinguished, and these lead to the formation of a surface consisting of conjugated rings.[16,17]

To model these potentially complex reaction processes, calculations on the contributing elementary reactions are desirable, as they provide the opportunity to obtain the required levels of insight and understanding for model genesis.[18−24] The initial step that allows formation of radical surface species involves hydrogen-abstraction reactions by means of gas-phase radicals, such as methyl and hydrogen.[24−27] In an earlier study,[27] we performed an elaborate level-of-theory investigation of hydrogen abstraction from benzene by methyl radical, as this reaction represents a fundamental point of comparison for radical-mediated hydrogen abstractions from the benzenoid components of PAHs. We found that virtually all the theoretical procedures that we examined were suitable for geometry optimization. However, for the reaction enthalpy, W1, G3-RAD, and UR-CCSD(T) yielded the best agreement with experiment. For the reaction barriers, URCCSD(T) and the low-cost BMK method provided values in close agreement with the benchmark value. Overall, G3-RAD, URCCSD(T), and the cost-effective density functional theory (DFT) methods BMK, BB1K, and MPW1K were found to give the best results for calculating the thermochemistry and kinetics of hydrogen abstraction by the methyl radical from benzene.

Some earlier studies have reported on the characteristics and reactivity of aryl radicals derived from PAHs, though theoretical studies have been complicated by the large spin contamination in the phenyl radical at the unrestricted Hartree−Fock level of theory.[28] On the basis of electron spin resonance studies and

* To whom correspondence should be addressed: e-mail karen.hemelsoet@UGent.be (K.H.), radom@chem.usyd.edu.au (L.R.), or michel.waroquier@UGent.be (M.W.).
† Center for Molecular Modeling, Ghent University.
‡ School of Chemistry, University of Sydney.
§ ARC Centre of Excellence in Free Radical Chemistry and Biotechnology, University of Sydney.
|| Laboratorium voor Petrochemische Techniek, Ghent University.

10.1021/jp065141n CCC: $33.50
Published on Web 11/30/2006 PAGE EST: 7.9

analysis of the spectra, in combination with theoretical calculations, Kasai et al.[29] showed that the aryl radicals that they investigated were all σ-radicals, with the unpaired electron found to occupy the essentially nonbonding σ-orbital corresponding to the broken bond. Also, by use of semiempirical calculations and by examining the bond dissociation energy (BDE), it was found that the strength of the aryl−H bond is essentially independent of molecular size but is more dependent on the environment around the C−H bond, and a classification into three types of aryl radicals was proposed.[30,31] Aihara et al.[32] used a PM3 approach in combination with a restricted open-shell Hartree−Fock (ROHF) procedure, and showed that the C−H BDE values were fairly constant for their test set. They reported that small variations in the calculated BDE values were primarily determined by the local structure near the abstraction site. This was supported by a good correlation between the BDE values and corresponding ∠CCC angles, calculated at the abstraction site of the reactant. DFT calculations performed by Cioslowski et al.[33] with the B-LYP functional indicated that there is a thermodynamic preference for the hydrogen in H-abstraction reactions to be preferentially removed from congested regions of the parent hydrocarbons, suggesting that the site specificity of the hydrogen abstraction is strongly influenced by steric factors. In a previous study,[34] we carefully investigated the bond dissociation enthalpies at 298 K for an extended set of hydrocarbons and corresponding ethynyl, aryl, vinyl, alkyl, propargyl, benzyl, and allyl radicals. In that study, the possible aryl radicals produced from PAHs were classified into six groups according to their C−H bond strengths.

The main goal of the present work is to obtain thermodynamic and kinetic data for hydrogen abstraction by methyl radical from a variety of possible sites in polycyclic aromatic hydrocarbons. The influence of the local environment on the C−H bond strengths of the PAHs and the thermodynamics and kinetics of the corresponding abstraction reactions will be emphasized. We compute optimized geometries, reaction enthalpies at 298 K (ΔH_{298}), barriers at 0 K ($\Delta E_0^{\ddagger}$), and activation energies (E_a), pre-exponential factors (A), and rate constants [$k(T)$] within a relevant temperature interval (700−1100 K). By studying the variations in the activation energy and pre-exponential factor in terms of the details of the polycyclic structure, we aim to gain insights as to which sites are preferred for the initial formation of surface radicals in a polycyclic aromatic network.

2. Theoretical Procedures

All calculations were performed with the Gaussian 03[35] software package. Geometries were optimized at the B3-LYP[36] level of theory, in conjunction with the 6-311G(d,p) basis set.[37] As mentioned earlier, a previous study on the reference hydrogen-abstraction reaction in benzene showed the limited influence of the level of theory on the optimized geometries.[27] Other studies on related radical reactions also reported that B3-LYP gives a reliable and quantitatively good description of geometries.[38,39] Frequencies were computed at the same level of theory as the geometry optimizations to provide zero-point vibrational energies (ZPVEs) and thermal corrections to the enthalpy and to confirm the nature of the stationary points. A scale factor of 0.9806 was used to obtain the ZPVEs from the calculated harmonic vibrational frequencies,[40] while unscaled frequencies were used to obtain the thermal corrections to the enthalpy. The use of scale factors provides a means of accounting for systematic deviations between measured and computed frequency-dependent properties and is an important consideration for the accurate description of reaction kinetics and thermochemistry.[40−42]

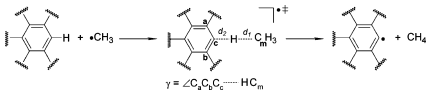

Figure 1. Hydrogen abstraction by the methyl radical from a model PAH to form an aryl radical plus methane. The forming bond length (d_1), breaking bond length (d_2), and out-of-plane angle (γ = angle between the $C_aC_bC_c$ plane and the H−CH_3 line) of the transition structure are highlighted.

Single-point energy calculations were performed by use of the BMK functional in conjunction with the 6-311+G(3df,2p) basis set. The BMK functional was recently developed by Boese and Martin[43] and is accurate to approximately 10 kJ mol^{-1} for the calculation of reaction barriers. The good performance of BMK appears to hinge on the combination of a high percentage of Hartree−Fock exchange (42%), together with terms dependent on the kinetic energy density, resulting in a "back-correction" for excessive HF exchange in systems where this would be undesirable. The BMK functional was also found to be a method of choice in our level-of-theory study on the abstraction reaction in benzene,[27] as it is an accurate computational method and yet affordable for systems of moderately large size, such as those studied in the present work.

We applied transition-state theory (TST),[44] including the incorporation of Eckart tunneling correction factors,[45] to calculate the rate constants $k(T)$. The Eckart method is a simple procedure that requires only a consideration of the stationary points on the reaction pathway and is therefore compatible with TST, although the method is often found to overestimate the tunneling contribution, especially at very low temperatures.[46] The link with the macroscopic quantities found in the Arrhenius rate law is made by a linear fit of ln $k(T)$ values, calculated for a range of temperatures, versus $1/T$. One refinement in our theoretical treatment comes from the observation that the transition structures (TSs) for the hydrogen-abstraction reactions have a very low frequency vibration, corresponding to internal rotation of the incoming methyl group about the forming bond. The standard harmonic oscillator (HO) model is known to be inappropriate for such modes and other approximations, such as the free rotor (FR)[19,47] or hindered rotor (HR)[48,49] model, are therefore used for this mode. The choice of a particular description depends on the height of the rotational barrier and the temperature. In a recent study of radical-addition reactions, we demonstrated the importance of correctly describing hindered internal rotations in order to obtain reliable partition functions.[19,50] In the present work, a mixed harmonic oscillator/free rotor (HO/FR) or mixed harmonic oscillator/hindered rotor (HO/HR) model, in which all the internal motions except for the methyl torsion in the TS are approximated as independent harmonic oscillators, was used.

3. Results and Discussion

Hydrogen abstraction by an approaching methyl radical from various sites in selected polycyclic aromatic hydrocarbons, leading to the formation of aryl radicals plus methane, have been studied. A schematic representation of the reactions that have been investigated is displayed in Figure 1, while the PAH molecules that have been studied, including our numbering scheme, are depicted in Figure 2. Our test set of PAHs can be divided into two subcategories. The first group includes the series of linear acenes, consisting of benzene (B), naphthalene (N), anthracene (A), tetracene (T), and pentacene (P). The other group consists of the nonlinear structures, including phenan-

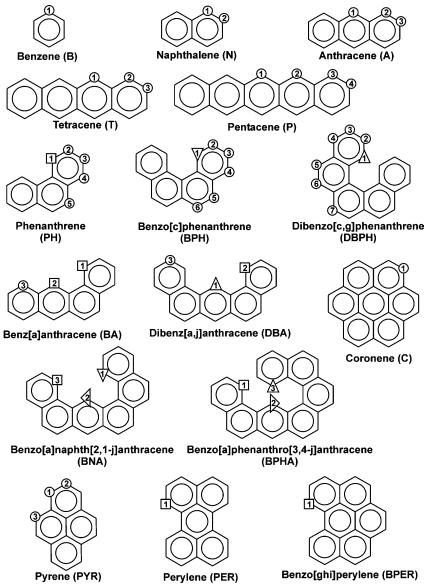

Figure 2. PAHs examined in the present study. Sites where hydrogen abstraction is considered are numbered. The sites are labeled on the basis of the hydrogen-abstraction enthalpy classifications (see text) (○ for B sites, □ for PH sites, ▽ for BPH sites, △ for DBPH sites, triangle pointing left for BNA sites, and triangle pointing right for BPHA sites).

threne (PH), benzo[*c*]phenanthrene (BPH), dibenzo[*c*,*g*]phenanthrene (DBPH), benz[*a*]anthracene (BA), dibenz[*a*,*j*]anthracene (DBA), coronene (C), benzo[*a*]naphth[2,1-*j*]anthracene (BNA), benzo[*a*]phenanthro[3,4-*j*]anthracene (BPHA), pyrene (PYR), perylene (PER), and benzo[*ghi*]perylene (BPER). The largest of these systems is coronene, which includes seven six-membered aromatic rings. Throughout this article, the notation PAH-X refers to the abstraction of hydrogen atom X from the polycyclic aromatic hydrocarbon PAH.

3.1. Geometries. The geometries of the PAHs, aryl radical products, and TSs were optimized at the B3-LYP/6-311G(d,p) level of theory. We note to begin that all the product radicals are of the σ-type, with the unpaired electron almost completely localized on a single carbon atom.[29] The corresponding spin densities of these product aryl radicals are given in Table S1 of the Supporting Information and clearly indicate the localization of the unpaired electron. Consequently, most geometrical perturbations resulting from the removal of a hydrogen atom are localized, systematic, and predictable.

A key geometrical feature is the planarity of most of the reactant PAHs and product aryl radicals. Four exceptions are found among the PAH molecules, specifically BPH, DBPH, BNA, and BPHA. Because of steric repulsive interactions between a pair of closely positioned hydrogen atoms, these molecules show significant deviations from planarity (Figure 3). In the first two structures, the deviations from planarity amount to approximately 18° within the phenanthrene component and 30° between the two phenanthrene components in DBPH. The BNA and BPHA structures can be regarded as

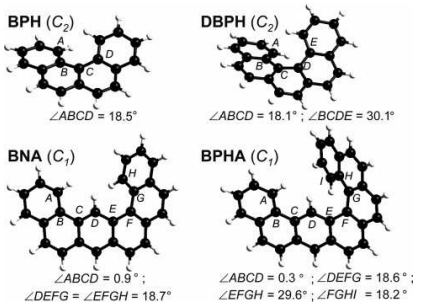

Figure 3. B3-LYP/6-311G(d,p) optimized geometries of nonplanar PAHs BPH, DBPH, BNA, and BPHA, including dihedral angles that measure the degree of nonplanarity.

combinations of two smaller PAH structures, specifically PH and BPH in the case of BNA and PH and DBPH in the case of BPHA. The deviations from planarity are mainly confined to the BPH and DBPH moieties, respectively, and similar dihedral angles of approximately 18° and 30° are found in these substructures. The nonplanarity is to a large extent removed when the aryl radicals BPH-1, BNA-1, and BNA-2 (see Figure 2) are formed, following the abstraction of a hydrogen atom. In the case of the DBPH-1, BPHA-2, and BPHA-3 radicals, the deviations from planarity for the twisted plane where the hydrogen is abstracted are significantly reduced. This is reflected in dihedral angles of 7.6°, 10.2°, and 6.5°, respectively, for ∠*ABCD*, ∠*DEFG*, and ∠*FGHI* (as defined in Figure 3) of the corresponding aryl radicals. Other important geometrical features in the PAHs and the product radicals are the changes in bond distances and angles at the hydrogen-abstraction site. The perturbations associated with removal of a hydrogen atom lead to shortening of the adjacent C−C bonds by approximately 0.02 Å, as well as widening of the bond angle at the carbon from which abstraction has taken place by about 6°. Similar results were noted previously by Cioslowski et al.[33] for a test set of 10 PAHs containing up to five six-membered rings.

For the transition structures for hydrogen abstraction, the forming (d_1) and breaking (d_2) bond lengths, as well as the out-of-plane angle (γ) of the approaching methyl radical, are the salient geometrical features. These parameters are illustrated in Figure 1, and the computed results are included in Table 1. It can be seen that, for most structures, d_1 is modestly shorter than d_2 (average difference approximately 0.07 Å), which is consistent with a "late" (in the Hammond sense) TS and in accordance with the reaction endothermicity. Exceptions are found for DBA-1, BNA-2, and BPHA-2, where the d_2 bond length is slightly shorter than the d_1 bond length (average difference approximately 0.02 Å). This behavior can be traced back to the more folded structures for the TSs in these cases, as illustrated in Figure 4. It can also be seen that for the abstraction of hydrogen atoms located at some of the more congested sites of the PAHs, the approaching methyl radical is forced to follow an out-of-plane pathway. For these TSs, the out-of-plane angle γ ranges from 11.9° (for PER-1) to 40.8° (for BNA-2). These large values of γ are basically due to steric hindrance between the incoming methyl radical and the closely positioned hydrogen atoms.

3.2. Reaction Enthalpies and Barriers. ΔH_{298} and $\Delta E_0^{\ddagger}$ values for the reactions between the various PAHs and the

TABLE 1: Forming (d_1) and Breaking (d_2) Bond Lengths and Out-of-Plane Angles γ in the Transition Structures for Hydrogen Abstraction from PAHs by Methyl Radical[a]

site	d_1 (Å)	d_2 (Å)	γ (deg)	site	d_1 (Å)	d_2 (Å)	γ (deg)
TS:B-1	1.307	1.379	0.1	TS:DBPH-1	1.322	1.362	21.6
TS:N-1	1.308	1.381	0.0	TS:DBPH-2	1.305	1.379	0.8
TS:N-2	1.305	1.380	0.0	TS:DBPH-3	1.304	1.381	2.4
TS:A-1	1.313	1.385	0.0	TS:DBPH-4	1.309	1.380	2.5
TS:A-2	1.308	1.381	0.0	TS:DBPH-5	1.306	1.383	4.5
TS:A-3	1.306	1.379	0.0	TS:DBPH-6	1.308	1.380	1.1
TS:T-1	1.312	1.385	0.3	TS:DBPH-7	1.306	1.383	3.9
TS:T-2	1.308	1.380	0.0	TS:BA-1	1.322	1.373	0.1
TS:T-3	1.306	1.379	0.0	TS:BA-2	1.333	1.368	22.6
TS:P-1	1.314	1.382	0.0	TS:BA-3	1.308	1.381	0.6
TS:P-2	1.313	1.383	0.0	TS:DBA-1	1.355	1.343	38.9
TS:P-3	1.308	1.380	0.0	TS:DBA-2	1.323	1.371	0.1
TS:P-4	1.306	1.379	0.0	TS:DBA-3	1.305	1.380	0.1
TS:PH-1	1.323	1.373	0.2	TS:BNA-1	1.332	1.354	26.9
TS:PH-2	1.305	1.380	0.0	TS:BNA-2	1.361	1.331	40.8
TS:PH-3	1.304	1.382	0.0	TS:BNA-3	1.322	1.371	17.2
TS:PH-4	1.308	1.382	0.0	TS:BPHA-1	1.318	1.373	14.1
TS:PH-5	1.308	1.381	0.0	TS:BPHA-2	1.355	1.338	37.5
TS:BPH-1	1.333	1.352	26.0	TS:BPHA-3	1.323	1.361	22.2
TS:BPH-2	1.306	1.378	2.5	TS:C-1	1.307	1.382	0.0
TS:BPH-3	1.303	1.382	2.6	TS:PYR-1	1.305	1.384	0.0
TS:BPH-4	1.309	1.380	1.8	TS:PYR-2	1.305	1.380	0.0
TS:BPH-5	1.306	1.383	3.2	TS:PYR-3	1.308	1.381	0.0
TS:BPH-6	1.308	1.381	2.2	TS:PER-1	1.322	1.370	11.9
				TS:BPER-1	1.321	1.374	0.0

[a] See Figure 1 for definitions of d_1, d_2, and γ. Transition structures were optimized at the B3-LYP/6-311G(d,p) level.

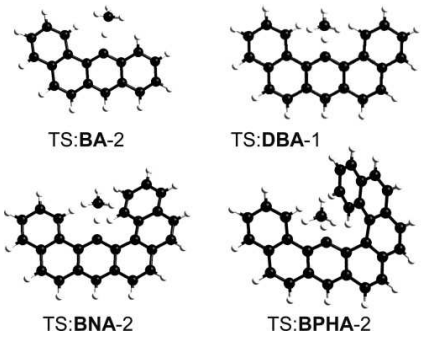

Figure 4. B3-LYP/6-311G(d,p) optimized geometries of the transition structures for hydrogen abstraction by methyl radical at congested sites.

methyl radical were calculated at the BMK/6-311+G(3df,2p)//B3-LYP/6-311G(d,p) level, by use of scaled ZPVEs and thermal corrections.[51] The results are given in Table 2.

3.2.1. Reaction Enthalpies. Inspection of the results in Table 2 shows that the hydrogen-abstraction enthalpies lie within a broad range between −1.8 (BNA-2) and +34.3 (A-1, T-1) kJ mol^{-1}. The reactions are endothermic with the exception of the BNA-2 reaction, which is slightly exothermic. A clustering of the reaction enthalpies into six groups is observed, as illustrated in Figure S1 of the Supporting Information. This had previously been noted, on the basis of BDE values.[34] Averages of the computed ΔH_{298} values for each of these groups X ($\langle \Delta H_{298} \rangle_X$) can be determined. In order of decreasing reaction enthalpies, we distinguish B-like sites ($\langle \Delta H_{298} \rangle_B = 32.0$ kJ mol^{-1}), PH-like sites ($\langle \Delta H_{298} \rangle_{PH} = 25.0$ kJ mol^{-1}), DBPH-like sites ($\langle \Delta H_{298} \rangle_{DBPH} = 18.4$ kJ mol^{-1}), BPHA-like sites ($\langle \Delta H_{298} \rangle_{BPHA} = 12.1$ kJ mol^{-1}), BPH-like sites ($\langle \Delta H_{298} \rangle_{BPH} = 4.5$ kJ mol^{-1}), and BNA-like sites ($\langle \Delta H_{298} \rangle_{BNA} = -1.8$ kJ mol^{-1}). Figure 2 shows the hydrogen atoms that belong to the various categories.

In earlier work, classifications based on other properties have been proposed. For example, in one study involving a smaller test set of six PAHs (B, N, A, PH, BPH, and DBPH),[24] the various abstraction sites were differentiated on the basis of a qualitative description of the local environment of the sites, specifically the number of intermediate carbon atoms between the hydrogen to be abstracted and the closest adjacent hydrogen atom. There is significant overlap between this classification and that based on reaction enthalpies, indicating the important role of the local environment of the hydrogen-abstraction site on the C−H bond strength. We note, however, that sometimes these clusters of values are coincidental rather than intrinsic. For example, the ΔH_{298} value for the DBPH-1 site amounts to 19.3 kJ mol^{-1}, which is close to the 19.0 kJ mol^{-1} for DBA-1, despite the local environments for the DBPH-1 and DBA-1 sites clearly being quite different.

Detailed analysis of the series of linear acenes reveals that the various sites (previously all classified as B-like sites) can be subdivided into three categories. The first group corresponds to hydrogen atoms located in the outer rings of the linear acenes, and the nomenclature B-like sites remains appropriate for this type. An average value of $\langle \Delta H_{298} \rangle_B = 30.5$ kJ mol^{-1} is obtained. The second and third groups correspond to naphthalene- (N-) and anthracene- (A-) like sites, with $\langle \Delta H_{298} \rangle_N = 31.8$ kJ mol^{-1} and $\langle \Delta H_{298} \rangle_A = 34.1$ kJ mol^{-1}, respectively. The latter group of A-type hydrogens are sometimes referred to as solo hydrogens,[32] that is, hydrogen atoms bonded to sp^2-carbon atoms with no adjacent C−H bonds. In agreement with the study of Aihara et al.,[32] the calculated enthalpy values corresponding to these solo atoms are found to be the largest in the particular PAH molecule being considered.

It is concluded overall that the reaction enthalpies for abstraction at the more congested sites correspond to smaller (less positive or more negative) enthalpy values, due to a relief from steric hindrance upon creation of the radical, in accordance with previous conclusions of Cioslowski et al.[52]

3.2.2. Reaction Barriers. The calculated hydrogen-abstraction barriers at 0 K ($\Delta E_0^{\ddagger}$) are included in Table 2. The barriers are relatively high, lying between 70.8 (P-4) and 89.2 (DBA-1) kJ mol^{-1}. It can be seen that the steric hindrance effects the methyl radical encounters when approaching the abstraction site become very important for the more congested sites. In such circumstances, they contribute to a significant increase in the reaction barrier with respect to the barrier of 71.8 kJ mol^{-1} for the abstraction in benzene. The most striking examples of increased barriers are seen for the abstractions at DBA-1, BA-2, BNA-2, and BPHA-2, with barriers amounting to 89.2, 82.9, 80.7, and 82.2 kJ mol^{-1}, respectively. The optimized geometries of the corresponding TSs (Figure 4) reveal high values for the out-of-plane angles (explicitly given in Table 1, e.g., 38.9° for DBA-1), which is a reflection of the steric hindrance encountered by the methyl radical.

Inspection of the results in Table 2 does not show any general correlation between the ΔH_{298} and $\Delta E_0^{\ddagger}$ results. Indeed, a scatter plot is obtained when these quantities are plotted against one another (Figure 5a). We observe that greater congestion generally leads to reduced reactivity for hydrogen abstraction by a methyl radical (because the site becomes less accessible), in contrast to the greater reactivity that would have been anticipated to accompany the lower reaction enthalpies (relief of steric strain) with a normal (Bell−Evans−Polanyi) reactivity−enthalpy relationship.[53] On the other hand, for the series of linear

TABLE 2: Calculated Reaction Enthalpies and Barriers for Hydrogen Abstraction from Various Sites of the PAHs Shown in Figure 2[a]

site	B-1	N-1	N-2	A-1	A-2	A-3	T-1
ΔH_{298} (kJ mol^{-1})	30.6	32.1	30.8	34.3	31.9	30.8	34.3
$\Delta E_0^{\ddagger}$ (kJ mol^{-1})	71.8	72.7	71.7	74.8	72.6	71.3	74.6
site	T-2	T-3	P-1	P-2	P-3	P-4	PH-1
ΔH_{298} (kJ mol^{-1})	31.6	30.4	34.0	33.8	31.5	29.9	24.7
$\Delta E_0^{\ddagger}$ (kJ mol^{-1})	72.1	71.0	74.4	74.2	71.5	70.8	76.5
site	PH-2	PH-3	PH-4	PH-5	BPH-1	BPH-2	BPH-3
ΔH_{298} (kJ mol^{-1})	31.1	32.2	32.1	31.7	4.9	30.2	32.1
$\Delta E_0^{\ddagger}$ (kJ mol^{-1})	71.5	72.0	72.4	72.2	75.2	71.6	72.2
site	BPH-4	BPH-5	BPH-6	DBPH-1	DBPH-2	DBPH-3	DBPH-4
ΔH_{298} (kJ mol^{-1})	31.6	32.7	32.0	19.3	31.0	32.0	31.9
$\Delta E_0^{\ddagger}$ (kJ mol^{-1})	72.8	73.1	72.6	74.1	71.9	73.0	73.3
site	DBPH-5	DBPH-6	DBPH-7	BA-1	BA-2	BA-3	DBA-1
ΔH_{298} (kJ mol^{-1})	33.0	31.8	33.1	24.5	26.8	32.2	19.0
$\Delta E_0^{\ddagger}$ (kJ mol^{-1})	73.7	72.5	73.8	76.9	82.9	72.8	89.2
site	DBA-2	DBA-3	C-1	BNA-1	BNA-2	BNA-3	BPHA-1
ΔH_{298} (kJ mol^{-1})	23.6	31.2	34.0	4.0	-1.8	24.5	26.0
$\Delta E_0^{\ddagger}$ (kJ mol^{-1})	76.2	71.3	73.2	72.8	80.7	76.6	77.6
site	BPHA-2	BPHA-3	PYR-1	PYR-2	PYR-3	PER-1	BPER-1
ΔH_{298} (kJ mol^{-1})	12.1	16.9	33.7	30.8	31.8	23.7	25.9
$\Delta E_0^{\ddagger}$ (kJ mol^{-1})	82.2	73.5	73.3	71.5	71.9	77.0	76.8

[a] Energies were obtained at the BMK/6-311+G(3df,2p)//B3-LYP/6-311G(d,p) level.

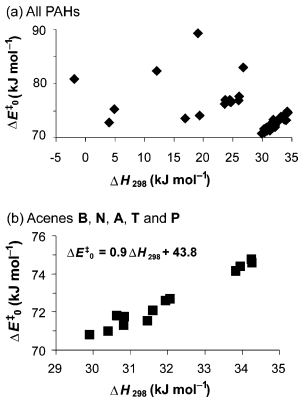

Figure 5. Barriers at 0 K ($\Delta E_0^{\ddagger}$) versus reaction enthalpies at 298 K (ΔH_{298}) for hydrogen-abstraction reactions at various sites of (a) all the PAHs examined and (b) only the series of linear acenes [BMK/6-311+G(3df,2p)//B3-LYP/6-311G(d,p)].

acenes, the Bell−Evans−Polanyi relationship does hold reasonably well, as illustrated in Figure 5b. For these uncongested regions, the approaching methyl radical does not encounter increased steric hindrance effects, and consequently a direct link between the strength of the C−H bond (as characterized by the ΔH_{298} values) and the reactivity toward abstraction (as characterized by the $\Delta E_0^{\ddagger}$ values) is expected and observed.

3.3. Kinetic Parameters and Rate Constants. Rate constants $k(T)$, and corresponding activation energies E_a and pre-exponential factors A, for the reactions between the various PAHs and methyl radical were calculated at the BMK/6-311+G(3df,2p)//B3-LYP/6-311G(d,p) level in the temperature interval of 700−1100 K, which is relevant for the steam cracking and coke formation processes. Two refinements are taken into consideration in the calculations: the effect of tunneling corrections on the one hand, and a refined description of the low-energy torsion of the methyl group in the TSs on the other. Details of the computed kinetic parameters can be found in Table S3 of the Supporting Information.

We find that the Eckart tunneling correction contributes an average downward shift of 4.5 kJ mol^{-1} to the activation energy, whereas it has only a modest effect on the pre-exponential factor, indicated by an average decrease by a factor of 1.3 in the ratio $A_{\text{with out tunneling}}/A_{\text{with tunneling}}$.

In order to establish a more detailed description of the low-lying vibrational mode corresponding to the internal rotation of the methyl group about the forming/breaking bond in the TSs, rotational potentials were computed. For the uncongested sites, the barrier height for the rotational potential was found to be very small, more precisely 0.1 kJ mol^{-1} or less, and the values of the methyl torsional frequency ν_m lie between 4.2 and 65.4 cm^{-1}. On this basis, the free rotor model was deemed appropriate to describe the methyl torsion, and a mixed harmonic oscillator/free rotor (HO/FR) model was used for the calculation of kinetic properties. For the congested sites (PH-, BPH-, DBPH-, BNA-, and BPHA-like sites), the methyl torsional barriers were found to be higher, with a maximum value of approximately 5 kJ mol^{-1} being obtained for DBA-1. The abstraction reactions at these sites show a larger value for the torsional frequency, a maximum value of 147.3 cm^{-1} being found for the abstraction at DBA-1. A one-dimensional hindered rotor model was chosen to model the internal rotation in these cases, and a mixed harmonic oscillator/hindered rotor (HO/HR) model was used for the calculation of kinetic properties. The influence of the refined treatment of internal rotations for the investigated hydrogen-abstraction reactions is not negligible. The activation energy is lowered by an average of 3.3 kJ mol^{-1}, while the pre-exponential factor decreases by a factor of 5.6 ($= A_{HO}/A_{mixed}$). The overall influence on the rate constant $k(T)$ amounts to average factors ($= k_{mixed}/k_{HO}$) of 0.59, 0.54, and 0.49 at 700, 900, and 1100 K, respectively.

3.3.1. Linear Acenes. For the series of linear acenes, we subdivided the abstraction sites as B, N, or A, all of which are uncongested locations where steric hindrance effects between the methyl radical and the PAH molecule are not important. The mixed HO/FR model was therefore used for the computa-

TABLE 3: Calculated Rate Constants, Activation Energies, and Pre-exponential Factors for Hydrogen Abstraction by Methyl Radical at Various Sites in Linear Acenes[a]

site	k_{700} (m^3 mol^{-1} s^{-1})	k_{900} (m^3 mol^{-1} s^{-1})	k_{1100} (m^3 mol^{-1} s^{-1})	E_a (kJ mol^{-1})	A (m^3 mol^{-1} s^{-1})
B-1	2.55×10^1	5.12×10^2	3.97×10^3	80.9	2.62×10^7
N-1	1.45×10^1	2.99×10^2	2.36×10^3	81.6	1.69×10^7
N-2	1.74×10^1	3.53×10^2	2.76×10^3	81.1	1.86×10^7
A-1	7.36×10^0	1.64×10^2	1.35×10^3	83.6	1.20×10^7
A-2	1.34×10^1	2.76×10^2	2.18×10^3	81.6	1.55×10^7
A-3	1.99×10^1	3.96×10^2	3.05×10^3	80.7	1.96×10^7
T-1	7.62×10^0	1.68×10^2	1.39×10^3	83.4	1.20×10^7
T-2	1.78×10^1	3.62×10^2	2.83×10^3	81.2	1.94×10^7
T-3	2.15×10^1	4.25×10^2	3.26×10^3	80.4	2.04×10^7
P-1	7.73×10^0	1.70×10^2	1.40×10^3	83.4	1.21×10^7
P-2	8.02×10^0	1.75×10^2	1.43×10^3	83.0	1.19×10^7
P-3	1.71×10^1	3.41×10^2	2.64×10^3	80.8	1.71×10^7
P-4	2.19×10^1	4.29×10^2	3.27×10^3	80.3	2.02×10^7

[a] Calculated by use of the mixed HO/FR model and including Eckart tunneling corrections. Energies were obtained at the BMK/6-311+G(3df,2p)//B3-LYP/6-311G(d,p) level.

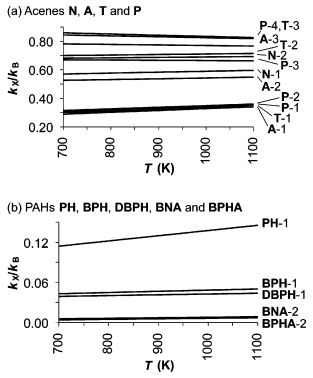

Figure 6. Ratios of calculated rate constants $k_X(T)/k_B(T)$ for hydrogen-abstraction reactions at the possible sites of (a) linear acenes and (b) nonlinear PAHs, within the temperature range 700−1100 K [BMK/6-311+G(3df,2p)//B3-LYP/6-311G(d,p) with HO/FR or HO/HR frequency models and including Eckart tunneling corrections; see text].

tion of the rate constants $k(T)$ in these cases. In Figure 6a, the rate constants for the hydrogen abstractions at N, A, T, and P are depicted, with the abstraction in benzene serving as a reference. Table 3 gives the rate constants at 700, 900, and 1100 K, together with the derived kinetic parameters. Abstraction from the benzene molecule is the fastest. Abstractions of a hydrogen atom located at a central ring, corresponding to A-like sites, or more precisely A-1, T-1, P-1, and P-2, are the slowest, approximately 3 times slower than abstraction in benzene. Abstraction reactions at noncentral rings (corresponding to B- and N-like sites) are preferred over abstraction at the central rings. This trend is supported by both kinetic parameters: the average activation energy is approximately 3 kJ mol^{-1} lower, while the pre-exponential factor is 1.7 times higher.

Another interesting aspect is the convergent behavior of the kinetic parameters and rate constants with increasing PAH size. Comparison of the kinetic parameters E_a and A for the abstraction reactions at B-1, N-1, A-1, T-1, and P-1 shows that limiting values are already reached for both parameters in the anthracene molecule, and this is also seen in Figure 6a. It thus appears sufficient to take into account three six-membered rings in order to adequately model the kinetics of the linear acenes.

3.3.2. Nonlinear PAHs. Calculated rate constants for a range of temperatures, as well as the associated kinetic parameters E_a and A, are given in Table 4 for the abstraction reactions for the nonlinear PAHs. Figure 6b depicts the ratio of the rate constant at the characteristic sites X with respect to the rate constant in benzene in the relevant temperature range. Inspection of the results obtained for the different categories PH-1, BPH-1, DBPH-1, BNA-2, and BPHA-2 reveals that the calculated $k(T)$ values for the less congested PAH molecules, for example, phenanthrene, are higher than those for the congested sites at all temperatures. Further examination of the results obtained for the abstraction at these (congested) non-B-like sites shows that the variation in the kinetic parameters is larger than in the series of linear acenes. The E_a values lie in the range 80.9−96.7 kJ mol^{-1}, while the A values vary between 5.3×10^5 and 1.0×10^7 m^3 mol^{-1} s^{-1}. The kinetic parameters corresponding to the six different categories based on reaction enthalpies are depicted in Figure 7. The pre-exponential factors clearly support the conclusion that the abstraction becomes more difficult as the PAH abstraction site becomes more congested. In addition, the E_a values for the very congested sites BNA-2 and BPHA-2 are substantially higher.

Detailed inspection of the results in Table 4 also shows that, even within a specific PAH, abstraction at B-like sites is always preferred over abstraction at more congested sites. For instance, for the various sites within the phenanthrene (PH) molecule, it can be seen that abstraction at the PH-like site (PH-1) is more difficult than abstractions at the B-like sites (PH-i, $i = 2-5$), as reflected in an average factor of 2.3 between the specific rate constants.

As a final remark, we note that comparison of the PH-1 and BPER-1 results offers valuable information about the possible consequences of adding an extra layer to the coke surface model. The deviations between the rate parameters for the two abstraction reactions are seen to be small, with a factor of approximately 1.6 being obtained for k(BPER-1)/k(PH-1) and small changes also being observed for the activation energy and pre-exponential factor.

4. Conclusion

In this study, hydrogen abstraction by an approaching methyl radical from a variety of sites in polycyclic aromatic hydrocarbons (PAHs) has been investigated by means of density functional theory calculations. Large systems, containing up to seven six-membered rings, have been examined, and the influence of the polycyclic environment on thermodynamic and kinetic properties has been explored. Optimized B3-LYP/6-

TABLE 4: Calculated Rate Constants, Activation Energies, and Pre-exponential Factors for Hydrogen Abstraction by Methyl Radical at Various Sites in Nonlinear PAHs[a]

site	k_{700} (m^3 mol^{-1} s^{-1})	k_{900} (m^3 mol^{-1} s^{-1})	k_{1100} (m^3 mol^{-1} s^{-1})	E_a (kJ mol^{-1})	A (m^3 mol^{-1} s^{-1})
PH-1	2.91×10^{0}	6.76×10^{1}	5.78×10^{2}	84.8	5.85×10^{6}
PH-2	8.62×10^{0}	1.73×10^{2}	1.34×10^{3}	80.8	8.78×10^{6}
PH-3	8.43×10^{0}	1.72×10^{2}	1.35×10^{3}	81.3	9.27×10^{6}
PH-4	6.39×10^{0}	1.30×10^{2}	1.01×10^{3}	81.2	6.89×10^{6}
PH-5	7.87×10^{0}	1.59×10^{2}	1.24×10^{3}	81.1	8.32×10^{6}
BPH-1	1.10×10^{0}	2.41×10^{1}	1.99×10^{2}	83.3	1.71×10^{6}
BPH-2	4.63×10^{0}	9.30×10^{1}	7.21×10^{2}	80.9	4.74×10^{6}
BPH-3	4.20×10^{0}	8.68×10^{1}	6.85×10^{2}	81.6	4.90×10^{6}
BPH-4	3.30×10^{0}	6.81×10^{1}	5.38×10^{2}	81.6	3.84×10^{6}
BPH-5	3.29×10^{0}	6.92×10^{1}	5.54×10^{2}	82.2	4.20×10^{6}
BPH-6	3.77×10^{0}	7.77×10^{1}	6.13×10^{2}	81.6	4.38×10^{6}
DBPH-1	9.96×10^{-1}	2.14×10^{1}	1.74×10^{2}	82.8	1.41×10^{6}
DBPH-2	4.31×10^{0}	8.77×10^{1}	6.87×10^{2}	81.3	4.72×10^{6}
DBPH-3	3.48×10^{0}	7.40×10^{1}	5.96×10^{2}	82.4	4.64×10^{6}
DBPH-4	2.79×10^{0}	5.86×10^{1}	4.69×10^{2}	82.1	3.54×10^{6}
DBPH-5	2.78×10^{0}	5.97×10^{1}	4.84×10^{2}	82.7	3.88×10^{6}
DBPH-6	3.37×10^{0}	6.92×10^{1}	5.44×10^{2}	81.5	3.81×10^{6}
DBPH-7	2.72×10^{0}	5.90×10^{1}	4.80×10^{2}	82.9	3.93×10^{6}
BA-1	1.92×10^{0}	4.61×10^{1}	4.02×10^{2}	85.6	4.44×10^{6}
BA-2	1.51×10^{-1}	4.53×10^{0}	4.57×10^{1}	91.6	9.71×10^{5}
BA-3	3.69×10^{0}	7.68×10^{1}	6.10×10^{2}	81.9	4.48×10^{6}
DBA-1	4.84×10^{-2}	1.76×10^{0}	2.02×10^{1}	96.7	7.44×10^{5}
DBA-2	3.79×10^{0}	8.65×10^{1}	7.32×10^{2}	84.4	7.03×10^{6}
DBA-3	9.51×10^{0}	1.90×10^{2}	1.47×10^{3}	80.8	9.54×10^{6}
BNA-1	1.19×10^{0}	2.38×10^{1}	1.86×10^{2}	80.9	1.23×10^{6}
BNA-2	1.42×10^{-1}	3.77×10^{0}	3.53×10^{1}	88.4	5.30×10^{5}
BNA-3	5.43×10^{-1}	1.27×10^{1}	1.09×10^{2}	84.9	1.11×10^{6}
BPHA-1	4.59×10^{-1}	1.12×10^{1}	9.83×10^{1}	86.0	1.13×10^{6}
BPHA-2	1.09×10^{-1}	3.09×10^{0}	3.00×10^{1}	90.0	5.33×10^{5}
BPHA-3	1.30×10^{0}	2.72×10^{1}	2.18×10^{2}	82.1	1.64×10^{6}
C-1	3.63×10^{1}	7.70×10^{2}	6.18×10^{3}	82.3	4.77×10^{7}
PYR-1	1.25×10^{1}	2.66×10^{2}	2.15×10^{3}	82.5	1.68×10^{7}
PYR-2	1.84×10^{1}	3.71×10^{2}	2.89×10^{3}	81.0	1.92×10^{7}
PYR-3	1.68×10^{1}	3.37×10^{2}	2.61×10^{3}	80.8	1.71×10^{7}
PER-1	2.24×10^{0}	5.31×10^{1}	4.60×10^{2}	85.3	4.93×10^{6}
BPER-1	4.71×10^{0}	1.11×10^{2}	9.59×10^{2}	85.2	1.01×10^{7}

[a] Calculated by use of the mixed HO/FR or HO/HR model and including Eckart tunneling corrections. Energies were obtained at the BMK/6-311+G(3df,2p)//B3-LYP/6-311G(d,p) level.

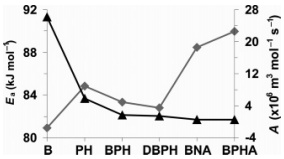

Figure 7. Average values of activation energies (◆, E_a, kJ mol^{-1}) and pre-exponential factors (▲, A, m^3 mol^{-1} s^{-1}) for PAH groups [BMK/6-311+G(3df,2p)//B3-LYP/6-311G(d,p) with HO/FR or HO/HR frequency models and including Eckart tunneling corrections; see text].

311G(d,p) geometries and subsequent BMK/6-311+G(3df,2p) single-point energy calculations have been used, leading to the following conclusions.

The congested sites in the PAHs correspond to lower reaction enthalpy values, largely reflecting the release of steric strain upon creation of the radical. The reaction barriers on the other hand show that abstraction at these congested locations is more difficult, as the site becomes less accessible for the approaching methyl radical. Consequently, a Bell−Evans−Polanyi relationship is not obtained. However, analysis of the subset of linear acenes does indicate a good correlation between reactivities and reaction enthalpies, since in this case we are dealing with uncongested locations and steric hindrance effects in the TSs are not important.

Rate constants, activation energies, and pre-exponential factors, calculated in the temperature interval 700−1100 K, support the observation that abstraction at the uncongested benzene-like sites is preferred for the initial formation of radical species. For the series of linear acenes, the kinetic parameters are found to vary modestly, whereas for the expanded test set, larger variations are observed. For calculation of the rate constants, two refinements are taken into account, specifically Eckart tunneling corrections and an improved description of the internal rotation of the incoming methyl group about the breaking/forming bond in the transition structure. The latter effect reduces the rate constant by a factor of about 1.9 (at a temperature of 900 K). The tunneling corrections contribute to a shift in the activation energies by approximately 4.5 kJ mol^{-1}. Overall, the combination of both effects results in an average downward shift of 7.8 kJ mol^{-1} for the activation energies and a reduction by a factor of approximately 7.4 for the pre-exponential factors, leading to a decrease in the rate constants by a factor of 2.6.

Acknowledgment. K.H. thanks L.R. and members of his research group for their kind hospitality during her stay at the University of Sydney, where this work originated. D.M. thanks the University of Sydney for a Sesqui Postdoctoral Fellowship. V.V.S., G.B.M., and M.W. thank the Fund for Scientific Research−Flanders, and the Research Board of Ghent University. L.R. thanks the Australian Research Council for a Discovery Grant and the ARC Centre of Excellence in Free

Radical Chemistry and Biotechnology for funding and gratefully acknowledges generous allocations of computing time from the Australian Partnership for Advanced Computing, the Australian National University Supercomputing Facility, and the Australian Centre for Advanced Computing and Communication. Finally, we thank Professor Jan Martin for making the BMK functional available for our use.

Supporting Information Available: Reaction enthalpies at 298 K (Figure S1), structures of the PAHs that have been examined (Figure S2), spin densities of all product radicals (Table S1), total energies, zero-point vibrational energies, and thermal corrections (Table S2), and effect on activation energies and pre-exponential factors of the model used to provide a refined description of the low-energy torsional motion of the methyl group in the transition structures and effect of Eckart tunneling corrections (Table S3). This material is available free of charge via the Internet at http://pubs.acs.org.

References and Notes

(1) Gonzales, J. M.; Barden, C. J.; Brown, S. T.; Schleyer, P. v. R.; Schaefer, H. F., III; Li, Q.-S. *J. Am. Chem. Soc.* **2003**, *125*, 1064 and references therein.

(2) Watson, M. D.; Fechtenkötter, A.; Müllen, K. *Chem. Rev.* **2001**, *101*, 1267.

(3) (a) Harvey, R. G. *Polycyclic Aromatic Hydrocarbons: Chemistry and Carcinogenicity*; Cambridge University Press: Cambridge, U.K., 1991. (b) Harvey, R. G. *Polycyclic Aromatic Hydrocarbons*; Wiley−VCH: New York, 1997.

(4) Durant, J. L.; Busby, W. F.; Lafleur, A. L.; Penman, B. W.; Crespi, C. L. *Mutat. Res.* **1996**, *371*, 123.

(5) Denissenko, M. F.; Pao, A.; Tang, M. S.; Pfeifer, G. P. *Science* **1996**, *274*, 430.

(6) Allamandola, L. J. *Top Curr. Chem.* **1990**, *153*, 1.

(7) (a) *Polycyclic Aromatic Hydrocarbons and Astrophysics*; Léger, A., d'Hendecourt, L., Boccara, N., Eds.; NATO ASI Series C; Reidel: Dordrecht, The Netherlands, 1987; Vol. 191. (b) Puget, J. L.; Léger, A. *Annu. Rev. Astron. Astrophys.* **1989**, *27*, 161.

(8) Allen, J. O.; Dookeran, M.; Smith, K. A.; Sarofim, A. F.; Taghizadeh, K.; Lafleur, A. L. *Environ. Sci. Technol.* **1996**, *30*, 1023.

(9) Lovas, F. J.; McMahon, R. J.; Grabow, J.-U.; Schnell, M.; Mack, J.; Scott, L. T.; Kuczkowski, R. L. *J. Am. Chem. Soc.* **2005**, *127*, 4345.

(10) (a) Kroto, H. W.; Heath, J. R.; O'Brien, S. C.; Curl, R. F.; Smalley, R. E. *Nature* **1985**, *318*, 162. (b) Zhang, Q. L.; O'Brien, S. C.; Heath, J. R.; Liu, Y.; Curl, R. F.; Kroto, H. W.; Smalley, R. E. *J. Phys. Chem.* **1986**, *90*, 525. (c) Smalley, R. E. *Acc. Chem. Res.* **1992**, *25*, 98.

(11) Pope, C. J.; Marr, J. A.; Howard, J. B. *J. Phys. Chem.* **1993**, *97*, 11001.

(12) (a) Richter, H.; Mazyar, O. A.; Sumathi, R.; Green, W. H.; Howard, J. B.; Bozzelli, J. W. *J. Phys. Chem. A* **2001**, *105*, 1561. (b) Richter, H.; Grieco, W. J.; Howard, J. B. *Combust. Flame* **1999**, *119*, 1.

(13) Harris, S. J.; Weiner, A. M.; Blint, R. J. *Combust. Flame* **1988**, *72*, 91.

(14) (a) Frenklach, M.; Clary, D. W.; Gardiner, W. C.; Stein, S. E. *Proc. Combust. Inst.* **1985**, *20*, 887. (b) Frenklach, M.; Warnatz, J. *Combust. Sci. Technol.* **1987**, *51*, 265. (c) Frenklach, M.; Wang, H. *Proceedings of the 23rd International Symposium on. Combustion*; The Combustion Institute: Pittsburgh, PA, 1990; p 1559. (d) Frenklach, M. *Proceedings of the 26th International Symposium on Combustion*; The Combustion Institute: Pittsburgh, PA, 1996; p 2258.

(15) Wauters, S.; Marin, G. B. *Ind. Eng. Chem. Res.* **2002**, *41*, 2379.

(16) Vereecken, L.; Peeters, J.; Bettinger, H. F.; Kaiser, R. I.; Schleyer, P. v. R.; Schaefer, H. F., III. *J. Am. Chem. Soc.* **2002**, *124*, 2781.

(17) Wauters, S.; Marin, G. B. *Chem. Eng. J.* **2001**, *82*, 267.

(18) Van Speybroeck, V.; Van Neck, D.; Waroquier, M.; Wauters, S.; Saeys, M.; Marin, G. B. *Int. J. Quantum Chem.* **2003**, *91*, 384.

(19) Van Speybroeck, V.; Van Neck, D.; Waroquier, M.; Wauters, S.; Saeys, M.; Marin, G. B. *J. Phys. Chem. A* **2000**, *104*, 10939.

(20) Van Speybroeck, V.; Borremans, Y.; Van Neck, D.; Waroquier, M.; Wauters, S.; Saeys, M.; Marin, G. B. *J. Phys. Chem. A* **2001**, *105*, 7713.

(21) Van Speybroeck, V.; Reyniers, M. F.; Marin, G. B.; Waroquier, M. *Chem. Phys. Chem.* **2002**, *3*, 863.

(22) Van Speybroeck, V.; Hemelsoet, K.; Waroquier, M.; Marin, G. B. *Int. J. Quantum Chem.* **2004**, *96*, 568.

(23) de Bruin, T. J. M.; Lorant, F.; Toulhoat, H.; Goddard, W. A., III. *J. Phys. Chem. A* **2004**, *108*, 10302.

(24) Hemelsoet, K.; Van Speybroeck, V.; Marin, G. B.; De Proft, F.; Geerlings, P.; Waroquier, M. *J. Phys. Chem. A* **2004**, *108*, 7281.

(25) Saeys, M.; Reyniers, M. F.; Marin, G. B.; Van Speybroeck, V.; Waroquier, M. *J. Phys. Chem. A* **2003**, *107*, 9147.

(26) Saeys, M.; Reyniers, M. F.; Van Speybroeck, V.; Waroquier, M.; Marin, G. B. *Chem. Phys. Chem.* **2006**, *7*, 188.

(27) Hemelsoet, K.; Moran, D.; Van Speybroeck, V.; Waroquier, M.; Radom, L. *J. Phys. Chem. A* **2006**, *110*, 8942.

(28) (a) Mebel, A. M.; Lin, M. C.; Yu, T.; Morokuma, K. *J. Phys. Chem. A* **1997**, *101*, 3189. (b) Nicolaides, A.; Smith, D. M.; Jensen, F.; Radom, L. *J. Am. Chem. Soc.* **1997**, *119*, 8083.

(29) Kasai, P. H.; Clark, P. A.; Whipple, E. B. *J. Am. Chem. Soc.* **1970**, *92*, 2640.

(30) Chen, R. H.; Kafafi, S. A.; Stein, S. E. *J. Am. Chem. Soc.* **1989**, *111*, 1418.

(31) Wang, H.; Frenklach, M. *J. Phys. Chem.* **1993**, *97*, 3867.

(32) Aihara, J-I; Fujiwara, K.; Harada, A.; Ichikawa, H.; Fukushima, K.; Hirota, F.; Ishida, T. *J. Mol. Struct. (THEOCHEM)* **1996**, *366*, 219.

(33) Cioslowski, J.; Liu, G.; Martinov, M.; Piskorz, P.; Moncrieff, D. *J. Am. Chem. Soc.* **1996**, *118*, 5261.

(34) Van Speybroeck, V.; Marin, G. B.; Waroquier, M. *Chem. Phys. Chem.* **2006**, accepted.

(35) Frisch, M. J.; Trucks, G. W.; Schlegel, H. B.; Scuseria, G. E.; Robb, M. A.; Cheeseman, J. R.; Montgomery, Jr., J. A.; Vreven, T.; Kudin, K. N.; Burant, J. C.; Millam, J. M.; Iyengar, S. S.; Tomasi, J.; Barone, V.; Mennucci, B.; Cossi, M.; Scalmani, G.; Rega, N.; Petersson, G. A.; Nakatsuji, H.; Hada, M.; Ehara, M.; Toyota, K.; Fukuda, R.; Hasegawa, J.; Ishida, M.; Nakajima, T.; Honda, Y.; Kitao, O.; Nakai, H.; Klene, M.; Li, X.; Knox, J. E.; Hratchian, H. P.; Cross, J. B.; Bakken, V.; Adamo, C.; Jaramillo, J.; Gomperts, R.; Stratmann, R. E.; Yazyev, O.; Austin, A. J.; Cammi, R.; Pomelli, C.; Ochterski, J. W.; Ayala, P. Y.; Morokuma, K.; Voth, G. A.; Salvador, P.; Dannenberg, J. J.; Zakrzewski, V. G.; Dapprich, S.; Daniels, A. D.; Strain, M. C.; Farkas, O.; Malick, D. K.; Rabuck, A. D.; Raghavachari, K.; Foresman, J. B.; Ortiz, J. V.; Cui, Q.; Baboul, A. G.; Clifford, S.; Cioslowski, J.; Stefanov, B. B.; Liu, G.; Liashenko, A.; Piskorz, P.; Komaromi, I.; Martin, R. L.; Fox, D. J.; Keith, T.; Al-Laham, M. A.; Peng, C. Y.; Nanayakkara, A.; Challacombe, M.; Gill, P. M. W.; Johnson, B.; Chen, W.; Wong, M. W.; Gonzalez, C.; Pople, J. A. Gaussian 03, Revision C2; Gaussian, Inc.: Wallingford, CT, 2004.

(36) (a) Becke, A. D. *J. Chem. Phys.* **1993**, *98*, 5648. (b) Stephens, P. J.; Devlin, F. J.; Chabalowski, C. F.; Frisch, M. J. *J. Phys. Chem.* **1994**, *98*, 11623.

(37) Krishnan, R.; Binkley, J. S.; Seeger, R.; Pople, J. A. *J. Chem. Phys.* **1980**, *72*, 650.

(38) Smith, D. M.; Nicolaides, A.; Golding, B. T.; Radom, L. *J. Am. Chem. Soc.* **1998**, *120*, 10223.

(39) Coote, M. L. *J. Phys. Chem. A* **2004**, *108*, 3865.

(40) Scott, A. P.; Radom, L. *J. Phys. Chem.* **1996**, *100*, 16502.

(41) Lynch, B. J.; Truhlar, D. G. *J. Phys. Chem. A* **2001**, *105*, 2936.

(42) Zhao, Y.; Lynch, B. J.; Truhlar, D. G. *Phys. Chem. Chem. Phys.* **2005**, *7*, 43.

(43) Boese, A. D.; Martin, J. M. L. *J. Chem. Phys.* **2004**, *121*, 3405.

(44) (a) Laidler, K. J. *Chemical Kinetics*; HarperCollins Publishers Inc.: New York, 1987. (b) McQuarrie D. A.; Simon, J. D. *Physical Chemistry*—A Molecular Approach; University Science Books: Sausalito, CA, 1997.

(45) Eckart, C. *Phys. Rev.* **1930**, *35*, 1303.

(46) Truong, T. N.; Duncan, W. T.; Tirtowidjojo, M. *Phys. Chem. Chem. Phys.* **1999**, *1*, 1061 and references therein.

(47) Troe, J. *J. Chem. Phys.* **1977**, *66*, 4758.

(48) Heuts, J. P. A.; Gilbert, R. G.; Radom, L. *Macromolecules* **1995**, *28*, 8771.

(49) (a) Vansteenkiste, P.; Van Speybroeck, V.; Marin, G. B.; Waroquier, M. *J. Phys. Chem. A* **2003**, *107*, 3139. (b) Van Speybroeck, V.; Vansteenkiste, P.; Van Neck, D.; Waroquier, M. *Chem. Phys. Lett.* **2005**, *402*, 479.

(50) Van Cauter, K.; Van Speybroeck, V.; Vansteenkiste, P.; Reyniers, M. F.; Waroquier, M. *Chem. Phys. Chem.* **2006**, *7*, 131.

(51) The component absolute energies, ZPVEs and thermal corrections are presented in Table S2 of the Supporting Information.

(52) Cioslowski, J.; Liu, G.; Moncrieff, D. *J. Org. Chem.* **1996**, *61*, 4111.

(53) (a) Bell, R. P. *Proc. R. Soc. London, Ser. A* **1936**, *154*, 414. (b) Evans, M. G.; Polanyi, M. *Trans. Faraday Soc.* **1938**, *34*, 11.

Paper III

Reactivity indices for radical reactions involving polyaromatics

Hemelsoet K. , Van Speybroeck V. , Marin G. B. ,
De Proft F., Geerlings P. and Waroquier M.

J. Phys. Chem. A, **2004**, *108*, 7281–7290

J. Phys. Chem. A **2004,** *108,* 7281−7290 **7281**

Reactivity Indices for Radical Reactions Involving Polyaromatics

Karen Hemelsoet,[†] Veronique Van Speybroeck,[†] Guy B. Marin,[‡] Frank De Proft,[§] Paul Geerlings,[§] and Michel Waroquier*,[†]

Laboratory of Theoretical Physics, Ghent University, Proeftuinstraat 86, B-9000 Ghent, Belgium, Laboratorium voor Petrochemische Techniek, Ghent University, Krijgslaan 281-S5, B-9000 Ghent, Belgium, and Eenheid Algemene Chemie (ALGC), Faculteit Wetenschappen, Vrije Universiteit Brussel, Pleinlaan 2, B-1050 Brussels, Belgium

Received: March 22, 2004; In Final Form: May 27, 2004

The reactivity of polyaromatics involved in various radical reactions is studied. The reactions under study are hydrogen abstractions by a methyl radical and additions to double bonds both intra- and intermolecular. The chemical reactivity of the involved molecules is described through different properties, which are calculated within the density functional theory (DFT) framework. The softness reactivity index is tested on its usefulness and reliability to provide information about the reactivity of the global molecule or about chemical selectivity. The applicability of the hard and soft acids and bases (HSAB) principle for bimolecular radical reactions is illustrated by comparing the results of the softness-matching criterion with kinetic and thermodynamic data. For large polyaromatic molecules several magnetic indices, in particular, magnetic susceptibilities, chemical shifts, and nucleus independent chemical shifts (NICS), are computed to quantify the aromatic character of the involved species. The applicability of these magnetic indices in the case of radical reactions is validated by comparing with kinetic results obtained from transition state theory.

1. Introduction

Polycyclic aromatic hydrocarbons (PAHs) are among the most studied chemical compounds during the last years.[1,2] Some PAHs are very carcinogenic substances and are known to be present in more than trace amounts in the earth's atmosphere, soil, and water.[3] PAHs have also been detected in celestial objects such as meteorites and in interstellar space.[3−7] They play an important role during combustion processes of organic substances such as coal, oil, and garbage since they are formed as byproducts due to incomplete combustion.[8−11] Knowledge of their characteristics and their formation processes has attained a lot of theoretical and experimental attention. Several theoretical studies have concentrated on reaction paths that enable the growing of the aromatic species. Usually this is done by classical kinetic studies using an appropriate rate theory and an accurate ab initio method to provide the microscopic ingredients, such as geometries and frequencies. This procedure requires theoretical calculations on the reactants, the transition states, and the products.[9,12] This methodology was followed by some of the authors on radical reactions which are important during coke formation, which is a side process of thermal cracking of hydrocarbons.[13−18]

In this work various of these radical reactions (hydrogen abstraction by a methyl radical and inter- and intramolecular additions) that enable the growth of the PAHs are studied from the point of reactivity indices such as hardness and softness.[19] These were well-known properties within chemistry, although they were mainly defined on a qualitative basis.[20] A theoretical framework to derive reactivity indices from first principles was provided within density functional theory (DFT). For a recent review, we refer to Geerlings et al.[21] Site-selectivity is another important aspect and can be characterized by local descriptors, such as the Fukui function.[22] The concept is a generalization of the frontier molecular orbital reactivity indices (FMO) of Fukui,[23] where all responses to any change of charges, geometry et al. take place in the HOMO (highest occupied molecular orbital) and LUMO (lowest unoccupied molecular orbital), while the core orbitals remain unaffected.

The reactivity indices provide knowledge that can be used to assess the importance of various reaction routes in technologically important processes such as coke formation and can support the elimination of certain reaction paths. The calculations based on reactivity indices are computationally less intensive (but also less detailed) because all information is obtained through study of the reactants only. Consequently, only information about the onset of the chemical reaction should be expected. In this paper we test the reliability of reactivity indices to provide a correct chemical reactivity picture of radical reactions. This approach is compared with earlier reported kinetic results and correlations between the two methods are established. From the concept of reactivity descriptors, it is clear that they can mainly describe kinetically controlled reactions. On the other hand, there might be a correlation between the rate constant and the equilibrium constant, a relation which is incorporated in the noncrossing rule (for further details, we refer to ref 24). In this view, reactivity indices can be expected to provide information about the thermodynamic aspects in some cases.

In our specific case, in which we are dealing with large polycyclic aromatic structures, important information about the reaction mechanism can also be revealed by studying the aromaticity.[25,26] Aromaticity is a complex property, which is usually described by three aspects: high stability, low reactivity, and sustained induced ring current.[27] Many efforts have been made to quantify aromaticity and a number of criteria is

* To whom all correspondence should be addressed. Fax: 32 (0) 9264 65 60. Email: michel.waroquier@UGent.be.
[†] Laboratory of Theoretical Physics.
[‡] Laboratorium voor Petrochemische Techniek.
[§] Eenheid Algemene Chemie.

10.1021/jp048743k CCC: $27.50
Published on Web 08/06/2004

commonly used to characterize the aromatic behavior of molecules. One distinguishes geometric (bond length alternation and bond order), energetic (stabilization energies), and magnetic (chemical shifts, diamagnetic susceptibility anisotropy, exaltation, nucleus independent chemical shifts (NICS) and ring current effects) criteria.[27] Important contributions within the study of the reactivity of PAHs and their correlation with aromaticity were made by Schleyer and co-workers,[28] and applications on several types of reactions have provided evidence for the utility of these magnetic descriptors, such as NICS.[29−31] Also DFT-based reactivity indices can be used as indicators of aromaticity.[32]

In general, studies on the DFT-based reactivity indices of radical reactions have so far been very limited. Pioneering work on reactions of free radicals has been done by Pearson.[33] Some reactivity indices have been calculated,[34−36] and Chandra et al.[37] have tested the HSAB principle for the addition of free radicals to olefins using the condensed values of the Fukui function and softness. Generally, the attack takes place at the less substituted carbon atom of the double bond, in good agreement with other results. They also found good correlations between the hardness and the activation energy in the case of reactions of the OH radical with halomethanes.[38] The addition mechanism of fluoromethyl radicals to fluoroethylenes has been studied by Korchowiec et al.[39] Hirata et al. studied the electronic excited states of PAH radical ions through use of time-dependent DFT.[40] Very recently, Nguyen et al. performed a critical analysis on the use of reactivity descriptors for rationalizing radical reactions.[41]

In this paper, a detailed investigation about the reactivity indices of several radical systems is provided and furthermore the applicability of the HSAB principle for bimolecular radical reactions is studied. The validity of the HSAB principle for other types of reactions has been discussed earlier,[42−46] and the extension of the principle on its applicability to the time-evolution of chemical reactions has recently been studied.[47] In this paper, we will also investigate possible correlations between kinetic data and results derived from DFT-based indices. Further information about the reactivity of the different radical reactions is provided through the study of the aromatic behavior of the involved molecules.

2. Theoretical background

The **reactivity indices** discussed here are defined as derivatives of the electronic energy $E[N, v(\mathbf{r})]$ with N the total number of electrons and $v(\mathbf{r})$ the external potential due to the nuclei.[19] Three categories are distinguished:[48] global indices, local indices, and kernels, which will be left out of this discussion.

The global indices—chemical potential μ, the hardness η, and the softness S—can be computed applying the finite difference method using the vertical ionization potential and electron affinity.[19]

For our purposes, the local indices, varying from point to point, are of higher importance. They provide direct information about the site-selectivity within a molecule.

The Fukui function $f(\mathbf{r})$ is the normalized local softness $s(\mathbf{r})$:[20]

$$s(\mathbf{r}) = f(\mathbf{r})S \tag{1}$$

As N does not represent a continuous variable but only takes integer values,[49] three distinct classes of indices appear, respectively, for (i) nucleophilic attack, where the molecule gains an electron, (ii) electrophilic attack, where the molecule loses an electron, and (iii) radical attack, where the total electron number remains unchanged. The condensed Fukui functions give an approximate value for the local Fukui function at the position of an atomic center and are obtained by integration of the Fukui function over an atomic region:[50]

$$f_k^+ = q_k(N+1) - q_k(N)$$

$$f_k^- = q_k(N) - q_k(N-1)$$

$$f_k^0 = \frac{1}{2}(q_k(N+1) - q_k(N-1))$$

with $q_k(N)$ the electron population on the kth atom of the molecule with N electrons. To calculate the density in an atomic region, different population analysis methods can be used. Geerlings et al. have studied the sensibility of the Fukui function in terms of the population analysis method.[51]

The above-mentioned indices are applied in the hard and soft acids and bases (HSAB) principle, which was originally suggested in 1963 by Pearson:[20]

"Hard acids prefer to coordinate with hard bases and soft acids prefer to coordinate with soft bases for both their thermodynamic and kinetic properties."

Several attempts to prove the HSAB principle were suggested in the literature; for a review, see ref 21. The principle states that the interaction between a system A and a system B will be favored in the case of global softnesses which are close to each other, the optimum being reached when $S_A = S_B$ (in terms of global indices).[52] The local version of the principle states that the optimal interaction sites may be characterized by the condition $s_{Ai} = s_{Bj}$ in case the ith atom of system A interacts with the jth atom of system B.[53] This softness-matching criterion provides the working equations for testing the validity of the HSAB principle and therefore we introduce the variable $\Delta s_{i,j}$:

$$\Delta s_{i,j} = s_i - s_j \tag{2}$$

which defines the difference between the condensed softness of the ith atom of the first molecule and the jth atom of the second molecule. The minimal $\Delta s_{i,j}$ indicates the preferred reaction sites i and j in the reactants.

It has been shown by Parr et al. that reactivity indices (and in particular the hardness) can also be used as indicators of aromaticity,[27] based on the fact that both hardness and aromaticity are measures of high stability and low reactivity. Another important characteristic of aromaticity is the possibility to sustain induced ring currents. On the basis of these three aspects, different criteria to describe the aromatic character of molecules are used.[26,32] The most important magnetic descriptors are based on NMR theory,[54] and according to Jiao et al.[29] "the magnetic criterion is the most specific and unambiguous manifestation of aromaticity". Another important factor is the geometry, as reflected in the planarity of the molecule and the equalization of bond lengths.

The magnetic probes used in this work are the diamagnetic susceptibility anisotropy $\Delta\chi$, the chemical shift δ, and the nucleus independent chemical shift (NICS). The first descriptor is defined as the difference between the out-of-plane component χ_3 and the average of the in-plane components χ_1 and χ_2:

$$\Delta\chi = \chi_3 - \frac{1}{2}(\chi_1 + \chi_2) \tag{3}$$

This quantity is however size dependent.[55] The chemical shift δ is defined as

$$\delta = \sigma_{TMS} - \sigma \tag{4}$$

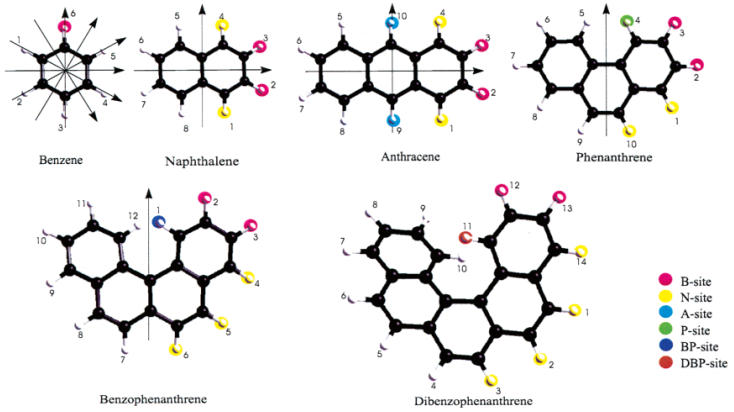

Figure 1. Benzene and some polycyclic aromatic molecules (PAHs) studied in the hydrogen abstraction reactions. The symmetry axes lying inside the molecular plane are shown. The different sites are indicated.

with σ the isotropic part of the shielding tensor. The reference molecule used in NMR experiences is tetramethylsilane (TMS). The chemical shifts are less obvious indicators of aromaticity because they mainly monitor local effects and to a much lesser extent global ones (like ring currents).[56] The NICS, as defined by Schleyer et al.,[57] is the absolute magnetic shielding in the center of a ring and consist of a diamagnetic and a paramagnetic contribution.[58] Schleyer et al. recommended the use of the NICS values calculated at 1 Å above the ring centers as aromaticity index, rather than the NICS values computed in the ring centers.[58] The main advantage of the NICS values is that they are less dependent on the ring size and that they do not require a reference system. The disadvantage is that NICS gives only a reliable absolute indication in the case of large ring sizes, where local shielding effects can be ignored.

3. Computational Details

All ab initio calculations are performed within the Gaussian 98 software package,[59] using Becke's three-parameter hybrid B3LYP functional.[60] The molecular orbitals are expanded in a triple-ζ 6-311G basis augmented with a set of single d and p polarization functions. The B3LYP functional is known to give a reliable and quantitatively good description of geometries, frequencies and reaction barriers for radical reactions.[61] Several studies have also indicated that B3LYP, and even Hartree−Fock, methods are sufficiently accurate for estimating the relative stabilities of different conformers, especially when large basis sets including polarization functions are used.[61d,62] According to a specific study on the activation energies of radical addition and abstraction reactions,[63] it was found that DFT/B3LYP methods are able to reproduce qualitative trends in the activation energies when compared to CBS-QB3 methods. When comparing with experimental activation energies the resemblence is even more striking. Only hydrogen abstractions in which a hydrogen radical is involved may be less accurate.

The condensed Fukui functions and softnesses are systematically calculated using the natural population analysis (NPA). This population analysis is known to give reliable results,[64] especially for molecules with low polarizibility which are subject of this study. Therefore, other population schemes such as CHELP[65] and MK (Merz−Singh−Kollman),[66] which are based on the electrostatic potential, are not taken into consideration. The Mulliken scheme is known to be less accurate, since it is strongly dependent on the basis set.

The NMR quantities are calculated using the CSGT method. The CSGT (continuous set of gauge transformations) method, developed by Keith and Bader,[67] achieves gauge-invariance by performing a continuous set of gauge transformations, one for each point in real space. An accurate three-dimensional description of the first-order electronic current density is obtained, from which the shielding tensors and magnetic susceptibility can be determined. For a review of CSGT and other DFT methods for calculating NMR properties, we refer to Helgaker et al.[68] Studies on a large number of molecules reveal that the CSGT method is computationally very efficient and accurate.[69] This method demands the use of a large basis to obtain reliable results.[67,70]

4. Results and Discussion

4.1. Applicability of HSAB Principle. Hydrogen Abstraction. Figure 1 shows benzene (B) and the polycyclic aromatic molecules (PAHs) naphthalene (N), anthracene (A), phenanthrene (P), benzophenanthrene (BP), and dibenzophenanthrene (DBP). The molecules BP and DBP are characterized by a nonplanar geometry, due to steric interactions between adjacent hydrogens. Hydrogen abstraction reactions by an approaching methyl radical on each of these molecules are studied. This leads to the formation of a variety of organic radicals (aryl radicals) and methane. Within a specific molecule abstraction can occur at different places, resulting in different radicals which cannot be related to each other by symmetry operations. For example if one looks at naphthalene, there are two possibilities: abstraction of hydrogen number 1 (and equally 4, 5, and 8) or abstraction of hydrogen number 2 (and equally 3, 6, and 7). Within the field of polyaromatics it may be convenient to introduce a specific nomenclature to identify the various positions.[15,71] One distinguishes between benzene-, naphthalene-, anthracene-, phenanthrene-, benzophenanthrene- and dibenzophenanthrene-like sites. This nomenclature is clarified in Figure 1, where all hydrogens are assigned to a specific site. The different sites X are characterized in the following way:

TABLE 1: Hardness η and Condensed Softness Differences $\Delta s_{C,Hi}$ Calculated at the B3LYP/6-311g Level in the Case of Hydrogen Abstraction Reactions, Where Experimental Results Are Given in Italics in Parentheses[75]**

η (eV)					
B	N	A	P	BP	DBP
5.556 (*5.3*)	4.237 (*4.2*)	3.396 (*3.3*)	3.998 (*3.8*)	3.581	3.485

	$\Delta s_{C,Hi}$					
i	B	N	A	P	BP	DBP
1	1.951	2.089	2.090	2.105	2.152	2.098
2	1.951	2.072	2.069	2.086	2.094	2.096
3	1.951	2.072	2.069	2.092	2.089	2.102
4	1.951	2.089	2.090	2.122	2.102	2.102
5	1.951	2.089	2.090	2.122	2.097	2.096
6	1.951	2.072	2.069	2.092	2.093	2.098
7		2.072	2.069	2.086	2.093	2.116
8		2.089	2.090	2.105	2.097	2.101
9			2.087	2.087	2.102	2.115
10			2.087	2.087	2.089	2.169
11					2.094	2.169
12					2.152	2.115
13						2.101
14						2.116

we count the number of intermediate carbon atoms at both sides between the specific hydrogen center and the adjacent hydrogen atoms. The thus obtained numbers *A* and *A′* are used to classify the X-like sites according to *A*/*A′*. As such the α- and *β*- protons in naphthalene[72] are identified as $^2/_2$ and $^3/_2$ sites, respectively. Applying this procedure for all the hydrogens, we obtain $^2/_2$ in the case of X = B, $^3/_2$ in the case of X = N, $^3/_3$ in the case of X = A, $^4/_2$ in the case of X = P, $^5/_2$ in the case of X = BP, and $^6/_2$ in the case of X = DBP.

From the knowledge of the reactivity indices, defined in section 2, and the HSAB principle, one should be able to predict which hydrogen atom is preferred for abstraction. The availability of an extended database of ab initio kinetic studies on these hydrogen abstraction reactions, performed by the authors,[17,73] can be used to validate the concept of reactivity indices within the context of the HSAB principle. The HSAB predictions can be done on the basis of properties of the reactants only, indicating the advantage of reactivity indices compared to more elusive, reaction path type kinetic studies. The computed global hardnesses of the studied molecules are given in Table 1, and it is seen that most molecules can be considered as soft (except for B which one could consider to be intermediately hard). Consequently, hard−hard effects are of less importance.[74] Note that the experimental hardnesses are quite well reproduced. The global hardness of the attacking methyl radical is 5.478 eV, indicating the intermediate hard character of this radical. Because of the above considerations the soft−soft model should provide an adequate description for the studied reactions. The condensed local softness of the carbon atom of the methyl radical amounts to 2.192 1/au. According to the softness-matching criterion the attack of the methyl radical will take place at the hydrogen atom of the hydrocarbon whose condensed softness is closest to the value of the methyl radical. For that purpose it is instructive to analyze the condensed softnesses of the various hydrogen atoms *i* of the polyaromatic with reference to the value 2.192. These $\Delta s_{C,Hi}$ values are given in Table 1 (the numbers in the first column refer to the labeling of the hydrogen atoms as given in Figure 1 and are in accordance with the IUPAC convention). It should be stressed that hydrogen atoms belonging to the same X-site do not necessarily have the same $\Delta s_{C,Hi}$ value, as these sites cannot be transformed into one another by a symmetry operator belonging to the molecular point group. With the exception of DBP, the lowest $\Delta s_{C,Hi}$ values are found at a benzene-like site of the molecules. According to the HSAB principle, abstraction of the hydrogen atom at these sites should be less activated. This rule does not hold for DBP where the lowest $\Delta s_{C,Hi}$ values are found at naphthalene-like sites (Table 1). This is probably due to the nonplanarity of the DBP-radical.

The validity of the HSAB conclusions is now tested by comparing with kinetic and thermodynamic quantities for the hydrogen reactions under study. Is there any correlation between the local softness and some specific kinetic parameters and/or thermodynamic quantities (activation energy, reaction enthalpy, ...)? First, comparison is made with the kinetic parameters of the abstraction reaction: the activation energy and the pre-exponential factor defining the reaction rate. These quantities were calculated within the framework of transition state theory (TST)[17] and are determined by microscopic quantities, such as the reaction barrier at 0 K (ΔE_0: this is the energy difference between the reactant and the transition state, including the zero-point energy difference) and the partition functions belonging to the reactants and transition states. Since the various reactivity indices playing a role in the HSAB principle are systematically determined at 0 K, it is more plausible to use the reaction barrier ΔE_0 at 0 K as comparative material instead of the activation energy. They are given in Figure 2. The reaction B → B_R and abstraction at other benzene-like sites turns out to yield the lowest reaction barrier (62.33 kJ/mol for N, 62.23 kJ/mol for A, and 62.82 kJ/mol for P), supporting a preference for abstraction of a hydrogen atom bound to a benzene-like site. Thus, the HSAB principle is a good prediction model for the kinetics of abstraction of H atoms by methyl radicals on polyaromatics.

At the next stage, one can look at the stability of the formed radicals after abstraction at various positions. The most stable radicals are depicted in Figure 2 (the ground state energies of all possible radicals are given in Table S1 of the Supporting Information). The radicals which are predicted to be formed by the HSAB principle are not the most stable ones. This clearly illustrates that the HSAB principle correlates nicely with kinetics but not necessarily with thermodynamic properties. This could be expected since reactivity indices only give information on the onset of a chemical reaction.[24] Following this discussion an Evans−Polanyi relation which establishes a correlation between the reaction barrier and the reaction enthalpy[76] should not be valid for the studied reactions. The validity of such correlation on hydrogen abstractions was thoroughly discussed in a recent work by some of the presenting authors.[73] It was found that Evans−Polanyi holds for abstractions at a substituted benzene ring with a methyl radical leading to phenylic, alkylic, allylic and benzylic radicals. This is illustrated in Figure 3 where the reaction barrier is plotted vs the reaction enthalpy at 0 K. At the same figure, the results of the hydrogen abstractions at the polyaromatics are shown (indicated by B, N, A, P, BP, and DBP). The quasi-linear correlation between the reaction barrier and the stability of the formed radicals is no longer valid. Some nonlinear clustering is observed for the hydrogen abstractions discussed in this work. This clustering within the subcategory of reactions leading to aryl radicals indicates that the reaction enthalpy cannot be regarded as a suitable reactivity index for hydrogen abstraction reactions. This is not too surprising, since it concerns subtle differences within a subset of reactions. For further information about reaction enthalpies and bond energies of benzene and several polyaromatics, we refer to ref 77. We stress that the HSAB principle apparently succeeds in predicting

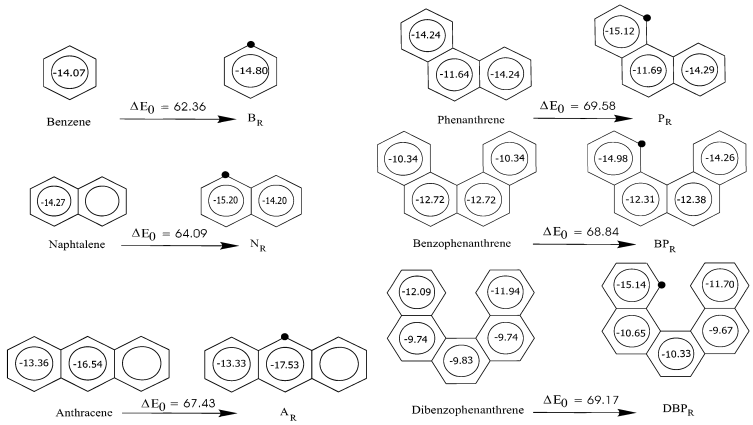

Figure 2. NICS values of molecules involved in hydrogen abstractions. NICS values of the planar molecules are calculated 1 Å above the plane of the ring; NICS values of the nonplanar molecules are calculated in the plane of the ring. The reaction barriers ΔE_0 at 0 K are given (in kJ/mol).

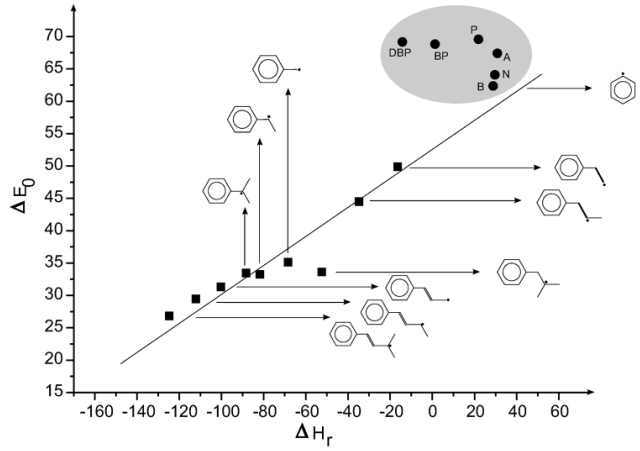

Figure 3. Correlation between ΔE_0 (in kJ/mol) and ΔH_r (at 0 K, in kJ/mol) for all types of hydrogen abstraction reactions (most of the values were taken from ref 73). Clustering is observed within the subcategory of phenylic radicals as discussed in this paper.

correctly the subtle differences in activation energies. This is in line with previous observations where the DFT-based reactivity indices were found to probe mainly the kinetic aspects of a reaction.[21] We would like to emphasize again that a correlation between HSAB results and thermodynamic properties can be expected in the case of noncrossing reactions. For the hydrogen abstraction reactions studied in this work, no such correlation was however found.

Addition Reactions. As a second class of bimolecular radical reactions, we consider addition reactions of radicals to several gas-phase components, such as ethene, propene, ethyne, and propyne. These reactions are of fundamental importance in this field of hydrocarbon chemistry as they lie on the basis of the growth of surface radicals toward larger polyaromatics.[13] We make some particular selection of addition reactions figuring in polyaromatic growth and for which ab initio results are available as comparative material for the analysis with the softness differences Δs. The kinetics of additional reactions were calculated by analogous procedures as outlined in ref 13. The studied radicals are the ethylbenzene radical (R1), phenylacetylene radical (R2), butylbenzene radical (R3) and 1-phenyl-1,3-butadiene-4-yl radical (R4) (Figure 4). The possible reaction paths are illustrated in Figure 4. A relevant question is which olefins are the most reactive for addition reactions.

In the case of an electrophilic addition to alkenes and alkynes the regioselectivity is usually described by applying the Mark-

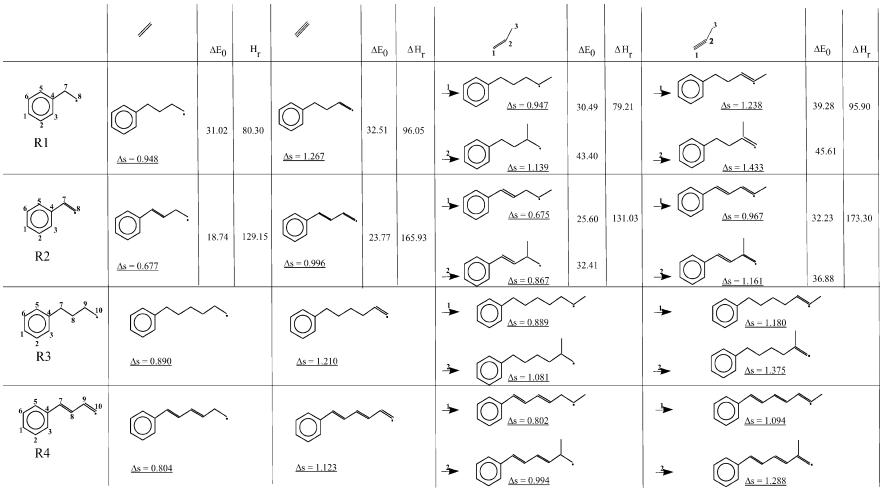

Figure 4. Schematic representation of the addition reactions. Minimal softness diferrences Δ*s* according the softness matching criterion and reaction barriers ΔE_0 (in kJ/mol) and reaction enthalpy values (in kJ/mol) are included.

ovnikov rule, which states that the least electronegative part of the reagent attaches itself to the carbon atom that has the most hydrogens already attached to it (least substituted carbon atom). During this addition reaction, an intermediate carbocation is formed and the positive charge is spread out over the neighboring carbon atoms, increasing the stability of the total system. Aizman et al. have recently studied the Markovnikov rule in the light of site activation models and found good correlations with variations in the Fukui function.[78] In the case of a radical addition reaction the regioselectivity of the reaction can analogously be described, using hyperconjugation arguments.

The condensed softness values are taken up in Table S2 of the Supporting Information. The maximum value of the local softness usually indicates the most reactive part of the molecule. For the radicals, this reactive part is always located at the radical center, as could be expected. As in the previous section, the validity of the HSAB-principle is shown by comparing the softness-matching criterion with the reaction barrier ΔE_0. The kinetic results and the softness differences Δ*s* are given in Figure 4. The Δ*s* values are the minimal differences between the condensed softnesses of the carbon atom of the radical center on one hand and the carbon atoms of the olefin on the other hand.

Several conclusions can be made.

1. The site-reactivity of the nonsymmetric molecules propene and propyne is in accordance with the Markovnikov rule: the addition of the radical will preferentially occur at the least substituted carbon atom involved in the double, respectively triple bond. The minimal softness Δ*s* shows a lower value for reaction path 1 compared with reaction path 2 (see Figure 4). This preference for reaction path 1 is also supported by the reaction barriers reporting large differences between the two paths (average difference of 7.67 kJ/mol). The first reaction path gives rise to a secondary radical which is more stable than a primary radical.

2. Minimal softness differences may serve as a measure for the reactivity of the different precursors. The lowest Δ*s* values are observed in the addition reactions to propene and ethene, and following the HSAB principle they are assigned as the most reactive precursors. The softness differences are distinctly larger for the two other remaining precursors ethyne and propyne. The deviations between the Δ*s* values of the reactions with ethene (ethyne) and reactions with propene (propyne) are small. This is due to the fact that condensed reactivity indices only provide information concerning a limited molecular region. The chain length is of little importance here, and the methyl substituent in the chain does not substantially influence the reactivity index of the carbon atom number 1 (see Figure 4). This carbon atom is mainly influenced by the double and triple bonds, respectively.

The Δs values are in agreement with the ΔE_0 values and support the observation that addition to precursors exhibiting a double bond is favored with regard to triple bonds.

As discussed in the previous section, no correlation can be found between the HSAB predictions and thermodynamics. The reaction enthalpies ΔH_r are depicted in Figure 4. It is also seen that no linear correlation can be found between the ΔH_r values and the ΔE_0 values. We will not go into detail about this problem, but refer to the review of Fischer and Radom about radical addition reactions, where the validity of the linear Evans−Polanyi relation is thoroughly discussed for this class of reactions.[79]

3. On basis of the Δ*s* values, we conclude that R2 is more reactive than R4, followed by R3 and R1. This is in line with chemical intuition since R2 and R4 are both vinylic radicals and are more reactive than the primary radicals R1 and R3. This is completely confirmed by the trend of the energy barrier ΔE_0 predicting much lower values for R2, emphasizing the large reactive character of this radical.

4.2. Effect of Aromaticity on the Reactivity of PAHs. The relation between aromaticity and reactivity can be studied through several indices.[27,32] In this paper, we focus on the magnetic indices originated from NMR theory. Furthermore, it is instructive to study the evolution of the aromaticity descriptors along the reaction path. In the following section, we try to

TABLE 2: Magnetic Properties of Hydrogen Abstraction and Cyclization Reactions[a]

molecule	$\Delta\chi$ (ppm cgs)	δ (ppm)	NICS(0) (ppm)	NICS(1) (ppm)
benzene[b]	−65.65 (*−62.9*)[d]	6.34	−12.80 (*−11.5*)[e]	−14.07
B_R[b]	−59.39	6.16	−16.16	−14.80
naphthalene[b]	−127.36 (*−130.3*)[d]	6.67	−13.03 (*−11.4*)[e]	−14.27
N_R[b]	−119.82	6.55	−14.87	−14.66
anthracene[b]	−191.55 (*−204.8*)[d]	6.93	−13.16 (*−11.2*)[e]	−14.42
A_R[b]	−183.99	6.85	−14.60	−14.73
phenanthrene[b]	−178.80	6.88	−11.89(*−10.0*)[e]	−13.37
P_R[b]	−171.55	6.73	−13.35	−13.70
benzophenanthrene[c]	−226.58	7.02	−11.53	
BP_R[b]	−243.67	7.00	−12.81	−10.73
dibenzophenanthrene[c]	−247.12	6.88	−10.67	
DBP_R[c]	−252.23	6.84	−11.50	

molecule	ΔE_0 (kJ/mol)	$\Delta\chi$ (ppm cgs)	*R*	δ (ppm)	*T*	$NICS^{av}$ (ppm)
B_{RE}	51.79	−65.38	−16.34E−2	6.29	−0.0768	−12.30
B_{TS}		−54.70		5.81		−6.84
N_{RE}	49.11	−131.13	−15.19E−2	6.70	−0.0730	−12.53
N_{TS}		−111.22		6.21		−8.95
A_{RE}	41.39	−191.38	−7.51E−2	6.97	−0.0596	−12.74
A_{TS}		−177.01		6.56		−10.19
P_{RE}	33.43	−174.55	−5.18E−2	6.80	−0.0210	−11.77
P_{TS}		−165.51		6.66		−11.11
BP_{RE}	50.03	−201.19	2.99E−2	6.60	0.0088	−9.63
BP_{TS}		−207.23		6.65		−9.89

[a] These values were calculated using the CSGT method at B3LYP/6-311 g** level. Other computed values are in italics. [b] Planar molecule. [c] Nonplanar molecule. [d] Reference 29c. [e] GIAO−SCF/6-31g*//B3LYP/6-31g*.[57]

establish a correlation between the magnetic indices—calculated at reactants, transition states and products—and the reaction kinetics.

Hydrogen Abstraction. The results of the magnetic susceptibility anisotropy, the average proton chemical shift and the average NICS value calculated on the aromatics and the subsequent formed radicals after hydrogen abstraction (computed at B3LYP/6-311g** level), are reported in Table 2. For this discussion we retained the most stable aryl radicals (see previous discussion) as displayed in Figure 2. For comparison also other computed values reported in the literature are included. Although the calculations have not been performed on the same computational levels, a qualitative agreement is found. The homologous series of linear acenes (with B, N, and A as the first three components) has been intensively studied[28] and the NICS values have also been subject of elaborated study, from semiempirical to ab initio studies.[80]

The differences between the magnetic indices of the reactants and the product species appear to be small, indicating that the change of aromaticity is not the driving force behind this type of reactions and thus no clear correlation between ΔE_0 (see also Figure 2) and the magnetic descriptors can be found. Furthermore, the magnetic susceptibility anisotropy $\Delta\chi$ and the average proton chemical shift δ show that the radicals are less aromatic than the reactants in the case of B, N, A, and P. The abstraction of a σ-electron indeed results in less shielding of the nuclei by the electron cloud and a decrease in aromaticity. The magnetic susceptibility anisotropy of BP and DBP suggests just the contrary since the anisotropy value of the radical is larger than the value of the reactant, whereas the average proton chemical shift remains almost constant. Both BP and DBP molecules are nonplanar, and by abstracting a hydrogen, the planarity of the substrate increases (in the case of BP_R this leads to a perfect planar molecule) and thus the aromaticity increases, which is reflected in the values for the magnetic susceptibility anisotropy. As $\Delta\chi$ is a size-dependent quantity, a comparative study of magnetic indices can be instructive if limited to the same family of molecules but with different types of sites, such as A and P. Because of the geometric structure A (A_R) is more aromatic than P (P_R): electronic currents experience less resistance in a fully stretched geometry.[81]

For the sake of completeness, the averages of the computed NICS values of all rings of the involved polycyclic molecule are included in Table 2. Schleyer et al. recommended the use of the NICS values computed 1 Å above the ring center (NICS-(1)) for planar molecules;[58] for nonplanar molecules the NICS values are computed at the ring centers (NICS(0)). All calculated NICS values are also given in Figure 2. The increase of NICS going from reactants to transition states is no effect of aromaticity, and will not further be treated here. Within this context, the influence of a biradical electron pair on the aromaticity for biradical benzynes has been studied earlier,[82] where more detailed information based on the dissected NICS values is presented.

Cyclization. In this section we focus on unimolecular radical cyclization reactions that eventually lead to a further growing of the polycyclic aromatic molecule. The reactants consist of an aromatic nucleus of conjugated benzene rings and an attached alkyl chain with the appropriate number of carbons to allow cyclization. After the reaction, an extra ring is formed as schematically shown in Figure 5. On the basis of geometrical considerations one distinguishes two classes: a first class wherein the aromatic nucleus is flat (B_{RE}, N_{RE}, and A_{RE}) and a second class where the clusters are folded due to large steric hindrance between the attached alkyl chain and the aromatic nucleus (P_{RE} and BP_{RE}). To test the influence of the aromatic character of the involved species on the reactivity various magnetic indices of reactants and transition states are computed. For more details we refer to refs 17 and 18.

The theoretical values for the magnetic susceptibility anisotropy, the average proton chemical shift of the protons attached to the aromatic nucleus, and the average NICS values computed at the ring center are given in the lower part of Table 2. The last two magnetic properties include mainly information about the aromatic nucleus whereas the magnetic susceptibility anisotropy includes also effects of the attached alkyl chain. All indices lead to the following general conclusion: the transition states B_{TS}, N_{TS}, A_{TS}, and P_{TS} are less aromatic than the

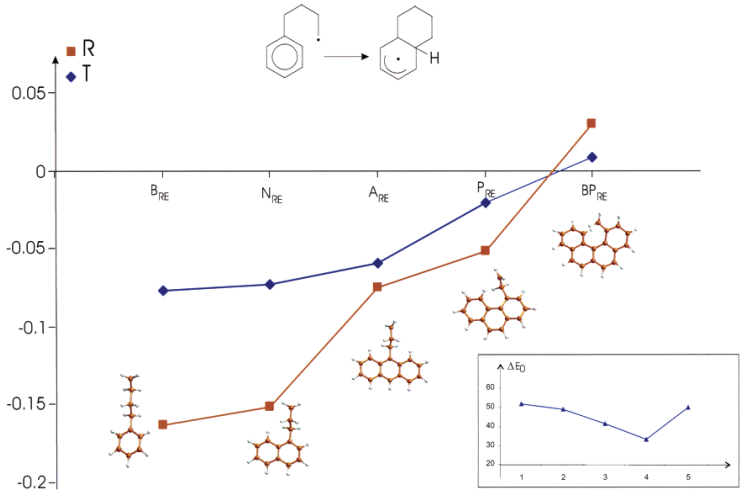

Figure 5. Relative dimensionless parameters *R* and *T* for the cyclization of the benzene, naphthalene, anthracene, phenanthrene, and benzophenanthrene reactant. The reaction barrier ΔE_0 is shown in the inset.

corresponding reactants. For these cyclization reactions, the transition states are less planar than the reactants due to the formation of the extra ring which prohibits the flowing of ring currents. Benzophenanthrene forms an exception: the transition state is more aromatic than the reactant. In this case, the reactant is strongly folded due to steric hindrance between the attached alkyl chain and the aromatic nucleus. During cyclization the deviations from planarity decrease.

It is now instructive to compare the magnetic indices with the kinetics calculated with TST. We only report reaction barriers at 0 K, in analogy with discussions in previous sections. The results are reported in Table 2 and are taken from ref 15. To compare various reactions, a suitable normalization is required for the magnetic susceptibility anisotropy since this property is size-dependent. We therefore introduce the relative dimensionless parameter *R*:

$$R = \frac{\Delta\chi(\mathrm{TS}) - \Delta\chi(\mathrm{RE})}{\Delta\chi(\mathrm{RE})} \tag{5}$$

Similarly, for the proton chemical shifts, we define *T*:

$$T = \frac{\delta(\mathrm{TS}) - \delta(\mathrm{RE})}{\delta(\mathrm{RE})} \tag{6}$$

δ represents the average chemical proton shift of the protons attached to the aromatic nucleus. The resulting values are given in Table 2 and their evolution in function of the type of the site is depicted in Figure 5. For the interpretation of these data it is important to stress that the properties *R* and *T* are mainly determined by the aromatic nucleus. A lower absolute value for *R* and *T* indicates a smaller aromaticity difference between reactant and transition state. Comparison between these magnetic parameters and the reaction barriers at 0 K indicates that the smaller the aromaticity difference between the aromatic nucleus in the transition state and reactant the lower the reaction barrier for cyclization. The sign of the parameters *R* and *T* indicates whether the aromaticity increases (positive sign) or decreases (negative sign) when going to the transition state. Only for BP does the aromaticity increase when going to the transition state. During this cyclization reaction, the molecule becomes more planar due to the presence of the benzylic type of radical. One can correlate this result with the highest barrier for cyclization. Both relative indices show a similar behavior and are in agreement with the kinetic results ΔE_0, as presented in Figure 5.

5. Conclusions

In this work, we studied the reactivity of various PAHs which are involved in radical reactions. The studied reactions are hydrogen abstractions, addition reactions, and cyclization reactions which play a significant role in several technologically important processes such as thermal cracking and soot formation. The reactivity is investigated by means of the HSAB principle, using the softness-matching criterion. The validity of the latter principle for the bimolecular radical reactions was shown, since the predictions of the HSAB principle are confirmed by kinetic results, such as reaction barriers. A correlation between the thermodynamic properties of the reactions (reaction enthalpy) is not always valid, which can be expected since DFT-based reactivity indices only give information on the onset of chemical reactions. Concerning various magnetic indices describing aromaticity, it was found that they give a consistent prediction of aromaticity which is in accordance with our chemical intuition. For hydrogen abstractions at PAHs, no correlation between the reaction barriers and the magnetic descriptors could be established, since aromaticity is not the driving force for these reactions. In the case of cyclization reactions of alkyl chains at an aromatic nucleus, the aromaticity change of the aromatic nucleus during the reaction is the determining reactivity factor and thus the magnetic indices are in good agreement with the reaction barriers at 0 K.

Acknowledgment. This work is supported by the Fund for Scientific Research−Flanders (FWO), the Research Board of Ghent University, and the Institute for Science and Technology (I.W.T.). P.G. thanks FWO−Vlaanderen for continuous support to his group.

Supporting Information Available: Tables of absolute energies of radicals induced by hydrogen abstraction (Table S1) and of condensed softness values for the molecules involved in the addition reactions (Table S2). This material is available free of charge via the Internet at http://pubs.acs.org.

References and Notes

(1) Gonzales, J. M.; Barden, C. J.; Brown, S. T.; Schleyer, P. v. R.; Schaefer, H. F., III; Li, Q.-S. *J. Am. Chem. Soc.* **2003**, *125*, 1064 and references therein.

(2) Watson, M. D.; Fechtenkötter, A.; Müllen, K. *Chem. Rev.* **2001**, *101*, 1267.

(3) (a) *Polycyclic Aromatic Hydrocarbons and Astrophysics*; Léger, A., d'Hendecourt, L., Boccara, N., Eds.; NATO ASI Series, Series C 191; Reidel: Dordrecht, The Netherlands, 1987; (b) Puget, J. L.; Léger, A. *Annu. Rev. Astron. Astrophys.* **1989**, *27*, 161.

(4) Durant, J. L.; Busby, W. F.; Lafleur, A. L.; Penman, B. W.; Crespi, C. L.; *Mutat. Res.* **1996**, *371*, 123.

(5) Denissenko, M. F.; Pao, A.; Tang, M. S.; Pfeifer, G. P. *Science* **1996**, *274*, 430.

(6) Allen, J. O.; Dookeran, N. M.; Smith, K. A.; Sarofim, A. F.; Taghizadeh, K.; Lafleur, A. L. *Environ. Sci. Technol.* **1996**, *30*, 1023.

(7) Allamandola, L. J. *Top. Curr. Chem.* **1990**, *153*, 1.

(8) Pope, C. J.; Marr, J. A.; Howard, J. B. *J. Phys. Chem.* **1993**, *97*, 11001.

(9) Richter, H.; Mazyar, O. A.; Sumathi, R.; Green, W. H.; Howard, J. B.; Bozzelli, J. W. *J. Phys. Chem. A.* **2001**, *105*, 1561.

(10) Harris, S. J.; Weiner, A. M.; Blint, R. J. *J. Combust. Flame* **1988**, *72*, 91.

(11) (a) Frenklach, M.; Clary, D. W.; Gardiner, W. C.; Stein, S. E. *Proc. Combust. Inst.* **1984**, *20*, 887. (b) Frenklach, M.; Warnatz, J. *Combust. Sci. Technol.* **1987**, *51*, 265. (c) Frenklach, M.; Wang, H. *23rd International Symposium on Combustion*; The Combustion Institute: Pittsburgh, PA, 1990; p 1559. (d) Frenklach, M. *26th International Symposium on Combustion*; The Combustion Institute: Pittsburgh, PA, 1996; p 2258.

(12) (a) Heuts, J. P. A.; Gilbert, R. G.; Radom, L. *J. Phys. Chem.* **1996**, *100*, 18997; (b) Heuts, J. P. A.; Gilbert, R. G.; Radom, L. *Macromolecules* **1996**, *28*, 8771.

(13) Van Speybroeck, V.; Van Neck, D.; Waroquier, M.; Saeys, M.; Wauters, S.; Marin, G. B. *J. Phys. Chem. A.* **2000**, *104*, 10939.

(14) Van Speybroeck, V.; Borremans, Y.; Van Neck, D.; Waroquier, M.; Wauters, S.; Saeys, M.; Marin, G. B. *J. Phys. Chem. A.* **2001**, *105*, 7713.

(15) Van Speybroeck, V.; Reyniers, M. F.; Marin, G. B.; Waroquier, M.; *ChemPhysChem* **2002**, *3*, 863.

(16) Van Speybroeck, V., Martelé Y., Waroquier, M.; Schacht, E. *J. Am. Chem. Soc.* **2001**, *123*, 10650.

(17) Van Speybroeck, V.; Hemelsoet, K.; Marin, G. B.; Waroquier, M. *Int. J. Quantum Chem.*, published on the Web.

(18) Van Speybroeck, V.; Hemelsoet, K.; Waroquier, M.; Marin, G. B. *J. Comput. Methods Sci. Eng.* **2002**, *2*, 315.

(19) Parr, R. G.; Yang, W. *Density-Functional Theory of Atoms and Molecules*; Oxford Science Publications: Oxford, England, 1988.

(20) Pearson, R. G. *J. Am. Chem. Soc.* **1963**, *85*, 3533.

(21) Geerlings, P.; De Proft, F.; Langenaeker, W. *Chem. Rev.* **2003**, *103*, 1793.

(22) Parr, R. G.; Yang, W., *J. Am. Chem. Soc.* **1984**, *106*, 4049.

(23) Fukui, K. Theory of Orientation and Stereoselection; Springer, Berlin. 1982. *Science* **1982**, *218*, 747.

(24) Klopman, G. *Chemical Reactivity and Reaction Paths*; Wiley: New York, 1974.

(25) Schleyer, P. v. R.; Jiao, H. *Pure Appl. Chem.* **1996**, *68*, 209.

(26) Gomes, J. A. N. F.; Mallion, R. B. *Chem. Rev.* **2001**, *101*, 1349.

(27) (a) Schleyer, P. v. R. *Chem. Rev.* **2001**, *101*, Special Edition "Aromaticity". (b) Zhou, Z. X.; Parr, R. G.; Garst, J. F. *Tetrahedron Lett.* **1988**, *29*, 4843. (c) Zhou, Z. X.; Parr, R. G. *J. Am. Chem. Soc.* **1989**, *111*, 7371.

(28) (a) Vereecken, L.; Peeters, J.; Bettinger, H. F.; Kaiser, R. I.; Schleyer, P. v. R.; Schaefer, H. F., III. *J. Am. Chem. Soc.* **2002**, *124*, 2781. (b) Schleyer, P. v. R.; Manoharan, M.; Jiao, H. J.; Stahl, F. *Org. Lett.* **2001**, *3*, 3643.

(29) (a) Schleyer, P. v. R.; Jiao, H.; Glukhovtsev, M. N.; Chandrasekhar, J.; Kraka, E. *J. Am. Chem. Soc.* **1994**, *116*, 10129. (b) Cossio, F. P.; Morao, I.; Jiao, H.; Schleyer, P. v. R. *J. Am. Chem. Soc.* **1999**, *121*, 6737. (c) Jiao, H.; Schleyer, P. v. R.; Mo, Y.; McAllister, M. A.; Tidwell, T. T. *J. Am. Chem. Soc.* **1997**, *119*, 7075.

(30) Moran, D.; Stahl, F.; Bettinger, H. F.; Schaefer, H. F., III; Schleyer, P. v. R. *J. Am. Chem. Soc.* **2003**, *125*, 6746.

(31) Williams, R. V.; Armantrout, J. R.; Twamley, B.; Mitchell, R. H.; Ward, T. R.; Bandyopadhyay, S. *J. Am. Chem. Soc.* **2002**, *124*, 13495.

(32) De Proft, F.; Geerlings, P. *Chem. Rev.* **2001**, *101*, 1451.

(33) Pearson, R. G. *J. Org. Chem.* **1989**, *54*, 1423.

(34) Roy, R. K.; Pal S., *J. Phys. Chem.* **1995**, *99*, 17822.

(35) Misra, G. P.; Sannigrahi, A. B. *J. Mol. Struct. (THEOCHEM)* **1996**, *361*, 63.

(36) Kar, T.; Sannigrahi, A. B. *Indian J. Chem.* **2000**, *39*, 68.

(37) Chandra, A. K.; Nguyen, M. T. *J. Chem. Soc., Perkin Trans.* **1997**, *2*, 1415.

(38) Chandra, A. K.; Uchimaru, T.; Sugie, M.; Sekiya, A. *Chem. Phys. Lett.* **2000**, *318*, 69.

(39) Korchowiec, J.; Uchimaru, T. *J. Phys. Chem. A* **1998**, *102*, 6682.

(40) Hirata, S.; Head-Gordon, M.; Szczepanski, J.; Vala, M. *J. Phys. Chem. A* **2003**, *107*, 4940.

(41) Nguyen, H. M. T.; Peeters, J.; Nguyen, M. T.; Chandra, A. K. *J. Phys. Chem. A* **2004**, *108*, 484.

(42) Geerlings, P.; De Proft, F. *Int. J. Quantum Chem.* **2000**, *80*, 227.

(43) (a) Galvan, M.; Dal Pino, A.; Joannopoulos, J. D. *Phys. Rev. Lett.* **1993**, *70*, 21. (b) Dal Pino, A.; Galvan, M.; Arias, T. A.; Joannopoulos, J. D. *J. Chem. Phys.* **1993**, *98*, 1606.

(44) Pal, S.; Chandrakumar, K. R. S. *J. Am. Chem. Soc.* **2000**, *122*, 4145.

(45) Nguyen, L. T.; Le, T. N.; De Proft, F.; Chandra, A. K.; Langenaeker, W.; Nguyen, M. T.; Geerlings, P. *J. Am. Chem. Soc.* **1999**, *121*, 5992.

(46) Pérez, P.; Toro-Labbé, A.; Contreras, R. *J. Phys. Chem. A* **1999**, *103*, 11246.

(47) Chattaraj, P. K.; Maiti, B. *J. Am. Chem. Soc.* **2003**, *125*, 2705.

(48) Chermette, H. *J. Comput. Chem.* **1999**, *20*, 129.

(49) Perdew, J. P.; Parr, R. G.; Levy, M.; Balduz, J. L. *Phys. Rev. Lett.* **1982**, *49*, 1691.

(50) Yang, W.; Mortier, W. J. *J. Am. Chem. Soc.* **1986**, *108*, 5708.

(51) De Proft, F., Martin, J. M. L.; Geerlings, P. *Chem. Phys. Lett.* **1996**, *256*, 400.

(52) (a) Chattaraj, P. K.; Lee, H.; Parr, R. G. *J. Am. Chem. Soc.* **1991**, *113*, 1855. (b) Damoun, S.; Van de Woude, G.; Mendez, F.; Geerlings, P. *J. Phys. Chem. A* **1997**, *101*, 886.

(53) Gazquez, J. L.; Mendez, F. *J. Phys. Chem.* **1994**, *98*, 4591.

(54) Seminario, J. M.; Politzer, P. *Modern Density Functional Theory, A Tool for Chemistry*; Elsevier: Amsterdam, 1995.

(55) Mcoche, B.; Gayoso, J.; Ouamerali, O. *Rev. Roum. Chim.* **1984**, *26*, 613.

(56) Fleischer, U.; Kutzelnigg, W.; Lazzaretti, P.; Mühlenkamp, V. *J. Am. Chem. Soc.* **1994**, *116*, 5298.

(57) Schleyer, P. v. R.; Maerker, C.; Dransfeld, A.; Jiao, H.; van Eikema Hommes, N. J. R. *J. Am. Chem. Soc.* **1996**, *118*, 6317.

(58) (a) Schleyer, P. v. R.; Jiao, H.; van Eikema Hommes, N. J. R.; Malkin, V. G.; Malkina, O. *J. Am. Chem. Soc.* **1997**, *119*, 12669. (b) Schleyer, P. v. R., Manoharan, M., Wang, Z−X.; Kiran, B.; Jiao, H. J.; Puchta, R.; van Eikema Hommes, N. J. R. *Org. Lett.* **2001**, *3*, 2465.

(59) Frisch, M. J.; Trucks, G. W.; Schlegel, H. B.; Scuseria, G. E.; Robb, M. A.; Cheeseman, J. R.; Zakrzewski, V. G.; Montgomery, J. A., Jr.; Stratmann, R. E.; Burant, J. C.; Dapprich, S.; Millam, J. M.; Daniels, A. D.; Kudin, K. N.; , Strain, M. C.; Farkas, O.; Tomasi, J.; Barone, V.; Cossi, M.; Cammi, R.; Mennucci, B.; Pomelli, C.; Adamo, C.; Clifford, S.; Ochterski, J.; Petersson, G. A.; Ayala, P. Y.; Cui, Q.; Morokuma, K.; Malick, D. K.; Rabuck, A. D.; Raghavachari, K.; Foresman, J. B.; Cioslowski, J.; Ortiz, J. V.; Stefanov, B. B.; Liu, G.; Liashenko, A.; Piskorz, P.; Komaromi, I.; Gomperts, R.; Martin, R. L.; Fox, D. J.; Keith, T.; Al-Laham, M. A.; Peng, C. Y.; Nanayakkara, A.; Gonzalez, C.; Challacombe, M.; Gill, P. M. W.; Johnson, B. G.; Chen, W.; Wong, M. W.; Andres, J. L.; Head-Gordon, M.; Replogle, E. S.; Pople, J. A. *Gaussian 98*; Gaussian Inc.: Pittsburgh, PA, 1998.

(60) (a) Becke, A. D. *J. Chem. Phys.* **1993**, *98*, 5648. (b) Lee, C.; Yang, W.; Parr, R. G. *Phys. Rev. B* **1988**, *37*, 785.

(61) (a) Petersson, G. A.; Malick, D. K.; Wilson, W. G.; Ochterski, J. W.; Montgomery, J. A.; Frisch, M. J. *J. Chem. Phys.* **1998**, *109*, 10570. (b) Cioslowski, J.; Liu, G.; Piskorz, P. *J. Phys. Chem. A*, **1998**, *102*, 9890. (c) Smith, D. M.; Nicolaides, A.; Golding, B. T.; Radom, L. *J. Am. Chem. Soc.* **1998**, *120*, 10223. (d) Wong, M. W.; Radom, L. *J. Phys. Chem. A* **1998**, *102*, 2237. (e) Koch, W.; Holthausen, M. C. *A Chemist's Guide to Density Functional Theory*; Wiley-VCH: New York 2001.

(62) (a) Parker, C. L.; Cooksy, A. L. *J. Phys. Chem. A* **1998**, *102*, 6186. (b) Lynch, B. J.; Fast, P. L.; Harris, M.; Truhlar, D. G. *J. Phys. Chem. A* **2000**, *104*, 4811.

(63) Saeys, M.; Reyniers, M−F.; Marin, G. B.; Van Speybroeck, V.; Waroquier, M. *J. Phys. Chem. A* **2003**, *107*, 9147.
(64) (a) Reed, A. E.; Weinstock, R. B.; Weinhold. F. *J. Chem. Phys.* **1985**, *83*, 735. (b) Reed, A. E.; Curtiss, L. A.; Weinhold. F. *Chem. Rev.* **1988**, *88*, 899.
(65) Chirlian, L. E.; Francl, M. M. *J. Comput. Chem.* **1987**, *8*, 894.
(66) Besler, B. H.; Merz, K. M., Jr.; Kollman, P. A. *J. Comput. Chem.* **1990**, *11*, 431.
(67) (a) Keith, T. A.; Bader, R. F. W. *Chem. Phys. Lett.* **1993**, *210*, 223. (b) Bader, R. F. W.; Keith, T. A. *J. Chem. Phys.* **1993**, *99*, 3669.
(68) Helgaker, T.; Jaszunski, M.; Ruud, K. *Chem. Rev.* **1999**, *99*, 293.
(69) Gregor, T.; Mauri, F.; Car, R. *J. Chem. Phys.* **1999**, *111*, 1815.
(70) Cheeseman, J. R.; Trucks, G. W.; Keith, T. A.; Frisch, M. J. *J. Chem. Phys.* **1996**, *104*, 5497.
(71) (a) Wauters, S.; Marin, G. B. *Chem. Eng. J.* **2001**, *82*, 267; (b) Wauters, S. Kinetics of coke formation during thermal cracking of hydrocarbons based on elementary reactions. Ph.D. Thesis, University of Ghent, 2001−2002.
(72) Morrisson, R. T.; Boyd, N. R. *Organic Chemistry*, 7th ed.; Allyn and Bacon, Boston, MA, 2003.
(73) Van Speybroeck, V.; Saeys, M.; Marin, G. B.; Waroquier, M.. To be submitted to *J. Phys. Chem. A.*
(74) Chattaraj, P. K. *J. Phys. Chem. A* **2001**, *105*, 511.
(75) Pearson, R. G. *J. Org. Chem.* **1989**, *54*, 1423.
(76) Evans, M. G.; Polanyi, M. *Trans. Faraday Soc.* **1935**, *31*, 875. Evans, M. G.; Polanyi, M. *Trans. Faraday Soc.* **1937**, *33*, 448.
(77) (a) Davico, G. E.; Bierbaum, V. M.; DePuy, C. H.; Ellison, C. B.; Squires, R. R. *J. Am. Chem. Soc.* **1995**, *117*, 2590. (b) Reed, D. R.; Kass, S. R. *J. Mass Spectrometry* **2000**, *35*, 534. (c) Violi, A.; Truong, T. N.; Sarofim, A. F. *J. Phys. Chem. A* **2004**, Published on Web.
(78) Aizman, A.; Contreras, R.; Galvan, M.; Cedillo, A.; Santos, J. C.; Chamorro, E. *J. Phys. Chem. A* **2002**, *106*, 7844.
(79) Fischer, H.; Radom, L. *Angew. Chem., Int. Ed.* **2001**, *40*, 1340.
(80) Patchkovskii, S.; Thiel, W. *J. Mol. Model.* **2000**, *6*, 67.
(81) Ligabue, A.; Pincelli, U.; Lazzaretti, P.; Zanasi, R. *J. Am. Chem. Soc.* **1999**, *121*, 5513.
(82) (a) Galbraith, J. M.; Schreiner, P. R.; Harris, N.; Wei, W.; Wittkopp, A.; Shaik, S. *Chem.−Eur. J.* **2000**, *6*, 1446. (b) De Proft, F., Schleyer, P. v. R.; van Lenthe, J.; Stahl, F.; Geerlings, P. *Chem.−Eur. J.* **2002**, *8*, 3402.

Paper IV

How useful are reactivity indicators for the description of hydrogen abstraction reactions on polycyclic aromatic hydrocarbons?

Hemelsoet K. , Van Speybroeck V. and Waroquier M.

Chem. Phys. Lett., **2006**, submitted

How useful are reactivity indicators for the description of hydrogen abstraction reactions on polycyclic aromatic hydrocarbons?

K. Hemelsoet, V. Van Speybroeck and M. Waroquier

Center for Molecular Modeling, Laboratory of Theoretical Physics, Ghent University, Proeftuinstraat 86, 9000 Ghent, Belgium

Abstract

Hydrogen abstraction reactions at polyaromatic hydrocarbons by a methyl radical are investigated from the viewpoint of DFT-based reactivity descriptors. The BMK functional succeeds in accurately reproducing experimental data for the global indicators. All species are considered as soft. The local HSAB principle shows an overall good qualitative agreement with kinetic barriers, and the local softness is successful for describing the general reactivity trends. However, the indicators do not succeed in predicting the particularly high barriers encountered in some abstraction reactions, as these barriers are mainly caused by steric hindrance effects in the transition structures.

1 Introduction

Polycyclic aromatic hydrocarbons (PAHs) have been intensively studied in modern chemistry, as they play a key role in a large number of different areas [1]. They are the largest known class of chemical carcinogens and mutagens [2,3], they are present in atmospheric aerosols and celestial objects [4] and they are important in the formation process of hollow-cage fullerenes [5]. In addition, PAHs are key intermediate products in soot formation and coal conversion processes [6,7]. More precisely, they can arise from incomplete combustion of organic matter and they are also formed in steam cracking units used in the petroleum industry for the production of light olefines such as ethylene and propylene. In such a reactor the formation of a coke layer -consisting of aromatic rings- on the inner walls of the reactor is observed, reducing the efficiency of the device. In all PAH growth processes [8,9], various classes of elementary reactions such as hydrogen abstraction, addition, cyclization and dehydrogenation reactions can be distinguished [9,10]. Calculations on these

elementary reactions are advisable, as they provide the opportunity to model the complex reaction process [11–16].

In a coke network, the initial radical surface species are formed through hydrogen abstraction reactions by small gas phase precursors, such as methyl and hydrogen radicals. Previously, we performed an elaborate level-of-theory study on the hydrogen abstraction reaction at benzene by a methyl radical, representing a reference reaction [17]. We found that the G3-RAD composite procedure, the URCCSD(T), and the cost-effective DFT methods BMK, BB1K and MPW1K give the best results for calculating accurate and reliable thermochemical and kinetic data. In a second paper of the authors, the study of hydrogen abstraction reactions by a methyl radical has been extended to PAHs, with focus on the influence of the local polyaromatic structure on the thermochemistry and kinetics [18]. In this work a large test set of 16 PAHs, containing up to a maximum of 7 six-membered rings, was studied. We found that, based on the reaction enthalpies, 6 different categories could be distinguished. For abstraction at uncongested locations, a normal Bell-Evans-Polanyi relationship was obtained. However, for the more congested locations this was not the case as some large energy barriers were explained in terms of steric hindrance in the transition structures. Based on kinetic information, we found that abstraction of uncongested hydrogens is preferential and that abstraction is more difficult with increasing PAH size.

Elementary reactions occurring in a coke network, testing a limited number of PAHs, have been already studied by the authors from the viewpoint of DFT-based reactivity indicators [15]. They have been proven successful for a broad variety of mainly soft-soft interactions. For a comprehensive overview, we refer to Geerlings *et al.* [19]. For earlier relevant studies on radical reactions and on the HSAB principle we refer to refs. [20–23]. Hydrogen abstraction reactions between the hydroxyl radical and halomethane compounds were studied by Chandra *et al.*, and a good correlation was observed between the hardness and the activation energy [24]. More recently, Nguyen et al. used the local softness and electronegativity to rationalize different hydrogen abstraction and addition reactions [25]. The reactivity of radical PAHs was investigated by Hirata *et al.* using time-dependent DFT [26]. Very recently, the electron affinity (EA) has been investigated and the direct link with the toxicity of the studied PAH systems was reported [27]. The correlation between reactivity indicators and thermodynamic and/or kinetic data was previously studied by the authors for various neutral, ionic and radical reactions [15,28–30].

The objectives of this letter are twofold. First, we assess whether DFT-based reactivity indicators are capable of providing reliable information about the reactivity sequence of the investigated set of PAHs. Therefore, a comparison with available experimental data is made. Second, we investigate whether the preferential sites for the radical attack are correctly indicated.

2 Theoretical background

DFT-based reactivity indicators are defined as derivatives of the electronic energy $E[N, v(\mathbf{r})]$ with N the total number of electrons and $v(\mathbf{r})$ the external potential [19,31]. Using the finite difference approach, the chemical potential μ, the global hardness η (equal to the Kohn-Sham HOMO-LUMO gap) and global softness S can be computed from the vertical ionization potential (IP) and electron affinity (EA):

$$\mu = -\frac{IP + EA}{2}, \qquad \eta = \frac{IP - EA}{2}, \qquad S = \frac{1}{2\eta}. \tag{1}$$

Site-selectivity can be described using local indicators. The Fukui function $f(\mathbf{r})$ and local softness $s(\mathbf{r}) = Sf(\mathbf{r})$ are predominantly used and have proven very successful for soft-soft interactions. The condensed form of $f(\mathbf{r})$ gives an approximate value at the position of an atomic center [32], for a radical attack one obtains:

$$f_k^0 = (q_k(N+1) - q_k(N-1))/2 \tag{2}$$

with $q_k(N)$ the electron population on the kth atom of the molecule with N electrons.

According to the hard soft acid base (HSAB) principle a reaction will be favored when the softness difference is minimal. This rule can be applied on a global level, resulting in reactivity sequences and on a local level, with the additional advantage of distinguishing the preferential site of attack.

3 Computational details

Full geometry optimizations and frequency calculations for minimum energy and transition-state structures were performed within the Gaussian03 software package [33] using density functional theory (DFT) with the hybrid B3-LYP functional [34,35] and 6-311G(*d,p*) basis set. Subsequent single-point energy calculations were done using both the B3-LYP and BMK functionals, in conjugation with the large 6-311+G(*3df,2p*) basis set. It is well-known that a proper description of the spatially diffuse electron distributions of anions requires a basis set with diffuse functions. Within this view, Modelli et al. recently tested a smaller set of PAHs using the B3-LYP functional and showed that inclusion of the smallest addition of diffuse functions is suitable for a correct description of stable PAH anion states and their corresponding EA values

[27]. In a previous study on hydrogen abstraction reactions by a methyl radical from benzene, the BMK functional was found to be a method of choice in order to obtain accurate and yet cost-effective results for the thermodynamic and kinetic properties of similar radical reactions. In the current paper, the performance of this functional for the calculation of reactivity descriptors is addressed for the first time. For the local reactivity descriptors, the atomic charges were systematically calculated using the CHELPG scheme [36], which is derived from the electrostatic potential and is known to provide accurate and reliable charges.

4 Results and discussion

In Figure 1 an overview is given of the PAHs under study. The complete set can be divided into two sub-categories. The first group includes the series of linear acenes, consisting of benzene (**B**), naphthalene (**N**), anthracene (**A**), tetracene (**T**) and pentacene (**P**). The other group consists of the non-linear structures, including phenanthrene (**PH**), benzo[c]phenanthrene (**BPH**), dibenzo[c,g]phenanthrene (**DBPH**), benz[a]anthracene (**BA**), dibenz[a,j]anthra-cene (**DBA**), coronene (**C**), benzo[a]naphth[2,1-j]anthracene (**BNA**), benzo[a]-phenanthro-[3,4-j]anthracene (**BPHA**), pyrene (**PYR**), perylene (**PER**) and benzo[ghi]-perylene (**BPER**). Hydrogen abstraction reactions by an approaching methyl radical, resulting in the formation of aryl radicals and methane, are investigated. Throughout the present letter, the notation PAH-X refers to the abstraction of hydrogen atom X from the polycyclic aromatic hydrocarbon PAH.

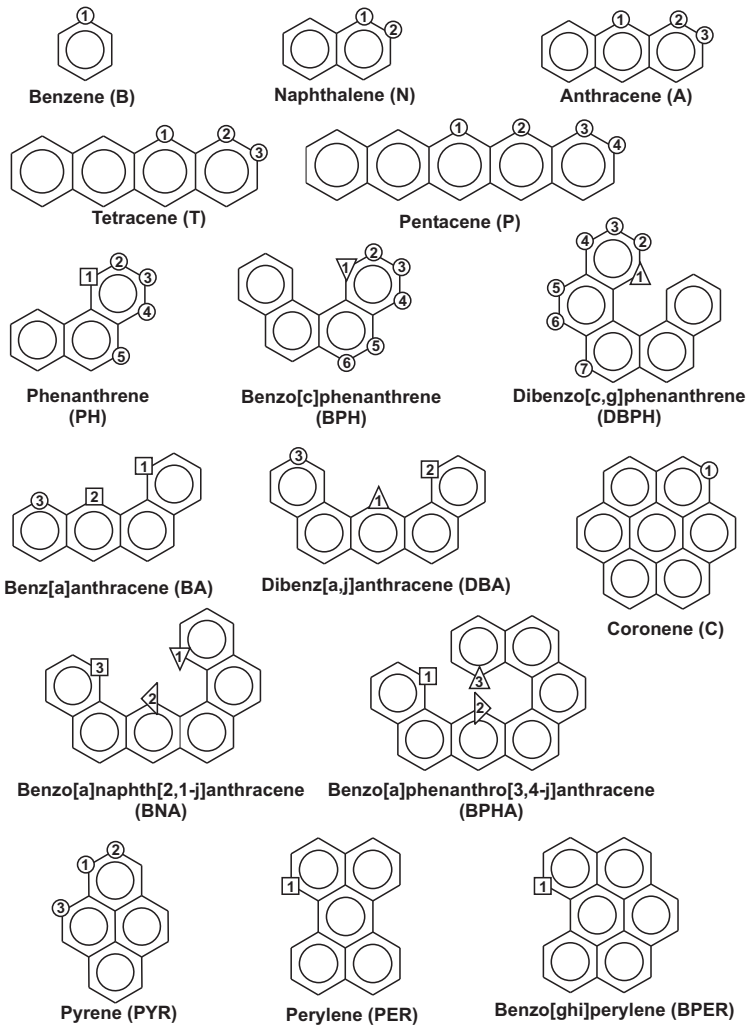

Fig. 1. Structures of polycyclic aromatic hydrocarbons.

	IP	EA	μ	η	S	ΔS
B	9.350	-1.637	-3.857	5.494	2.477 *(2.626)*	0.265
N	8.087	-0.460	-3.814	4.273	3.184 *(3.261)*	0.443
A	7.277	0.379	-3.828	3.449	3.945 *(3.939)*	1.204
T	6.726	0.974	-3.850	2.876	4.731 *(4.610)*	1.990
P	6.331	1.404	-3.867	2.464	5.523 *(5.195)*	2.781
PH	7.853	-0.297	-3.778	4.075	3.339 *(3.570)*	0.598
BPH	7.521	0.145	-3.833	3.688	3.689 *(3.720)*	0.948
DBPH	7.395	0.220	-3.808	3.588	3.792 *(-)*	1.051
BA	7.273	0.400	-3.836	3.437	3.959 *(3.854)*	1.218
DBA	7.287	0.410	-3.849	3.439	3.956 *(3.996)*	1.215
BNA	7.048	0.648	-3.848	3.200	4.251 *(-)*	1.510
BPHA	6.996	0.657	-3.827	3.170	4.293 *(-)*	1.551
C	7.295	0.318	-3.806	3.488	3.900 *(3.990)*	1.159
PYR	7.333	0.240	-3.786	3.547	3.836 *(3.929)*	1.095
PER	6.826	0.821	-3.824	3.002	4.532 *(4.545)*	1.791
BPER	7.068	0.577	-3.822	3.246	4.192 *(4.031)*	1.451

Table 1
IP, EA, μ , η, all in eV and S and ΔS in au^{-1}, calculated at BMK/6-311+G(*3df,2p*)//B3-LYP/6-311G(*d,p*) level. Experimental S are given in italics between parentheses. ΔS values give differences between the global softness of the PAH and the methyl radical ($S = 2.741$ au^{-1}).

The ionization potential IP, electron affinity EA, and derived global indicators μ, η and S were calculated. First of all the performance of the B3-LYP and BMK functionals was tested . We found that the influence of the functional used for the single-point energy calculation is very limited, and no qualitative changes were obtained for the calculated reactivity sequences. An average absolute deviation of 0.001 eV is found between the two methods for μ. For η and S, the BMK values are on average 0.148 eV higher and 0.180 eV lower than the calculated B3-LYP values, respectively. Comparison with experimental IP and EA data showed that overall, a better agreement was found with the IP BMK values, whereas the experimental EA values are better reproduced using the B3-LYP functional.

The results using the BMK/6-311+G(*3df,2p*)//B3-LYP/6-311G(*d,p*) level of theory are given in Table 1. Available experimental data for the global softness, based on experimental IP and EA values, are also given. The calculated EA values show that the majority of the studied PAHs correspond to stable anion states (corresponding to positive EA values); the only exceptions are **B**, **N** and **PH** ($EA < 0$). In general, all optimized species are considered as soft, since all are found in the range between 2.477 and 5.523 au^{-1}. Table 1 also shows that the S values match very well the corresponding experimental values. The calculated values of **N**, **A**, **BPH**, **DBA**, **C**, **PYR** and **PER** reproduce their experimental counterparts within 0.1 au^{-1} (≈ 0.004 eV^{-1}). The largest

discrepancy is noticed for **P**, although the overestimation of the experimental value by 0.3 au^{-1} ($\approx$ 0.01 eV^{-1}) is still limited. This excellent agreement is mainly due to error cancellation between the IP and EA contributions. For the series of linear acenes, it is seen that an increase in molecular size corresponds to an increase of the EA value. This indicates that the larger the linear polyaromatic becomes, the more stable the corresponding anion is. In combination with decreasing IP values, this behavior is also observed for S, demonstrating a higher reactivity for the larger linear molecules. It is also seen that the absolute values of the chemical potential of the PAHs (Table 1) are lower than that of the methyl radical (μ = -4.749 eV), indicating the electrophilic behavior of the methyl radical.

Furthermore the applicability of the global HSAB principle is tested. Therefore, calculated ΔS values - indicating the difference between the global softness of the PAH molecule on one hand and the global softness of the attacking methyl radical (S = 2.741 au^{-1}) on the other - are compared with calculated barriers at 0 Kelvin (ΔE_0 in kJ mol^{-1}). All barriers are given in Table 2. In a search for a possible correlation between ΔS and the reaction barriers ΔE_0, we plot them in Fig. 2, but there is manifestly no correlation between the two quantities.

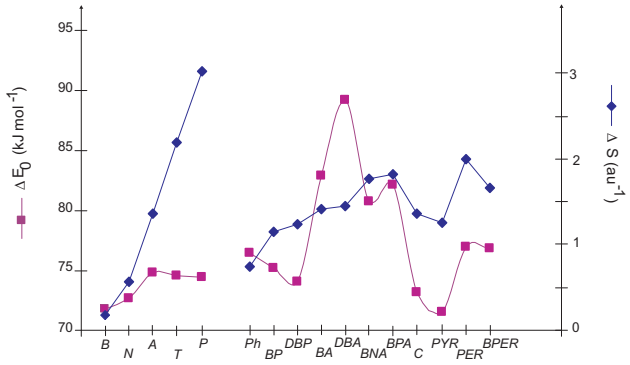

Fig. 2. Global softness differences ΔS (au^{-1}) and energy barriers at 0 Kelvin ΔE_0 (kJ mol^{-1}) for hydrogen abstraction reactions at PAHs by a methyl radical.

Summarizing, the experimental data are reproduced in a satisfactory way and the global descriptors succeed in correctly describing the reactivity of the PAH molecules. However, the hydrogen abstraction reactions under study do not follow the global HSAB principle, indicating that the dominant factors for these reactions are not hard/soft acid/base considerations.

While global properties may explain reactivity, site-selectivity is described by local quantities such as the Fukui function and local softness. We investigate whether these indicators are able to predict which hydrogen atom is preferred for abstraction. Therefore, the applicability of the local HSAB principle is

i	**N**	**A**	**T**	**P**	**PH**
1	2.742 (72.68)	2.810 (74.76)	2.790 (74.57)	2.778 (74.37)	2.758 (76.46)
2	2.673 (71.75)	2.723 (72.60)	2.709 (72.06)	2.777 (74.15)	2.707 (71.55)
3		2.678 (71.29)	2.673 (70.29)	2.705 (71.51)	2.685 (71.97)
4				2.669 (70.79)	2.748 (72.44)
5					2.764 (72.16)
i	**BPH**	**DBPH**	**BA**	**DBA**	**BNA**
1	2.797 (75.22)	2.788 (74.06)	2.744 (76.91)	2.817 (89.17)	2.822 (72.76)
2	2.713 (71.57)	2.731 (71.89)	2.825 (82.88)	2.772 (76.19)	2.896 (80.74)
3	2.710 (72.24)	2.698 (73.01)	2.740 (72.84)	2.740 (71.29)	2.805 (76.55)
4	2.756 (72.77)	2.761 (73.31)			
5	2.727 (73.09)	2.766 (73.67)			
6	2.721 (72.55)	2.732 (72.52)			
7		2.718 (73.84)			
	BPHA	**C**	**PYR**	**PER**	**BPER**
1	2.833 (77.56)	2.730 (73.16)	2.730 (73.33)	2.740 (76.95)	2.745 (76.81)
2	2.962 (82.18)		2.677 (71.50)		
3	2.782 (73.46)		2.760 (71.86)		

Table 2
$\Delta s_{C,H_i}$ using the CHELPG scheme. ΔE_0, scaled ZPVE included, are given in parentheses. Calculated at BMK/6-311+G(*3df,2p*)//B3-LYP/6-311G(*d,p*) level.

tested. The softness differences $\Delta s_{C,H_i}$ between the local softness of the carbon atom of the methyl group ($s_C = 2.849$ au^{-1}) and the local softness of the various hydrogen atoms of the PAHs are given in Table 2.

The Δs values are scarcely varying for the linear PAHs. The variations are somewhat larger for the non-linear PAHs but still limited to maximum 0.28 au^{-1}. Despite their small differences, we notice correct correlation between Δs and ΔE_0 for the various linear acenes. Even the site-selectivity is correctly predicted by the local softness in each linear acene under study, giving preference to a hydrogen abstraction at the outer rings. This correct behavior seems to be also valid for the non-linear series, but there are clearly some pertinent exceptions, for example **BNA**. In **BNA** the lowest energy barrier is not found at site 3, which corresponds with the lowest Δs. The Δs-ΔE_0 correlation is not perfect. Even when the local HSAB principle works well in most cases, there are exceptions where the principle fails. The largest barrier is observed for the **DBA**-1 abstraction reaction. The barrier amounts to 89.17 kJ mol^{-1} due to steric hindrance in the transition structure. This is not reflected in the local softness value of 2.817 au^{-1}, which globally belongs to the largest values obtained, but is not uniquely the largest one. Summarizing, the local HSAB principle does not work perfectly, and this is probably due to an insufficient

incorporation of the local environment in the evaluation of the local softness, in contrary to the description of the kinetics of the reaction. In this context, it is not surprising that the classification of the various H-abstraction reactions or PAHs into six distinct sites on basis of ab initio obtained reaction enthalpies is not reproduced at all by the local softness. Kinetics contains information of reactant(s), transition state(s) and product(s), and we agree that the descriptors carry only information on the reactant(s).

In addition to previous discussion, Figure 3 illustrates the three-dimensio-nal isosurfaces of the radical Fukui function $f^0(\mathbf{r})$ for the PAHs **T**, **DBA**, **DBPH** and **BPHA**. For the linear **T** molecule, it is seen that no distinction can be made between the different hydrogens, the preference for abstraction at non-central rings is too subtle. For the non-planar **DBPH** reactant, it is also hard to differentiate between hydrogen numbers 2 until 7, whereas hydrogen atom number 1 is clearly characterized by a deviating reactivity. The Fukui function is almost negligible for this hydrogen, confirming that abstraction at the congested site of this molecule is very hard. The **DBA** and **BPHA** $f^0(\mathbf{r})$ have surprising features, as hydrogen 1 and 2, respectively, show a non-negligible lobe whereas these atoms correspond to very high barriers. The $f^0(\mathbf{r})$ surfaces show deviating behavior from the condensed Δs values.

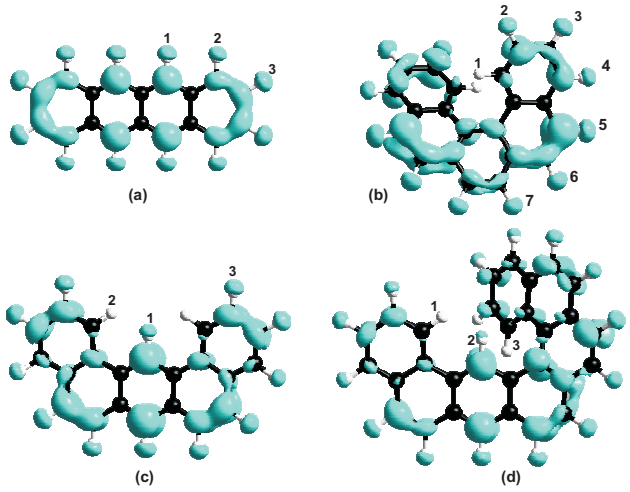

Fig. 3. Isosurfaces (value 0.003 au) for the radical Fukui functions $f^0(\mathbf{r})$ in the case of the (a) T, (b) DBP, (c) DBA and (d) BPA reactants.

Summarizing, we can conclude that based on local descriptors it is possible to indicate the preferred site of abstraction for most PAHs, as the minimal Δs value corresponds to the minimal ΔE_0 barrier. The condensed local descriptors are found suitable to describe the preferential site of attack, whereas the three-dimensional should be treated with utmost care. Exceptional high barriers can not be explained, as these exceptions are largely due to steric hindrance effects

in the corresponding transition structures.

5 Conclusions

We have critically analyzed the performance of various DFT-based reactivity descriptors. A large set of polyaromatic molecules (PAHs) was tested and the reactivity sequence of the involved species is investigated. We compared computational results using the B3-LYP and BMK functionals for the single-point energy calculations, in conjugation with the 6-311+G(*3df,2p*) basis set, with experimental data for the ionization potential, electron affinity and derived properties such as the chemical potential and global hardness. The influence of the level of theory was found to be very limited and no qualitative changes in the reactivity sequences were obtained. All PAH molecules are considered as soft and a good agreement with experiment is found. The behavior of the series of linear acenes is highlighted, indicating the increased reactivity for the larger species. It is furthermore also concluded that global hard/soft acid/base considerations can not explain the reactivity of the studied hydrogen abstraction reactions, as the global HSAB principle fails. From a local viewpoint however, a good qualitative agreement is obtained between local softness differences and reaction barriers at 0 Kelvin. The local softness is well-suited to predict the preferred hydrogen for abstraction by a methyl radical. Due to the fact that the descriptors solely use information of the reactants, none of them succeed in explaining some exceptional high reaction barriers, as these are due to steric hindrance effects in the transition structures.

References

[1] Gonzales J. M., Barden C. J., Brown S. T., Schleyer P. v. R., Schaefer H. F. III, and Li Q.-S., *J. Am. Chem. Soc.* **125**, pp. 1064 (2003).

[2] Harvey R. G., *Polycyclic Aromatic Hydrocarbons: Chemistry and Carcinogenicity*, Cambridge University Press: Cambridge (1991).

[3] Denissenko M. F., Pao A., Tang M. S., and Pfeifer G. P., *Science* **274**, pp. 430 (1996).

[4] Léger A., d'Hendecourt L., and Boccara N., *Polycyclic Aromatic Hydrocarbons and Astrophysics*, NATO ASI Ser., Ser. C 191 Reidel, Dordrecht (1987).

[5] Kroto H. W., Heath J. R., O'Brien S. C., Curl R. F., and Smalley R. E., *Nature* **318**, pp. 162 (1985).

[6] Richter H., Mazyar O. A., Sumathi R., Green W. H., Howard J. B., and Bozzelli J. W., *J. Phys. Chem. A* **105**, pp. 1561 (2001).

[7] Harris S. J., Weiner A. M., and Blint R. J., *J. Combust. Flame* **72**, pp. 91 (1988).

[8] Frenklach M. and Warnatz J., *Combust. Sci. Technol.* **51**, pp. 265 (1987).

[9] Vereecken L., Peeters J., Bettinger H. F., Kaiser R. I., Schleyer P. v. R., and Schaefer H. F. III, *J. Am. Chem. Soc.* **124**, pp. 2781 (2002).

[10] Wauters S. and Marin G. B., *Chem. Eng. J.* **82**, pp. 267 (2001).

[11] Van Speybroeck V., Van Neck D., Waroquier M., Saeys M., Wauters S., and Marin G. B., *J. Phys. Chem. A* **104**, pp. 10939 (2000).

[12] Van Speybroeck V., Borremans Y., Van Neck D., Waroquier M., Wauters S., Saeys M., and Marin G. B., *J. Phys. Chem. A* **105**, pp. 7713 (2001).

[13] Van Speybroeck V., Reyniers M.-F., Marin G. B., and Waroquier M., *ChemPhysChem* **3**, pp. 863 (2002).

[14] Van Speybroeck V., Hemelsoet K., Waroquier M., and Marin G. B., *Int. J. Quant. Chem.* **96**, pp. 568 (2004).

[15] Hemelsoet K., Van Speybroeck V., Marin G. B., De Proft F., Geerlings P., and Waroquier M., **108**, pp. 7281 (2004).

[16] de Bruin T. J. M., Lorant F., Toulhoat H., and W. A. III Goddard, *J. Phys. Chem. A* **108**, pp. 10302 (2004).

[17] Hemelsoet K., Moran D., Van Speybroeck V., Waroquier M., and L. Radom, *J. Phys. Chem. A* **110**, pp. 8942 (2006).

[18] Hemelsoet K., Van Speybroeck V., Moran D., Marin G. B., L. Radom, and Waroquier M., *J. Phys. Chem. A*.

[19] Geerlings P., De Proft F., and Langenaeker W., *Chem. Rev.* **103**, pp. 1793 (2003).

[20] Roy R. K. and Pal S., *J. Phys. Chem.* **99**, pp. 17822 (1995).

[21] Misra G. P. and Sannigrahi A. B., *J. of Molecular Structure (Theochem)* **361**, pp. 63 (1996).

[22] Chandra A. K. and Nguyen M. T., *J. Chem. Soc. Perkin Trans. 2* , p. 1415 (1997).

[23] Korchowiec J. and Uchimaru T., *J. Phys. Chem. A* **102**, pp. 6682 (1998).

[24] Chandra A. K., Uchimaru T., Sugie M., and Sekiya A., *Chem. Phys. Lett.* **318**, pp. 69 (2000).

[25] Nguyen H. M. T., Peeters J., Nguyen M. T., and Chandra A. K., *J. Phys. Chem. A* **108**, pp. 484 (2004).

[26] Hirata S., Head-Gordon M., Szczepanski J., and Vala M., *J. Phys. Chem. A* **107**, pp. 4940 (2003).

[27] Modelli A., Mussoni L., and Fabbri D., *J. Phys. Chem. A* (2006).

[28] Van Cauter K., Hemelsoet K., Van Speybroeck V., Reyniers M.-F., and Waroquier M, *Int. J. Quant. Chem.* **102**, pp. 7281 (2005).

[29] Hemelsoet K., Lesthaeghe D., Van Speybroeck V., and Waroquier M., **419**, pp. 10 (2006).

[30] Van Speybroeck V., Moonen K., Hemelsoet K., Stevens C. V., and Waroquier M., *J. Am. Chem. Soc.* **128**, pp. 8468 (2006).

[31] Parr R. G. and Yang W., *Density-Functional Theory of Atoms and Molecules*, Oxford Science Publications (1988).

[32] Yang W. and Mortier W. J., *J. Am. Chem. Soc.* **108**, pp. 5708 (1986).

[33] Frisch M. J., Trucks G. W., Schlegel H. B., Scuseria G. E., Robb M. A., Cheeseman J. R., Montgomery J. J. A., Vreven T., Kudin K. N., Burant J. C., Millam J. M., Iyengar S. S., Tomasi J., Barone V., Mennucci B., Cossi M., Scalmani G., Rega N., Petersson G. A., Nakatsuji H., Hada M., Ehara M., Toyota K., Fukuda R., Hasegawa J., Ishida M., Nakajima T., Honda Y., Kitao O., Nakai H., Klene M., Li X., Knox J. E., Hratchian H. P., Cross J. B., Bakken V., Adamo C., Jaramillo J., Gomperts R., Stratmann R. E., Yazyev O., Austin A. J., Cammi R., Pomelli C., Ochterski J. W., Ayala P. Y., Morokuma K., Voth G. A., Salvador P., Dannenberg J. J., Zakrzewski V. G., Dapprich S., Daniels A. D., Strain M. C., Farkas O., Malick D. K., Rabuck A. D., Raghavachari K., Foresman J. B., Ortiz J. V., Cui Q., Baboul A. G., Clifford S., Cioslowski J., Stefanov B. B., Liu G., Liashenko A., Piskorz P., Komaromi I., Martin R. L., Fox D. J., Keith T., Al-Laham M. A., Peng C. Y., Nanayakkara A., Challacombe M., Gill P. M. W., Johnson B., Chen W., Wong M. W., Gonzalez C., and Pople J. A., *Gaussian 03, Revision C2, Gaussian,*, Inc.: Wallingford CT (2004).

[34] Becke A. D., *J. Chem. Phys.* **98**, pp. 5648 (1993).

[35] Lee C., Yang W., and Parr R. G., *Phys. Rev. B* **37**, pp. 785 (1988).

[36] Chirlian L. E. and Francl M. M., *J. Comput. Chem.* **8**, pp. 894 (1987).

Paper V

Reactivity and aromaticity of polyaromatics in radical cyclization reactions

Van Speybroeck V. , Hemelsoet K. , Waroquier M. and Marin G. B.

Int. J. Quant. Chem., **2004**, *96*, 568–576

Reactivity and Aromaticity of Polyaromatics in Radical Cyclization Reactions

V. VAN SPEYBROECK,[1] K. HEMELSOET,[1] M. WAROQUIER,[1] G. B. MARIN[2]

[1]*Laboratory of Theoretical Physics, Universiteit Gent, Proeftuinstraat 86, B-9000 Gent, Belgium*
[2]*Laboratorium voor Petrochemische Techniek, Universiteit Gent, Krijgslaan 281-S5, B-9000 Gent, Belgium*

Received 6 September 2002; accepted 28 May 2003

DOI 10.1002/qua.10758

ABSTRACT: Theoretical ab initio calculations are presented on cyclization reactions of polyaromatics that occur by a radical mechanism. Such processes are one of the elementary steps for polyaromatic hydrocarbon formation in thermal cracking units and during soot formation. Ring closure can take place at various sites of the polyaromatic surface. It is the aim of this study to obtain insight into the influence of the local structure on the reactivity of the polyaromatics. Aromaticity is a determining factor for the reactivity and can be probed by various magnetic properties such as the diamagnetic susceptibilities, proton chemical shifts, and nucear-independent chemical shifts. A correlation is established between the magnetic properties and activation energy of the studied reactions. Int J Quantum Chem 96: 568–576, 2004

Key words: radical reactions; density functional calculations; kinetics; magnetic properties

Introduction

A better understanding of polycyclic aromatic hydrocarbons (PAHs) is of growing scientific interest during the last years. Some of them show evidence for mutagenic or tumorigenic properties; also, their presence in atmospheric aerosols, many celestial objects such as planetary nebulae, reflection nebulae, and active galaxies have been shown, and they play an important role in the formation of hollow-cage fullerenes [1–8]. PAHs are also key intermediates and products in carcinogen and soot formation processes and in coal conversion processes [9–12]. They can arise from incomplete combustion of organic matter and as side products in a thermal cracking unit used in the petroleum indus-

Correspondence to: V. Van Speybroeck; e-mail: veronique.vanspeybroeck@rug.ac.be

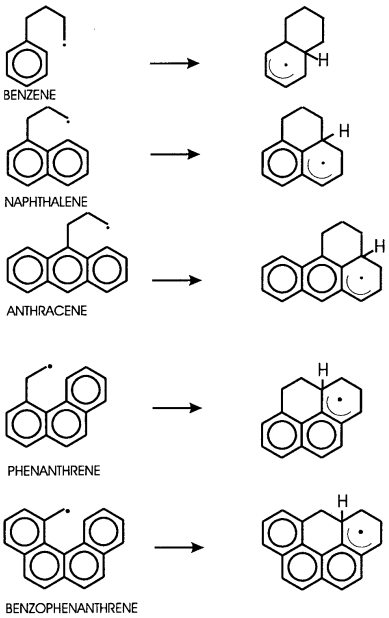

FIGURE 1. Cyclization reactions with polyaromatics.

try for the production of light olefines such as ethene. A quantitative understanding of the formation of PAH molecules is essential for an efficient design of clean and practical combustion devices such as engines and incinerators and of thermal cracking units to maximize the run length.

In this article we study cyclization reactions of alkyl radicals attached to a substrate consisting of various benzene rings (Fig. 1). These types of reactions lead to incorporation of new carbon atoms in the already formed surface. The focus is to get insight into the influence of the local polyaromatic structure on the kinetics and reactivity of the PAHs during ring closure.

Theoretical models can give a valuable contribution to quantify the kinetics of chemical reactions and obtain insight into the factors that govern PAH formation. One can estimate the reactivity of the involved clusters toward ring closure by calculating the corresponding rate constants. This can be done by means of transition-state theory (TST) and performing ab initio calculations on all reactants and activated complexes. This procedure was followed in one the previous articles of the authors [13]. It was found that the activation energy is largely determined by the local polyaromatic structure and its aromaticity. This conclusion was, however, made on the basis of chemical intuition, such as considerations about the planarity of the substrate. Aromatic species have the ability to sustain a diatropic ring current. This property can be quantified using various magnetic criteria such as the diamagnetic susceptibilities, proton chemical shifts, and nuclear-independent chemical shifts [14, 15]. In this work various magnetic properties of the reactants and transition states are calculated with the aim to correlate the kinetic results with the degree of aromaticity of the species. The article is organized as follows: First, we briefly comment on the applied theoretical procedures. In the Results and Discussion section, a short overview of the kinetic results is presented, which is needed for the transparency of this article. The last section gives a thorough discussion of the magnetic properties of the various complexes.

Theoretical Details

All ab initio calculations were carried out with the Gaussian 98 software package within the density functional theory (DFT) framework by using Becke's three-parameter hybrid B3LYP functional [16–18]. The molecular orbitals are expanded in the triple-ζ 6-311G basis augmented with single first d and p polarization functions [19]. Several studies have indicated that B3LYP and even Hartree–Fock (HF) methods are sufficiently accurate for the estimation of the relative stabilities of different conformers, especially when large basis sets including polarization functions are used [20–22]. According to specific studies on similar radical reactions, the B3LYP method gives a reliable and quantitatively good description of geometries, frequencies, reaction barriers, and pre-exponential factors. In this case, where the system of interest is large, B3LYP provides a viable alternative for more computational intensive methods like CBS, G2, or CBS-RAD procedures [23–26]. Our calculations show that the spin contamination is limited, giving values for the spin-squared expectation close to 0.75. DFT calculations are known to show systematically less spin

contamination in the Kohn–Sham wave function than other unrestricted HF-based methods [27]. Energy minima were located by full geometry optimizations with the Berny algorithm [28, 29]. The vibrational frequencies of the optimized structures are also calculated at the same level of theory. It is well known that the B3LYP harmonic vibrational frequencies are systematically larger than the observed experimental frequencies. The overestimation, however, is found to be relatively uniform, and as a result generic frequency scaling factors are often applied. A scaling factor of 0.9614 is applied to the frequencies in the evaluation of the partition functions while the zero-point vibrational energies are scaled with 0.9806 [30].

The kinetic parameters are calculated by means of TST [31–35], which has proven its success in many studies for the quantitative prediction of macroscopic kinetic quantities of chemical reactions [23, 36–40]. In TST the rate coefficient for the reaction $A \rightarrow B$ is given by

$$k(T) = \frac{k_B T}{\hbar} \frac{q_{\ddagger}}{q_A} e^{-(\Delta E_0/k_B T)}, \quad (1)$$

where k_B represents the Boltzman constant, T is the temperature, $\hbar$ is the Planck constant, ΔE_0 represents the molecular energy difference at the absolute zero between the activated complex and the reactant (with inclusion of the zero-point vibrational energies), and $q_{\ddagger}$ and q_A are the molecular partition functions of the transition state and reactant, respectively. The molecular properties, such as geometries (moments of inertia), ground-state energies, and frequencies, required for the evaluation of the partition functions and the reaction barrier ΔE_0 are obtained by ab initio molecular calculations. The molecular partition function contains rotational, electronic, vibrational, and translational contributions. Internal rotations are treated in the harmonic oscillator approximation to keep the problem computationally feasible. Moreover, as the coke environment becomes larger the rotational potential barriers are expected to increase, making the influence of internal rotations less important [13].

The magnetic properties [magnetic susceptibilities (χ, ppm cgs), ^{1}H NMR chemical shifts (δ, ppm), nucleus-independent chemical shifts (NICS)] are calculated on the optimized geometries at the B3LYP/6-311G** level using the continuous set of gauge transformations (CSGT)/6-311G** method [41]. The CSGT method, developed by Kiefer and Bader, achieves gauge invariance by performing a continuous set of gauge transformations, one for each point in real space. An accurate 3-D description of the first-order electronic current density is obtained, from which the shielding tensors and magnetic susceptibility can be determined. Studies on a large number of molecules reveal that the CSGT method is computationally efficient and much more accurate than any single-origin method for any basis set, especially for larger molecules [41].

Results and Discussion

AB INITIO STUDY ON CYCLIZATION REACTIONS

The studied reactions are radical cyclizations, which are one of the finalizing steps toward formation of a new cyclic structure on a former aromatic. The local structure of the reactive site is varied to get insight into its influence on the reactivity. Five clusters are considered as schematically shown in Figure 1. The nomenclature is based on the smallest aromatic that exhibits the same local structure. For cyclization the minimum number of carbon atoms that have to be added to allow the formation of a new six-membered ring varies from 4 to 0 depending on the local structure of the polyaromatic.

A detailed discussion of the geometries and frequencies was given in Ref. [13]. We only give a brief overview of the results for the understanding of this article.

For the geometry of the reactants a major distinction can be made between the benzene-, naphtalene-, and anthracene-like sites and the phenanthrene- and benzophenanthrene-like sites. The structures of the optimized reactants are shown in Figure 2. In the first class, the reactants are all flat-type clusters, i.e., the substrate remains in an almost planar conformation because the attached alkyl chain causes minimal perturbations on the geometry of a pure aromatic. The second class are the so-called folded clusters. Due to large steric hindrance between the attached alkyl chain and the substrate, strong deviations from planarity are present in the substrate and the aromaticity is partially broken in the reactant.

The transition states for cyclization are obtained by gradually decreasing the values of the forming C—C bond. The optimized structures of the activated complexes are shown in Figure 3. For the flat clusters the deviations from planarity at the reac-

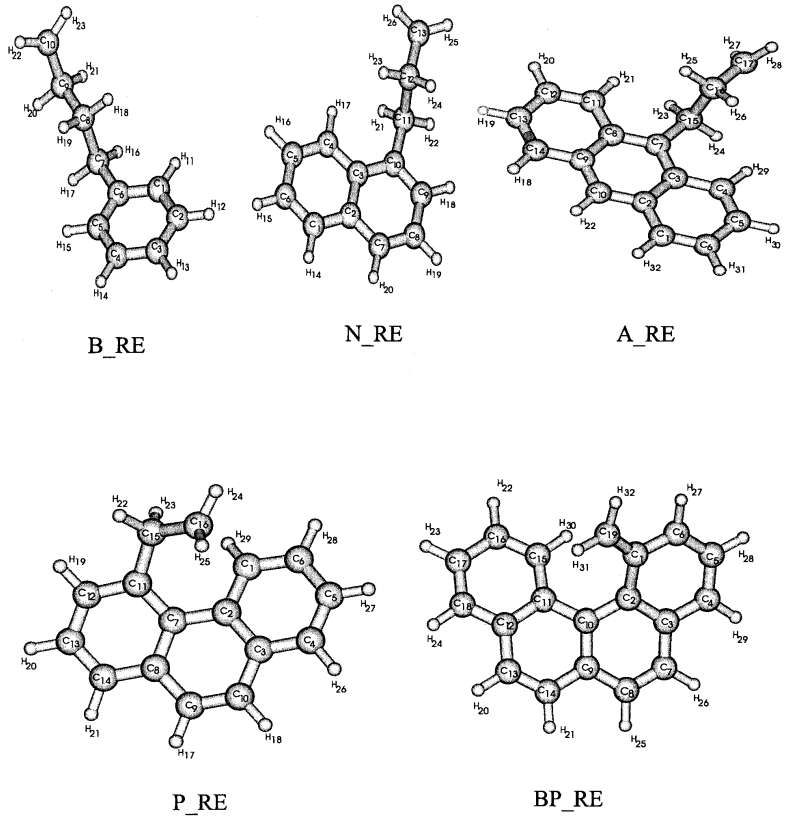

FIGURE 2. Optimized structures of reactants.

tive center of the substrate are small, while the folded clusters exhibit a helix-like structure in the transition state for cyclization. More details about geometries and vibrations can be found in Ref. [13].

KINETICS OF THE CHEMICAL REACTIONS

The influence of the local polyaromatic structure on the reactivity toward cyclization can be estimated by calculating the kinetic parameters by means of TST and DFT. This method has proven its accuracy for the calculation of the reaction kinetics of various radical reactions [39, 40].

All necessary microscopic quantities like the partition functions are obtained by the ab initio calculations. In this case we are interested in the kinetics in the temperature range from 700–1100 K, which is typical for the formation of PAHs during thermal

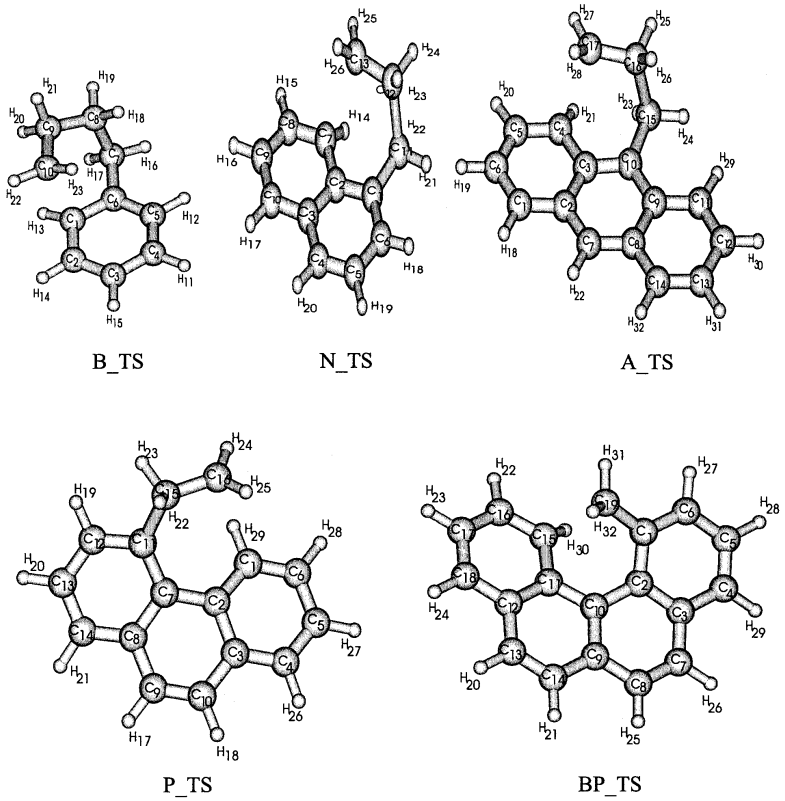

FIGURE 3. Optimized structures of transition states.

cracking of hydrocarbons. The resulting kinetic parameters—the activation energy and pre-exponential factor—are listed in Table I.

The kinetic parameters for the cyclization reactions vary strongly for the various clusters. For the flat clusters the activation energy is lowered the more aromatic rings are involved, supporting the general concept of maximum overlap of the π-orbital that is being attacked and the π-system of the substrate, leading to a stabilization of the transition state.

For the folded sites two aspects are important: the reactivity of the substrate and the radical species. The variation of the pre-exponential factor must be traced back to the number of carbon atoms of the alkyl chain and the corresponding conformational flexibility of the reactant complex. For more details see Ref. [13].

TABLE I
Kinetic and magnetic properties of the cyclization reactions.

	E_A	A	$\Delta\chi$	R	NICS^{av}	NICS^{TS}	^{1}H	T
B			−65.65365		−12.8035		6.3453	
B_{RE}			−65.38265		−12.3032		6.2936	
B_{TS}	47.44	1.0×10^{10}	−54.69770	16.34×10^{-2}	−6.8403	−2.3700	5.8119	0.4817
N			−127.36175		−13.0264		6.6738	
N_{RE}			−131.13430		−12.5336		6.7010	
N_{TS}	46.32	9.8×10^{10}	−111.21795	15.19×10^{-2}	−8.9492	−3.4600	6.2119	0.4891
A			−191.51945		−13.1573		6.9333	
A_{RE}			−191.37540		−12.7381		6.9720	
A_{TS}	39.23	1.9×10^{11}	−177.01230	7.51×10^{-2}	−10.1958	−4.4782	6.5566	0.4154
P			−178.80050		−11.8881		6.8796	
P_{RE}			−174.54725		−11.7674		6.8051	
P_{TS}	31.50	3.0×10^{11}	−165.50605	5.18×10^{-2}	−11.1099	−4.0955	6.6622	0.1429
BP			−317.28835		−11.5334		7.0161	
BP_{RE}			−201.19380		−9.6293		6.5986	
BP_{TS}	50.11	1.9×10^{12}	−207.22710	-2.99×10^{-2}	−9.8891	4.9709	6.6507	−0.0521

E_A (kJ/mol), A (1/s), $\Delta\chi$ (ppm cgs), NICS^{av} (ppm), NICS^{TS} (ppm), and ^{1}H (ppm) are, respectively, the activation energy, pre-exponential factor, diamagnetic susceptibility anisotropy, average of the NICS values computed at the rings of the substrate, NICS value of the newly forming ring in the transition state, and proton chemical shifts. R and T are defined according to formulas (4) and (5). The subscripts *RE* and *TS* are abbreviations for the reactant and transition state, respectively.

MAGNETIC PROPERTIES

Previous discussion reveals that the aromaticity of the substrate is an important factor for the reactivity of the polyaromatic during cyclization. Aromaticity can be defined as the ability of a compound to sustain an induced ring current, although various definitions have been put forward for the concept of aromaticity. For a more general review see Ref. [14]. The aromaticity can be efficiently probed by various magnetic properties, such as the diamagnetic susceptibility anisotropy, the proton chemical shifts, and nucleus-independent chemical shift computed at ring centers. In what follows we compute these properties for all involved reactants and transition states and try to establish a correlation between the various magnetic properties and the kinetics of the cyclization reactions.

Diamagnetic Susceptibility Anisotropy

The diamagnetic susceptibility tensor is defined as

$$\bar{\bar{\chi}} = \frac{\delta^2 E}{\delta \vec{B} \delta \vec{B}_{\vec{B}=0}}. \tag{2}$$

Aromatic molecules were found to possess high diamagnetic susceptibility ansitropies $\Delta\chi$, i.e., large differences between the perpendicular and average in-plane component of the diamagnetic susceptibility. $\Delta\chi$ is defined as

$$\Delta\chi = \chi_{zz} - \frac{1}{2}(\chi_{xx} + \chi_{yy}), \tag{3}$$

where χ_{xx}, χ_{yy}, and χ_{zz} are the three principal moments of the diamagnetic susceptibility tensor. However, the values are highly dependent on the size of the system. Therefore, it needs suitable calibration standards [42]. The values of $\Delta\chi$ of all involved species during reaction are listed in Table I. We also included the values for the pure aromatics, without the additional alkyl chain. The nomenclature is as follows: B, N, A, P, BP stands for benzene, naphtalene, anthracene, phenanthrene, and benzophenanthrene. We stress that the values of $\Delta\chi$ can only be compared for molecules of the same size. This means that we can compare N_{RE} with N_{TS} or A with P but not N_{RE} with N. From comparison of A with P, it follows that anthracene is more aromatic than phenanthrene due to the specific ordering of the rings.

All transition states are less aromatic than the reactants except for benzophenanthrene. This is due to the benzylic type of radical involved in the cyclization. To compare the values of $\Delta\chi$ for all reactions we introduced a new property that is size independent and unitless:

$$R = \frac{\Delta\chi(TS) - \Delta\chi(RE)}{\Delta\chi(RE)}. \quad (4)$$

A correlation can now be established between this new property R and the activation energy. The larger the value of R, the larger the difference in aromaticity between the transition state and reactant and the higher the activation energy. For benzophenanthrene a negative value is found, indicating that not only the reactivity of the substrate is important but also the type of radical. In this case the substrate is highly reactive due to its folded nature, while the attacking radical is less reactive due to its benzylic type.

Proton Chemical Shifts

Proton chemical shifts are also often used to probe the aromaticity of a molecule. Protons attached to aromatic rings are more shielded due to the induced magnetic field and they undergo a downfield shift of typically 2–4 ppm. Proton chemical shifts vary significantly depending on where they are located. Inner protons (such as H_{30}, H_{31} in BP_{RE}) are more shielded than protons attached at the outer ring structure (such as H_{21}, H_{25} in BP_{RE}). In Table I, we report average proton chemical shifts of all protons attached directly to the ring structures as an indication for aromaticity of the compound. The average proton chemical shifts suggest the following series for aromaticity: BP > A > P > N > B. The more rings involved in the cluster the more aromatic the polyaromatic becomes. Anthracene and phenanthrene have the same number of rings, but due to the specific spatial ordering of the rings anthracene is more aromatic than phenanthrene. This is in agreement with the results of $\Delta\chi$.

On the basis of the shifts we can conclude again that the substrate of all transition states is less aromatic than that of the reactant, except for benzophenanthrene. To compare the aromaticity difference between the reactants and transition states we introduce the parameter T:

$$T = \delta(RE) - \delta(TS). \quad (5)$$

A similar trend is found as for the parameter R. The smaller the aromaticity difference between reactants and transition states the smaller the activation energy. Again, benzophenanthrene behaves differently. Although the transition state is more aromatic than the reactant the activation energy is the largest. This is due to the specific type of radical, i.e., benzylic, involved in the cyclization reaction. For cyclization not only the reactivity of the substrate is important but also the type of radical must be taken into account. This will be clarified in the following paragraph.

Nucleus-Independent Chemical Shifts

Nucleus-independent chemical shifts (NICSs) values are absolute magnetic shieldings at ring centers (nonweighted mean of the heavy atom coordinates). Negative NICS values give an indication to aromaticity, while positive values tend toward antiaromaticity [15]. The average of the NICS values computed at all rings of the substrate are listed in Table I. In addition, we also computed NICS values of the newly forming ring in the transition state to have an indication whether the transition state shows already some degree of aromaticity.

According to the average NICS value, the following series for the polyaromatics is suggested: A > N > B > P > BP. This result is not fully consistent with the conclusions made on the basis of the proton chemical shifts. This is probably caused by the specific ordering of the rings in phenanthrene and benzophenanthrene.

The substrate is always more aromatic in the reactant, except for benzophenanthrene. The NICS values computed in the newly forming ring are negative for all sites except benzophenanthrene. This means that for the benzene, naphtalene, anthracene, and phenanthrene already some degree of aromaticity is established in the new ring. To establish a correlation with the activation energies, two aspects must be taken into account: the substrate difference in aromaticity between transition state and reactant and the ability to delocalize the electrons in the newly forming ring. The larger the aromaticity difference the less reactive the substrate becomes. Based on the averaged NICS values, this suggest the following series: BP > P > A > N > B. The more negative the NICS value of the newly forming ring, the more the transition state is stabilized due to electron delocalization in the newly forming ring. This suggests the following series:

A > N > B > P > BP. These results agree with the qualitative conclusions made in Ref. [13].

Conclusions

We studied the influence of the local polyaromatic structure on the kinetics of various cyclization reactions. These reactions lead ultimately to incorporation of carbon atoms and the growth of the polyaromatic coke surface. Five clusters or sites were considered at which cyclization can take place. The minimum number of carbon atoms that must be added to allow cyclization varies from 4 to 1 depending on the local structure of the cluster. The reactivity of the PAHs is largely determined by the degree of aromaticity of the substrate and the reactivity of the radical. We calculated various magnetic properties to quantify the aromaticity. The larger the difference in substrate aromaticity between the transition states and reactants the less reactive the reactant becomes toward cyclization. The larger the degree of delocalization in the newly forming ring of the transition state the easier the reaction take place.

ACKNOWLEDGMENTS

This work was supported by the Fund for Scientific Research—Flanders (FWO) and the Research Board of Ghent University.

References

1. Durant, J. L.; Busby, W. F.; Lafleur, A. L.; Penman, B. W.; Crespi, C. L. Mutat Res 1996, 371, 123.
2. Denissenko, M. F.; Pao, A.; Tang, M.; Pfeifer, G. F. Science 1996, 274, 430.
3. Allen, J. O.; Dookeran, N. M.; Smith, K. A.; Sarofim, A. F.; Taghizadeh, K.; Lafleur, A. L. Environ Sci Tech 1996, 30, 1023.
4. (a) Léger, A.; d'Hendecourt, L.; Boccara, N., Eds. Polycyclic Aromatic Hydrocarbons and Astrophysics, NATO ASI Series, Series C, 191; Reidel: Dordrecht, The Netherlands, 1987; (b) Puget, J. L.; Léger, A. Annu Rev Astron Astrophys 1989, 27, 161–198.
5. Allamandola, L. J. Top Curr Chem 1990, 153, 1–25.
6. Aihara, J. Bull Chem Soc Jpn 1990, 63, 2781–2784.
7. (a) Kroto, H. W.; Heath, J. R.; O'Brien, S. C.; Curl, R. F.; Smalley, R. E. Nature 1985, 318, 162; (b) Zhang, Q. L.; O'Brien, S. C.; Heath, J. R.; Liu, Y.; Curl, R. F.; Kroto, H. W.; Smalley, R. E. J Phys Chem 1986, 90, 525; (c) Smalley, R. E. Acc Chem Res 1992, 25, 98.
8. Pope, C. J.; Marr, J. A.; Howard, J. B. J Phys Chem 1993, 97, 11001–11013.
9. Richter, H.; Mazyar, O.; Sumathi, R.; Green, W.; Howard, J. B.; Bozzelli, J. W. J Phys Chem A 2001, 105, 1561.
10. Faliks, A.; Yetter, R. A.; Floudas, C. A.; Hall, R.; Rabitz, H. J Phys Chem A 2000, 104, 10740–10746.
11. Richter, H.; Grieco, W. J.; Howard, J. B. Combust Flam 1999, 119, 1.
12. Marinov, N. M.; Pitz, W. J.; Westbrook, C. K.; Castaldi, M. J.; Senkan, S. M. Combust Sci Tech 1996, 116, 211–287.
13. Van Speybroeck, V.; Reyniers, M. F.; Marin, G. B.; Waroquier, M. Chem Phys Chem 2002, 3, 863–870.
14. De Proft, F.; Geerlings, P. Chem Rev 2001, 101, 1451–1464.
15. von Ragué Schleyer, P.; Maerker, C.; Dransfeld, A.; Jiao, H.; van Eikema Hommes, N. J. R. J Am Chem Soc 1996, 118, 6317.
16. Frisch, M. J.; Trucks, G. W.; Schlegel, H. B.; Scuseria, G. E.; Robb, M. A.; Cheeseman, J. R.; Zakrzewski, V. G.; Montgomery, J. A. Jr.; Stratmann, R. E.; Burant, J. C.; Dapprich, S.; Millam, J. M.; Daniels, A. D.; Kudin, K. N.; Strain, M. C.; Farkas, O.; Tomasi, J.; Barone, V.; Cossi, M.; Cammi, R.; Mennucci, B.; Pomelli, C.; Adamo, C.; Clifford, S.; Ochterski, J.; Petersson, G. A.; Ayala, P. Y.; Cui, Q.; Morokuma, K.; Malick, D. K.; Rabuck, A. D.; Raghavachari, K.; Foresman, J. B.; Cioslowski, J.; Ortiz, J. V.; Baboul, A. G.; Stefanov, B. B.; Liu, B.; Liashenko, A.; Piskorz, P.; Komaromi, I.; Gomperts, R.; Martin, R. L.; Fox, D. J.; Keith, T.; Al-Laham, M. A.; Peng, C. Y.; Nanayakkara, A.; Gonzalez, C.; Challacombe, M.; Gill, P. M. W.; Johnson, B.; Chen, W.; Wong, M. W.; Andres, J. L.; Gonzalez, C.; Head-Gordon, M.; Replogle, E. S.; Pople, J. A. Gaussian 98, revision A.7; Gaussian, Inc.: Pittsburgh, PA, 1998.
17. For example, Parr, R. G.; Yang, W. Density-Functional Theory of Atoms and Molecules; Oxford University Press: Oxford, UK, 1989.
18. Becke, A. D. J Chem Phys 1993, 98, 5648.
19. Krishnan, R.; Binkley, J. S.; Seeger, R.; Pople, J. A. J Chem Phys 1980, 72, 650.
20. Wong, M. W.; Radom, L. J Phys Chem A 1998, 102, 2237–2245.
21. Parker, C. L.; Cooksy, A. L. J Phys Chem A 1998, 102, 6186–6190.
22. Lynch, B. J.; Fast, P. L.; Harris, M.; Truhlar, D. G. J Phys Chem A 2000, 104, 4811–4815.
23. Smith, D. M.; Nicolaides, A.; Golding, B. T.; Radom, L. J Am Chem Soc 1998, 120, 10223–10233.
24. Ochterski, J. W.; Petersson, G. A.; Montgomery, J. A. J Chem Phys 1996, 104, 2598–2619.
25. Curtiss, L. A.; Raghavachari, K.; Trucks, G. W.; Pople, J. A. J Chem Phys 1991, 94, 7221–7230.
26. Mayer, P. M.; Parkinson, C. J.; Smith, D. M.; Radom, L. J Chem Phys 1998, 108, 604–615.
27. Fischer, H.; Radom, L. Angew Chem Int Ed 2001, 40, 1340–1371.
28. Peng, C.; Ayala, P. Y.; Schlegel, H. B.; Frisch, M. J. J Comput Chem 1996, 17, 49.
29. Peng, C.; Schlegel, H. B. Isr J Chem 1994, 33, 449.
30. Scott, A. P.; Radom, L. J Phys Chem 1996, 100, 16502–16513.

31. Eyring, H. J Chem Phys 1935, 3, 107; a more comprehensive treatment can be found in Wynne-Jones, W. F. K.; Eyring, H. J Chem Phys 1935, 3, 492 (this article is reproduced in full in Back, M. H.; Laidler, K. L. Selected Readings in Chemical Kinetics; Pergamon: Oxford, UK, 1967).
32. Evans, M. G.; Polanyi, M. Trans Faraday Soc 1935, 31, 875; Evans, M. G.; Polanyi, M. Trans Faraday Soc 1937, 33, 448.
33. Laidler, K. J. Chemical Kinetics; HarperCollins: New York, 1987.
34. McQuarrie, D. A.; Simon, J. D. Physical Chemistry—A Molecular Approach; University Science Books: Sausalito, CA, 1997.
35. For reviews, see, e.g., (a) Pechukas, P. Dynamics of Molecular Collisions, Part B; Plenum Press: New York, 1976; (b) Laidler, K. J.; King, M. C. J Phys Chem 1983, 87, 2657; (c) Truhlar, D. G.; Hase, W. L.; Hynes, J. T. J Phys Chem 1983, 87, 2664; (d) Gilbert, R. G.; Smith, S. C. Theory of Unimolecular and Recombination Reactions; Blackwell: Oxford, UK, 1990.
36. Van Speybroeck, V.; Martelé, Y.; Waroquier, M.; Schacht, E. J Am Chem Soc 2001, 123, 10650–10657.
37. Heuts, J. P. A.; Gilbert, R. G.; Radom, L. J Phys Chem 1996, 100, 18997–19006.
38. Heuts, J. P. A.; Gilbert, R. G.; Radom, L. Macromolecules 1995, 28, 8771–8781.
39. Van Speybroeck, V.; Van Neck, D.; Waroquier, M.; Wauters, S.; Saeys, M.; Marin, G. B. J Phys Chem A 2000, 104, 10939–10950.
40. Van Speybroeck, V.; Borremans, Y.; Van Neck, D.; Waroquier, M.; Wauters, S.; Saeys, M.; Marin, G. B. J Phys Chem A 2001, 105, 7713–7723.
41. Cheeseman, J. R.; Frisch, M. J.; Trucks, G. W.; Keith, T. A. J Chem Phys 1995, 104, 5497; Keith, T. A.; Bader, R. F. W. Chem Phys Lett 1993, 210, 223; Keith, T. A.; Bader, R. F. W. Chem Phys Lett 1992, 194, 1–8.
42. Dauben, H. J. Jr.; Wilson, J. D.; Laity, J. L. In Synder, J., Ed. Non-Benzonoid Aromatics, vol. 2; Academic Press: New York, 1971; and references therein; Aihara, J. J Am Chem Soc 1985, 207, 298; Haigh, C. W.; Mallion, R. B. J Chem Phys 1982, 76, 4063.

Paper VI

Modeling elementary reactions in coke formation from first principles

Van Speybroeck V. , Hemelsoet K. , Minner B. ,
Marin G. B. and Waroquier M.

Mol. Sim., **2007**, accepted

Modeling elementary reactions in coke formation from first principles

V. VAN SPEYBROECK [a], K. HEMELSOET [a], B. MINNER [a], G.B. MARIN [b] and M. WAROQUIER [a] *

[a] Center for Molecular Modeling, Ghent University, Proeftuinstraat 86, 9000 Ghent, Belgium, [b]Laboratorium voor Petrochemische Techniek, Ghent University, Krijgslaan 281-S5, 9000 Ghent, Belgium

(*Received*)

Theoretical calculations are presented on elementary reactions which are important during coke formation in a thermal cracking unit. This process is known to proceed through a free radical chain mechanism. The elementary reaction steps that lead to the growth of the coke surface can be divided into five classes of reversible reactions : hydrogen abstraction, substitution, gas phase olefin addition to radical surface species, gas phase radical addition to olefinic bonds and cyclization. To identify the elementary reaction classes that determine the coking rate, all microscopic routes that start from benzene and lead to naphthalene have been investigated. It is found that initial creation of surface radicals, either by hydrogen abstraction or substitution and subsequent hydrogen abstractions, determines the global coking rate. The influence of the local polyaromatic structure on the kinetics of the hydrogen abstraction reactions is determined by performing calculations on a large set of polyaromatic hydrocarbons (PAHs). On basis of the BDE values six types of possible reactive sites at the coke surface can be distinguished. For the initial hydrogen abstraction the local polyaromatic structure strongly influences the reaction kinetics and abstraction is preferred from less congested sites of the polyaromatic.

Keywords: radical reactions, hydrogen abstraction, density functional calculations, polyaromatic hydrocarbons, bond dissocation enthalpy, coke

1 Introduction

Thermal cracking of hydrocarbons is the simplest and oldest method for petroleum refinery processes and is considered as the main process for the production of light olefins such as ethene. The thermal cracking of hydrocarbons is known to proceed through a free radical chain mechanism. Radicals are mainly formed via C-C bond breaking and propagation occurs through abstraction and β-scission reactions. Decomposition of radicals by β-scission results in the desired gas-phase olefins. During this process, highly undesirable carbon-rich products are formed on the inner walls of the reactor giving rise to the formation of a coke layer. This coke layer has a negative influence on the efficiency of the cracking unit. The process of coke formation is a complex phenomenon (1; 2; 3). Initially coke is formed by a heterogeneous catalytic mechanism in which the properties of the inner tube skin play an important role. Once the metal surface is covered with coke the catalytic activity of the metal particles diminishes and a heterogeneous non-catalytic mechanism becomes important. The coke layer thus formed has a polynuclear aromatic character. Usually one focuses on the second process since the period of catalytic coke formation is very small with respect to the total run length. In today's operation of a plant simulation models play a very important role. Recently a coking model based on elementary reactions was developed at the Laboratorium voor Petrochemische Techniek (3; 4). In view of the fundamental nature of the elementary steps considered such a model is of general applicability . One of the main challenges in the development of an accurate and broadly applicable model is the assignment of rate coefficients for individual reactions occurring in the reaction network. The fundamental nature of the elementary steps considered allows the use of theoretical calculations to provide kinetic and thermodynamic data and to obtain microscopic insight in the basic reaction steps of the coke formation model. The elementary reaction steps that lead to incorporation of carbon atoms and growth of the coke surface can be divided in five classes of reversible reactions (cfr. Fig. 1):

(i) Hydrogen abstraction reactions by gas phase radicals and reverse reactions

*Corresponding author. Email: veronique.vanspeybroeck@ugent.be

Molecular Simulation
ISSN 0892-7022 print/ISSN 1029-0435 online © 200x Taylor & Francis
http://www.tandf.co.uk/journals
DOI: 10.1080/0892702YYxxxxxxxx

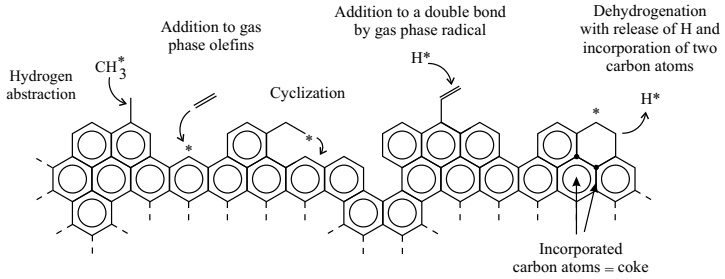

Figure 1 : Radical elementary reaction steps leading to coke growth

(ii) Substitution reactions by radicals at the coke surface and reverse reactions
(iii) Addition reactions of radical surface species to gas phase olefins and the inverse β-scission of a radical surface species in smaller surface species and gas phase olefins
(iv) Addition reactions of gas phase radicals to olefinic bonds in a surface species and the inverse decomposition of radical surface species to gas phase radicals and olefinic surface species
(v) Cyclization of radical surface species and decyclization.

Due to the increasing capabilities of computing power and optimization of numerical models it is now possible to perform high level ab initio calculations on systems of industrial importance. Kinetic parameters, such as the preexponential factor and activation energy, can be obtained by means of Transition State Theory (TST). The microscopic quantities are obtained by means of ab initio calculations. In this work preference has been given to Density Functional Theory calculations, since this approach is computationally attractive for the larger structures that are involved. This approach has been successfully applied to a variety of important chemical reactions. In the first part of this paper, microscopic routes starting from benzene leading to the formation of naphthalene are investigated with the aim to obtain insight into the elementary reaction classes that determine the rate of coke formation. In the second part of the paper, larger polyaromatic clusters are considered in order to determine the influence of the coke matrix on the kinetics of the elementary reactions.

2 Methodology

All calculations were performed using the Gaussian 03 software package (5). Geometries were optimized at the B3-LYP level of theory, in conjunction with the 6-311G(d,p) basis set (6; 7). A previous study on the hydrogen-abstraction reaction from benzene with the methyl radical showed the limited influence of the level of theory on the optimized geometries (8). Other studies on related radical reactions also reported that B3-LYP gives a reliable and quantitatively good description of geometries. (9; 10; 11). Frequencies were computed at the same level of theory as the geometry optimizations to provide zero-point vibrational energies (ZPVEs) and thermal corrections to the enthalpy, and to confirm the nature of the stationary points. A scale factor of 0.9806 was used to obtain the ZPVEs from the calculated harmonic vibrational frequencies, while unscaled frequencies were used to obtain the thermal corrections to the enthalpy. The use of scale factors provides a means of accounting for systematic deviations between measured and computed frequency-dependent properties, and is an important consideration for the accurate description of reaction kinetics and thermochemistry (12). Single-point energy calculations were performed using the BMK functional in conjunction with the 6-311+G(3df,2p) basis set (13). The BMK functional was recently developed by Boese and Martin and is accurate to approximately 10 kJ/ mol for the calculation of reaction barriers. The good performance of BMK appears to hinge on the combination of a high percentage of Hartree-Fock exchange (42%), together with terms dependent on the kinetic energy density, resulting

in a "back-correction" for excessive HF exchange in systems where this would be undesirable. The BMK functional was also found to be a method of choice in our level-of-theory study on the abstraction reaction in benzene,(8) as it is an accurate computational method and yet affordable for systems of moderately large size, such as those studied in the present work. We applied transition state theory (TST) to calculate the rate constants k(T) (14; 15; 16; 17). The link with the macroscopic quantities found in the Arrhenius rate law is made by a linear fit of ln k(T) values, calculated for a range of temperatures, versus 1/T. One refinement in our theoretical treatment comes from the observation that some of the low vibrational modes correspond to internal rotations rather than pure oscillations.

The standard harmonic oscillator (HO) model is known to be inappropriate for such modes and other approximations, such as the free rotor (FR) or hindered rotor (HR) model are advisable for the description of these modes (18). For identification of internal rotations, one must analyze the low vibrational spectrum of the molecule. Due to steric and electronic hindrance in the molecule, these rotations are opposed by a rotational potential. The choice of a particular description depends on the height of the rotational barrier and the temperature, as illustrated in Figure 2. For low activated rotations the FR approach is used whereas for more hindered rotations the hindered rotor approach is applied. In a recent study of radical-

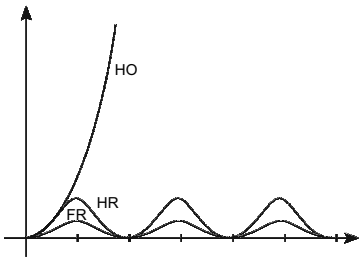

Figure 2 : Potential within Harmonic Oscillator (HO), Hindered Rotor (HR) and Free Rotor (FR) model.

addition reactions, we demonstrated the importance of correctly describing hindered internal rotations in order to obtain reliable partition functions. (18) Summarizing we use a mixed harmonic oscillator/free rotor (HO/FR) or mixed harmonic oscillator/hindered rotor (HO/HR) model, in which all the internal motions except for the internal rotations are approximated as independent harmonic oscillators.

3 Results and Discussion

3.1 *Reaction routes from benzene to naphtalene*

In order to obtain microscopic insight into the importance of the various elementary reactions leading to coke, a reaction route starting from benzene and producing naphthalene is proposed, as shown in Scheme 1. At first instance the coke surface is approximated by one benzene ring. In the following section, the implications of this approximation will be validated on the rate determining steps of the coke network.
The reaction sequence is initiated by hydrogen abstractions from benzene with gas phase radicals creating radical surface species. In turn these radicals react further with unsaturated gas phase components. Ethene has been used as coke precursor, as it is the olefinic hydrocarbon with the largest concentration in the thermal cracking unit (19). The initial hydrogen abstraction was studied both using a methyl and hydrogen radical. Earlier experimental work indicated that these radicals are very reactive in the coke formation during thermal cracking (20).

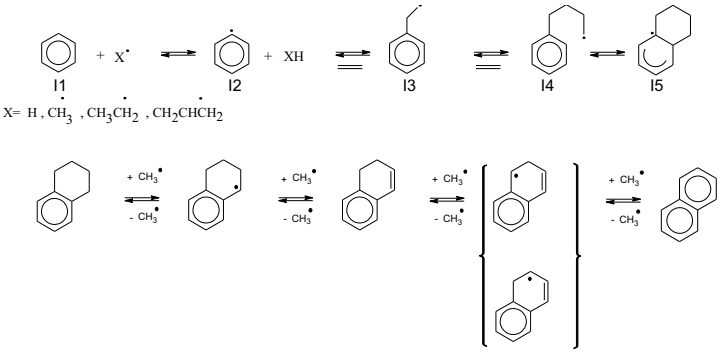

Scheme 1 : Reaction route starting from benzene to naphthalene

The reaction barriers at 0K, the frequency factors, activation barriers and the rate constants at three typical temperatures for coke formation are given in Table 1 and for each reaction the transition state is shown in Figure 3.

Elementary Reaction	ΔE_0	A	Ea	k(875K)	k'(875K)	k(1050K)	k'(1050K)	k(1075K)	k'(1075K)
I1 to I2 (with hydrogen)	62.13	1.08E+12	79.62	1.90E+07	**3.75E-05**	1.18E+08	**1.15E-01**	1.45E+08	**3.46E-01**
I1 to I2 (with methyl)	71.80	2.62E+10	80.9	3.86E+05	**2.17E-06**	2.46E+06	**1.34E-02**	3.06E+06	**7.61E-02**
I2 to I3	17.52	8.92E+09	33.25	9.21E+07	**2.32E+01**	1.97E+08	**6.20E+05**	2.16E+08	**1.27E+06**
I3 to I4	34.34	6.91E+09	52.44	5.10E+06	**1.28E+00**	1.70E+07	**5.32E+04**	1.95E+07	**1.15E+05**
I4 to I5	50.44	9.90E+08	49.53	1.09E+06	**1.09E+06**	3.39E+06	**3.39E+06**	3.87E+06	**3.87E+06**
I5 to I6 (with methyl)	66.18	1.18E+10	80.54	1.83E+05	**1.03E-06**	1.16E+06	**6.27E-03**	1.43E+06	**3.57E-02**
I5 to I6	121.02	6.52E+13	129.34	1.23E+06	**1.23E+06**	2.38E+07	**2.38E+07**	3.36E+07	**3.36E+07**
S1 to S2	55.29	1.29E+10	68.63	1.03E+06	**5.77E-06**	4.95E+06	**2.68E-02**	5.94E+06	**1.48E-01**
S2 to S3	64.41	5.65E+09	78.90	1.10E+05	**6.16E-07**	6.68E+05	**3.62E-03**	8.25E+05	**2.05E-02**
S3 to S4	45.45	4.60E+09	61.23	1.01E+06	**5.69E-06**	4.12E+06	**2.23E-02**	4.85E+06	**1.21E-01**

Table 1. Kinetic parameters of the elementary reactions of Scheme 1. ΔE_0 and E_a are reported in kJ/mol, whereas A is in units of $dm^3/mol/s$ for bimolecular reactions and $1/s$ for unimolecular reactions. k and k' are the rate constant and modified rate constant as explained in the text. For the initial hydrogen abstraction with methyl and hydrogen Eckart tunneling was also incorporated.

Rate constants of unimolecular reactions (e.g. cyclization reactions) and bimolecular reactions (e.g. hydrogen abstractions and addition reactions) cannot be directly compared as they have different units. To circumvent this problem modified rate constants are introduced for bimolecular reactions, by multiplication with the concentration of one the reactants:

$$\frac{dc_{product}}{dt} = k(T)c_A c_B = k'(T)c_A \tag{1}$$

For the initial hydrogen abstraction, the reactant B is either the concentration of hydrogen or methyl radicals while for the addition reactions the concentration of ethene is used. . Gas phase concentration profiles were obtained from a simulation program, which is based on a detailed network of elementary reactions, developed at the Laboratorium voor Petrochemische Techniek (21; 22). The reactor geometry and the operating conditions are taken for a typical ethane cracking unit. The process gas temperature profile as a function of the axial reactor coordinate is schematically shown in Figure 4 and varies between 800 K at the reactor inlet to reach a coil outlet temperature of 1100 K. Typical concentrations of ethene and ethyne were obtained at the reactor inlet, in the middle of the reactor length and at the outlet the reactor. These values are presented in Table 2.

The modified rate constants are also tabulated in Table 1 and are visualized in terms of temperature in Figure 5. It is found that the initial hydrogen abstraction are relatively slow, due to the low concentration

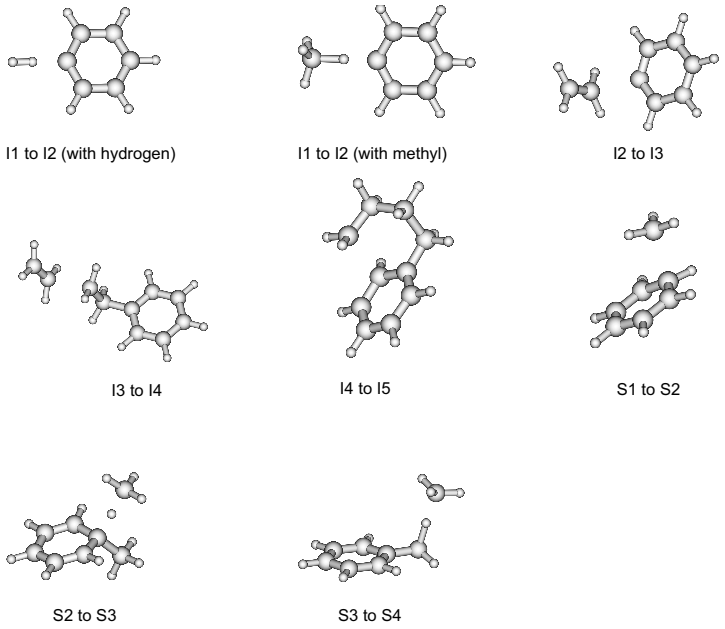

Figure 3: Transition states for the elementary reactions leading to cokes

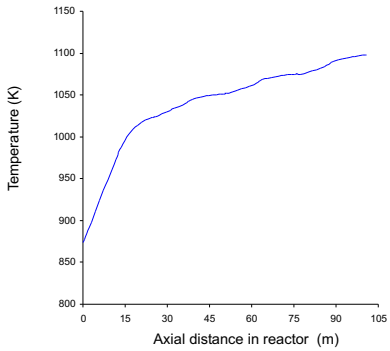

Figure 4 : Temperature profile of the process gas along the reactor coil for typical ethane cracking conditions

of the gas phase radicals. The individual rate constants however were found to be one of the highest in the total reaction network. This conclusion remains unaltered either considering methyl radicals or hydrogen

Axial Distance	T	Ethene	H	CH3
1.09 m	875	2.52E-07	1.98E-12	5.62E-12
44.02 m	1050	3.14E-03	9.80E-10	5.42E-09
100.96 m	1075	5.88E-03	2.38E-09	2.49E-08

Table 2. Concentrations of ethene, the hydrogen and methyl radical at various axial reactor distances during ethane cracking. The concentrations are in units of $kmol/dm^3$

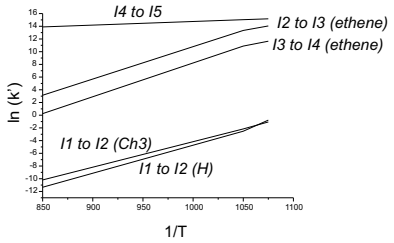

Figure 5 : Modified rate constants for the elementary reactions leading to coke in the temperature interval 850-1100 K.

radicals. The initially created radical surface species can further grow by means of various subsequent additions. The first addition of ethene or ethyne to the phenyl radical is characterized by a high rate constant. This can be explained by the reactivity of the phenyl radical. The subsequent additions are slower whereas further cyclizations and dehydrogenation, proceed very fast. The dehydrogenation can proceed either by a hydrogen abstraction with a methyl radical or a β-scission with release of a hydrogen radical. The rate constants for both routes were calculated. The unimolecular reaction pathway, referred as I5 to I5 in table 1 has a relatively high activation energy but also a much higher pre-exponential factor. Moreover due to the low concentration of methyl radicals, the β-scission is preferred. The final goal of this work should be the determination of the global coking rate. This requires the kinetic parameters of all elementary reaction steps as presented here, but also the concentration of all intermediate radicals. Therefore the mass balances must be solved taking into account the pseudo-steady state assumption. This procedure was presented in the work of Wauters and Marin (1) but on basis of semi-empirical kinetic parameters. The prediction is the global coking rate with accurately determined kinetic parameters, as presented here, will be a topic of future research.

In Scheme 1 the first step of the reaction network is the hydrogen abstraction creating a phenyl radical. Alternatively also a substitution reaction could take place with creation of toluene from which a hydrogen abstraction with methyl forms the benzyl radical :

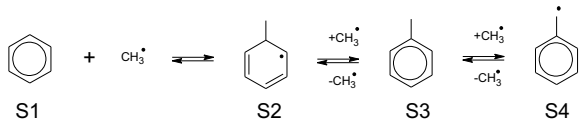

Scheme 2 : Radical substitution at the coke surface and further hydrogen abstraction with creation of a benzylic type of radical.

The substitution reaction consists of two consecutive reactions : an addition of a gas-phase radical creating a hexadienyl radical (S1 to S2) and release of the H atom with the formation of toluene (S2 to

S3). From that point benzylic type of radicals can be formed by abstraction by another gas phase radical. The kinetic parameters for these three reactions are given in table 3.

The hydrogen abstraction from toluene (S3 to S4 in Scheme 2) is substantially lower activated than the corresponding reaction starting from benzene. As benzylic type of radicals are much more stable than phenylic radicals, the activation barriers for the creation of the benzylic radicals is the lowest according to the Evans-Polanyi relation (23; 24). Also the first steps leading to toluene are all lower activated than the abstraction at benzene. When inspecting however the modified rate constants that also take into account the concentration of the gas phase radicals, these initial steps remain very slow.

Previous discussion reveals that the initial creation of surface species determines the global coking rate.

3.2 *Influence of the coke matrix on the kinetics*

The reaction network discussed in the previous section was based on the assumption that the coke surface could be approximated by only one benzene ring. It is however important to validate this approximation. Therefore calculations were performed on larger polyaromatic compounds to establish the importance of the local environment of the active surface site in the coke formation. This is done for the initial hydrogen abstraction with the methyl radical creating a variety of possible aryl radicals.

Starting from a general polyaromatic (cfr. Figure 6) , a large number of possible reactive sites can be identified. It would be desirable to classify all possible aryl radicals of PAHs into a limited set of groups, each characterized by a given reactivity. A measure of the chemical reactivity of a

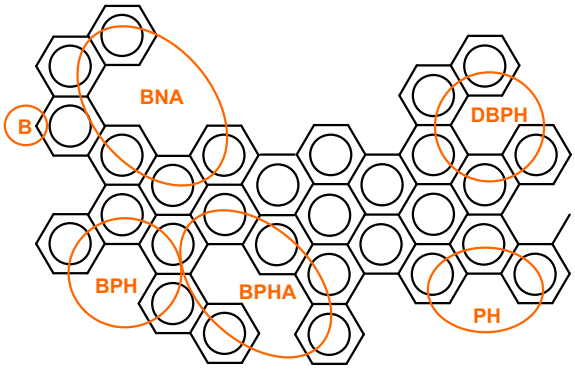

Figure 6 : Representation of general PAH and classification into various sites

site at an aromatic cluster is the bond dissociation energy (BDE) of the corresponding C-H bond. BDEs of various aryl radicals formed from 13 PAHs i.e. benzene, naphthalene, anthracene, tetracene, phenanthrene, benzo[c]phenanthrene, dibenzo[c,g]phenanthrene, benz[a]anthracene, dibenz[a,j]anthracene, coronene, benzo[a]napht[2,1-j]anthracene,
benzo[a]phenanthr[2,1-j]-anthracene, benzo[ghi]perylene (fig. 1) are studied, in order to determine the influence of the local polyaromatic environment on the $C-H$ bond strength.

The BDE values segregate into six groups with different reactivity, and which can be related to the local structure around the site : benzene-like site (B sites), phenanthrene-like sites (P sites), dibenzophenanthrene-like sites (DBP sites), benzophenanthreneanthracene-like sites (BPA sites), benzophenanthrene-like sites (BP sites) and benznaphtanthracene-like sites (BNA sites) (cfr. Figure 8). The indication of the various sites is also indicated on the PAH of Figure 6. More information about the classification can be found in reference (25). The classification of PAHs into various groups was already

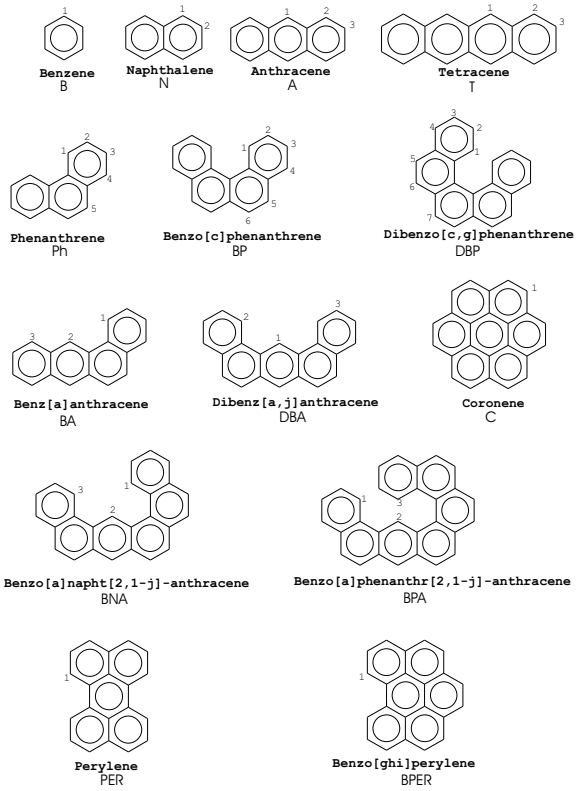

Figure 7 :Polyaromatic hydrocarbons dataset. Distinct states at each PAH type are indicated and labeled.

suggested by Wang en Frenklach on the basis of semi-empirical calculations. (26). Only three classes were suggested due to the limited dataset that was considered. Other interesting references concerning BDEs of aryl radicals are the works of Chen et al. , Aihara et al. and Cioslowski et al. (27; 28; 29). The latter reference approximates the closest our work since the results are also based on ab initio techniques.

Kinetics of hydrogen abstraction by the methyl radical from PAHs. In this part attention is focussed on the influence of the local environment of the C-H bond on the kinetics of corresponding abstraction reactions by a methyl radical. Rate constants k(T), and corresponding activation energies E_a and pre-exponential factors A, for the reactions between the various PAHs and methyl radical were calculated at the BMK/6-311+G(3df,2p)//B3-LYP/6-311G(d,p) level in the temperature interval of 700 to 1100 K, which is relevant for the steam cracking and coke formation processes. Two refinements are taken into consideration in the calculations: the effect of tunneling corrections on the one hand, and a refined

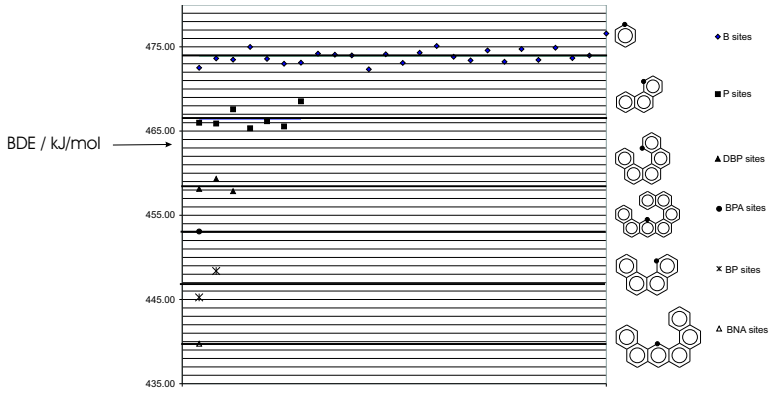

Figure 8 : BDEs for various PAHs

description of the low-energy torsion of the methyl group in the TSs on the other. The calculated rate constants, activation energies and pre-exponential factors for the hydrogen abstractions are taken up in table 3.

The relative rates for hydrogen abstraction by a methyl radical at site X with respect to a benzene-like site are presented in Figure 9. It can be concluded that abstraction is always preferred at less congested

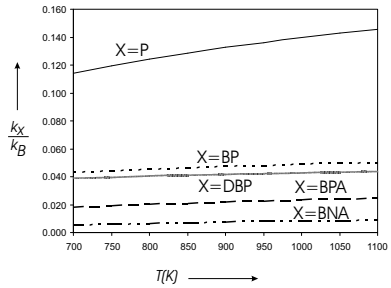

Figure 9 : Rate constant for hydrogen abstractions with a methyl radical at site X, relative to the rate constant at the B site, as function of temperature

PAH molecules and most preferably at benzene-like sites. Earlier work also showed that even within a specific PAH, abstraction at B-like sites is always preferred over abstraction at more congested sites. For instance, for the various sites within the phenanthrene (P) molecule, the abstraction at the P-like site is more difficult than abstraction at the B-like sites (30)

site	k_{700}	k_{900}	k_{1100}	E_a	A
B-1	2.55E+04	5.12E+05	3.97E+06	80.9	2.62 E+10
N-1	1.45E+04	2.99E+05	2.36E+06	81.6	1.69 E+10
N-2	1.74E+04	3.53E+05	2.76E+06	81.1	1.86 E+10
A-1	7.36E+03	1.64E+05	1.35E+06	83.6	1.20 E+10
A-2	1.34E+04	2.76E+05	2.18E+06	81.6	1.55 E+10
A-3	1.99E+04	3.96E+05	3.05E+06	80.7	1.96 E+10
T-1	7.62E+03	1.68E+05	1.39E+06	83.4	1.20 E+10
T-2	1.78E+04	3.62E+05	2.83E+06	81.2	1.94 E+10
T-3	2.15E+04	4.25E+05	3.26E+06	80.4	2.04 E+10
PH-1	2.91 E+03	6.76 E+04	5.78 E+05	84.8	5.85 E+09
PH-2	8.62 E+03	1.73 E+05	1.34 E+06	80.8	8.78 E+09
PH-3	8.43 E+03	1.72 E+05	1.35 E+06	81.3	9.27 E+09
PH-4	6.39 E+03	1.30 E+05	1.01 E+06	81.2	6.89 E+09
PH-5	7.87 E+03	1.59 E+05	1.24 E+06	81.1	8.32 E+09
BPH-1	1.10 E+03	2.41 E+04	1.99 E+05	83.3	1.71 E+09
BPH-2	4.63 E+03	9.30 E+04	7.21 E+05	80.9	4.74 E+09
BPH-3	4.20 E+03	8.68 E+04	6.85 E+05	81.6	4.90 E+09
BPH-4	3.30 E+03	6.81 E+04	5.38 E+05	81.6	3.84 E+09
BPH-5	3.29 E+03	6.92 E+04	5.54 E+05	82.2	4.20 E+09
BPH-6	3.77 E+03	7.77 E+04	6.13 E+05	81.6	4.38 E+09
DBPH-1	9.96 E+02	2.14 E+04	1.74 E+05	82.8	1.41 E+09
DBPH-2	4.31 E+03	8.77 E+04	6.87 E+05	81.3	4.72 E+09
DBPH-3	3.48 E+03	7.40 E+04	5.96 E+05	82.4	4.64 E+09
DBPH-4	2.79 E+03	5.86 E+04	4.69 E+05	82.1	3.54 E+09
DBPH-5	2.78 E+03	5.97 E+04	4.84 E+05	82.7	3.88 E+09
DBPH-6	3.37 E+03	6.92 E+04	5.44 E+05	81.5	3.81 E+09
DBPH-7	2.72 E+03	5.90 E+04	4.80 E+05	82.9	3.93 E+09
BA-1	1.92 E+03	4.61 E+04	4.02 E+05	85.6	4.44 E+09
BA-2	1.51 E+02	4.53 E+03	4.57 E+04	91.6	9.71 E+08
BA-3	3.69 E+03	7.68 E+04	6.10 E+05	81.9	4.48 E+09
DBA-1	4.84 E+01	1.76 E+03	2.02 E+04	96.7	7.44 E+08
DBA-2	3.79 E+03	8.65 E+04	7.32 E+05	84.4	7.03 E+09
DBA-3	9.51 E+03	1.90 E+05	1.47 E+06	80.8	9.54 E+09
BNA-1	1.19 E+03	2.38 E+04	1.86 E+05	80.9	1.23 E+09
BNA-2	1.42 E+02	3.77 E+03	3.53 E+04	88.4	5.30 E+08
BNA-3	5.43 E+02	1.27 E+04	1.09 E+05	84.9	1.11 E+09
BPHA-1	4.59 E+02	1.12 E+04	9.83 E+04	86.0	1.13 E+09
BPHA-2	1.09 E+02	3.09 x 100	3.00 E+04	90.0	5.33 E+08
BPHA-3	1.30 E+03	2.72 E+04	2.18 E+05	82.1	1.64 E+09
C-1	3.63 E+04	7.70 E+05	6.18 E+06	82.3	4.77 E+10
PER-1	2.24 E+03	5.31 E+04	4.60 E+05	85.3	4.93 E+09
BPER-1	4.71 E+03	1.11 E+05	9.59 E+05	85.2	1.01 E+10

Table 3. Rate constants and pre-exponential factor in $dm^3\ mol^{-1}\ s^{-1}$ and activation barrier in kJ mol^{-1}. All values were obtained using energies at the BMK/6-311+G(3df,2p)//B3-LYP/6-311G(d,p) level and using a mixed HO/FR or HO/HR model, with inclusion of Eckart tunneling corrections.

4 Conclusions

In this paper, various elementary reaction steps important for coke formation during thermal cracking of hydrocarbons are studied. At first instance all elementary reaction steps of a reaction network starting from

benzene and leading to naphthalene were studied in order to determine the slowest reaction steps of the network. The importance of all elementary reaction steps can only be validated when taking into account both rate constants for all elementary reactions and concentrations of gas-phase olefins and radicals. On basis of such analysis it can be concluded that the initial hydrogen abstraction is the slowest step of the reaction network. A competitive pathway for the initial hydrogen abstraction is the substitution reaction leading to toluene. The rates of these reactions are somewhat higher than for the hydrogen abstraction but due to the low concentration of methyl radicals in the reactor coils, also the substitution reaction is one of the slowest steps of the network. The coking rate is thus determined by the rate by which initial surface species are created, either by direct hydrogen abstraction or by an initial substitution and subsequent hydrogen abstraction.

At second instance, the kinetic calculations were extended to larger polyaromatics, to investigate the influence of the local environment of the coke surface on the kinetic parameters. A classification for the reactivity of PAHs based on BDEs was proposed. Six different classes of C-H bonds could be identified. The influence of the local environment of the active site on the kinetics was investigated by studying a series of hydrogen abstraction reactions with the methyl radical. The latter reaction class was derived to determine the global coking rate of the reaction network. It was found that the rate constants can vary largely depending on the local structure of the polyaromatic surface. Moreover at typical temperatures encountered during cracking, hydrogen abstractions preferentially occur at the less congested PAH sites, such as benzene.

References

[1] S. Wauters, G. B. Marin. *Ind. Eng. Chem. Res.,* **41**, 2379 (2002).
[2] S. Wauters, G. B. Marin. *Chem. Eng. J.,* **82**, 267 (2001).
[3] S. Wauters, PhD Thesis. *Kinetics of coke formation during thermal cracking of hydrocarbons based on elementary reactions*, Ghent University (2001)
[4] Reyniers,M.F., Froment, G.F. *Ind. Eng. Chem. Res.* **34**, 773 (1995)
[5] Gaussian 03, Revision B.03, M. J. Frisch, G. W. Trucks, H. B. Schlegel, G. E. Scuseria, M. A. Robb, J. R. Cheeseman, J. A. Montgomery, Jr., T. Vreven, K. N. Kudin, J. C. Burant, J. M. Millam, S. S. Iyengar, J. Tomasi, V. Barone, B. Mennucci, M. Cossi, G. Scalmani, N. Rega, G. A. Petersson, H. Nakatsuji, M. Hada, M. Ehara, K. Toyota, R. Fukuda, J. Hasegawa, M. Ishida, T. Nakajima, Y. Honda, O. Kitao, H. Nakai, M. Klene, X. Li, J. E. Knox, H. P. Hratchian, J. B. Cross, V. Bakken, C. Adamo, J. Jaramillo, R. Gomperts, R. E. Stratmann, O. Yazyev, A. J. Austin, R. Cammi, C. Pomelli, J. W. Ochterski, P. Y. Ayala, K. Morokuma, G. A. Voth, P. Salvador, J. J. Dannenberg, V. G. Zakrzewski, S. Dapprich, A. D. Daniels, M. C. Strain, O. Farkas, D. K. Malick, A. D. Rabuck, K. Raghavachari, J. B. Foresman, J. V. Ortiz, Q. Cui, A. G. Baboul, S. Clifford, J. Cioslowski, B. B. Stefanov, G. Liu, A. Liashenko, P. Piskorz, I. Komaromi, R. L. Martin, D. J. Fox, T. Keith, M. A. Al-Laham, C. Y. Peng, A. Nanayakkara, M. Challacombe, P. M. W. Gill, B. Johnson, W. Chen, M. W. Wong, C. Gonzalez, and J. A. Pople, Gaussian, Inc., Wallingford CT, 2004.
[6] an example of a reference work : R.G. Parr and W. Yang *Density-Functional Theory of Atoms and Molecules*, ed. by Oxford University Press in 1989.
[7] A. D. Becke, *J. Chem. Phys.* **98**, 5648 (1993)
[8] K. Hemelsoet, D. Moran, V. Van Speybroeck, M. Waroquier, L. Radom, *J. Phys. Chem. A,* **110**, 8942 (2006)
[9] L.A. Curtiss, K. Raghavachari, P.C. Redfern, J.A. Pople, *J.Chem.Phys.* **106**, 1063 (1997).
[10] M. L. Coote, *J.Phys.Chem. A*, **108**, 3865-3872 (2004).
[11] B.J. Lynch, D.G. Truhlar, *J.Phys.Chem.A* **105**, 2936-2941 (2001)
[12] A.P. Scott, L. Radom, *J. Phys. Chem.* **100**, 16502-16513 (1996).
[13] A.D. Boese, J.M.L. Martin, *J. Chem. Phys.* **2004**, *121*, 3405-3416.
[14] H. Eyring, J.Chem.Phys. **1935** ,107. A more comprehensive treatment can be found in W.F.K. Wynne-Jones, H. Eyring, J.Chem.Phys. **1935**,3, 492. This article is reproduced in full in M.H. Back, K.L. Laidler, *Selected readings in chemical kinetics*; Pergamon Oxford, 1967.
[15] K.J. Laidler, *Chemical kinetics*; ed by HarperCollins Publishers, Inc,1987.
[16] D.A. Mc. Quarrie, J.D. Simon, *Physical Chemistry-A molecular approach*, University Science Books, Sausalito, California, 1997.
[17] For reviews, see for example (a) P. Pechukas, *Dynamics of Molecular Collisions, Part B*; W.H. Miller, Plenum Press: New York, 1976. (b) K.J. Laidler, M.C. King, J.Phys. Chem. **1983**,87,2657. (c) D.G. Truhlar, W.L.Hase, J.T. Hynes, J.Phys. Chem **1983**,87, 2664. (d) R.G. Gilbert, S.C. Smith, *Theory of Unimolecular and Recombination Reactions*, Blackwell: Oxford, 1990.
[18] V. Van Speybroeck, D. Van Neck, M. Waroquier, S. Wauters, M. Saeys, G.B. Marin, *J.Phys.Chem.A* **2000**,104,10939-10950.
[19] (a) F.D. Kopinke, G. Zimmerman, S. Nowak, *Carbon.* **26**,117-124 (1988) (b) F.D. Kopinke, G. Zimmerman, G.C. Reyniers, G.F. Froment, *Ind.Eng.Chem.Res.*, **32**, 56-61 (1993) (c) F.D. Kopinke, G. Zimmerman, G.C. Reyniers, G.F. Froment, *Ind.Eng.Chem.Res.*, **32**, 2620-2625 (1993)
[20] G.F. Froment, *Fouling of heat transfer surfaces by coke formation in petrochemical reactors*, in E. Summerscales, J.G. Knudson (Eds.), Fouling of Heat Transfer Equipment, Hemisphere Publ. Corp. (1981).
[21] P.J. Clymans, G.F. Froment, *Comput.Chem.Eng.*, **8**, 137-142 (1984).
[22] (a) G.C. Reyniers, G.F. Froment, F.D. Kopinke, G. Zimmerman, *Ind. Eng.Chem.Res.*, textbf33(11), 2584-2590 (1994). (b) P.M. Plehiers, G.C. Reyniers, G.F. Froment, *Ind. Eng.Chem.Res.*, **29**, 636-641 (1990).
[23] M.G. Evans, *Discuss.Faraday Soc.* **1947***2*, 271.; M.G. Evans, J. Gergely, E.C. Seaman, *J.Polym.Sci.*,

1948, *3*, 866; M.G. Evans, M. Polanyi, *Trans.Faraday Soc.*, **1938**, *34*, 11.
[24] N.N. Semenov, *Some problems in Chemical Kinetics and Reactivity*(Engl. Trans.), Princeton Press, Princeton, **1958**, 29-33.
[25] V. Van Speybroeck, G.B. Marin, M. Waroquier, *ChemPhysChem*, **7**, 2205-2214 (2006)
[26] H. Wang, M. Frenklach, *J.Phys.Chem.*, **97**, 3867-3874, 1993.
[27] C.-C. Chen, J. W. Bozzelli, *J. Phys. Chem. A* **2003** *107*, 4531-4546.
[28] J. Aihara, *Bull.Chem.Soc.Jpn.*, **1990**, *63*, 2781-2784.
[29] J. Cioslowski, G. Liu, M. Martinov, P. Piskorz, D. Moncrieff, *J.Am.Chem.Soc.* **1996** *118*, 5261-5264.
[30] K. Hemelsoet, V. Van Speybroeck, D. Moran, G.B. Marin, L. Radom, M. Waroquier, *J. Phys. Chem. A*,, in press.

Paper VII

Comparative study of kinetics and reactivity indices of free radical polymerization reactions

Van Cauter K. , Hemelsoet K. , Van Speybroeck V. ,
Reyniers M. F. and Waroquier M.

Int. J. Quant. Chem., **2005**, *102*, 454–460

Comparative Study of Kinetics and Reactivity Indices of Free Radical Polymerization Reactions

K. VAN CAUTER,[1] K. HEMELSOET,[1] V. VAN SPEYBROECK,[1] M. F. REYNIERS,[2] M. WAROQUIER[1]

[1]*Laboratory of Theoretical Physics, Universiteit Gent, Proeftuinstraat 86, B-9000 Gent, Belgium*
[2]*Laboratorium voor Petrochemische Techniek, Universiteit Gent, Gent, Belgium*

Received 7 September 2003; accepted 27 August 2004
Published online 6 December 2004 in Wiley InterScience (www.interscience.wiley.com).
DOI 10.1002/qua.20388

ABSTRACT: Density functional theory calculations are used to determine the kinetics and reactivity indices of the first propagation steps of the polyethylene and poly(vinyl chloride) polymerization. Transition state theory is applied to evaluate the rate coefficient from the microscopically determined energies and partition functions. A comparison with the experimental Arrhenius plots validates the level of theory. The ability of reactivity indices to predict certain aspects of the studied propagation reactions is tested. Global softnesses of the reactants give an indication of the relative energy barriers of subsequent monomer additions. The correlation between energy and hardness profiles along the reaction path confirm the principle of maximum hardness. Local indices predict the regioselectivity of the attack of the growing radical to vinyl chloride. © 2004 Wiley Periodicals, Inc. Int J Quantum Chem 102: 454–460, 2005

Key words: density functional theory; free radical polymerization; kinetics; reactivity indices

Introduction

The principal aim of this work is to study reactivity characteristics of some radical addition reactions that are elementary steps in the free radical polymerization of polyethylene (PE) and poly(vinyl chloride) (PVC). Usually the reactivity of chemical species is studied by calculating the rate constants of some basic chemical reactions in which they are involved. Within this approach the geometries and frequencies that serve as input for the rate expression, as derived from transition state theory (TST), are obtained by means of ab initio calculations [1].

On the other hand, one can also estimate the reactivity of molecules on the basis of various reactivity indices (RI) [2, 3]. Density functional theory (DFT) provides a solid theoretical framework to derive a

Correspondence to: V. Van Speybroeck; e-mail: veronique.vanspeybroeck@UGent.be

This article was presented at the 10th International Conference on the Applications of Density Functional Theory in Chemistry and Physics, September 7–12, 2003, Brussels, Belgium.

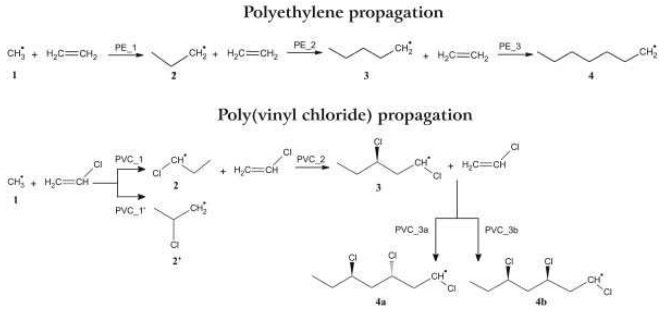

FIGURE 1. Initiation and first propagation steps of the polyethylene and poly(vinyl chloride) production.

variety of chemical reactivity descriptors, which can be divided into three categories: global indices, local descriptors, and kernels. The calculation of RI is computationally less intensive than the first method, because only the electronic structure of the reactants is needed and the transition state (TS) is not considered. Consequently, only information about the onset of the chemical reaction can be expected.

RI must be interpreted by use of chemical principles, such as the hard and soft acids and bases (HSAB) principle and the principle of maximum hardness (PMH). According to the global HSAB principle, the interaction between two systems will be favored in case of global softnesses that are close to each other. Following the PMH principle, molecular systems at equilibrium tend toward states of higher hardness, and, as a consequence, transition states are expected to present a minimum hardness value [4]. This principle was confirmed for the isomerization reaction of guanine, and good linear correlations between the rotational energy of the hydroxyl group and the chemical potential, hardness, and electrophilicity index along the reaction path were established [5].

In the present work we elaborate on the use of RI to confirm some kinetic aspects of the free radical polymerization reactions obtained through TST. It is important to note that no temperature effects are involved within the theory of RI so only a correlation with the reaction barrier can be expected; information on the frequency factor cannot be assessed [6].

Free radical polymerization is a technologically very important process and the knowledge of the propagation rate constant and its chain length dependence, which is difficult to assess on experimental grounds, is necessary for further insight into the polymerization process. DFT/B3LYP calculations provide a reliable and cost-effective method for determining the kinetic parameters of radical addition reactions via TST [7]. A recent level-of-theory study for the addition of an ethyl radical to ethene (resembling PE_2, see Fig. 1) established that DFT-based methods give systematically better predictions for the rate constant than all Hartree–Fock-based methods (e.g., QCISD, CC, MP2, MP4) [8]. This is mainly attributed to the presence of spin contamination in the Hartree–Fock ground state [9]. This is confirmed here by a comparative study of theoretical and experimental data [10]. Within the scope of this work the success of DFT/B3LYP calculations in predicting the kinetics of radical reactions is a solid basis for the calculation of DFT-based reactivity indices. For the propagation step during the PVC production, tacticity also emerges as an important aspect [11]. The relative importance of competitive pathways leading to atactic, syndiotactic, and isotactic polymers is studied on basis of the kinetics and reactivity indices.

Kinetics

REACTION SCHEME

The studied reactions are schematically presented in Figure 1. The initiating addition of a methyl radical to the monomer unit (ethene or vinyl chloride) is followed by two subsequent propagation steps. For PVC, various reaction routes are possible because of the asymmetry of vinyl chloride (VC). PVC_1 refers to the "tail" addition of VC,

TABLE I

Preexponential factor A in m^3/mol · s and activation energy E_a in kJ/mol. ΔE_0 is the reaction barrier at 0 K (in kJ/mol). S is the global softness and the s_k are the condensed values; the numbering of the carbon atoms k starts from the radical center. All calculations are performed at the B3LYP/6-311g level of theory.**

Kinetics				Reactivity Indices						
						s_k				
Reaction	A	E_a	ΔE_0	Reactant	S	$k = 1$	$k = 2$	$k = 3$	$k = 4$	$k = 5$
				ethene	2.041	0.826	0.826			
PE_1	1.94×10^6	34.46	31.88	**1**	2.484	2.192				
PE_2	4.80×10^4	37.68	33.75	**2**	2.955	1.988	−0.202	0.076		
PE_3	6.96×10^4	37.93	33.58	**3**	3.033	1.988	−0.189	0.069	0.022	−0.006
				VC	2.245	0.823	0.456			
PVC_1	6.65×10^5	29.69	26.04	**1**	2.484	2.192				
PVC_2	1.80×10^4	34.74	28.71	**2**	3.206	1.565	−0.166	0.079		
PVC_3a	1.24×10^4	35.88	29.44	**3**	3.301	1.584	−0.150	−0.0001	0.007	−0.003
PVC_3b	1.89×10^4	47.01	35.08*	**3′**	3.323	1.578	−0.153	−0.017	0.012	−0.007

* For PVC_3b the reaction barrier is calculated with reference to the reactant conformation **3′** that is closest to the TS structure of the concerned reaction.

producing a 1-chloroprop-1-yl radical (**2**), and PVC_1′ is the corresponding "head" addition producing a 2-chloroprop-1-yl radical (**2′**). It is well known that PVC grows mainly by head-to-tail propagation; therefore no head-to-head additions are considered in the further reaction scheme [11]. This aspect will be confirmed by our theoretical calculations for the first addition.

After the second addition (PVC_2), a chiral carbon center is created as a result of the presence of the end-standing Cl-atom in reactant **2.** Each following VC addition will create an additional chiral carbon centrum to which a Cl atom is attached. The relative orientation of the chlorine atoms in the subsequent chiral centers determines the tacticity of the final polymer chain. In case of the third addition, PVC_3a leads to an alternating arrangement of the Cl atoms, and PVC_3b leads to equally orientated chlorine atoms at the two subsequent chiral centra in the product (1,3,5-trichlorohept-1-yl radical). The preference for one route or another results in the formation of an isotactic, syndiotactic, or atactic polymer: subsequent additions of type a will eventually lead to a syndiotactic polymer, those of type b to an isotactic polymer. However, under realistic operation conditions a mixture of both type of additions can be expected, leading to an atactic polymer, but still with a certain degree of syndiotactic sequences (enabling partial crystallization).

METHODOLOGY

All calculations are performed with the Gaussian 98 software package. For the evaluation of the molecular partition functions, all internal modes are treated as harmonic oscillators, with frequencies determined for the all-trans configurations with respect to the CCCC torsional angles. Figure 2 gives the Arrhenius plots for the studied reactions. The theoretical rate constants of the first addition reactions (PE_1 and PVC_1) are compared with the experimental data in the temperature range 300–600 K [10]. Concerning the influence of the basis set, the use of a triple-zeta basis set, within the DFT/B3LYP method, gives the best agreement with the experimental rate constant for both PE_1 and PVC_1. The DFT/B3LYP/6-311g** method is retained for all calculations of kinetics and reactivity indices.

POLYETHYLENE PROPAGATION

The theoretical Arrhenius plots for the PE propagation reactions are given in Figure 2(a). The derived kinetic parameters are listed in Table I. The propagation reactions are much slower than the initiation step PE_1, which exhibits both a lower activation energy and a substantially higher frequency factor. The reaction rates of PE_2 and PE_3 are close to each other, although PE_3 is slightly faster than PE_2. Despite the good correspondence of theoretical rate constants for PE_1 with experi-

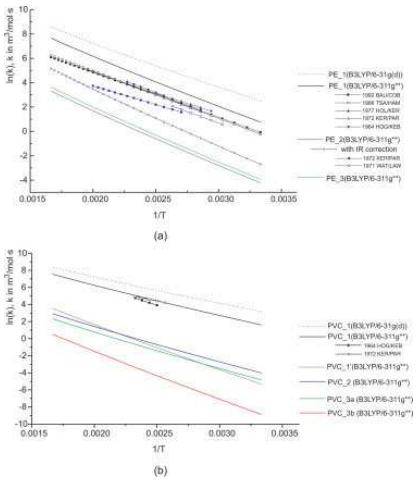

FIGURE 2. Experimental [10] and theoretical rate constants for the propagation reactions of PE (a) and PVC (b).

mental values, the reaction rates of PE_2 show larger deviations. This is due to the limitations of the harmonic oscillator (HO) model. Treating internal rotations (IR) correctly brings the theoretical prediction of the rate constant closer to the experiment, as demonstrated in Figure 2(a) for PE_2. We also stress that the apparent convergence of propagation rate constant is merely a reflection of the limitations of the HO model, because convergence is not yet expected in this early stage of propagation. An IR treatment will change the HO picture because the conformational flexibility of the chain increases systematically during propagation. The incorporation of internal rotations, however, is not essential within the scope of this work but forms the subject of another study.

POLY(VINYL CHLORIDE) PROPAGATION

The Arrhenius plots for the PVC reactions are displayed in Figure 2(b). The kinetic parameters are listed in Table I. Figure 3(a) gives the energy diagrams for the subsequent VC additions. The energies of the reactants are systematically chosen as reference. Both the reaction barrier and frequency factor point out a strong preference of reaction

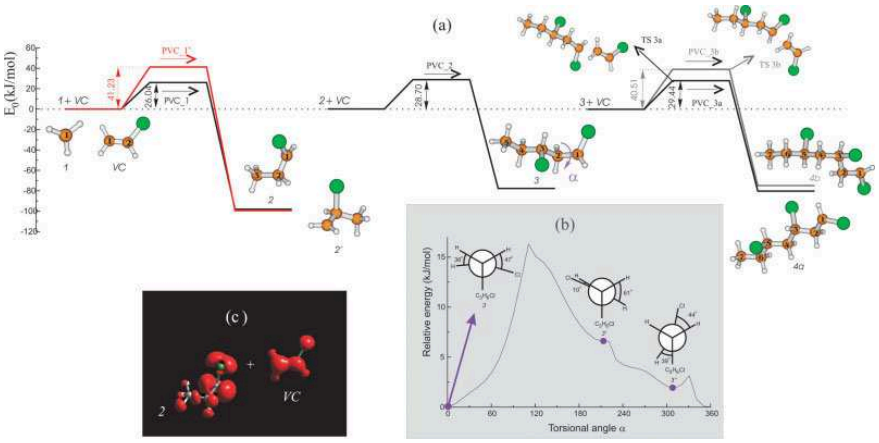

FIGURE 3. (a) Energy diagram for the additions PVC_1, PVC_2, PVC_3. The energies of the reactants are systematically chosen as reference point. E_0 is the ground-state energy with inclusion of zero-point contributions. (b) Torsional potential of the CHCl rotation in reactant **3,** with Newman projections of the fully optimized local minima. (c) 3-D local softness for the reactants of PVC_2.

route PVC_1 with respect to PVC_1′ ($k_1/k_{1'}$ is 1000 at 300 K, 100 at 500 K), in agreement with experimental findings [11]. As a consequence, head-to-head additions are not further considered for the second and third propagation step. Reaction PVC_2 is slower than the initiating addition to a methyl radical (**1**), because the latter is less stable than radical **2** and also experiences less steric hindrance when approaching VC. For the third reaction, the end-standing CHCl group of reactant **3** is forced into different positions depending on the relative orientation of the VC-chlorine with respect to the chlorine at the chiral carbon in the reactant (Fig. 3). These distinct attacks to VC give rise to two different transition states and two different products which are enantiomers of the 1,3,5-trichloroheptyl radical. From this perspective and for a better understanding of the reaction mechanism, it is instructive to study the rotational potential of the CHCl group in 1,3-dichloropentyl radical [see Fig. 3(b)]. Apart from the energetically most favored conformer **3,** two local energy minima (**3′** and **3″**) are observed as a function of the rotational angle as schematically illustrated in the Newman projections. Conformer **3** is geometrically similar to the TS_3a structure and structure **3′** resembles TS_3b. Conformer **3″** leads to a transition state that corresponds to another conformation of TS_3b, which can be reached by applying a single internal rotation.

The reaction path 3b has the highest barrier because, in the corresponding transition state, the chlorine atoms at two subsequent chiral carbon centra are relatively close to each other. The repulsion between those chlorine atoms results in a gauche orientation of the $C_2C_3C_4C_5$ torsional angle in the product **4b.** The reaction path 3a is energetically favoured since the chlorine atoms in conformation **4a** are at alternating sides of the polymer backbone. Taking into account also preexponential factors, we find that reaction path 3a proceeds 10 times faster than path 3b at 500 K.

From these kinetic results of the first additions, preliminary remarks could be made concerning the tacticity of the polymer, namely that free radical polymerization of VC leads predominantly to syndiotactic sequences, with some "meso" errors in the chain, implying the folding of the polymer at those places. Those random foldings would partially hinder the crystallization realized by trans syndiotactic structures. However, solvent effects and high-pressure conditions are likely to influence this picture, especially when the radical chain gets longer.

Reactivity Indices

DFT-related RI are defined as derivatives of the total electronic energy with respect to the number of electrons or the external potential [2].

Global indices—such as the chemical potential μ, the hardness η, and the softness S—contain information about the molecule as a whole. They are often computed using the finite-difference approximation. In the case of S, one obtains $S = 1/(I - A)$, where I is the ionization potential and A is the electron affinity. These properties serve as an input for the global HSAB principle by means of the softness-matching criterium, which states that molecules with the smallest difference between the global softnesses will preferentially react.

Local indices, such as the Fukui function $f(\mathbf{r})$ and the local softness $s(\mathbf{r})$, are applied to predict the most reactive site in a molecule. These two indices are correlated through the equation $s(\mathbf{r}) = Sf(\mathbf{r})$, indicating $f(\mathbf{r})$ and $s(\mathbf{r})$ to be an intra- and intermolecular descriptor, respectively. In practice, one often uses condensed values that give an approximate value for the local function at the position of an atomic center. These quantities are obtained by integration of the local function over an atomic region. In this work we systematically use the natural population analysis (NPA) method. This population analysis is known to give reliable and quantitatively good results [12].

The principal goal of this work is to verify the adequacy of DFT-related RI in giving reliable information on some kinetic aspects of the free radical polymerization reactions, which are subject of this study. We mainly concentrate on the PVC propagation reactions as more distinct reaction features emerge because of the presence of the chlorine atom in VC, making the discussion more interesting. Inspection of the kinetic parameters (Table I) shows only slight differences in the reaction barriers. Consequently, only subtle variations of the RI can be expected.

GLOBAL INDICES

In case of the polymerization of PE a qualitative agreement between ΔE_0 and the softness-matching between ethene and the different radical reactants is found. Table 1 gives a summary of all relevant parameters needed for the discussion. The best matching is found in case of the methyl radical, confirming the kinetic result that PE_1 is character-

ized by the lowest barrier. The reactions PE_2 and PE_3 show almost equal reaction barriers, and the same trend is observed for the RI. In case of PVC, multiple reaction paths are possible and the computation of the RI requires special attention. In order to be able to differentiate between the possible paths, the RI are computed for the different conformations of the reactants. This approach is demonstrated for the PVC_3 addition reaction, which reveals two paths leading to the products **4a** and **4b,** as displayed in Figure 3. The corresponding transition states originate from various conformers (**3, 3′, 3″**) of the radical **3** as explained previously. The RI computed at those conformers are expected to exhibit slight changes, of which we investigate in how far they give an indication about the preferential reaction path. According to the softness-matching criterium (between VC and the different radicals), the RI suggest a preference for reaction path 3a (Table I). This confirms the kinetic results, where the reaction barrier of PVC_3a (leading to product **4a**) is smaller than the barrier of PVC_3b (leading to product **4b**). For addition PVC_3b the conclusion is made on basis of a modified barrier, where the corresponding conformer (**3′**) of the reactant and transition state is taken into account (Table I).

Generally, we conclude that the behavior of the global softness of the different radicals reveals a good qualitative agreement with the relative reaction barriers, supporting the HSAB principle despite the "hard" character of ethene (η = 2.041 eV) and VC (η = 6.061 eV).

The PMH is tested by creating hardness profiles, which reproduce the hardness values along the reaction path. An interesting corollary of the PMH is the fact that the TS of a reaction should have a minimum hardness value [4]. Figure 4 gives the energy E and hardness η computed for the reactant (RE), transition state (TS), and product (PR) of reaction PE_3 and PVC_3a. We stress that only η of the radical reactant is taken into account because it is characterized by the smallest hardness (most reactive). The correct correlation between energy and hardness is observed, and the TS is characterized by the minimal hardness value.

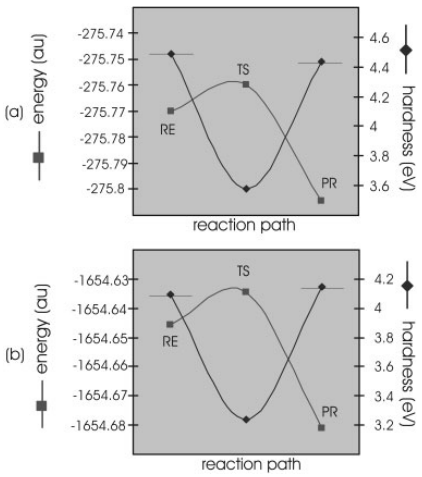

FIGURE 4. Energy-hardness profile of (a) PE_3 and (b) PVC_3a computed at B3LYP/6-311g** level.

LOCAL INDICES

In Table I, the condensed values s_k are given for the carbon atoms, which are numbered starting from the radical center (illustrated in Fig. 3 for PVC). The condensed softness values confirm that the radical center (k = 1) appears as the most reactive site. This is further illustrated by the 3-D plot of $s(\mathbf{r})$ in Figure 3(c). According to the softness-matching criterium, addition of the radical center is expected at the carbon atom of VC bonded to two hydrogen atoms, and thus the correct attack on the VC is suggested.

The previous discussion shows that the RI succeed in predicting the regioselectivity of the VC additions. Because of the use of a population analysis approximation, the subtle differences between the RI become even smaller and, consequently, no correlation between the local RI and kinetic data can be expected. Within this view, we notice that in case of the PVC_3 addition, no distinction can be made between the two possible reaction paths on the basis of local indices.

Conclusions

DFT/B3LYP calculations combined with TST principles produce accurate reaction rates for addition reactions involved in the free radical polymerization processes. This method is generally accepted and requires a conformational and vibrational study of all reactants and transition states.

DFT-based reactivity indices, such as global softness, provide qualitative correlations with the reaction barriers of the studied radical reactions. In case of PVC, the regioselectivity is correctly predicted through the use of the condensed softness values, making a priori exclusion of certain competitive reaction routes possible. Finally, the correlation between the energy and hardness along the reaction path has been studied and the PMH has been illustrated.

ACKNOWLEDGMENTS

This work is supported by the Fund for Scientific Research–Flanders (FWO) and the Research Board of Ghent University.

References

1. (a) Heuts, J. P. A.; Gilbert, R. G.; Radom, L. J Phys Chem 1996, 100, 18997–19006; (b) Van Speybroeck, V.; Van Neck, D.; Waroquier, M. J Phys Chem A 2002, 106, 8945–8950.
2. Parr, R. G.; Yang, W. Density-Functional Theory of Atoms and Molecules; Oxford Science Publications: Oxford, 1988.
3. Geerlings, P.; De Proft, F.; Langenaeker, W. Chem Rev 2003, 103, 1793–1873.
4. (a) Datta, D. J Phys Chem 1992, 96, 2409–2410; (b) Chattaraj, P. K.; Nath, S.; Sannigrahi, A. B. J Phys Chem 1994, 98, 9143–9145.
5. Cadet, J.; Grand, A.; Morell, C.; Letelier, J. R.; Moncada, J. L.; Toro-Labbé, A. J Phys Chem A 2003, 107(27), 5334–5341.
6. Hemelsoet, K.; Van Speybroeck, V.; Marin, G. B.; De Proft, F.; Geerlings, P.; Waroquier, M. Reactivity indices for radical reactions involving polyaromatics. J Phys Chem A 2004, 108(35), 7281.
7. Fischer, H.; Radom, L. Angew Chem Int Ed 2001, 40, 1340–1371.
8. Van Speybroeck, V.; Van Cauter, K.; Coussens, B.; Waroquier, M. Ab initio study of free-radical polymerizations: Last effective methods to determine the reaction rates (I), accepted in Chem Phys Chem (September 2004).
9. Chuang, Y.-Y.; Coitńo, E. L.; Truhlar, D. G. J Phys Chem A 2000, 104, 446–450.
10. NIST. Chemical Kinetics Database on the Web. http://www.kinetics.nist.gov.
11. Endo, K. Prog Polym Sci 2002, 27, 2021–2054.
12. (a) Reed, A. E.; Weinstock, R. B.; Weinhold, F. J Chem Phys 1985, 83, 735–746; (b) Reed, A. E.; Curtiss, L. A.; Weinhold, F. Chem Rev 1988, 88, 899–926.

Paper VIII

Global DFT-based reactivity indicators: an assessment of theoretical procedures in zeolite catalysis

Hemelsoet K. , Lesthaeghe D. , Van Speybroeck V. and Waroquier M.

J. Phys. Chem. C, **2007**, 111, 3028–3037

3028 *J. Phys. Chem. C* **2007,** *111,* 3028−3037

Global DFT-Based Reactivity Indicators: An Assessment of Theoretical Procedures in Zeolite Catalysis

Karen Hemelsoet,* David Lesthaeghe, Veronique Van Speybroeck, and Michel Waroquier*

Center for Molecular Modeling, Ghent University, Proeftuinstraat 86, B-9000 Ghent, Belgium

Received: August 30, 2006; In Final Form: November 23, 2006

The dependence of global reactivity descriptors on electronic structure method as well as basis set is investigated for typical reactions in zeolite catalysis. This research is especially focused on hard−hard interactions between small probe molecules (such as chloromethane, methanol, ethylene, and propene) and different zeolite clusters containing both oxygen and amine functionalities. The performance of novel hybrid metafunctionals (such as BMK and MPWB1K) on crucial reactivity predictors is assessed through comparison with both Hartree−Fock and B3-LYP results. For the complex bifunctional zeolite systems, we find accurate results using any of the DFT functionals, in conjunction with a basis set of at least double-ζ quality further augmented with both polarization and diffuse functions. Reactivity sequences, based on global softness differences as well as activation hardness values, are generally found to be independent of the level of theory whenever a DFT functional is used.

1. Introduction

Ab initio quantum mechanical calculations are nowadays widely used to rationalize all kinds of chemical problems. The standard wave function based Hartree−Fock (HF) method has proven successful, even though computational bond lengths and reaction barriers often overestimate experimental values. Although later refinements (called post-HF methods) lead to more accurate and reliable results, this is at the expense of computational efficiency, which becomes especially problematic when systems of medium or large molecular size are studied. Density functional theory (DFT), on the other hand, has gained a lot of attention over the years, based on an excellent cost-to-performance ratio.[1] Additionally, DFT provides important advantages as a conceptual theory,[2,3] enabling a precise definition for many commonly used chemical concepts such as electronegativity[4] and hardness.[5] These properties, currently referred to as DFT-based reactivity indicators, are defined as functional derivatives of the total electronic energy to the total number of electrons or the external potential.[2,6] In this paper, we will only focus on the so-called "global" indicators (as opposed to "local" indicators), which are used to describe the overall reactivity of a chemical system. These have been commonly applied to a broad variety of organic and inorganic chemical systems, discussing the reactive behavior of one single molecule or a set of related systems, occasionally even providing reactivity sequences for the latter (for a comprehensive review, see ref 3). Compared to traditional reaction rate theories such as transition state theory, calculations based on reactivity indicators are computationally less intensive (but in the same time less detailed) because all information is obtained through study of the reactants only.

Most studies in the field of DFT-based reactivity descriptors focus on their applicability and interpretative use, whereas little attention is generally given to the level of theory at which the indicators are computed. As a standard procedure, they are calculated by simply using the level as was used for the geometry optimization. The choice of basis set and the selection of a quantum mechanical Hamiltonian are nevertheless two essential points which can hardly be neglected, as the main advantage of the indicators is precisely their low computational cost. Furthermore, a strong level-of-theory dependence of the reactivity descriptors would almost certainly undermine their reliability. Relevant works investigating the performance of different theoretical procedures for describing reactivity-related properties are, however, rather scarce, and we will give a brief overview of the literature in the remainder of this paragraph. Most studies primarily assess the influence of the level of theory on local reactivity descriptors.[7] For the global indicators, however, only De Proft and Geerlings previously studied the effect of different theoretical methods on the electronegativity and hardness.[8] They concluded that all DFT methods perform better than the high-level coupled cluster method. A superior behavior was demonstrated for the B3-LYP and B3-PW91 functionals in particular. Additionally, Jalbout et al.[9] reported the excellent performance of the CBS-QB3 and G3B3 methods for a set of heteronuclear and homonuclear diatomic molecules. In an early work by Chattaraj and Schleyer, comparing HF and MP2 results, the effect of correlation was found to be important for the validity of the HSAB principle in the case of soft−soft interactions, whereas interactions involving the hard Ag^+ acid could be sufficiently described using the far less time-consuming HF level.[10] To our knowledge, all research presenting level-of-theory studies on global reactivity indicators is limited to this handful of papers.

For the practical computation of global reactivity descriptors, the finite difference method is by far the most popular. In this approach, the functional derivatives are written as appropriate combinations of the vertical ionization potential and electron affinity. These quantities are absolutely crucial in both experimental and computational chemistry and have consequently gained widespread attention. The computation of these energy differences is, however, not always straightforward: they are

* Authors to whom all correspondence should be addressed. E-mail: Karen.Hemelsoet@UGent.be (K.H.); Michel.Waroquier@UGent.be (M.W.).

10.1021/jp0656227 CCC: $37.00
Published on Web 01/26/2007

largely influenced by the incorporation of electron correlation in the calculation method and require the use of large basis sets, which becomes prohibitive for larger molecular systems.[11] Therefore, almost all studies so far have focused on testing a subset of two data sets developed by Pople and co-workers, denoted as G2−1[12] and G2−2.[13] These sets cover 148 neutral and 146 ionic species and contain extremely accurate experimental data. Whereas the G2−1 test set contains smaller molecules, the G2−2 test set also includes several larger systems such as substituted benzenes. For a recent overview on the electron affinities, we refer to the work of Schaefer and co-workers.[14] In addition to a detailed overview of experimental techniques, several DFT methods were also tested, demonstrating a satisfactory accuracy (within 0.2 eV) for larger molecules of the B3-LYP, BLYP, and BP86 functionals. This accuracy can be spectacularly improved when composite methods are used, e.g., G2 theory has average deviations of 0.06 eV for both ionization energies and electron affinities.[13] The computationally extremely demanding Wn procedures[15−17] show an absolute superior behavior, as W1 is characterized by a mean absolute deviation of 0.013 eV for the G2−1 set and 0.018 eV for the G2−2 set (minus 5 molecules, due to the size of the systems concerned).[16] These methods were, of course, specifically developed and parametrized on relatively small systems. Nevertheless, these studies emphasize how quantum mechanical methods have been developed beyond the level of just reproducing experimental data and are now capable of making accurate predictions where the experimental results are unknown or uncertain. It should also be noted that the electron affinity is typically only a fraction of the size of the ionization potential. Moreover, although every atom and molecule has an ionization potential, they need not necessarily have an electron affinity: there are quite some atomic and molecular negative ions that are simply not stable. Within this respect, density functional methods have been suggested to be fundamentally in error for the computation of anionic systems.[18] However, no convincing evidence was found to support this concern.[19] Moreover, a recent discussion has shown that DFT-based reactivity indicators, and the hardness in particular, can contribute to an improved understanding of this problem.[20]

In this paper, the influence of the level of theory on global DFT-based reactivity indicators is studied. More specifically, the effect of both basis set size and electronic structure method is thoroughly discussed. In order to probe the latter effect, HF (representing a wave function-based method) as well as three density-functional-based techniques are tested. The performance of the MPWB1K[21] and BMK functionals,[22] representing the latest class of hybrid metafunctionals, are assessed for the first time. These metafunctionals are primarily known for their successful description of kinetic properties. Even though the BMK functional is brand new, it has already shown promising results for various properties such as geometries and reaction barriers.[22,23] Overall, our main interest is to qualitatively investigate whether reactivity sequences remain unchanged when different levels of theory are used. This would also be the first time that large inorganic molecules such as zeolites are considered as a test set for an expanded assessment, as these molecules of considerable size are, quite logically, not included in the aforementioned G2−1 and G2−2 test sets.

As just mentioned, the present level-of-theory study on global reactivity indicators is performed on typical zeolite systems. Zeolites are microporous crystalline aluminosilicates, built from corner-sharing SiO_4 and AlO_4 tetrahedra. These solid-state catalysts portray a wide variety of properties and applications,

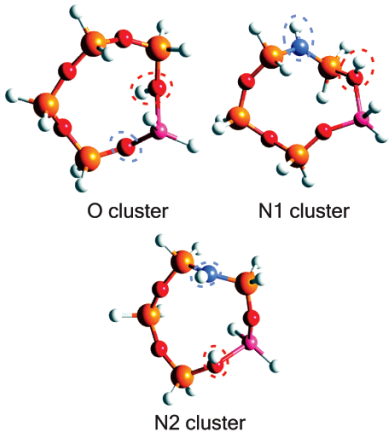

Figure 1. Optimized cluster geometries at B3-LYP/6-31G(d) level of theory, with acid site (red dotted line) and basic site (blue dotted line). For the O and N1 clusters both active sites are located on the same tetrahedron, whereas for the N2 cluster, the acid and base sites are further separated.

due mainly to their shape-selectivity and Brönsted acid sites ≡Si−OH−Al≡, in combination with neighboring Lewis base ≡Si−O−Al≡ sites. The size of the zeolite clusters needed for an adequate description of the chemically active part, combined with the presence of different elements which all play a crucial role in defining the chemical properties, add to the challenge of describing these systems through global reactivity descriptors. This explains why the zeolite systems under study form an ideal test set for both absolute and relative values of these descriptors, outside the scope of G2−1 and G2−2. In addition to a traditional acidic zeolite cluster, we will also compare results with amine substituted zeolites,[24] allowing us to validate whether reactivity sequences in zeolites remain unaltered for different levels of theory. The appeal of nitrogen-substituted zeolites is mainly based on the minor change on the molecular level (substituting a single oxygen bridge by a N−H bridge), yet which leads to completely different reactivity profiles. By applying detailed theoretical calculations on reactions in both zeolite types using classical transition state theory, amine-based zeolites have shown to be catalytically more active than the conventional analogue with O linkages.[25,26] Therefore, these catalysts represent a new class of highly promising materials. In previous work, we specifically studied the interactions of chloromethane, methanol, ethylene, and propene with three zeolite model clusters (O, N1, and N2),[27] which are depicted in Figure 1. In addition to a kinetic description of these reactions, we also investigated their reactive behavior from the viewpoint of DFT-based reactivity descriptors.[28] Using both local and global descriptors, calculated at the B3-LYP/6-31G(d)//B3-LYP/6-31G(d) level of theory, we demonstrated that the interaction can be characterized as hard−hard, and that certain quantities are fully capable of predicting the reactivity sequences as a result of the amine-substitution. In general, the descriptors were found to provide valuable information on the catalytic abilities of the various clusters.[28]

Summarizing, in this paper, we will validate whether the absolute values of global descriptors, which we previously calculated for some small molecules and a typical zeolite

containing only oxygen bridges on one specific level of theory, remain unchanged when different levels of theory are employed. We will investigate the low-cost HF method as well as three different DFT functionals, more precisely: B3-LYP, BMK, and MPWB1K. Although B3-LYP is the traditional functional of choice for calculations on zeolite systems, this is, to our knowledge, the first application of the hybrid metafunctionals MPWB1K and BMK in zeolite catalysis. In a next step, we will use the amine substituted zeolites to verify whether the choice in level of theory might influence reactivity sequences.

2. Global Reactivity Descriptors

The DFT-based reactivity indicators are defined as derivatives of the electronic energy $E[N,v(\mathbf{r})]$ with N the total number of electrons and $v(\mathrm{r})$ the external potential.[2,3,6] Global reactivity indicators provide information on the overall reactivity of a chemical system and are used to discuss reactivity sequences. The chemical potential (μ) equals the negative of the electronegativity, expressing the initial attraction toward electronic charge:

$$\mu = -\chi = \left(\frac{\partial E}{\partial N}\right)_v$$

The second derivative or hardness (η) measures the resistance to charge transfer, and the reciprocal is identified with the global softness (S)

$$\eta = \frac{1}{2S} = \left(\frac{\partial^2 E}{\partial^2 N}\right)_v$$

Using the finite difference approach, μ, η, and S can be computed from the vertical ionization potential (IP) and electron affinity (EA)

$$\mu = -\frac{\mathrm{IP} + \mathrm{EA}}{2}$$

$$\eta = \frac{\mathrm{IP} - \mathrm{EA}}{2}$$

$$S = \frac{1}{\mathrm{IP} - \mathrm{EA}}$$

The computation of these descriptors requires three single-point energy calculations. Nevertheless, as these calculations must be performed at a fixed geometry (the optimized geometry of the N-electron system), the computational effort in order to follow this procedure remains limited. The quantities are implemented in empirically well-known chemical principles. The hard soft acid base (HSAB) principle was originally discussed by Pearson[29] and states that a reaction between systems A and B will be favored when the global softness difference $\Delta S = S_A - S_B$ is minimal.[30] This rule was obtained through optimization of the covalent contribution of the interaction energy, consequently neglecting other effects such as polarization. According to the principle of maximal hardness (PMH),[31] molecules will rearrange themselves to achieve maximal hardness. Consequently, the transition state of a reaction should exhibit minimal hardness.[32] The activation hardness $\Delta\eta_{act} = \eta_{\text{adsorbed reactant}} - \eta_{\text{transition state}}$ describes hardness variations along the reaction path.[33] The smaller the activation hardness, the easier a reaction should occur.

3. Computational Methods

All calculations were performed using the Gaussian 03 software package.[34] The zeolite catalysts were simulated by a cluster built from 5 tetrahedral atoms (5T, T-atoms = Al or Si), which is capable of providing an adequate qualitative picture of chemical rearrangements that occur locally on the active site.[35,36] For the three zeolite clusters, the four probe molecules, as well as the adsorbed complexes, full geometry optimizations and frequency calculations using the hybrid B3-LYP functional[37,38] and 6-31G(d) basis set were performed as obtained in ref 25. The B3-LYP functional is known to provide accurate geometries within zeolite catalysis: Zygmunt et al. assessed the applicability of various readily available functionals for studying molecular adsorption in zeolite clusters and found that the B3-LYP functional gives intermolecular energies and vibrational frequencies similar to those obtained using MP2. Their final conclusion stated that the B3-LYP functional was the best choice for DFT treatment of zeolite clusters.[39] Nevertheless, we will also verify the suitability of the B3-LYP geometries by investigating the influence of the level of theory used for the geometry optimization. First, the performance of other functionals for geometry optimization, in particular BMK and MPWB1K, will be assessed. Second, we will upgrade the small basis set 6-31G(d) to 6-31+G(d,p), testing the influence of additional diffuse and polarization functions on the final geometry.

For the single-point energy calculations, four theoretical procedures were assessed. First of all, the standard Hartree−Fock (HF) method, in which correlation energy is completely neglected, was selected, due to the low computational cost. Note that the "DFT-based reactivity descriptors" are not rigorously defined within the HF scheme. However, we have used the finite difference approach to calculate these descriptors from the ionization potential and electron affinity obtained at the HF level. Furthermore, the popular B3-LYP hybrid functional[37,38] was applied. This functional is the standard choice to perform calculations within zeolite catalysis. In addition, two recently developed up-and-coming meta-gradient corrected functionals (BMK[22] and MPWB1K[21]) were also chosen, as their performance within the theory of conceptual DFT, as well as within zeolite catalysis, has not been investigated earlier.

Since the electron affinity values are very sensitive to the basis set,[40] as the addition of the electron entails a profound change in the spatial extent of the wave function of the anion, many Gaussian Pople basis sets were tested,[41] including 6-31G(d) (**1**), 6-31+G(d,p) (**2**), 6-311G(d,p) (**3**), 6-311+G(d,p) (**4**), 6-311++G(d,p) (**5**), and 6-311++G(3df,2p) (**6**). The performance of a selection of Dunning's correlation consistent basis sets,[42] cc-pVDZ (**7**), aug-cc-pVDZ (**8**), cc-pVTZ (**9**), and aug-cc-pVTZ (**10**) was also studied. The augmented basis sets **8** and **10** include one set of diffuse functions for each value of the angular momentum ℓ.

Additionally, for the smaller probe molecules (methanol, chloromethane, ethylene, and propene) high-level single-point energy calculations were performed, using the QCISD(T)[43] and CCSD(T)[44] post-HF methods in conjunction with the 6-311+G(d,p) and/or 6-311+G(3df,2p) basis sets. For these computations, the optimized B3-LYP/6-31G(d) geometries were used.

4. Results and Discussion

4.1. Comparison with Experiment: Small Probe Molecules. Resulting IP and EA values as well as their derived properties μ and η were calculated for four small probe molecules: chloromethane, methanol, ethylene, and propene. The calculated IP values were compared with available experimental data and mean absolute deviations (MADs) are reported in Table 1. The experimental IP values were obtained using

TABLE 1: Performance of Different Functional Methods[a]

	IP				μ and η			
	HF	B3-LYP	BMK	MPWB1K	HF	B3-LYP	BMK	MPWB1K
1. 6-31G(d)	1.43	0.25	0.25	0.25	1.62	1.21	1.31	1.28
2. 6-31+G(d,p)	1.36	0.11	0.14	0.16	0.72	0.21	0.34	0.31
3. 6-311G(d,p)	1.39	0.15	0.15	0.20	1.23	0.76	0.87	0.87
4. 6-311+G(d,p)	1.36	0.08	0.11	0.14	0.69	0.16	0.28	0.25
5. 6-311++G(d,p)	1.36	0.08	0.11	0.14	0.69	0.25	0.20	0.21
6. 6-311++G(3df,2p)	1.40	0.07	0.11	0.14	0.71	0.26	0.19	0.21
7. cc-pVDZ	1.42	0.20	0.20	0.21	1.43	0.97	1.10	1.07
8. aug-cc-pVDZ	1.38	0.09	0.12	0.15	0.70	0.31	0.20	0.16
9. cc-pVTZ	1.42	0.11	0.14	0.16	1.11	0.65	0.77	0.76
10. aug-cc-pVTZ	1.41	0.08	0.13	0.14	0.72	0.35	0.25	0.26
average values:								
over all basis sets	1.39	0.12	0.15	0.17	0.96	0.51	0.55	0.54
without diffuse functions	1.42	0.18	0.19	0.21	1.34	0.90	1.01	1.00
with diffuse functions	1.38	0.08	0.12	0.14	0.70	0.26	0.24	0.23

[a] Mean average deviations (MADs) in eV for the set of small probe molecules CH_3Cl, CH_3OH, C_2H_4, and C_3H_6. For the IPs the MADs are referred with respect to experiment, whereas for the global indicators μ and η the reference is the high level of theory QCISD(T)/6-311++G(3df,2p)//B3-LYP/6-31G(d).

photoelectron spectroscopy, amounting to 11.29 eV for chloromethane,[45] 10.96 eV for methanol,[46] 10.68 eV for ethylene,[47] and 9.91 eV for propene.[48]

From Table 1, it is immediately clear that the performance of the HF method is well below standard, showing deviations between 1.36 and 1.43 eV. In large contrast, the computed MAD values for the DFT functionals all indicate an excellent correlation with experiment, as the maximum MAD amounts to 0.25 eV, which corresponds to the smallest basis set 6-31G(d) taken into consideration. It is furthermore difficult to differentiate between the three DFT methods, as all of them succeed in an almost exact reproduction of the experimental data. The influence of the basis set is rather limited: the effect of adding extra polarization functions to a triple-ζ basis set (transition from basis set **5** to **6**) is, for instance, negligible. However, inclusion of diffuse functions leads to a substantial improvement of the results. This is a general observation, valid for both double- and triple-ζ basis sets. Furthermore, the Pople (**1**−**6**) and Dunning (**7**−**10**) basis set series perform very similarly, but because of the computational cost of the augmented basis sets, the latter series are not recommended for systems of considerable size. Overall, usage of 6-31G(d) and cc-pVDZ basis sets is discouraged.

As the global properties μ and η are not directly experimentally accessible and reliable experimental electron affinity data were not found, additional single-point energy calculations using the QCISD(T) and CCSD(T) levels, and using the B3-LYP/6-31G(d) optimized geometries, were performed (not included in Table 1). Among these, the QCISD(T)/6-311++G(3df,2p) level was chosen for benchmarking purposes as the MAD for the ionization potential with respect to the experimental values turned out to be the lowest (0.04 eV). MAD values for μ and η, resulting from comparison with the benchmark QCISD(T)/6-311++G(3df,2p) method, are given in Table 1. Closer inspection demonstrates how the three DFT functionals perform very similarly, whereas the HF MAD values are again substantially higher. All basis sets without diffuse functions perform poorly, irrespective of their double or triple-ζ character.

We conclude that for the computation of global descriptors, in the case of the four small probe molecules, accurate results can be obtained using either one of B3-LYP, BMK, or MPWB1K DFT functionals, in combination with a basis set of double-ζ or triple-ζ quality, augmented with both diffuse and polarization functions.

4.2. Reactivity Indicators: Purely Oxygen-Bridged Zeolites. Resulting IP, EA, μ and η values were calculated for the isolated, purely oxygen-bridged zeolite reactant (O cluster in Figure 1). Four electronic structure methods and nine basis sets were tested (in the remainder of the article the aug-cc-pVTZ basis set **10** is omitted, due to the large computational cost), and the results are reported in Table 2. Using the same extended set of various computational methods, global softness differences ΔS for the interactions between the O cluster and the small probe molecules were computed and consequently listed in Table 3. Finally, activation hardnesses $\Delta\eta_{act}$ were also calculated, using the optimized geometries of the adsorbed reactants and transition structures, and these values are given in Table 4.

4.2.1. Ionization Potential, Electron Affinity, Chemical Potential, and Hardness. The calculated IP values for this inorganic species (Table 2) show only a minor dependence on the level of theory, as they all lie in the narrow range between 9.35 and 9.90 eV. Inclusion of diffuse functions does not significantly alter the results. The EA values, on the other hand, vary more substantially, ranging from −0.19 to −2.81 eV. This effect is mostly attributed to the inclusion of diffuse functions, which are necessary for an accurate description of the more diffuse electron distribution of the anion state.

The influence of level of theory on the final geometry optimization was assessed for the purely oxygen-bridged zeolite cluster. The BMK/6-31G(d) and MPWB1K/6-31G(d) levels were used to assess the influence of a different functional and the B3-LYP/6-31+G(d,p) level was used to define the influence of a different basis set on the optimization. The sensitivity to geometry optimization is found to be extremely limited: Figure S1 in the Supporting Information depicts the global hardness of the zeolite catalyst which coincides for all levels of theory. The sole exception is formed by the low-cost HF single-point calculation on the MPWB1K optimized geometry, but the general trend is maintained nonetheless. Therefore, only the B3-LYP/6-31G(d) optimized geometries were retained in the remainder of this work.

The calculated μ varies between −3.40 and −4.69 eV, whereas η values range between 4.81 and 6.22 eV, indicating a relatively hard character of the investigated zeolite. The role of basis set is again restricted to the presence of diffuse functions, giving rise to a decrease of the hard character of the species with approximately 0.40 eV. We note that for all functionals under consideration, the 6-31+G(d,p), 6-311+G(d,p), 6-311++G(d,p), 6-311++G(3df,2p) and aug-cc-pVDZ results are extremely similar to one another. Based on these results, a double-ζ basis set, augmented with one set of diffuse

TABLE 2: Ionization Potentials, IP, Electron Affinities, EA, Chemical Potential, μ, and Global Hardness, η, for the Purely Oxygen-Bridged Zeolite[a]

	IP				EA			
	HF	B3-LYP	BMK	MPWB1K	HF	B3-LYP	BMK	MPWB1K
1. 6-31G(d)	9.65	9.37	9.77	9.78	−2.80	−1.35	−1.69	−1.59
2. 6-31+G(d,p)	9.68	9.48	9.86	9.86	−1.25	−0.41	−0.79	−0.67
3. 6-311G(d,p)	9.64	9.47	9.86	9.83	−2.27	−0.94	−1.32	−1.22
4. 6-311+G(d,p)	9.65	9.50	9.90	9.86	−1.20	−0.38	−0.76	−0.64
5. 6-311++G(d,p)	9.65	9.50	9.88	9.86	−1.03	−0.35	−0.68	−0.58
6. 6-311++G(3df,2p)	9.61	9.50	9.90	9.84	−0.96	−0.30	−0.61	−0.54
7. cc-pVDZ	9.62	9.35	9.74	9.75	−2.81	−1.33	−1.67	−1.58
8. aug-cc-pVDZ	9.57	9.43	9.77	9.77	−0.68	−0.19	−0.48	−0.39
9. cc-pVTZ	9.60	9.47	9.86	9.82	−2.36	−0.97	−1.32	−1.24
average values:								
over all basis sets	9.63	9.45	9.84	9.82	−1.70	−0.69	−1.04	−0.94
without diffuse functions	9.63	9.41	9.81	9.79	−2.56	−1.15	−1.50	−1.41
with diffuse functions	9.63	9.48	9.86	9.84	−1.02	−0.32	−0.66	−0.56

	μ				η			
	HF	B3-LYP	BMK	MPWB1K	HF	B3-LYP	BMK	MPWB1K
1. 6-31G(d)	−3.43	−4.01	−4.04	−4.09	6.22	5.36	5.73	5.68
2. 6-31+G(d,p)	−4.21	−4.54	−4.54	−4.60	5.47	4.95	5.32	5.26
3. 6-311G(d,p)	−3.69	−4.27	−4.27	−4.31	5.96	5.20	5.59	5.53
4. 6-311+G(d,p)	−4.22	−4.56	−4.57	−4.61	5.43	4.94	5.33	5.25
5. 6-311++G(d,p)	−4.31	−4.58	−4.60	−4.64	5.34	4.92	5.28	5.22
6. 6-311++G(3df,2p)	−4.33	−4.60	−4.65	−4.65	5.28	4.90	5.26	5.19
7. cc-pVDZ	−3.40	−4.01	−4.04	−4.09	6.21	5.34	5.70	5.66
8. aug-cc-pVDZ	−4.45	−4.62	−4.65	−4.69	5.13	4.81	5.12	5.08
9. cc-pVTZ	−3.63	−4.25	−4.27	−4.29	5.98	5.22	5.59	5.53
average values:								
over all basis sets	−3.96	−4.38	−4.40	−4.44	5.67	5.07	5.44	5.38
without diffuse functions	−3.54	−4.13	−4.15	−4.19	6.09	5.28	5.65	5.60
with diffuse functions	−4.30	−4.58	−4.60	−4.64	5.33	4.90	5.26	5.20

[a] All values are given in eV.

TABLE 3: ΔS Results in Absolute Values (au^{-1}) for the Reactions between the Probe Molecules and the Purely Oxygen-Bridged Zeolite

	zeolite O + CH_3Cl				zeolite O + CH_3OH			
	HF	B3-LYP	BMK	MPWB1K	HF	B3-LYP	BMK	MPWB1K
1. 6-31G(d)	0.321	0.677	0.556	0.557	0.399	0.741	0.635	0.641
2. 6-31+G(d,p)	0.274	0.594	0.467	0.478	0.185	0.546	0.406	0.414
3. 6-311G(d,p)	0.325	0.639	0.506	0.530	0.288	0.633	0.514	0.525
4. 6-311+G(d,p)	0.246	0.576	0.427	0.448	0.158	0.524	0.384	0.388
5. 6-311++G(d,p)	0.148	0.483	0.354	0.360	0.025	0.409	0.285	0.277
6. 6-311++G(3df,2p)	0.158	0.490	0.359	0.368	0.047	0.424	0.297	0.293
7. cc-pVDZ	0.303	0.640	0.534	0.537	0.295	0.639	0.544	0.547
8. aug-cc-pVDZ	0.226	0.533	0.417	0.410	0.097	0.454	0.337	0.322
9. cc-pVTZ	0.272	0.600	0.485	0.502	0.226	0.587	0.471	0.484
average values:								
over all basis sets	0.252	0.581	0.456	0.466	0.191	0.551	0.430	0.432
without diffuse functions	0.305	0.639	0.520	0.531	0.302	0.650	0.541	0.549
with diffuse functions	0.211	0.535	0.405	0.413	0.102	0.471	0.342	0.339

	zeolite O + C_2H_4				zeolite O + C_3H_6			
	HF	B3-LYP	BMK	MPWB1K	HF	B3-LYP	BMK	MPWB1K
1. 6-31G(d)	0.058	0.552	0.401	0.405	0.023	0.435	0.297	0.300
2. 6-31+G(d,p)	0.144	0.532	0.378	0.396	0.066	0.406	0.274	0.287
3. 6-311G(d,p)	0.095	0.567	0.403	0.412	0.017	0.448	0.301	0.308
4. 6-311+G(d,p)	0.166	0.543	0.385	0.405	0.125	0.411	0.276	0.289
5. 6-311++G(d,p)	0.011	0.392	0.408	0.419	0.139	0.168	0.056	0.031
6. 6-311++G(3df,2p)	0.003	0.401	0.413	0.429	0.059	0.178	0.062	0.041
7. cc-pVDZ	0.020	0.522	0.376	0.376	0.059	0.403	0.273	0.270
8. aug-cc-pVDZ	0.012	0.419	0.283	0.476	0.212	0.208	0.099	0.209
9. cc-pVTZ	0.043	0.521	0.360	0.375	0.032	0.404	0.261	0.272
average values:								
over all basis sets	0.061	0.494	0.379	0.410	0.081	0.340	0.211	0.223
without diffuse functions	0.054	0.540	0.385	0.392	0.033	0.422	0.283	0.288
with diffuse functions	0.067	0.458	0.373	0.425	0.120	0.274	0.153	0.171

functions and polarization functions (e.g., basis set **2**), seems sufficient for a reliable calculation of the global reactivity descriptors.

From a more interpretative point of view, μ can be applied to characterize the relative electrophilic or nucleophilic behavior of the involved molecules.[49] The chemical potentials for the

TABLE 4: $\Delta\eta_{act}$ Values (eV) for the Reactions between the Probe Molecules and the Purely Oxygen-Bridged Zeolite

	zeolite O + CH_3Cl				zeolite O + CH_3OH			
	HF	B3-LYP	BMK	MPWB1K	HF	B3-LYP	BMK	MPWB1K
1. 6-31G(d)	1.902	0.601	0.854	0.892	1.274	1.093	1.201	1.185
2. 6-31+G(d,p)	1.108	0.226	0.591	0.607	0.909	1.024	1.174	1.086
3. 6-311G(d,p)	2.155	0.501	0.731	0.784	1.075	1.085	1.232	1.159
4. 6-311+G(d,p)	1.044	0.387	0.591	0.600	0.871	1.006	1.159	1.041
5. 6-311++G(d,p)	0.949	0.347	0.528	0.526	0.888	0.948	1.054	0.988
6. 6-311++G(3df,2p)	1.507	0.311	0.607	0.514	0.890	0.955	1.063	0.983
7. cc-pVDZ	1.845	0.607	0.842	0.893	1.306	1.167	1.252	1.246
8. aug-cc-pVDZ	1.316	0.283	0.418	0.324	0.820	0.894	1.012	0.908
9. cc-pVTZ	2.319	0.419	0.798	0.829	1.267	1.165	1.294	1.249
average values:								
over all basis sets	1.572	0.409	0.662	0.663	1.033	1.037	1.160	1.094
without diffuse functions	2.055	0.532	0.806	0.850	1.230	1.127	1.245	1.210
with diffuse functions	1.185	0.311	0.547	0.514	0.876	0.965	1.092	1.001

	zeolite O + C_2H_4				zeolite O + C_3H_6			
	HF	B3-LYP	BMK	MPWB1K	HF	B3-LYP	BMK	MPWB1K
1. 6-31G(d)	1.616	1.092	1.275	1.304	2.151	1.452	1.722	1.730
2. 6-31+G(d,p)	1.089	0.852	1.015	1.024	1.526	1.509	1.436	1.408
3. 6-311G(d,p)	1.611	0.980	1.143	1.169	2.057	1.371	1.588	1.583
4. 6-311+G(d,p)	1.011	0.845	1.002	0.982	1.437	1.171	1.409	1.361
5. 6-311++G(d,p)	0.868	0.819	1.024	0.894	1.283	1.093	1.306	1.254
6. 6-311++G(3df,2p)	0.883	0.821	1.000	0.908	1.312	1.122	1.428	1.286
7. cc-pVDZ	1.531	1.096	1.255	1.282	2.058	1.454	1.678	1.697
8. aug-cc-pVDZ	1.285	0.743	0.964	0.795	1.206	1.049	1.368	1.184
9. cc-pVTZ	1.442	1.014	1.196	1.204	1.983	1.407	1.605	1.622
average values:								
over all basis sets	1.259	0.918	1.097	1.063	1.668	1.292	1.504	1.458
without diffuse functions	1.550	1.046	1.217	1.240	2.062	1.421	1.648	1.658
with diffuse functions	1.027	0.816	1.001	0.921	1.353	1.189	1.389	1.298

four probe molecules are tabulated in Table S2 of the Supporting Information. All Pople basis sets including diffuse functions succeed in a correct prediction of the stronger electrophilic behavior of the polar molecules (methanol and chloromethane) and a more nucleophilic behavior for the apolar molecules (ethene and propene). This is clearly illustrated in Figure 2, where the variation of the chemical potential depending on basis set size is depicted. As functional sensitivity was found to be small, only BMK results are included in Figure 2. The basis sets without diffuse functions, on the other hand, do not show a clear separation between molecules with polar and apolar character. Large deviations are clear for methanol in particular.

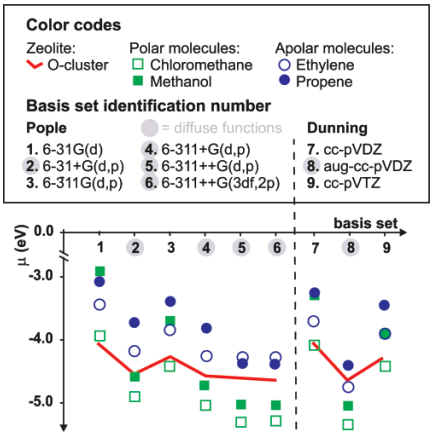

Figure 2. μ values for the O cluster (red line) and the four probe molecules chloromethane, methanol, ethylene and propene, calculated using the BMK functional (polar molecules: green; apolar molecules: blue).

4.2.2. Softness Differences. In Table 3, we list ΔS for the interaction between the four small probe molecules and the purely oxygen-bridged zeolite cluster. Large variations occur depending on both basis set and electronic structure method, but the overall predictions for ΔS are systematically larger for the two polar molecules compared to the apolar systems. Closer inspection of Table 3 reveals that the BMK and MPWB1K functionals predict almost identical values, whereas the HF predictions show large deviations from the DFT results. Concerning basis set dependence, the lack of diffuse functions will most often lead to higher ΔS values. At any rate, caution is absolutely necessary when applying the softness matching criterion to predict reaction preferences, as conclusions may depend on the applied level of theory. For sake of completeness, Table S1 of the Supporting Information tabulates the influence of the level of theory used for the geometry optimization on the average ΔS values. Yet again, this influence is negligible and our choice for B3-LYP/6-31G(d) geometries is warranted.

4.2.3. Activation Hardnesses. The $\Delta\eta_{act}$ values (Table 4) use information from the adsorbed reactants as well as from transition state structures. The smaller the $\Delta\eta_{act}$ value, the easier the reaction should proceed and the lower the reaction barrier should be. In ref 28, we compared $\Delta\eta_{act}$ values with energy barriers at 0 Kelvin (ΔE_0, Table 5; all properties were calculated using the B3-LYP/6-31G(d)//B3-LYP/6-31G(d) level of theory). Based on the ΔE_0 values, the following reactivity sequence corresponding to the interactions between the various small probe molecules and the purely oxygen-bridged cluster was obtained: propene < ethylene < chloromethane < methanol. No correlation exists between ΔE_0 and $\Delta\eta_{act}$, leading to the

TABLE 5: ΔE_0 Values (kJ/mol) for Chemisorption Reactions, ZPE Included, Taken from ref 28

	ΔE_0			
B3-LYP/6-31G(d)	CH_3Cl	CH_3OH	C_2H_4	C_3H_6
O	169.9	199.8	96.6	86.0
N1	220.3	165.8	141.0	117.6
N2	117.5	150.3	124.3	119.6

conclusion that the reactivity descriptor $\Delta\eta_{act}$ is inadequate in differentiating between the reactivities of the various probe molecules. The present study strongly confirms this conclusion: no correlation is obtained between the ΔE_0 and $\Delta\eta_{act}$ values, regardless of the level of theory used (see Table 4). We readily see that the overall $\Delta\eta_{act}$ value is smallest in the case of adsorption of chloromethane, while slight deviations can be noticed in the estimates predicted for methanol and ethylene. The largest values are found for propene. We note that for the current study the energy barriers were recalculated using the various levels of theory (included in Table S3 in the Supporting Information), but they do not differ qualitatively from the values at the B3-LYP/6-31G(d) level (displayed in Table 5). Finally, we report that the absolute values of HF differ substantially from the DFT results. The various $\Delta\eta_{act}$ predictions can again be classified in two categories, depending on the inclusion or exclusion of diffuse functions in the basis set.

4.3. Reactivity Sequences: Amine-Modified Zeolites. Comparison with kinetic data, such as ΔE_0 (Table 5), becomes more challenging when various zeolite clusters are compared. As in previous works of the authors, amine-substituted zeolite clusters (Figure 1) have been intensively investigated.[25,27] They form a suitable set of zeolite clusters to further validate the various rules on global reactivity descriptors. In particular, we will investigate whether the reactivity sequences between the three zeolite model clusters, as predicted in ref 28 using B3-LYP/6-31G(d), are maintained throughout the various levels of theory.

4.3.1. Hardness Sequence. In Tables S4 and S5 of the Supporting Information, the calculated IP and EA values as well as their derived global properties are given for the isolated amine-substituted zeolite models N1 and N2. It was earlier reported that all three investigated clusters are considered intermediately hard and that substitution of an oxygen by a nitrogen atom lowers the hardness, increasing the reactivity of the amine-modified cluster.[28] These conclusions were based on B3-LYP/6-31G(d) results, we now demonstrate that the hardness sequence $\eta(O) > \eta(N2) > \eta(N1)$ is retained for all investigated levels. The average difference between the $\eta(O)$ and $\eta(N2)$ values is 0.14 eV, whereas the average difference between the amine-substituted hardness values N2 and N1 is much smaller (0.07 eV). The reported hardness sequence indicates that substitution of an oxygen by a nitrogen atom lowers the hardness, increasing the reactivity of the amine-modified cluster.

4.3.2. Softness Differences. Global softness differences are calculated for the interactions between the three zeolite clusters and the probe molecules. Chloromethane and ethylene were chosen as the case study polar and apolar system, respectively. It was previously observed, using the B3-LYP/6-31G(d) level of theory, that for the interactions with the polar molecules, the HSAB principle fails due to a lack of any correlation between ΔS and ΔE_0.[28] This failure illustrates the limitations of the HSAB principle, where polarization effects are only partially included. For the apolar molecules however, the HSAB was shown to be successful.[28] In Figures 3 and 4 results for chloromethane and ethylene are illustrated. The following conclusions can be made.

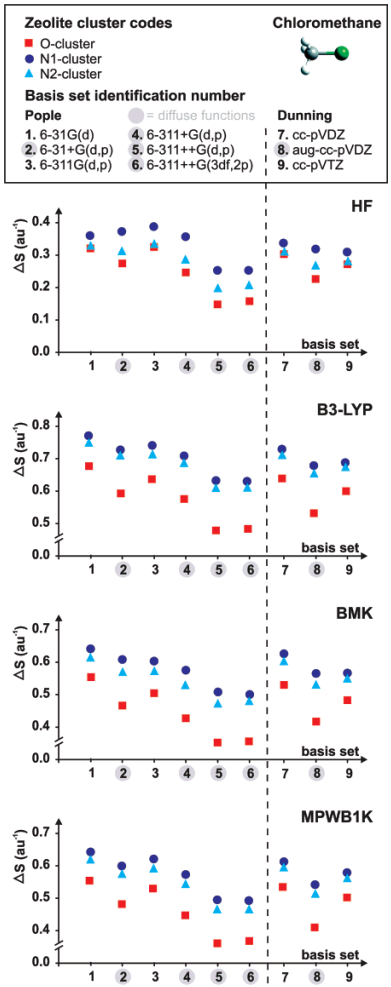

Figure 3. ΔS values for the interactions with chloromethane. Red squares correspond to the O cluster, dark blue circles to the N1 cluster, and light blue triangles to the N2 cluster.

First, we find that the overall qualitative basis set dependence of the various DFT functionals is extremely similar. A striking exception is noticed for the interaction with C_2H_4, where augmentation from the Dunning cc-pVDZ basis set leads to a largely deviating behavior for the MPWB1K functional.

Second, for ethylene the basis set dependence is largest in HF. From a quantitative perspective, the HF values are systematically smaller than the DFT results.

Third, the reactivity sequence $\Delta S(O) < \Delta S(N2) < \Delta S(N1)$ is found throughout, for both ethylene and chloromethane. Only

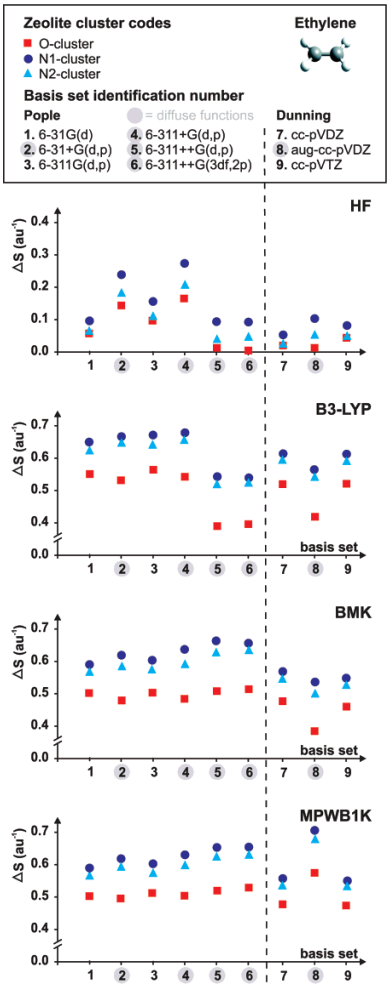

Figure 4. ΔS values for the interactions with ethylene. Red squares correspond to the O cluster, dark blue circles to the N1 cluster, and light blue triangles to the N2 cluster.

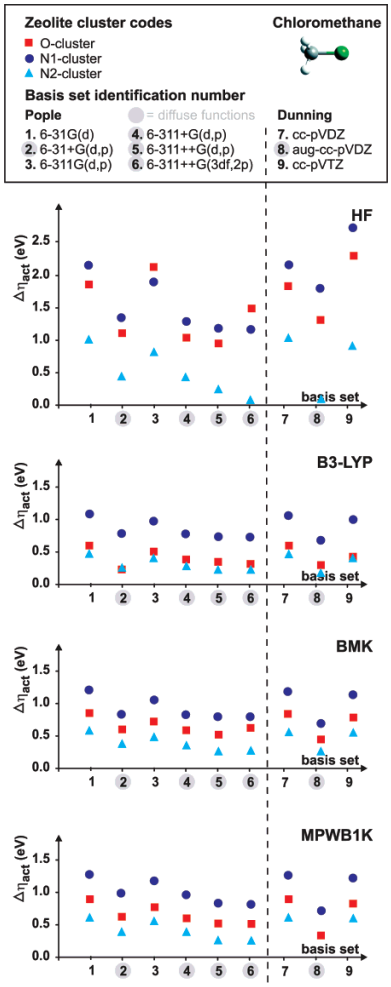

Figure 5. $\Delta\eta_{act}$ values or the interactions with chloromethane. Red squares correspond to the O cluster, dark blue circles to the N1 cluster, and light blue triangles to the N2 cluster.

in the case of ethylene this sequence matches the kinetic results in Table 5. For the studied hard−hard interactions within zeolite catalysis, reactivity sequences based on ΔS values are entirely independent of the computational method used for the calculation of the global reactivity descriptors. This is no guarantee, however, for sequences based on the HSAB principle to coincide with sequences obtained from kinetic data.

4.3.3. Activation Hardnesses. Activation hardnesses were calculated for the interactions between the three zeolite clusters and the probe molecules. Computations on both the optimized structures of the adsorbed reactants and transition structures were performed. Application of the B3-LYP/6-31G(d) level of theory on these systems has already been performed,[28] and an excellent correlation between the $\Delta\eta_{act}$ and ΔE_0 values for all studied reactions was observed. However, does this agreement still hold when the level of theory, used for the single-point energy calculations, is altered? Chloromethane and ethylene (optimized at B3-LYP/6-31G(d)) were again chosen as reference polar and apolar systems, respectively. The results are illustrated in Figures 5 and 6.

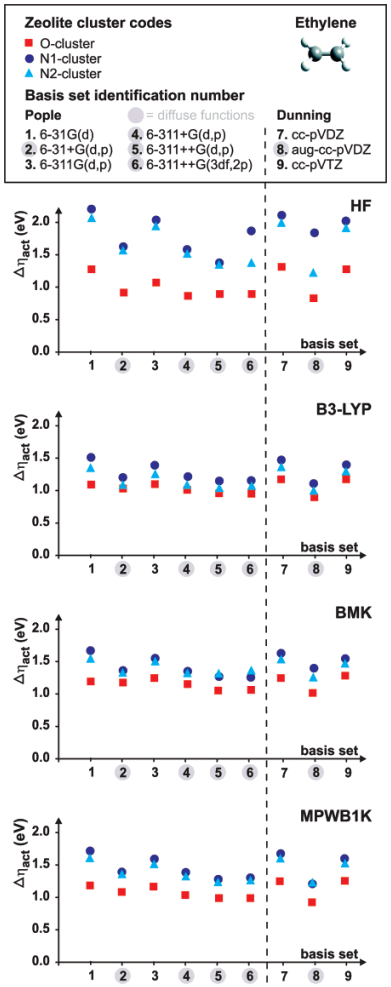

Figure 6. $\Delta\eta_{act}$ values for the interactions with ethylene. Red squares correspond to the O cluster, dark blue circles to the N1 cluster, and light blue triangles to the N2 cluster.

The conclusions about basis set and functional dependence are quite similar to those obtained in the previous section for the ΔS values. The basis set sensitivity of the four methods follows a similar pattern. The HF results show again a larger scattering from the DFT results, the latter which are closer to each other.

For the interaction with chloromethane, the sequence based on reaction barriers is the following: $\Delta E_0(N1) > \Delta E_0(O) > \Delta E_0(N2)$ and this trend is correctly reproduced by all three DFT methods using the $\Delta\eta_{act}$ descriptor. The MPWB1K/aug-cc-pVDZ result for the N2 cluster has been omitted due to spin-contamination in the calculation of the cation. The HF results show occasional deviations from this sequence, more precisely when the 6-311G(d,p) (**3**), 6-311++G(3df,2p) (**6**) basis sets are used. As mentioned earlier, HF performs poorly for the computation of $\Delta\eta_{act}$ values, underlying the importance of including correlation effects for an accurate energy calculation of the adsorbed reactants and transition structures.

For the interaction with ethylene, the correct sequence is different: $\Delta\eta_{act}(N1) > \Delta\eta_{act}(N2) > \Delta\eta_{act}(O)$. Here all levels of theory succeed in reproducing correctly this sequence. Only the BMK functional predicts an occasional reversed sequence between the N1 and N2 clusters, albeit based on very small differences.

5. Conclusions

We have thoroughly assessed the level-of-theory dependence of important molecular properties, such as the ionization potential and electron affinity, as well as global reactivity descriptors, such as the chemical potential and global hardness. This investigation was concentrated on typical interactions within zeolite catalysis between small probe molecules (chloromethane, methanol, ethylene, and propene) and three model zeolite clusters. All calculations were submitted to an extended set of computational methods. First of all, the dependence on electronic structure method was investigated by testing the HF and three DFT methods, in particular B3-LYP, BMK, and MPWB1K. The performance of the latter two hybrid meta-DFT functionals for the computation of reactivity descriptors was hereby addressed for the first time. The basis set dependence on the other hand was also intensively studied, using a broad set of both Pople and Dunning basis sets.

Comparison with available experimental data and high-level post-HF calculations shows that, at least for the small molecules, quantitatively accurate and reliable results can be obtained using any of the aforementioned DFT functionals in conjunction with a basis set of at least double-ζ quality, further augmented with a set of polarization and diffuse functions. The interactions between the oxygen-cluster and the probe molecules are addressed by investigating the global softness differences and activation hardnesses. We generally find similar performance for the three investigated DFT functionals, with the BMK and MPWB1K results particularly close to each other. The HF results, on the other hand, are more scattered and sensitive to the applied basis set.

As the reactivity descriptors are often applied to investigate intermolecular reactivity sequences, we found it crucial to investigate whether these sequences depend on a particular choice of computational method. In this view, three model clusters containing both oxygen and amine bridges were studied in detail. The ordering of the global hardness values is retained, no matter what electronic structure method or basis set is used. The same conclusion holds for the global softness differences, for interactions with both polar and apolar probe molecules. The reactivity ordering, based on activation hardnesses, turns out to show a minor dependence on the level of theory used. Comparison between the DFT functionals demonstrates an extreme similarity between BMK and MPWB1K results, while they both deviate substantially from the B3-LYP results. However, this deviation is only manifested from a quantitative, but not from a qualitative perspective. We gladly report that, for the studied hard−hard interactions, reactivity sequences are mainly independent of DFT functional and/or basis set used. In particular, the previously mentioned necessity to include

diffuse functions is not as strict when focus solely lies on obtaining reliable qualitative reactivity trends. Furthermore, the reactivity sequences obtained using the reactivity descriptors are overall in agreement with sequences based on ab initio reaction energies. An exception is found for the interactions between the oxygen-bridged zeolite cluster and the polar molecules, where the reactivity ordering is not in accordance with the HSAB principle.

Acknowledgment. This work is supported by the Fund for Scientific Research—Flanders (FWO), the Research Board of Ghent University, and the Institute for Science and Technology (I.W.T.).

Supporting Information Available: Global hardness of the purely oxygen-bridged cluster using various levels for the geometry optimization (Figure S1); average softness differences between the purely oxygen-bridged cluster and the probe molecules using various levels for the geometry optimization (Table S1); chemical potential for the probe molecules (Table S2); reaction barriers using various levels for the single-point energies (Table S3); ionization potentials, electron affinities, chemical potentials and global hardnesses for the amine-substituted zeolites N1 (Table S4) and N2 (Table S5). This material is available free of charge via the Internet at http://pubs.acs.org.

References and Notes

(1) Kohn, W.; Becke, A. D.; Parr, R. G. *J. Phys. Chem.* **1996**, *100*, 12974.
(2) Parr, R. G.; Yang, W. *Density-Functional Theory of Atomsand Molecules*; Oxford Science Publications, New York, 1988.
(3) Geerlings, P.; De Proft, F.; Langenaeker, W. *Chem. Rev.* **2003**, *103*, 1793.
(4) Parr, R. G.; Donnelly, R. A.; Levy, M.; Palke, W. E. *J. Chem. Phys.* **1978**, *68*, 3801.
(5) Parr, R. G.; Pearson, R. G. *J. Am. Chem. Soc.* **1983**, *105*, 7512.
(6) Chermette, H. *J. Comput. Chem.* **1999**, *20*, 129.
(7) (a) De, Proft, F.; Martin, J. M. L.; Geerlings, P. *Chem. Phys. Lett.* **1996**, *256*, 400. (b) De Proft, F.; Martin, J. M. L.; Geerlings, P. *Chem. Phys. Lett.* **1996**, *250*, 393. (c) Langenaeker, W.; De Proft, F.; Geerlings, P. *J. Mol. Struct. (THEOCHEM)* **1996**, *362*, 175. (d) Arulmozhiraja, S.; Kolandaivel, P. *Mol. Phys.* **1997**, *90*, 55. (e) Thanikaivelan, P.; Padmanabhan, J.; Subramanian, V.; Ramasami, T. *Theor. Chem. Acc.* **2002**, *107*, 326. (f) Martin, F.; Zipse, H. *J. Comp. Chem.* **2005**, *26*, 97. (g) Cioslowski, J.; Martinov, M.; Mixon, S. T. *J. Phys. Chem.* **1993**, *97*, 10948. (h) Gilardoni F.; Weber, J.; Chermette, H.; Ward, T. R. *J. Phys. Chem. A* **1998**, *102*, 3607.
(8) De Proft, F.; Geerlings, P. *J. Chem. Phys.* **1997**, *106*, 3270.
(9) (a) Jalbout, A. F.; Darwish, A. M.; Alkahby, H. Y. *J. Mol. Struct. (THEOCHEM)* **2002**, *585*, 205. (b) Jalbout, A. F.; Jalbout, F. N.; Alkahby, H. Y. *J. Mol. Struct. (THEOCHEM)* **2001**, *574*, 141.
(10) Chattaraj, P. K.; Schleyer, P. v. R. *J. Am. Chem. Soc.* **1994**, *116*, 1067.
(11) Simons, J.; Jordan, K. D. *Chem. Rev.* **1987**, *87*, 535.
(12) Curtiss, L. A.; Raghavachari, K.; Trucks, G. W.; Pople J. A. *J. Chem. Phys.* **1991**, *94*, 7221.
(13) Curtiss, L. A.; Redfern, P. C.; Raghavachari, K.; Pople J. A. *J. Chem. Phys.* **1998**, *109*, 42.
(14) Rienstra-Kiracofe, J. C.; Tschumper, G. S.; Schaefer, H. F.; Nandi, S.; Ellison, G. B. *Chem. Rev.* **2002**, *102*, 231.
(15) Martin, J. M. L.; de Oliveira, G. *J. Chem. Phys.* **1999**, *111*, 1843.
(16) Parthiban, S.; Martin, J. M. L. *J. Chem. Phys.* **2001**, *114*, 6014.
(17) Boese, A. D.; Oren, M.; Atasoylu, O.; Martin, J. M. L.; Kallay, M.; Gauss, J. *J. Chem. Phys.* **2004**, *120*, 4129.
(18) (a) Shore, H. B.; Rose, J. H.; Zaremba, E. *Phys. Rev. B* **1977**, *15*, 2858. (b) Schwarz, K. *Chem. Phys. Lett.* **1978**, *57*, 605.
(19) Galbraith, J. M.; Schaefer, H. F. *J. Chem. Phys.* **1996**, *105*, 862.
(20) Tozer, D. J.; De Proft, F. *J. Phys. Chem. A* **2005**, *109*, 8923.
(21) Zhao, Y.; Truhlar, D. G. *J. Phys. Chem. A* **2004**, *108*, 6908.
(22) Boese, A. D.; Martin, J. M. L. *J. Chem. Phys.* **2004**, *121*, 3405.
(23) Hemelsoet, K.; Moran, D.; Van Speybroeck, V.; Waroquier, M.; Radom, L. *J. Phys. Chem. A* **2006**, *110*, 8942.
(24) Astala, R.; Auerbach, S. M. *J. Am. Chem. Soc.* **2004**, *126*, 1843.
(25) Lesthaeghe, D.; Van Speybroeck, V.; Waroquier, M. *J. Am. Chem. Soc.* **2004**, *126*, 9162.
(26) Chan, B.; Radom, L. *J. Am. Chem. Soc.* **2006**, *128*, 5322.
(27) Lesthaeghe, D.; Van, Speybroeck, V.; Marin, G. B.; Waroquier, M. *J. Phys. Chem. B* **2005**, *109*, 7952.
(28) Hemelsoet, K.; Lesthaeghe, D.; Van Speybroeck, V.; Waroquier M. *Chem. Phys. Lett.* **2006**, *419*, 10.
(29) Pearson, R. G. *J. Am. Chem. Soc.* **1963**, *85*, 3533.
(30) (a) Chattaraj, P. K.; Lee, H.; Parr, R. G. *J. Am. Chem. Soc.* **1991**, *113*, 1855. (b) Damoun, S.; Van de Woude, G.; Mendez, F.; Geerlings, P. *J. Phys. Chem. A* **1997**, *101*, 886.
(31) (a) Pearson, R. G. *Acc. Chem. Res.* **1993**, *26*, 250. (b) Parr, R. G.; Chattaraj, P. K. *J. Am. Chem. Soc.* **1991**, *113*, 1854. (c) Chattaraj, P. K.; Ayers, P. W. *J. Chem. Phys.* **2005**, *123*, 086101.
(32) Datta, D. *J. Phys. Chem.* **1992**, *96*, 2409.
(33) Zhou, Z.; Parr, R. G. *J. Am. Chem. Soc.* **1990**, *112*, 5720.
(34) Frisch, M. J.; Trucks, G. W.; Schlegel, H. B.; Scuseria, G. E.; Robb, M. A.; Cheeseman, J. R.; Montgomery, J. A., Jr.; Vreven, T.; Kudin, K. N.; Burant, J. C.; Millam, J. M.; Iyengar, S. S.; Tomasi, J.; Barone, V.; Mennucci, B.; Cossi, M.; Scalmani, G.; Rega, N.; Petersson, G. A.; Nakatsuji, H.; Hada, M.; Ehara, M.; Toyota, K.; Fukuda, R.; Hasegawa, J.; Ishida, M.; Nakajima, T.; Honda, Y.; Kitao, O.; Nakai, H.; Klene, M.; Li, X.; Knox, J. E.; Hratchian, H. P.; Cross, J. B.; Bakken, V.; Adamo, C.; Jaramillo, J.; Gomperts, R.; Stratmann, R. E.; Yazyev, O.; Austin, A. J.; Cammi, R.; Pomelli, C.; Ochterski, J. W.; Ayala, P. Y.; Morokuma, K.; Voth, G. A.; Salvador, P.; Dannenberg, J. J.; Zakrzewski, V. G.; Dapprich, S.; Daniels, A. D.; Strain, M. C.; Farkas, O.; Malick, D. K.; Rabuck, A. D.; Raghavachari, K.; Foresman, J. B.; Ortiz, J. V.; Cui, Q.; Baboul, A. G.; Clifford, S.; Cioslowski, J.; Stefanov, B. B.; Liu, G.; Liashenko, A.; Piskorz, P.; Komaromi, I.; Martin, R. L.; Fox, D. J.; Keith, T.; Al-Laham, M. A.; Peng, C. Y.; Nanayakkara, A.; Challacombe, M.; Gill, P. M. W.; Johnson, B.; Chen, W.; Wong, M. W.; Gonzalez, C.; Pople, J. A. *Gaussian 03*, revision B.03; Gaussian, Inc.: Wallingford, CT, 2004.
(35) Sauer, J. *Chem. Rev.* **1989**, *89*, 199.
(36) van Santen, R. A.; Kramer, G. J. *Chem. Rev.* **1995**, *95*, 637.
(37) Becke, A. D. *J. Chem. Phys.* **1993**, *98*, 5648.
(38) Lee, C.; Yang, W. T.; Parr, R. G. *Phys. Rev. B* **1988**, *37*, 785. (b) Miehlich, B.; Savin, A.; Stoll, H.; Preuss H. *Chem. Phys. Lett.* **1989**, *157*, 200.
(39) Zygmunt, S. A.; Mueller, R. M.; Curtiss, L. A.; Iton, L. E. *J. Mol. Struct. (THEOCHEM)* **1998**, *430*, 9.
(40) Dunning, T. H., Jr.; Peterson, K. A.; Woon, D. E. Basis Sets: Correlation Consistent Sets. In *The Encyclopedia of Computational Chemistry*; Schleyer, P. v. R., Ed; John Wiley: Chichester, U.K., 1998.
(41) Frisch, M. J.; Pople, J. A.; Binkley, J. S. *J. Chem. Phys.* **1984**, *80*, 3265 and references therein.
(42) (a) Woon, D. E.; Dunning, T. H. *J. Chem. Phys.* **1993**, *98*, 1358. (b) Kendall, R. A.; Dunning, T. H.; Harrison, R. *J. Chem. Phys.* **1992**, *96*, 6796. (c) Dunning, T. H. *J. Chem. Phys.* **1989**, *90*, 1007. (d) Peterson, K. A.; Woon, D. E.; Dunning, T. H. *J. Chem. Phys.* **1994**, *100*, 7410. (e) Wilson, A. K.; van Mourik, T.; Dunning, T. H., Jr. *J. Mol. Struct. (THEOCHEM)* **1996**, *388*, 339.
(43) (a) Pople, J. A.; Head-Gordon, M.; Raghavachari, K. *J. Chem. Phys.* **1987**, *87*, 5968. (b) Gauss, J.; Cremer, D. *Chem. Phys. Lett.* **1988**, *150*, 280. (c) Salter, E. A.; Trucks, G. W.; Bartlett, R. J. *J. Chem. Phys.* **1989**, *90*, 1752.
(44) (a) Purvis, G. D.; Bartlett, R. J. *J. Chem. Phys.* **1982**, *76*, 1910. (b) Raghavachari, K.; Trucks, G. W.; Pople, J. A.; Head-Gordon, M. *Chem. Phys. Lett.* **1989**, *157*, 479.
(45) Kimura, K.; Katsumata, S.; Achiba, Y.; Yamazaki, T.; Iwata, S. *Ionization energies, Ab initio assignments, and valence electronic structure for 200 molecules in Handbook of HeI Photoelectron Spectra of Fundamental Organic Compounds*; JapanScientific Soc. Press: Tokyo, 1981.
(46) Vorob'ev, A. S.; Furlei, I. I.; Sultanov, A. S.; Khvostenko, V. I.; Leplyanin, G. V.; Derzhinskii, A. R.; Tolstikov, G. A. *Bull. Acad. Sci. USSR, Div. Chem. Sci.* **1989**, *38*, 1388.
(47) Bieri, G.; Asbrink, L. *J. Electron Spectrosc. Relat. Phenom.* **1980**, *20*, 149.
(48) Krause, D. A.; Taylor, J. W.; Fenske, R. F. *J. Am. Chem. Soc.* **1978**, *100*, 718.
(49) Chandra, A. K.; Uchimaru, T.; Sugie, M.; Sekiya, A. *Chem. Phys. Lett.* **2000**, *318*, 69.

Paper IX

Bifunctional acid-base catalyzed reactions in zeolites from the HSAB viewpoint

Hemelsoet K. , Lesthaeghe D. , Van Speybroeck V. and Waroquier M.

Chem. Phys. Lett., **2006**, *419*, 10–15

Available online at www.sciencedirect.com
SCIENCE DIRECT®
Chemical Physics Letters 419 (2005) 10–15
CHEMICAL PHYSICS LETTERS
www.elsevier.com/locate/cplett

Bifunctional acid–base catalyzed reactions in zeolites from the HSAB viewpoint

K. Hemelsoet, D. Lesthaeghe, V. Van Speybroeck, M. Waroquier *

Center for Molecular Modeling, Laboratory of Theoretical Physics, Ghent University, Proeftuinstraat 86, 9000 Gent, Belgium

Received 7 October 2005

Abstract

The applicability of the hard and soft acids and bases principle is investigated for the interaction of 5T zeolite clusters with probe molecules such as chloromethane, methanol and olefins. The reactions are intermediately hard–hard and, therefore, mainly charge-controlled. This is confirmed by the success of the atomic charges and the electrostatic interaction energy at the acid site as correct descriptors of regio-selectivity and reactivity sequences. Both acid and basic reactive sites can be clearly indicated using frontier orbitals. Moreover, an excellent correlation is found between the activation hardnesses and the energy barriers at the absolute zero.

1. Introduction

Zeolites are microporous crystalline aluminosilicates, built from corner-sharing SiO_4 and AlO_4 tetrahedra. These solid-state catalysts portray a wide variety of properties and applications, due mainly to their shape-selectivity and Brønsted acid sites ≡Si–OH–Al≡, in combination with neighboring Lewis base ≡Si–O–Si≡ sites [1]. To extend the range of possible applications, Astala and Auerbach [2] provided evidence through periodic DFT calculations that zeolites are capable of accommodating both methylene and amine groups at high concentrations. Theoretically determined sorption energies of typical guest molecules like NH_3 and BF_3 in amine-modified zeolites indicate that ≡Si–NH–Si≡ groups form significantly stronger Lewis bases than the usual ≡Si–O–Si≡ bridges. The combination of these Lewis basic sites with the well-known Brønsted acid sites due to aluminum impurities might lead to a substantial increase in bifunctional acid–base properties, as published in a previous communication [3]. In this Letter, we will study the formation of an alkoxide or an equivalent alkylammonium species, an archetypal step in zeolite chemistry for which both acid and basic site play a crucial role. In a traditional zeolite with only oxygen bridges, both sites are located near the aluminum defect. Amine moieties on the other hand cannot be located next to this aluminum, in order to prevent protonation of the ≡Si–NH–Al–OH–Si≡ bridge to a lesser reactive ≡Si–NH_2–Al–O–Si≡ connection. As previously shown, amine substituted zeolites have noticeably lower reaction barriers for SN_2 type reactions [3]. Recent work also shows that the stronger basic character of the amine bridge is compensated by undesired energetic effects caused by a larger charge separation between the positively charged intermediate and the negative aluminum [4]. The nitrogen site serves as an equivalently reactive site (compared to O) but located in a geometrically more favorable position.

In this Letter, we assess whether DFT-based reactivity descriptors, such as global hardness, Fukui function and local softness are capable of providing reliable information about typical reactions between small molecules and different zeolite frameworks. Generally speaking, several of these reactivity indicators have proven successful for various soft–soft reactions occurring in the gas phase [5–7]. In the specific field of zeolites, some relevant works have already been published. The influence of isomorphous substitution of Al (by B and Ga) and Si (by Ge) on the catalytic activity of zeolite systems has been investigated using a range of reactivity indicators [8,9]. Beside local

* Corresponding author.
E-mail address: michel.waroquier@ugent.be (M. Waroquier).

0009-2614/$ - see front matter © 2005 Elsevier B.V. All rights reserved.
doi:10.1016/j.cplett.2005.10.145

softness values, relative electrophilicity and relative nucleophilicity, defined as the ratio of electrophilic and nucleophilic local softness values and their inverse, were found to be suitable descriptors for the acidity and basicity, respectively. The descriptors were also successful in describing the acidity and basicity of cation-exchanged zeolites [10–14], where cations act as Lewis acid sites while framework oxygen atoms show basic character. The applicability of a hard soft acid base approach was tested for the interaction of small probe molecules with clusters representing the active sites [15–17]. The systems studied in this paper are bifunctional in the sense that the acid and basic sites are both located on framework atoms, either being oxygen bridges or an oxygen and a nitrogen bridge in case of an amine substituted zeolite. To the best of our knowledge only Vos et al. [18,19] studied reactivity indicators on similar systems limited to solely oxygen bridges to predict reaction preference for the alkylation of toluene and benzene.

2. Theoretical background

DFT-based reactivity indicators are defined as derivatives of the electronic energy $E[N, v(\mathbf{r})]$ with N the total number of electrons and $v(\mathbf{r})$ the external potential [5,20]. Using the finite difference approach, the global hardness η and global softness S can be computed from the vertical ionization potential (IP) and electron affinity (EA):

$$\eta = \frac{IP - EA}{2}, \quad S = \frac{1}{2\eta}. \tag{1}$$

The hardness equals the Kohn–Sham HOMO–LUMO gap:

$$\eta = \frac{\epsilon_{\mathrm{LUMO}} - \epsilon_{\mathrm{HOMO}}}{2}. \tag{2}$$

According to the hard soft acid base (HSAB) principle, a reaction between systems A and B will be favored when the global softness difference $\Delta S = S_{\mathrm{A}} - S_{\mathrm{B}}$ is minimal. This rule was obtained through optimization of the covalent contribution of the interaction energy, consequently neglecting other effects such as polarization.

Site-selectivity can be described using local indicators. The Fukui function $f(\mathbf{r})$ and local softness $s(\mathbf{r}) = S\, f(\mathbf{r})$ mainly describe orbital-controlled effects, whereas the local hardness $\eta(\mathbf{r})$ is dominantly charge-controlled. The condensed form of $f(\mathbf{r})$ gives an approximate value at the position of an atomic center [21]:

$$f_k^+ = \tilde{q}_k(N+1) - \tilde{q}_k(N) \text{ (nucleophilic attack)},$$
$$f_k^- = \tilde{q}_k(N) - \tilde{q}_k(N-1) \text{ (electrophilic attack)},$$

with $\tilde{q}_k(N)$ the electron population on the kth atom of the molecule with N electrons. Within frontier orbital theory (FOT), the following approximation can be obtained:

$$f_k^+ = \rho_{\mathrm{LUMO}}(\mathbf{r}) \quad \text{and} \quad f_k^- = \rho_{\mathrm{HOMO}}(\mathbf{r}).$$

Reactivity sequences can also be obtained using the local HSAB principle.

The electrostatic energy between two atoms is also used to describe charge effects:

$$\Delta E_{\mathrm{el}} \propto \frac{q_i q_j}{R_{ij}}, \tag{3}$$

with R_{ij} being the distance between atom i and atom j and q_i and q_j the atomic charges.

According to the principle of maximal hardness (PMH), molecules will rearrange themselves to achieve maximal hardness. Consequently, the transition state of a reaction should exhibit minimal hardness [22]. The activation hardness $\Delta\eta_{\mathrm{act}} = \eta_{\mathrm{adsorbed\ reactant}} - \eta_{\mathrm{transition\ state}}$ describes hardness variations along the reaction path [23]. The smaller the activation hardness, the easier a reaction should occur.

In this Letter, we will verify whether a correlation exists between HSAB results, the electrostatic interaction energy term and the activation hardness on one hand and the reaction barrier at 0 K on the other hand. We will also investigate the applicability of the frontier orbitals and Fukui functions on indicating the preferred interaction sites. We will study both orbital- and charge-controlled effects.

3. Computational details

A similar approach was adopted as in [3], simulating the zeolite catalyst by a cluster built from 5 tetrahedral atoms (5T), which is capable of providing an adequate qualitative picture of chemical rearrangements that occur locally on the active site [24,25]. As shown in Fig. 1, three cases were studied: a fully oxygen surrounded cluster (O) and two amine substituted clusters (N1 and N2), with different proton locations. Full geometry optimizations and frequency calculations for minimum energy and transition-state structures were performed within the GAUSSIAN03 software package [26] using density functional theory (DFT) with the hybrid B3LYP functional [27] and 6-31g(d) basis set. The atomic charges were systematically calculated using the Merz–Singh–Kollman (MK) analysis scheme, which is derived from the electrostatic potential [28,29].

4. Results and discussion

We studied the interaction of chloromethane, methanol, ethylene and propene with 3 zeolite model clusters O, N1 and N2, depicted in Fig. 1. The acid and basic sites where the reactions occur are also indicated. The global hardness values in Table 1 immediately show that the HOMO–LUMO method (Eq. (2)) results in smaller values than obtained using the finite difference approach (Eq. (1)). This underestimation is due to derivative discontinuities of the exchange-correlation energy as elaborated by Perdew et al. [30]. Closer inspection of the computed values indicates an intermediately hard character for all three clusters. Substitution of an oxygen by a nitrogen atom lowers the hardness, increasing the reactivity of the amine-modified

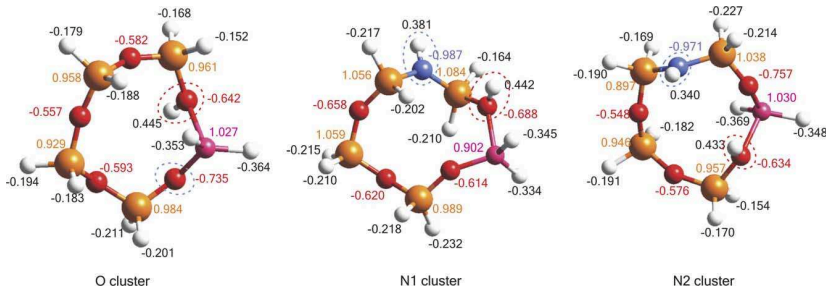

Fig. 1. Optimized cluster geometries, with acid site (red dotted line) and basic site (blue dotted line). MK charges at B3LYP/6-31g(d) level. (For interpretation of the references to colour in this figure legend, the reader is referred to the web version of this article.)

Table 1
Absolute hardness (eV) of isolated reactants, using the finite difference (FD) and HOMO–LUMO method

B3LYP/6-31g(d)	FD	HOMO–LUMO
O cluster	5.413	3.505
N_1 cluster	5.165	3.366
N_2 cluster	5.217	3.467
CH_3Cl	7.311	4.384
CH_3OH	7.574	4.623
C_2H_4	6.850	3.883
C_3H_6	6.496	3.805

cluster. The smaller guest molecules are all found to be hard. The two polar species exhibit the largest hardness values due to the occurrence of hetero atoms which are electronegative. The reactions can be described as intermediately hard–hard and we, therefore, expect electrostatic effects to be dominant.

The reactions of interest are all concerted, making use of both acid and base properties of the zeolite. The first step is the protonation of the adsorbed molecules in order to form a covalent alkoxide or alkylammonium species. The energetic results were already studied in detail in [4]: the amine substitution drastically lowers energies of transition states that occur typically through an SN_2-like activated complex which is highly strained in traditional oxygen bridged zeolites. In these cases, the nitrogen substitution introduces more basic sites, allowing reactions spanning two tetrahedral sites, for the case of cluster N2. The normally strained SN_2-type transition states are then more easily accessible through a linear transfer. The interaction of chloromethane is a typical example of such a reaction and the barriers correspondingly predict that reaction at the N2 cluster is substantially lower activated. For the N1 cluster the same reaction is less favored due to a strained 1T-transition state, which is combined with charge separation effects between the carbenium-like transition state and the negatively charged aluminum. The situation differs for methanol, where an optimal SN_2-type transition state automatically occurs. The reactions with the apolar guest molecules ethylene and propene are dominated by charge separation and nitrogen substitution does not improve catalytic performance.

In the following discussion, we will systematically use the reaction barriers at 0 K (ΔE_0) obtained from transition state theory as reference for the validation of the HSAB principle. Since all studied interactions are (intermediately) hard–hard, it is interesting to investigate whether a correlation can be established between the energy barriers and the HSAB results, keeping in mind that the HSAB principle is based upon a simple electron transfer effect [31]. The computed properties ΔE_0 and ΔS are listed in Table 2. We find that no correlation exists between ΔS and ΔE_0 for the reac-

Table 2
ΔE_0 values (kJ/mol), ZPE included, ΔS (1/au), ΔE_{act} (eV), ΔE_{el}^a at acid site and ΔE_{el}^b at basic site ($10^3 \times$ au)

B3LYP/6-31g(d)	ΔE_0	ΔS	$\Delta\eta_{act}$	ΔE_{el}^a	ΔE_{el}^b	ΔE_0	ΔS	$\Delta\eta_{act}$	ΔE_{el}^a	ΔE_{el}^b
	CH_3Cl					CH_3OH				
O	169.9	0.653	0.635	−16.1	−20.0	199.8	0.717	1.094	−20.6	−20.3
N1	220.3	0.773	1.080	−12.1	−13.5	165.8	0.838	0.720	−28.6	−16.5
N2	117.5	0.747	0.458	−13.3	−7.5	150.3	0.811	0.556	−27.5	−13.6
	C_2H_4					C_3H_6				
O	96.6	0.528	1.096	−31.5	11.2	86.0	0.419	1.454	−53.8	−22.3
N1	141.0	0.648	1.494	−24.0	12.0	117.6	0.540	1.880	−40.9	−12.6
N2	124.3	0.622	1.354	−26.0	9.0	119.6	0.513	1.840	−42.0	−12.1

tion with the polar molecules chloromethane and methanol. However, for the reactions with the apolar guest molecules ethylene and propene, we see that the softness matching criterion yields the same reactivity sequence as shown by the energy barriers. These results are a manifestation of the importance of polarization effects, which are only partially included within the HSAB principle.

The PMH principle is also based on global descriptors, but additionally takes into account the hardness values along the reaction path, including information from transition structures. The values for the activation hardness $\Delta\eta_{act}$ for the various reactions are given in Table 2 and the PMH is also schematically shown in Fig. 2, where calculations were performed on the three stationary points (adsorbed reactants, transition states, products). We find an excellent correlation between the activation hardness and the activation barriers at the absolute zero for all studied reactions. For the reaction with chloromethane, it is clear that including information from the transition structure leads to a correct reactivity description. On other zeolite systems, Vos et al. [18,19] also found a similar correlation for the methylation of benzene and toluene but not for the ethylation and isopropylation of benzene.

While global properties may explain reactivity, site selectivity is described by local quantities such as the Fukui function and the HOMO and LUMO frontier orbitals. Fig. 3 shows the 3-dimensional iso-surfaces of the frontier orbitals and the Fukui function governing electrophilic attack. Inspection of the HOMO for all three clusters shows that a suitable site for electrophilic attack (basic site) can be identified. However, in the case of the N1 cluster, the nitrogen site is not recognized as a basic site. The Fukui function $f^{-}(\mathbf{r})$ contains more detailed information, taking also orbital relaxation effects into account. Nevertheless, the Fukui function iso-surface of the O cluster is not concentrated on a specific region and, therefore, does not succeed in predicting the basic site for this cluster. For the N1 and N2 clusters, the basic oxygen can be identified, but the nitrogen site only shows significant basic character for the N2 cluster. The acid site of the zeolite cluster (the protonated oxygen) can be determined, as illustrated by the LUMO surfaces.

Studying local softness differences within an HSAB viewpoint on the other hand is not straightforward, as we are dealing with multiple site interactions. Ponti [32] suggested a definition for the softness differences, for which we generally found no agreement with the energy barriers

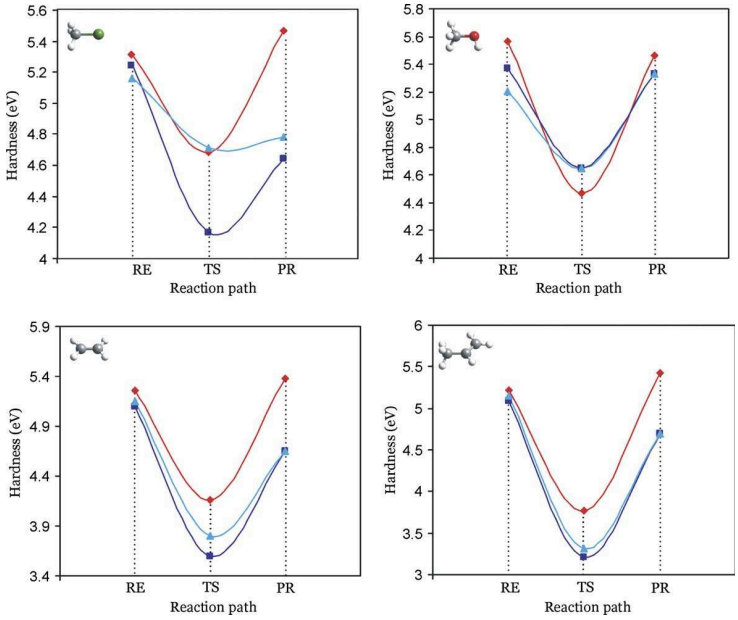

Fig. 2. Illustration of PMH, for O (♦ red line), N1 (■ dark blue line) and N2 cluster (▲ light blue line). (For interpretation of the references to colour in this figure legend, the reader is referred to the web version of this article.)

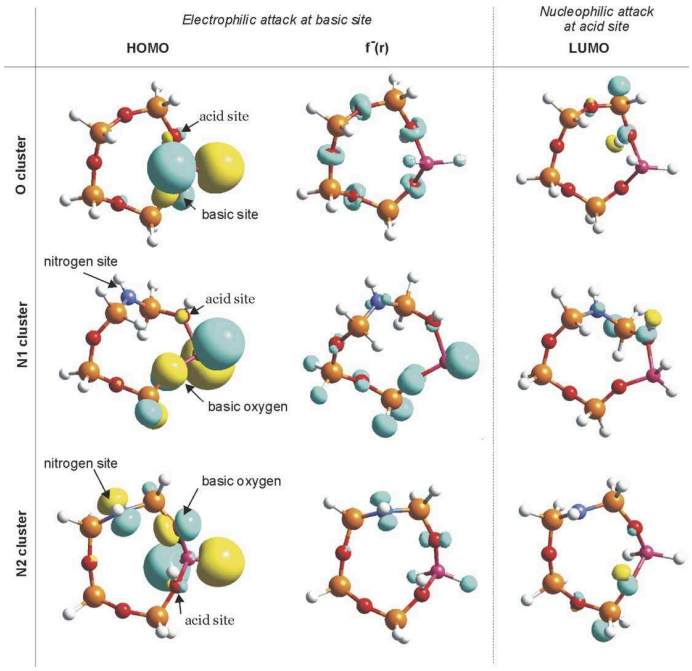

Fig. 3. Iso-surfaces (value 0.2) of the highest occupied orbital (HOMO), the Fukui function ($f^-(\mathbf{r})$) for electrophilic attack and the lowest unoccupied orbital (LUMO).

at 0 K. It has been found by other researchers that the Fukui function, as well as the local softness, are less suitable reactivity descriptors for reactions between (intermediate) hard species [33–35].

Atomic charges are useful indicators to alternatively identify the preferred site when charge effects are important and we investigate their applicability on the studied reactions. Fig. 1 shows the isolated zeolite frameworks with the charges on all atoms, according to the MK population analysis scheme. For all three clusters, the basic site is identified by the largest negative atomic charge, leading to the correct oxygen or nitrogen atom for the purely oxygen or

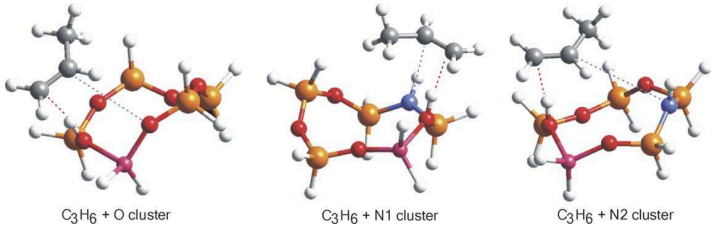

Fig. 4. Adsorbed reactants for reactions with propene, interaction at acid site (red line) and basic site (blue line). (For interpretation of the references to colour in this figure legend, the reader is referred to the web version of this article.)

amine-substituted zeolite clusters, respectively. The acid site is also correctly identified by the largest positive atomic charge on a hydrogen atom.

We computed the electrostatic energy (eq. (3)) of the interacting functional groups, using atomic charges and distances calculated on the stable adsorbed structures (illustrated for propene in Fig. 4). The obtained values for the concerted reaction occurring both at the acid and basic site are given in Table 2. For the reactions taking place at the acid site, we find a good agreement between ΔE_{el}^{a} and ΔE_0 for methanol, ethylene and propene, confirming the importance of charge effects. For chloromethane, no correlation could be expected since the values for the reaction barriers are governed by geometric strain in the transition states and the reactivity indicators are based solely on the reactants. The situation is less straightforward for the reactions occurring at the basic sites and differs for all studied examples. Only in the case of propene, an agreement between ΔE_{el}^{b} and ΔE_0 is noticed. The repulsive terms obtained for ethylene are due to the fact that the reaction occurring at the acid site (interaction of the protonated hydrogen with the π bond of ethylene) is dominant, as can be seen in the transition structure.

5. Conclusion

We have critically analyzed different DFT-based reactivity descriptors for the interaction of zeolites containing both oxygen and amine bridges with different probe molecules such as chloromethane, methanol, ethylene and propene. We performed a series of 5T cluster calculations to obtain reactivity sequences which were compared with energy barriers at the absolute zero. All the studied reactions are characterized as (intermediately) hard–hard, which is confirmed by the success of the atomic charges and the electrostatic energy term at the acid site to describe both the correct regio-selectivity and reactivity sequences. Within a global hard and soft viewpoint, a correlation could be established between the global softness differences and the reaction barriers for apolar molecules. For polar molecules no such correspondence was found. These results clearly illustrate the influence of only taking into account the covalent contribution towards the interaction energy in the theoretical backbone of the HSAB principle, hereby neglecting electrostatic and polarization effects. The excellent agreement between the activation hardness and energy barriers for all studied reactions is also remarkable, indicating the necessity of taking into account transition state effects for the interaction with polar molecules.

References

[1] A. Corma, Chem. Rev. 95 (1995) 559.
[2] R. Astala, S.M. Auerbach, J. Am. Chem. Soc. 126 (2004) 1843.
[3] D. Lesthaeghe, V. Van Speybroeck, M. Waroquier, J. Am. Chem. Soc. 126 (2004) 9162.
[4] D. Lesthaeghe, V. Van Speybroeck, G.B. Marin, M. Waroquier, J. Phys. Chem. B 109 (2005) 7952.
[5] P. Geerlings, F. De Proft, W. Langenaeker, Chem. Rev. 103 (2003) 1793.
[6] K. Hemelsoet, V. Van Speybroeck, G.B. Marin, F. De Proft, P. Geerlings, M. Waroquier, J. Phys. Chem. A 108 (2004) 7281.
[7] K. Van Cauter, K. Hemelsoet, V. Van Speybroeck, M.F. Reyniers, M. Waroquier, Int. J. Quant. Chem. 102 (2005) 454.
[8] W. Langenaeker, N. Coussement, F. De Proft, P. Geerlings, J. Phys. Chem. 98 (1994) 3010.
[9] R.C. Deka, R. Vetrivel, S. Pal, J. Phys. Chem. A 103 (1999) 5978.
[10] R.C. Deka, R.K. Roy, K. Hirao, Chem. Phys. Lett. 332 (2000) 576.
[11] R.C. Deka, K. Hirao, J. Mol. Catal. A 181 (2002) 275.
[12] R.C. Deka, R.K. Roy, K. Hirao, Chem. Phys. Lett. 389 (2004) 186.
[13] J.C. Santos, R. Contreras, E. Chamorro, P. Fuentealba, J. Chem. Phys. 116 (2002) 4311.
[14] A. Chatterjee, F. Mizukami, Chem. Phys. Lett. 385 (2004) 20.
[15] S. Pal, K.R.S. Chandrakumar, J. Am. Chem. Soc. 122 (2000) 4145.
[16] S. Krishnamurthy, R.K. Roy, R. Vetrivel, S. Iwata, S. Pal, J. Phys. Chem. A 101 (1997) 7253.
[17] R.C. Deka, D. Ajitha, K. Hirao, J. Phys. Chem. B 107 (2003) 8574.
[18] A.M. Vos, K.H.L. Nulens, F. De Proft, R.A. Schoonheydt, P. Geerlings, J. Phys. Chem. B 106 (2002) 2026.
[19] A.M. Vos, R.A. Schoonheydt, F. De Proft, P. Geerlings, J. Phys. Chem. B 107 (2003) 2001.
[20] R.G. Parr, W. Yang, Density-Functional Theory of Atoms and Molecules, Oxford Science Publications, 1988.
[21] W. Yang, W.J. Mortier, J. Am. Chem. Soc. 108 (1986) 5708.
[22] D. Datta, J. Phys. Chem. 96 (1992) 2409.
[23] Z. Zhou, R.G. Parr, J. Am. Chem. Soc. 112 (1990) 5720.
[24] J. Sauer, Chem. Rev. 89 (1989) 199.
[25] R.A. van Santen, G.J. Kramer, Chem. Rev. 95 (1995) 637.
[26] M.J. Frisch et al., GAUSSIAN03, Revision B.03, Gaussian, Inc., Wallingford, CT, 2004.
[27] A.D. Becke, J. Chem. Phys. 98 (1993) 5648.
[28] U.C. Singh, P.A. Kollman, J. Comput. Chem. 5 (1984) 129.
[29] B.H. Besler, K.M. Merz Jr., P.A. Kollman, J. Comput. Chem. 11 (1990) 431.
[30] J.P. Perdew, M. Levy, Phys. Rev. Lett. 51 (1983) 1884.
[31] P.W. Ayers, J. Chem. Phys. 122 (2005) 141102.
[32] A. Ponti, J. Phys. Chem. A 104 (2000) 8843.
[33] P.K. Chattaraj, J. Phys. Chem. A 105 (2001) 511.
[34] J. Melin, F. Aparicio, V. Subramanian, M. Galvan, P.K. Chattaraj, J. Phys. Chem. A 108 (2004) 2487.
[35] P. Thanikaivelan, J. Padmanabhan, V. Subramanian, T. Ramasami, Theor. Chem. Acc. 107 (2002) 326.

Paper X

Unexpected four-membered over six-membered ring formation during the synthesis of azaheterocyclic phosphonates: experimental and theoretical evaluation

Van Speybroeck V. , Moonen K. , Hemelsoet K.
Stevens C. V. and Waroquier M.

J. Am. Chem. Soc., **2006**, *128*, 8468–8478

J|A|C|S
ARTICLES
Published on Web 06/13/2006

Unexpected Four-Membered over Six-Membered Ring Formation during the Synthesis of Azaheterocyclic Phosphonates: Experimental and Theoretical Evaluation

Veronique Van Speybroeck,*,† Kristof Moonen,‡ Karen Hemelsoet,†
Christian V. Stevens,*,‡ and Michel Waroquier†

Contribution from the Center for Molecular Modeling, Ghent University, Proeftuinstraat 86, B-9000 Ghent, Belgium, and Research Group SynBioC, Department of Organic Chemistry, Faculty of Bioscience Engineering, Ghent University, Coupure links 653, B-9000 Ghent, Belgium

Received December 12, 2005; Revised Manuscript Received April 26, 2006;

E-mail: veronique.vanspeybroeck@ugent.be; chris.stevens@ugent.be

Abstract: The cyclization of functionalized aminophosphonates is studied on both experimental and theoretical grounds. In a recently described route to phosphono-β-lactams [Stevens C. V.; Vekemans, W.; Moonen, K.; Rammeloo, T. *Tetrahedron Lett.* **2003,** *44*, 1619], it was found that starting from an ambident allylic anion only four-membered rings were formed without any trace of six-membered lactams. New anion trapping experiments revealed that the γ-anion is highly reactive in intermolecular reactions. Ab initio calculations predict higher reaction barriers for the γ-anion due to restricted rotation about the C−N bond and due to highly strained transition states during ring closure. The sodium or lithium counterion, explicit dimethyl ether solvent molecules, and bulk solvent effects were properly taken into account at various levels of theory.

1. Introduction

Intramolecular ring-closure competition between a four-membered and a six-membered ring is generally accepted to lead to the six-membered ring.[2] Several ring-closure studies have been performed on the formation of lactones from ω-bromoalkanoate ions to evaluate the influence of the ring size.[3,4] When the exo-tet situation is considered during ring closure,[5] the six-membered ring preference can be explained by a smaller Baeyer strain (angle strain) as well as a smaller Pitzer strain (due to eclipsed conformations of the hydrogens). The possibility to form a four- or a six-membered ring exists when an α-alkenyl anion can ring close in an exo-tet mode either directly or through its mesomeric canonical form. However, a surprising preference for the formation of a four-membered ring was found during the synthesis of azaheterocyclic phosphonates.[6−8] When treated with a base, *N*-chloroacetyl-1-aminoalkenyl phosphonates derived from cinnamaldehyde exclusively lead to phosphono-β-lactams without any trace of the corresponding six-membered lactams. In a quite similar reaction where the anion was stabilized by a carbonyl group instead of a phosphonate group, the same experimental preference was observed toward the formation of the four-membered ring. However no explanation for this peculiar reactivity was given.[9,10] The higher reactivity of the α-canonical anion compared to the γ-canonical anion could be believed to be important for the observed reactivity; however, steric factors may also play a role since exclusive γ-alkylation was observed using β,γ-unsaturated α-silyloxy-phosphonates.[11]

The main goal of the present paper is to unravel the origin of this remarkable selectivity toward four-membered ring formation. This is done both on experimental and theoretical grounds. In addition to the previously reported synthesis of 4-phosphono-β-lactams new experiments were set up to trap the intermediate anions prior to cyclization to obtain information about the factors controlling the stability of the mesomeric resonance contributors. Further microscopic insight into stabilization and charge distribution is obtained by means of ab initio theoretical calculations.

The theoretical study of organometallic species as encountered here is challenging as the effects of the metallic counterion and solvent all contribute to the final reaction preference. To evaluate

† Center for Molecular Modeling.
‡ Research Group SynBioC.

(1) Deleted in proof.
(2) Smith, M. B.; March, J. Kinetic Requirements for reactions. *Advanced Organic Chemistry*, 5th ed.; J. Wiley and Sons: New York, 2001; pp 278−282.
(3) Galli, C.; Illuminati, G.; Mandolini, L.; Tamborra, P. *J. Am. Chem. Soc.* **1977**, *99*, 2591−2597.
(4) Mandolini L. *J. Am. Chem. Soc.* **1978**, *100*, 550−554.
(5) Baldwin, J. E. *J. Chem. Soc., Chem. Commun.* **1976**, 734−736.
(6) Stevens, C. V.; Vekemans, W.; Moonen, K.; Rammeloo, T. *Tetrahedron Lett.* **2003**, *44*, 1619−1622.
(7) Moonen, K.; Laureyn, I.; Stevens, C. V. *Chem. Rev.* **2004**, *104*, 6177−6215.
(8) Moonen, K.; Stevens, C. V. *Synthesis* **2005**, 3603−3612.
(9) Bossio, R.; Marcos, C. F.; Marcaccini, S.; Pepino R. *Tetrahedron Lett.* **1997**, *38*, 2519−2520.
(10) Marcaccini, S.; Pepino, R.; Pozo M. C. *Tetrahedron Lett.* **2001**, *42*, 2727−2728.
(11) Hata, T.; Nakajima, M.; Sekine, M. *Tetrahedron Lett.* **1979**, 2047−2050.

10.1021/ja0584119 CCC: $33.50

the contribution of various parameters on the geometries, energies, and the reaction outcome, the reaction route was modeled in different environments: in the gas phase, with transmetalation with sodium or lithium as the counterion, and finally with inclusion of solvent interactions. The theoretical results are correlated with the experimental data.

From a theoretical point of view the stabilization of allylic anions by phosphorus substituents has attracted considerable interest.[12−19] The review of Katritzky[20] on the regioselectivity of reactions of heteroatom-stabilized allylic anions with electrophiles presents both experimental and theoretical considerations on this item. Unsymmetrically substituted allyl anions can react with electrophiles both intra- or intermolecularly at two sites, making these species of considerable importance. An early theoretical work on the stabilization of allylic anions by heteroatom-containing subgroups was presented by Denmark and Cramer where neutral, anionic, and lithiated P-allyl and P-methylphosphonic diamides were discussed.[16]

Recently, Pratt and co-workers performed several advanced calculations on the aggregation states of lithium carbenoids in the gas phase and in ethereal solvent.[21] From a methodological point of view, this work deserves attention as it incorporates the effects of the metallic cation which is further embedded in solution. It was explicitly shown that charge-separated species may be dramatically stabilized by solvent interactions. Pratt, Văn Ngũỹen, and Ramachandran have additionally studied the performance of various electronic structure methods for the accurate reproduction of barrier heights for lithium enolates.[22] Recently, in a theoretical study performed by Ando, the origin of π-facial stereoselectivity in the alkylation of enolates was investigated.[23] In this study, the effects of the counterion, explicit coordination of solvent molecules with the lithium ion, and bulk solvent effects were found to be important for the reaction mechanism and energetics. Bearing this in mind, it is necessary to evaluate the influence of each of these effects on the reaction outcome for the present study.

The main motivation for studying the remarkable selectivity of the ring-closure reaction lies in the pharmaceutical importance of the β-lactam ring as part of several important antibiotics, including penicillin.[24] Also some electron-deficient monocyclic β-lactams appeared to be very active, including the commercially available azthreonam,[25−28] in which the β-lactam heterocycle proved to be the key structural feature of this class of antibiotics. Furthermore, increasing resistance is a major threat in hospitals and in the community[29] and is mainly caused by the emergence and spread of β-lactamases, which are β-lactam-deactivating enzymes evolutionarily related to penicillin-binding proteins (PBPs).[30−33] Therefore, current research is focusing on new functionalized β-lactams having β-lactamase-inhibiting activity or combining antibacterial activity with enhanced stability toward β-lactamases.[34,35] In addition to these well-known antibacterial properties, β-lactams have also found application in inhibiting serine proteases. Members of this major class of enzymes are involved in numerous physiological processes including protein turnover, digestion, blood coagulation and wound healing, fertilization, cell differentiation and growth, cell signaling, the immune response, and apoptosis.[36,37]

2. Experimental and Calculation Methods

General. ^{1}H NMR spectra were recorded at 300 MHz with $CDCl_3$ as solvent and tetramethylsilane (TMS) as internal standard. ^{13}C NMR spectra were recorded at 75 MHz and ^{31}P NMR spectra at 121 MHz. MS spectra were measured using electron spray ionization (4000 V). THF was dried and distilled over sodium (benzophenone ketyl control). The absolute value of the coupling constants (J) in Hz and assignments of ^{1}H and ^{13}C peaks were determined using COSY, HSQC, HMBC, and DEPT experiments.

Typical Procedure for the Synthesis of Phosphono-β-lactams 4. A NaH suspension [0.24 g (6 mmol, 1.2 equiv)] in mineral oil is washed three times with petroleum ether to remove the oil, and 15 mL of dry THF is added. Then, 5 mmol of the corresponding *N*-chloroacetyl amino alkenylphosphonate **1** in 5 mL of THF is added dropwise, and the reaction mixture is refluxed for 2 or 3 h protected from moisture with a $CaCl_2$ tube. After cooling, the mixture is poured into 25 mL of water and extracted with 20 mL of diethyl ether. The remaining water phase is then washed two times with 10 mL of diethyl ether. The combined organic phases are dried with $MgSO_4$. The β-lactams are obtained in good purity after filtration and evaporation of the solvent. Further purification can be performed using column chromatography.

Ab Initio Molecular Orbital Calculations. All ab initio calculations were carried out with the GAUSSIAN 03 software package.[38] Density-functional theory (DFT) methods[39] have been shown to be more efficient than wave function based procedures such as highly correlated post-Hartree−Fock methods due to their excellent cost-to-performance ratio. Despite the importance of phosphorus compounds in chemistry, only limited levels of theory studies were conducted on such elements. The work of Leyssens and Peeters addresses the accuracy of various post-

(12) Schleyer, P. V.; Clark, T.; Kos, A. J.; Spitznagel, G. W.; Rohde, C.; Arad, D.; Houk, K. N.; Rondan, N. G. *J. Am. Chem. Soc.* **1984**, *106*, 6468−6475.
(13) Streitwieser, A., Jr.; Rajca, A.; McDowell, R. S.; Glaser, R. *J. Am. Chem. Soc.* **1987**, *109*, 4184−4188.
(14) Denmark, S. E.; Dorow, R. L. *J. Am. Chem. Soc.* **1990**, *112*, 864−866.
(15) Denmark, S. E.; Dorow, R. L. *J. Org. Chem.* **1990**, *55*, 5926−5928.
(16) Denmark, S. E., Cramer, C. J. *J. Org. Chem.* **1990**, *55*, 1806−1813.
(17) Kranz, M.; Denmark, S. E. *J. Org. Chem.* **1995**, *60*, 5867−5877.
(18) Koch, R.; Anders, E. *J. Org. Chem.* **1995**, *60*, 5861−5866.
(19) (a) Leyssens, T.; Peeters, D. *J. Mol. Struct. (THEOCHEM)* **2004**, *673*, 79−86. (b) Leyssens, T.; Peeters, D. *J. Mol. Struct. (THEOCHEM)* **2004**, *686*, 71−82.
(20) Katritzky, A. R.; Piffl, M.; Lang, H. Y.; Anders, E. *Chem. Rev.* **1999**, *99*, 665−722.
(21) Pratt, L. M.; Streitwieser, A. J. *Org. Chem.* **2003**, *68*, 2830−2838.
(22) Pratt, L. M.; Văn Ngũỹen, N.; Ramachandran, B. *J. Org. Chem.* **2005**, *70*, 4279−4283.
(23) Ando, K. *J. Am. Chem. Soc.* **2005**, *127*, 3964−3972.
(24) Dürckheimer, W.; Blumbach, J.; Lattrell, R.; Scheunemann, K. H. *Angew. Chem.* **1985**, *24*, 180−202.
(25) Imada, A.; Kitano, K.; Kintaka, K.; Muroi, M.; Asai, M. *Nature* **1981**, *289*, 590−591.
(26) Sykes, R. B.; Cimarusti, C. M.; Bonner, D. P.; Bush, K.; Floyd, D. M.; Georgopapadakou, N. H.; Koster, W. H.; Liu, W. C.; Parker, W. L.; Principe, P. A.; Rathnum, M. L.; Slusarchyk, W. A.; Trejo, W. H.; Wells, J. S. *Nature* **1981**, *291*, 489−491.
(27) Gordon, E. M.; Ondetti, M. A.; Pluscec, J.; Cimarusti, C. M.; Bonner, D. P.; Sykes, R. B. *J. Am. Chem. Soc.* **1982**, *104*, 6053−6060.
(28) Brogden, R. N.; Heel, R. C. *Drugs* **1986**, *31*, 96−130.
(29) Neu, H. C. *Science* **1992**, *257*, 1064−1073.
(30) Bulychev, A.; Massova, I.; Miyashita, K.; Mobashery, S. *J. Am. Chem. Soc.* **1997**, *119*, 7619−7625.
(31) Golemi, D.; Maveyraud, L.; Vakulenko, S.; Tranier, S.; Ishiwata, A.; Kotra, L. P.; Samama, J.-P.; Mobashery, S. *J. Am. Chem. Soc.* **2000**, *122*, 6132−6133.
(32) Meroueh, S. O.; Minasov, G.; Lee, W.; Shoichet, B. K.; Mobashery, S. *J. Am. Chem. Soc.* **2003**, *125*, 9612−9618.
(33) Fisher, J. F.; Meroueh, S. O.; Mobashery, S. *Chem. Rev.* **2005** *105*, 395−424.
(34) Sandanayaka, V. P.; Prashad, A. S. *Curr. Med. Chem.* **2002**, *9*, 1145−1165.
(35) Hammond, M. L. *J. Antimicrob. Chemother.* **2004**, *53*, Suppl. S2, ii7−ii9.
(36) Bonneau, P. R.; Hasani, F.; Plouffe, C.; Malenfant, E.; LaPlante, S. R.; Guse, I.; Ogilvie, W. W.; Plante, R.; Davidson, W. C.; Hopkins, J. L.; Morelock, M. M.; Cordingley, M. G.; Deziel, R. *J. Am. Chem. Soc.* **1999**, *121*, 2965−2973.
(37) Powers, J. C.; Asgian, J. L.; Ekici, O. D.; James, K. E. *Chem. Rev.* **2002**, *102*, 4639−4750.
(38) Frisch, M. J.; et al. *Gaussian 03*; Gaussian, Inc.: Pittsburgh, PA, 2003.
(39) Example of a reference work: Parr, R. G.; Yang, W. *Density-Functional Theory of Atoms and Molecules*; Oxford University Press: New York, 1989.

Scheme 1. Synthesis of 4-Phosphono-β-lactams[a]

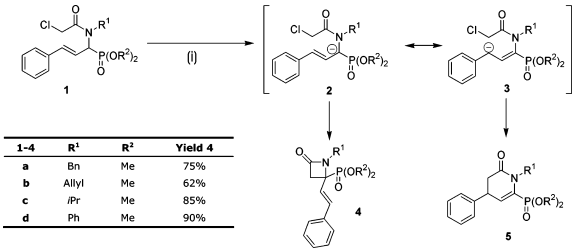

1–4	R^1	R^2	Yield 4
a	Bn	Me	75%
b	Allyl	Me	62%
c	*i*Pr	Me	85%
d	Ph	Me	90%

[a] Reagents and conditions: (i) 1.1 equiv NaH, THF, Δ, 3 h.

Hartree−Fock and DFT methods on the geometries and energies of phosphorus-containing compounds.[19] The systems studied in that work are relatively small, and the use of highly correlated electronic structure methods such as MP2, MP4, QCISD, CCSD(T) was feasible. Their results show that the geometries resulting from DFT(B3LYP), MP2, and QCISD computations using the 6-31++g(d,p) are usually very close to each other. Another study by Pratt et al. revealed the structures of fluoromethyllithium and chloromethyllithium carbenoids in the gas phase and in ethereal solvent,[40] and it was found that the optimized geometries from the mPW1PW91/6-31+g(d) and QCISD/6-31+g(d) level agree to a large extent.

The systems of interest to the current work are too large to perform geometry optimizations at the post-Hartree−Fock level. DFT methods are therefore more suitable, and in the light of the previous discussion the B3LYP and mPW1PW91 exchange correlation functionals were selected to establish their influence on the geometry. The B3LYP functional is the most popular version of a hybrid DFT method combining the Becke exchange functional with the LYP correlation functional and which also contains 20% of exact Hartree−Fock exchange.[41] According to various references, the B3LYP methods provide excellent low-cost performance for geometry optimizations.[42] This is further confirmed by specific studies performed by Leyssens and Peeters on the properties of the phosphonate functional group.[19] The mPW1PW91 functional is also a hybrid functional containing 25% of exact exchange. The latter uses the modified Perdew−Wang exchange functional that has improved the long-range behavior as proposed by Adamo and Barone.[43] DFT models may substantially underestimate the activation energies for SN_2 substitution reactions. More information can be found in a study performed by Kormos and Cramer[44] where the relatively good performance of the mPW1PW91 functional is also shown. Another interesting paper within this respect is the study recently performed by Pratt and co-workers on the performance of various electronic structure methods for the evaluation of barrier heights for gas-phase reactions of lithium enolates.[22] They showed that when DFT methods succeeded in locating a transition-state structure, the geometries of the forming and breaking bond were in reasonable agreement with MP2 calculations. Also single-point MP2 energies at B3LYP geometries provide a reasonable estimate of the lithium enolate activation barriers in the gas phase. However, since the systems under consideration are quite large, such a strategy is computationally not feasible.

Another issue of importance is the basis set used for the calculations. As the present study involves anions, which have a more spread-out electron density than neutral atoms, it is essential to add diffuse functions in the basis set.[45] The following basis sets were used: 6-31+g(d), 6-311 g(d,p), 6-311++g(d,p). The first one represents a double-ζ basis, whereas the others are triple-ζ basis sets. They further differ in the number of diffuse and/or polarization functions added.

The vibrational frequencies of the optimized structures were calculated at the same level of theory at which the geometries were optimized. The transition states were verified to have only one imaginary frequency and hence correspond to a first-order saddle point on the potential energy surface.

3. Experimental Results

The synthesis of the phosphono-β-lactams under investigation was performed, starting from the appropriate *N*-chloroacetyl-1-amino alkenylphosphonates, **1**, which were obtained according to a literature procedure.[6] Upon treatment with a strong base, typically sodium hydride, a phosphorus-stabilized anion is formed, which can be represented by two canonical resonance contributors **2** and **3** (Scheme 1). The ring closure, performed in 3 h at 66 °C, showed that only one product was formed with a characteristic chemical shift between 24.01 and 24.75 ppm (^{31}P NMR), while the chemical shift for a vinylic phosphonate is expected at significantly higher field (10−20 ppm). The same products were obtained at room temperature using LiHMDS as a base in diethyl ether as a solvent.

The proposed β-lactam structure was confirmed upon further spectroscopic investigation. The very high infrared absorption of the carbonyl (>1750 cm^{-1}) is typical for highly strained rings. Furthermore, the ring CH_2(3) appears as a second-order spin system in the ^{1}H NMR spectrum, involving a geminal coupling constant of 14.6−15.3 Hz and also quite large ^{31}P couplings (5.5−5.8 Hz), indicating the near presence of the phosphorus atom. According to the integral of the signals in the region of 6−7 ppm in the proton spectrum, two alkenyl protons are present in the molecule. A E-coupling of 16.2 Hz was found for all five products, next to smaller ^{31}P couplings. All aforementioned phosphorus couplings disappeared when the proton spectrum was run with selective ^{31}P decoupling. All ^{13}C peaks could be attributed to the appropriate carbon in the azetidinones using 2D techniques (HSQC and HMBC) together with DEPT spectra. The quaternary carbon atom bearing the phosphonate group is expressed as a doublet (J = 166.7−168.5 Hz) in the ^{13}C spectrum, with a chemical shift clearly within the aliphatic

(40) Pratt, L. M.; Ramachandran, B.; Xidos, J.; Cramer, C. J.; Truhlar, D. G. *J. Org. Chem.* **2002**, *67*, 7607−7612.
(41) Becke, A. D. *J. Chem. Phys.* **1993**, *98*, 5648−5652.
(42) Coote, M. L. *J. Phys. Chem. A* **2004**, *108*, 3865−3872.
(43) Adamo, C.; Barone, V. *J. Chem. Phys.* **1998**, *108*, 664−675.
(44) Kormos, B. L.; Cramer, C. J. *J. Phys. Org. Chem.* **2002**, *15*, 712−720.
(45) Lynch, B. J.; Zhao, Y.; Truhlar, D. G. *J. Phys. Chem. A* **2003**, *107*, 1384−1388.

region (58.06−59.82 ppm). From this carbon, a clear HMBC coupling was observed with the CH_2(3) of the four-membered ring.

An overview of the regioselectivity of intermolecular reactions between heteroatom-stabilized allyl anions and electrophiles has been presented by Katritzky et al.[20] Even though an intramolecular reaction is considered in our system, some important directing factors could be identified such as nature of the counterion, reaction conditions, the nature of the electrophile, steric characteristics of the anion and the electrophile, coordination between the electrophile and the substrate prior to bond formation, etc. Lithium and sodium have been evaluated as counterions giving the same selectivity. The reaction conditions, on the other hand, have an influence on the reaction rate but not on the selectivity. Formation of the anion occurs fast and can be followed visually by the evolution of hydrogen gas from the reaction mixture upon addition of sodium hydride at room temperature. After the H_2-gas evolution ceases, the reaction needs a further 3 h of reflux in THF (bp 66 °C), while the reaction did not complete during an overnight reflux period in diethyl ether (bp 35 °C). The high number of functionalities in the substrate calls for a more profound investigation of other determining factors. Furthermore, the intramolecular reaction under investigation involves additional complications compared to the intermolecular reactions, such as anion geometry and substrate conformation.

A phosphonate group is known to greatly stabilize carbanions in the α-position through electrostatic interactions.[15,20] This might explain the lack of reactivity in the γ-position. To study the selectivity of the reaction, an experiment was set up to trap the allyl anion with common electrophiles, such as a proton (or a deuteron) or methyl iodide. For this purpose, *N*-acetyl-1-amino alkenylphosphonate, **8**, was synthesized using a modified procedure. Imine **6** was phosphonylated regioselectively using dimethyl phosphite in methanol (97% yield),[46] and the resulting aminophosphonate **7** was then acetylated using acetyl chloride and DMAP/pyridine (63% overall yield). The resulting *N*-acetyl-1-amino alkenylphosphonate, **8**, is sterically and electronically very similar to the *N*-chloroacetyl substrates but is not prone to intramolecular reactions because of the lack of a leaving group. Initial attempts to prepare the anion with LiHMDS and to trap it with methyl iodide resulted in complex mixtures. When the anion was quenched with water, an unseparable mixture of starting material and two new products was found in low yield after extraction. The generation of several side products was probably induced by the acidic acetyl protons leading to unselective deprotonation by LiHMDS. However, when sodium hydride was used instead, deprotonation proceeded selectively, and a clean mixture of starting material **8** and its isomer **10** was found after quenching with water. Furthermore, both isomers could be separated using column chromatography, which allowed the unambiguous determination of the structure of the resulting isomer with the use of selected NMR techniques.

The ratio of both isomers was rather surprisingly in favor of the γ-protonated isomer **10**, suggesting it as an important contributor to the canonical resonance system of the allyl anion. When deuterium oxide was used to quench the allyl anion, the corresponding monodeuterated products were obtained in the same ratio. The reaction was then repeated under the same conditions, however, using methyl iodide as an intermediate soft electrophile. This might provide a better model for the intramolecular alkylation. In this case, the γ-methylated product **11** was formed as a mixture of (*E*,*Z*)-isomers (δ ^{31}P = 16.3 and 16.2). Purification using column chromatography or crystallization failed. The structure was confirmed, however, by comparing the ^{13}C, ^{31}P, and DEPT spectra from the crude reaction mixture with vinyl phosphonate **10** and by determining its mass spectrum using LC−MS. No other phosphorus-containing compounds were detected using ^{31}P NMR.

The results obtained from the intermolecular reactions with allylic anion **9** are in contradiction with the exclusive β-lactam formation in the intramolecular reaction. To elucidate these peculiarities, ab initio molecular orbital calculations were performed as presented in the following section, giving microscopic insight into the reaction preference.

4. Ab Initio Results

Free Anions. The energetically most favored structure of the free carbanion is visualized in Figure 1 (labeled as **2a** in Scheme 1). This structure was found by applying various internal rotations about single bonds and selecting stepwise the most stable conformation along the rotational potential. For the discussion of the geometry some of the carbon atoms are labeled as shown in Figure 2 (Anion I). The most important geometrical parameters are listed in Table 1.

One particular internal rotation deserves special attention, i.e., about the C_1-C_2 bond, as it gives rise to either the *E* or *Z* geometry of the γ-anionic form (α and γ refer to the phosphorus atom). The *E* geometry cannot lead to six-membered rings. The latter conformer was found to be highly unstable (14.8 kJ/mol), indicating that the *Z* geometry is preferred which can either close at the γ- or α-position.

Within the context of a further cyclization toward four- or six-membered ring formation, the C_5-C_1 and C_5-C_3 distances are relevant, as they represent the distances from the α- and γ-carbon centers of the allylic unit to the chlorinated carbon atoms. They amount to 2.78 and 3.65 Å, respectively, and indicate that the most stable conformer of the anion has a characteristic geometry that is suitable for four-membered ring formation. Also, the internal rotation about the C_1-N bond, will play a crucial role in the reaction mechanism, as it determines the relative position of the chlorinated carbon atom (C_5) toward the α- or γ-carbon center (respectively, C_1 or C_3). In the energetically most favored conformation the dihedral angle $C_2C_1NC_4$ amounts to −82.19°, and C_5 points away from the carbon atom at the γ-position of the phosphorus (cf. Figure 1).

To unravel the mechanism of the further ring closure, it is instructive to study the polarization of charge of the carbanion. Therefore, we calculated partial atomic charges according to the ChelpG scheme[47] on the optimized geometries. The latter method uses electrostatic derived charges and has proven its accuracy for calculating atomic populations.[48,49] The results are given in Table 2. The phosphorus atom has a highly positive charge (0.88), whereas the negative charge is delocalized over the allyl unit with a slight polarization toward the γ-carbon atom

(46) Van Meenen, E.; Moonen, K.; Acke, D.; Stevens, C. V. *Arkivoc* **2006**, 31−35.

(47) Breneman, C. M.; Wiberg, K. B. *J. Comput. Chem.* **1990**, *11*, 361−373.
(48) Sigfridsson, E.; Ryde, U. *J. Comput. Chem.* **1998**, *19*, 377−395.
(49) Martin F.; Zipse, H. *J. Comput. Chem.* **2005**, *26*, 97−105.

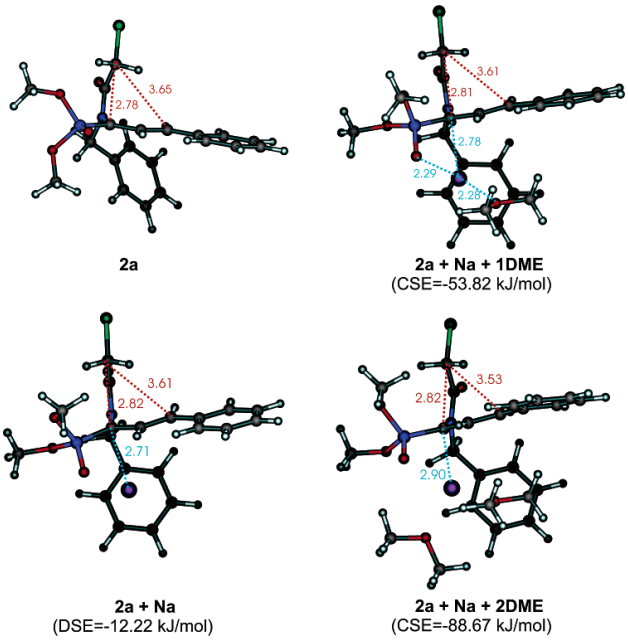

Figure 1. Optimized conformers of the anions in different molecular environments: **2a** in the gas phase, **2a** + Na including one sodium ion, **2a** + Na + 1DME and **2a** + Na + 2DME including one sodium ion and one or two DME molecules. All optimizations are performed at the B3LYP/6-31+g(d) level.

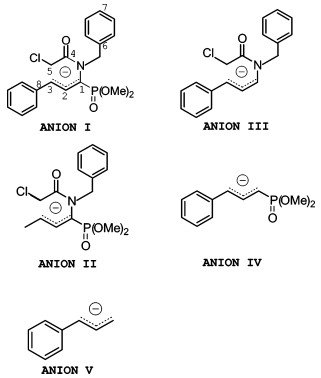

Figure 2. Allyl stabilized carbanions.

(C_3). Also, the oxygen of the P═O bond carries a large negative charge and is the basic reason for the positively charged phosphorus atom. The origin of this charge distribution is studied more in detail by calculating the energetically most favored structure of some other free anions with different substitution patterns (cf. Figure 2). It turns out that the net amount of negative charge on the allyl unit systematically increases by removing the phosphonate group and/or the nitrogen centered group (Anion III, Anion IV, Anion V). In the presence of the phosphonate group (Anion IV) a highly polarized carbon−phosphorus bond is obtained with a large positive charge (1.12) on the P atom. Previous results are in accordance with the findings of Cramer and Denmark.[16]

Protonation Energies. The reactivity of the α- and γ-carbon atoms (α and γ are referred with respect to the phosphonate group) toward electrophilic attack can be estimated by calculating the protonation energies at both carbon positions (see Scheme 2):

$$\Delta E_x = E(Anion + H_x) - E(Anion) - E(H^+) \qquad (1)$$

with $x = \alpha$ or γ. In Scheme 2, the α- and γ-protonated forms are related to **8** and **10**, respectively. The results are shown schematically in Figure 3. For the Anions I and II having both the phosphonate group and the nitrogen-containing subgroup, the protonated molecule at the γ-position is more stable by 23 and 37 kJ/mol, respectively. When removing either the phosphonate or nitrogen centered subgroup, the stability sequence inverts. These findings are in accordance with the experiments described in the previous section: the γ-carbon has a larger proton affinity than the α-carbon. However, these thermody-

Table 1. Most Important Geometrical Characteristics of Reactants and Transition States at the B3LYP/6-31+g(d) level[a]

Gas Phase Structures

	Anion I (**2a**)	TS4	TS6
C_5-C_1	2.7762	2.1233	2.8210
C_5-C_3	3.6454	3.7046	2.5544
C_1-C_5	1.8131	2.4117	2.3520
$C_3C_2C_1N$	0.34	9.27	−1.32
$C_2C_1NC_4$	−82.19	−116.51	−36.02
$C_1NC_4C_5$	−1.11	10.28	−15.24

Transmetalated Structures

	Anion I +Na	TS4 + Na	TS6 + Na
C_5-C_1	2.8176	1.9825	2.7987
C_5-C_3	3.6139	3.6417	2.1833
C_1-C_5	1.7986	2.4820	2.4213
$C_3C_2C_1N$	−4.41	6.59	−2.25
$C_2C_1NC_4$	−80.36	−117.36	−31.36
$C_1NC_4C_5$	2.86	11.28	−16.72
$Na-C_1$	2.7097	2.9223	2.8038
$Na-C_3$	3.5203	2.7938	2.7610
$Na-C_6$	2.8747	2.7873	2.7168
$Na-C_7$	2.9833	3.6904	3.0384
	Anion I +Li	**TS4 + Li**	**TS6 + Li**
C_5-C_1	2.8327	1.9674	2.7920
C_5-C_3	3.6866	2.8895	2.4085
C_1-C_5	1.7986	2.4902	2.4432
$C_3C_2C_1N$	−2.08	5.93	−1.64
$C_2C_1NC_4$	−83.80	−120.25	−31.42
$C_1NC_4C_5$	2.53	11.08	−16.28
$Li-C_1$	2.3744	2.5211	2.4360
$Li-C_3$	3.6033	2.5803	2.4183
$Li-C_6$	2.4987	2.5595	2.3279
$Li-C_7$	2.7311	3.7625	2.7642

Transmetalated Structures Coordinated with Dimethylether Molecules

	Anion I + Na+1DME	TS4 + Na + 1DME	TS6 + Na + 1DME
C_5-C_1	2.8142	1.9995	2.7905
C_5-C_3	3.6081	3.6616	2.2261
$Cl-C_5$	1.7994	2.4685	2.4100
$C_3C_2C_1N$	−5.12	5.23	−2.68
$C_2C_1NC_4$	79.53	−116.69	−31.66
$C_1NC_4C_5$	2.47	10.87	−17.73
$Na-C_1$	2.7773	3.0057	2.6789
$Na-C_3$	3.5396	2.8753	3.8638
$Na-C_6$	3.0571	2.9603	2.7726
$Na-C_7$	3.2443	3.8839	3.5234
$Na-O_1$	2.2795	2.2779	2.2758
O_1-C_6	5.0397	5.1811	4.7951
O_1-C_8	4.4539	4.3069	5.0642

[a] All distances are reported in Å, angles and dihedrals in degrees. O_1 is the oxygen of the DME molecule.

namic findings cannot explain the exclusive reaction toward four-membered rings. Most probably the transition state toward six-membered ring formation is characterized by energetically unfavorable effects, which inhibit the ring closure at the γ-site.

Transmetalation. Although the free gas-phase anions provide useful information, the counterion may contribute to the factors that affect the regioselectivity of heteroatom-stabilized allylic anions. Therefore, the free anion with the presence of a sodium counterion was optimized. Various stable structures were obtained when starting from different initial positions of the sodium cation. The most stable configuration is visualized in Figure 1 (labeled as **2a**+Na). The sodium counterion prefers a position between the allylic subsystem and the benzyl group

Table 2. Atomic Charges Calculated According to the ChelpG Scheme at the B3LYP/6-31+g(d) Level of Theory for Various Anions

	anion I (2a)	anion II	anion III	anion IV	anion V
C5	0.21	0.13	0.30		
Cl	−0.29	−0.29	−0.31		
C1	−0.39	−0.32	−0.43	−0.63	−0.75
C2	0.10	−0.15	0.11	0.24	0.28
C3	−0.47	−0.20	−0.55	−0.59	−0.66
N	0.20	0.15	0.23		
P	0.88	0.89		1.12	
O	−0.65	−0.67		−0.70	

	anion I + Na	anion I + Li	anion I + Na+1DME	anion I + Na+2DME
C5	−0.05	0.03	0.03	0.06
Cl	−0.20	−0.21	−0.22	−0.22
C1	−0.34	−0.42	−0.34	−0.30
C2	0.04	0.01	0.09	0.10
C3	−0.51	−0.40	−0.47	−0.49
N	−0.04	0.02	−0.01	−0.02
P	0.81	0.96	0.80	0.83
O	−0.64	−0.69	−0.70	−0.61
Na/Li	0.59	0.54	0.55	0.49
O1			−0.36	−0.20
O2			–	−0.19

Scheme 2 [a]

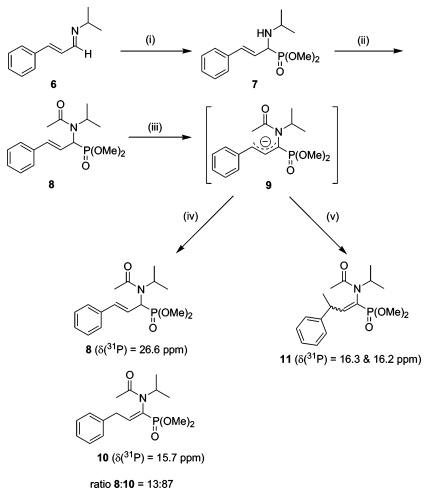

[a] Reagents and conditions: (i) 2 equiv $HPO(OMe)_2$, MeOH, Δ, 3 h; (ii) 1.5 equiv AcCl, 0.2 equiv DMAP, 2 equiv pyridine, THF, rt (1 h), Δ (1 h); (iii) 1) 1.1 equiv NaH, −78 °C, THF; 2) −78 °C → rt (2h); (iv) H_2O, 2 h rt; (v) 3 equiv MeI, 2 h, rt.

(cf. Table 1: $Na-C_1 = 2.71$ Å, $Na-C_6 = 2.87$ Å, $Na-C_7 = 2.98$ Å). The sodium atom makes an additional contact with the oxygen of the P═O bond ($Na-O = 2.27$ Å). The lithiated anions have similar geometrical characteristics (cf. Table 1: $Li-C_1 = 2.37$ Å, $Li-C_6 = 2.50$ Å, $Li-C_7 = 2.73$ Å). The atomic charges are not drastically altered by incorporating the counterion (cf. Table 3). For further cyclization, it is also important to analyze the effect of the counterion with respect to the

Table 3. Reaction Barriers for Four- and Six-Membered Cyclization ($\Delta E^{\ddagger}(4)$, $\Delta E^{\ddagger}(6)$, $\Delta G^{\ddagger}(4)$, $\Delta G^{\ddagger}(6)$) Expressed in kJ/mol at Various Levels of Theory[a]

	gas phase results					
level of theory	$\Delta E^{\ddagger}(4)$	$\Delta E^{\ddagger}(6)$	$\Delta(\Delta E^{\ddagger})$	$\Delta G^{\ddagger}(4)$	$\Delta G^{\ddagger}(6)$	$\Delta(\Delta G^{\ddagger})$
B3LYP/6-311g**//B3LYP/6-311g**	75.72	98.12	22.40	70.28	96.99	26.71
mPW1PW91/6-31+g(d)//B3LYP/6-311g**	91.43	111.69	20.25			
BP86/6-31+g(d)//B3LYP/6-311g**	70.54	86.32	15.78			
B3LYP/6-31+g(d)//B3LYP/6-31+g(d)	81.05	101.83	20.78	75.61	100.70	25.09
B3LYP/6-311++g(d)//B3LYP/6-311++g(d,p)	82.43	103.12	20.69			
mPW1PW91/6-31+g(d)//MPW1PW91/6-311g**	90.78	110.45	19.67	85.34	109.32	23.98
	without inclusion of bulk solvent effects			with inclusion of bulk solvent effects		
B3LYP/6-31+g(d)//B3LYP/6-31+g(d)	$\Delta E^{\ddagger}(4)$	$\Delta E^{\ddagger}(6)$	$\Delta(\Delta E^{\ddagger})$	$\Delta G^{\ddagger}(4)$	$\Delta G^{\ddagger}(6)$	$\Delta(\Delta G^{\ddagger})$
transmetalated structures (Na)	157.14	160.54	3.40	95.31	121.45	26.14
transmetalated structures (Li)	167.66	177.65	9.99	102.17	147.31	45.13
transmetalated structures (Na) + 1DME molecule	149.69	140.75	−8.94	88.00	103.31	15.31
transmetalated structures (Na) + 2DME molecule	145.06	140.39	−4.66	58.78	85.62	26.84

[a] $\Delta(\Delta E^{\ddagger})$ is the difference between the reaction barrier for six- and four-membered ring formation, i.e. $\Delta E^{\ddagger}(4) - \Delta E^{\ddagger}(6)$. In the notation Level1//Level2, Level1 is the electronic level of theory used for the energetics, whereas Level2 is the level of theory used for the geometry optimization.

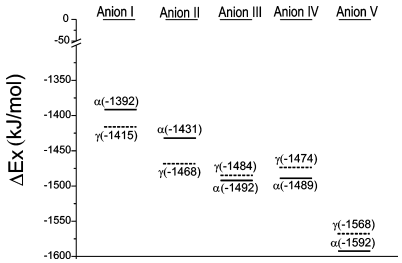

Figure 3. Protonation energies (ΔE_x) for various anions (B3LYP/6-31+g(d) level).

chemically active area of the molecule. The C_5-C_1 and C_5-C_3 distances are not considerably altered. This conclusion also holds for the $C_2C_1NC_4$ dihedral angle which determines the position of the C_5-C_1 unit to the allylic system. This proves that the counterion exerts limited influence on the structural parameters of the system under consideration.

Effect of Solvation. The computations discussed thus far refer to unsolvated compounds. However, THF was used as solvent in our experiments, and solvation may be expected to be important in these ether-like solvents. The solvation originates from two contributions: coordination of ether oxygens to the sodium cation (coordination solvation) and the electrostatic effect of the solvent dielectric medium (dielectric solvation). The latter effect is more easily to deal with from a computational point of view as it is usually approximated by enclosing the molecule in a cavity within a continuous dielectric medium. Recently, an article by Kelly, Cramer, and Truhlar appeared on the accurate determination of solvation free energies, which may be interesting for a more detailed reading on this subject.[50] The dielectric solvation energies (DSE) were obtained using a CPCM (also known as COSMO) option in Gaussian 03 on the unsolvated B3LYP/6-31+g(d) structures.[51] The coordination solvation energy (CSE) is estimated by coordinating the sodium ion to one ore more ether oxygens. Dimethyl ether (DME) was chosen as the coordinating solvent instead of THF. DME has about the same basicity as THF but is significantly smaller for computations. An important question concerns the degree of coordination. For solvent-separated ion pairs, four-coordinated lithium cations have been recognized in NMR studies.[52,53] However, for contact ion pairs as encountered here, the degree of coordination may be dependent on the nature of the counterion, and the coordination may be expected to be smaller due its electrostatic effect.[54] The degree of coordination for the system under consideration is estimated by coordinating the sodium cation with one, two, three, or four DME molecules and calculating the CSE energies. These values are shown in Figure 1. Coordination of the first two ether molecules is highly exothermic (CSE amounts to −53.8 and −88.7 kJ/mol). As the coordination with the second DME is still highly exothermic, an additional DME molecule was placed close to the ion pair. Coordination of the third DME molecule causes only a slight additional stabilization (−98.9 kJ/mol versus −88.7 kJ/mol) and is located at a large distance of 4.74 Å from to the sodium ion (compared with Na−O distances of 2.17 and 2.18 Å for the first two DME molecules). The CSE amounts to −102.7 kJ/mol for four DME molecules, indicating that the coordination effectiveness is largely reduced from the third DME molecule on.

The DSE is obtained as the sum of two terms, an electrostatic term, which has a negative sign and which is derived from the interaction of the solute charges with the solvent, and a nonelectrostatic term, that is generally positive and consisting of the free energy needed for the formation of the cavity in the continuum, a dispersion term and a repulsion term. The value for the DSE on the monomeric ion pair formed by the anion and the sodium ion amounts to 12.22 kJ/mol and is non-negligible. These values are in line with the numbers reported by Pratt and Streitwieser.[21] The geometrical parameters with

(50) Kelly, C. P.; Cramer, C. J.; Truhlar, D. G. *J. Chem. Theory Comput.* **2005**, *1*, 1133−1152.
(51) (a) Cossi, M.; Rega, N.; Scalmani, G.; Barone, V. *J. Comput. Chem.* **2003**, *24*, 669−681. (b) Barone, V.; Cossi, M. *J. Phys. Chem. A* **1998**, *102*, 1995−2001.
(52) Reich, H. J.; Green, D. P.; Medina, M. A.; Goldenberg, W. S.; Gudmundsson, B. O.; Dykstra, R. R.; Philips, N. H. *J. Am. Chem. Soc.* **1998**, *120*, 7201−7210.
(53) Carlier, P. R.; Lo, C. W.-S. *J. Am. Chem. Soc.* **2000**, *122*, 12819−12823.
(54) Schade, C.; Schleyer, P. V. R. *Adv. Organomet. Chem.* **1988**, *27*, 169−170.

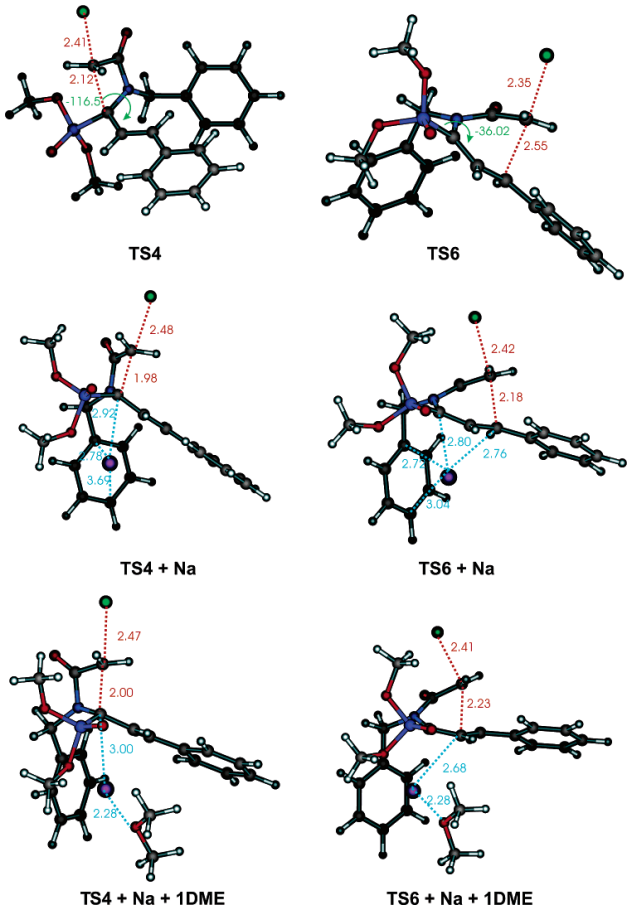

Figure 4. Optimized conformers of the transition states in different molecular environments: TS4 and TS6 transition states for four- and six-membered lactam formation in the gas phase; TS4+Na and TS6+Na including one sodium ion; TS4+Na+1DME and TS6+Na+1DME including one sodium ion and one DME molecule. All optimizations are performed at the B3LYP/6-31+g(d) level.

inclusion of solvent molecules, confirm once more that the chemical active area for cyclization remains nearly the same.

Transition-State Structures. To unravel the experimentally obtained reaction preference toward four-membered lactams, calculations are performed to determine the reaction barriers. The transition states toward four- and six-membered ring formation in the gas phase are visualized in Figure 4, and some relevant geometrical parameters are given in Table 1.

Both transition states resemble an intramolecular SN_2-like reaction characterized by an umbrella-like inversion at C_5. In the reacting anion the C_5 carbon atom is oriented toward the α-carbon atom, i.e. the reactive center for four-membered ring formation. In the case of six-membered ring formation large distortions are needed from the original geometry of the anion to adapt the SN_2-like transition structure (cf. Table 1): the dihedral angle $C_2C_1NC_4$ varies from −82.2 to −36.0°. To get an idea about energetic variations associated with these distortions, the rotational potential in terms of this geometrical variable was calculated. This was done by a stepwise variation of the $C_2C_1NC_4$ torsional angle and optimizing all other degrees of freedom. To reduce the computational cost, the B3LYP/3-21+g(d) level of theory was adapted. The results are shown

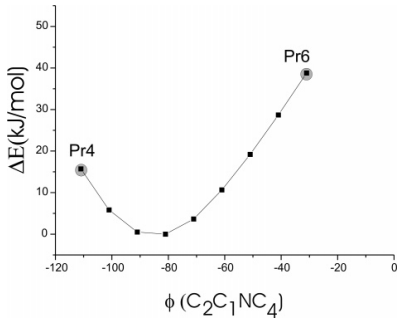

Figure 5. Part of the rotational potential in terms of the $C_2C_1NC_4$ dihedral angle. The precursors for four- and six-membered ring formation (Pr4 and Pr6) are indicated by a gray circle.

in Figure 5 for the appropriate range of the dihedral angle. Starting from the most stable favorable conformation ($\phi = -82.9°$) the torsional angle reaches values of -116 and $-36°$ in the four- or six-membered transition states, respectively (cf. Table 1). Due to the strongly asymmetric shape of the rotational potential around the minimum, the associated energy to induce such distortions amounts to approximately 15 and 38 kJ/mol. Therefore, a large amount of energy is needed to reach the transition state toward the six-membered lactams. The structures of the transition states with incorporation of the counterions are also visualized in Figure 4. The chemically active part for the ring-closure reaction is not altered substantially; only the phenyl groups slightly relax in the presence of the sodium cation. Furthermore, the distances of the forming C−C bond are shorter (∼0.15 Å) at all levels of theory. This is in accordance with the results of Ando.[23]

Reaction Barriers. In the further course of the discussion, both the bare reaction barriers $\Delta E^{\ddagger}$ (i.e. the electronic energy differences between transition state and corresponding reactant) and the corresponding free energies ($\Delta G^{\ddagger}$) including zero-point, thermal, and entropic contributions are evaluated. When PCM computations are used, the energies have the status of free energies, since they implicitly take into account the thermal and entropic contributions of the solvent.[55] The values are given in Table 3 at various levels of theory.

First, the influence of the level of theory on the energetic results is discussed. It is generally known that B3LYP geometries are quite accurate[19,42,56] and that variations on the reaction barriers are small by adopting another level for the geometry optimization. This is confirmed by our calculations: mPW1PW91/6-31+g(d)//B3LYP/6-311 g** and mPW1PW91/6-31+g(d)//mPW1PW91/6-31+g(d) predict barriers for four-membered cyclization of 91.43 and 90.78 kJ/mol, respectively. The functional form has a much larger influence on the reaction barriers leading to respective values between 70 to 91 kJ/mol. The selection of the most suitable level of theory is jeopardized by the lack of direct experimental data on the reaction barriers. However, the differences between the reaction barriers for four- and six-membered ring formation (i.e. $\Delta(\Delta E^{\ddagger}) = \Delta E^{\ddagger}(6) - \Delta E^{\ddagger}(4)$, where $\Delta E^{\ddagger}(4)$ and $\Delta E^{\ddagger}(6)$ are the barriers for four- and six-membered cyclization) show much less variation (16−22 kJ/mol, depending on the electronic level of theory used), predicting a large preference for four-membered ring formation at all levels of theory. The reason for this preference must be traced back to the high amount of energy needed to reach a conformation suitable for six-membered ring formation (cf. Figure 5).

At second instance, the influence of the cation and solvent effects on the reaction barriers is discussed. Inclusion of the sodium cation has a dramatic influence on the reaction barriers. Both barriers increase with approximately 60−80 kJ/mol at all levels of theory. Similar findings were found by Ando.[23] Moreover, there is not a clear preference anymore for four- or six-membered ring formation ($\Delta(\Delta E^{\ddagger}) = 3.4$ kJ/mol). However, since the reactions were performed in THF, solvation of the counterion is expected to be important. At first, bulk solvent effects are taken into account using the CPCM model, lowering the reaction barriers to about 95 and 121 kJ/mol (at the B3LYP/6-31+g(d)//B3LYP/6-31+g(d) level) for four- and six-membered ring formation, respectively. Furthermore, the preference for cyclization at the α-position is correctly predicted by including bulk solvent effects ($\Delta(\Delta G^{\ddagger}) = 26.1$ kJ/mol) and thus emphasizing the necessity to treat solvent effects in a proper way.

Finally explicit solvent molecules were taken into account as explained previously. The barriers were calculated for one and two DME molecules. Oncemore, inclusion of bulk solvent effects is required to predict the correct reaction preference. The difference between the activation free energy for four- and six-membered ring formation ($\Delta(\Delta G^{\ddagger})$) amounts to 15.31 and 26.84 kJ/mol in the case of adding one or two DME molecules, respectively. The value of $\Delta(\Delta G^{\ddagger})$ may be expected to alter only slightly with inclusion of more DME molecules, consistently with the result found for the CSE values. All theoretical calculations are now consistent, explaining the four-membered ring preference. The values of $\Delta(\Delta G^{\ddagger})$ amount to 25.09, 26.14, and 26.84 kJ/mol at the B3LYP/6-31+g(d) level for the gas-phase computations, the calculations with inclusion of the sodium counterion and the inclusion of the sodium and two DME molecules, respectively.

Summarizing, for this particular reaction a correct qualitative picture is predicted using the gas-phase computations. Solvent effects do alter the absolute values of the reaction barriers but do not affect the global α/γ selectivity. This might be anticipated as the geometries of the chemical active part of the system are not significantly altered by inclusion of the molecular environment. However, based on this single application, these conclusions may not be generalized.

Origin of the Four-Membered Ring Preference. Finally, suggestions are validated to unravel the true origin of the four-membered ring formation preference. As already pointed out, the rotation about the C−N bond is largely hindered. Moreover the associated potential is asymmetric, i.e a rotation toward the γ-carbon atom is disfavored (cfr. Figure 5). To investigate more in depth these energetically unfavorable effects, the reaction barriers for a number of allyl-stabilized anions differing in the substituents X, Y, and Z attached at various positions of the anion (cf. Figure 6) were calculated.

(55) Tomasi, J.; Persico, M. *Chem. Rev.* **1994**, *94*, 2027−2094.
(56) Gomez-Balderas, R.; Coote, M. L.; Henry, D. J.; Radom, L. *J. Phys. Chem. A* **2004**, *108*, 2874−2883.

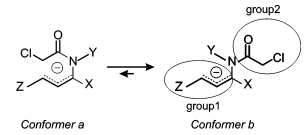

	X	Y	Z	$\Delta(\Delta G^{\ddagger})$
ANION I	$P(OMe)_2$ (O)	$CH_2(C_6H_5)$	C_2H_5	26.84
ANION Ia	$P(OMe)_2$ (O)	$CH_2(C_6H_5)$	CH_3	33.97
ANION Ib	$P(OH)_2$ (O)	$CH_2(C_6H_5)$	C_2H_5	33.21
ANION Ic	PH_2 (O)	$CH_2(C_6H_5)$	C_2H_5	20.40
ANION Id	$C(CH_3)_2$	$CH_2(C_6H_5)$	C_2H_5	26.13
ANION Ie	CH_3	$CH_2(C_6H_5)$	C_2H_5	21.16
ANION If	CH_3	CH_3	C_2H_5	7.90
ANION Ig	CH_3	CH_3	CH_3	18.81
ANION Ih	CH_3	CH_3	H	26.01

Figure 6. Difference between four- and six-membered activation free energies for a variety of allyl stabilized anion. The calculations are performed at the B3LYP/6-31+g(d)//B3LYP/6-31+g(d) level of theory. For Anions I, Ic, Id and Ie also two DME molecules and bulk solvent effects were included.

When substituting the bulky phosphonate group by a tertiary butyl group which is approximately as voluminous, the four-membered ring is still preferred by 26.13 kJ/mol (Anion Id). This indicates that the true nature of the four-membered ring formation preference is not related to the specific properties of the phosphonate group. Nevertheless, the phosphonate group plays a crucial role in the anion stability, allowing selective deprotonation of the substrates. Also Bossio et al. and Marcaccini et al. found preference for four-membered ring formation in the case where the anion was stabilized by a carbonyl group.[9,10] Even when substantially reducing the size of the X and Y substituent, four-membered rings are always preferentially formed. This indicates that the size of the X and Y group are not the primary cause for the largely hindered rotation about the C−N bond. The anion can exist in at least two conformers which are schematically shown in Figure 6 and which differ in the relative orientation of the groups 1 and 2 which are attached to the nitrogen−carbon bond. Our calculations point out that Conformer a, which is ready for six-membered ring formation, is highly unstable due to the large amount of energy needed to bring the groups 1 and 2 closer toward each other.

Furthermore, it was investigated whether the site selectivity seen in the reactive anion under study can further be rationalized by inspecting appropriate DFT-based reactivity indicators. Therefore, a variety of global and local indices, such as the global hardness (η), local softness ($s(\boldsymbol{r})$), and Fukui function ($f(\boldsymbol{r})$), were applied to the most stable conformer. For more explanation on their definitions we refer to the textbook of Parr and Yang[39] and a review by Geerlings et al.[57] The reactions studied here concern an ambident nucleophile, where the soft and hard centers are located in the same system. Moreover, the reactions are intramolecular SN_2 cyclization reactions, and the Fukui function for electrophilic attack ($\bar{f}(\boldsymbol{r})$) is believed to indicate the most favorable site. The condensed Fukui and

(57) Geerlings, P.; De Proft, F.; Langenaeker, W. *Chem. Rev.* **2003**, *103*, 1793.

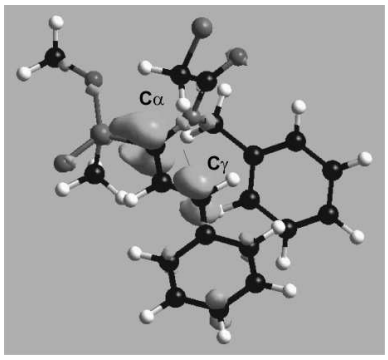

Figure 7. Iso-surfaces (value 0.005) of the Fukui function ($f^{-}(r)$) for electrophilic attack in the most stable conformer of the anion, which is the precursor for four-membered ring formation.

softness values calculated using the natural population analysis (NPA) and CHELPG scheme are given in Table S1 of the Supporting Information. The α-carbon atom is the softest center, whereas the γ-carbon atom is somewhat harder; thus, the condensed local indices indeed predict that cyclization preferentially occurs at the α-position. This can further be illustrated by visualizing $\bar{f}(\boldsymbol{r})$ of the reactive anion (Figure 7). The largest value for the Fukui function is indeed found at the α-carbon atom. The specific reaction is an example of a reaction which is frontier-orbital controlled, and the Fukui function is an appropriate indicator to describe the site selectivity.[58,59] The specific selectivity encountered here has been seen in various other systems such as HCHO, NCS, and malonaldehyde anion.[60]

In the anion trapping experiment with a proton, which is known to be very hard, the reaction may be expected to occur preferentially at the hardest center, which is the γ-carbon atom in our case. However, since the alkylation with methyl iodide which is a soft electrophile, also occurs at the γ-position, it can be concluded that the site-selectivity is primarily dictated by geometric constraints, whereas the frontier-orbital interactions are of minor importance.

Summarizing, the four-membered ring preference is due to a largely hindered internal rotation around the C−N bond of the 1-aminoalkenyl-phosphonate, which prevents the anion in reaching the conformer suitable for six-membered ring formation.

5. Conclusions

In this study a peculiar ring closure of functionalized aminophosphonates toward four-membered phosphono-β-lactams has been unraveled both on experimental and theoretical bases. Starting from an ambident allylic anion, no trace of six-membered lactams was found, and only the highly strained four-membered rings are formed through intramolecular alkylation. Nevertheless, new anion trapping experiments indicate that the

(58) Chattaraj, P. K. *J. Phys. Chem. A* **2001**, *105*, 511−513.
(59) Fukui, F. *Theory of Orientation and Stereoselection*; Springer-Verlag: Berlin, 1973; p 134; *Science* (Washington, D.C.) **1982**, *218*, 747.
(60) Pearson, R. G. *Chemical Hardness: Applications from Molecules to Solids*; Wiley-VCH Verlag GMBH: Weinheim, 1997.

γ-position is more reactive in intermolecular reactions. This was confirmed by the calculation of theoretical protonation energies, which ascribe the stabilization of this isomer to the presence of the phosphonate- and nitrogen-containing subgroup. However, it was found that the remarkable selectivity is typically associated with intramolecular reactions and was primarily due to a restricted rotation around the C−N bond of the 1-amino-alkenyl-phosphonate studied. Therefore, the transition state for six-membered ring formation is energetically disfavored. The typical SN_2-like transition state is geometrically strained for six-membered ring formation and consequently substantially (approximately 25 kJ/mol) more activated. The system of interest is challenging as it contains solvated sodium or lithium ions. However, the α/γ-selectivity is not notably influenced by accounting for solvent effects.

Acknowledgment. This work is supported by the Fund for Scientific Research-Flanders (FWO) and the Research Council of Ghent University.

Supporting Information Available: Complete ref 38, reactivity indices for the reactive anion, structural characterization of all compounds, Cartesian coordinates of all optimized reactants, transition structures. This material is available free of charge via the Internet at http://pubs.acs.org.

JA0584119

Paper XI

Spin-polarized conceptual DFT study of the regioselectivity in ring closures of radicals

Pintér B. , De Proft F. , Van Speybroeck V. ,
Hemelsoet K. , Waroquier M. , Chamorro E. ,
Veszprémi T. and Geerlings P.

J. Org. Chem., **2007**, 72, 348–356

JOC*Article*

Spin-Polarized Conceptual Density Functional Theory Study of the Regioselectivity in Ring Closures of Radicals

B. Pintér,[†,‡] F. De Proft,*[,‡] V. Van Speybroeck,[§] K. Hemelsoet,[§] M. Waroquier,[§] E. Chamorro,[||,‡] T. Veszprémi,[†] and P. Geerlings[‡]

Inorganic Chemistry Department, Budapest University of Technology and Economics (BUTE), Szent Gellért tér 4, 1521 Budapest, Hungary, Eenheid Algemene Chemie (ALGC), Faculteit Wetenschappen, Vrije Universiteit Brussel (VUB), Pleinlaan 2, 1050 Brussels, Belgium, Center For Molecular Modeling, Ghent University, Proeftuinstraat 86, 9000 Ghent, Belgium, and Departmento de Ciencias Químicas, Facultad de Ecología y Recursos Naturales, Universidad Andrés Bello, Avenida República 275, Santiago, Chile

fdeprof@vub.ac.be

Received July 5, 2006

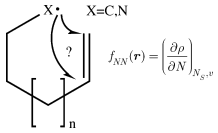

The regioselectivity of ring-forming radical reactions is investigated within the framework of the so-called spin-polarized conceptual density functional theory. Two different types of cyclizations were studied. First, a series of model reactions of alkyl- and acyl-substituted radicals were investigated. Next, attention was focused on the radical cascade cyclizations of *N*-alkenyl-2-aziridinylmethyl radicals (a three-step mechanism). In both of these reactions, the approaching radical (carbon or nitrogen centered) adds to a carbon−carbon double bond within the same molecule to form a radical ring compound. In this process, the number of electrons is changing from a local point of view (a charge transfer occurs from one part of the molecule to another one) at constant global spin number N_s (both the reactant and the product ring compound are in the doublet state). It is shown that the experimentally observed regioselectivities for these ring-closure steps can be predicted using the spin-polarized Fukui functions for radical attack, $f^0_{NN}(\mathbf{r})$.

Introduction

In 1976, Baldwin introduced a set of simple rules governing the regioselectivity of ring closures.[1] On the basis of the acceptor part of these molecules, containing the carbon atom at which the ring-closure reaction occurs, he divided these reactions into three main groups: the *tet*rahedral[2] systems, *tri*gonal systems, and *dia*gonal systems. On the other hand, for the donor part of the system, one can classify the reactions as nucleophilic, electrophilic, or radicalar intramolecular additions. In the past three decades, these rules have proven to be useful to predict the major outcome of ring-forming reactions.[3] However, numerous papers have stressed the limitations of and exceptions to these rules.[4] For radical cyclization processes, Beckwith at al.[5]

[†] Budapest University of Technology and Economics.
[‡] Vrije Universiteit Brussel.
[§] Ghent University.
[||] Universidad Andrés Bello.

(1) Baldwin, J. E. *J. Chem. Soc., Chem. Commun.* **1976**, 734.

(2) This is the prevalent nomenclature, describing the geometry of the acceptor atom, sp^3 center as *tet*- (tetrahedral), sp^2 center as *trig*- (trigonal), and sp center as *dig*- (digonal). Another nomenclature indicates where the displaced electrons end up: if the electron pair ends up outside, then this is denoted as *endo*-; if the electron pair ends up within (smaller ring formation), the terminology *exo* is used.

(3) For reviews, see: (a) Jasperse, C. J.; Curran, P. D.; Fevig, L. T. *Chem. Rev.* **1991**, *91*, 1237. (b) Kochi, J. K. *Free Radicals*, Wiley: New York, 1973. (c) Julia, M. *Pure Appl. Chem.* **1974**, *40*, 553. (d) Beckwith, A. L. J. *Tetrahedron* **1981**, *37*, 3073. (e) Hart, D. J. *Science* **1984**, *223*, 883. (f) Giese, B. *Radicals in Organic Synthesis: Formation of Carbon-Carbon Bonds*; Pergamon: New York, 1986. (g) Jung, M. E; Cho, M. Y.; Jung, H. Y. *Tetrahedron Lett.* **1996**, *37*, 3. (h) Ingold, K. U.; Beckwith, A. L. J. Free-Radical Rearrangements. In *Rearrangements in Ground and Excited States*; de Mayo, P., Ed.; Academic Press: New York, NY, 1980; Vol. 1, p 161.

(4) (a) Wilt, W. J. *Tetrahedron* **1985**, *41*, 3979. (b) Curran, D. P.; Chang, C. T. *J. Org. Chem.* **1989**, *54*, 3140. (c) Struble, D. L.; Beckwith A. L. J.; Gream, G. E. *Aust. J. Chem.* **1972**, *25*, 1081.

10.1021/jo0613885 CCC: $37.00
Published on Web 12/21/2006

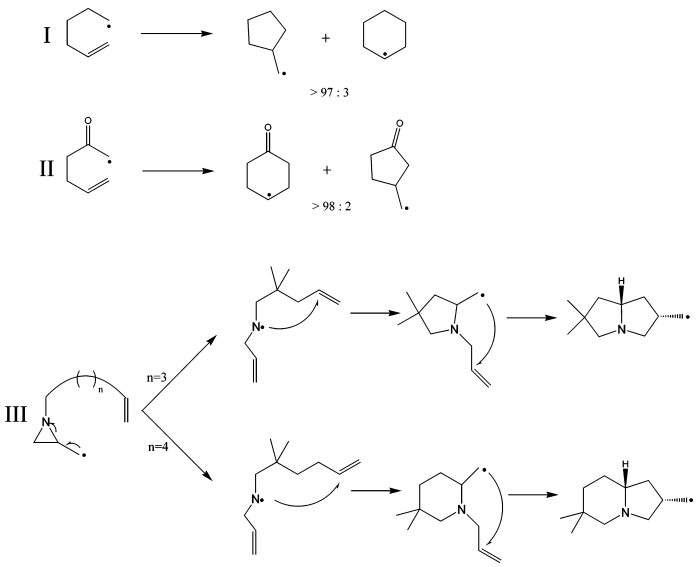

FIGURE 1. Different cyclization reactions involving radicals: (I) cyclization of hexenyl radicals, (II) cyclization of acyl-substituted hexenyl radicals, and (III) cascade radical reactions.

constructed some practical guidelines considering the influence of steric and electronic factors on the regioselectivity; they stated that the reaction occurs preferentially in the *exo* mode, that substituents on the double bond have an unfavorable effect, that adjacent semioccupied orbitals, filled nonbonding or orbitals containing lone pairs favor the homolytic cleavage, and that the stereochemical outcome of the reaction depends on the substituents at different position. A series of other contributions have investigated the aspects of regioselectivity of these reactions. Houk and co-workers[6] expanded the MM2 force field[7] to describe the rate of product formation in the cyclization of alkyl- and aryl-substituted radicals. The MM2 force field with fixed transition state parameters was also used to describe the regioselectivity.[8] The 6-*endo* versus 5-*exo* modes of the *dig* process (i.e., the cyclization of hexenyl and related radicals) has attracted considerable attention.[9,10] Generally, 5-hexenyl radicals cyclize with high regioselectivity to give five-membered rings rather than six-membered rings (Figure 1, reaction I).[11] Such cyclizations are usually kinetically controlled.[12,5] The overwhelming preference for 5-*exo* ring closure over the 6-*endo* cyclization is a consequence of the interplay of three main factors, the stereoelectronic,[13] polar,[14] and steric effects.[14] All three effects favor the five-membered ring formation, i.e., the thermodynamically less stable products. Note that these cyclizations need to follow the Bürgi−Dunitz trajectory,[15] which suggests that a nucleophile will approach the C═C double bond at roughly the tetrahedral angle (rather than perpendicular). This was supported by theoretical investigations of transition structures for radical additions to unsaturated systems, where it was established that angles of attack of the reagents are close to tetrahedral.[16] Considering the reaction path of an intramolecular radical "ene" addition, two different transition states, chair-like and boat-like, were found in both (*exo* and *endo*) processes.[17] The formation of these transition states is the first step of two different processes that finally produce two regiochemically different products. It is generally accepted that the chair-like

(5) Beckwith, A. L. J.; Easton, C. J.; Serelis, A. K. *J. Chem. Soc., Chem. Commun.* **1980**, 482.
(6) (a) Spellmeyer, D. C.; Houk, K. N. *J. Org. Chem.* **1987**, *52*, 959. (b) Broeker, J. L.; Houk, K. N. *J. Org. Chem.* **1991**, *56*, 3651.
(7) Allinger, N. A. *J. Am. Chem. Soc.* **1977**, *99*, 8127.
(8) (a) Beckwith, A. L. J.; Schiesser, C. H. *Tetrahedron* **1985**, *41*, 3925. (b) Beckwith, A. L. J.; Schiesser, C. H. *Tetrahedron Lett.* **1985**, *26*, 373.
(9) (a) Bennasar, M.-L.; Juan, C.; Bosch, J. *Chem. Commun.* **2000**, 2459. (b) Ellis, D. A.; Hart, D. J.; Zhao, L. *Tetrahedron Lett.* **2000**, *41*, 9357. (c) Snider, B. B.; Buckman, B. O. *J. Org. Chem.* **1992**, *57*, 4883.
(10) Haney, B. P.; Curran, D. P. *J. Org. Chem.* **2000**, *65*, 2007.
(11) Walling, C.; Cioffari, A. *J. Am. Chem. Soc.* **1972**, *94*, 6059.
(12) Turro, N. J. *Modern Molecular Photochemistry*; University Press: Menlo Park, 1978.
(13) Kirby, A. J. *Stereoelectronic Effects*; University Press: Oxford, 1996.
(14) Denisov, E.T.; Denisova, T. G.; Pokidova, T. S. *Handbook of Free Radical Initiators*; Wiley-Interscience: New York, 2003.
(15) (a) Bürgi, H. B.; Dunitz, J. D.; Lehn, J. M.; Wipff, G. *Tetrahedron* **1974**, *30*, 1563. (b) Bürgi, H. B.; Dunitz, J. D. *Acc. Chem. Res.* **1983**, *16*, 153.
(16) Houk, K. N.; Paddon-Row R. N.; Spellmeyer, D. C.; Rondan, N. G.; Nagase S. *J. Org. Chem.* **1986**, *51*, 2874.
(17) Leach, A. G.; Wang, R.; Wohlhieter, G. E.; Khan, S. I.; Jung, M. E.; Houk, K. N. *J. Am. Chem. Soc.* **2003**, *125*, 4271.

SCHEME 1. Different Radical Cyclizations Investigated

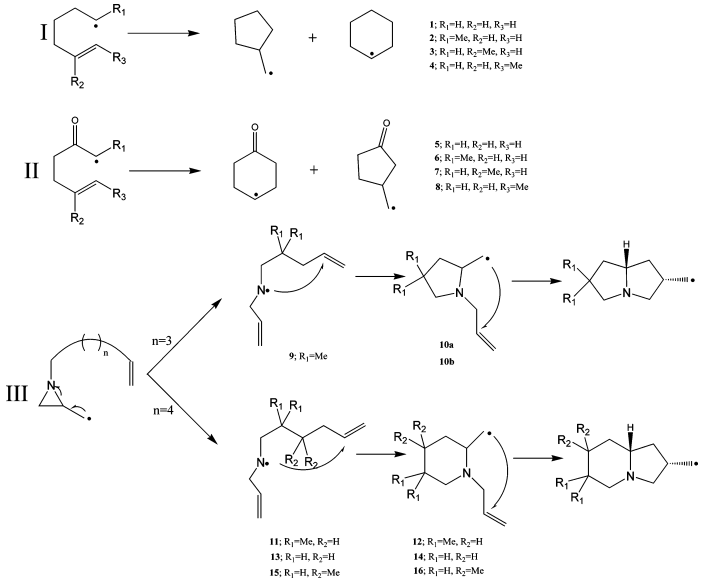

orientation of the transition state is more stable than the boat-like (also suggested by Beckwith), and the former clearly suggests a preferable interaction between the reacting centers in the transition state, i.e., more favorable overlap between the π-orbital of the ene part and the SOMO (where the radical is localized).[18,4c] In contrast, for the 5-*exo* pathways of acyl-substituted radicals, the boat-like conformation of TS has the lowest energy. These systems are also in contrast with the prediction of Baldwin's rules and undergo a 6-*endo*[19] ring-forming process (Figure 1, reaction II) via a chair-like transition state.

At this point it is also worthwhile to mention that the analogous ring closure of the prototypical 1,3-hexadiene-5-yn-1-yl radical, which gives the phenyl radical in a regioselective manner,[20] occurs in a multistep mechanism.[21] Theoretical work showed that the latter process occurs in the 5-*exo* mode (contrary to common belief) followed by two additional steps (rearrangement via cyclization and ring-opening steps) resulting in the formation of the phenyl radical.[21] For the cyclization of 1-vinyl-5-methyl-5-hexenyl radicals[22] Gomez, Lopez and co-workers demonstrated that the "direct" 6-*endo-trig* ring closure is an effective competing reaction[23] among the rapid rearrangement of the methylenecyclopentyl radical via a reversible 3-*exo-trig* cyclization following the 5-*exo* attack, which was supposed by Beckwith and O'Shea.[24] For competitive 5-*exo-dig* and 6-*endo-dig* cyclizations of vinyl and aryl radicals,[25] no rearrangement-type reactions were reported, and the trends in the activation barriers indicate a strong stereoelectronic preference for the 5-*exo-dig* cyclizations. This is fully consistent with the shorter incipient $C_1 \cdots C_{exo}$ distances in the starting materials and with the smaller deformation needed to form the new bonds via transition state.[26]

From a stereochemical point of view one of the guidelines of Beckwith states that "1- or 3-substituted systems afford mainly *cis*-disubstituted products, whereas 2- or 4-substituted systems give mainly *trans*-products."[5] Experimental studies have shown that the chair-like transition state conformation is energetically unfavorable with bulky substituents, as it would force the bulky phenyl group into an axial position. The unexpected stereochemistry can be rationalized if one assumes a boat-like transition state for the cyclization.[27]

(18) (a) Struble, D. L.; Beckwith, A. L. J.; Gream, G. E. *Tetrahedron Lett.* **1968**, 3701. (b) Beckwith, A. L. J. *Essays on Free Radical Chemistry*; Special Publication 24; Chemical Society: London, 1970; p 239.
(19) Clive, D. L. J.; Cheshire, D. R. *J. Chem. Soc., Chem. Commun.* **1987**, 1520.
(20) Walch, S. P. *J. Chem. Phys.* **1995**, *103*, 8544.
(21) Olivella, S.; Sole, A. *J. Am. Chem. Soc.* **2000**, *122*, 11416.
(22) Stork, G.; Baine, N. H. *J. Am. Chem. Soc.* **1982**, *104*, 2321.
(23) Gómez, A.M.; Company, M. D.; Uriel, C.; Valverde, S.; López, J. C. *Tetrahedron Lett.* **2002**, *43*, 4997.
(24) (a) Beckwith, A. L. J.; O'Shea, D. M. *Tetrahedron Lett.* **1986**, *27*, 4525. (b) Crich, D.; Fortt, S. M. *Tetrahedron Lett.* **1987**, *28*, 2895.
(25) (a) König, B.; Pitsch, W.; Klein, M.; Vasold, R.; Prall, M. Schreiner, P. R. *J. Org. Chem.* **2001**, *66*, 1742. (b) Kovalenko, S. V.; Peabody, S.; Manoharan, M.; Clark, R. J.; Alabugin, I. V. *Org. Lett.* **2004**, *6*, 2457.
(26) Alabugin, I. V.; Manoharan, M. *J. Am. Chem. Soc.* **2005**, *127*, 12583.

The kinetics and mechanism of the analogous reactions of nitrogen-centered radicals are not well established.[28] Previously, some of the present authors have examined the cascade cyclizations of *N*-alkenyl-2-aziridinylmethyl radicals[29] (Figure 1, reaction III) using density functional theory (DFT) calculations. In this contribution, they reviewed the details of three-membered ring-opening processes, primarily the β-cleavage of aziridinyl radicals, and the above-mentioned unclarified treatment of cyclization of nitrogen-centered radicals.

In the present contribution, the regioselectivity of two distinct types of radical cyclization reactions (both alkyl- and acyl-substituted radical cyclizations ("simple"[3a,30]) and the above-mentioned cascade reactions, depicted in Figure 1) will be investigated using reactivity indices introduced within the framework of spin-polarized DFT. It will be shown that the regioselectivities estimated using this approach are in good agreement with the experimental results. The different nitrogen- and carbon-centered radicals investigated in this work are depicted in Scheme 1. Radicals **9**, **11**, **13**, and **15** are the intermediates of the second step, whereas **10**, **12**, **14**, and **16** correspond to the intermediates of the third step of the cascade reactions. Radicals **1**−**4** and **5**−**8** are the alkyl- and acyl-substituted model systems, respectively, and **10a** and **10b** are the *trans* and *cis* conformers of radical **10**, respectively. We briefly discuss the effect of the orientation of the attacking radical relative to the double bond on the regioselectivity prediction. We also discuss why the non-spin-polarized Fukui functions seem to be inefficient for these systems and why, on the other hand, the spin-polarized indices give the correct regioselectivity.

Theory and Computational Details

Density functional theory provides a very convenient framework for the discussion of chemical reactivity. A series of global and local quantities, the so-called reactivity descriptors or indices, have been introduced to describe the extent of the response of a molecular system toward perturbations in either its number of electrons, N, its external (i.e., due to the nuclei) potential, $v(\underline{r})$, or both.[31] An important example of these reactivity indices is the Fukui function, introduced by Parr and Yang,[32] defined as the response of the system's electron density $\rho(\underline{r})$ due to a perturbation in its total number of electrons N at a constant external potential $v(\underline{r})$. Due to the discontinuity of the electron density with respect to the number of electrons, three different Fukui functions can be introduced, representing the case of a nucleophilic $f^+(\underline{r})$, electrophilic $f^-(\underline{r})$, and a neutral (radical) attack $f^0(\underline{r})$:

$$f^+(\underline{r}) = (\partial\rho(\underline{r})/\partial N)^+_{v(\underline{r})} \approx \rho_{N+1}(\underline{r}) - \rho_N(\underline{r}) \quad (1)$$

$$f^-(\underline{r}) = (\partial\rho(\underline{r})/\partial N)^-_{v(\underline{r})} \approx \rho_N(\underline{r}) - \rho_{N-1}(\underline{r}) \quad (2)$$

$$f^0(\underline{r}) = \frac{1}{2}(f^+ + f^-) \approx \frac{1}{2}(\rho_{N+1}(\underline{r}) - \rho_{N-1}(\underline{r})) \quad (3)$$

where $\rho_{N+1}(\underline{r})$, $\rho_N(\underline{r})$, and $\rho_{N-1}(\underline{r})$ are the electron densities of the $N+1$, N, and $N-1$ electron system, respectively, all obtained at the geometry of the N electron system, due to the fact that the derivative is taken at a constant external potential. However, in chemistry it is customary to work with properties associated with atoms and functional groups in the molecule. In this context, a useful approximation to describe the site reactivity is given by the condensed-to-atom Fukui indices by using an atomic charge partitioning scheme:[33]

$$f_k^+ \approx N_k(N+1) - N_k(N) \quad (4)$$

$$f_k^- \approx N_k(N) - N_k(N-1) \quad (5)$$

$$f_k^0 \approx \frac{1}{2}(N_k(N+1) - N_k(N-1)) \quad (6)$$

where $N_k(N+1)$, $N_k(N)$, and $N_k(N-1)$ represent the electron populations on atom k in the $N+1$, N, and $N-1$ electron system.

Another related quantity is the local softness,[34,35] $s(\underline{r})$:

$$s(\underline{r}) = (\partial\rho(\underline{r})/\partial\mu)_{v(\underline{r})} = (\partial\rho(\underline{r})/\partial N)_{v(\underline{r})}(\partial N/\partial\mu)_{v(\underline{r})} = Sf(\underline{r}) \quad (7)$$

where S is the global softness, which can be computed using the vertical ionization energy (IE) and electron affinity (EA) of the system:[34]

$$S \approx 1/(\mathrm{IE} - \mathrm{EA}) \quad (8)$$

One can interpret the reaction ability toward soft reagents of the different parts of the molecules with the condensed form of the local softness, written as

$$s_k^i = Sf_k^i \quad (9)$$

where i equals either $+$, $-$, or 0 depending on whether the system undergoes a nucleophilic, electrophilic, or radical attack. In addition to the Fukui function, this quantity permits comparison of the reactivity of different sites in different molecules and is thus preferred to study intermolecular reactivity.

When using these indices to describe the molecular site selectivity, one usually works within the framework of the hard and soft acids and bases (HSAB) principle[36] for which theoretical justifications have been provided in recent years.[36c−e] One can also adopt

(27) (a) RajanBabu, T. V.; Fukunaga, T. *J. Am. Chem. Soc.* **1989**, *111*, 296. (b) RajanBabu, T. V. *J. Am. Chem. Soc.* **1987**, *109*, 609. (c) RajanBabu, T. V. *J. Org. Chem.* **1988**, *53*, 4522. (d) RajanBabu, T. V.; Fukunaga, T.; Reddy G. S. *J. Am. Chem. Soc.* **1989**, *111*, 1759.

(28) For reviews, see: (a) Fallis, G. A.; Brinza, M. I. *Tetrahedron* **1997**, *53*, 17543. (b) Newcomb, M.; Musa, O. M.; Martinez, F. N.; Horner, J. H. *J. Am. Chem. Soc.* **1997**, *119*, 4569. (c) Newcomb, M.; Burchill T. M.; Deeb M. T. *J. Am. Chem. Soc.* **1988**, *110*, 6528. (d) Maxwell, B. J.; Tsanaktsidis, J. *J. Am. Chem. Soc.* **1996**, *118*, 4276. (e) Bowman, R. W.; Stephenson, T. P.; Young, R. A. *Tetrahedron* **1996**, *52*, 11445

(29) Van Speybroeck, V.; De Kimpe, N.; Waroquier, M. *J. Org. Chem.* **2005**, *70*, 3674.

(30) (a) Giese, B. *Radicals in Organic Synthesis: Formation of Carbon-Carbon Bonds*; Pergamon: Oxford, 1986. (b) Curran, D. P. *Synthesis* **1988**, 417. (c) Melikyan, G. G. *Synthesis* **1993**, 833. (d) Iqbal, J.; Bhatia, B.; Nayyar, N. K. *Chem. Rev.* **1994**, *94*, 519. (e) Snider, B. B. *Chem. Rev.* **1996**, *96*, 339. (f) Curran, D. P.; Porter, N. A.; Giese, B. *Stereochemistry of Radical Reactions*; VCH: Weinheim, 1996.

(31) (a) Parr, R. G.; Yang, W. *Density Functional Theory of Atoms and Molecules*; Oxford University Press: New York, 1989. (b) Parr, R. G.; Yang, W. *Ann. Rev. Phys. Chem.* **1995**, *46*, 701. (c) Kohn, W.; Becke, A. D.; Parr, R. G. *J. Phys. Chem.* **1996**, *100*, 12974. (d) Chermette, H. *J. Comp. Chem.* **1999**, *20*, 129. (e) Geerlings, P.; De Proft, F.; Langenaeker, W. *Adv. Quant. Chem.* **1999**, *33*, 303. (f) Geerlings, P.; De Proft, F.; Langenaeker, W. *Chem. Rev.* **2003**, *103*, 1793.

(32) Parr, R. G.; Yang, W. *J. Am. Chem. Soc.* **1984**, *106*, 4049.

(33) Yang, W.; Mortier, W. J. *J. Am. Chem. Soc.* **1986**, *106*, 5708.

(34) Yang, W.; Parr, R. G. *Proc. Natl. Acad. Sci. U.S.A.* **1985**, *82*, 6723.

(35) Lee, C.; Yang, W.; Parr, R. G. *J. Mol. Struct.* (*Theochem*) **1988**, *163*, 305.

(36) (a) Pearson, R. G. *J. Am. Chem. Soc.* **1963**, *85*, 3533. (b) Pearson, R. G. *Science* **1966**, *151*, 172. (c) Chattaraj, P. K.; Lee, H.; Parr, R. G. *J. Am. Chem. Soc.* **1991**, *113*, 1855. (c) Ayers, P. W. *J. Chem. Phys.* **2005**, *122*, 141102. (d) Chattaraj, P. K.; Ayers, P. W. *J. Chem. Phys.* **2005**, *123*, 086101. (e) Ayers, P. W.; Parr, R. G.; Pearson, R. G. *J. Chem. Phys.* **2006**, *124*, 194107.

a local version of this principle,[37] as will be discussed later on in this contribution.

For the title reactions, it is natural to explore the condensed-to-atoms electronic Fukui functions within the framework of spin-polarized DFT,[38] since in addition to the above-mentioned indices, these explicitly consider responses of the systems to changes in the spin number N_s (i.e., the difference between the number of α and β electrons).[40]

In this approach, four types of "spin-polarized" Fukui functions can be written as

$$f_{NN}(\underline{r}) \equiv \left[\frac{\delta\mu_N}{\delta v(\underline{r})}\right]_{N,N_s,B(\underline{r})} = \left[\frac{\delta\rho(\underline{r})}{\partial N}\right]_{N_s,v(\underline{r}),B(\underline{r})} \tag{10}$$

$$f_{SN}(\underline{r}) \equiv -\frac{1}{\mu_B}\left[\frac{\delta\mu_N}{\delta B(\underline{r})}\right]_{N,N_s,B(\underline{r})} = \left[\frac{\delta\rho_S(\underline{r})}{\partial N}\right]_{N_s,v(\underline{r}),B(\underline{r})} \tag{11}$$

$$f_{NS}(\underline{r}) \equiv \left[\frac{\delta\mu_S}{\delta v(\underline{r})}\right]_{N,N_s,v(\underline{r})} = \left[\frac{\delta\rho(\underline{r})}{\partial N_s}\right]_{N,v(\underline{r}),B(\underline{r})} \tag{12}$$

$$f_{SS}(\underline{r}) \equiv -\frac{1}{\mu_B}\left[\frac{\delta\mu_S}{\delta B(\underline{r})}\right]_{N,N_s,v(\underline{r})} = \left[\frac{\delta\rho_S(\underline{r})}{\partial N_s}\right]_{N,v(\underline{r}),B(\underline{r})} \tag{13}$$

In these equations, $B(\underline{r})$ is the external magnetic field, μ_B is the Bohr magneton,

$$\mu_N = \left(\frac{\partial E}{\partial N}\right)_{N_s,v(\underline{r}),B(\underline{r})} \text{ and } \mu_S = \left(\frac{\partial E}{\partial N_s}\right)_{N,v(\underline{r}),B(\underline{r})} \tag{14}$$

are the chemical and spin potentials, and

$$\rho(\underline{r}) = \rho^{\uparrow}(\underline{r}) + \rho^{\downarrow}(\underline{r}) \text{ and } \rho_S(\underline{r}) = \rho^{\uparrow}(\underline{r}) - \rho(\underline{r})^{\downarrow} \tag{15}$$

are the electron and spin densities, respectively. μ_N is associated with the energy change upon electron-transfer processes at constant multiplicity, whereas μ_S measures the energetic cost for the system to change its spin number, i.e., to undergo a spin polarization at a constant number of electrons.

One of the aims of this paper is the application of the latter "spin-polarized" Fukui function describing the chemical reactivity for a process at constant spin number N_s, i.e., f_{NN}, to systems undergoing intramolecular radical addition reactions.

Within a frozen orbital approximation, the spin Fukui functions can be computed using the HOMO and LUMO shape factors, proposed by Galvan et al.:[39a]

$$f^{-}_{NN,k} = \frac{1}{2}[\sigma_k^{\mathrm{HOMO},\uparrow} + \sigma_k^{\mathrm{HOMO},\downarrow}] \tag{16}$$

$$f^{+}_{NN,k} = \frac{1}{2}[\sigma_k^{\mathrm{LUMO},\uparrow} + \sigma_k^{\mathrm{LUMO},\downarrow}] \tag{17}$$

In ref 39j, a comparison between the frozen orbital approximation and the finite difference approximation was presented, showing that similar results for both methods are obtained when occupied orbitals are involved. Very recently, both approximations were studied for a set of carbene and related systems and were found to give similar results.[40] As such, the FOA can be considered to be a viable approach for the present set of molecules.

The spin-polarized Fukui function for a radical attack is the average of these two functions:

$$f^{0}_{NN,k} = \frac{1}{2}[f^{+}_{NN,k} + f^{-}_{NN,k}] \tag{18}$$

To calculate the shape factors via molecular spin orbital approximation, different partitioning schemes have been introduced.[41] For instance, summing the basis-set components corresponding to atom k:

$$\sigma_k^{\mathrm{HOMO},\uparrow} = \frac{1}{n_{\mathrm{deg,HOMO},\uparrow}} \sum_{g_{\mathrm{HOMO},\uparrow}}^{n_{\mathrm{deg,HOMO},\uparrow}} \sum_{\mu\in k} \sum_{\nu} c_{\mu,g_{\mathrm{HOMO},\uparrow}} c_{\nu,g_{\mathrm{HOMO},\uparrow}} S_{\mu\nu} \tag{19}$$

$$\sigma_k^{\mathrm{HOMO},\downarrow} = \frac{1}{n_{\mathrm{deg,HOMO},\downarrow}} \sum_{g_{\mathrm{HOMO},\downarrow}}^{n_{\mathrm{deg,HOMO},\downarrow}} \sum_{\mu\in k} \sum_{\nu} c_{\mu,g_{\mathrm{HOMO},\downarrow}} c_{\nu,g_{\mathrm{HOMO},\downarrow}} S_{\mu\nu} \tag{20}$$

$$\sigma_k^{\mathrm{LUMO},\uparrow} = \frac{1}{n_{\mathrm{deg,LUMO},\uparrow}} \sum_{g_{\mathrm{LUMO},\uparrow}}^{n_{\mathrm{deg,LUMO},\uparrow}} \sum_{\mu\in k} \sum_{\nu} c_{\mu,g_{\mathrm{LUMO},\uparrow}} c_{\nu,g_{\mathrm{LUMO},\uparrow}} S_{\mu\nu} \tag{21}$$

$$\sigma_k^{\mathrm{LUMO},\uparrow} = \frac{1}{n_{\mathrm{deg,LUMO},\downarrow}} \sum_{g_{\mathrm{LUMO},\downarrow}}^{n_{\mathrm{deg,LUMO},\downarrow}} \sum_{\mu\in k} \sum_{\nu} c_{\mu,g_{\mathrm{LUMO},\downarrow}} c_{\nu,g_{\mathrm{LUMO},\downarrow}} S_{\mu\nu} \tag{22}$$

where σ_k represents the shape factors of corresponding molecular orbitals, $c_{\mu,g}$ are the molecular orbital coeficients, $n_{\mathrm{deg,mo}}$ is the number of degenerate frontier orbitals of the given specified spin state (i.e., a crude average for possible effects due to the presence of degenerate molecular frontier spin orbitals).

These expressions constitute condensed-to-atom k Fukui responses where condensation is achieved by summing overall the basis-set components centered at the kth atom of interest and that the overlap integral $S_{\mu\nu}$ is performed over entire three-dimensional molecular space.[42] This partitioning scheme has also been found particularly useful to compute condensed values of DFT-based reactivity indices.[42,43] Note that these equations are obtained by applying a Mulliken type of approach; a revival of interest for Mulliken type of projection operators exists recently.[44]

(37) (a) Gázquez, J. L. In *Chemical Hardness: Structure and Bonding*; Sen, K. D., Ed.; Springer-Verlag: New York, 1993; Vol. 80, p 27. (b) Méndez, F.; Gázquez, J. L. *J. Am. Chem. Soc.* **1994**, *116*, 9298. (c) Gázquez, J. L.; Méndez, F. *J. Phys. Chem.* **1994**, *98*, 4591. (d) Méndez, F.; Gázquez, J. L. *Proc. Indian Acad. Sci.* **1994**, *106*, 183. (e) Li, Y.; Evans, J. N. S. *J. Am. Chem. Soc.* **1995**, *117*, 7756. (f) Damoun, S.; Van de Woude, G.; Méndez, F.; Geerlings, P. *J. Phys. Chem. A* **1997**, *101*, 886. (g) Geerlings, P.; De Proft, F. *Int. J. Quantum Chem.* **2000**, *80*, 227.

(38) (a) Von Bart, U; Hedin, L. *J. Phys. C* **1972**, *5*, 1629. (b) Rajagopal, A. K.; Callaway, J. *Phys. Rev. B* **1973**, *7*, 1912. (c) Gunnarson, O.; Lundqvist, B. I. *Phys. Rev. B* **1976**, *13*, 4274.

(39) (a) Galván, M.; Vela, A.; Gázquez, J. L. *J. Phys. Chem.* **1988**, *92*, 6470. (b) Galván, M.; Vargas, R. *J. Phys. Chem.* **1992**, *96*, 1625. (c) Vargas, R.; Galván, M. *J. Phys. Chem.* **1996**, *100*, 14651. (d) Vargas, R.; Galván, M.; Vela, A. *J. Phys. Chem. A* **1998**, *102*, 3134. (e) Vargas, R.; Cedillo, A.; Garza, J.; Galván, M. In *Reviews of Modern Quantum Chemistry: A Celebration to The Contributions of Robert G. Parr*; Sen, K. D., Ed.; World Scientific: Singapore, 2002; p 936. (f) Galvan, M.; Vela, A.; Gazquez, J. L. *J. Phys. Chem.* **1988**, *92*, 6470. (g) Chamorro, E.; De Proft, F.; Geerlings, P. *J. Chem. Phys.* **2005**, *123*, 154104. (h) Chamorro, E.; Perez, P.; De Proft, F.; Geerlings, P. *J. Chem. Phys.* **2006**, *124*, 314602. (i) Garza, J.; Vargas, R.; Cedillo, A.; Galván, M.; Chattaraj, P. K. *Theor. Chem. Acc.* **2006**, *115*, 257.

(40) Chamorro, E.; Santos, J. C.; Escobar, C. A.; Perez, P. *Chem. Phys. Lett.* **2006**, *431*, 210.

(41) (a) Hirshfeld, F. L. *Theor. Chim. Acta* **1977**, *44*, 129. (b) Contreras, R. R.; Fuentealba, P.; Galvan, M.; Perez, P. *Chem. Phys. Lett.* **1999**, *304*, 405.

(42) Chamorro, E.; Pérez P. *J. Chem. Phys.* **2005**, *123*, 114107.

(43) Bulat, F. A.; Chamorro, E.; Fuentealba, P.; Toro-Labbe, A. *J. Phys. Chem. A* **2004**, *108*, 342.

(44) (a) Mayer, I. *Chem. Phys. Lett.* **2003**, *382*, 265. (b) Carbó-Dorca, R.; Bultinck, P. *J. Math. Chem.* **2004**, *36*, 231 (c) Vyboishchikov, S. F.; Salvador, P.; Duran, M. *J. Chem. Phys.* **2005**, *122*, 244110.

TABLE 1. Relative Energies and Free Energies of the Different Conformers of a Series of Simple Alkyl- and acyl-substituted Model Systems[a]

		B3LYP/6-311++g(d,p)		MP2/6-311++g(d,p)	
reaction	structure	ΔE	ΔG	ΔE	ΔG
I	**1a**	6.24	5.95	2.20	3.43
	1b	1.65	1.89	0.00	0.00
	1c	0.35	0.00	0.42	1.17
	1d	6.80	7.63	2.06	2.88
	1e	0.00	0.46	0.63	1.20
II	**5a**	1.15	2.93	0.00	0.00
	5b	5.94	7.26	1.00	2.55
	5c	0.00	0.00	0.55	0.51
	5d	2.81	2.31	0.45	1.27

[a] At the (U)B3LYP/6-311++g (d,p) and (U)MP2/6-311++g (d,p) levels. For the numbering of the different conformers, see Figures 2 and 3. All values are in kcal/mol.

Note from eqs 10−13 that $f_{NN}(\underline{r})$ is the equivalent of the Fukui function in the non-spin-polarized case but with the additional restriction that the spin number N_s should also remain constant. It is thus more suited to describe charge-transfer processes without a change in the total spin multiplicity of the system. Hence, it measures the initial response in the reorganization of the charge density upon removing (f^{-}_{NN}) or adding (f^{+}_{NN}) exactly the same fraction of the number of electrons to the spin-up and spin-down frontier molecular orbitals. For the description of a radical attack, one uses the average of f^{-}_{NN} and f^{+}_{NN}.

All calculations were performed using the Gaussian03[45] software package. For the intermediates of the cascade reactions, i.e., for radicals **9**−**16**, we used the (U)B3LYP/6-311G(d,p) level (see ref 30), whereas radicals **1**−**8** were optimized at the (U)B3LYP/6-311++G(d,p) level[46] of theory. In these cases a frequency analysis was performed, and all structures were verified as minima on the potential energy surface. For radicalar systems, one could expect a less optimal performance of DFT-based calculation methods.[47] In order to confirm the level of theory, the different conformations of reactants of simplest cyclizations (**1** and **5**) were optimized at (U)-MP2/6-311++g(d,p). As can be seen from Table 1, the relative energies change within a few kcal/mol, the difference between geometries calculated with both methods being negligible.

Natural population analysis (NPA)[48] charges were obtained on all radicals with the NBO program in Gaussian03 at the B3LYP/6-311++G(d,p) level,[49] in order to compute the condensed Fukui functions. Although the differences in the optimized geometries for these systems are negligible as far as the inclusion of diffuse functions in the basis set is concerned, their inclusion is important in the computation of the Fukui functions, as this involves the calculation of a stable radical anion. CASSCF(3,3)/6-311++G//(U)MP2/6-311++g(d,p) and CASSCF(5,5)/6-311++G//(U)MP2/6-311++g(d,p) calculations were carried out for **1a** and **5d**, respectively, to make sure that these systems can be described by a single determinant; the weights of the ground state configuration are 0.975 and 0.96 for **1a** and **5d**, respectively, confirming the assumed single-reference character of these species. The spin-polarized Fukui functions f_{NN} were computed using approximations (eqs 16 and 17); to calculate the $S_{\mu\nu}$ values simple modifications to the 1601.F routine of Gaussian have been introduced.[41b] According to the results of CASSCF calculations, the required population analysis can be performed with confidence.

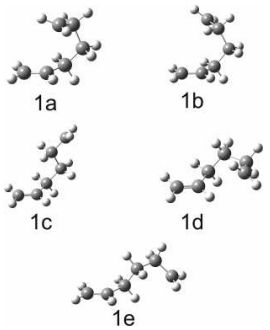

FIGURE 2. Different conformers of **1** for the doublet ground state at the (U)B3LYP/6-311++g (d,p) level.

Results and Discussion

In the first part, we have investigated the importance of the orientation of the attacking radical relative to the double bond, considering the cases of both a single cyclization and a domino reaction.

We will first discuss the results for the single cyclization. The reactants in different conformations were identified for the two simplest model systems (**1** and **5**) shown in Figures 2 and 3.

In Figure 2, the five investigated orientations of the alkyl toward the double bond (which can be found after applying two internal rotations) for the additions of alkyl-substituted radicals are depicted: **a**, **b**, and **c** correspond to conformers generated by rotating around the C_2-C_3 bond (see Scheme 2) in the most curved chain, while **d** and **e** correspond to one of the "near-attack" orientations and the linear conformer, respectively.

As expected, the most stable conformer of **1** is the linear conformer (see Table 1 for the relative energies and relative free energies) at the B3LYP level; at the MP2 level, conformer **b** is the more more stable one, the difference with the linear conformer is only 0.63 kcal/mol. For the two near-attack conformations (**a** and **d**) , the Bürgi−Dunitz angles and

(45) Frisch, M. J.; Trucks, G. W.; Schlegel, H. B.; Scuseria, G. E.; Robb, M. A.; Cheeseman, J. R.; Montgomery, J. A., Jr.; Vreven, T.; Kudin, K. N.; Burant, J. C.; Millam, J. M.; Iyengar, S. S.; Tomasi, J.; Barone, V.; Mennucci, B.; Cossi, M.; Scalmani, G.; Rega, N.; Petersson, G. A.; Nakatsuji, H.; Hada, M.; Ehara, M.; Toyota, K.; Fukuda, R.; Hasegawa, J.; Ishida, M.; Nakajima, T.; Honda, Y.; Kitao, O.; Nakai, H.; Klene, M.; Li, X.; Knox, J. E.; Hratchian, H. P.; Cross, J. B.; Bakken, V.; Adamo, C.; Jaramillo, J.; Gomperts, R.; Stratmann, R. E.; Yazyev, O.; Austin, A. J.; Cammi, R.; Pomelli, C.; Ochterski, J. W.; Ayala, P. Y.; Morokuma, K.; Voth, G. A.; Salvador, P.; Dannenberg, J. J.; Zakrzewski, V. G.; Dapprich, S.; Daniels, A. D.; Strain, M. C.; Farkas, O.; Malick, D. K.; Rabuck, A. D.; Raghavachari, K.; Foresman, J. B.; Ortiz, J. V.; Cui, Q.; Baboul, A. G.; Clifford, S.; Cioslowski, J.; Stefanov, B. B.; Liu, G.; Liashenko, A.; Piskorz, P.; Komaromi, I.; Martin, R. L.; Fox, D. J.; Keith, T.; Al-Laham, M. A.; Peng, C. Y.; Nanayakkara, A.; Challacombe, M.; Gill, P. M. W.; Johnson, B.; Chen, W.; Wong, M. W.; Gonzalez, C.; Pople, J. A. *Gaussian 03*, Revision C.02; Gaussian, Inc.: Wallingford, CT, 2004.

(46) For a detailed account on these types of basis sets, see, for example: Hehre, W. J.; Radom, L.; Schleyer P. v. R.; Pople, J. A. **1986** *Ab initio Molecular Orbital Theory*; Wiley: New York, 1986.

(47) (a) Zhang, Y.; Yang, W. *J. Chem. Phys.* **1998**, *109*, 2604. (b) Gritsenko, O. V.; Ensing, B.; Schipper, P. R. T.; Baerends, E. J. *J. Phys. Chem. A* **2000**, *104*, 8558.

(48) (a) Reed, A. E.; Weinstock, R. B.; Weinhold, F. *J. Chem. Phys.* **1985**, *83*, 735. (b) Reed, A. E.; Weinhold, F. *J. Chem. Phys.* **1985**, *83*, 1736. (c) Reed, A. E.; Curtiss, L. A.; Weinhold, F. *Chem. Rev.***1988**, *88*, 899.

(49) (a) Becke, A. D. *J. Chem. Phys.* **1993**, *98*, 5648. (b) Lee, C.; Yang, W.; Parr, R. G. *Phys. Rev. B* **1988**, *37*, 785. (c) Stephens, P. J.; Devlin, F. J.; Chabalowski, C. F.; Frisch, M. J. *J. Phys. Chem.* **1994**, *98*, 11623.

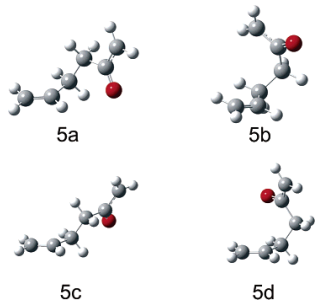

FIGURE 3. Different conformers of **5** for the doublet ground state at the (U)B3LYP/6-311++g (d) level.

SCHEME 2. Numbering of Structures Studied

C_1-C_{exo} distances are equal to $\alpha = 106.5°$ and 138.7° and $r_{C_1-C_{exo}} = 3.156$ and 3.244 Å, respectively. This suggests that the cyclization of alkyl-substituted radicals starts from the **a** type conformers, since for these structures the angle α is the closest to the tetrahedral angle. Very recently Guan et al.[50] studied the 6,6-diphenyl-5-hexenyl radical systems to determine the rate constant of the 5-*exo* radical cyclizations with different substituents. Our near-attack orientation conformer is the equivalent of their radical reactant (RR), and comparing the geometrical data, one can find that the geometry turns out to be relatively insensitive for the substitutions.

Similarly, **5** was used to determine the most beneficiary initial structure for acyl-substituted radicals. These conformers are depicted in Figure 3, and the relative energies and free energies are again listed in Table 1. In this case the in-plane geometry at the radical center (C_1, C_2, C_3, and O are in plane) causes a longer distance between the acceptor and donor part of the molecule. The linear orientation (conformer **c**) again is the most stable conformer at the B3LYP level; **b** and **d** are the two near-attack conformations with $\alpha = 98.04°$ and 106.1°, $r_{C_1-C_{exo}} =$ 3.896 and 4.036 Å, respectively. The radical cyclization of acyl-substituted chains occurs via the **d** conformer, because it is more stable than **b**, and the corresponding Bürgi−Dunitz angle is closer to the favored tetrahedral angle than in **b**. These comparisons establish the further investigation of the methyl-substituted alkyl and acyl radicals for only the linear (**1e**, **2e**, **3e**, **4e**, **5c**, **6c**, **7c**, **8c**) and in the most favored near-attack initial orientations (**1a**, **2a**, **3a**, **4a**, **5d**, **6d**, **7d**, **8d**).

In the case of the cascade reactions the radicals **9**−**16** are the intermediates, located on the reaction coordinate after the three-membered ring opening. These structures were used to predict the regioselectivity for the addition of the nitrogen radical to the double bond.

Next, we assess the regioselectivity of the intramolecular addition of the carbon or nitrogen radical to the ene side of the compound using the non-spin-polarized DFT-based reactivity indices and the local hard and soft acids and bases principle.[37] In our case, following the finite difference approach, the smallest absolute value of the difference in local Fukui functions between the nitrogen or carbon radical on one hand and one of the carbon atoms of the double bond (C_{exo} or C_{endo}) on the other corresponds to the atom more susceptible to radical attack. One should however note that, in some cases, this principle was found be problematic, indicating that a nonreactive site will be the most important.[51] One should indeed carefully check that the smallest difference in Fukui functions corresponds to the

TABLE 2. Condensed Fukui Functions for Both Model and Cascade Cyclizations[a]

				f^0		
			experimentally preferred carbon	N, C	C_{exo}	C_{endo}
I	linear	**1e**	exo	0.585	−0.004	0.113
		2e	exo	0.486	−0.017	0.094
		3e	exo	0.565	0.002	0.107
		4e	exo	0.553	0.001	0.094
I	near-attack	**1a**	exo	0.525	−0.018	0.118
		2a	exo	0.457	−0.019	0.089
		3a	exo	0.545	−0.007	0.086
		4a	exo	0.502	−0.017	0.103
II	linear	**5c**	endo	0.474	0.017	0.112
		6c		0.407	−0.003	0.090
		7c		0.466	0.030	0.113
		8c	endo	0.452	0.029	0.101
II	near-attack	**5d**	endo	0.468	0.023	0.090
		6d		0.401	−0.001	0.066
		7d		0.446	0.045	0.095
		8d	endo	0.443	0.040	0.082
III	2 step	**9**	exo	0.447	0.002	0.092
		11	exo	0.456	0.010	0.071
		13	exo	0.452	0.012	0.072
		15	exo	0.443	0.004	0.068
III	3 step	**10a**	exo	0.554	−0.027	0.036
		10b	exo	0.514	−0.019	0.101
		12	exo	0.524	−0.018	0.062
		14	exo	0.542	−0.016	0.093
		16	exo	0.531	−0.020	0.090

[a] At the (U)B3LYP/6-311++g (d,p) level. All values are in au.

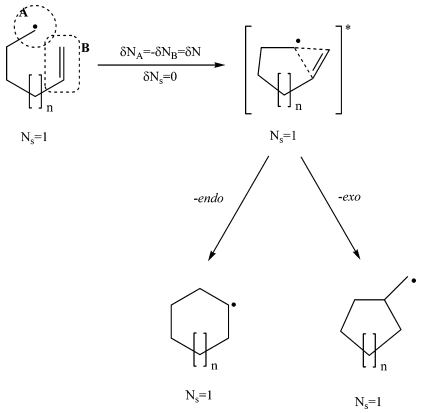

FIGURE 4. Spin-polarized specification of the initial stage in the radical cyclizations.

(50) Guan, X.; Phillips, D. L.; Yang, D. *J. Org. Chem.* **2006**, *71*, 1984.

TABLE 3. Condensed Spin-Polarized Fukui Functions f^0_{NN} for Both Model and Cascade Cyclizations[a]

				f^0_{NN}				
			experimentally preferred carbon	N, C	C_{exo}	C_{endo}	Δf_{NN} (exo)	Δf_{NN} (endo)
I	linear	**1e**	exo	0.283	0.480	−0.134	0.197	0.417
		2e	exo	0.825	0.438	−0.066	0.387	0.891
		3e	exo	0.329	0.627	−0.147	0.298	0.476
		4e	exo	0.358	0.094	0.059	0.264	0.299
I	near-attack	**1a**	exo	0.337	0.438	−0.055	0.101	0.392
		2a	exo	0.691	0.279	−0.016	0.412	0.707
		3a	exo	0.385	0.494	−0.079	0.109	0.464
		4a	exo	0.324	0.304	0.112	0.020	0.212
II	linear	**5c**	endo	−0.002	0.136	0.051	0.138	0.053
		6c		0.521	0.131	−0.015	0.390	0.536
		7c		0.092	0.361	0.139	0.269	0.047
		8c	endo	−0.046	0.156	0.189	0.202	0.235
II	near-attack	**5d**	endo	0.072	0.188	0.042	0.116	0.030
		6d		0.359	0.145	−0.156	0.214	0.515
		7d		0.028	0.406	0.101	0.378	0.073
		8d	endo	0.026	0.239	0.158	0.213	0.132
III	2 step	**9**	exo	0.411	0.162	0.070	0.249	0.341
		11	exo	0.434	0.050	0.061	0.384	0.373
		13	exo	0.444	0.139	0.066	0.305	0.378
		15	exo	0.485	0.126	0.030	0.359	0.455
III	3 step	**10a**	exo	0.094	0.157	−0.110	0.063	0.204
		10b	exo	0.275	0.244	−0.077	0.031	0.352
		12	exo	0.175	0.142	−0.132	0.033	0.307
		14	exo	0.099	0.163	−0.127	0.064	0.226
		16	exo	0.105	0.180	−0.095	0.075	0.200

[a] At the (U)B3LYP/6-311++g (d,p) level. Also given are the Fukui function differences $\Delta f_{NN}(\text{exo}) = |f^0_{NN}(\text{N, C}) - f^0_{NN}(\text{exo})|$ and $\Delta f_{NN}(\text{endo}) = |f^0_{NN}(\text{N, C}) - f^0_{NN}(\text{endo})|$. All values are in au.

combination of the Fukui function on the radical center with the highest value of the Fukui function on the atoms of the double bond, corresponding to a soft−soft interaction (i.e., an interaction between atoms of similar (high) softness). Moreover, it should be remarked that this proposed Δf criterion (i.e., smallest absolute difference between the Fukui functions of the different interacting sites) only makes sense in the case of an intramolecular interaction; for an intermolecular process, one should use the difference of the condensed local softness values computed with this Fukui function. Table 2 shows the condensed f^0_k values (calculated using NPA charges) for the simple cyclization in two different orientations, alkyl- and acyl-substituted chains in near-attack and in linear arrangements and for the cascade intermediates. The numbering of all the analyzed atoms is depicted in Scheme 2.

From Table 2, it can be seen that the carbon atom at the *exo* position (C_{exo}) has a f^0_k value smaller than that of the carbon atom at the terminal position (C_{endo}). Hence the C_{endo} atom is more susceptible to radical attack than C_{exo}. Thus, the prediction for the alkyl-substituted hexenyl radical (I) based on the non-spin-polarized Fukui function is not in agreement with the experimentally observed outcome that the hexenyl radical and its substituted analogues cyclize with high regioselectivity to give five-membered rings. For acyl-substituted radicals (II), where experimentally a clear preference for the 6-*endo* process is found, the calculated regioselectivity is in good agreement with experiment. The calculated Fukui functions for the second and third step of radical cascade cyclizations of *N*-alkenyl-2-aziridinylmethyl radicals to pyrrolizidines and indolizidines show that in both steps the f^0_k value of the C_{endo} is always higher than that of the C_{exo}. It is thus expected that the radical attack will preferentially be at the C_{endo} carbon atom. These results are not in agreement with experimental data, because the observed regioselectivity and the calculated activation barriers show that the cyclization of the nitrogen radical (second step) and the carbon radical (third step) always prefer the attack on the C_{exo} resulting in the formation of the "smaller" ring.

Next, we tried to gain more insight in the failure of the condensed Fukui function in the prediction of the regioselectivity of these radical cyclization reactions. In a bimolecular radical addition one can expect little charge transfer between the two molecules. When charge is transferred from the donor to the acceptor, the spin state of both of the reactants is changing. Thus, considering the separated reactants, the nonpolarized Fukui function measures the response of the density for each reactant to a change in number of electrons at fixed external potential but variable spin number and can be expected to give the right regioselectivity. In the reaction studied in this work, part of the molecule acts as an electron acceptor and another part as an electron donor. In an intramolecular addition, during the charge transfer from the donor part to the acceptor part of the molecule, the spin state of the molecule remains constant (Figure 4).

In our case the approaching radical (nucleophilic, electrophilic) adds to the π bond of the carbon−carbon double bond to form a closed-ring doublet radical. In such a process, the number of electrons is changing from a local point of view (charge transfer occurs from one part of the molecule to another one) at constant global spin number N_s (both the reactant and the closed ring are in the doublet state), and the generalized Fukui function $f_{NN}(r)$ should be used to investigate the regioselectivity. This index measures the initial response of the electron density to a constrained charge transfer, i.e., the spin number N_s remains constant during the change in the number

(51) (a) Chattaraj, P. K, *J. Phys. Chem. A* **2001**, *105*, 511. (b) Melin, J.; Aparicio, F.; Subramanian, V.; Galvan, M.; Chattaraj, P. K. *J. Phys. Chem. A* **2001**, *108*, 2487.

of electrons. An example is the modeling of an intramolecular rearrangement (which occurs at constant multiplicity).

We have consequently studied the regioselectivity in the different cases considered above using the spin-polarized reactivity indices, as this cyclization involves a doublet radical compound. Also in this case, the smallest absolute value of the difference in local spin-polarized Fukui functions between the nitrogen or carbon radical on one hand and one of the carbon atoms of the double bond (C_{exo} or C_{endo}) on the other should identify the atom more susceptible to radical attack. The calculated $f_{NN}(\underline{r})$ values for the simple cyclization of alkyl-substituted radicals (I) in linear and in near-attack orientation are given in Table 3. One can indeed observe that $\Delta f^0_{NN}(\underline{r})$ is always smaller between the radical and C_{exo} of the double bond than between the radical and the terminal carbon atom (C_{endo}), i.e., it shows a preference for the formation of 5-*exo* rather than the 6-*endo* products, in good agreement with the experimental results.

The non-spin-polarized Fukui functions are relatively insensitive to structural orientation in radicals **1**−**9**, whereas $f_{NN}(\underline{r})$ changes significantly when going from the linear to the other conformer generated by performing the internal rotations. In the near-attack conformers C_{exo} is softer or more susceptible to radical attack than in linear conformers.

At this point we have to note that the investigations of the cyclization of 5-methyl-5-hexenyl radical (**3**) from different groups come to different conclusions; Beckwith at al. supposed a preferential *endo* ring closure[52] supported by theoretical calculations, whereas work from Walling at al. clearly showed[11] the exclusive formation of the cyclopentylmethyl radical in agreement with Baldwin's rules. In the results of the latter paper one can realize the influence of the methyl substituent, maintaining the steric effect, but the reaction occurs in *exo* mode and our calculations are in agreement with their results.

In the case of acyl-substituted radicals (Table 3, II), in the near-attack orientation the terminal carbon (C_{endo}) atom has a much better "matching" for radical attack, except for **6**, than C_{exo}. According to the computational results the 6-*endo* pathway is generally favored in this case; the only exception occurs when an alkyl substitutent connects to the radical carbon atom. However, there are no available experimental data for this system, and theoretical calculations showed that the lowest activation barrier corresponds to the *endo* cyclization. Note that in the more complex Jung−Rayle radical cyclization[53] (where, instead of a methyl group, a five-membered ring is connected to the carbon-centered radical), only 5-*exo* cyclization was mentioned. The $f^0_{NN}(\underline{r})$ values for the linear conformation are very different from the $f^0_{NN}(\underline{r})$ values for the near-attack orientation and thus clearly show their usefulness for prediction.

The $f^0_{NN}(\underline{r})$ values for the nitrogen radical and for the carbon 6-*endo* and 5-*exo* cyclizations of the cascade reaction are also given in Table 3. Experimentally both cyclization steps of the domino reaction (III) were found to be a regioselective process as it leads, if it occurs, always to the smaller ring. One can find a good agreement between our computational results and available experimental data. The better matching always corresponds to the *exo* ring closure. In the case of **11** the $f^0_{NN}(\underline{r})$ values are quite similar for both C_{exo} and C_{endo} carbon atoms.

(52) Beckwith, A. L. J.; Blair, I. A.; Phillipou, G. *Tetrahedron Lett.* **1974**, *15*, 2251.

(53) Jung, M. E.; Rayle, H. L. *J. Org. Chem.* **1997**, *62*, 4601.

Conclusion

In this contribution, we have presented a study of the regioselectivity of the radical cyclizations of alkyl- and acyl-substituted hexenyl radicals and the regioselectivity of the cascade radical reaction of *N*-alkenyl-2-aziridinylmethyl radicals, using DFT-based reactivity descriptors. In the first part, we analyzed the different initial orientations for the two simplest alkyl- and acyl-substituted systems. The two near-attack conformations **1a** and **5c** match the Bürgi−Dunitz trajectory. In the case of the second and third step of the cascade reactions, we used the geometry of the intermediates.

In the next step, we investigated the regioselectivity using the Fukui functions within the framework of the local hard and soft acids and bases (HSAB) principle. The interaction was investigated as the interaction of two radicalar species in both near-attack and linear conformations. The Fukui indices predict that both alkyl- and acyl-substituted radicals occur via 6-*endo* mode. A similar preference was found in the cascade reaction; the ring-forming steps occur on the terminal carbon. This result indicates that the regioselectivity can be explained only in the case of the intramolecular addition of acyl-substituted systems.

Finally, we applied the reactivity descriptors emerging from spin-polarized density functional theory because in an intramolecular process the number of electrons is changing from a local point of view at a constant global spin number N_s. The analysis of the condensed-to-atom spin-polarized Fukui functions indicates that the correct regioselectivity of the intramolecular radical additions emerges from considering the interaction of two radicalar species in the near-attack conformation. In these cases, good agreement was found when comparing the predicted regioselectivities with experimental data.

Acknowledgment. B.P. thanks the Bizáki Puky Péter Memorial Foundation (Bizáki Puky Péter Emlékalapítvány) and the Széchenyi István Fellowship Foundation (Széchenyi István Ösztöndíj Alapítvány) for financial support. E.C. thanks the Millennium Nucleus for Applied Quantum Mechanics and Computational Chemistry (Mideplan-Conicyt, Chile), Grant No. P02-004-F, to Fondecyt(Chile), Grant No. 1030173, and the Universidad Andres Bello (UNAB), grant UNAB-DI 16-04, for continuous support. This work has been realized within the framework of a Bilateral Cooperation Agreement between the Governments of the Flemish Community of Belgium and Hungary under Project VLW79.

Supporting Information Available: Optimized geometries and energies of all compounds considered in this work. This material is available free of charge via the Internet at http://pubs.acs.org.

JO0613885

Bibliography

[1] Parr R. G. and Yang W., *Density-Functional Theory of Atoms and Molecules*, Oxford Science Publications (1988).

[2] Dreizler R. M. and Gross E. K. U., *Density Functional Theory: An Approach to the Quantum Many Body Problem*, Springer-Verlag: Berlin (1990).

[3] Bader R. F. W., *Atoms in Molecules: a Quantum Theory*, Clarendon Press; Oxford (1990).

[4] Janak J. F., *Phys. Rev. B* **18**, pp. 7165 (1978).

[5] Perdew J. P., Parr R. G., Levy M., and Balduz J. L. Jr., *Phys. Rev. Lett.* **49**, pp. 1691 (1982).

[6] Nguyen-Dang T. T., Bader R. F. W., and Essén H., *Int. J. Quant. Chem.* **22**, pp. 1049 (1982).

[7] Russier V., *Phys. Rev. B* **45**, pp. 8894 (1992).

[8] Perdew J. P. and Levy M., *Many-Body Phenomena at Surfaces*, edited by D. Langreth and H. Suhl, Academic, New York (1984).

[9] von Barth U., *Many-Body Phenomena at Surfaces*, edited by D. Langreth and H. Suhl, Academic, New York (1984).

[10] Chermette H., *J. Comput. Chem.* **20**, pp. 129 (1999).

[11] Mermin N. D., *Phys. Rev.* **137** (1965).

[12] Geerlings P., De Proft F., and Langenaeker W., *Chem. Rev.* **103**, pp. 1793 (2003).

[13] Parr R. G., Donnelly R. A., Levy M., and Palke W. E., *J. Chem. Phys.* **68**, pp. 3801 (1978).

[14] Kohn W., Becke A. D., and Parr R. G., *J. Phys. Chem.* **100**, pp. 12974 (1996).

[15] Gyftopoulos E. P. and Hatsopoulos G. N., *Proc. Natl. Acad. Sci. U. S. A.* **60**, pp. 786 (1965).

[16] Iczkowski R. P. and Margrave J. L., *J. Am. Chem. Soc.* **83**, pp. 3547 (1961).

[17] Parr R. G. and Pearson R. G., *J. Am. Chem. Soc.* **105**, pp. 7512 (1983).

[18] Ayers P. W. and Parr R. G., *J. Am. Chem. Soc.* **122**, pp. 2010 (2000).

[19] Pearson R. G., *J. Chem. Educ.* **64**, pp. 561 (1987).

[20] Koopmans T. A., *Physica* **1**, pp. 104 (1933).

[21] Politzer P., *J. Chem. Phys.* **86**, pp. 1072 (1987).

[22] Pearson R. G., *J. Am. Chem. Soc.* **85**, pp. 3533 (1963).

[23] Ayers P. W., Parr R. G., and Pearson R. G., *J. Chem. Phys.* **124**, pp. 194107 (2006).

[24] Komorowski L., Lipinski J., and Pyka M. J., *J. Phys. Chem.* **97**, pp. 3166 (1993).

[25] Chattaraj P. K., Cedillo A., and Parr R. G., *J. Chem. Phys.* **103**, pp. 7645 (1995).

[26] Mineva T., Sicilia E., and Russo N., *J. Am. Chem. Soc.* **120**, pp. 9053 (1998).

[27] Nalewajski R. F., *Chemical Hardness*, Sen K. D. , Ed. ; Structure and Bonding 80 ; Springer-Verlag: Berlin (1993).

[28] Baeckelandt B. G., Mortier W. J., and Schoonheydt R. A., *Chemical Hardness*, Sen K. D. , Ed. ; Structure and Bonding 80 ; Springer-Verlag: Berlin (1988).

[29] Bultinck P. and Carbó-Dorca R., **364**, pp. 357 (2002).

[30] Maynard A. T., Huang M., Rice W. G., and Covell D. G., *Proc. Natl. Acad. Sci. U.S.A.* **95**, pp. 11578 (1998).

[31] Parr R. G., Von Szentpaly L., and Liu S. B., *J. Am. Chem. Soc.* **121**, pp. 1922 (1999).

[32] Ayers P. W., Anderson J. S. M., and Bartolotti L. J., *Int. J. Quant. Chem.* **101**, pp. 520 (2005).

[33] Chattaraj P. K. and Maiti B., *J. Phys. Chem. A* **105**, pp. 169 (2001).

[34] Ayers P. W., Anderson J. S. M., Rodriguez J. I., and Jawed Z., *Phys. Chem. Chem. Phys.* **7**, pp. 1918 (2005).

[35] Parr R. G. and Bartolotti L. J., *J. Phys. Chem.* **87**, pp. 2810 (1983).

[36] Nalewajski R. F. and Parr R. C., *J. Chem. Phys.* **77**, pp. 399 (1982).

[37] Carbo R., Colabuig B., Vera L., and Besalu E., *Adv. Quantum Chem.* **25**, pp. 254 (1994).

[38] Besalu E., Carbo R., Mestres J., and Sol M., *Top. Curr. Chem.* **173**, pp. 31 (1995).

[39] Sol M., Mestress J., and Oliva J. M., *Int. J. Quant. Chem.* **58**, pp. 36 (1996).

[40] Carbo R., Besalu E., and Girones X., *Adv. Quantum Chem.* **38**, pp. 1 (2000).

[41] Carbo R., Arnau M., and Leyda L., *Int. J. Quant. Chem.* **17**, pp. 1185 (1980).

[42] Hodgkin E. E. and Richards W. G., *Int. J. Quantum Chem., Quantum Biol. Symp.* **295**, pp. 122 (1987).

[43] Boon G., De Proft F., Langenaeker W., and Geerlings P., **295**, pp. 122 (1998).

[44] Boon G., Langenaeker W., De Proft F., De Winter H., Tollenaere J. P., and Geerlings P., *J. Phys. Chem. A* **105**, pp. 8805 (2001).

[45] Boon G., Van Alsenoy C., De Proft F., Bultinck P., and Geerlings P., *J. Phys. Chem. A* **107**, pp. 11120 (2003).

[46] Parr R. G. and Yang W., *J. Am. Chem. Soc.* **106**, pp. 4049 (1984).

[47] Ayers P. W. and Levy M., *Theor. Chem. Acc.* **103**, pp. 353 (2000).

[48] Fukui K., Yonezawa Y., and Shingu H., *J. Chem. Phys.* **20**, pp. 722 (1952).

[49] Parr R. G. and Parr J. B., *Theor. Chem. Acc.* **102**, pp. 5 (1999).

[50] Kato S., *Theor. Chem. Acc.* **103**, pp. 219 (2000).

[51] Yang W., Parr R. G., and Pucci R., *J. Phys. Chem.* **81**, pp. 2862 (1984).

[52] Chattaraj P. K., Cedillo A., and Parr R. G., *J. Chem. Phys.* **103**, pp. 10621 (1995).

[53] Pacios L. F., **276**, pp. 381 (1997).

[54] Pacios L. F. and Gomez P. C., *J. Comput. Chem.* **19**, pp. 488 (1998).

[55] De Proft F., Geerlings P., Liu S., and Parr R. G., *Polish J. Chem.* **72**, pp. 1737 (1999).

[56] Ayers P. W. and Levy M., *Theor. Chem. Acc.* **103**, pp. 353 (2000).

[57] Michalak A., De Proft F., Geerlings P., and Nalewajski R. F., *J. Phys. Chem. A* **103**, pp. 762 (1999).

[58] Yang W. and Parr R. G., *Proc. Natl. Acad. Sci. U. S. A.* **82**, pp. 6723 (1985).

[59] Yang W. and Mortier W. J., *J. Am. Chem. Soc.* **108**, pp. 5708 (1986).

[60] Mulliken R. S., *J. Chem. Phys.* **23**, pp. 1833.

[61] Reed A. E., Curtiss L. A., and Weinhold F., *Chem. Rev.* **88**, pp. 899 (1988).

[62] Hirshfeld F. L., *Theor. Chim. Acta* **44**, pp. 129 (1977).

[63] Breneman C. M. and Wiberg K. B., *J. Comput. Chem.* **11**, pp. 361 (1990).

[64] Besler B. H., Merz Jr. K. M., and Kollman P. A., *J. Comput. Chem.* **11**, pp. 431 (1990).

[65] Singh U. C. and Kollman P. A., *J. Comput. Chem.* **5**, pp. 129 (1984).

[66] De Proft F., Martin J. M. L., and Geerlings P., **256**, pp. 400 (1996).

[67] De Proft F., Martin J. M. L., and Geerlings P., **230**, pp. 393 (1996).

[68] Langenaeker W., De Proft F., and Geerlings P., *J. Mol. Struct. (Theochem)* **362**, pp. 175 (1996).

[69] Arulmozhiraja S. and Kolandaivel P., *Mol. Phys.* **90**, pp. 55 (1997).

[70] Martin F. and Zipse H., *J. Comput. Chem.* **26**, pp. 97 (2005).

[71] Cioslowski J., Martinov M., and Mixon S. T., *J. Phys. Chem.* **97**, pp. 10948 (1993).

[72] Gilardoni F., Weber J., Chermette H., and Ward T. R., *J. Phys. Chem. A* **102**, pp. 3607 (1998).

[73] Thanikaivelan P., Padmanabhan J., Subramanian V., and Ramasami T., *Theor. Chem. Acc.* **107**, pp. 326 (2002).

[74] Mineva T., Parvanov V., Petrov I., Neshev N., and Russo N., *J. Phys. Chem. A* **105**, pp. 1959 (2001).

[75] Grigorov M., Weber J., Chermette H., and Trouchet J. M. J., *Int. J. Quant. Chem.* **61**, pp. 551 (1997).

[76] Grigorov M., Weber J., Vuillermet N., Chermette H., and Troucher J. M. J., *J. Chem. Phys.* **108**, pp. 8790 (1998).

[77] Balawender R. and Komorowski L., *J. Chem. Phys.* **109**, pp. 5203 (1998).

[78] Liu G. H., *J. Chem. Phys.* **106**, pp. 165 (1997).

[79] Nalewajski R. F., Korchowiec J., and Zhou Z., *Int. J. Quant. Chem.* , p. 349 (1988).

[80] Senet P., *J. Chem. Phys.* **107**, pp. 2516 (1997).

[81] Ayers P. W., Morrison R. C., and Roy R. K., *J. Chem. Phys.* **116**, pp. 8731 (2002).

[82] Roy R. K., Pal S., and Hirao K., *J. Chem. Phys.* **110**, pp. 8236 (1999).

[83] Roy R. K., Hirao K., and Pal S., *J. Chem. Phys.* **113**, pp. 1372 (2000).

[84] Fuentealba P., Perez P., and Contreras R., *J. Chem. Phys.* **113**, pp. 2544 (2000).

[85] Roy R. K., Hirao K., Krishnamurty S., and Pal S., *J. Chem. Phys.* **115**, pp. 2901 (2001).

[86] Bultinck P., Carbó-Dorca R., and Langenaeker W., *J. Chem. Phys.* **118**, pp. 4349 (2003).

[87] Roy R. K., Krishnamurti S., Geerlings P., and Pal S., *J. Phys. Chem. A* **102**, pp. 3746 (1998).

[88] Roy R. K., De Proft F., and Geerlings P., *J. Phys. Chem. A* **102**, pp. 7035 (1998).

[89] Ghosh S. K. and Berkowitz M., *J. Chem. Phys.* **83**, pp. 864 (1985).

[90] Hohenberg P. and Kohn W., *Phys. Rev. B* **136**, pp. 864 (1964).

[91] Harbola M. K., Chattaraj P. K., and Parr R. G., *Isr. J. Chem.* **31**, pp. 395 (1991).

[92] Langenaeker W., De Proft F., and Geerlings P., *J. Phys. Chem.* **99**, pp. 395 (1995).

[93] Senet P., *J. Phys. Chem.* **105**, pp. 6471 (1996).

[94] Fuentealba P. and Parr R. G., *J. Chem. Phys.* **94**, pp. 5559 (1991).

[95] Fuentealba P. and Cedillo M., *J. Chem. Phys.* **110**, pp. 9807 (1999).

[96] Chamorro E., Contreras R., and Fuentealba P., *J. Chem. Phys.* **113**, pp. 10861 (2000).

[97] Berkowitz M. and Parr R. G., *J. Chem. Phys.* **88**, pp. 2554 (1998).

[98] Nalewajski R. F., *Int. J. Quant. Chem.* **44**, pp. 67 (1992).

[99] Baekelandt B. G., Mortier W. J., Lievens J. L., and Schoonheydt R. A., *J. Am. Chem. Soc.* **113**, pp. 6730 (1991).

[100] Liu S., De Proft F., and Parr R. G., *J. Phys. Chem. A* **101**, pp. 6991 (1997).

[101] Von Bart U. and Hedin L., *J. Phys. Chem.* **5**, pp. 1629 (1972).

[102] Rajagopal A. K. and Callaway J., *Phys. Rev. B* **7**, pp. 1912 (1973).

[103] Gunnarson O. and Lundqvist B. I., *Phys. Rev. B* **13**, pp. 4274 (1976).

[104] Galvan M., Vela A., and Gazquez J. L., *J. Phys. Chem.* **92**, pp. 6470 (1988).

[105] Vargas R., Cedillo A., Garza J., and Galvan M., *Rev. Mod. Quantum Chem.* **2**, pp. 936 (2002).

[106] Galvan M. and Vargas R., *J. Phys. Chem.* **96**, pp. 1625 (1992).

[107] Vargas R. and Galvan M., *J. Phys. Chem.* **100**, pp. 14651 (1996).

[108] Vargas R., Galvan M., and Vela A., *J. Phys. Chem. A* **102**, pp. 3134 (1998).

[109] Chamorro E., De Proft F., and Geerlings P., *J. Phys. Chem.* **123**, pp. 154104 (2005).

[110] Chamorro E., Perez P., De Proft F., and Geerlings P., *J. Chem. Phys.* **124**, pp. 314602 (2006).

[111] Garza J., Vargas R., Cedillo A., Galvan M., and Chattaraj P. K., *Theor. Chem. Acc.* **115**, pp. 257 (2006).

[112] Robles J. and Bartolotti L. J., *J. Am. Chem. Soc.* **106**, pp. 3723 (1984).

[113] Garcia V. M., Castell O., Reguero M., and Caballol R., *Mol. Phys.* **87**, pp. 1395 (1996).

[114] Kohn W., Savin A., and Ullrich C. A., *Int. J. Quant. Chem.* **101**, pp. 20 (2005).

[115] Melin J., Aparicio F., Galvan M., Fuentealba P., and Contreras R., *J. Phys. Chem. A* **106**, pp. 5353 (2002).

[116] De Proft F., Fias S., Van Alsenoy C., and Geerlings P., *J. Phys. Chem. A* **109**, pp. 6335 (2005).

[117] Schleyer P. v. R., *Chem. Rev.* **101** (2001).

[118] Zhou Z. X., Parr R. G., and Garst J. F., *Tetrahedron Letters* **29**, pp. 4843 (1988).

[119] Zhou Z. X. and Parr R. G., *J. Am. Chem. Soc.* **111**, pp. 7371 (1989).

[120] Zhou Z. and Navangul H. V., *J. Phys. Org. Chem.* **3**, pp. 784 (1990).

[121] Zhou Z., *J. Phys. Org. Chem.* **8**, pp. 103 (1995).

[122] Gomes J. A. N. F. and Mallion R. B., *Chem. Rev.* **101**, pp. 1349 (2001).

[123] De Proft F. and Geerlings P., *Chem. Rev.* **101**, pp. 1451 (2001).

[124] Fleischer U., Kutzelnigg W., Lazzaretti P., and Mühlenkamp V., *J. Am. Chem. Soc.* **116**, pp. 5298 (1994).

[125] Chen Z., Wannere C. S., Corminboeuf C., Puchta R., and Schleyer P. v. R., *Chem. Rev.* **105**, pp. 3842 (2005).

[126] Schleyer P. v. R., Jiao H., van Eikema Hommes N. J. R., Malkin V. G., and Malkina O., *J. Am. Chem. Soc.* **119**, pp. 12669 (1997).

[127] Schleyer P. v. R., Manoharan M., Wang Z-X, Kiran B., Jiao H. J., Puchta R., and van Eikema Hommes N. J. R., *Organic Letters* **3**, pp. 2465 (2001).

[128] Lazzeretti P., *Phys. Chem. Chem. Phys.* **6**, pp. 217 (2004).

[129] Stanger A., *J. Org. Chem.* **71**, pp. 883 (2006).

[130] Gambiagi M., de Gambiagi M. S., dos Santos Silva C. D., and Paiva de Figueiredo A., *Phys. Chem. Chem. Phys.* **2**, pp. 3381 (2000).

[131] Bultinck P., Ponec R., and Van Damme S., *J. Phys. Org. Chem.* **18**, pp. 706 (2005).

[132] Bultinck P., Rafat M., Ponec R., Van Gheluwe B., Carbó-Dorca, and Popelier P., *J. Phys. Chem. A* **110**, pp. 7642 (2006).

[133] Ponec R., Bultinck P., and Gallegos Saliner A., *J. Phys. Chem. A* **109**, pp. 6606 (2005).

[134] Ponec R., Bultinck P., Gutta P., and Tantillo D. J., *J. Phys. Chem. A* **110**, pp. 3785 (2006).

[135] Mandado M., Bultinck P., González-Moa M., and Mosquera R. A., **433**, pp. 5 (2006).

[136] Bultinck P., Ponec R., and Carbó-Corca, *J. Comput. Chem.* **28**, pp. 152 (2006).

[137] Sanderson R. T., *Science* **114**, pp. 670 (1951).

[138] Sanderson R. T., *Science* **116**, pp. 41 (1952).

[139] Sanderson R. T., *J. Chem. Educ.* **29**, pp. 539 (1952).

[140] Sanderson R. T., *Science* **121**, pp. 207 (1955).

[141] Mortier W. J., Ghosh S. K., and Shankar S., *J. Am. Chem. Soc.* **108**, pp. 4315 (1986).

[142] Mortier W. J., *Electronegativity*, Sen K. D. , Jørgenson C. K. , Eds.: Structure and Bonding 66; Springer-Verlag: Berlin (1987).

[143] Bultinck P., Langenaeker W., Lahorte P., De Proft F., Geerlings P., Waroquier M., and Tollenaere J. P., *J. Phys. Chem. A* **106**, pp. 7887 (2002).

[144] Bultinck P., Langenaeker W., Lahorte P., De Proft F., Geerlings P., Van Alsenoy C., and Tollenaere J. P., *J. Phys. Chem. A* **106**, pp. 7895 (2002).

[145] Bultinck P., Vanholme R., Popelier P. L. A., De Proft F., and Geerlings P., *J. Phys. Chem. A* **108**, pp. 10359 (2004).

[146] Pearson R. G., *J. Chem. Educ.* **45**, pp. 581 (1968).

[147] Pearson R. G., *J. Chem. Educ.* **45**, pp. 643 (1968).

[148] Pearson R. G., *Science* **151**, pp. 172 (1966).

[149] Chattaraj P. K., *J. Phys. Chem. A* **105**, pp. 511 (2001).

[150] Melin J., Aparicio F., Subramanian V., Galvan M., and Chattaraj P. K., *J. Phys. Chem. A* **108**, pp. 2487 (2004).

[151] Ponti A., *J. Phys. Chem. A* **104**, pp. 8843 (2000).

[152] Chattaraj P. K., Lee H., and Parr R. G., *J. Am. Chem. Soc.* **113**, pp. 1855 (1991).

[153] Gazquez J. L., *J. Phys. Chem. A* **101**, pp. 9464 (1997).

[154] Gazquez J. L., *J. Phys. Chem. A* **101**, pp. 4657 (1997).

[155] Ayers P. W., *J. Chem. Phys.* **122**, pp. 141102 (2005).

[156] Klopman G., *J. Am. Chem. Soc.* **90**, pp. 223 (1968).

[157] Pearson R. G., *J. Chem. Educ.* **64**, pp. 561 (1987).

[158] Pearson R. G., *J. Chem. Educ.* **76**, pp. 267 (1999).

[159] Pearson R. G., *Acc. Chem. Res.* **26**, pp. 250 (1993).

[160] Parr R. G. and Chattaraj P. K., *J. Am. Chem. Soc.* **113**, pp. 1854 (1991).

[161] Liu S. and Parr R. G., *J. Chem. Phys.* **106**, pp. 5578 (1997).

[162] Ghanty T. K. and Ghosh S. K., *J. Phys. Chem.* **100**, pp. 12295 (1996).

[163] Pearson R. G. and Palke W. E., *J. Phys. Chem.* **96**, pp. 3283 (1992).

[164] Chattaraj P. K., Nath S., and Sannigrahi A. B., *Chem. Phys. Lett.* **212**, pp. 223 (1993).

[165] Chattaraj P. K., Nath S., and Sannigrahi A. B., *J. Phys. Chem.* **98**, pp. 9143 (1994).

[166] Datta D., *Inorg. Chem.* **31**, pp. 2797 (1992).

[167] Harbola M. K., *Proc. Natl. Acad. Sci. U.S.A.* **89**, pp. 1036 (1992).

[168] Chandra A. K., *J. Mol. Struct. (THEOCHEM)* **312**, pp. 297 (1994).

[169] Hati S. and Datta D., *J. Org. Chem.* **57**, pp. 6056 (1992).

[170] Hohm U., *J. Phys. Chem. A* **104**, pp. 8418 (2000).

[171] Chattaraj P. K. and Ayers P. W., *J. Chem. Phys.* **123**, pp. 086101 (2005).

[172] Nguyen L. T., Le T. N., De Proft F., Chandra A. K., Langenaeker W., Nguyen M. T., and Geerlings P., *J. Am. Chem. Soc.* **121**, pp. 5992 (1999).

[173] Safi B., Choho K., and Geerlings P., *J. Phys. Chem. A* **105**, pp. 591 (2001).

[174] Nguyen M. T., Chandra A. K., Sakai S., and Morokuma K., *J. Org. Chem.* **64**, pp. 65 (1999).

[175] Chattaraj P. K., Perez P., Zevallos J., and Toro-Labbé A., *J. Mol. Struct. (Theochem)* **580**, pp. 171 (2002).

[176] Le T. N., Nguyen L. T., Chandra A. K., De Proft F., Geerlings P., and Nguyen M. T., *J. Chem. Soc. - Perkin Trans. 2* **6**, pp. 1249 (1999).

[177] Gomez B., Fuentealba P., and Contreras R., *Theor. Chem. Acc.* **110**, pp. 421 (2003).

[178] Eyring H., *J. Chem. Phys.* **3**, pp. 107 (1935).

[179] Wynne-Jones W. F. K. and Eyring H., *J. Chem. Phys.* **3**, pp. 492 (1935).

[180] Evans M. G. and Polanyi M., *Trans. Faraday Soc.* **31**, pp. 875 (1935).

[181] Evans M. G. and Polanyi M., *Trans. Faraday Soc.* **33**, pp. 448 (1937).

[182] Laidler K. J., *Chemical Kinetics*, Harper Collins Publishers, Inc. (1987).

[183] Mc Quarrie D. A. and Simon J. D., *Physical Chemistry - A molecular approach*, University Science Books, Sausalito, California (1997).

[184] Truhlar D. G. and Garrett B. C., *Annual Rev. Phys. Chem.* **35**.

[185] Wigner W., *J. Chem. Phys.* **5**, pp. 720 (1937).

[186] Eckart C., *Phys. Rev.* **35**, pp. 1303 (1930).

[187] Truong T. N., Duncan W. T., and Tirtowidjojo M., *Phys. Chem. Chem. Phys.* **1**, pp. 1061 (1999).

[188] Duncan W. T., Bell R. L., and Truong T. N., *J. Comput. Chem.* **19**, pp. 1039 (1998).

[189] Truhlar D. G. and Kuppermann A., *J. Am. Chem. Soc.* **93**, pp. 1840 (1971).

[190] Troe J., *J. Chem. Phys.* **66**, pp. 4758 (1977).

[191] Van Speybroeck V., Van Neck D., Waroquier M., Saeys M., Wauters S., and Marin G. B., *J. Phys. Chem. A* **104**, pp. 10939 (2000).

[192] Heuts J. P. A., Gilbert R. G., and Radom L., *Macromolecules* **28**, pp. 8771 (1995).

[193] Vansteenkiste P., Van Speybroeck V., Marin G. B., and Waroquier M., *J. Phys. Chem. A* **107**, pp. 3139 (2003).

[194] Van Speybroeck V., Vansteenkiste P., Van Neck D., and Waroquier M., *Chem. Phys. Lett.* **402**, pp. 479 (2005).

[195] Van Speybroeck V., Borremans Y., Van Neck D., Waroquier M., Wauters S., Saeys M., and Marin G. B., *J. Phys. Chem. A* **105**, pp. 7713 (2001).

[196] Van Cauter K., Van Speybroeck V., Vensteenkiste P., Reyniers M., and Waroquier M., *ChemPhysChem.* **7**, pp. 131 (2006).

[197] Froment G. F., *Rev. Chem. Eng.* **6**, pp. 295 (1990).

[198] Figueiredo J. L., *Edol Kohle, Erdgas, Petrochem.* **42**, pp. 294 (1989).

[199] Bennet M. J. and Price J. B., *J. Mater. Sci.* **16**, pp. 170 (1981).

[200] Reyniers G. C., Froment G. F., Kopinke F. D., and Zimmerman G., *Ind. Eng. Chem. Res.* **33**, pp. 2584 (1994).

[201] Wauters S., *Kinetics of coke formation during thermal cracking of hydrocarbons based on elementary reactions.*, PhD thesis, University of Ghent (2001).

[202] Wauters S. and Marin G. B., *Chem. Eng. J.* **82**, pp. 267 (2001).

[203] Wauters S. and Marin G. B., *Ind. and Eng. Chem. Res.* **41**, pp. 2379 (2002).

[204] Saeys M., Reyniers M.-.F, Marin G. B., Van Speybroeck V., and Waroquier M., *J. Phys. Chem. A* **107**, pp. 9147 (2003).

[205] Saeys M., Reyniers M.-F., Marin G. B., Van Speybroeck V., and Waroquier M., *AICHE Journal* **50**, pp. 426 (2004).

[206] Saeys M., Reyniers M.-F., Van Speybroeck V., Waroquier M., and Marin G. B., *ChemPhysChem* **7**, pp. 188 (2006).

[207] Van Speybroeck V., Van Neck D., Waroquier M., Wauters S., Saeys M., and Marin G. B., *Int. J. Quant. Chem.* **91**, pp. 384 (2003).

[208] Van Speybroeck V., Hemelsoet K., Waroquier M., and Marin G. B., *Int. J. Quant. Chem.* **96**, pp. 568 (2004).

[209] Van Speybroeck V., Reyniers M.-F., Marin G. B., and Waroquier M., *ChemPhysChem* **3**, pp. 863 (2002).

[210] Reyniers M.-F. S. G. and Froment G. G., *Ind. Eng. Chem. Res.* **34**, pp. 773 (1995).

[211] Frenklach M., Clary D. W., Gardiner W. C., and Stein S. E., *Proc. Combust. Inst.* **20**, pp. 887 (1984).

[212] Frenklach M. and Wang H., *23rd Int. Symp. on Combustion*, The Combustion Institute, Pittsburgh, PA (1990).

[213] Frenklach M. and Warnatz J., *Combust. Sci. Technol.* **51**, pp. 265 (1987).

[214] Frenklach M., *26th Int. Symp. on Combustion*, The Combustion Institute, Pittsburgh, PA (1996).

[215] Vereecken L., Peeters J., Bettinger H. F., Kaiser R. I., Schleyer P. v. R., and Schaefer H. F. III, *J. Am. Chem. Soc.* **124**, pp. 2781 (2002).

[216] Gonzales J. M., Barden C. J., Brown S. T., Schleyer P. v. R., Schaefer H. F. III, and Li Q.-S., *J. Am. Chem. Soc.* **125**, pp. 1064 (2003).

[217] Watson M. D., Fechtenkötter A., and Müllen K., *Chem. Rev.* **101**, pp. 1267 (2001).

[218] Harvey R. G., *Polycyclic Aromatic Hydrocarbons: Chemistry and Carcinogenicity*, Cambridge University Press: Cambridge (1991).

[219] Harvey R. G., *Polycyclic Aromatic Hydrocarbons*, Wiley-VCH: New York (1997).

[220] Durant J. L., Busby W. F., Lafleur A. L., Penman B. W., and Crespi C. L., *Mutat. Res.* **371**, pp. 123 (1996).

[221] Denissenko M. F., Pao A., Tang M. S., and Pfeifer G. P., *Science* **274**, pp. 430 (1996).

[222] Allamandola L. J., *Top. Curr. Chem.* **153**, pp. 1 (1990).

[223] Léger A., d'Hendecourt L., and Boccara N., *Polycyclic Aromatic Hydrocarbons and Astrophysics*, NATO ASI Ser., Ser. C 191 Reidel, Dordrecht (1987).

[224] Puget J. L. and Léger A., *Annu. Rev. Astron. Astrophys.* **27**, pp. 161 (1989).

[225] Allen J. O., Dookeran N. M., Smith K. A., Sarofim A. F., Taghizadeh K., and Lafleur A. L., *Environ. Sci. Technol.* **30**, pp. 1023 (1996).

[226] Lovas F. J., McMahon R. J., Grabow J.-U., Schnell M., Mack J., Scott L. T., and Kuczkowski R. L., *J. Am. Chem. Soc.* **127**, pp. 4345 (2005).

[227] Kroto H. W., Heath J. R., O'Brien S. C., Curl R. F., and Smalley R. E., *Nature* **318**, pp. 162 (1985).

[228] Zhang Q. L., O'Brien S. C., Heath J. R., Liu Y., Curl R. F., Kroto H. W., and Smalley R. E., *J. Phys. Chem.* **90**, pp. 525 (1986).

[229] Smalley R. E., *Acc. Chem. Res.* **25**, pp. 98 (1992).

[230] Marr J. A. Pope C. J. and Howard J. B., *J. Phys. Chem.* **97**, pp. 11001 (1993).

[231] Richter H., Mazyar O. A., Sumathi R., Green W. H., Howard J. B., and Bozzelli J. W., *J. Phys. Chem. A* **105**, pp. 1561 (2001).

[232] Richter H., Grieco W. J., and J. B. Howard, *Combust. Flame* **119**, pp. 1 (1999).

[233] Harris S. J., Weiner A. M., and Blint R. J., *J. Combust. Flame* **72**, pp. 91 (1988).

[234] Moran D., Stahl F., Bettinger H. F., Schaefer H. F. III, and Schleyer P. v. R., *J. Am. Chem. Soc.* **125**, pp. 6746 (2003).

[235] Wong M. W., Pross A., and Radom L., *J. Am. Chem. Soc.* **115**, pp. 11050 (1993).

[236] Wong M. W. and Radom L., *J. Phys. Chem.* **99**, pp. 8582 (1995).

[237] Wong M. W. and Radom L., *J. Phys. Chem. A* **102**, pp. 2237 (1998).

[238] Gómez-Balderas R., Coote M. L., Henry D. J., Fischer H., and Radom L., *J. Phys. Chem. A* **107**, pp. 6082 (2003).

[239] Gómez-Balderas R., Coote M. L., Henry D. J., and Radom L., *J. Phys. Chem. A* **108**, pp. 2874 (2004).

[240] Coote M. L., Wood G. P. F., and Radom L., *J. Phys. Chem. A* **106**, pp. 12124 (2002).

[241] Henry D. J., Coote M. L., Gómez-Balderas R., and Radom L., *J. Am. Chem. Soc.* **126**, pp. 1732 (2004).

[242] Giese B., *Angew. Chem. Int. Ed.* **24**, pp. 553 (1985).

[243] Tedder J. M., *Angew. Chem. Int. Ed.* **21**, pp. 401 (1982).

[244] Fischer H. and Radom L., *Angew. Chem. Int. Ed.* **40**, pp. 1340 (2001).

[245] Pearson R. G., *J. Org. Chem.* **54**, pp. 1423 (1989).

[246] Roy R. K. and Pal S., *J. Phys. Chem.* **99**, pp. 17822 (1995).

[247] Misra G. P. and Sannigrahi A. B., *J. of Molecular Structure (Theochem)* **361**, pp. 63 (1996).

[248] Kar T. and Sannigrahi A. B., *Indian Journal of Chemistry* **39**, pp. 68 (2000).

[249] Chandra A. K., Uchimaru T., Sugie M., and Sekiya A., *Chem. Phys. Lett.* **318**, pp. 69 (2000).

[250] Korchowiec J. and Uchimaru T., *J. Phys. Chem. A* **102**, pp. 6682 (1998).

[251] Chandra A. K. and Nguyen M. T., *J. Chem. Soc. Perkin Trans. 2* , p. 1415 (1997).

[252] Nguyen H. M. T., Peeters J., Nguyen M. T., and Chandra A. K., *J. Phys. Chem. A* **108**, pp. 484 (2004).

[253] Nguyen H. M. T., Chandra A. K., Carl S. A., and Nguyen M. T., *J. of Molecular Structure (Theochem)* **732**, pp. 219 (2005).

[254] Chandra A. K. and Nguyen M. T., *Faraday Discussions* **135**, pp. 191 (2007).

[255] Ghanty T. K. and Ghosh S. K., *J. Phys. Chem. A* **106**, pp. 4200 (2002).

[256] Pintér B., De Proft F., Van Speybroeck V., Hemelsoet K., Waroquier M., Chamorro E., Veszprémi T., and Geerlings P., *J. Org. Chem.*

[257] Kopinke F. D., Zimmerman G., and Nowak S., *Carbon* **26**, pp. 117 (1988).

[258] Kopinke F. D., Zimmerman G., Reyniers G. C., and Froment G. F., *Ind. Eng. Chem. Res.* **32**, pp. 56 (1993).

[259] Kopinke F. D., Zimmerman G., Reyniers G. C., and Froment G. F., *Ind. Eng. Chem. Res.* **32**, pp. 2620 (1993).

[260] Ochterski J. W., Petersson G. A., and Montgomery J. A., *J. Chem. Phys.* **104**, pp. 2598 (1996).

[261] Montgomery J. A., Frisch M. J., Ochterski J. W., and Petersson G. A., *J. Chem. Phys.* **112**, pp. 6532 (2000).

[262] Mayer P. M. Henry D. J., Parkinson C. J. and Radom L., *J. Phys. Chem. A* **105**, pp. 6750 (2001).

[263] Henry D. J., Sullivan M. B., and Radom L., *J. Chem. Phys.* **118**, pp. 4849 (2003).

[264] Henry D. J., Parkinson C. J., and Radom L., *J. Phys. Chem. A* **106**, pp. 7927 (2002).

[265] Martin J. M. L. and Parthiban S., *Quantum Mechanical Prediction of Thermochemical Data*, Cioslowski, J. Ed.; Kluwer-Academic: Dordrecht, Netherlands (2001).

[266] Scott A. P. and Radom L., *J. Phys. Chem.* **100**, pp. 16502 (1996).

[267] Zhao Y., Lynch B. J., and Truhlar D. G., *J. Phys. Chem. A* **108**, pp. 2715 (2004).

[268] Lynch B. J. and Truhlar D. G., *J. Phys. Chem. A* **105**, pp. 2936 (2001).

[269] Zhao Y., Lynch B. J., and Truhlar D. G., *Phys. Chem. Chem. Phys.* **7**, pp. 43 (2005).

[270] Tokmakov I. V., Park J., Gheyas S., and Lin M. C., *J. Phys. Chem. A* **103**, pp. 3636 (1999).

[271] Krech M. and Price S. J. W., *Can. J. Chem.* **45**, pp. 157 (1967).

[272] Zhang H. X., Ahonkhai S. I., and Back M. H., *Can. J. Chem.* **67**, pp. 1541 (1989).

[273] Kasai P. H., Clark P. A., and Whipple E. B., *J. Am. Chem. Soc.* **92**, pp. 2640 (1970).

[274] Bell R. P., *Proc. Roy. Soc. A* **154**, pp. 414 (1936).

[275] Evans M. G. and Polanyi M. G., *Trans. Faraday Soc.* **34**, pp. 11 (1938).

[276] Biermann D. and Schmidt W., *J. Am. Chem. Soc.* **102**, pp. 3163 (1980).

[277] Herndon W. C. and Ellzey M. L. Jr., *J. Am. Chem. Soc.* **96**, pp. 6631 (1974).

[278] Wang D. Z. and Streitwieser A., *Theor. Chem. Acc.* **102**, pp. 78 (1999).

[279] Corma A., *Chem. Rev.* **95**, pp. 559 (1995).

[280] Sauer J., *Chem. Rev.* **89**, pp. 199 (1989).

[281] van Santen R. A. and Kramer G. J., *Chem. Rev.* **95**, pp. 637 (1995).

[282] Astala R. and Auerbach S. M., *J. Am. Chem. Soc.* **126**, pp. 1843 (2004).

[283] Lesthaeghe D., Van Speybroeck V., and Waroquier M., *J. Am. Chem. Soc.* **126**, pp. 9162 (2004).

[284] Chan B. and Radom L., *J. Am. Chem. Soc.* **128**, pp. 5322 (2006).

[285] Lesthaeghe D., Van Speybroeck V., Marin G. M., and Waroquier M., *J. Phys. Chem. B* **109**, pp. 7952 (2005).

[286] De Proft F. and Geerlings P., *J. Chem. Phys.* **106**, pp. 3270 (1997).

[287] Jalbout A. F., Jalbout F. N., and Alkahby H. Y., *J. Mol. Struct. (Theochem)* **574**, pp. 141 (2001).

[288] Jalbout A. F., Darwish A. M., and Alkahby H. Y., *J. Mol. Struct. (Theochem)* **585**, pp. 205 (2002).

[289] Vos A. M., Nulens K. H. L., De Proft F., Schoonheydt R. A., and Geerlings P., *J. Phys. Chem. B* **106**, pp. 2026 (2002).

[290] Vos A. M., Schoonheydt R. A., De Proft F., and Geerlings P., *J. Phys. Chem. B* **107**, pp. 2001 (2003).

[291] Langenaeker W., Coussement N., De Proft F., and Geerlings P., *J. Phys. Chem.* **98**, pp. 3010 (1994).

[292] Deka R. C., Vetrivel R., and Pal S., *J. Phys. Chem. A* **103**, pp. 5978 (1999).

[293] Deka R. C., Roy R. K., and Hirao K., **332**, pp. 576 (2000).

[294] Deka R. C. and Hirao K., *J. Mol. Cat. A* **181**, pp. 275 (2002).

[295] Deka R. C., Roy R. K., and Hirao K., **389**, pp. 186 (2004).

[296] Santos J. C., Contreras R., Chamorro E., and Fuentealba P., *J. Chem. Phys.* **116**, pp. 4311 (2002).

[297] Chatterjee A. and Mizukami F., **385**, pp. 20 (2004).

[298] Pal S. and Chandrakumar K. R. S., *J. Am. Chem. Soc.* **122**, pp. 4145 (2000).

[299] Krishnamurty S., Roy R. K., Vetrivel R., Iwata S., and Pal S., *J. Phys. Chem. A* **101**, pp. 7253 (1997).

[300] Deka R. c., Ajitha D., and Hirao K., *J. Phys. Chem. B* **107**, pp. 8574 (2003).

[301] Mignon P., Geerlings P., and Schoonheydt R., *J. Phys. Chem. B.*

[302] Zhao Y. and Truhlar D. G., *J. Phys. Chem. A* **108**, pp. 6908 (2004).

[303] Boese A. D. and Martin J. M. L., *J. Chem. Phys.* **121**, pp. 3405 (2004).

[304] Dunning T. H. Jr., Peterson K. A., and Woon D. A., *Basis Sets: Correlation Consistent Sets. In The Encyclopedia of Computational Chemistry; Schleyer P. v. R.*, Ed; John Wiley: Chichester (1998).

[305] Baldwin J. E., *J. Chem. Soc., Chem. Commun.* **734** (1976).

[306] Jasperse C. J., Curran P. D., and Fevig L. T., *Chem. Rev.* **91**, pp. 1237 (1991).

[307] Julia M., *Pure Appl. Chem.* **40**, pp. 553 (1974).

[308] Beckwith A. L. J., *Tetrahedron* **37**, pp. 3073 (1981).

[309] Hart D. J., *Science* **223**, pp. 883 (1984).

[310] Jung M. E., Cho M. Y., and Jung H. Y., *Tetrahedron Letters* **37**, pp. 3 (1996).

[311] Kochi J. K., *Free Radicals*, Wiley: New York (1973).

[312] Giese B., *Radicals in Organic Synthesis: Formation of Carbon-Carbon Bonds*, Pergamon: New York (1986).

[313] Ingold K. U. and Beckwith A. L. J., *Rearrangements in Ground and Excited States*, Ed. P. de Mayo, Academic Press, New York, Vol.1 (1980).

[314] Wilt W. J., *Tetrahedron* **41**, pp. 3979 (1985).

[315] Curran D. P. and Chang C. T., *J. Org. Chem.* **54**, pp. 3140 (1989).

[316] Struble D. L., Beckwith A. L. J., and Graem G. E., *Australian Journal of Chemistry* **25**, pp. 1081 (1972).

[317] Stevens C. V., Vekemans W., Moonen K., and Rammeloo T., *Tetrahedron Lett.* **44**, pp. 1619 (2003).

[318] Moonen K., Laureyn I., and Stevens C. V., *Chem. Rev.* **104**, pp. 6177 (2004).

[319] Moonen K. and Stevens C. V., *Synthesis* **20**, pp. 3603 (2005).

[320] Smith M. B. and March J., *Kinetic Requirements for reactions*, Advanced Organic Chemistry, 5th ed. ; J. Wiley and Sons: New York (2001).

[321] Bossio R., Marcos C. F., Marcaccini S., and Pepino R., *Tetrahedron Lett.* **38**, pp. 2519 (1997).

[322] Marcaccini S., Pepino R., and Pozo M. C., *Tetrahedron Lett.* **42**, pp. 2727 (2001).

[323] Galli C., Illuminati G., Mandolini L., and Tamborra P., *J. Am. Chem. Soc.* **99**, pp. 2591 (1977).

[324] Mandolini L., *J. Am. Chem. Soc.* **100**, pp. 550 (1978).

[325] Pratt L. M. and Streitwieser A. J., *Org. Chem.* **68**, pp. 2830 (2003).

[326] Denmark S. E. and Cramer C. J., *J. Org. Chem.* **55**, pp. 1806 (1990).

[327] Katritzky A. R., Piffl M., Lang H. Y., and Anders E., *Chem. Rev.* **99**, pp. 665 (1999).

[328] Dürckheimer W., Blumbach J., Lattrell R., and Scheunemann K. H., *Angew. Chem.* **24**, pp. 180 (1985).

[329] Van Speybroeck V., De Kimpe N., and Waroquier M., *J. Org. Chem.* **70**, pp. 3674 (2005).

[330] Brown W. R., Stephenson P. T., and Young A. R., *Tetrahedron* **52**, pp. 11445 (1996).

[331] Kim S. and Lee T. A., *Synlett.* **950** (1997).

[332] De Smaele D., Bogaert P., and De Kimpe N., *Tetrahedron Lett.* **39**, pp. 9797 (1998).

[333] Dowd P. and Zhang W., *Chem. Rev.* **93**, pp. 2091 (1993).

[334] Harling J. D. and Motherwell W. B., *J. Chem. Soc., Chem. Commun.* **1380** (1988).

[335] Jorgenson W. L. and Laird R. E., *J. Org. Chem.* **55**, pp. 9 (1990).

[336] Marples B. A. and Toon R. C., *Tetrahedron Lett.* **40**, pp. 4873 (1999).

[337] Pasto D. J., *J. Org. Chem.* **61**, pp. 252 (1996).

[338] Ramaiah M., *Tetrahedron* **43**, pp. 3541 (1987).

[339] Bowman W. R., Brown D. S., Burns C. A., Marples B. A., and Zaida N. A., *Tetrahedron* **48**, pp. 6883 (1992).

[340] Beckwith A. L. J., Easton C. J., and Serelis A. K., *J. Chem. Soc. , Chem. Commun.* **482** (1980).

[341] Spellmeyer D. C. and Houk K. N., *J. Org. Chem.* **52**, pp. 959 (1987).

[342] Broeker J. L. and Houk K. N., *J. Org. Chem.* **56**, pp. 3651 (1991).

[343] Allinger N. A., *J. Am. Chem. Soc.* **99**, pp. 8127 (1977).

[344] Beckwith A. L. J. and Schiesser S. H., *Tetrahedron* **41**, pp. 3952 (1985).

[345] Bennasar M.-L., Juan C., and Bosch J., *Chem. Commun.* **2459** (2000).

[346] Ellis D. A., Hart D. J., and Zhao L., *Tetrahedron Lett.* **41**, pp. 9357 (2000).

[347] Snider B. B. and Buckman B. O., *J. Org. Chem.* **57**, pp. 4883 (1992).

[348] Haney B. P. and Curran D. P., *J. Org. Chem.* **65**, pp. 2007 (2000).

[349] Walling C. and Cioffari A., *J. Am. Chem. Soc.* **94**, pp. 6059 (1972).

A

Overzicht

A.1 Algemene inleiding

In dit doctoraatswerk worden chemische reacties, die voorkomen in uiteenlopende domeinen, gemodelleerd en hun eigenschappen worden bestudeerd gebruik makend van theoretische berekeningen. In dit opzicht leidde de toepassing van kwantummechanica tot een grote vooruitgang en meer inzicht in het proces van chemische binding. De eerste belangrijke mijlpaal binnen het onderzoeksgebied van chemische reactiviteit was de ontwikkeling van de Lewistheorie, die later veralgemeend werd door Coulson en Longuet-Higgins. Vervolgens werden symmetrieregels in rekening gebracht om het verloop van een reactie te voorspellen. De grensorbitaaltheorie (FMO) van Fukui en de Woodward-Hoffmann-regels kunnen in dit kader gesitueerd worden. Pearson postuleerde, zich baserend op experimentele gegevens, het hard/zacht zuur/base (HSAB) principe om de stabiliteit van gevormde chemische species te verklaren.

Op dit ogenblik is een brede waaier aan technieken voorhanden om moleculaire systemen en chemische reacties te bestuderen. Essentieel voor een dergelijke beschrijving zijn ab initio-methoden, waarmee zonder enige empirische input de grondtoestandsenergie en verschillende fysische en chemische eigenschappen kunnen berekend worden. Binnen deze ab initio-methoden kan een onderscheid gemaakt worden tussen op de golffunctie gebaseerde technieken (zoals Hartree-Fock) en dichtheidsfunctionaaltheorie (DFT). Beide veeldeeltjestechnieken hebben een enorme impact gehad op de ontwikkeling van de moderne chemie en de protagonisten ervan – Prof. J. A. Pople en Prof. W. Kohn – werden in 1998 onderscheidden met de Nobelprijs voor de Chemie.

In deze doctoraatsthesis wordt in hoofdzaak DFT gebruikt omdat deze methode een sterk theoretisch kader vormt voor de introductie van belangrijke chemische concepten, zoals de chemische potentiaal, hardheid en zachtheid.

Deze veeldeeltjestechniek is tevens een belangrijk computationeel werktuig, aangezien er accurate en betrouwbare resultaten bekomen worden tegenover een haalbare computationele inspanning. DFT is gebaseerd op de basistheorema's van Hohenberg en Kohn en de introductie van ééndeeltjesorbitalen door Kohn en Sham zorgde voor een praktisch berekeningsschema, waarin de enige onbekende de exchange-correlatie functionaal is.

Binnen DFT kan elke chemische reactie beschreven worden aan de hand van veranderingen in de ééndeeltjeselektronendichtheid. Het is echter eenvoudiger om, in plaats van de elektronendichtheid, de externe potentiaal en het totaal aantal elektronen als basisveranderlijken te beschouwen. Veranderingen in deze basisgrootheden stellen 'universele' of 'model'storingen voor en beschrijven de essentie van een chemische reactie zodat er geen verdere details omtrent het aanvallend species nodig zijn. De responsfuncties van de totale elektronenenergie ten gevolge van veranderingen in de kernconfiguratie (corresponderend met de externe potentiaal) en/of het totale aantal elektronen worden bijgevolg gedefinieerd als reactiviteitsdescriptoren. Aangezien de indicatoren overeenstemmen met de eerste termen van een Taylorexpansie in de elektronenenergie zullen zij het meest betrouwbaar zijn indien de perturbaties zwak zijn, zodanig dat hogere-orde effecten verwaarloosd kunnen worden.

Chemische reactiviteit wordt traditioneel gezien beschreven a.d.h.v. thermodynamische en kinetische grootheden, zoals reactiebarrières, reactie-enthalpieën en snelheidscoëfficiënten. Een brede waaier aan geavanceerde veeldeeltjesmethoden werd ontwikkeld en getest om accurate resultaten te bekomen voor deze grootheden. De enorme vooruitgang op het gebied van computercapaciteit maakt het mogelijk om ook grote systemen te onderzoeken, die belangrijk zijn op wetenschappelijk en industrieel gebied. Snelheidscoëfficiënten worden in hoofdzaak berekend via transitietoestandstheorie (TST) of uitbreidingen ervan. De methode is conceptueel vrij eenvoudig en maakt gebruik van de statische eigenschappen van 3 afzonderlijke toestanden van het systeem, nl. de reactanten, producten en transitietoestand.

Chemische reactiviteit kan dus enerzijds bestudeerd worden d.m.v. grootheden afgeleid uit thermodynamica en kinetiek en anderzijds door gebruik te maken van DFT-gebaseerde reactiviteitisdescriptoren. In dit doctoraatswerk wordt uitvoerig nagegaan in welke mate beide beschrijvingen complementair zijn. Het is aangewezen om initieel de voor- en nadelen van conceptuele DFT te bespreken. Een belangrijk voordeel is dat de nodige berekeningen computationeel veel minder intensief – maar uiteraard ook minder gedetailleerd – zijn aangezien enkel de reactanten bestudeerd worden. Er mag bijgevolg enkel informatie over het begin van de reactie verwacht worden en de indicatoren zullen vooral succesvol zijn in het geval van een transitietoestand die gelijkaardig is aan de reactanten en waarbij er tijdens het verdere verloop van de reactie weinig reorganisatie optreedt. Een ander voordeel is dat de indicatoren regioselectiviteit kunnen beschrijven, m.a.w. op basis van de reactanten kan er voorspeld worden waar een chemische reactie preferentieel zal door-

gaan. Een laatste belangrijke troef is het ruime toepassingsgebied van deze grootheden, aangezien er geen beperkingen zijn op de bestudeerde species of reacties. Ui-teraard kent conceptuele DFT ook minpunten. In de eerste plaats is het nog steeds onduidelijk wanneer de indicatoren succesvol kunnen toegepast worden en wanneer niet. Tot op heden is hun voorspellende waarde bijgevolg nog steeds beperkt en dikwijls worden ze in hoofdzaak complementair aan de traditionele beschrijving gebruikt. Reactiviteitsdescriptoren zijn waardevol op kwalitatief gebied en zij worden dan ook voornamelijk aangewend om reactiviteitstendensen te bespreken. Daarentegen kunnen zij niet gebruikt worden om accurate, kwantitatieve data te bekomen.

De toepasbaarheid en het interpretatief nut van DFT-gebaseerde reactiviteitsindicatoren wordt gedetailleerd bestudeerd voor verschillende chemische systemen en bijhorende reacties. De gekozen toepassingen kaderen binnen de verschillende onderzoeksdomeinen waarin het Centrum voor Moleculaire Modellering (hoofd Prof. M. Waroquier) werkzaam is en kunnen in 3 ruime categorieën verdeeld worden. De eerste categorie bevat radicalaire reacties. Er werden voornamelijk reacties bestudeerd die bijdragen tot de groei van een grafietachtige cokeslaag aan de binnenwand van een thermische krakingsoven. Dit onderzoekswerk werd uitgevoerd in samenwerking met het Laboratorium voor Petrochemische Techniek van de Universiteit Gent (hoofd Prof. G. B. Marin). Voor een welbepaald type van radicalaire reacties werden accurate en betrouwbare thermodynamische en kinetische grootheden bepaald. Dit werk gebeurde in samenwerking met de onderzoeksgroep van Prof. L. Radom (School of Chemistry, University of Sydney), die een autoriteit is binnen het onderzoek van radicalaire reacties en de bepaling van geschikte theoretische methoden om deze interacties te beschrijven. In een beperkte mate werden ook vrije radicalaire polymerizatiereacties bestudeerd. Het testen van de reactiviteitsindicatoren gebeurde in samenwerking met Prof. P. Geerlings en Prof. F. De Proft (Eenheid Algemene Chemie, Vrije Universiteit Brussel), die een ruime expertise bezitten op het gebied van conceptuele DFT. De grote uitdaging ligt in de vraag of de reactiviteitsindicatoren geschikte grootheden zijn om het gedrag van radicalaire systemen te bestuderen. De ladingstransfer tussen een radicaal en een neutrale molecule is nl. een complexer fenomeen dan de overdracht tussen twee ionen, twee neutrale systemen of een ion en een neutraal systeem. In de literatuur werd er tot op heden nog weinig onderzoek verricht naar de toepasbaarheid van conceptuele DFT voor radicalaire systemen en/of reacties. Het belangrijke HSAB-principe werd bijvoorbeeld vooral bestudeerd voor typische, anorganische Lewis zuur-base reacties.

De tweede categorie zijn typische reacties die kaderen binnen het domein van de heterogene katalyse over zeolieten. Deze systemen zijn microporeuze materialen waarbij chemische reacties optreden in de poriën. Er wordt nagegaan tot welke categorie, nl. zacht-zacht of hard-hard, deze reacties behoren en welke effecten (covalente, elektrostatische, ...) de interacties domineren.

Het derde en laatste toepassingsluik bevat cyclisatiereacties, waarbij zowel

een ionaire als een radicalaire ringsluiting wordt bestudeerd. Deze voorbeelden vormen een nieuwe uitdaging voor de reactiviteitsindicatoren wegens het unimoleculaire karakter van de reacties. Binnen dit onderzoeksluik werd er samengewerkt met de onderzoeksgroepen van Prof. C. V. Stevens en Prof. N. De Kimpe van de Universiteit Gent. Additioneel werden sommige van deze ringsluitingen onderzocht gebruik makend van spinindicatoren, in samenwerking met de onderzoeksgroep van Prof. P. Geerlings en Prof. F. De Proft.

In het vervolg van deze nederlandstalige samenvatting wordt een kort theoretisch overzicht gegeven van de grootheden die gebruikt worden in dit werk. Vervolgens worden de belangrijkste resultaten voor de 3 toepassingsluiken besproken. De gedetailleerde uitwerking kan teruggevonden worden in deel II, waarin de originele artikels weergegeven worden. Deze samenvatting wordt afgesloten met een algemeen besluit en perspectieven voor verder onderzoek.

A.2 Theoretische achtergrond

A.2.1 DFT-gebaseerde reactiviteitsindicatoren

De reactiviteitsindicatoren bestudeerd in deze thesis representeren de respons van een systeem t.o.v. een welbepaalde perturbatie, i.h.b. de verandering van het totale aantal elektronen N of de kernconfiguratie (corresponderend met de externe potentiaal $v(\mathbf{r})$). De indicatoren worden bijgevolg gedefinieerd als functionele afgeleiden van de totale elektronenenergie $E[N, v(\mathbf{r})]$ naar N (bij constante $v(\mathbf{r})$) of naar $v(\mathbf{r})$ (bij constante N). Tabel A.1 geeft de responsfuncties tot op tweede orde weer.

					$E[N, v(\mathbf{r})]$					
			↙				↘			
n=1			μ						$\rho(\mathbf{r})$	
	↙			↘			↙			↘
n=2	η				$f(\mathbf{r})$					$\chi_1(\mathbf{r}, \mathbf{r}')$
	↙	≡	$(\frac{\partial}{\partial N})_{v(\mathbf{r})}$		en		↘	≡	$(\frac{\partial}{\partial v(\mathbf{r})})_N$	

Tabel A.1: Schematisch overzicht van de reactiviteitsindicatoren.

De afleidbaarheid naar N vergt extra aandacht omdat voor reële systemen, zoals geïsoleerde atomen en moleculen, N noodzakelijkerwijs een natuurlijk getal is. Drie afzonderlijke klassen verschijnen, corresponderend met een nucleofiele ($dN > 0$), electrofiele ($dN < 0$) of radicalaire ($dN = 0$) aanval. De uitbreiding naar fractionele waarden van N werd uitgebreid bestudeerd en er werd aangetoond dat de E versus N curve stuksgewijze linear is. In de praktijk wordt er gebruik gemaakt van een Taylorexpansie van de energiefunctionaal getrunceerd op tweede orde (kwadratische interpolatie).

Tabel A.1 geeft duidelijk aan dat er een onderscheid kan gemaakt worden tussen drie categorieën: globale indicatoren, lokale indicatoren en kernels. De eerste groep beschrijft het reactief gedrag van een molecule in zijn totaliteit en wordt gebruikt om een verzameling van gelijkaardige moleculen onderling te vergelijken. De tweede groep bevat plaatsafhankelijke informatie en geeft aan waar de reactieve sites zich bevinden. De derde groep ten slotte zijn grootheden die afhankelijk zijn van twee plaatscoördinaten, die geassocieerd kunnen worden met een lokale respons (op plaats $\mathbf{r}$) ten gevolge van een lokale perturbatie (op plaats $\mathbf{r}'$).

Globale indicatoren

De eerste orde afgeleide van $E[N, v(\mathbf{r})]$ naar N, bij constante $v(\mathbf{r})$, is de *chemische potentiaal* μ. Deze grootheid beschrijft de ontsnappingsneiging van de elektronenwolk uit een evenwichtstoestand. De chemische potentiaal geeft een interpretatie aan de Lagrangevermenigvuldiger optredend in de Eulervergelijking zoals die voorkomt in het DFT formalisme ($v(\mathbf{r}) + \frac{\partial F_{HK}[\rho]}{\partial \rho(\mathbf{r})} = \mu$). Daarnaast is μ equivalent met een welgekend en belangrijk chemisch concept, nl. de electronegativiteit χ ($\mu = -\chi$).

De tweede orde afgeleide van $E[N, v(\mathbf{r})]$ naar N, bij constante $v(\mathbf{r})$, is de *globale hardheid* η. Deze grootheid drukt de weerstand tegenover ladingstransfer uit. Gebruik makend van het theorema van Koopmans kan aangetoond worden dat de globale hardheid overeenstemt met de energiekloof tussen de bezette en onbezette orbitalen. De *globale zachtheid* S is de reciproke grootheid van de globale hardheid en kan gerelateerd worden aan de polariseerbaarheid van een systeem. De definities voor de globale hardheid en zachtheid vormden een belangrijke stap voorwaarts in de studie van Lewis zuur-base reacties.

	Definitie	FD methode	Koopmans' theorema
μ	$(\frac{\partial E}{\partial N})_{v(\mathbf{r})}$	$-\frac{1}{2}(IP + EA)$	$\frac{1}{2}(\epsilon_{\text{HOMO}} + \epsilon_{\text{LUMO}})$
η	$\frac{1}{2}(\frac{\partial^2 E}{\partial N^2})_{v(\mathbf{r})} = \frac{1}{2}(\frac{\partial \mu}{\partial N})_{v(\mathbf{r})}$	$\frac{1}{2}(IP - EA)$	$\frac{1}{2}(\epsilon_{\text{LUMO}} - \epsilon_{\text{HOMO}})$
S	$\frac{1}{2\eta} = (\frac{\partial N}{\partial \mu})_{v(\mathbf{r})}$	$(IP - EA)^{-1}$	$(\epsilon_{\text{LUMO}} - \epsilon_{\text{HOMO}})^{-1}$

Tabel A.2: Definities en eenvoudige berekeningsmethoden voor globale reactiviteitsindicatoren.

In deze thesis worden bovenstaande grootheden berekend d.m.v. de eindige-differentiemethode (finite difference = FD), waarbij de basisveranderlijken de vertikale ionisatiepotentiaal (IP) en elektronenaffiniteit (EA) zijn. Een nadeel van deze methode is dat er drie energieberekeningen nodig zijn, nl. op het N-, het $N+1$- en het $N-1$-systeem. Een extra probleem kan opduiken i.v.m. de stabiliteit van het $N+1$- en/of $N-1$-systeem. Vandaar is het soms aangewezen om, in navolging van het theorema van Koopmans, gebruik te maken van de

energie van de grensorbitalen (HOMO=highest occupied molecular orbital en LUMO=lowest unoccupied molecular orbital). Tabel A.2 geeft een overzicht van de besproken globale indicatoren en hun berekeningsmethoden.

Lokale indicatoren

De eerste orde afgeleide van $E[N, v(\mathbf{r})]$ naar $v(\mathbf{r})$, bij constante N, is de *elektronendichtheid* $\rho(\mathbf{r})$. De *vormfactor* $\sigma(\mathbf{r}) = \rho(\mathbf{r})/N$ beschrijft relatieve informatie omtrent de elektronendichtheid.

De tweede orde gemengde afgeleide van $E[N, v(\mathbf{r})]$ is de Fukui functie $f(\mathbf{r})$:

$$f(\mathbf{r}) = (\frac{\partial^2 E}{\partial N \partial v(\mathbf{r})}) = (\frac{\partial \rho(\mathbf{r})}{\partial N})_{v(\mathbf{r})} = (\frac{\partial \mu}{\partial v(\mathbf{r})})_N.$$

Deze grootheid is genormaliseerd op 1 en kan beschouwd worden als een intramoleculaire descriptor. De Fukui functie veralgemeent de grensorbitaaltheorie (frontier molecular orbital theory = FMO), die door Kenichi Fukui ontwikkeld werd en waarin het belang van de grensorbitalen HOMO en LUMO benadrukt wordt. Voor een nucleofiele, respectievelijk electrofiele en radicalaire aanval bekomt men:

$$\begin{aligned} f^+(\mathbf{r}) &\approx \rho_{N+1}(\mathbf{r}) - \rho_N(\mathbf{r}) \approx \rho_{\text{LUMO}}, \\ f^-(\mathbf{r}) &\approx \rho_N(\mathbf{r}) - \rho_{N-1}(\mathbf{r}) \approx \rho_{\text{HOMO}}, \\ f^0(\mathbf{r}) &\approx (\rho_{N+1}(\mathbf{r}) - \rho_{N-1}(\mathbf{r}))/2 \approx (\rho_{\text{LUMO}} + \rho_{\text{HOMO}})/2. \end{aligned}$$

De lokale zachtheid $s(\mathbf{r})$ is een andere veelgebruikte lokale descriptor, die intermoleculaire reactiviteit kan beschrijven aangezien hij informatie van $f(\mathbf{r})$ aanvult met globale informatie (S):

$$s(\mathbf{r}) = (\frac{\partial \rho(\mathbf{r})}{\partial \mu})_{v(\mathbf{r})} = Sf(\mathbf{r}).$$

Deze drie-dimensionele grootheden kunnen gevisualiseerd worden d.m.v. iso-oppervlakken. Deze oppervlakken zijn echter dikwijls moeilijk te interpreteren en daarom gebruikt men in de praktijk gecondenseerde descriptoren die een benaderende waarde op de plaats van een atomair centrum voorstellen:

$$\begin{aligned} f_k^+ &= \tilde{q}_k(N+1) - \tilde{q}_k(N) \text{ en } s_k^+ = S(\tilde{q}_k(N+1) - \tilde{q}_k(N)), \\ f_k^- &= \tilde{q}_k(N) - \tilde{q}_k(N-1) \text{ en } s_k^- = S(\tilde{q}_k(N) - \tilde{q}_k(N-1)), \\ f_k^0 &= (\tilde{q}_k(N+1) - \tilde{q}_k(N-1))/2 \text{ en } s_k^0 = S(\tilde{q}_k(N+1) - \tilde{q}_k(N-1))/2. \end{aligned}$$

In deze uitdrukkingen stelt $\tilde{q}_k(N)$ de elektronenpopulatie voor van atoom k van de molecule met N elektronen. Deze populatie kan volgens verschillende schema's berekend worden; de bekendste zijn Mulliken, Natural Population Analysis (NPA), Hirshfeld, AIM en technieken gebaseerd op een fitting aan de elektrostatische potentiaal (CHELPG, MK,...).

Spin-gepolariseerde indicatoren

De traditionele formulering van DFT kan uitgebreid worden naar een spin-gepolariseerde vorm, die gebruikt wordt om systemen met een algemenere potentiaal te beschrijven. Er kan b. v. een magnetisch veld $B(\mathbf{r})\mathbf{e}_z$ toegevoegd worden aan de scalaire potentiaal $v(\mathbf{r})$. De totale elektronenenergie kan vervolgens uitgedrukt worden in termen van de elektronendichtheid $\rho(\mathbf{r})$ en de spindichtheid $\rho_S(\mathbf{r})$:

$$E[\rho(\mathbf{r}),\rho_S(\mathbf{r})] \quad = \quad F[\rho(\mathbf{r}),\rho_S(\mathbf{r})] + \int \rho(\mathbf{r})v(\mathbf{r})d\mathbf{r} - \mu_B \int B(\mathbf{r})\rho_S(\mathbf{r})d\mathbf{r},$$

met $F[\rho(\mathbf{r}),\rho_S(\mathbf{r})]$ de universele functionaal en μ_B het Bohr magneton. Ook binnen dit spin-gepolariseerde formalisme kunnen er responsfuncties gedefinieerd worden die overeenstemmen met veranderingen in N, N_S (het spingetal, gelijk aan het verschil van aantal spin-up en het aantal spin-down elektronen), $v(\mathbf{r})$ en $\mathbf{B}(\mathbf{r})$. Een overzicht van de belangrijkste indicatoren wordt gegeven in Tabel A.3.

Globale indicatoren	Lokale indicatoren
$\mu_N = (\frac{\partial E}{\partial N})_{N_S,v(\mathbf{r}),\mathbf{B}(\mathbf{r})}$	$\rho(\mathbf{r}) = (\frac{\partial E}{\partial v(\mathbf{r})})_{N,N_S,\mathbf{B}(\mathbf{r})}$
$\mu_S = (\frac{\partial E}{\partial N_S})_{N,v(\mathbf{r}),\mathbf{B}(\mathbf{r})}$	$\rho_S(\mathbf{r}) = -\frac{1}{\mu_B}(\frac{\partial E}{\partial \mathbf{B}(\mathbf{r})})_{N,N_S,v(\mathbf{r})}$
$\eta_{NN} = (\frac{\partial \mu_N}{\partial N})_{N_S,v(\mathbf{r}),\mathbf{B}(\mathbf{r})}$	$f_{NN}(\mathbf{r}) = (\frac{\partial \mu_N}{\partial v(\mathbf{r})})_{N,N_S,\mathbf{B}(\mathbf{r})}$
$\eta_{NS} = (\frac{\partial \mu_N}{\partial N_S})_{N,v(\mathbf{r}),\mathbf{B}(\mathbf{r})}$	$f_{SN}(\mathbf{r}) = (\frac{\partial \mu_N}{\partial \mathbf{B}(\mathbf{r})})_{N,N_S,v(\mathbf{r})} = -\mu_B(\frac{\partial \rho_S}{\partial N_S})_{N,v(\mathbf{r}),\mathbf{B}(\mathbf{r})}$
$= (\frac{\partial \mu_S}{\partial N})_{N_S,v(\mathbf{r}),\mathbf{B}(\mathbf{r})} = \eta_{SN}$	
$\eta_{SS} = (\frac{\partial \mu_S}{\partial N_S})_{N,v(\mathbf{r}),\mathbf{B}(\mathbf{r})}$	$f_{NS}(\mathbf{r}) = (\frac{\partial \mu_S}{\partial v(\mathbf{r})})_{N,N_S,\mathbf{B}(\mathbf{r})} = (\frac{\partial \rho}{\partial N_S})_{N,v(\mathbf{r}),\mathbf{B}(\mathbf{r})}$
	$f_{SS}(\mathbf{r}) = (\frac{\partial \mu_S}{\partial \mathbf{B}(\mathbf{r})})_{N,N_S,v(\mathbf{r})} = -\mu_B(\frac{\partial \rho_S}{\partial N_S})_{N,v(\mathbf{r}),\mathbf{B}(\mathbf{r})}$

Tabel A.3: Definities van spin-gepolariseerde indicatoren.

Veranderingen in N corresponderen met ladingstransfer, terwijl veranderingen in N_S spintransfer beschrijven. De grootheden μ_N en μ_S stellen de chemische en spin potentiaal voor. Merk op dat μ_N, η_{NN} en $f_{NN}(\mathbf{r})$ analoog zijn aan μ, η en $f(\mathbf{r})$ gedefinieerd binnen het niet-gepolariseerde formalisme, hier wordt echter N_S constant gehouden bij het nemen van de afgeleide.

Aromaticiteitsindicatoren

Parr toonde aan dat de globale hardheid ook gebruikt kan worden om aromaticiteit te beschrijven, beide begrippen zijn immers een maatstaf voor een hoge stabiliteit/lage reactiviteit. In het toepassingsluik van dit doctoraatswerk worden verschillende polyaromatische systemen uitvoerig bestudeerd en enkele belangrijke magnetische descriptoren – de magnetische anisotropie $\Delta\chi$, chemische shift δ en de Nucleus Independent Chemical Shift (NICS) – worden hiervoor berekend. In tegenstelling tot de NICS, beschrijven $\Delta\chi$ en δ in hoofdzaak

lokale effecten. Het gebruik van NICS als aromaticiteitscriterium kent de laatste jaren een enorme opmars.

A.2.2 Implementatie in belangrijke chemische principes

Bovenstaande definities voor de DFT-gebaseerde reactiviteitsindicatoren zorgen ervoor dat verschillende goedgekende, experimenteel vastgestelde, chemische principes nu ook kwalitatief – en tot op zekere hoogte kwantitatief – getest kunnen worden.

Principe van equalisatie van de electronegativiteit

Sanderson postuleerde dat bij de vorming van een nieuwe molecule, de electronegativiteiten van de samenstellende atomen equaliseren, resulterend in een karakteristieke moleculaire electronegativiteit die het geometrische gemiddelde is van de originele atomaire waarden. Dit model beschouwt enkel veranderingen in N en verwaarloost bijgevolg verscheidene andere perturbaties. Binnen deze benadering is de elektronenstroom ΔN proportioneel met $\Delta\chi$ (of $\Delta\mu$), terwijl de bindingsenergie ΔE kwadratisch is in $\Delta\chi$. Het hoofddoel van dit principe is het bekomen van moleculaire ladingsverdelingen aan een relatief lage computationele kost. De initiële formulering kent echter aan alle atomen van een welbepaald element dezelfde lading toe en dit beperkt de toepasbaarheid ervan. Meer gesofisticeerde schema's werden ontwikkeld en getest, waaronder de electronegativity equalization method (EEM) van Mortier en medewerkers.

HSAB-principe

Pearson postuleerde het hard/zacht zuur/base principe (hard/soft acids and bases = HSAB): harde zuren verkiezen te reageren met harde basen (meestal leidend tot een chemische binding met een ionair karakter) en zachte zuren verkiezen te reageren met zachte basen (meestal leidend tot een chemische binding met een covalent karakter). Dit principe kan zowel op een globaal als een lokaal niveau toegepast worden. De invoering van de definities voor hardheid en zachtheid binnen het DFT-kader maakte een theoretische bewijsvoering mogelijk. De eerste inspanningen hieromtrent, gebaseerd op de minimalisatie van de bindingsenergie ΔE, houden enkele (te) sterke vereenvoudigingen in. De bindingsenergie bestaat uit verschillende contributies en in de oorspronkelijke bewijsvoering wordt echter enkel rekening gehouden met de covalente bijdrage (en de elektrostatische en polarisatiebijdragen worden verwaarloosd). Deze covalente term kan opgesplitst worden in een ladingstransfer- en een reshuffling-term. Recentelijk werd aangetoond dat het HSAB-principe in essentie een effect is van ladingstransfer. Gebruik makend van de dubbele uitwisselingsreactie ($A_hB_s + A_sB_h \rightleftarrows A_hB_h + A_sB_s$) werd aangetoond dat zacht-zacht pro-

ducten inderdaad gestabiliseerd worden door ladingstransfer, terwijl de hard-hard producten gestabiliseerd worden door elektrostatische interacties. Deze classificatie is duidelijk gelijkaardig aan deze van Klopman, die een onderscheid maakte tussen grensorbitaal-gecontroleerde en ladingsgecontroleerde reacties.

Principe van maximale hardheid

Pearson postuleerde het principe van maximale hardheid (principle of maximal hardness = PMH): moleculen (her)organiseren zichzelf zodanig dat zij een maximale hardheid bezitten. De oorspronkelijke bewijsvoering van dit principe veronderstelt dat μ en $v(\mathbf{r})$ constant zijn. Deze onrealistische vereiste blijkt echter niet cruciaal te zijn, aangezien het principe reeds voor tal van systemen werd aangetoond. Het PMH-principe kan (net zoals het HSAB-principe) aagewend worden om de richtingsafhankelijkheid van de reactie aan te duiden. In die gevallen waar het berekenen van de hardheid problematisch is, biedt het gelijkaardige principe van minimale polariseerbaarheid een alternatief. Verder volgt uit het principe van maximale hardheid dat de transitietoestand van een reactie gekenmerkt wordt door een minimale hardheid. Hardheidsvariaties langs het reactiepad kunnen bestudeerd worden gebruik makend van de activeringshardheid:

$$\Delta\eta_{\text{act}} = \eta_{\text{reactant}} - \eta_{\text{transitietoestand}}.$$

Hoe kleiner $\Delta\eta_{\text{act}}$, hoe sneller de reactie verloopt.

A.2.3 Chemische kinetiek

De meer traditionele en gekende aanpak om een chemische reactie te bestuderen bestaat erin de snelheidscoëfficiënt $k(T)$ te berekenen. De populairste berekeningsmethode is transitietoestandstheorie (TST) en dit vanwege zijn conceptuele eenvoud. Dit model maakt verschillende veronderstellingen. Ten eerste wordt de faseruimte tussen de reactanten en de producten verdeeld door een oppervlak dat het pad van minimale energie doorsnijdt op de transitietoestand. Dit punt is een eerste orde zadelpunt: de energie bereikt er een maximale waarde in de reactiecoördinaat, terwijl alle andere vrijheidsgraden er minimaal zijn. Vervolgens wordt aangenomen dat elk traject (vertrekkende van de reactanten) dat het verdelend oppervlak doorsnijdt, doorreageert naar de producten. Ten slotte wordt verondersteld dat de evenwichtsenergieverdeling van de reactanten een Boltzmannverloop volgt. Gebruik makend van bovenstaande veronderstellingen kan men afleiden dat de snelheidsconstante voor een bimoleculaire reactie $A + B \rightarrow C + D$ gegeven wordt door:

$$k(T) \quad = \quad \frac{k_B T}{h} \frac{q_{\ddagger}/V}{(q_A/V)(q_B/V)} \mathrm{e}^{-\frac{\Delta E_0^{\ddagger}}{k_B T}},$$

met k_B de Boltzmann constante, h de constante van Planck, V het referentievolume waarin het translationeel gedeelte van de partitiefunctie geëvalueerd wordt, q_A, q_B en $q_\ddagger$ de moleculaire partitiefuncties van de reactanten (A en B) en de transitietoestand (TS), en $\Delta E_0^\ddagger$ het ZPVE-gecorrigeerde energieverschil tussen de TS en de reactanten (i.e. de reactiebarrière) op 0 K. Dit eenvoudige model heeft beperkingen, waaronder het niet in rekening brengen van recrossing en kwantummechanische tunneleffecten. Correcties voor dit laatste effect worden in de volgende paragraaf besproken.

De microscopische grootheden (q en $\Delta E_0^\ddagger$) kunnen in verband gebracht worden met macroscopische eigenschappen (nl. de pre-exponentiële factor A en de activeringsenergie E_a), die optreden in de Arrhenius snelheidswet:

$$k(T) \quad = \quad A \exp(-\frac{E_a}{RT}),$$

met R de universele gasconstante. A en E_a worden bekomen door een lineaire fitting van $\ln k(T)$ versus $1/T$ te berekenen en vervolgens het intercept met de $\ln k(T)$-as, respectievelijk de helling, te nemen.

Accurate resultaten voor $k(T)$ worden bekomen door gebruik te maken van geavanceerde ab initio-methoden voor de berekening van bovenstaande microscopische grootheden. In de volgende paragrafen worden twee verfijningen aan de originele formulering besproken.

Tunneleffect

Het kwantummechanische tunneleffect (doorheen de potentiële energiebarrière) wordt in rekening gebracht door de transmissiecoëfficiënt $\kappa(T)$. Deze factor houdt rekening met het tunnelen van deeltjes met een energie die lager is dan de energiebarrière, alsook met de niet-klassieke reflectie van deeltjes met een energie hoger dan de barrière. Het tweede effect correspondeert met destructieve interferentie waardoor de reactie niet doorgaat. De tunnelingsbijdrage is dominant, aangezien de lage energietoestanden een grotere bezetting kennen. Bijgevolg zorgen de correcties ervoor dat de snelheidscoëfficiënt toeneemt ($\kappa(T) > 1$). De algemene uitdrukking is:

$$\kappa(T) \quad = \quad \frac{\int_{E=0}^{\infty} P(E) \mathrm{e}^{-\frac{E}{k_B T}} dE}{\int_{E^\ddagger}^{\infty} \mathrm{e}^{-\frac{E}{k_B T}} dE} = \frac{\mathrm{e}^{\frac{E^\ddagger}{k_B T}}}{k_B T} \int_{E=0}^{\infty} P(E) \mathrm{e}^{-\frac{E}{k_B T}} dE,$$

met $E^\ddagger$ de drempelenergie en $P(E)$ de transmissiewaarschijnlijkheid.

Er zijn verschillende benaderingen mogelijk voor de berekening van $\kappa(T)$, o.a. de eenvoudige methoden van Wigner en Eckart. Binnen het Wignerschema wordt de werkelijke energiebarrière gemodelleerd door een parabolische variant en $\kappa(T)$ wordt berekend door enkel gebruik te maken van de imaginaire frequentie van de TS. Deze methode houdt echter enkel rekening met bijdragen

aan de top van de barrière en bijgevolg wordt het tunneleffect onderschat. De Eckartbenadering hanteert een realistischere exponentiële fit voor de barrière en voor de berekening van $\kappa(T)$ dient men opnieuw enkel gebruik te maken van eigenschappen van de stationaire punten langs het reactiepad. In tegenstelling tot de Wignerbenadering zorgt het Eckartmodel dikwijls voor een overschatting van de kwantummechanische tunneling.

Interne rotaties

Een andere verfijning kan aangebracht worden bij de berekening van de rotationele bijdrage q_{rot} van de moleculaire partitiefuncties q. Meer in het bijzonder kunnen de bewegingen die overeenstemmen met interne rotaties in de molecule correcter in rekening worden gebracht. De totale partitiefunctie kan geschreven worden als:

$$q = q_{elec} q_{trans} q_{rot} q_{vib}.$$

Binnen de harmonische-oscillatorbenadering (HO) worden alle vibrationele modes benaderd als onafhankelijke harmonische oscillatoren, waarbij enkel kleine afwijkingen vanuit een evenwichtsstructuur toegelaten zijn. Verder is de potentiële energie kwadratisch in alle variabelen. Voor elke vibrationele mode i (met $i = 1, \ldots, 3N-6$ voor een niet-lineaire molecule) heeft men:

$$q_{vib,i} = \frac{\mathrm{e}^{-\frac{h\nu_i}{2k_BT}}}{1-\mathrm{e}^{-\frac{h\nu_i}{k_BT}}}.$$

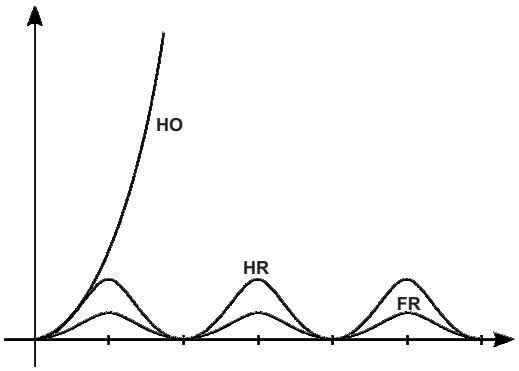

Figuur A.1: Potentiële energiecurve, overeenstemmend met verschillende beschrijvingen van de interne beweging.

Deze uitdrukking is echter niet geschikt om interne rotaties te beschrijven, aangezien zij overeenstemmen met een anharmonische, niet-kwadratische potentiaal die leidt tot vibraties met een grote amplitude die veel afwijken van

de evenwichtsstructuur. Indien de barrière zeer laag is, kan het extreme model van een vrije rotor (free rotor = FR) gebruikt worden. Voor deze mode wordt de HO-uitdrukking voor de partitiefunctie vervangen door:

$$q_{FR} = \frac{1}{\sigma_{int}}\sqrt{\frac{k_B T \pi}{h\nu}} = \frac{1}{\sigma_{int}}\sqrt{\frac{2k_B T \pi I_m}{\hbar^2}},$$

met symmetriegetal σ_{int} en gereduceerd inertiaalmoment I_m. De intermediaire situatie kan beschreven worden a.d.h.v. een gehinderd-rotormodel (hinderd rotor = HR). De bijhorende partitiefunctie kan als volgt berekend worden:

$$q_{HR} = \frac{1}{\sigma_{int}}\sum_k g_k(m)\exp(-\frac{\epsilon_k(m)}{k_B T}),$$

met $g_k(m)$ de ontaarding van het energieniveau $\epsilon_k(m)$ en σ_{int} het symmetriegetal van de interne rotatie. Bovenstaande uitdrukking is slechts geldig indien alle interne rotaties ontkoppeld worden. Figuur A.1 geeft de curves van de potentiële energie in de reactiecoördinaat weer voor de verschillende beschrijvingen.

Bij analyse van het vibrationeel spectrum van een molecule kunnen sommige laaggelegen modes geïdentificeerd worden als interne rotaties. Deze torsionele modes worden op een specifieke manier behandeld, nl. als FR of HR, terwijl alle andere modes gemodelleerd worden door een harmonische oscillator. Op deze manier wordt dus een gemengd harmonisch oscillator/vrije rotor (HO/FR) of harmonisch oscillator/gehinderd rotor (HO/HR) schema geconstrueerd om de interne bewegingen in de molecule te beschrijven.

A.3 Toepassingen

A.3.1 Radicalaire reacties binnen het cokesmodel

Inleiding

Het stoomkraken of de pyrolyse van koolwaterstoffen wordt beschouwd als één van de belangrijkste industriële processen voor de productie van lichte olefines, zoals etheen en propeen. Het belang van deze species in de chemische industrie dient benadrukt te worden, zo vormen zij o.a. de basisproducten van thermoplastiek, vezels, schuimen, etc. In moderne krakingsraffinaderijen worden koolwaterstofvoedingen – waarbij ethaan en nafta het populairste zijn – gekraakt volgens een complexe cascade van radicalaire reacties. De voeding passeert in een krakingsoven drie delen: een radiatiesectie, een transitiezone en een convectiezone. In de radiatiezone wordt er een koolstofachtig residu gevormd op de binnenwand van de reactorbuizen en dit heeft uiteraard een negatief effect op de efficiëntie van de krakingseenheid. De vorming van deze

grafietachtige residulaag (cokes) is bijgevolg zeer ongewenst, de warmtetoevoer en de inlaatdruk dienen verhoogd te worden om ervoor te zorgen dat de conversie en selectiviteit van het krakingsproces behouden blijft. Finaal dient de oven uit productie genomen te worden voor ontcoking. Tijdens dit proces wordt de cokeslaag van de reactorbuizen afgebrand met een gecontroleerd lucht/stoom mengsel. Experimenteel werd waargenomen dat cokes gevormd kan worden volgens drie verschillende mechanismen. Ten eerste is er een katalytisch proces waarbij er een dunne, vezelachtige laag gevormd wordt op de reactorwand. Vervolgens zorgt een heterogeen, niet-katalytisch vormingsproces voor een dikkere, grafietachtige structuur. Hierbij reageert het cokesoppervlak met precursoren uit de gasfase. Ten slotte kan er ook, maar dit slechts in uitzonderlijke omstandigheden (zeer hoge temperaturen of zeer zware voedingen) een homogeen, niet-katalytisch proces optreden. In de relevante temperatuursintervallen werd waargenomen dat het heterogeen, niet-katalytisch vormingsproces dominant is.

Het Laboratorium voor Petrochemische Techniek (LPT) heeft een lange traditie in de ontwikkeling van single-event microkinetische modellen van belangrijke chemische processen. Het thermisch-krakingsmodel werd reeds uitvoerig bestudeerd, terwijl het cokesvormingsproces tot op heden minder intensief werd onderzocht. De doctoraatsthesis van Dr. S. Wauters vormt een referentiewerk binnen dit gebied: de groei van het cokesnetwerk wordt erin bestudeerd a.d.h.v. een single-event microkinetisch model. Binnen een dergelijk model worden alle mogelijke reacties (> 5000) opgedeeld in een beperkt aantal elementaire klassen. In het specifiek geval van cokesvorming zijn er 5 elementaire klassen: waterstofabstractie, substitutie, additie van een gasfase-olefine aan een oppervlakteradicaal, additie van een gasfaseradicaal aan een olefine en cyclisatie. Figuur A.2 geeft een overzicht van deze verschillende radicalaire reacties die leiden tot de groei van het cokesoppervlak. Het is moeilijk om vanuit experimenteel standpunt inzicht te verkrijgen in individuele reactiestappen en moleculaire modellering kan een toegevoegde waarde bieden. Binnen het Centrum voor Moleculaire Modellering (CMM) werden reeds verschillende studies uitgevoerd om thermodynamische en kinetische grootheden te bepalen voor elementaire reactiestappen binnen het cokesmodel. Het netwerk wordt voorgesteld door een polyaromatische structuur van geconjugeerde benzeenringen. Voor de theoretische berekeningen werd de polyaromatische structuur verwaarloosd en benaderd door één enkele benzeenring. De invloed van de lokale polyaromatische omgeving kan echter in rekening gebracht worden door gebruik te maken van een set van polyaromatische koolwaterstoffen (PAHs). PAHs behoren tot de meest onderzochte chemische systemen aangezien zij in tal van uiteenlopende domeinen (biologie, astrofysica, vorming van fullerenen, etc.) voorkomen. PAHs worden tevens gevormd als intermediaire producten bij de onvolledige verbranding van organische materialen.

De initiële oppervlakteradicalen worden gevormd via waterstofabstracties door precursoren aanwezig in het gasmengsel. Vervolgens hebben er verschillende additiereacties plaats en uiteindelijk zorgt een cyclisatiereactie voor de

vorming van een nieuwe ring, die na dehydrogenatie zorgt voor incorporatie van extra koolstofatomen binnen de reeds gevormde cokeslaag. In dit werk worden drie elementaire reactieklassen die voorkomen in het groeiproces van cokes bestudeerd. Waterstofabstracties door een aanvallend methylradicaal worden in detail onderzocht: de gevoeligheid van verschillende grootheden (i.h.b. reactiebarrière, reactie-enthalpie en snelheidscoëfficiënt) aan het berekeningsniveau voor de geometrieoptimalisatie en elektronische energie wordt bestudeerd en vervolgens wordt de lokale polyaromatische omgeving in rekening gebracht. Ten slotte wordt er bestudeerd of er een correlatie is tussen deze accurate en betrouwbare thermodynamische en kinetische gegevens enerzijds en resultaten gebaseerd op DFT-gebaseerde reactiviteitsdescriptoren anderzijds. Deze strategie wordt eveneens toegepast voor inter- en intramoleculaire additiereacties.

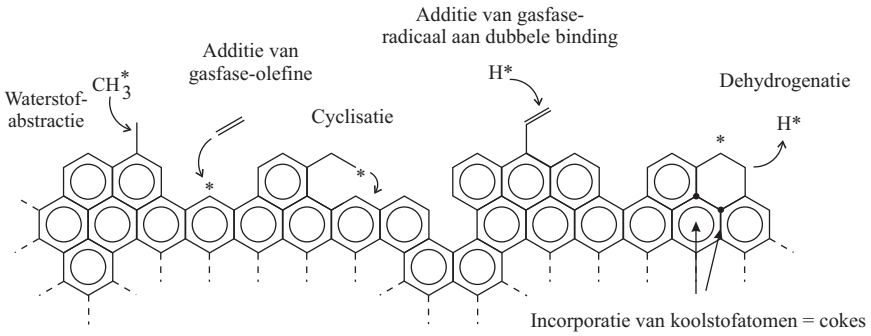

Figuur A.2: Groei van het cokesnetwerk op basis van elementaire reacties.

Radicalaire systemen en bijhorende reacties werden tot op heden weinig bestudeerd d.m.v. reactiviteitsindicatoren. Pionierswerk op vrije radicalen werd verricht door Pearson en een klein aantal studies werd uitgevoerd op het berekenen van globale en lokale indicatoren. Chandra et al. testte de toepasbaarheid van het HSAB-principe voor additiereacties, terwijl Nguyen et al. eveneens waterstofabstracties onderzocht. De recente ontwikkelingen binnen de spin-gepolariseerde formulering van DFT en de daarin ingevoerde definities voor indicatoren maken het mogelijk om spin-polarisatie te beschrijven. Hun toepasbaarheid werd reeds aangetoond voor verschillende reacties.

Waterstofabstractie aan benzeen: invloed van het berekeningsniveau op thermodynamische en kinetische grootheden

De invloed van het berekeningsniveau (Level of Theory=LOT) op de thermodynamische en kinetische parameters van de waterstofabstractie door het methylradicaal aan benzeen wordt nagegaan. Deze reactie vormt de referentie-

reactie voor waterstofabstracties aan polyaromatische structuren opgebouwd uit geconjugeerde zesringen, zoals geïllustreerd in Figuur A.3. Een brede waaier aan ab initio-methodes (DFT en HF/post-HF), in combinatie met verschillende dubbele- en drievoudige-zeta Pople-basissets, wordt onderzocht.

Ten eerste wordt de invloed van het berekeningsniveau op de geometrieoptimalisatie bestudeerd. Hiervoor worden belangrijke geometrische parameters en URCCSD(T)/6-311+G(*d,p*)-enthalpieën en barrières, berekend op de verschillende geoptimaliseerde structuren, met elkaar vergeleken. Ten tweede, gebruik makend van geselecteerde geometrieën, wordt de invloed van het berekeningsniveau op de reactie-enthalpie ΔH_{298} en reactiebarrière $\Delta E_0^{\ddagger}$ nagegaan. Finaal wordt ook de gevoeligheid van de pre-exponentiële factor A, de activeringsenergie E_a en de snelheidscoëfficiënt $k(T)$ aan het gebruikte niveau bestudeerd. Uiteindelijk wordt een niveau geselecteerd dat accurate en betrouwbare resultaten oplevert en dat eveneens computationeel haalbaar is voor berekeningen op grotere, polyaromatische structuren. Geavanceerde composietmethoden, zoals CBS-QB3, G3(MP2)-RAD, G3-RAD en W1, worden eveneens getest.

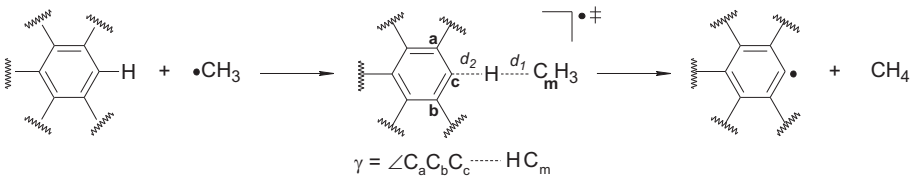

Figuur A.3: Waterstofabstracties door het methylradicaal aan polyaromatische structuren opgebouwd uit geconjugeerde zesringen.

Geometrieën De geoptimaliseerde TS-geometrieën tonen aan dat voor alle niveaus de lengte van de vormende binding kleiner is dan deze van de gebroken binding. Dit stemt overeen met een late TS en met de endothermiciteit van de reactie. Gebruik makend van de URCCSD(T)/6-311+G(*d,p*)-energieën, vertonen de QCISD-, CCSD- en BMK-geometrieën de laagste waarden. Ook de B3-LYP-functionaal leidt tot goede resultaten. De berekende waarden voor ΔH_{298} en $\Delta E_0^{\ddagger}$ tonen een zeer kleine variatie (wegens annulatie van fouten tussen reactanten en producten, resp. reactanten en TSs). HF en bepaalde post-HF-methoden, zoals MP2, falen echter wel tengevolge van zware spincontaminatie in het fenylradicaal en de TS. Samenvattend, de gevoeligheid van de geoptimaliseerde evenwichtsstructuren van de bestudeerde waterstofabstractie aan het berekeningsniveau is zeer beperkt. De populaire B3-LYP- en BMK-functionalen, in combinatie met de 6-31+G(*d,p*) basisset, zijn zeer interessant wegens de lage computationele kost.

Reactie-enthalpieën en barrières Gebruik makend van B3-LYP en BMK (6-31+G(*d,p*)) geoptimaliseerde geometrieën, worden een set van ΔH_{298}- en $\Delta E_0^{\ddagger}$-waarden (inclusief geschaalde ZPVEs en thermische correcties) berekend. De overeenkomst tussen het W1-resultaat voor ΔH_{298} en de experimentele waarde is zeer goed en de W1-methode wordt bijgevolg gekozen als referentiemethode. De overige composietmethoden presteren eveneens bijzonder goed, de CBS-QB3 methode worstelt echter met het probleem van spin-contaminatie in de UMP2 golffunctie. De URCCSD(T)/6-311+G(*3df,2p*)-methode is rekenintensief, maar presteert heel goed. De standaard DFT-methoden vertonen een niet-verwaarloosbaar basisseteffect. De 6-31G(*d*)-basisset is te beperkt om accurate resultaten te produceren, de upgrade naar 6-31+G(*d,p*)-waarden liggen daarentegen reeds veel dichter bij het W1-referentiepunt. De uitgebreide 6-311+G(*3df,2p*)-basisset levert geen substantiële meerwaarde op. De invloed van de functionaal is doorslaggevend: B3-LYP overschat de barrière (dit wordt echter reeds gedeeltelijk gecompenseerd door gebruik te maken van de restricted variant RB3-LYP). De hybride-meta-functionalen BB1K, MPW1K en MPWB1K presteren goed (de MPW1K-resultaten liggen zeer dicht bij de ΔH_{298}-referentiewaarden). In het algemeen presteert de BMK-functionaal het best, resulterend in $\Delta E_0^{\ddagger}$-waarden die minder dan 1 kJ mol^{-1} afwijken van de W1-referentiewaarde.

Kinetische parameters en snelheidscoëfficiënten E_a- en A-waarden worden berekend via TST in het temperatuursgebied 600-800 K, waarin experimentele informatie beschikbaar is. De interne rotatie van de methylgroep rond de vormende binding wordt wegens de zeer lage rotationele potentiaal gemodelleerd als een vrije rotor en bijgevolg wordt een gemengd HO/FR-model gebruikt. Deze verfijning zorgt voor een gemiddelde daling van 3 kJ mol^{-1} voor E_a, wat beperkt is. Een veel groter effect is merkbaar voor A. Het tunnelen van het proton doorheen de potentiaalbarrière wordt in rekening gebracht via de Eckartbenadering. Hierdoor daalt E_a gemiddeld met 5 kJ mol^{-1}, terwijl de A waarden slechts weinig beïnvloed worden.

Twee experimentele datasets zijn voorhanden, er bestaat echter een grote discrepantie tussen beide. Dit is o.a. te wijten aan het verschillende, en telkens kleine, temperatuursinterval waarin beide experimenten werden uitgevoerd. De noodzakelijke extrapolatie voor de berekening van E_a en A kan dan grote fouten met zich meebrengen. De experimentele kinetische waarden worden niet betrouwbaar genoeg geacht en geavanceerde composietmethoden bieden een goed alternatief. Vergelijking met deze referentiewaarden toont de geschiktheid aan van de BB1K-, MPW1K-, BMK- en URCCSD(T)-methoden, telkens in combinatie met de 6-311+G(*3df,2p*)-basisset. Vergelijking van de theoretische en experimentele $k(T)$-waarden is wel mogelijk en hieruit blijkt dat alle composietmethoden uitstekend presteren en opnieuw leveren de BB1K-, MPW1K- en BMK-functionalen goede resultaten.

Waterstofabstracties aan polyaromaten: thermodynamische en kinetische resultaten

De invloed van de lokale polyaromatische omgeving op de thermodynamische en kinetische grootheden van waterstofabstracties door een aanvallend methylradicaal wordt bestudeerd gebruik makend van een uitgebreid set van PAHs. De testset is weergegeven in Figuur A.4 en een groep van lineaire acenen kan duidelijk onderscheiden worden van de overige niet-lineaire structuren. Abstracties aan verschillende sites van een welbepaalde PAH-molecule zijn mogelijk. De verschillende waterstofatomen zijn allen genummerd in Figuur A.4. Uit voorgaande paragraaf is gebleken dat BMK/6-311+G(*3df,2p*)//B3-LYP/6-31G(*d,p*) een geschikt niveau is aangezien deze methode aanleiding geeft tot accurate grootheden tegenover een haalbare computationele inspanning. De abstractie van het waterstofatoom X aan de polyaromaat PAH wordt genoteerd als **PAH**-X.

Geometrieën De meeste geoptimaliseerde reactanten zijn planaire structuren, slecht 4 uitzonderingen worden gerapporteerd (**BPH**, **DBPH**, **BNA** en **BPHA**). De non-planariteit is een gevolg van sterke sterische repulsie tussen nabijgelegen waterstofatomen. De planariteit wordt echter in grote mate hersteld bij de productradicalen aangezien er een waterstof geabstraheerd werd. Ten gevolge van de abstractie worden de bindingslengtes van de nabije C-C bindingen aan de abstractiesite korter ($\sim 0.02\,\mathring{A}$), en de bindingshoek wordt groter ($\sim 6°$). Voor de meeste TSs is de lengte van de vormende binding groter dan deze van de gebroken binding ($\sim 0.07\,\mathring{A}$), in overeenstemming met de endothermiciteit van de corresponderende waterstofabstracties (enkel **DBA**-1, **BNA**-2 and **BPHA**-2 vertonen het tegenovergestelde gedrag). Inspectie van de TSs toont eveneens aan dat het aanvallend methylradicaal voor abstractie aan ingekapselde sites sterisch gehinderd wordt en bijgevolg volgt het methylradicaal een pad dat niet in het vlak opgespannen door de aanvalsite van het PAH en de oorspronkelijke positie van de methylgroep ligt.

Reactie-enthalpieën en barrières De ΔH_{298}-resultaten liggen in een breed interval, enkel **BNA**-2 toont een licht exotherm gedrag (ΔH_{298} = -1.8 kJ mol^{-1}). Een clustering in 6 groepen (**B**-, **PH**-, **DBPH**-, **BPHA**-, **BPH**- en **BNA**-achtige sites) wordt geobserveerd, zoals aangegeven in Figuur A.4 d.m.v. verschillende symbolen. Voor de lineaire acenen kan er nog een verdere onderverdeling (in **B**-, **N**- en **A**-type sites) gemaakt worden, waarbij de grootste ΔH_{298}-waarden overeenstemmen met **A**-type sites. Alle resultaten tonen aan dat de enthalpiewaarden voor abstracties aan de ingekapselde sites relatief klein zijn en dit tengevolge van een vermindering van sterische hinder bij creatie van het radicaal. De $\Delta E_0^{\ddagger}$-waarden zijn relatief hoog (interval van 70.8 tot 89.2 kJ mol^{-1}). De hoogste barrières zijn opnieuw een gevolg van sterische hinder tussen het aanvallend methylradicaal en nabijgelegen waterstofatomen.

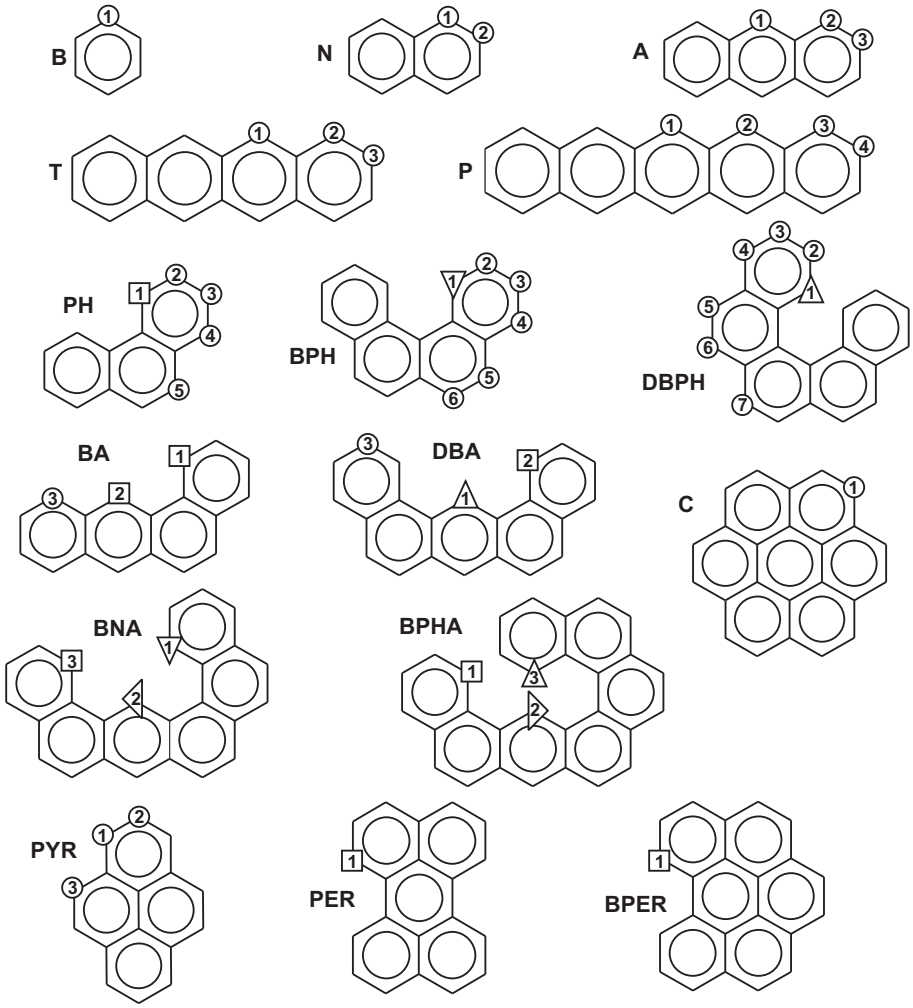

Figuur A.4: Schematische representatie van PAHs. Type sites: ◯ : **B**, □ : **PH**, △ : **DBPH**, ▷ : **BPHA**, ▽ : **BPH**, ◁ : **BNA**.

Voor de volledige testset wordt er geen correlatie gevonden tussen de ΔH_{298}- en $\Delta E_0^{\ddagger}$-resultaten. Er geldt dat, hoe groter de inkapseling van het te abstraheren waterstofatoom, hoe lager de reactiviteit voor abstractie ($\Delta E_0^{\ddagger}$ groot) en hoe groter de opheffing van sterische spanning (ΔH_{298} klein). Dit is in tegenstrijd met een normaal reactiviteit-enthalpie gedrag, uitgedrukt door een Bell-Evans-Polanyi relatie. Dit gedrag wordt in grote mate wel waargenomen voor de serie lineaire acenen, waar sterische hinder geen rol van betekenis speelt.

Kinetische parameters en snelheidscoëfficiënten Snelheidscoëfficiënten $k(T)$ en afgeleide grootheden E_a en A worden berekend in het temperatuursinterval 700-1100 K. Er wordt opnieuw rekening gehouden met het tunneleffect en met de interne rotatie van de methylgroep rond de vormende binding. Het laatste effect stemt overeen met het gebruik van een gemengd HO/FR-model voor de niet-ingekapselde of vrije sites en een gemengd HO/HR-model voor de ingekapselde sites. Beide verfijningen hebben een niet-verwaarloosbare invloed op de resultaten, zoals is weergegeven in Tabel A.4. Tunneling beïnvloedt in hoofdzaak E_a, terwijl het in rekening brengen van de interne rotatie vooral A wijzigt.

	IR model	Eckart tunneling	totaal
$(E_a)_i - (E_a)_f$	3.3	4.5	7.8
A_f/A_i	0.4	0.7	0.3
$k_f/k_i\,(700)$	0.6	1.6	1.0
$k_f/k_i\,(900)$	0.5	1.4	0.7
$k_f/k_i\,(1100)$	0.5	1.2	0.6

Tabel A.4: Invloed van verfijningen aan TST model op E_a (in kJ mol^{-1}), A en $k(T)$ voor verschillende temperaturen. De subscripts i en f refereren naar de initiële, resp. finale waarden.

Gedetailleerde studie van de E_a-, A- en $k(T)$-resultaten voor de lineaire acenen leidt tot 2 belangrijke observaties. Ten eerste is abstractie van een waterstofatoom gelokaliseerd aan een centrale ring moeilijker dan abstractie aan een niet-centrale ring. Ten tweede vertonen de parameters een convergent gedrag vanaf 3 aaneengeschakelde ringen (antraceen) en bijgevolg is het voldoende om 3 zesringen in beschouwing te nemen om het gedrag van waterstofabstracties aan lineaire acenen correct te modelleren.

Een analoge studie voor de niet-lineaire PAH-moleculen toont aan dat de waterstofabstractie moeilijker wordt naarmate de inkapseling toeneemt. De gevonden variaties in E_a en A zijn sterker dan deze geobserveerd voor de lineaire serie. De invloed van het toevoegen van een extra laag aan het cokesoppervlak kan nagegaan worden door b. v. de **PH**-1 resultaten te vergelijken met de **BPER**-1 resultaten, de conclusie is dat de extra laag een verwaarloosbare invloed heeft op de kinetische resultaten.

Reactiviteitsdescriptoren versus thermodynamica en kinetiek

Reactiviteitsdescriptoren voor PAHs Tabel A.5 tabelleert de globale des-criptoren μ en S, berekend op BMK/6-311+G(*3df,2p*)//B3-LYP/6-311G(*d,p*)-niveau, voor de bestudeerde PAH-moleculen (Figuur A.4). De zachtheidswaarden S tonen aan dat alle structuren beschouwd kunnen worden als zacht. De overeenkomst met experimentele waarden (bekomen via IP- en EA-data) is

zeer goed, dit is echter voornamelijk te wijten aan een foutenannulering tussen de IP- en EA-contributie. De lineaire acenen worden zachter en bijgevolg reactiever naarmate de grootte toeneemt.

PAH	μ	S	PAH	μ	S
B	-3.857	2.477 *(2.626)*	**BA**	-3.836	3.959 *(3.854)*
N	-3.814	3.184 *(3.261)*	**DBA**	-3.849	3.956 *(3.996)*
A	-3.828	3.945 *(3.939)*	**BNA**	-3.848	4.251 *(-)*
T	-3.850	4.731 *(4.610)*	**BPHA**	-3.827	4.293 *(-)*
P	-3.867	5.523 *(5.195)*	**C**	-3.806	3.900 *(3.990)*
PH	-3.778	3.339 *(3.570)*	**PYR**	-3.786	3.836 *(3.929)*
BPH	-3.833	3.689 *(3.720)*	**PER**	-3.824	4.532 *(4.545)*
DBPH	-3.808	3.792 *(-)*	**BPER**	-3.822	4.192 *(4.031)*

Tabel A.5: μ (eV) en S (au^{-1}), berekend op BMK/6-311+G(*3df,2p*)//B3-LYP/6-311G(*d,p*) niveau. Beschikbare experimentele S-waarden staan tussen haakjes.

Vanuit een lokaal standpunt is de radicalaire Fukui functie $f^0(\mathbf{r})$ aangewezen om de meest reactieve site aan te duiden. Figuur A.5 toont echter aan dat dit niet zo eenvoudig is. Tetraceen (**T**), **DBPH** en **BPHA** representeren de lineaire en niet-lineaire categorieën, respectievelijk. Het iso-oppervlak voor **T** vertoont minimale variaties, de lobes rond de waterstofatomen zijn nagenoeg identiek. Iets grotere, doch nog steeds beperkte, variaties zijn er voor **DBPH** en **BPHA**. Het is echter wel duidelijk dat de waterstofatomen op een ingekapselde positie (b. v. positie 1) een lage reactiviteit hebben.

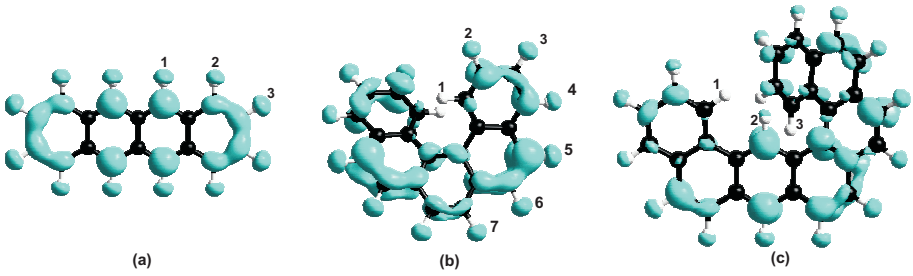

Figuur A.5: Iso-oppervlakken van $f^0(\mathbf{r})$ voor (a) **T** , (b) **DBPH** en (c) **BPHA**.

Waterstofabstracties De reeds besproken waterstofabstracties aan polyaromaten door een aanvallend methylradicaal worden nu bestudeerd d.m.v. DFT-gebaseerde reactiviteitsdescriptoren. De toepasbaarheid van het HSAB-principe wordt onderzocht: barrières op 0 Kelvin ($\Delta E_0^{\ddagger}$) worden vergeleken met zachtheidsverschillen (zie vorige paragraaf). Alle grootheden werden berekend op BMK/6-311+G(*3df,2p*)//B3-LYP/6-311G(*d,p*)-niveau.

Vanuit een globaal perspectief wordt er geen correlatie tussen $\Delta E_0^{\ddagger}$ en ΔS gevonden. De lokale HSAB-variant vergelijkt $\Delta E_0^{\ddagger}$-resultaten met $\Delta s_{C,H_i}$, corresponderend met de verschillen tussen de gecondenseerde zachtheid van het koolstofatoom van de methylgroep enerzijds en de gecondenseerde zachtheid van een waterstofatoom H_i van de PAH-molecule anderzijds. Voor de berekening van de gecondenseerde waarden werd het CHELPG-populatieschema gebruikt. Er wordt eerst nagegaan of de lokale zachtheid erin slaagt het correcte waterstofatoom voor abstractie aan te duiden binnen een welbepaalde PAH molecule. De geobserveerde variaties zijn klein, toch is het duidelijk dat voor de lineaire acenen de minimale $\Delta s_{C,H_i}$-waarden corresponderen met waterstofatomen gelokalizeerd aan een niet-centrale ring. Bijgevolg wordt abstractie aan de niet-centrale ringen gepreferreerd, in overeenkomst met de energetische $\Delta E_0^{\ddagger}$-resultaten. Deze goede correlatie tussen beide grootheden is eveneens geldig voor abstractie aan sommige niet-lineaire PAH-moleculen, er zijn echter enkele pertinente uitzonderingen. Wanneer de reactiviteit van de verschillende PAH-reactanten met elkaar wordt vergeleken, leveren de descriptoren en de barrières eveneens gelijkaardige intermoleculaire reactiviteitssequenties op. De uitzonderingen op de HSAB-regel tonen aan dat hard/zacht zuur/base beschouwingen niet dominant zijn voor de corresponderende reacties. Inderdaad, in deze gevallen zijn (zoals reeds vermeld) sterische effecten doorslaggevend en deze worden niet beschreven d.m.v. de indicatoren.

Additiereacties Een tweede groep van radicalaire reacties die optreden tijdens de groei van het cokesnetwerk zijn additiereacties van oppervlakteradicalen aan gasfaseprecursoren zoals etheen, ethyn, propeen en propyn. De $\Delta E_0^{\ddagger}$- en Δs-waarden (corresponderend met het verschil tussen de NPA-gecondenseerde zachtheid van een koolstofatoom van het olefine enerzijds en de NPA-gecondenseerde zachtheid van het radicalair koolstofatoom van de reactant radicalen anderzijds) voor de additie van 2 geselecteerde radicalen worden weergegeven in Tabel A.6. Alle grootheden werden berekend op B3-LYP/6-311G(*d,p*)-niveau.

Een belangrijke vraag is welke olefines de grootste reactiviteit vertonen voor radicalaire additie. Daarnaast wordt nagegaan of reactiviteitsindicatoren de correcte regioselectiviteit, i.h.b. het gepreferreerd reactiepad in geval van de niet-symmetrische precursoren propeen en propyn, kunnen voorspellen.

		etheen	*ethyn*	*propeen*	*propyn*
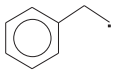 *R1*	ΔE_0	31.02	32.51	30.49	39.28
	Δs	0.948	1.267	0.947	1.238
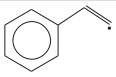 *R2*	ΔE_0	18.74	23.77	25.60	32.23
	Δs	0.677	0.996	0.675	0.967

Tabel A.6: $\Delta E_0^{\ddagger}$ (kJ mol^{-1}, inclusief geschaalde ZPVE) en Δs (au^{-1}) voor de additiereacties, berekend op B3-LYP/6-311G(*d,p*)-niveau.

Uit tabel A.6 volgt dat additie aan olefines met een dubbele binding geprefereerd wordt boven additie aan olefines met een drievoudige binding. De lengte van de precursor is van ondergeschikt belang: de gecondenseerde zachtheid kan geen onderscheid maken tussen additie aan b. v. etheen en propeen aangezien enkel de lokale omgeving van het radicalair centrum in rekening gebracht wordt. Vergelijking van de verschillende radicalaire koolwaterstoffen toont aan dat, op basis van het lokaal HSAB-principe, R2 reactiever is dan R1. Het laatste radicaal is inderdaad van het primaire type en is minder reactief dan het vinylische radicaal R2. Additie aan de niet-symmetrische moleculen geeft aanleiding tot twee verschillende reactiepaden (enkel de resultaten die overeenkomen met het meest voordelige reactiepad zijn weergegeven in Tabel A.6). De Δs-resultaten zijn in overeenstemming met de traditionele Markovnikov regel (aangepast voor radicalaire reacties op basis van hyperconjugatie-argumenten): de additie heeft preferentieel plaats aan het minst-gesubstitueerde koolstofatoom dat deelneemt aan de dubbele, respectievelijk drievoudige, binding. Bovenstaande conclusies stemmen in grote mate overeen met de $\Delta E_0^{\ddagger}$-resultaten. De berekende enthalpiewaarden geven het exotherm karakter van de additiereacties aan. Er wordt echter geen correlatie gevonden tussen de enthalpiewaarden en de barrières en bijgevolg wordt er niet voldaan aan de traditionele formulering van de Bell-Evans-Polanyi-relatie. Hierbij aansluitend is het zo dat de HSAB-voorspellingen geen overeenkomst vertonen met de enthalpiewaarden.

Cyclisatiereacties De derde groep van radicalaire reacties die leiden tot de groei van het cokesnetwerk zijn unimoleculaire cyclisatiereacties. Vijf reactanten, bestaande uit een aromatische kern en een alkylketen met het gepaste aantal koolstofatomen voor cyclisatie, worden bestudeerd op B3-LYP/6-311G(*d,p*)-niveau.

De radicalaire Fukui functie $f^0(\mathbf{r})$ slaagt er niet in het correcte koolstofatoom voor cyclisatie aan te duiden. Andere cyclisatiereacties zullen later besproken worden en er zal worden aangetoond dat het gebruik van spin-

gepolariseerde reactiviteitsindicatoren een goed alternatief biedt voor de beschrijving van unimoleculaire cyclisatiereacties. Door de aanwezigheid van de aromatische kern, kunnen echter ook aromaticiteisdescriptoren waardevolle informatie leveren. De magnetische susceptibiliteitsanisotropie $\Delta\chi$ en de chemische shift van de protonen δ tonen een goede correlatie met de barrières $\Delta E_0^{\ddagger}$: hoe kleiner het verschil in aromaticiteit tussen reactant en TS, hoe lager de barrière voor cyclisatie. Dit toont het belang aan van het aromatisch karakter van de onderzochte reactanten en tevens het belang van de aromaticiteitsveranderingen die zij ondergaan tijdens het verloop van de reactie.

Besluit

Verschillende radicalaire reacties die optreden binnen het groeiproces van cokes werden onderzocht gebruik makend van traditionale thermodynamische en/of kinetische grootheden enerzijds en voorspellende reactiviteitsdescriptoren anderzijds.

De waterstofabstractie aan benzeen door een aanvallend methylradicaal werd uitgebreid bestudeerd en dient als referentie voor abstracties aan polyaromatische systemen. Deze reacties creëren initiële oppervlakteradicalen aan het cokesoppervlak. De invloed van het berekeningsniveau op thermodynamische en kinetische parameters werd uitgebreid getest. Geavanceerde composietmethoden, i.h.b. W1, dienen als referentie in het geval experimentele data ontbreken of onbetrouwbaar zijn. Uit deze uitgebreide studie volgt dat de gevoeligheid van de geometrieoptimalisatie aan het gebruikte niveau minimaal is (enkel HF en enkele post-HF-methoden leiden tot niet-accurate waarden wegens spin-contaminatie). De invloed van het niveau (zowel methode als basisset) voor de single-point energieberekeningen is daarentegen veel groter. Samenvattend geldt dat accurate, betrouwbare en tevens computationeel haalbare resultaten voor deze groep van waterstofabstracties kunnen bekomen worden op BMK/6-311+G(*3df,2p*)//B3-LYP/6-311G(*d,p*)-niveau.

Gebruik makend van dit niveau werd vervolgens de invloed van de lokale polyaromatische omgeving nagegaan op reactiebarrières, reactie-enthalpieën, snelheidscoëfficiënten, activeringsenergieën en pre-exponentiële factoren. Abstractie aan een ingekapselde, moeilijk bereikbare site stemt overeen met een lage enthalpiewaarde (door de vermindering van sterische spanning wanneer het radicaal gevormd wordt) en een hoge reactiebarrière (door sterische hinder). Dit gedrag is in tegenspraak met de traditionele Bell-Evans-Polanyi relatie. De subcategorie van lineaire acenen vertoont wel een normaal reactiviteit-enthalpie gedrag aangezien de abstracties gebeuren aan vrije, niet-ingekapselde sites en sterische hinder geen rol van betekenis speelt.

Reactiviteitsdescriptoren tonen aan dat de bestudeerde polyaromatische moleculen zacht zijn. Het lokaal HSAB-principe kan voor de meerderheid van de bimoleculaire radicalaire reacties (waterstofabstracties door een methyl-

radicaal en additiereacties aan gasfaseprecursoren) succesvol worden toegepast: de kwalitatieve overeenkomst tussen zachtheidsverschillen enerzijds en energiebarrières anderzijds is goed. De lokale zachtheid is een geschikte descriptor om de geprefeerde site aan te duiden voor abstractie of additie. De unimoleculaire cyclisatiereacties kunnen niet beschreven worden met de traditionele reactiviteitsdescriptoren; de aromaticiteitsveranderingen tijdens de reactie zijn dominant. De indicatoren slagen er niet in om specifieke en uitzonderlijk hoge barrières te verklaren optredend bij de waterstofabstracties aangezien deze te wijten zijn aan sterische hinder. In het algemeen wordt er geen correlatie gevonden tussen de indicatoren en thermodynamische grootheden (zoals de reactie-enthalpie).

A.3.2 Typische reacties in kleine zeolietclusters

Inleiding

Zeolieten zijn microporeuze, kristallijne aluminosilicaten die opgebouwd zijn uit SiO_4- and AlO_4-tetrahedra. Deze vaste-stof katalysatoren beschikken over een specifieke vormselectiviteit en bijzondere zuur/base-karakteristieken die aanleiding geven tot een brede waaier aan eigenschappen en toepassingen. Deze periodieke structuren kunnen gemodelleerd worden d.m.v. kleine clusters. In dit werk worden 5T-clusters (T=Al of Si) gehanteerd, waarin zowel Brönstedt zure sites (≡Si-OH-Al≡) als Lewis basische sites (≡Si-O-Al≡) aanwezig zijn. Naast een zuivere-zuurstofcluster (O-cluster) worden er ook twee stikstof-gesubstitueerde clusters (N1- en N2-cluster) onderzocht die onstaan door substitutie van één enkele zuurstofbrug door een N-H verbinding. De clusters worden weergegeven in Figuur A.6. Ab initio-berekeningen toonden reeds aan dat de stikstof-gesubstitueerde zeolietstructuren veelbelovende nieuwe materialen zijn wegens een hogere reactiviteit in vergelijking met de traditionele zuurstofvarianten. Deze verhoogde reactiviteit voor sommige S_N2-reacties is vooral te wijten aan de gunstigere geometrische positie van de Lewis base. De vorming van een alkoxide- of alkylammoniummolecule wordt bestudeerd, aangezien dit een typisch voorbeeld is van een reactie die zowel de zure als basische eigenschappen van de zeolietcluster gebruikt. In het bijzonder worden reacties met chloromethaan, methanol, etheen en propeen onderzocht.

Een belangrijk voordeel van het gebruik van reactiviteitsdescriptoren – in tegenstelling tot thermodynamische en/of kinetische grootheden – is dat de indicatoren bekomen kunnen worden met een beperkte computationele inspanning. In dit werk wordt nagegaan of de globale descriptoren onafhankelijk zijn van het gebruikte berekeningsniveau. Indien dit het geval is, versterkt dit voorgaande vaststelling. Indien er echter een grote afhankelijkheid van het berekeningsniveau wordt gevonden, ondermijnt dit in sterke mate de betrouwbaarheid van de indicatoren.

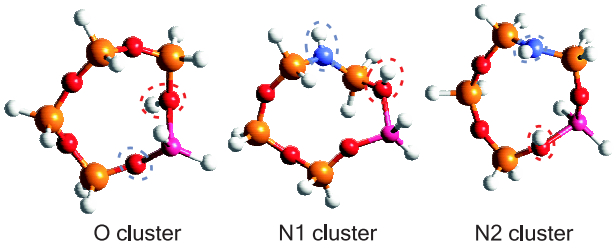

Figuur A.6: 5T zeolietclusters, geoptimaliseerd op B3-LYP/6-31G(d) niveau, met aanduiding van de zure site (rode stippellijn) en basische site (blauwe stippellijn).

De chemische reactiviteit van de reacties tussen de 5T-zeolietclusters en de kleine probemoleculen wordt vervolgens intensief bestudeerd d.m.v. globale en lokale indicatoren. Er wordt nagegaan of de reactiviteitsindicatoren erin slagen om informatie te verschaffen over de katalytische mogelijkheden van de onderzochte zeolietstructuren. De bifunctionaliteit van de zeolietkatalysatoren vormt een grote uitdaging voor de conceptueel eenvoudige descriptoren. De lokale zachtheid en de Fukui functie worden getest op hun toepasbaarheid en interpretatief nut i.v.m. de bespreking van de regioselectiviteit.

Invloed van het berekeningsniveau op globale reactiviteitsdescriptoren

Ten eerste wordt aangetoond dat de invloed van het berekeningsniveau gebruikt voor de geometrieoptimalisatie zeer klein is. Vandaar worden de computationeel interessante B3-LYP/6-31G(d) geoptimaliseerde geometrieën gehanteerd. Dit niveau is trouwens de standaardkeuze voor ab initio-berekeningen binnen zeolietkatalyse. Vervolgens wordt de invloed van het berekeningsniveau gebruikt voor de single-point energieberekeningen nagegaan. De resultaten van de hybride-meta-functionalen MPWB1K en BMK worden vergeleken met B3-LYP- en HF-waarden. MPWB1K en BMK worden voor de eerste keer toegepast binnen zeolietkatalyse en binnen het kader van reactiviteitsdescriptoren. De elektronenaffiniteit EA is gevoelig aan de keuze van basisset aangezien het toevoegen van een elektron leidt tot een grote verandering in de ruimtelijke omvang van de golffunctie. Om dit gedrag grondig te kunnen bestuderen, worden 9 Pople- en Dunning-basissets getest.

Kleine probe moleculen: vergelijking met experiment Experimentele IP-resultaten zijn beschikbaar voor chloromethaan, methanol, etheen en propeen. Voor berekening van de descriptoren μ en η wordt een post-HF-niveau

(QCISD(T)/6-311++G(*3df,2p*)//B3-LYP/6-31G(*d*)) gebruikt als referentie. De η-resultaten bevestigen het hard en intermediair karakter van de polaire en apolaire moleculen, respectievelijk. De computationele waarden vertonen in het algemeen een zeer kleine gevoeligheid aan het berekeningsniveau. Vergelijking met de referentiewaarden toont aan dat gebruik van een DFT functionaal (B3-LYP, BMK of MPWB1K) in combinatie met een dubbele- of drievoudige-zeta basisset, inclusief polarisatie- en diffuse functies, tot accurate resultaten leidt.

Reactiviteitsindicatoren: zuivere-zuurstofzeolieten De berekende hardheidsresultaten van de O-cluster liggen tussen 4.81 en 6.22 eV en duiden het intermediair hard karakter van deze molecule aan. Het toevoegen van diffuse functies aan de basisset leidt tot een verlaging van de hardheid met gemiddeld 0.4 eV. Het gebruik van een dubbele-zeta basisset, inclusief polarisatie- en diffuse functies, lijkt voldoende te zijn om betrouwbare resultaten te bekomen. Globale zachtheidsverschillen ΔS en activeringshardheden $\Delta\eta_{\text{act}}$ werden berekend voor de reacties tussen de O-cluster en de 4 probemoleculen. Dit maakt het mogelijk om de reactiviteit van de kleine moleculen te vergelijken. De HF-resultaten verschillen substantieel van de resultaten bekomen met de 3 DFT-functionalen, terwijl de BMK- en MPWB1K-resultaten bijna identiek zijn. Inclusie van diffuse functies leidt dikwijls tot hogere ΔS- en $\Delta\eta_{\text{act}}$-resultaten. Ten slotte is de reactiviteitssequentie van de kleine moleculen sterk afhankelijk van het gebruikte berekeningsniveau.

Reactiviteitssequenties: stikstof-gesubstitueerde zeolieten Vervolgens wordt de reactiviteitssequentie van de verschillende zeolietclusters (O, N1 en N2) onderzocht. In het bijzonder wordt nagegaan of deze sequentie gevoelig is aan het gebruikte berekeningsniveau.

In het algemeen vertonen de reactiviteitssequenties een zeer beperkte gevoeligheid aan het berekeningsniveau. De DFT-resultaten liggen zeer dicht bij elkaar en ter illustratie worden daarom de BMK-resultaten voor ΔS en $\Delta\eta_{\text{act}}$ weergegeven in Figuur A.7. De η-waarden tonen aan dat door de substitutie van een zuurstofbrug door een N-H-verbinding de reactiviteit van de zeolietcluster toeneemt. Alle berekeningsniveaus voorspellen de volgende sequentie: $\eta(O) > \eta(N2) > \eta(N1)$. Bijgevolg zijn ook de ΔS-sequenties onafhankelijk van het gebruikte theoretische niveau. De hard-hard interacties tussen de 3 clusters en chloromethaan en etheen, representatief voor een apolair, respectievelijk polair systeem, vertonen telkens de sequentie $\Delta S(N1) > \Delta S(N2) > \Delta S(O)$. Dit duidt aan dat, op basis van het globaal HSAB-principe, de interacties met de O-cluster geprefereerd worden. Anderzijds zijn de $\Delta\eta_{\text{act}}$-waarden wel verschillend voor de reacties met chloromethaan en etheen. Voor de apolaire molecule geldt: $\Delta\eta_{\text{act}}(N1) > \Delta\eta_{\text{act}}(O) > \Delta\eta_{\text{act}}(N2)$, terwijl voor de polaire molecule geldt: $\Delta\eta_{\text{act}}(N1) > \Delta\eta_{\text{act}}(N2) > \Delta\eta_{\text{act}}(O)$.

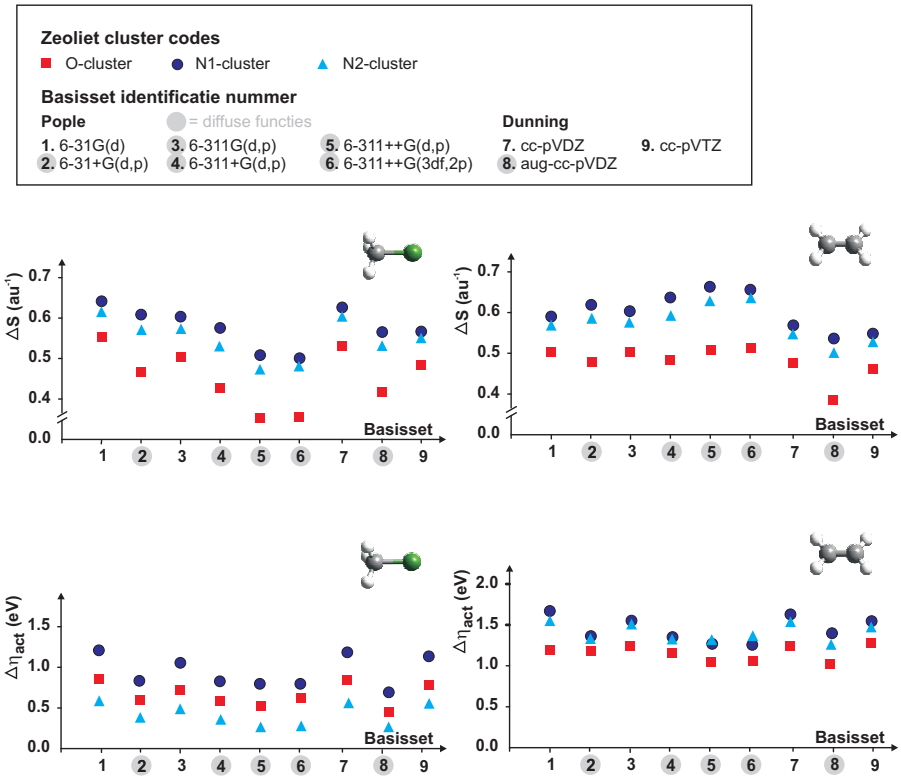

Figuur A.7: Globale zachtheidsverschillen en activeringshardheden voor de interacties tussen de zeolietclusters en chloromethaan en etheen, berekend met de BMK-functionaal.

Reactiviteitsdescriptoren versus thermodynamica en kinetiek

In deze paragraaf wordt nagegaan of de globale en lokale reactiviteitsdescriptoren waardevolle informatie leveren omtrent het reactief gedrag van de zeolietclusters. In het bijzonder wordt gecontroleerd of de indicatoren de correcte kwalitatieve reactiviteitssequenties tussen de zuurstof- en amine-gemodificeerde clusters kunnen weergeven. Hiervoor wordt de correlatie bekeken met de reactiebarrière op 0 Kelvin ($\Delta E_0^{\ddagger}$). Alle resultaten werden berekend op B3-LYP/6-31G(d)-niveau en worden weergegeven in Tabel A.7.

De interacties tussen de clusters en de apolaire moleculen etheen en propeen vertonen een correlatie tussen de ΔS- en $\Delta E_0^{\ddagger}$-resultaten, dit illustreert de toepasbaarheid van het globaal HSAB-principe. Een dergelijke correlatie wordt echter niet gevonden voor de interacties met de polaire moleculen. Dit falen van het HSAB-principe is mogelijk te wijten aan de dominantie van polaire

	$\Delta E_0^{\ddagger}$	ΔS	$\Delta\eta_{\text{act}}$	$\Delta E_0^{\ddagger}$	ΔS	$\Delta\eta_{\text{act}}$
		CH3Cl			CH3OH	
O	169.9	0.653	0.635	199.8	0.717	1.094
N1	220.3	0.773	1.080	165.8	0.838	0.720
N2	117.5	0.747	0.458	150.3	0.811	0.556
		C2H4			C3H6	
O	96.6	0.528	1.096	86.0	0.419	1.454
N1	141.0	0.648	1.494	117.6	0.540	1.880
N2	124.3	0.622	1.354	119.6	0.513	1.840

Tabel A.7: Reactiebarrières (kJ mol^{-1}), zachtheidsverschillen (au^{-1}) en activeringshardheden (eV) voor reacties tussen zeolietclusters en probemoleculen.

interacties bij deze specifieke groep van interacties, terwijl het HSAB-principe geen rekening houdt met dergelijke effecten. Inspectie van de $\Delta\eta_{\text{act}}$-waarden toont aan dat deze grootheid niet kan gebruikt worden om de correcte reactiviteitssequentie van de 4 kleine probemoleculen te reproduceren. De reactiviteitssequentie van de 3 zeolietkatalysatoren wordt daarentegen wel correct voorspeld: er wordt een uitstekende overeenkomst bekomen tussen $\Delta\eta_{\text{act}}$ en $\Delta E_0^{\ddagger}$.

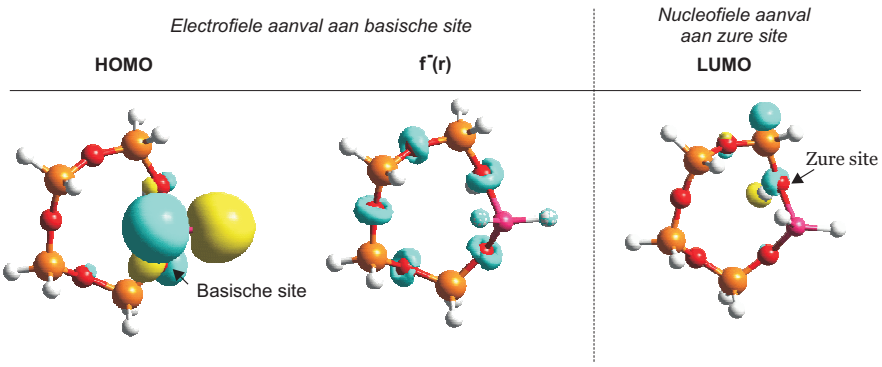

Figuur A.8: Iso-oppervlakken van de HOMO, $f^{-}(\mathbf{r})$ en LUMO voor de O-cluster.

Ten slotte wordt er nagegaan of de lokale indicatoren de correcte regioselectiviteit aangeven. Aangezien de reacties hard-hard zijn, en bijgevolg elektrostatische effecten verwacht worden een grote rol te spelen, werden de atomaire ladingen (via het MK schema) en de elektrostatische potentiaal berekend. Beide grootheden slagen erin de correcte zure site aan te duiden voor de 3 clusters. Verder worden in Figuur A.8 de drie-dimensionale iso-oppervlakken

van lokale grootheden weergegeven voor de zuivere-zuurstofcluster. De grensorbitalen HOMO en LUMO slagen erin om de correcte zure, respectievelijk basische site aan te duiden. De Fukui functie bevat extra informatie t.o.v. de grensorbitalen, de nucleofiele Fukui functie ($f^-(\mathbf{r})$) slaagt er echter niet in om de basische site aan te duiden, het iso-oppervlak is niet geconcentreerd rond een welbepaald atomair centrum. Voor de stikstof-gesubstitueerde zeolieten zijn de HOMO en LUMO eveneens succesvol en ook de $f^-(\mathbf{r})$ duidt nu een site met basisch karakter aan. De indicatoren kunnen echter niet het basische karakter van de N-H-verbinding in de N1-cluster aanduiden.

Besluit

Drie 5T-zeolietclusters en 4 kleine probemoleculen werden gebruikt als testset om de gevoeligheid van globale reactiviteitsdescriptoren aan het berekeningsniveau na te gaan. De invloed van de geometrieoptimalisatie is bijzonder klein, en B3-LYP/6-31G(d) geometrieën werden gebruikt voor de single-point energieberekeningen. HF- en 3 DFT-methoden, in het bijzonder B3-LYP, BMK en MPWB1K werden getest, in combinatie met 9 verschillende bassissets. Algemeen werd vastgesteld dat de invloed van het berekeningsniveau op de globale descriptoren klein is. De 3 DFT-functionalen vertonen een zeer gelijkaardig gedrag, de HF-resultaten liggen iets meer verspreid en vertonen een grotere gevoeligheid aan de gebruikte basisset. Wanneer de 3 zeolietkatalysatoren met elkaar worden vergeleken is het duidelijk dat de reactiviteitssequenties (bekomen op basis van de globale zachtheidsverschillen en activeringshardheden) in grote mate onafhankelijk zijn van het berekeningsniveau.

Vervolgens werd nagegaan in welke mate reactiviteitsindicatoren waardevolle informatie kunnen verschaffen over deze complexe hard-hard interacties, door correlaties met energiebarrières op 0 Kelvin te bestuderen. Het HSAB-principe kan succesvol toegepast worden voor de interacties tussen de clusters en de apolaire moleculen etheen en propeen. Voor de interactie met de polaire moleculen chloromethaan en methanol lukt dit echter niet, vermoedelijk wegens de dominantie van polaire effecten (die het HSAB-principe niet in rekening brengt). De activeringshardheid daarentegen vertoont een uitstekende correlatie met de barrières voor alle onderzochte reacties. De grensorbitalen HOMO en LUMO slagen erin om de correcte zure, respectievelijk basische site aan te duiden. Deze grootheden zijn complementair met de atomaire ladingen en de elektrostatische energieterm, die frequenter gebruikt worden om de reactiviteit van hard-hard interacties te beschrijven.

A.3.3 Unimoleculaire cyclisatiereacties

Inleiding

De laatste categorie van toepassingen omvat twee cyclisatiereacties. Beide voorbeelden vertonen een bijzonder en onverwacht gedrag en bijgevolg werd er nagegaan of ab initio-berekeningen meer inzicht kunnen verschaffen in het waargenomen reactiemechanisme. In dit doctoraatswerk ligt de focus op de toepasbaarheid van reactiviteitsindicatoren, voor de details en bijzonderheden van het reactiemechanisme wordt verwezen naar de oorspronkelijke artikels.

Het eerste voorbeeld is de cyclisatie van azaheterocyclische aminofosfaten waar een opmerkelijke voorkeur voor de vorming van een vierring (i.p.v. een stabielere zesring) werd waargenomen. De invloed van verschillende effecten, zoals substituenten, tegenionen en het aanwezige solvent, werd in rekening gebracht. De waargenomen selectiviteit kan echter reeds waargenomen worden binnen een gasfase-omgeving. Deze reactie is belangrijk binnen het syntheseproces van β-lactamen en kent bijgevolg farmaceutische toepassingen. De β-lactamring is nl. het actieve onderdeel van verschillende belangrijke antibiotica zoals penicilline. Het tweede voorbeeld zijn cascadecyclisaties van stikstof- en koolstofgecentreerde radicalen die uiteindelijk leiden tot de vorming van pyrrolizidines. De competitieve vorming van inolizidines werd experimenteel niet waargenomen. Ab initio-energetische berekeningen toonden reeds aan dat de route naar vorming van inolizidines inderdaad gekenmerkt wordt door een hogere reactiebarrière.

Cyclisatie van gefunctionaliseerde aminofosfaten

De bijzondere voorkeur voor vorming van een vierring i.p.v. een stabielere zesring bij gefunctionaliseerde aminofosfaten wordt onderzocht. Wanneer N-chloroacetyl-1-aminoalkenyl-fosfaat in contact komt met een sterke base wordt er (na abstractie van een waterstofatoom) een fosfor-gestabiliseerd anion gevormd dat in twee mesomere vormen kan voorkomen. Het volledige reactieschema wordt gegeven in Figuur A.9. De competitieve reactiepaden zijn duidelijk weergegeven. Na afsplitsing van het Cl-ion (aangehecht aan koolstofatoom C_5) kan de intramoleculaire cyclisatie doorgaan aan het α-koolstofatoom C_1 (leidend tot de vierring) of aan het γ-koolstofatoom C_3 (leidend tot de zesring).

De geometrische parameters van de α-canonische vorm suggereren de vorming van de vierring, aangezien de corresponderende bindingslengte korter en de corresponderende dihedrale hoek gunstiger is. Gedetailleerde studie van de TS toont tevens aan dat de interne rotatie rond de C_1N-binding sterk gehinderd is, resulterend in een niet-symmetrische potentiaal die de voorkeur voor de vierringvorming ondersteunt (Figuur A.10(a)). De figuur verduidelijkt dat het energetisch veel moeilijker is om de precursor geschikt voor de vorming van

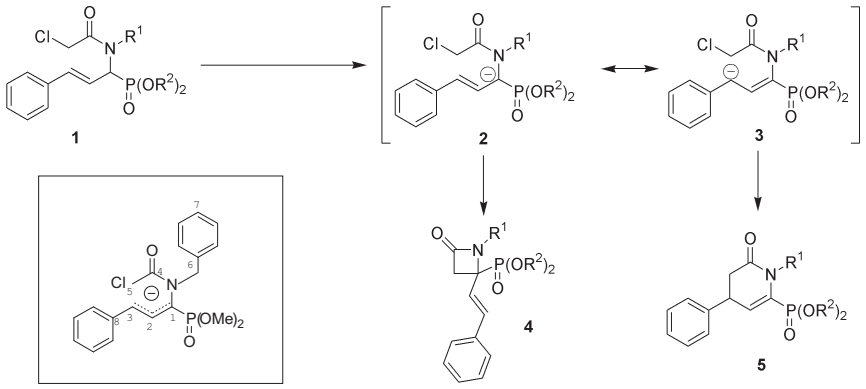

Figuur A.9: Reactieschema. Inzet: het anionreactant, met aanduiding van de atomen die belangrijk zijn tijdens het cyclisatieproces.

de zesring (Pr6) te bereiken. De invloed van substituenten, tegenionen en het aanwezige solvent is beperkt en de voorkeur voor vierringvorming blijft onaangetast.

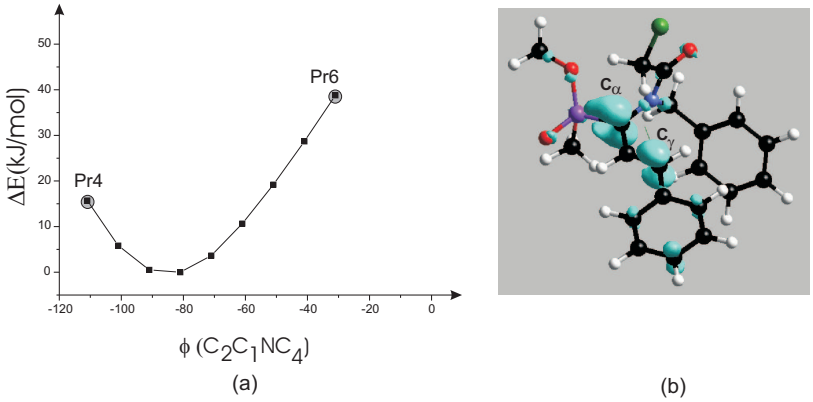

Figuur A.10: (a) Deel van de potentiaal bij rotatie t.o.v. de $C_2C_1NC_4$ dihedrale hoek. De precursoren voor vier- en zesringvorming (Pr4 en Pr6) zijn aangeduid. (b) Iso-oppervlak van de radicalaire Fukui functie.

DFT-descriptoren werden berekend op B3-LYP/6-31+G(d)-niveau om na te gaan of deze grootheden er eveneens in slagen om enkel op basis van informatie

van het reactant (i.e. het fosfor-gestabiliseerd anion) de vierringvorming te voorspellen. De globale hardheid ($\eta = 2.74$ eV) benadrukt het zacht (reactief) karakter van dit anion. De Fukui functie voor een electrofiele aanval ($f^-(\mathbf{r})$) wordt geplot in Figuur A.10(b). Het iso-oppervlak rond het α-koolstofatoom is groter dan het oppervlak rond het γ-koolstofatoom en de Fukui functie slaagt er dus in de regioselectiviteit van de reactie correct te voorspellen. De NPA- en CHELPG-gecondenseerde waarden van $f^-(\mathbf{r})$ leiden tot dezelfde conclusie: het α-atoom is reactiever (hogere waarde voor f_k^-) dan het γ-atoom.

In tegenstelling tot de voorkeur voor de vorming van de vierring in de besproken unimoleculaire reactie werd experimenteel vastgesteld dat bimoleculaire reacties (zoals protonering of de reactie met CH_3I) preferentieel plaatsvinden aan de γ-positie. Dit gedrag kan eveneens verklaard worden d.m.v. lokale reactiviteitsdescriptoren, aangezien een proton en het bindend koolstofatoom van methyliodide een hard karakter hebben. Volgens het lokaal HSAB-principe geldt inderdaad dat deze harde atomen bij voorkeur een binding zullen vormen met het hardere γ-koolstofatoom van het reactant.

Stikstof- and koolstof-gecentreerde radicalen in cascadecyclisaties

De radicalaire cascadecyclisatie startend vanaf N-alkenyl-2-aziridinylmethyl wordt geïllustreerd in Figuur A.11. In de eerste stap zorgt de cyclisatie van een stikstof-gecentreerd radicaal tot de vorming van een vijfring of een zesring en vervolgens cycliseren de gevormde koolstof-gecentreerde radicalen verder zodat er een bicyclische structuur gevormd wordt. Experimenteel werd een duidelijke voorkeur voor de vorming van de kleinere ring door additie van het radicalair centrum aan het 5-exo-koolstofatoom waargenomen. Ab initio-energetische berekeningen, uitgevoerd op B3-LYP/6-311G(*d,p*) niveau, bevestigen de experimentele observaties. Er wordt nagegaan of reactiviteitsdescriptoren er eveneens in slagen om de correcte regioselectiviteit aan te duiden. De indicatoren werden berekend op B3-LYP/6-311++G(*d,p*)//B3-LYP/6-311G(*d,p*) en gecondenseerde Fukui functies maakten gebruik van de NPA-analyse.

De gecondenseerde waarden van de traditionele radicalaire Fukui functie $f^0(\mathbf{r})$ voorspellen echter additie aan het 6-exo-koolstofatoom en zijn dus niet geschikt. Om meer inzicht te krijgen in het reactiemechanisme van deze cyclisatiereactie wordt er gebruik gemaakt van spin-gepolariseerde Fukui functies. Dit is aangewezen aangezien de bestudeerde unimoleculaire reacties gekenmerkt worden door een constant spingetal N_S, terwijl N wel verandert op lokaal vlak. De atomaire waarden van de gepolariseerde Fukui functie $f_{NN}(\mathbf{r}) = (\frac{\partial \rho(\mathbf{r})}{\partial N})_{N_S, v(\mathbf{r}), \mathbf{B}(\mathbf{r})}$ slagen er wel in om de correcte regioselectiviteit aan te duiden: de overeenkomst tussen de $f^0_{NN,k}$-waarde van het radicalair centrum en het 5-exo-atoom is beter dan de overeenkomst met het 6-exo-atoom.

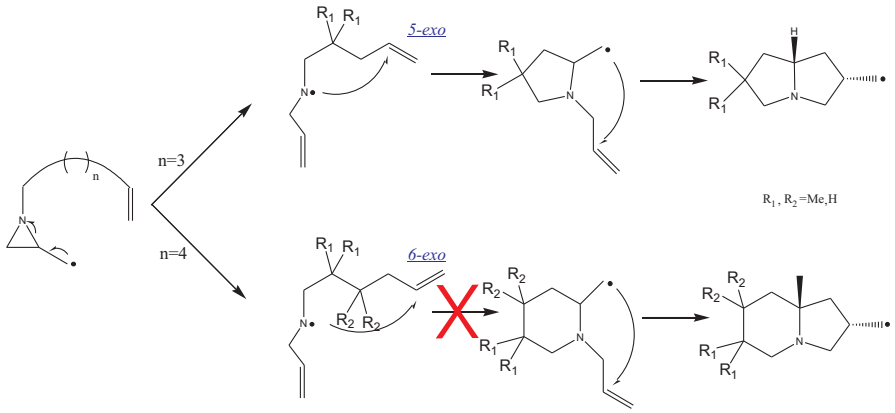

Figuur A.11: Cascadecyclisatiereacties van stikstof- en koolstof-gecentreerde radicalen.

Besluit

De regioselectiviteit van twee unimoleculaire cyclisatiereacties werd onderzocht. De cyclisatie van een fosfor-gestabiliseerd anion leidt uitsluitend tot de vorming van de vierring, terwijl de stabielere zesring experimenteel niet wordt waargenomen. De reactiviteitsdescriptoren, i.h.b. de Fukui functie, slagen erin deze opmerkelijke voorkeur te voorspellen en leveren bijgevolg belangrijke extra informatie ter aanvulling van de energetische resulaten. Bimoleculaire reacties, zoals de additie van een proton, hebben plaats op het γ-koolstofatoom en dit kan eveneens verklaard worden op basis van het lokaal HSAB-principe. De regioselectiviteit van cascadecyclisaties van stikstof- en koolstofgecentreerde radicalen kan correct aangeduid worden d.m.v. de spin-gepolariseerde Fukui functie. Deze reacties zijn gekenmerkt door een constant spingetal, terwijl het totale elektronenaantal wel verandert op een lokaal niveau.

A.4 Besluit en toekomstperspectieven

In dit doctoraatswerk werden reactiviteitsindicatoren, gedefinieerd binnen de dichtheidsfunctionaaltheorie, gevalideerd voor een brede waaier aan chemische reacties die voorkomen in zeer uiteenlopende toepassingsgebieden. De chemische potentiaal, de globale hardheid en de globale zachtheid worden gebruikt om de reactiviteit van een volledige, geïsoleerde molecule te bespreken of om een verzameling van gelijkaardige systemen met elkaar te vergelijken. De Fukui functie wordt gebruikt als een intra-moleculaire descriptor terwijl de

lokale zachtheid inter-moleculaire informatie kan verschaffen over regioselectiviteit. Om het nut van voorgaande grootheden goed te kunnen testen worden zij geïmplementeerd binnen goedgekende chemische principes, zoals de equalisatie van de electronegativiteit, het principe van maximale hardheid en het hard/zacht zuur/base of HSAB-principe. De validering van de bekomen resultaten gebeurt a.d.h.v. een vergelijking met ab initio thermodynamische en kinetische grootheden. In het algemeen hebben DFT-gebaseerde reactiviteitsdescriptoren hun nut reeds bewezen voor de interpretatie van een groot aantal experimentele en/of theoretische resultaten. Het blijft echter een grote uitdaging om op voorhand te voorspellen of zij succesvol zullen zijn of zullen falen voor een specifieke reactie. Om werkelijk gebruik te kunnen maken van deze indicatoren als een onafhankelijk en voorspellend instrument zijn eenvoudige richtlijnen nodig die aangeven welke indicatoren een grote kans hebben om de correcte reactiviteit aan te geven. De reactiviteitsdescriptoren beschrijven elektronische effecten op basis van informatie van enkel de reactanten; ze zijn echter niet in staat om sterische effecten in rekening te brengen. De inherente beperkingen moeten steeds in het achterhoofd gehouden worden. In dit doctoraatswerk wordt er b. v. in de transitietoestanden van bepaalde bimoleculaire radicalaire reacties sterke sterische hinder ondervonden, wat leidt tot hoge reactiebarrières. Op basis van de definities kan er verwacht worden dat de descriptoren hier niet gebruikt kunnen worden om additionele informatie te bieden over de chemische reactiviteit, en dit werd inderdaad waargenomen.

De grootste groep van onderzochte toepassingen bestaat uit radicalaire reacties. De meerderheid van deze radicalaire reacties treedt op tijdens cokesvorming, een neveneffect van thermisch kraken van koolwaterstoffen. Cokes is een grafietachtige residulaag die gevormd wordt op de binnenste reactorwand van de krakingsoven. Gebruik makend van transitietoestandstheorie werden waterstofabstracties door een aanvallend methylradicaal aan polyaromatische systemen zeer intensief bestudeerd, resulterend in accurate, betrouwbare en tegelijkertijd computationeel haalbare thermodynamische en kinetische resultaten. Andere bestudeerde bimoleculaire radicalaire reacties zijn additions van gasfaseradicalen aan kleine olefines en de initiatie- en eerste propagatiestappen van de polymerisatiereacties die leiden tot de vorming van polyethyleen en polyvinylchloride. In het algemeen werd vastgesteld dat de radicalaire Fukui functie erin slaagt om de geprefereerde reactiesite aan te duiden. Dit toont duidelijk het belang aan van de grensorbitalen voor dit specifieke reactietype. Het lokale HSAB-principe kon eveneens succesvol toegepast worden en correcte reactiviteitssequenties werden bekomen wanneer gelijkaardige moleculen met elkaar vergeleken werden. De lokale zachtheid is bijgevolg een geschikte indicator voor de studie van bimoleculaire radicaire reacties. Het succes van de lokale descriptoren is in schril contrast met het gebruik van de globale grootheden. Het globaal HSAB-principe slaagt er niet in de correcte reactiviteitssequenties aan te duiden en het gebruik van globale descriptoren wordt bijgevolg afgeraden bij de studie van bimoleculaire radicalaire reacties. Naast deze bimoleculaire reacties werden er ook unimoleculaire radicalaire reacties bestudeerd. In deze

gevallen slaagt de radicalaire Fukui functie er niet in om de correcte reactiesite voor cyclisatie aan te duiden. De onderzochte cyclisaties stemmen overeen met een gebonden elektronentransfertproces: tijdens de reactie blijft het spingetal constant, terwijl het totale elektronenaantal wel wijzigt op lokaal niveau. De spin-gepolariseerde Fukui functie werd aangewend en deze grootheid was inderdaad succesvol.

De huidige definities voor de descriptoren van een radicalaire aanval komen overeen met het rekenkundig gemiddelde van de overeenkomstige grootheden voor een elektrofiele en nucleofiele aanval. Deze beschrijving kan echter verfijnd worden door meer rekening te houden met het specifiek reactiemechanisme van een welbepaald radicalair type. Het is bijvoorbeeld duidelijk dat waterstofabstracties in wezen sterk verschillen van additiereacties, en het is duidelijk dat het gebruik van één enkele indicator om beide reactietypes te beschrijven op problemen zal stuiten. Er werd reeds gesuggereerd dat er i.p.v. het rekenkundig gemiddelde veeleer een gewogen gemiddelde dient genomen te worden waarbij het specifiek elektrofiel of nucleofiel karakter van de reactanten in rekening wordt gebracht. De spin-gepolariseerde vorm van DFT dient eveneens nog verder onderzocht te worden. Dit werk is in opbouw in de onderzoeksgroep van Prof. Geerlings en Prof. De Proft.

In dit doctoraatswerk werden ook bimoleculaire reacties onderzocht die optreden binnen zeolietkatalyse, nl. interacties tussen kleine probemoleculen (zowel apolair als polair) en zeolietclusters. Naast de traditionele zuiverezuurstofcluster werd ook de invloed van de substitutie van een zuurstofbrug door een aminegroep nagegaan. Het globaal HSAB-principe is enkel in staat om de interacties tussen de clusters en de apolaire moleculen correct te beschrijven. De interacties met de polaire moleculen worden gedomineerd door polaire bijdragen en aangezien deze niet in rekening genomen worden in het HSABprincipe is de globale zachtheid geen geschikte indicator voor dit specifieke reactietype. Ook vanuit lokaal standpunt treden er veel problemen op. Het complexe reactiemechanisme van deze geconcerteerde reacties, waarbij de aanval aan de zure en aan de basische site simultaan gebeurt, kan niet beschreven worden gebruik makend van de geteste lokale indicatoren. In het algemeen is er nog verder onderzoek nodig voor de correcte beschrijving van multiple-site interacties. De polaire probemoleculen zijn harde systemen, en de lokale hardheid is eventueel een geschiktere index. Tot op heden is de berekening van deze grootheid echter nog problematisch en is er geen praktisch schema beschikbaar.

Een laatste toepassing was de unimoleculaire cyclisatie van een anion dat aanleiding geeft tot de vorming van een vierring, nl. de β-lactamring. Deze reactie vormt een uitstekend voorbeeld om competitieve reactiepaden te bestuderen, aangezien initieel de vorming van een stabiele zesring verwacht wordt. Het anionreactant is zeer zacht en de Fukui functie slaagt erin het geprefereerde atoom voor cyclisatie, nl. dit dat aanleiding geeft tot de vierring, aan te duiden als het meest reactief. Wanneer het anionreactant gebruikt werd binnen bimoleculaire reacties, b. v. protonatiereacties, is de lokale zachtheid

een geschikte descriptor om de waargenomen regioselectiviteit te beschrijven.

In dit doctoraatswerk werd tevens een belangrijk voordeel van het gebruik van reactiviteitsindicatoren onderzocht, nl. de lage computationele kost van deze grootheden. In de eerste plaats gebruiken zij enkel informatie bekomen op basis van de reactanten. Een zeer uitgebreide studie toont aan dat reactiviteitssequenties gebaseerd op globale descriptoren in grote mate onafhankelijk zijn van het gebruikte berekeningsniveau. Verschillende theoretische methoden – gaande van Hartree-Fock tot de nieuwste ontwikkelingen binnen dichtheidsfunctionaaltheorie – werden getest voor zowel geometrieoptimalisatie als energieberekeningen. De grote onafhankelijkheid van het berekeningsniveau draagt in grote mate bij tot de betrouwbaarheid van de onderzochte conceptuele grootheden die in het algemeen een belangrijke toegevoegde waarde bieden aan thermodynamische en kinetische grootheden.

B

List of Publications

Updated March 2007

Publications in International Peer-Reviewed Journals

1. Hemelsoet K. , Van Speybroeck V. , Marin G. B. , De Proft F. , Geerlings P. and Waroquier M.
Reactivity indices for radical reactions involving polyaromatics
J. Phys. Chem. A, **2004**, *108*, 7281–7290

2. Van Speybroeck V. , Hemelsoet K. , Waroquier M. and Marin G. B.
Reactivity and aromaticity of polyaromatics in radical cyclization reactions
Int. J. Quant. Chem., **2004**, *96*, 568–576

3. Van Cauter K. , Hemelsoet K. , Van Speybroeck V. , Reyniers M. F. and Waroquier M.
Comparative study of kinetics and reactivity indices of free radical polymerization reactions
Int. J. Quant. Chem., **2005**, *102*, 454–460

4. Hemelsoet K. , Lesthaeghe D. , Van Speybroeck V. and Waroquier M.
Bifunctional acid-base catalyzed reactions in zeolites from the HSAB viewpoint
Chem. Phys. Lett., **2006**, *419*, 10–15

5. Van Speybroeck V. , Moonen K. , Hemelsoet K. , Stevens C. V. and Waroquier M.
Unexpected four-membered over six-membered ring formation during the

synthesis of azaheterocyclic phosphonates: experimental and theoretical evaluation
J. Am. Chem. Soc., **2006**, *128*, 8468–8478

6. Hemelsoet K. , Moran D. , Van Speybroeck V. , Waroquier M. and Radom L.
An assessment of theoretical procedures for predicting the thermochemistry and kinetics of hydrogen abstraction by methyl radical from benzene
J. Phys. Chem. A, **2006**, *110*, 8942–8951

7. Hemelsoet K. , Van Speybroeck V. , Moran D. , Marin G. B. , Radom L. and Waroquier M.
Thermochemistry and kinetics of hydrogen abstraction by methyl radical from polycyclic aromatic hydrocarbons
J. Phys. Chem. A, **2006**, *110*, 13624–13631

8. Hemelsoet K. , Lesthaeghe D. , Van Speybroeck V. and Waroquier M.
Global DFT-based reactivity indicators: an assessment of theoretical procedures in zeolite catalysis
J. Phys. Chem. C, **2007**, *111*, 3028–3037

9. Pintér B. , De Proft F. , Van Speybroeck V. , Hemelsoet K. , Waroquier M. , Chamorro E. , Veszprémi T. and Geerlings P.
Spin-polarized conceptual DFT study of the regioselectivity in ring closures of radicals
J. Org. Chem., **2007**, *72*, 348–356

10. Van Speybroeck V. , Hemelsoet K. , Minner B. , Marin G. B. and Waroquier M.
Modeling elementary reactions in coke formation from first principles
Molecular Simulation, **2007**, accepted

11. Hemelsoet K. , Van Speybroeck V. and Waroquier M.
Study of hydrogen abstraction reactions on PAHs from the viewpoint of reactivity indicators
Chem. Phys. Lett., **2007**, submitted

Publications in A2 Journals

1. Van Speybroeck V. , Hemelsoet K. , Waroquier M. and Marin G. B.
Reactivity and kinetics of polyaromatic hydrocarbons in elementary radical reactions
J. Comp. Methods in Sciences and Engineering, **2002**, *2*, 315–318

Oral Contribution

Reactivity of Radical Reactions involving Polycyclic Aromatic Hydrocarbons
Reactivity Symposium, Theoretical aspects of reactivity, Brussels
5-7 April 2006

Poster Presentations

Research results were presented as poster presentations on several international conferences.